

# Interim Report



## System-wide environmental issues for sustainable salmonid aquaculture

*John K Volkman, J. Parslow, P. Thompson,  
M. Herzfeld, K. Wild-Allen, S. Blackburn, C. Crawford, P. Bonham,  
D. Holdsworth, P. Sakov, J.R. Andrewartha and A. Revill*

*January 2006*

*Aquafin CRC Project 4.2  
(FRDC Project No. 2001/097)*



System-wide environmental issues for sustainable salmonid aquaculture:  
interim report.

Bibliography.  
ISBN 1 921061 28 6.

1. Salmon farming - Tasmania. 2. Salmon farming - Tasmania  
- Monitoring. 3. Salmon farming - Environmental aspects -  
Tasmania. I. Volkman, John K. II. CSIRO. Marine and  
Atmospheric Research. III. Fisheries Research and  
Development Corporation (Australia). IV. Aquafin  
Cooperative Research Centre (Australia). V. Tasmanian  
Aquaculture and Fisheries Institute. (Series: FRDC  
Project ; no. 2001/097). (Series : Aquafin CRC Project ; 4.  
2).

333.956561409946

© Copyright Aquafin Cooperative Research Centre, Fisheries Research and Development Corporation, Commonwealth Scientific and Industrial Research Organisation

**This work is copyright. Except as permitted under the Copyright Act 1968 (Cth), no part of this publication may be reproduced by any process, electronic or otherwise, without the specific written permission of the copyright owners. Neither may information be stored electronically in any form whatsoever without such permission.**

**Every attempt has been made to provide accurate information in this document. However, no liability attaches to Aquafin CRC, its participant organisations or any other organisation or individual concerned with the supply of information or preparation of this document for any consequences of using the information contained in the document.**

*Published by CSIRO Marine and Atmospheric Research*



# System-wide environmental issues for sustainable salmonid aquaculture

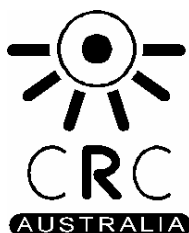
*John K Volkman, J. Parslow, P. Thompson,  
M. Herzfeld, K. Wild-Allen, S. Blackburn,  
C. Crawford, P. Bonham, D. Holdsworth,  
P. Sakov, J.R. Andrewartha and A. Revill*

January 2006

*Aquafin CRC Project 4.2  
(FRDC Project No. 2001/097)*



**Australian Government**  
**Fisheries Research and  
Development Corporation**



Tasmanian Aquaculture  
& Fisheries Institute  
University of Tasmania

# Table of Contents

## Abbreviations

<b>Non-Technical Summary .....</b>	<b>1</b>
------------------------------------	----------

<b>Acknowledgements .....</b>	<b>5</b>
-------------------------------	----------

<b>1. Introduction .....</b>	<b>6</b>
------------------------------	----------

1.1. Background to the Study.....	6
-----------------------------------	---

1.2. Need for the Study .....	7
-------------------------------	---

1.3. Objectives as Set out in Original Proposal .....	9
---	---

<b>2. Results and Discussion .....</b>	<b>9</b>
--	----------

2.1. Physical Modelling of the Huon and D'Entrecasteaux Channel .....	10
---	----

2.2. Phytoplankton .....	24
--------------------------	----

2.3. Sediment Biogeochemistry .....	39
-------------------------------------	----

2.4. Biogeochemical Modelling.....	46
------------------------------------	----

2.5. Adaptive Management of Salmon Aquaculture in the Huon and D'Entrecasteaux Channel .....	71
--	----

<b>3. Summary .....</b>	<b>83</b>
-------------------------	-----------

<b>References.....</b>	<b>85</b>
------------------------	-----------

## Appendix 1. Intellectual Property

## Appendix 2. Staff employed on project

## Appendix 3. Communications

## Appendix 4. List of attached project reports

## Abbreviations

ANOVA	Analysis of Variance
CMR	CSIRO Marine Research
CMAR	CSIRO Marine and Atmospheric Research (from July 1 <sup>st</sup> , 2005)
CRQ	Community respiration quotients = $\text{TCO}_2/\text{O}_2$ flux ratio
DBL	diffusive boundary layer
DIN	dissolved inorganic nitrogen
DO	dissolved oxygen
DPIWE	Department of Primary Industries, Water and Environment
ESD	Ecologically Sustainable Development
HES	Huon Estuary Study
MECO	Model for Estuaries and Coastal Ocean
OM	Organic matter
PAR	photosynthetically active radiation
RPI	relative preference indices
SCFA	Standing Committee on Fisheries and Aquaculture
TAFI	Tasmanian Aquaculture and Fisheries Institute
UTas	University of Tasmania

## Non-Technical Summary

<b>2001/097</b>	Aquafin CRC - FRDC Salmon Subprogram: System-wide environmental issues for sustainable salmonid aquaculture
-----------------	---

**PRINCIPAL INVESTIGATOR:** Dr John Volkman  
**ADDRESS:** CSIRO Marine and Atmospheric Research  
GPO Box 1538  
HOBART Tasmania 7001  
Australia  
Telephone: 03 62325281 Fax: 03 62325090

### OBJECTIVES:

1. Our overall objective is to acquire the necessary system understanding and knowledge, and apply it, in collaboration with industry and regulators, to support development of an adaptive management program which addresses system-wide impacts and production capacity for, and allows sustainable development of, salmon farms in the Huon Estuary and D'Entrecasteaux Channel.
2. Also, to develop and implement 3-D hydrodynamic and ecological models of the Huon Estuary and D'Entrecasteaux Channel, and use these to assess and predict the environmental impacts of salmon farm nutrient loads in relation to other nutrient sources (especially catchments and marine boundaries), and to assess the level of connectivity and exchange between the Huon Estuary and D'Entrecasteaux Channel, and among subsystems within D'Entrecasteaux Channel.
3. Determine the role of sediments in the estuary and nearby channel as a source of nutrient release and oxygen consumption as an input for the models and for comparison with processes occurring in sediments under fish cages.
4. Identify and quantify the key processes that link nutrient cycles with phytoplankton abundance and composition and determine the fate of the nutrients produced in finfish cage farms in waters of the Huon Estuary and D'Entrecasteaux Channel.

A 3D primitive equation model has been developed for the Huon Estuary and D'Entrecasteaux Channel to examine the hydrodynamics of the region. Using a nesting process the region could be represented with high resolution while incorporating forcing due to wind stress, tides, low frequency sea level oscillations and pressure gradients due to temperature and salinity distributions. Major forcing consists of river flow, which may be as large as  $1000 \text{ m}^3 \text{ s}^{-1}$  from the Huon River, wind which has an annual average speed of speed of  $4.3 \text{ ms}^{-1}$  from the south and tide which has a range of  $\sim 1 \text{ m}$  during the spring tide. The full year of 2002 was simulated and calibrated to data collected during 16 months in the parallel Broadscale Monitoring Program. Surface heat fluxes play a crucial role in regulating water temperature in the region. Differential

heating is apparent in the side bays, both in measured data and in the model and this may contribute towards heating of the main channel.

The Huon Estuary behaves as a salt wedge estuary with marine flow in bottom waters directed upstream in the Huon estuary, favouring the southern bank. Entrainment occurs from the salt wedge into the downstream freshwater flow, the majority of which then turns north upon entering the channel and exits into Storm Bay at the northern end of the channel. The head of the salt wedge is located near Huonville under low flow and is pushed downstream under high flow conditions. Under high flow conditions fresher water may be found as far north as North West Bay, and may be advected north as much as 24 km in just over two days. Flushing times varied from around three days for the lower Huon Estuary under high flow conditions to ~20 days for the whole domain in winter. A flushing estimate for the whole domain based on the average time for neutrally buoyant particles to exit the domain was computed as ~26 days.

Modelling of passive tracers showed that for releases at sites in the northern D'Entrecasteaux channel the distributions are confined to the northern region. Release sites in the lower channel and in the lower Huon Estuary resulted in relatively uniform concentrations throughout the domain outside a well defined mixing zone of high concentration. For release sites further up the Huon the largest concentrations were confined to the upper Huon. The southern channel and Huon Estuary can be characterized as well connected to the whole domain, whereas the northern channel has relatively poor connectivity with the southern channel.

Particle tracking results also confirmed the diurnal dominance of tidal forcing, with particles exhibiting up-channel and up-river movement on the flood tide, and down-channel/river on the ebb. During flood events the favoured trajectory out of the Huon was up-channel. The freshwater plume also favoured the northern bank of the Huon due to the influence of Coriolis forces. The location of the freshwater plume was, however, sensitive to wind direction, with north-easterly winds pushing the freshwater plume southwards.

A 3D biogeochemical model has been developed and refined so that it reproduces the observed spatial and temporal dynamics of dissolved nutrients, chlorophyll, phytoplankton biomass and oxygen in the Huon Estuary and D'Entrecasteaux Channel. This was coupled to a coarser resolution version of the hydrodynamic model. Observed nitrogen, chlorophyll and the biomass of the larger phytoplankton are particularly well reproduced in the D'Entrecasteaux Channel and side bays. The phosphorus cycle, which has a greater number of dissolved and particulate phases, is adequately simulated. However, modelled small phytoplankton biomass throughout the region lacked the observed seasonal winter maxima, and dinoflagellate biomass is poorly represented, particularly in the Huon where observed autumn blooms are absent. Further refinements of the model will be required to capture these ecological events. Modelled oxygen concentrations suggest over-estimation of horizontal mixing in bottom waters at the mouth of the Huon Estuary.

To demonstrate the effect of fish farm discharges on the biogeochemical cycling and water quality of the Huon Estuary and D'Entrecasteaux Channel a simulation was made with fish farm discharges omitted. By comparing this simulation with the original model run the effects of fish farm discharges throughout the region are clearly shown.

In general farm discharges had greatest effect on the nutrient fields in summer and on the phytoplankton in autumn.

Modelled annual median chlorophyll concentrations are  $\sim 1 \text{ mgChl m}^{-3}$  in surface waters throughout the D'Entrecasteaux Channel with slightly higher values in the southern basin compared to the northern end of the Channel. In the Huon Estuary modelled chlorophyll concentrations were lower contrary to observations, because dinoflagellates blooms were not simulated. Modelled annual median oxygen saturation dropped from  $\sim 100\%$  in surface waters to  $\sim 80\%$  in bottom waters of the lower Huon Estuary. The most oxygen-depleted waters were simulated in the upper Huon reflecting the influx of fresh river water. Values in bottom waters of the D'Entrecasteaux Channel were generally higher than in the Huon Estuary.

Nutrients showed a considerable range due to seasonally dependent utilization of nutrients by phytoplankton over an annual cycle. Concentrations during the summer months dropped to near-zero indicating that phytoplankton growth was limited by nutrients, in particular by nitrogen. Median annual dissolved inorganic nitrogen (DIN) was  $\sim 10 \text{ mgN m}^{-3}$  in surface waters of the D'Entrecasteaux Channel and about four times that in the Huon Estuary. Bottom water concentrations were highest in the mid Huon Estuary and in relatively shallow water, where the opaque river water limited phytoplankton growth and uptake. Phosphorus showed a similar behaviour.

Grazing by microzooplankton consumes an unusually high portion of daily primary production in the Huon Estuary. Prediction of phytoplankton blooms is possible only if the mechanism of escape from predation is known and quantifiable. Differential grazing pressure may contribute to small scale or short term variability in phytoplankton biomass making monitoring more difficult.

The environmental health of the D'Entrecasteaux Channel is high relative to the Huon Estuary and lower River Derwent reflecting the generally good conditions prevailing in the Channel and its adjacent embayments. There is evidence that chlorophyll *a* concentrations increased between 1996–1998 and 2001–2004 in the Huon Estuary with most of this increase occurring in the upper estuary. Locally supplied or recycled nitrogen (ammonium and urea) supports most of the phytoplankton growth in the Huon Estuary. Our monitoring work indicates that integrated water samples are needed for assessment of chlorophyll *a* concentrations, especially in the Huon and we recommend a minimum of monthly sampling of stations more than 10 km apart (if along the centre axis of the estuary).

We analysed the organic content and composition of several sediments from the Huon Estuary and some from more marine sites at Port Esperance (D'Entrecasteaux Channel) and Tasman Peninsula. These analyses show that organic matter contents in sediments from more exposed marine conditions are much lower than those in the Huon or in silt-dominated sites close to land. The inshore sediments have higher contents of organic matter, but this is mostly of terrestrial origin as shown by the high contents of long-chain alcohols and plant-derived sterols such as sitosterol and stigmasterol. In contrast, the organic matter in the sandy off-shore sediment is dominated by marine sources.

Three field trips during 2004, including March, July and November were carried out to measure benthic nutrient fluxes at sites in the Huon Estuary using sediments returned to

the laboratory for incubation. These results suggest that aerobic respiration is the dominant form of metabolism. Sediment respiration rates (measured as TCO<sub>2</sub> fluxes) at the lower estuary site ranged between 228  $\mu\text{mol m}^{-2} \text{h}^{-1}$  TCO<sub>2</sub> during winter and 644  $\mu\text{mol m}^{-2} \text{h}^{-1}$  TCO<sub>2</sub> during summer. Somewhat higher respiration rates were measured in the upper estuary (267  $\mu\text{mol m}^{-2} \text{h}^{-1}$  TCO<sub>2</sub> and 839  $\mu\text{mol m}^{-2} \text{h}^{-1}$  TCO<sub>2</sub> respectively). Ammonium production rates ranged between 16 to 81  $\mu\text{mol m}^{-2} \text{h}^{-1}$ , which was much less than measured fluxes through the sediment – water interface (1.6 to -6.7  $\mu\text{mol m}^{-2} \text{h}^{-1}$ ) indicating efficiently recycling of nitrogen liberated during the breakdown of organic matter in the sediments through the coupling of nitrification and denitrification.

The overall goal of this study is to help industry and managers design and implement an effective adaptive management strategy for sustainable development of salmon aquaculture with acceptable system-wide environmental impacts. The observations and modelling conducted by the study have led to improved quantitative understanding of the spatial and temporal variation in key environmental variables, and their response to natural environmental forcing and fish farm loads. The models are sufficiently developed to assess the likely environmental consequence of alternative future aquaculture development scenarios, and the potential for interaction with other pressures such as increases in catchment nutrient loads. These models can also assist in the evaluation of alternative monitoring and assessment strategies.

There has been agreement among industry, regulators and scientists on an interim set of environmental indicators, and implementation of an interim monitoring strategy. Monitoring results have been reassuring, suggesting that voluntary caps on fish farm loads in the Huon Estuary adopted by industry have avoided unacceptable environmental impacts at system-wide scales. To complete the work, an adaptive management strategy and associated monitoring is now required that includes:

- Clear operational objectives related to environmental impacts, and agreed indicators and performance measures;
- A monitoring strategy which provides cost-effective and reliable feedback on progress towards objectives;
- Understanding and models for assessment and prediction, to support management and industry decision-making.

These aims are being addressed in a follow-on project (CRC 4.2(2); FRDC 2004/074).

**KEYWORDS:** salmonid aquaculture, environmental issues, adaptive management, eutrophication, hydrodynamic modelling, biogeochemical modelling, phytoplankton ecology, indicators, monitoring, nutrients, dissolved oxygen, water quality, sediments.

## **Acknowledgements**

This project was carried out by a multidisciplinary team of scientists drawn from CSIRO Marine Research (CMR), Tasmanian Aquaculture and Fisheries Institute (TAFI) and PhD students from the University of Tasmania (Hobart and Launceston campuses). We gratefully acknowledge the many people who have contributed to the field work, sample analysis and data interpretation. We are particularly grateful to staff from the Department of Primary Industries, Water and Environment (DPIWE) of the Tasmanian State Government, Dr Gwen Fenton and more recently Colin Shepherd for their involvement in the project and valuable discussions. This project would not have succeeded without the close support of the Tasmanian salmon aquaculture companies and we would particularly like to acknowledge Dr Dominic O'Brien for his most valuable contributions.

This project employed funds invested out of the Aquafin CRC's Commonwealth grant and by FRDC and other participants of the CRC including the two research providers CSIRO Marine and Atmospheric Research and the Tasmanian Aquaculture and Fisheries Institute.

## **1. Introduction**

This report covers the work of project CRC 4.2 (FRDC 2001-097). This is part of a 7-year program which will be completed through project CRC 4.2(2) (FRDC 2004-074) by mid-2008. By agreement with Aquafin CRC and FRDC, the current project is presented as an Interim Report, comprising an overview of results and discussion, together with a non-technical summary. Six technical reports have also been prepared, providing detailed methods and results as well as animations of some of the modelling results which are included on the accompanying CD. The program will be reported as a whole, including benefits, adoption and outcomes, at the end of the follow on project in 2008.

### **1.1. Background to the Study**

This project was a major part of the first phase of research undertaken by the Environment Program of the CRC for Sustainable Aquaculture of Finfish (“Aquafin CRC”) to address environmental issues of relevance to the Tasmanian salmonid aquaculture industry. It was developed jointly by the two research agencies CSIRO Marine Research (CMR) and the Tasmanian Aquaculture and Fisheries Institute (TAFI) in close consultation with senior staff from the salmon industry, Government regulators and the FRDC to examine the system-wide environmental issues facing finfish aquaculture. Local or on-site research needs were concurrently addressed through FRDC project 2000/164 which determined the effects of stocking and fallowing on benthic faunal distributions and sediment biogeochemical processes.

This project explicitly addressed the fact that any expansion of the salmonid industry will be limited by the industry’s contribution to nutrient loads in surrounding water bodies and possible effects on phytoplankton abundance, dissolved oxygen levels and other ecological changes. One option available to the Tasmanian State Government was to limit nutrient release through agreed limitations to stocking numbers or feed quotas for different regions. Any limits set are necessarily best estimates and may be overly conservative because of a lack of detailed knowledge of the effects of nutrient release on ecosystem functioning. At the commencement of this project it was not possible to define appropriate limits for particular sites within a region, or to establish limits for those areas outside the Huon Estuary where environmental data were very limited. This study was designed to address these data needs and provide vital assistance with the planned establishment of an adaptive management strategy for environmental management of the industry.

Modelling, in combination with laboratory and associated field work, provides a means to identify the minimum data needs for assessing environmental conditions, allows scenarios to be tested and key linkages in the ecology of the region to be identified. However, for these models to provide a useful representation of the Huon and D’Entrecasteaux Channel we needed to resolve uncertainties about the influence of waters from D’Entrecasteaux Channel on conditions in the Huon Estuary, the role of organic-rich sediments in the natural cycling of nutrients and consumption of oxygen in the estuary and the manner in which phytoplankton groups respond to elevated nutrient levels.

The project was able to take advantage of the extensive set of environmental information, data and concepts generated by the FRDC-funded Huon Estuary Study - Environmental Research for Integrated Catchment Management and Aquaculture (Project No. 96/284; abbreviated to HES hereafter), but comparable data were not available for the D'Entrecasteaux Channel even though northern sections of the D'Entrecasteaux Channel was already heavily used by salmonid farming with aspirations for more carrying capacity. We noted that some areas such as North West Bay had high feed inputs and might not be as well flushed as other areas of the Channel. Port Esperance waters were being intensively farmed and there was a risk that they may be contributing substantially to nutrient loading in the lower Channel. There is considerable lease area in the southern Channel and plans for more, but use of these sites is currently limited due to constraints imposed by the need for freshwater bathing of the fish to treat amoebic gill disease.

As a precursor to this project, Department of Primary Industries, Water and Environment (DPIWE) and industry agreed to adopt an adaptive management approach to regulation and management of system-wide environmental impacts of salmon farms in the Huon Estuary and D'Entrecasteaux Channel. After the project started it was soon recognized that an adaptive management strategy needed to be put in place immediately and the original research proposal was modified by bringing forward tasks to support design and implementation of adaptive management of system-wide impacts, originally proposed for the second triennium of the CRC. We created a new adaptive management subproject to act as a focus for interaction between project researchers, State Government regulators and industry representatives to define suitable environmental indicators, advise on an interim monitoring project and help to interpret and assess data obtained from such monitoring.

Modelling and monitoring both play essential and synergistic roles in adaptive management. System understanding, encapsulated in models, underpins the choice of informative environmental indicators. Monitoring of these indicators provides direct assessment of the environmental state against agreed environmental objectives and targets. Models are needed for interpretation of monitoring results, especially for attribution of cause where environmental change is detected. Model predictions provide a basis for the development of management decision rules, while monitoring provides feedback on the outcomes of past management decisions, and data for testing and refining system understanding and model prediction.

## **1.2. Need for the Study**

There is a demonstrable need for more effective monitoring of the environmental effects of finfish aquaculture in Australia. For effective long-term management, it is critical that effective monitoring programs are set in place, both to allow evaluation of the performance of environmental management strategies, and to assess our understanding of marine farming environments as expressed through model performance and reliability.

Australian authorities need to adopt a more consistent approach to the regulation of finfish aquaculture. A national approach is needed that can build on existing experience in the different States. The Aquafin CRC provides one mechanism to achieve this by substantially improving communication between researchers, different finfish

industries and regulators, adoption of common approaches such as SCFA ESD and modelling and development of generic management and monitoring tools that can be readily adapted to different fish species and environments.

There is varying acceptance of finfish aquaculture in Australia. It is strongly supported by the Tasmanian and South Australian State Governments and it is generally well accepted by the general public in those States, particularly in regional areas where the industry provides considerable employment. However, some developments have been the subject of court cases (e.g. early efforts to farm tuna inside Boston Island, Port Lincoln in South Australia) or subject to strong opposition (e.g. proposals for finfish farming in Moreton Bay, Queensland). Victoria has severe restrictions on finfish farming due to perceptions of environmental risk.

In the international arena, there has been considerable controversy about real and perceived environmental impacts of salmonid farming. For example, in British Columbia a five year moratorium on new leases was imposed due to environmental concerns. In Scotland, the parliament was placed under considerable pressure to mount a major review of the environmental performance of the industry with a raft of issues such as sea-lice, disease and chemical issues, and possible links between nutrients and harmful algal blooms regularly featuring in the popular press. The present project grew out of the need by finfish industries, regulators and the Aquafin CRC to be proactive and work together to understand farm-environment interactions to avoid any unfounded controversies in Australia.

In South Australia, the aquaculture development application procedures are being enhanced to address the issues raised during the court proceedings associated with tuna farming in the Louth Bay region north of Port Lincoln. The establishment of an Aquaculture Act, an improved planning process and the initiation of an improved environmental monitoring program provide more certainty for developers and improved transparency and accountability on environmental issues. In Tasmania, any further expansion in the Huon Estuary (which, prior to our study, was the main location for salmon farming) will require a full consideration of the effects of nutrients on the ecosystem's assimilative capacity. To address community concerns, any changes in regulation or industry practices must be underpinned by environmental research addressing key knowledge gaps to ensure that appropriate measures are being taken.

The expansion of the salmon and tuna aquaculture industries in Australia will depend on a combination of economic, environmental and societal factors. It is the purpose of the CRC Environment Program to provide objective data and information addressing those environmental issues that could impinge on the success of finfish aquaculture. The present project was designed to study effects at the system-wide level and in particular help to identify the carrying capacity of southern Tasmanian regions for salmonid aquaculture.

The siting of finfish farming requires that a number of physical (water depth, benthic habitat, current speed, etc.), environmental (water and sediment quality, system carrying capacity, pollutants) and climatic criteria be met. Sufficient sites in Tasmania and South Australia are available to allow the industries to expand, but their characteristics are poorly defined and the overall carrying capacity of the regions is poorly known. Successful finfish aquaculture requires that the water body in which it is

located has, and maintains, a high environmental quality. Cage aquaculture has the potential to impact on this through release of nutrients, chemicals and organic matter and the associated changes in ecosystem function.

There has been considerable attention overseas to the possibility of links between nutrient release from salmon farming and the increasing prevalence of harmful algal blooms. This has gained much media attention and forced the salmon industry onto the defensive in the absence of compelling data either supporting or refuting the assertions being made. Previous modelling studies by CMR as part of FRDC-funded project 96/284 have demonstrated that the phytoplankton abundance in the Huon Estuary in summer is augmented by nutrients from salmon farming. However, specific details of how the composition of nutrient inputs (from cage aquaculture and other sources) can affect phytoplankton abundance and composition is still a key knowledge gap. Through a combination of field measurements and laboratory studies (some as part of the PhD project by Paul Armstrong) we aimed to establish how diatoms, dinoflagellates (including toxic species such as *Gymnodinium catenatum*) and other microalgae respond to increased nutrient inputs in the particular environments being studied.

### **1.3. Objectives as Set out in Original Proposal**

1. Our overall objective is to acquire the necessary system understanding and knowledge, and apply it, in collaboration with industry and regulators, to support development of an adaptive management program which addresses system-wide impacts and production capacity for, and allows sustainable development of, salmon farms in the Huon Estuary and D'Entrecasteaux Channel.
2. Also, to develop and implement 3-D hydrodynamic and ecological models of the Huon Estuary and D'Entrecasteaux Channel, and use these to assess and predict the environmental impacts of salmon farm nutrient loads in relation to other nutrient sources (especially catchments and marine boundaries), and to assess the level of connectivity and exchange between the Huon Estuary and D'Entrecasteaux Channel, and among subsystems within D'Entrecasteaux Channel.
3. Determine the role of sediments in the estuary and nearby channel as a source of nutrient release and oxygen consumption as an input for the models and for comparison with processes occurring in sediments under fish cages.
4. Identify and quantify the key processes that link nutrient cycles with phytoplankton abundance and composition and determine the fate of the nutrients produced in finfish cage farms in waters of the Huon Estuary and D'Entrecasteaux Channel.

## **2. Results and Discussion**

This chapter provides an overview of the research carried out and a summary of the key findings. A full technical account of the physical modelling, biogeochemical modelling and environmental studies in the Huon and D'Entrecasteaux Channel is shown in the accompanying technical reports available on the CD accompanying this report.

## **2.1. Physical Modelling of the Huon and D'Entrecasteaux Channel**

For a detailed technical account of the physical modelling the reader is referred to the accompanying technical report “Numerical Hydrodynamic Modelling of the D'Entrecasteaux Channel and Huon Estuary” by Herzfeld et al. (2005).

The D'Entrecasteaux Channel comprises the water body between the Tasmanian mainland and Bruny Island. The Huon Estuary joins the D'Entrecasteaux Channel near the southern limit of the channel, having fresh water input from the Huon River some 60 km upstream from the mouth of the estuary (Figure 1). The combined region is now a significant area for salmonid finfish farming as shown from the wide distribution of salmon farms in 2004 (Figure 2).

The Huon River is a significant source of fresh water where it enters the head of the Huon Estuary at Huonville. Saline water enters the Channel from the open ocean and propagates up the estuary as a salt wedge creating a classic salt wedge type estuary. These estuaries are characterised by high stratification and a stable water column; the water column only becoming well mixed during times of high flow when the salt wedge is pushed back downstream. The Huon/D'Entrecasteaux region is also characterised by complex geography, making modelling of the region challenging.

The channel domain is relatively shallow, with maximum depths of less than 60 m. The Huon Estuary is generally less than half this depth, with a narrow channel creating a connection between the estuary mouth and the main body of the channel. The region of interest in this study, the channel domain, terminates at the northern and southern limits of Bruny Island (Figure 1) to create two open boundaries.

In order to project trends in ecosystem health a series of numerical models were implemented to provide predictive capacity. These consisted of a hydrodynamic model described here to predict water transports, mixing regimes and temperature/salinity distributions and a biogeochemical model (described in section 2.4) to predict primary productivity and nutrient cycling.

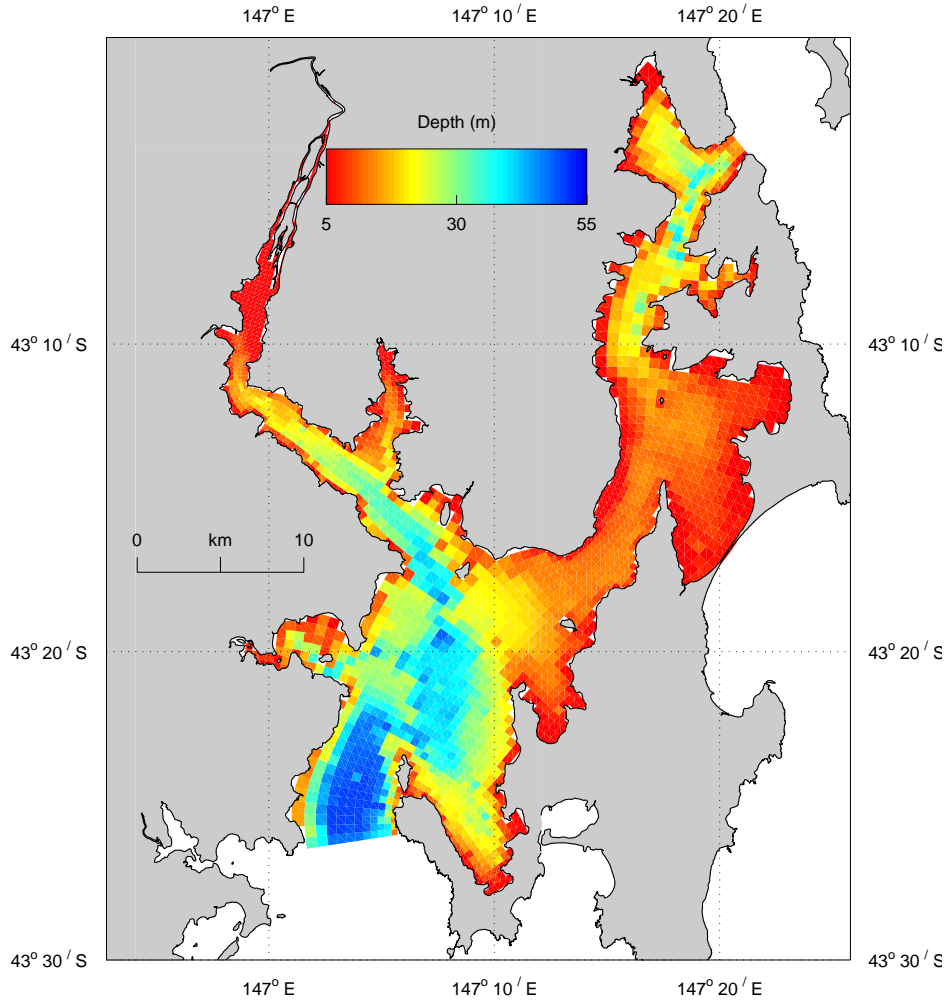


Figure 1. Map of the Huon-D'Entrecasteaux Channel domain showing bathymetry (in metres) and boundaries to the north and south of the channel.

We used the MECO (Model for Estuaries and Coastal Ocean; Walker and Waring, 1998) hydrodynamic model to simulate the physics of the D'Entrecasteaux Channel and Huon Estuary. This model was developed by the Environmental Modelling group at CMR over the last decade. MECO is intended to be a general purpose model applicable to scales ranging from estuaries to regional ocean domains, and has been successfully applied to a variety of applications encompassing these scales to date. MECO is a three-dimensional finite difference hydrodynamic model based on the primitive three dimensional equations of momentum, continuity and conservation of heat and salt, employing the hydrostatic and Boussinesq assumptions. The equations of motion are discretised on a finite difference stencil corresponding to the Arakawa C grid. A great advantage of MECO is that it can perform particle tracking and may be directly coupled to ecological and sediment transport models.

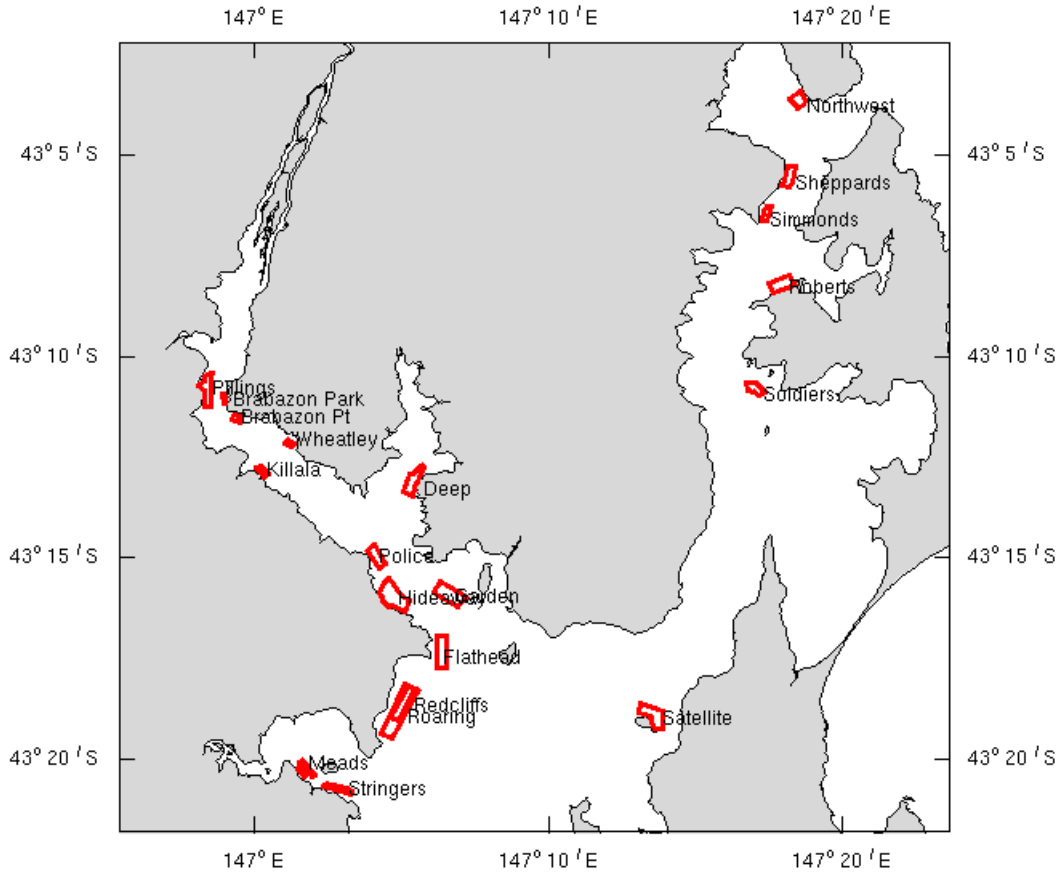


Figure 2. Salmon aquaculture farms in the Huon Estuary and D'Entrecasteaux Channel in 2004.

Outputs from the model include three-dimensional distributions of velocity, temperature, salinity, density, passive tracers, mixing coefficients and sea level. Examples of these are shown in the accompanying technical report (Herzfeld et al., 2005). Inputs required by the model include forcing due to wind, atmospheric pressure gradients, surface heat and water fluxes and open boundary conditions (e.g. tides).

The model uses a curvilinear orthogonal grid in the horizontal and a choice of fixed 'z' coordinates or terrain-following  $\sigma$  coordinates in the vertical. The curvilinear horizontal grid was particularly useful in this application since it enabled high resolution to be specified in areas of the study region where small scale motions were present and larger resolution where they were not (Figure 3). Long period simulations are required (>1 year) to assess the impact of aquaculture on the aquatic environment, and these simulations required acceptable run time ratios of greater than 100:1 (i.e. 100 model days in one day real time). Therefore, computation efficiency was an important issue in this study into which considerable effort was devoted. Much of this effort was directed in configuring the curvilinear grid to adequately resolve the domain without over-resolving and imposing computational penalties. A Laplacian diffusion scheme is employed in the horizontal on geopotential surfaces. Smagorinsky mixing coefficients may be utilised in the horizontal.

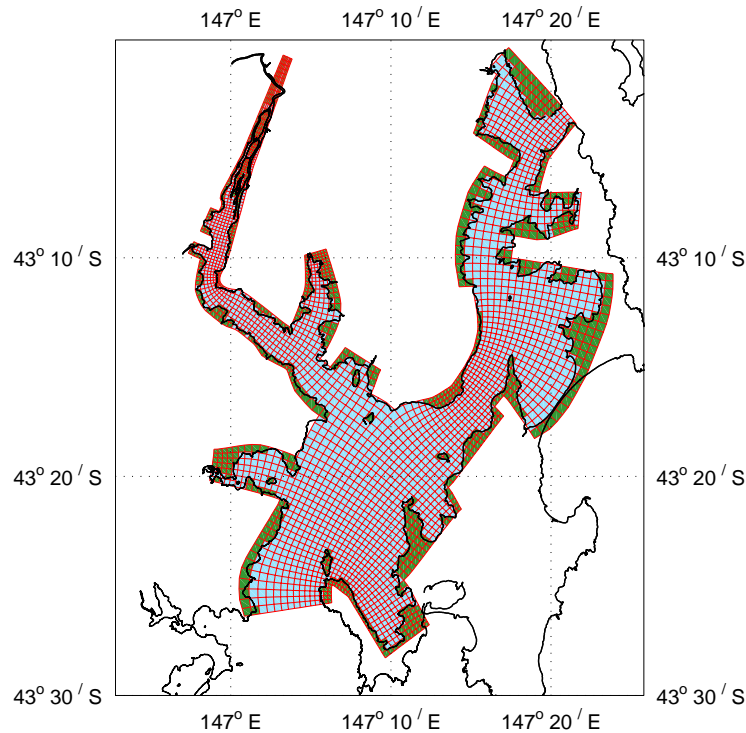


Figure 3. Model grid showing variation in cell size.

In order to remove problems of defining boundary conditions, the modelling required the construction of three nested model grids. A large scale regional grid was constructed which supplied the initial and open boundary conditions for an intermediate scale grid, which in turn supplied boundary forcing for the local grid of the study region. The regional domain includes three open boundaries; two cross-shore and one offshore beyond the shelf break.

Successively nesting local scale models inside larger regional models has two main advantages:

- (a) Regional models are capable of resolving large scale phenomena (e.g. boundary currents, mesoscale eddies, large scale upwelling, coastally trapped waves) that are not captured by local models. Motion resulting from these phenomena can be communicated into the local model through the open boundaries.
- (b) Open boundaries are notorious sources of error due to reflection and over-specification problems. By prescribing measured data on regional open boundaries and using output of the regional model to drive the local model these problems were minimized.

Environmental data to calibrate the model were provided by the joint TAFI-CSIRO Broad-Scale Monitoring Program carried out as part of the Aquafin CRC Environment Program. This program collected temperature, salinity, nutrients and phytoplankton samples on a monthly basis from throughout 2002 along a transect down the

D'Entrecasteaux Channel and at specific sites in the side bays. Full details are provided in the accompanying technical report by Thompson et al. (2005).

These temperature and salinity data were used for model initialisation and forcing through the open boundaries as well as model calibration. Additionally, these data provided useful insight into the thermodynamics and exchange processes occurring in the Huon and D'Entrecasteaux Channel. The first three months of 2002 were used to obtain an acceptable calibration, and the remainder of the year was used to validate this calibration. The model was also forced with wind, river flow from the Huon River and elevation, temperature and salinity at the two oceanic open boundaries.

Additional data were collected in the North West Bay region independently by TAFI. These data consisted of conductivity, temperature and depth and nutrient samples collected at specific sites and acoustic Doppler current profiler data from specific sites (courtesy of Dr Alan Jordan, TAFI) and covered the period November 2001 to February 2002.

The field data showed that there is a gradient in temperature (up to 1°C) down the D'Entrecasteaux Channel during summer and autumn, with the northern end warmer. The deeper waters at the southern end have the lowest temperature in the channel, presumably due to the sub-thermocline oceanic influence. Towards autumn this vertical gradient at the southern end is less pronounced as surface cooling decreases surface temperature heading into winter. In winter, bottom waters become warmer than surface waters, but still several degrees cooler than the summer bottom temperature. This bottom temperature increase in winter is also observed at the northern end of the channel. On 10 January 2001, a warm surface layer was particularly pronounced and shallow, and is associated with a thin layer of fresher water attributed to the influence of Huon River outflow. The flow data indicates that a large flow of  $883 \text{ m}^3 \text{ s}^{-1}$  occurred on 8 January 2001, thus the measurements taken on 10 January 2001 certainly captures this event. Generally, salinity is lower in the mid-channel region and attains the highest values in bottom waters at the ends of the channel throughout the year, thus density compensating the temperature distribution. Thin fresh water layers can also be observed mid-channel during times of high Huon River flow.

Flow from the Huon River was input directly into the model as an open boundary condition. River flow records were obtained at Frying Pan Creek, upstream from the riverine input open boundary in the Huon/D'Entrecasteaux domain (courtesy of DPIWE). This flow record was multiplied by a scaling factor of 1.2 to allow for catchment area contributing to flow below Frying Pan Creek, resulting in flow applicable to Huonville. Several large flood events occurred in 2002, primarily in the winter and spring months. The largest flow of close to 1000 cumecs occurred on 13 August. The salinity of the Huon inflow was assumed to be fresh (i.e. 0 psu). Derwent River flow was input as boundary conditions to the larger scale models within which the local domain was nested. Daily flow was obtained from the Tasmanian Hydro below Meadowbank and hourly data from DPIWE of the Tyenna flow.

Initial runs of the model were not satisfactory until it was realised that the heat terms had to be modified. The largest input of heat into the region is due to the short wave radiation component. During the winter months this decreases by approximately one-third compared to summer. The latent heat flux constitutes the largest heat loss term,

with larger losses observed during summer. Long wave radiation is predominantly a loss although occasionally diffuse sky input results in net longwave input. The sensible heat flux can act as a source or sink of heat and remains relatively invariant throughout the year. This heat flux was applied as the surface boundary condition for vertical diffusion of heat which greatly improved the representation of the annual cycle of sea surface temperature in the model. It was observed that temperature is significantly higher at the head of North West Bay than in the channel during summer, presumably due to differential heating associated with the gradient of bathymetry. This indicated that the shallow side bays adjacent to the main channel play an important role in acting as a heat source for the main channel during summer, subject to exchange processes.

### *2.1.1. General model solutions*

The full annual cycle of temperature and salinity in the Huon-D'Entrecasteaux region can be found in Herzfeld et al. (2005). Illustrative examples for the months of January to April, 2002 are shown in Figure 4.

Generally the model tends to be slightly fresh and cool mid-channel in the winter months. The warmer winter southern bottom water and associated seasonal variability described above is also evident. The Huon-D'Entrecasteaux system is microtidal with spring tide ranges up to 1 m. The diurnal tide has a range that is slightly larger than the semi-diurnal tide, and sea level in the region varies between periods of pure diurnal to pure semi-diurnal character.

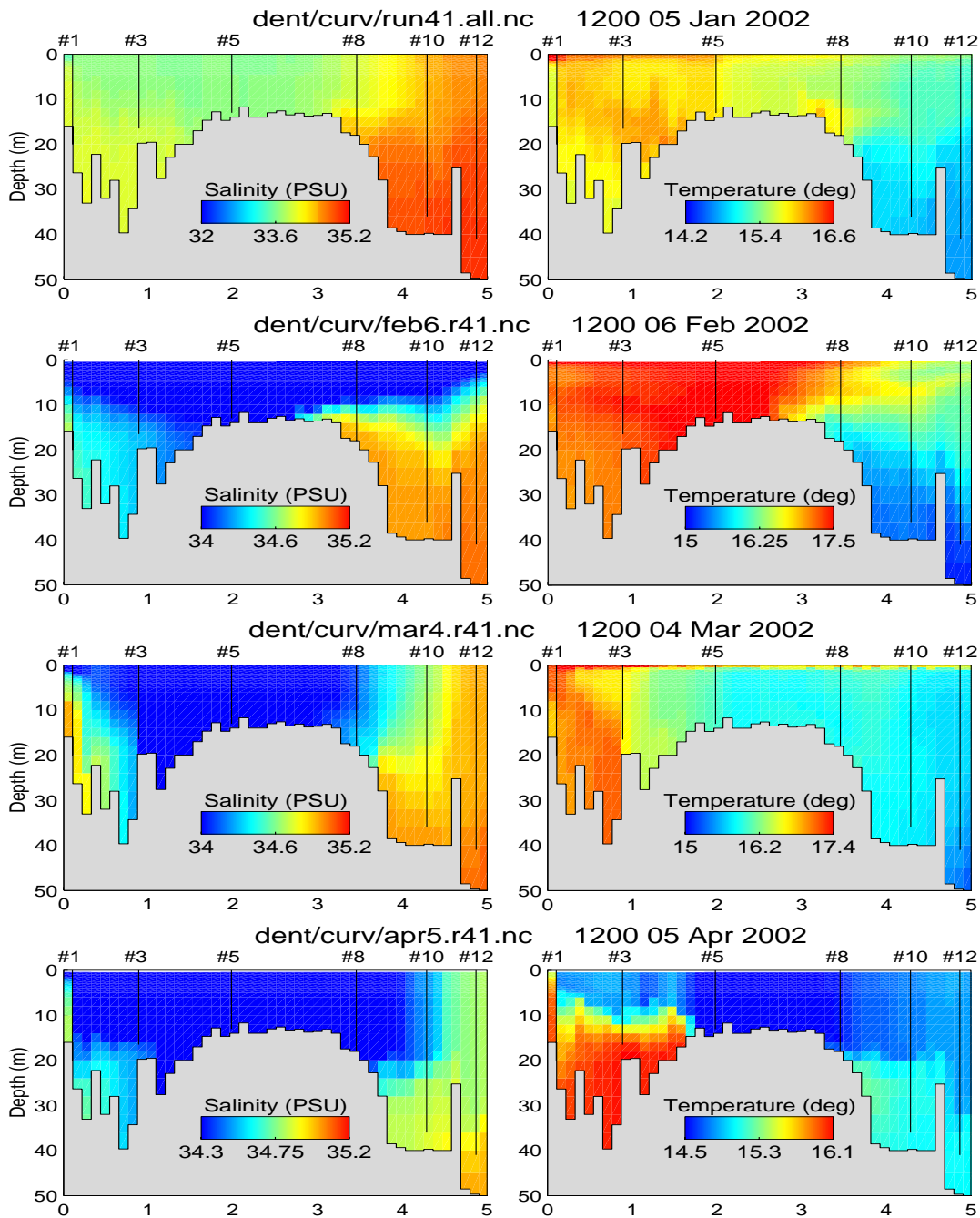


Figure 4. Modelled salinity and temperature sections for the months of January to April, 2002.

Since the Huon Estuary is a salt-wedge estuary, it is characterized by a freshwater layer overlying a saline wedge that intrudes up estuary. During periods of high flow a distinct fresh water plume discharges from the Huon Estuary and propagates up the D'Entrecasteaux Channel towards the northern boundary (Figure 5). This fresh water plume appears to favour the northern side of the estuary within the Huon, consistent with observation. Little fresh water makes its way to the southern boundary, and this occurs only under the influence of north-easterly winds. Under high flow the salt wedge in the Huon Estuary is pushed downstream.

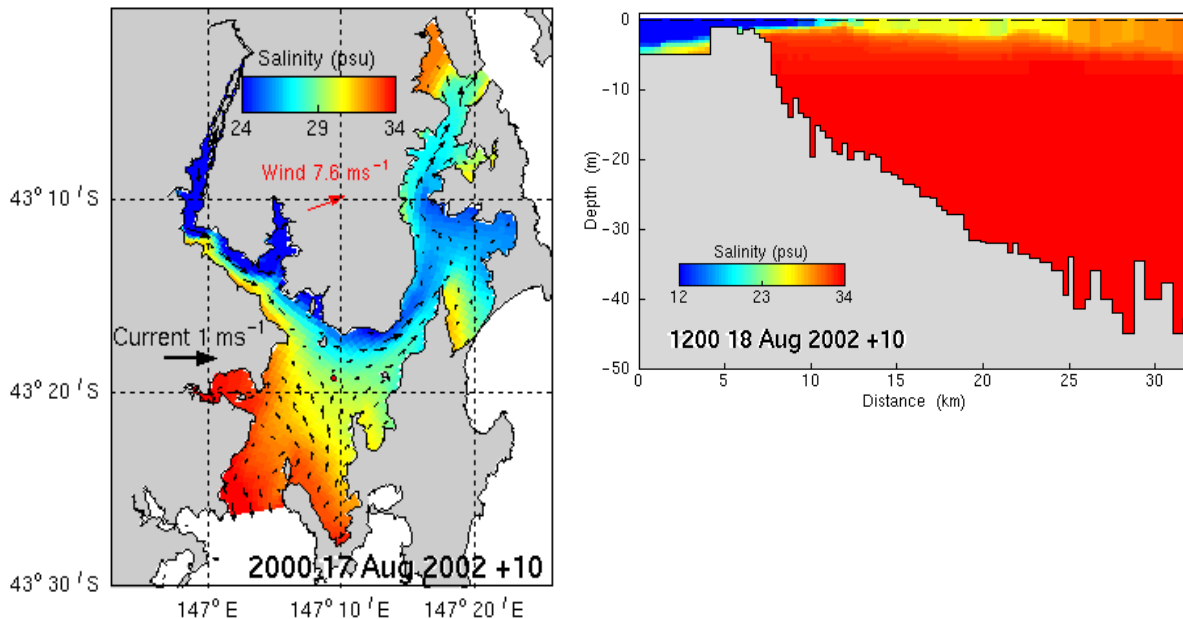


Figure 5. Modelled surface salinity and surface currents during a  $\sim 1000 \text{ m}^3 \text{ s}^{-1}$  flood. Tide is ebbing with a range of 0.83 m.

Maximum current velocities are observed midway up the D'Entrecasteaux channel at the narrowest point near Gordon, and may reach more than  $0.5 \text{ m s}^{-1}$  at times. Note that the sediment composition at this location is consistent with persistent strong currents. These currents are predominately tidal in nature, exhibiting a distinct oscillation at the tidal frequency. Motion is generally directed up-channel and up-river during the flood tide and down-channel and down-river during the ebb. Sea level gradients are low throughout the domain.

The general net flow through the system is inflow in bottom waters at the southern boundary following a route up the Huon Estuary in the salt wedge. Entrainment into the fresh river flow then carries water down-river into the channel where net flow up-channel out of the northern boundary occurs.

Our analyses indicate that locally the tide and wind are dominant drivers of surface flow, opposed by the Coriolis force. The mean surface flow in the Huon Estuary is a balance between density forcing and Coriolis (as expected in a salt wedge estuary) with wind contributing to down-river flow. In the northern channel density driven flow combines with rotation forces to produce seasonal up-channel residual flow. Cross channel forces balance in this area, with Coriolis opposing wind driven flow with some contribution of density effects to Coriolis. The southern channel exhibits both along and cross-channel net flow. Coriolis forcing opposes density forces in the along-channel direction while the wind driven flow opposes density driven flow in the cross-channel direction. Coriolis forcing is directed up-channel throughout the channel, whereas density effects are directed up-channel in the northern channel and down-channel in the southern channel. Horizontal friction becomes more important in bottom waters.

Passive tracers were used to obtain an estimate of the flushing characteristics of the estuary. A passive tracer was initialized in a sub-region of the estuary (Figure 6) with a concentration of one and zero elsewhere, and the total mass in this sub-region was

calculated throughout the simulation (Figure 7). Full forcing was applied to the domain (i.e. wind, tide, low frequency sea level and temperature/salinity effects) and the tracer distribution was simulated for a fixed period (14 days in this case). The e-folding time for flushing this sub-region is encountered when the total mass was reduced to  $1/e$  (~38%) of the initial mass.

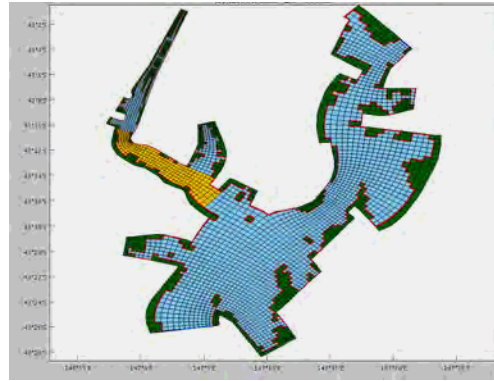


Figure 6. Huon flushing region (shown in yellow).

Flushing times were calculated for the dates 14 February, 15 April, 14 July and 17 October. The e-folding time for this sub-region varies from approximately 3.5 to 9.5 days depending on the magnitude of the Huon River flow, with faster flushing rates for higher flows. Maximum surface tracer concentration is found at the head of the estuary after 14 days, with significant concentrations ( $> 0.7$ , i.e. 70% of the original concentration) for low flows.

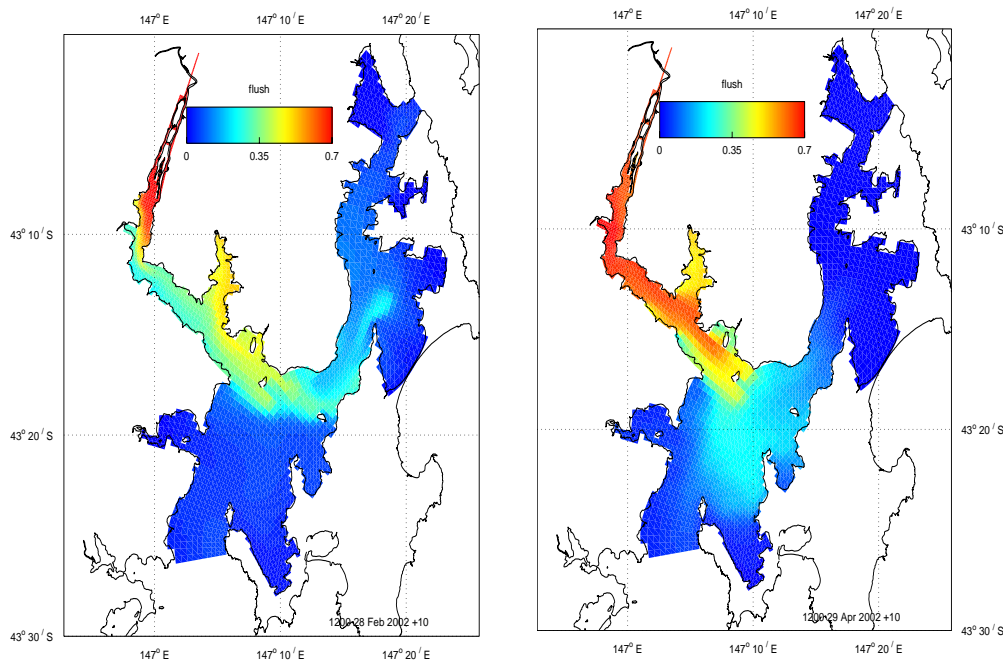


Figure 7a. Flushing tracer distribution: February      Fig. 7b. Flushing tracer distribution: April

Flushing times for the main channel range from 7.5 days in February to 8.8 in October. Surface concentration generally is higher (up to 0.7 in April) in the northern end of the

channel and remains low in the southern end and upper Huon Estuary. The northern boundary is responsible for little import of new water, as demonstrated by alternatively changing northern and southern open boundary conditions to zero flux conditions (which do not allow tracer with zero concentration in through the boundary). Using a zero flux on the northern boundary, the total mass never reached the e-folding fraction after 14 days. In fact total mass approached steady state, indicating that after an initial decrease while tracer is mixed into the side bays and Huon, there is negligible import of new water and this boundary must be associated with mass export. Using a zero flux on the southern boundary the flushing time is 8.2 days, only marginally longer than the 8.0 days calculated for runs when both boundaries were open. Hence the southern boundary is almost exclusively responsible for bringing in new water with zero concentration tracer. A summary of calculated flushing times for the various regions and the whole domain is shown in Table 1.

Table 1. Summary of flushing times for major side bays

<b>Region</b>	<b>Date</b>	<b>River Flow (m<sup>3</sup> s<sup>-1</sup>)</b>	<b>Flushing Time (days)</b>
Lower Huon Estuary	Feb 2002	131	6.5
Lower Huon Estuary	Apr 2002	128	9.5
Lower Huon Estuary	Jul 2002	229	4.7
Lower Huon Estuary	Oct 2002	537	3.4
Main D'Ent Channel	Feb 2002	131	7.5
Main D'Ent Channel	Apr 2002	128	8.5
Main D'Ent Channel	Jul 2002	229	8.0
Main D'Ent Channel	Oct 2002	537	8.8
Whole domain	Jul 2002	229	19.8
NWB	Jul 2002	229	5.0
Port Esperance	Jul 2002	229	5.1
Barnes Bay	Jul 2002	229	10.3
Great Bay	Jul 2002	229	7.4
Isthmus Bay	Jul 2002	229	9.5
Little Taylors Bay	Jul 2002	229	6.3
Great Taylors Bay	Jul 2002	229	6.9
Isthmus + Great Bays	Jul 2002	229	13.6

Residual, or mean/net, flow is the long term circulation the system experiences, and contributes towards flushing the region and distributing tracers input from the open ocean throughout the system. In this case the seasonal residual was calculated by averaging the velocities from every time-step over a 90 day period.

Surface residual currents are directed down-river in the Huon Estuary during all seasons, with maximum speeds of up to approximately 0.2 ms<sup>-1</sup> in the winter and spring when rainfall (hence river flow) is greatest. This river flow enters the channel and flows predominantly up-channel towards the north. Some flow is observed down-channel to the southern boundary.

The bottom flow is strongly directed into the domain at the southern boundary and continues northward towards the Huon Estuary mouth. Here the flow splits with the majority of water continuing upstream into the Huon Estuary along the southern bank, a smaller secondary bottom flow continuing through the narrowest point of the channel past Gordon into Isthmus Bay and a smaller still recirculation heading south into Great Taylor Bay. Further up the Huon Estuary bottom flow is directed down-river. At the northern end of the D'Entrecasteaux Channel bottom flow is directed down-channel and into North West Bay. Away from the southern boundary bottom velocities are generally quite weak throughout the domain, of the order of  $1 \text{ cm s}^{-1}$ .

Residual flow for the D'Entrecasteaux – Huon Estuary system is thus as follows: flow enters the region in bottom water at the southern end of the channel and continues along the bottom and upstream into the Huon Estuary in the salt wedge, favouring the southern bank. Entrainment occurs from the salt wedge into the downstream freshwater flow, the majority of which then turns north upon entering the channel and exits into Storm Bay at the northern end of the channel. A smaller proportion of Huon flow exits the southern channel.

The surface residual flow is predominantly the result of density gradient forces, wind and effects of rotation. Horizontal and vertical friction becomes important in the bottom waters. A schematic of the residual flow is presented in Figure 8.

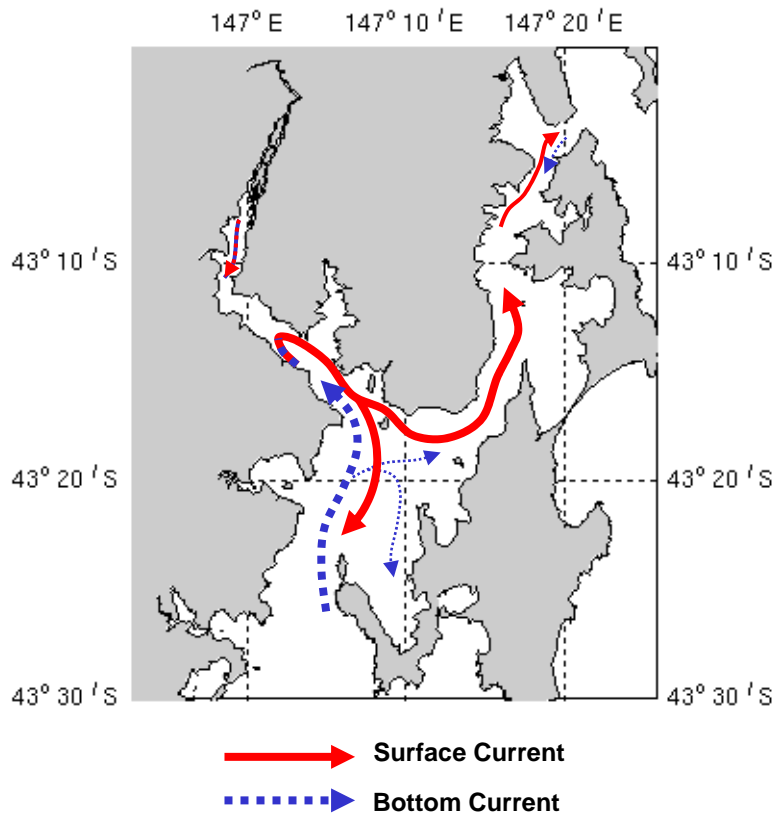


Figure 8. Residual flows in the Huon and D'Entrecasteaux Channel.

Point sources of tracers were continuously input into the water column at locations corresponding to a number of fish farm sites (Figure 9 and Table 2) with unit loads (assumed to be  $1 \text{ g s}^{-1} \sim 31,500 \text{ kg yr}^{-1}$ , giving output concentrations in units of  $\text{g m}^{-3}$ , or  $\text{mg L}^{-1}$ ) for the 12 month simulation period of 2002. Tracers were released over a depth range of 0 m to the shallower of 14 m depth (assumed to be the maximum depth of a farm cage) or the bottom. Surface tracer concentrations were output at two hour intervals and post-processed to compute the 5th, 50th (median) and 95th percentile distributions for the whole simulation, providing a statistical description of the distributions resulting from tracer transport over this period. Note that the response of the tracers to the interaction of the point source input with the system dynamics is linear, so that if the load were increased by some arbitrary factor then the corresponding concentrations can be scaled accordingly.

The release sites can be broadly categorized into three separate groups; those in the lower channel which resulted in relatively uniform concentrations throughout the domain outside a well defined mixing zone of high concentration, those in the upper Huon which have high concentrations in the upper Huon and lower concentrations throughout much of the remaining domain, and those in the upper channel whose tracer distributions are largely confined to the northern channel. This is a consequence of the residual flow, whose trajectories tracer tends to follow in the long term. The residual flow enters the domain in bottom waters in the southern channel, loops through the salt wedge in the Huon and exits the domain through the northern channel. This may be thought of as a ‘conveyor’ where tracer entering at any point on the conveyor will impact all locations downstream from its point of entry. Specifically, any tracer entering bottom waters in the southern channel (as most sites do extending to 14 m depth) will be transported with the residual flow and eventually make its way through the whole system and exit the northern boundary.

This behaviour is observed in Figures 9 to 11, which show the percentile distributions for Northwest (northern channel), Stringers (southern channel) and Killala (upper Huon Estuary). Distributions from the Northwest release were mainly confined to the head of North West Bay. Distributions resulting from release further south down the channel at Stringers exhibit a dramatic change. Tracer is distributed throughout the domain, with relatively uniform distributions found outside the mixing zone region of several kilometres associated with high concentration. Tracer is found within the Huon Estuary, having median concentrations of  $\sim 0.0005$  and maxima of  $\sim 0.001$ . The release at Killala results in distributions that are larger in the Huon Estuary than the D’Entrecasteaux Channel. Median concentrations are 0.001 in the upper and lower Huon while channel concentrations are  $\sim 0.0007$ . Elevated concentrations are observed in the channel near the Huon mouth.

For a full treatment of all release sites refer to Herzfeld et al. (2005). To put the predicted tracer concentrations in Figures 9 to 11 in some perspective, one can think of these as representing concentrations of DIN. They show that a “standard load” of  $1 \text{ g N s}^{-1}$ , or  $31.5 \text{ tonnes N y}^{-1}$ , if mixed and dispersed conservatively, results in typical median concentrations around  $0.0005$  to  $0.001 \text{ mg N m}^{-3}$  throughout the system, and  $0.001$  to  $0.002 \text{ mg N m}^{-3}$  in the Huon Estuary and North West Bay. The 95 percentile concentrations are about twice as large. Loads from individual farm sites range from around 10 to 90 tonnes N p.a. (Table 2), so dispersed concentrations resulting from individual sites would scale from about one third to three times these values. The total

load of around 720 tonnes N p.a. might be expected to increase median background DIN by about 10 to 20 mg m<sup>-3</sup>. Of course, in practice DIN is generally not conserved, but is taken up by phytoplankton and cycled through pelagic and benthic systems. If translated directly into chlorophyll, an increase in DIN of 10 mg m<sup>-3</sup> would produce an increase in phytoplankton biomass of around 1.5 mg Chl-a m<sup>-3</sup>. In the full biogeochemical modelling, where zooplankton grazing and other limiting factors and loss terms are included, predicted increases in phytoplankton biomass are significantly less than this. DIN in the biogeochemical model increased locally by up to 10 to 20 mg m<sup>-3</sup>, and the system wide median increase is somewhat less than this. The discrepancy may be due in part to an overestimation of passive tracer resulting from the open boundary condition employed. The boundary condition for nitrate in the biogeochemical model is specified using measured data, hence the flux of nitrate into and out of the domain is reasonably accurately known. This is not the case with the passive tracer, and an underestimation of tracer flux out of the domain may result.

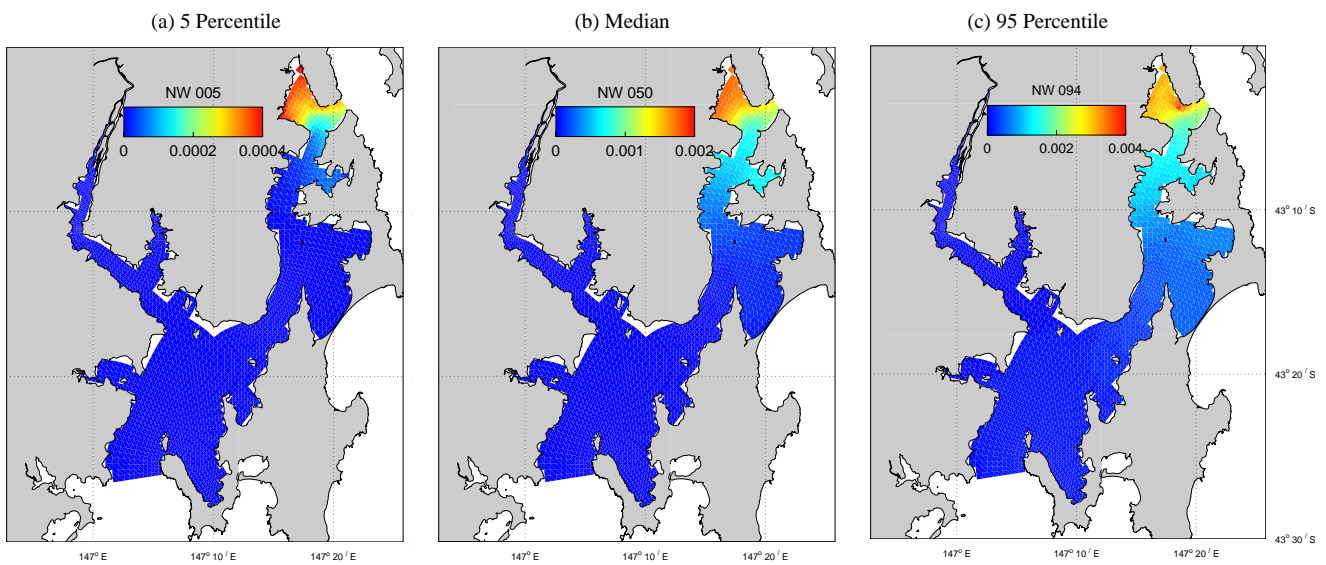


Figure 9. Percentile distributions for a tracer release at the Northwest site

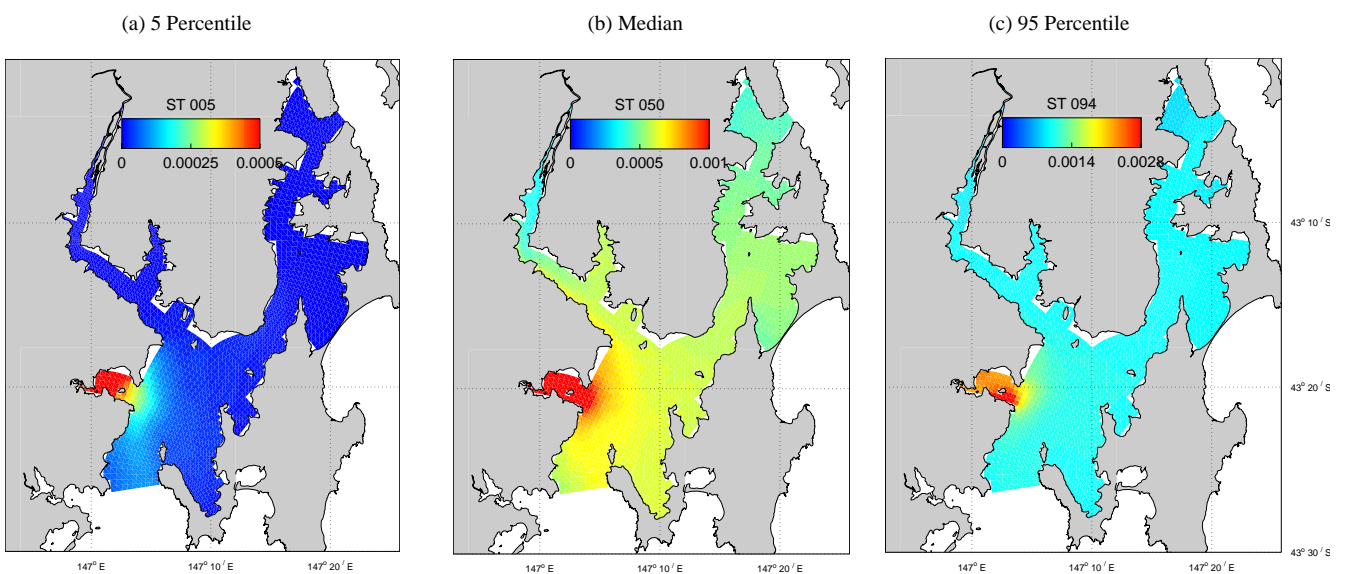


Figure 10. Percentile distributions for a tracer release at the Stringers site

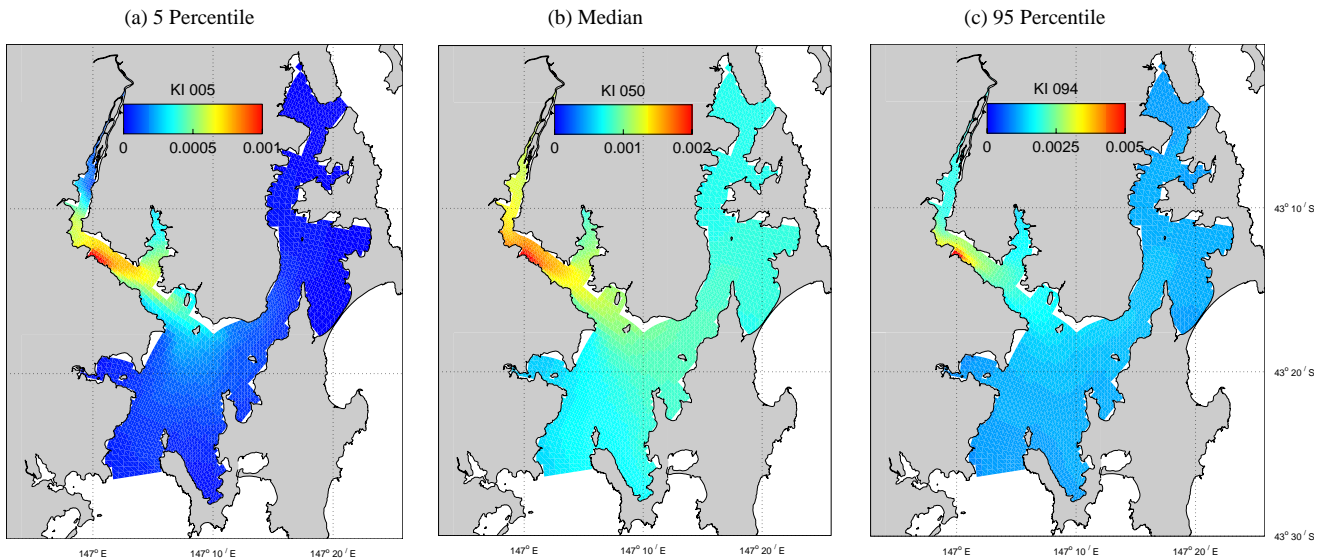


Figure 11. Percentile distributions for a tracer release at the Killala site

The connectivity of the domain was examined by observing the behaviour of neutrally buoyant particles released at the same locations as the point source releases and over the same depth range. The particles were released from random locations over the depth range at a rate of two particles/hour from an initial pool of 10,000 particles. These particles were subsequently advected with the circulation to provide insight into how various regions of the domain are connected. The particles were also subjected to random motion representing the effect of diffusion (i.e. sub-grid scale effects). Therefore, any two particles released from the same place at the same time are expected to undergo different trajectories due to this random motion. When a particle crosses the open boundaries at the northern and southern end of the model domain it was placed in the initial pool for subsequent re-release. The particle distributions after six months of simulation (corresponding to mid-winter) are displayed in Figure 12a (Stringers) and Figure 12b (Hideaway Bay). This distribution is the projection of particles at all depths onto the surface. Particles are colour coded according to their age since being released over the range 0–20 days (i.e. blue particles are 0 days old, red particles are > 20 days old).

Our analyses show that particles released in the southern channel and Huon Estuary exhibit relatively uniform distribution throughout the whole domain whereas those released at sites in the northern channel result in distributions confined to the northern domain. Therefore the southern channel and Huon Estuary are well connected to the whole domain, whereas the northern channel has relatively poor connectivity with the southern channel. This is consistent with the residual flow analyses which suggest a net flow up-channel exiting through the northern boundary.

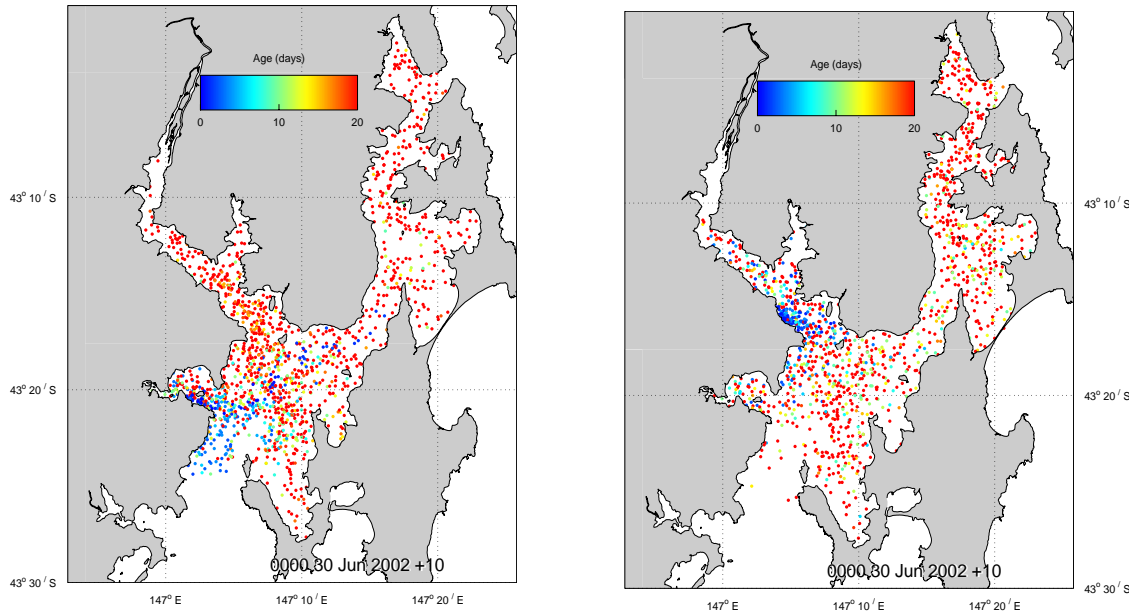


Figure 12. Particle release at (a) Stringers and (b) Hideaway Bay

## 2.2. Phytoplankton

There are four main aspects to the phytoplankton research reported here. First a baseline study of the D'Entrecasteaux Channel, the region adjacent to the Huon Estuary. The expansion of the aquaculture industry out of the Huon Estuary into the D'Entrecasteaux Channel meant that characterizing its environmental status was timely. Second, answering the question: "What nutrients support phytoplankton blooms, oceanic nitrate or locally supplied and largely recycled ammonium?" The third issue addressed in this section of the report is the relative importance of grazing in the Huon Estuary as a control on phytoplankton. Finally there is a preliminary comparison of chlorophyll *a* concentrations in 1996–1998 versus 2001–2004 in the Huon Estuary.

### 2.2.1. Phytoplankton in the D'Entrecasteaux Channel

The D'Entrecasteaux Channel lies between Tasmania and Bruny Island: at the south end it opens to Storm Bay through a 5 km wide and 50 m deep channel while the north end opens to the River Derwent through ~ 1 km wide and less than 20 m deep channel. There are no significant river inputs directly into the Channel although there are significant indirect inputs from the Huon River and North West Bay River. Nutrient inputs are largely seasonal resulting from deep oceanic water pushed into the region during winter.

A set of 12 stations were sampled monthly in the D'Entrecasteaux Channel during the 16 months from January 2002 to March 2003. A full report is provided in the attached technical report by Thompson and Bonham (2005). Phytoplankton community composition was broadly similar between the Huon and D'Entrecasteaux Channel in terms of algal class and seasonal timing of peak abundances (Figure 13). In general microflagellates dominate year round in terms of numbers. There were reliable spring diatom blooms. The data suggest that in the period from 1996–1998 (Huon Estuary Study) to 2002–2003 the main genus in the spring bloom changed from *Chaetoceros*

spp. to *Skeletonema* spp. In both water bodies there were autumn diatom blooms of *Pseudo-nitzschia*. The major difference was the presence of summer or autumn dinoflagellate blooms, especially *Gymnodinium catenatum*, in the Huon Estuary that have not been observed to reach similar densities in D'Entrecasteaux Channel.

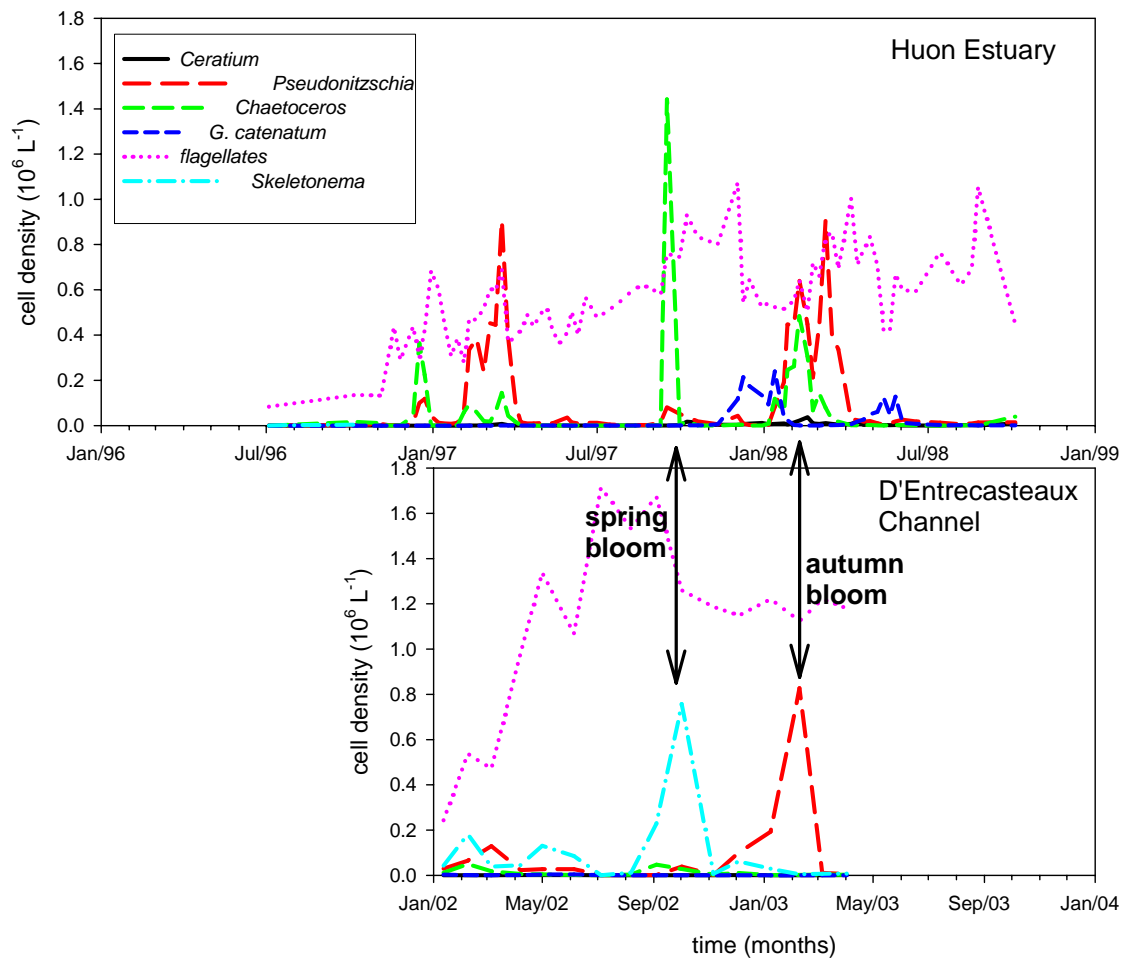


Figure 13. A comparison of dominant phytoplankton genera and their temporal abundance in the Huon Estuary (1996–1998 data from CSIRO Huon Estuary Study Team 2000) and D'Entrecasteaux Channel 2002–2003. Note panels are aligned by season not year.

Of the 12 channel sites characterized in 2002-2003 none showed any serious indications of eutrophication or anthropogenic nutrient inputs. The commonly accepted primary symptoms of eutrophication include hypoxia, anoxia, excessive phytoplankton blooms and high ambient nutrient concentrations (Gray et al., 1992). Since coastal ecosystems are generally nitrogen-limited then it would be anticipated that they will respond to the addition of more nitrogen. Human activities such as catchment clearing, sewage discharge, agriculture and finfish aquaculture can add nitrogen loads to the ecosystem. These loads can impact on the ecosystem to cause greater primary production (often equated to a greater concentration of chlorophyll *a*), more frequent algal blooms and decreasing water transparency. If the resulting carbon load is sufficient then hypoxia or anoxia may arise. In some ecosystems the source of nitrogen to fuel the increased algal blooms is associated with low dissolved oxygen and ammonium release from sediments. Therefore bottom water ammonium is also a symptom of an ecosystem with a supply of nitrogen that can be exacerbated by carbon loading. In the case of chlorophyll *a* as a measure of ecosystem status there are

standards recommended by ANZECC (2000) for mean annual chlorophyll *a* concentrations and the status of a water body:

Ultra-oligotrophic	< 0.7 mg m <sup>-3</sup>
Oligotrophic	0.7 – 2.1 mg m <sup>-3</sup>
Mesotrophic	2.1 – 6.25 mg m <sup>-3</sup>
Eutrophic	6.25 – 19.2 mg m <sup>-3</sup>
Hyper-eutrophic	> 19.2 mg m <sup>-3</sup>

All of the D’Entrecasteaux Channel sites sampled had mean annual chlorophyll *a* concentrations less than 2 µg L<sup>-1</sup> the internationally accepted criterion for oligotrophic waters. Some sites, however, were better than others. The site judged to be in the best environmental health was Little Taylors Bay with a relatively short flushing time, high dissolved oxygen, low ammonium and low chlorophyll *a* (Figure 14, Table 2).

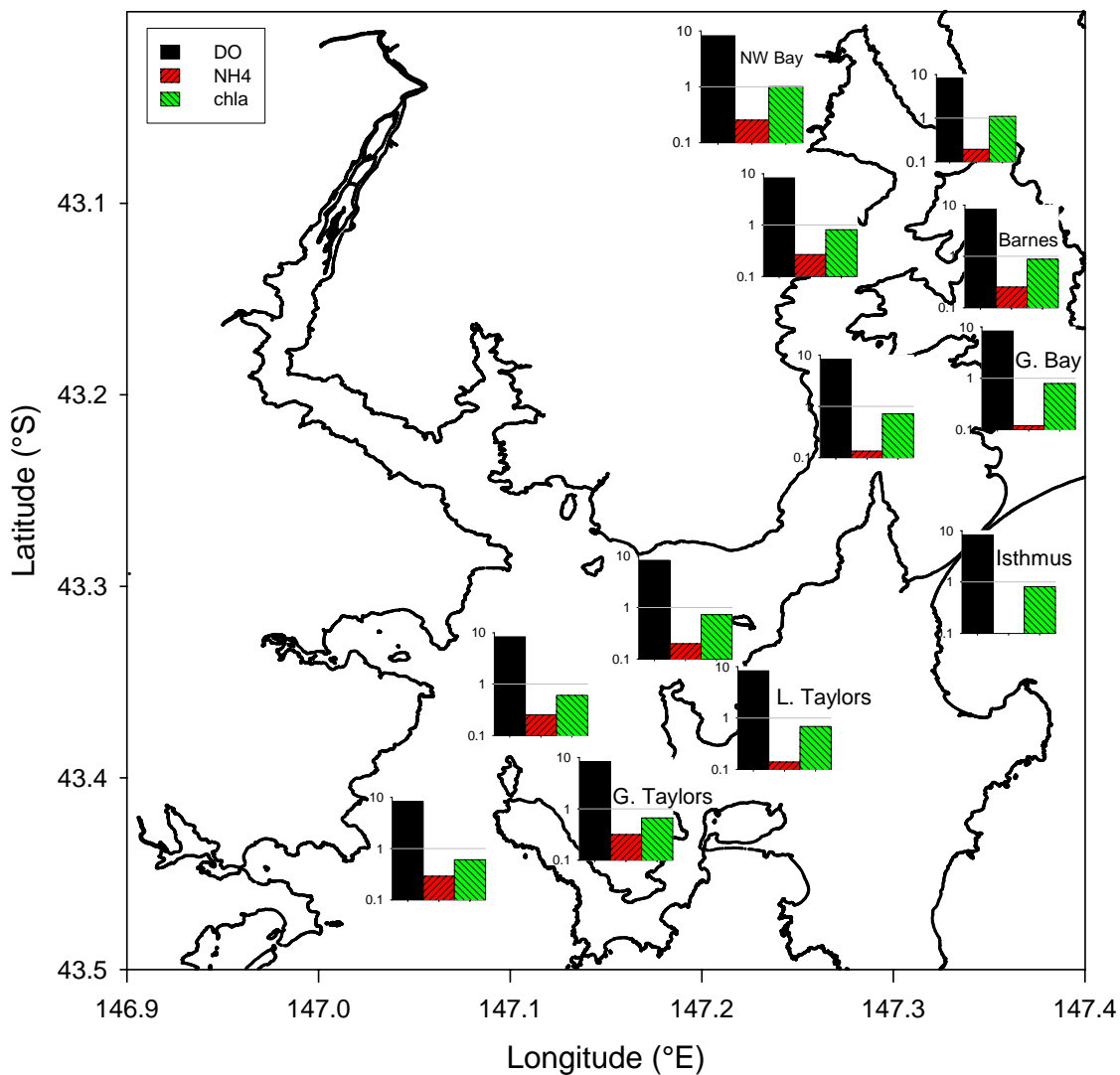


Figure 14. Map showing mean concentrations of dissolved oxygen, chlorophyll *a* and NH<sub>4</sub><sup>+</sup> at 12 locations in D’Entrecasteaux Channel during 2002 and 2003. Note the logarithmic scale on the inserted bar graphs.

In an effort to succinctly express these differences a summary statistic was developed consisting of mean annual chlorophyll *a* concentration, mean ammonium concentration and mean dissolved oxygen concentration. These site characteristics were weighted to achieve approximately equal emphasis using a very simple formula:

$$\text{score} = [\text{DO}]/10 + \text{chl}a + [\text{NH}_4^+]$$

Where [DO] is the concentration of dissolved oxygen in mg L<sup>-1</sup>, chl*a* = the concentration of chlorophyll *a* in mg L<sup>-1</sup> and [NH<sub>4</sub><sup>+</sup>] is the concentration of ammonium in μM and all measurements are annual means. The summary statistic was used to estimate the relative environmental health of all the sites but adjusted for flushing times for the various embayments (Table 2). A comparison of more water bodies should be undertaken to determine whether such a simple statistic can be used to rank the environmental health of water bodies around Tasmania. Regionally based intercomparisons are likely to be valid although it is unclear whether all State waters can be assessed using this simple approach, in particular, naturally anoxic water bodies may be problematic.

Table 2. Environmental characteristics at sites 1-12 in the D'Entrecasteaux Channel sampled in 2002 and 2003. See Figure 14 for approximate site locations or Technical Report (Thompson and Bonham 2005) for exact locations

Site	Description	DO	NH <sub>4</sub>	Chl <i>a</i>	Score	Grade	Flushing time	Comment
		mg L <sup>-1</sup>	μM	(μg L <sup>-1</sup> )			(Days)	
1	Mid channel off Dennes Pt	8.216	0.193	1.094	2.50	B+		High [chl <i>a</i> ] suggests frontal zone in this passage
2	NW Bay	8.216	0.255	1.005	2.48	C+	5.0	Moderate NH <sub>4</sub> , relatively low DO, greater chl <i>a</i> suggest this Bay is under stress, probably healthy due to short flushing time.
3	Mid channel off Oyster Cove Pt	8.232	0.266	0.811	2.29	B		Relatively high NH <sub>4</sub> is a concern
4	Barnes Bay	8.229	0.253	0.882	2.35	B-	10.3	Moderate NH <sub>4</sub> , moderate chl <i>a</i> and relatively long flushing time make this Bay one to be watched
5	Mid channel south of Green Is	8.292	0.135	0.720	2.06	B+		No problems detected
6	Great Bay	8.316	0.120	0.786	2.11	A-	7.4	Good DO, low NH <sub>4</sub> , low chl <i>a</i> and short flushing time
7	Isthmus Bay	8.299	0.093	0.808	2.11	B+	9.5	Good, but longer flushing time than site 6
8	Mid channel west of Satellite Is	8.314	0.199	0.727	2.13	B+		No problems detected
9	Little Taylors Bay	8.308	0.140	0.686	2.03	A+	6.3	Best overall site in survey
10	Mid channel, half way from Partridge Is and Ventenat Pt	8.291	0.253	0.602	2.06	B		Moderate NH <sub>4</sub>
11	Great Taylors Bay	8.298	0.318	0.664	2.19	B+	6.9	1 of 16 [NH <sub>4</sub> ] was very high, potential concern in this Bay
12	Mid channel off Browns Point	8.291	0.290	0.608	2.10	B		Moderate NH <sub>4</sub>

In comparison with nearby ecosystems the D'Entrecasteaux Channel had a mean chlorophyll *a* concentration of 0.83  $\mu\text{g L}^{-1}$ , lower than that observed in the Huon Estuary Study (HES) (1.32  $\mu\text{g l}^{-1}$ ; CSIRO Huon Estuary Study Team, 2000) and about 30% of the mean value observed in the lower River Derwent (2.63  $\mu\text{g L}^{-1}$ )\*.

We also examined other measures of ecosystem response to nutrient inputs. Of these, the frequency of algal blooms seems promising. The term “algal bloom” does not have an international or widely adopted definition although for the purpose of this report we will use a rise to three times the annual median concentration (Smayda 1997). Of the southeast Tasmanian ecosystems where we have sufficient data the mean concentrations of chlorophyll rank these three ecosystems: lower Derwent\* > Huon > Channel (i. e. Channel is lowest, = better). The frequency of bloom events provided a different ranking with the Huon experiencing many more observations of high chlorophyll *a* concentrations (Figure 15) and observations of much greater peak concentrations. The relative frequencies of blooms was Huon > Derwent >> Channel. There was a significant difference between these ecosystems ( $\chi^2 = 31.3$  with 2 degrees of freedom,  $P < 0.001$ ) in terms of bloom frequency. Together the relatively low mean chlorophyll *a* concentration and high bloom frequency indicates that the Huon Estuary has a low baseline of chlorophyll *a* biomass and yet is beset with more algal blooms than would be expected. By comparison the D'Entrecasteaux Channel had fewer blooms with only 3.6% of all observations exceeding three times the median chlorophyll *a* concentration.

\* data for 14 sites in the lower Derwent over the period from 1996 to 2004 were kindly supplied by the Tasmanian Department of Primary Industries, Water and Environment (DPIWE).

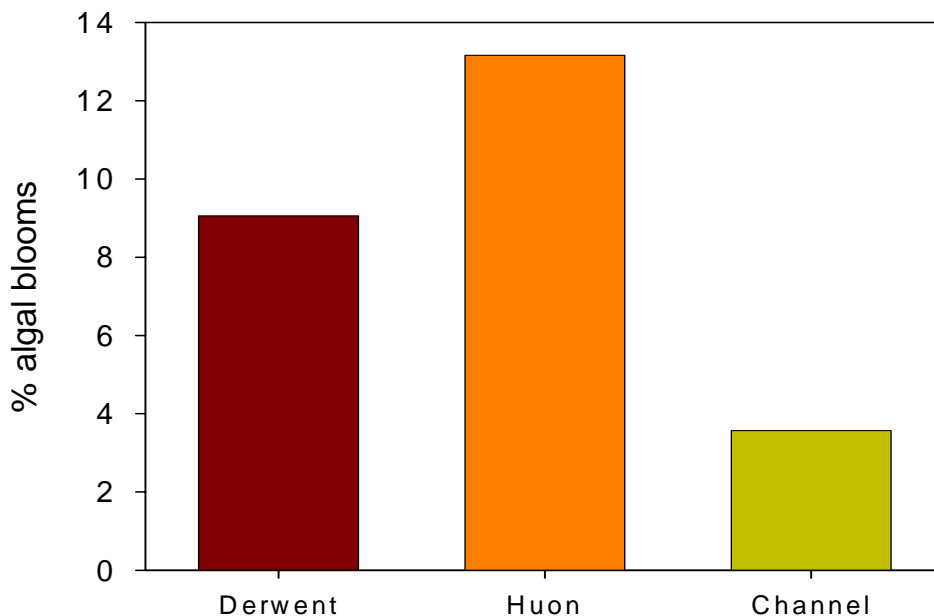


Figure 15. The percentage of algal blooms observed in the lower River Derwent, the D'Entrecasteaux Channel or the Huon Estuary.

### Management Implications

The environmental health of the D'Entrecasteaux Channel was high relative to the Huon and lower River Derwent reflecting the generally good conditions prevailing in the Channel and its adjacent embayments. North West Bay shows modest but early symptoms of eutrophication and, it is suggested, maintains a reasonably good health primarily due to its short flushing time. Barnes Bay is also reasonably healthy but its relatively long flushing time suggests this Bay would be more susceptible to eutrophication than most other embayments along the D'Entrecasteaux Channel.

### 2.2.2. Phytoplankton and nutrients

In this project research has focused upon whether the phytoplankton are using nutrients that have an oceanic source or more locally supplied or regenerated nutrients. Given that phytoplankton in Australian estuaries are nitrogen limited we are primarily interested in whether the phytoplankton grow using oceanic nitrate or more locally input or recycled nitrogen such as ammonium or urea. Paul Armstrong's PhD research included four field trips in the Huon Estuary on the 28-29 May 2003, 23-24 September 2003, 18-19 November 2003, and 24-25 February 2004. During these field trips a  $^{15}\text{N}$  dilution technique was used to measure uptake of three different nitrogen (N) sources ( $\text{NO}_3^-$ ,  $\text{NH}_4^+$  and urea) by the natural phytoplankton assemblage. Two sites, Garden Island and Hideaway Bay, were used for this field work. The N uptake measurements were taken at 5 m and 20 m water depth during both the day and night.

Conclusions so far from the results are that absolute uptake rates of  $\text{NH}_4^+$  were approximately five times greater than  $\text{NO}_3^-$  and urea uptake was approximately three times greater than  $\text{NO}_3^-$  on all four field trips (Figure 16).

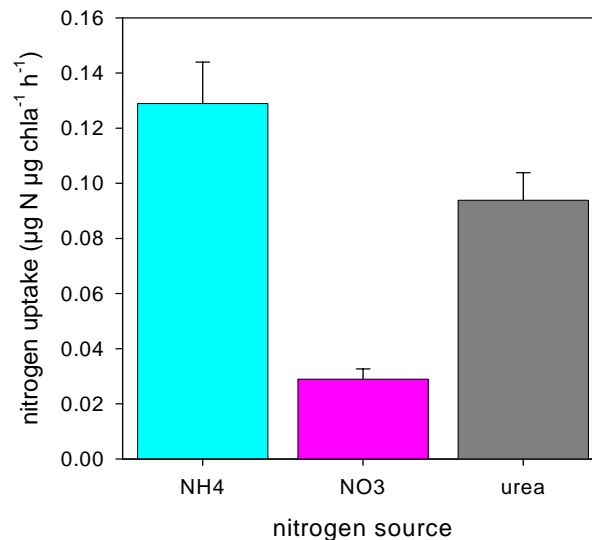


Figure 16. Absolute uptake rates for ammonium, nitrate and urea averaged across all experiments (various depths, times of day and seasons).

In some cases the uptake of nutrients is simply in proportion to their availability but many species of phytoplankton have preferences for particular forms of nitrogen. This relative preference index (RPI) can be calculated for each form of nitrogen:

$$RPI_{NO_3^-} = \frac{\frac{\rho NO_3^-}{\rho NO_3^- + \rho NH_4^+ + \rho ureaN}}{\frac{[NO_3^-]}{[NO_3^-] + [NH_4^+] + [ureaN]}}$$

Where  $\rho$  = the measured uptake rate and  $[NO_3^-]$  is  $([NO_3^-] + [NO_2^-])$  after McCarthy et al. (1977). The index gives 1 when uptake is in proportion to availability, >1 when a nitrogen species is preferentially taken up and <1 when the converse is true.

For all the samples from the Huon Estuary the RPI for  $NH_4^+$  was approximately nine times greater than that of  $NO_3^-$  (Figure 17). Similarly the RPI for urea was ~ 2.4 or four times greater than the 0.61 RPI for nitrate. The results indicate an active preference for uptake of  $NH_4^+$  and urea over nitrate.

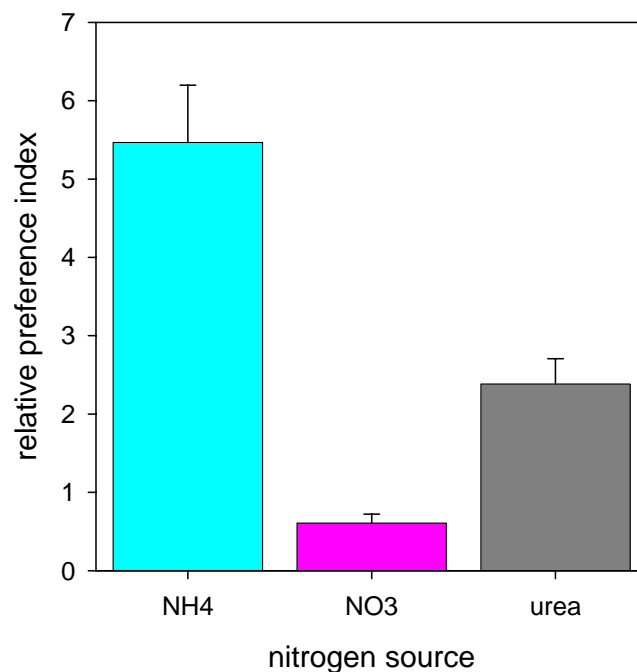


Figure 17. Relative preference indices for ammonium, nitrate and urea uptake experiments averaged across all depths, times of day and seasons. Details of calculations are given in text.

During February 2004 measured  $NH_4^+$  uptake rates ( $0.12 \mu\text{gN L}^{-1} \text{h}^{-1}$ ) would have exhausted ambient ammonium concentrations ( $3.92 \mu\text{g L}^{-1}$ ) in ~ 32 hours. During the preceding period from September 2003 through to February 2004 there was, however, only a relatively small decrease in ambient concentration of  $NH_4^+$  in comparison to the large decrease in ambient concentration of  $NO_3^-$ . These observations indicate a high rate of  $NH_4^+$  relative to  $NO_3^-$  re-supply to the ecosystem.

A large bloom of *G. catenatum* has not recently been observed in the Huon Estuary (unfortunate from the study's perspective) but a dense bloom did occur a few kilometres away in Southport. An extra field trip (30-31 March 2004) was undertaken

in Southport to investigate N uptake by *G. catenatum* during this bloom. The complete set of these results will be available in Paul's soon to be completed PhD thesis.

Paul has also carried out several laboratory experiments. *G. catenatum* was grown on  $\text{NO}_3^-$  or  $\text{NH}_4^+$  as sole N sources. Growth on  $\text{NH}_4^+$  ( $0.123 \text{ d}^{-1}$ ) as a sole N source was measured and found not to be significantly different ( $P = 0.161$ ) from growth solely on  $\text{NO}_3^-$ . Paul has commenced experiments to determine the ability of *G. catenatum* to grow on urea as a sole N source. The information from these lab experiments will help us understand whether a certain species of N may confer an advantage to *G. catenatum* and further insight into its bloom dynamics.

### **Management Implications**

The phytoplankton of the Huon Estuary use mostly, and have a strong preference for,  $\text{NH}_4^+$  or urea. Thus summer and autumn algal blooms are mostly fueled by nitrogen locally supplied or recycled.

### **2.2.3. Grazing experiments**

Phytoplankton growth can be controlled by the intensity of zooplankton grazing (top-down control). Larger phytoplankton tend to be eaten by the larger classes of zooplankton (copepods etc), while the smaller phytoplankton species are consumed by the smaller animals (microzooplankton). This can have important consequences for biogeochemical cycling since the larger animals produce discrete faecal pellets which rapidly remove organic material from the photic zone to sediments while in the smaller size classes much of the organic matter and nutrients is recycled in place. As part of our research into the pathways of nutrient cycling and to improve our understanding of the processes associated with phytoplankton blooms in the Huon Estuary we have undertaken the first measurements of microzooplankton grazing in this ecosystem based on the grazing-dilution technique of Landry and Hassett (1982). Prior to the development of this breakthrough technique the technical difficulties caused by the overlapping size range of microzooplankton, mostly ciliates, heterotrophic flagellates and zooplankton nauplii, with their phytoplankton prey made ecological studies into the role of these small predators nearly impossible.

The grazing-dilution technique is time consuming and labour intensive (Landry and Hassett 1982), but it has been increasingly used to assess the grazing impacts by microzooplankton. The results have provided important new insights into the cycling of matter through the aquatic food chain (Verity and Smetacek 1996), dramatically focusing attention upon "top down" control of phytoplankton growth particularly in oceanic environments (e.g. Fileman and Burkill 2001). In some locations microzooplankton have been reported capable of consuming ~ 100% of the phytoplankton daily production (Verity et al., 1996).

A total of four grazing rate experiments were undertaken during 2003 and 2004. A complete set of data is presented in the attached Technical Report (Thompson and Bonham 2005). The apparent growth rates of phytoplankton in individual incubation bottles were calculated using chlorophyll *a* as the measure of standing stock. A typical result from a grazing rate experiment demonstrates the linear nature of the relationship

between the proportion of unfiltered seawater added (“fraction unfiltered seawater”) and the apparent phytoplankton growth rate (Figure 18). There are two important estimates of *in situ* processes estimated from these data. The first is the Y-axis intercept, the estimated phytoplankton growth rate in the absence of any grazing =  $1.53 \pm 0.08 \text{ d}^{-1}$ . The second is the slope of the line, estimates the grazing rate by microzooplankton on phytoplankton =  $-1.44 \pm 0.11 \text{ d}^{-1}$ .

In the first experiment during September 2003 grazing rates were quite variable and not significantly different from zero (Table 3). During all other experiments grazing rates were significantly different from zero and significantly different in time (i.e. from each other). Grazing rates rose in November and were maximal in February before declining again in winter (July 2004). Grazing pressure was sufficient to reduce phytoplankton growth rates by an average of  $79\% \pm 6\%$  ( $\pm 1 \text{ S.E.}$ ) across all experiments. Net phytoplankton growth rates (grazing rate – growth rate) were mostly small, with significant net growth only during the late summer bloom in February 2004 (Table 3).

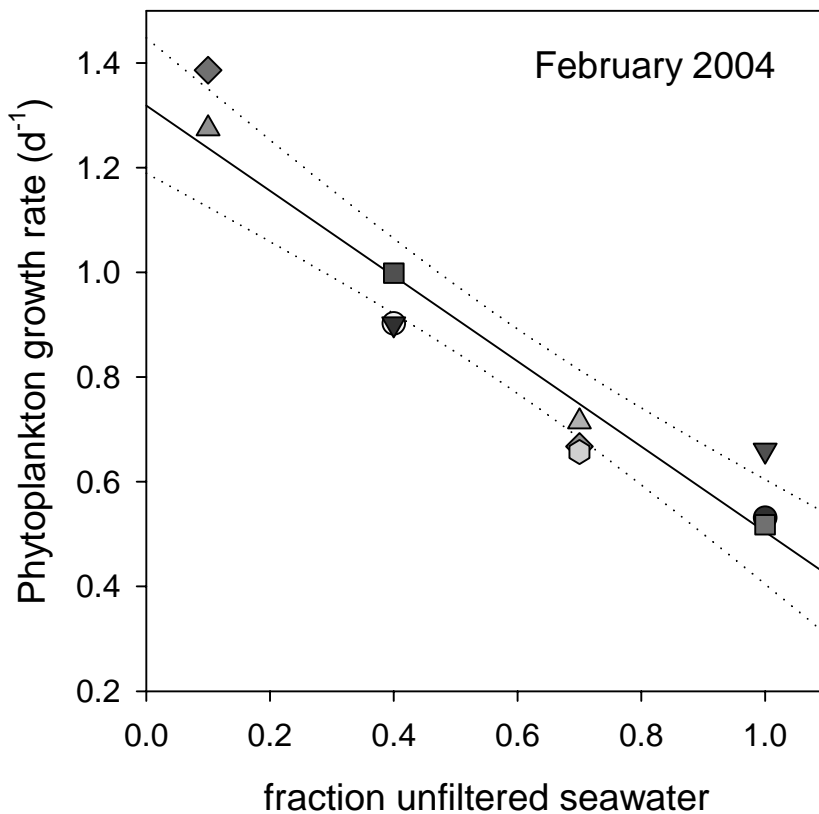


Figure 18. The phytoplankton growth rates are calculated from initial versus final chlorophyll *a* concentrations (see Technical Report for details) plotted versus the amount of unfiltered seawater in the sample. Solid line is a linear regression, dotted lines are 95% confidence intervals for the regression. This experiment was conducted in February 2004 as one of four throughout 2003–2004.

Table 3. Grazing rates and gross phytoplankton growth rates (chlorophyll *a*) in the Huon Estuary during 2003-2004. Means  $\pm$  standard errors are reported for grazing and growth rates.

Date	Standing stock chlorophyll <i>a</i> $\mu\text{g L}^{-1}$	Slope = grazing coefficient: <i>G</i> $\text{d}^{-1}$	Y axis intercept = phytoplankton growth rate: $\mu$ $\text{d}^{-1}$	$R^2$	Net growth rate ( $\mu - g$ ) $\text{d}^{-1}$
September 2003	0.36	-0.03 ( $\pm 0.13$ )	0.04 ( $\pm 0.08$ )	0.01	0.01
November 2003	1.18	-0.66 ( $\pm 0.14$ )	1.03 ( $\pm 0.09$ )	0.69	0.37
February 2004	1.98	-0.81 ( $\pm 0.09$ )	1.32 ( $\pm 0.06$ )	0.90	0.50
July 2004	0.25	-0.51 ( $\pm 0.10$ )	0.54 ( $\pm 0.06$ )	0.72	0.03

During late summer when the phytoplankton biomass was greatest ( $1.92 \mu\text{g chlorophyll } a \text{ L}^{-1}$ ) there were sufficient amounts of several individual pigments to calculate growth and grazing rates for each (see technical report for details). Grazing was approximately equal to or greater than gross growth rates for alloxanthin, diadinoxanthin, diatoxanthin and zeaxanthin, while for chlorophyll *b*, chlorophyll *c*, fucoxanthin and  $\beta, \beta$ -carotene growth rates were substantially greater than grazing. The calculated net growth rates ( $\mu - g$ ) were greatest for fucoxanthin ( $0.84 \text{ d}^{-1}$ ) and about 33% greater than for the most generic pigment, chlorophyll *a* (Table 3, Figure 18). The results clearly indicate that differential grazing was sufficient to shift phytoplankton community composition relatively quickly reducing Cyanophyta and Cryptophyta relative to taxa such as Bacillariophyta, Dinophyta, Prymnesiophyceae, Chrysophyceae and Raphidophyceae.

The dominant microheterotroph grazers were ciliates (43%), followed by heterotrophic dinoflagellates (30%) and tintinnids (18%). Small numbers of most other grazers were observed with radiolarians, copepod nauplii, bivalve larvae, Appendicularians (larval tunicates), and rotifers each averaging less than 1% of the total (Figure 19). Numbers of *Polykrikos schwartzii* peaked at  $510 \pm 361 \text{ L}^{-1}$  in February 2004. Temporal variability was high but overall the total number of grazers was maximal during November 2003, significantly greater than the numbers observed in February or July 2004 ( $P < 0.001$ ). The rise in grazers during November 2003 was primarily due to an increase in ciliates and was accompanied by a significant decline in grazer diversity (see Technical Report, Thompson and Bonham 2005 for details).

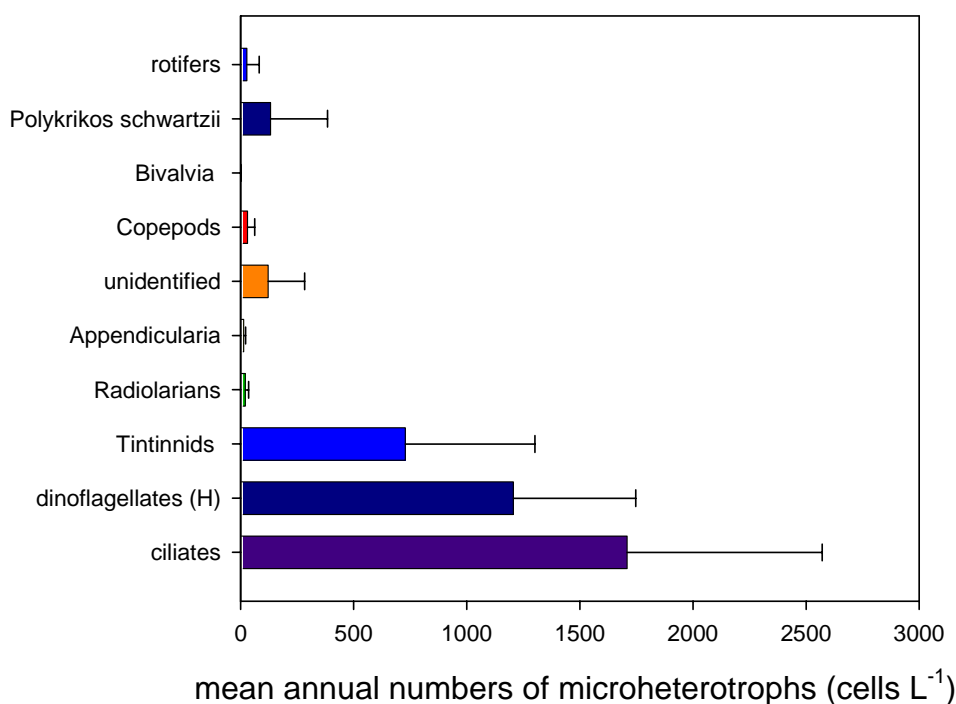


Figure 19. The abundances of dominant groups of microheterotroph grazers (microzooplankton) in the Huon Estuary, sampled four times during 2003–2004

Gross phytoplankton growth rates ( $\mu$ ) varied over the annual cycle from about zero to  $1.5 \text{ d}^{-1}$ . The upper gross growth rate ( $1.5 \text{ d}^{-1}$ ) is approximately the maximum that can be expected for temperate phytoplankton species under the prevailing temperature conditions (Eppley, 1972). Net phytoplankton growth rates based on chlorophyll *a* were sometimes small, but increased sharply during the blooms both during spring and in the late summer bloom reaching  $0.37$  to  $0.5 \text{ d}^{-1}$  (~40% of gross growth rates) during November 2003 and February 2004. That net growth rates may be small at certain times of the year is perfectly consistent with the observations of changes in wide spread chlorophyll *a* concentrations in the Huon Estuary and nearby D'Entrecasteaux Channel. For example, averaged over 12 sites in D'Entrecasteaux Channel the observed increase in chlorophyll *a* concentration was a net growth rate of  $0.005 \text{ d}^{-1}$  during the annual transition from winter minimum to spring maximum.

Given that our experiments measured gross growth rates that are consistent with the demonstrated capability of the species present in this ecosystem and that net growth rates observed from local sampling and estimated by the grazing dilution technique were generally lower, sometimes considerably lower, we can conclude that microheterotroph grazing was always capable of consuming a substantial portion of the daily primary production. In other ecosystems around the world, reported grazing rates are often lower, but range from ~ 40% to 100+% of primary production (see review by Calbet and Landry 2004). As our observations indicate grazing rates in the Huon were always greater than 69% of gross production and reached 96% in winter they are at the upper end of those observed elsewhere. This comparison suggests that the Huon Estuary is characterized by a high degree of general top-down control on phytoplankton.

Using individual pigments to calculate pigment specific growth and grazing rates suggested that grazing pressure was not uniform across a range of phytoplankton classes. Diatoms (based on cell counts and fucoxanthin, see Thompson and Bonham 2004) had the greatest gross and net growth rates, a result consistent with the observed concurrent diatom bloom. Zeaxanthin was present (as in 1997; Butler et al., 2000) and was also grazed efficiently. Possible sources of zeaxanthin are cyanobacteria, although these were seldom observed during phytoplankton counts, or some species of the Chlorophyta. Chlorophyll *b* was also present and grazed although at this time we cannot resolve whether this is divinyl chlorophyll *b* from prochlorophytes or monovinyl chlorophyll *b* from chlorophytes, prasinophytes or euglenophytes such as *Eutreptiella*; however monovinyl is considered more likely.

It is clear that the nutrient concentration in the surface layer was not sufficient to support the development of a phytoplankton bloom from November to May. Ignoring physical concentration as a mechanism to achieve bloom densities phytoplankton must access nutrients from recycling, a local source or deeper in the water column. Given the dual controls on phytoplankton biomass (bottom up by nutrients or top down by predators) it would only seem possible for the blooms to occur when phytoplankton escape grazing and access sufficient nutrients. It is possible that vertical migration by dinoflagellates achieves both these objectives while allowing the cells to remain within the estuary in spite of the relatively strong estuarine circulation.

The microzooplankton community was similar in composition to those observed in coastal water bodies from Nova Scotia, Canada (Gifford, 1988) to South Africa (Froneman and McQuaid, 1997) with dominance by ciliates (aloricate) followed by tintinnids. Densities of both types of ciliates (aloricate + tintinnids) were  $\sim 2400 \text{ L}^{-1}$ , very similar to the  $2100 \text{ L}^{-1}$  reported for waters around New Zealand (James et al., 1996, Hall et al., 2004). The major difference between microheterotrophs in the Huon Estuary and other coastal locations in the world seems to be the greater importance of heterotrophic dinoflagellates. Heterotrophic dinoflagellates have been reported to be dominant grazers in some pelagic ecosystems but not in oligotrophic ones where the picoplankton are considered too small for efficient grazing by some dinoflagellates (Stelfox-Widdicombe et al. 2000). Large numbers of heterotrophic dinoflagellates are characteristic of the Australasian region north of the subtropical convergence (Wood, 1954). Although *Noctiluca scintillans* was present during February 2004 (P. Thompson, pers. obs.) its large size meant that it was considered a component of the macrozooplankton ( $> 200 \mu\text{m}$ ) and it was excluded from these experiments.

The available data indicate that grazing pressure was always high in the Huon Estuary with microheterotrophs capable of consuming  $\sim 80\%$  of primary production. Although this conclusion should be tempered by the lack of resolution in time and space it indicates that top down control is an important component of the pelagic ecology in this ecosystem. For a phytoplankton bloom to occur a species or community must escape this strong grazing pressure for sufficient time to bloom. At the phytoplankton community level there are only a few mechanisms that would allow a general escape from microheterotroph predation. For example there is often a lag between the increasing growth rate of phytoplankton relative to zooplankton in early spring, the net result is a spring bloom. Spring blooms occur most years in the Huon Estuary and D'Entrecasteaux Channel indicating this uncoupling does occur. During summer it is possible that grazing pressure is reduced as a result of a trophic cascade. Grazing by

macrozooplankton on microzooplankton has been shown to reduce grazing on phytoplankton by 50% (Hansen et al., 1993). We have observed episodic high densities of salps (tunicates) that appear to remove most of the particles from the water column. Subsequent to these salp “blooms” there may be an opportunity for phytoplankton growth to escape top down control. It is also possible that *Noctiluca scintillans* may act in the same manner. In general the published accounts of trophic cascades involve nonvisual feeders such as ctenophores or medusae (Table 1 in Verity and Smetacek, 1996).

Species-specific mechanisms used to escape predation are much better studied in terrestrial ecosystems and include: satiation, spatial separation, size, physical defences, chemical defences, colouration or behaviour, and symbiosis. Routine monitoring of the Huon Estuary and D’Entrecasteaux Channel found mostly diatom blooms. As a group diatoms often use the satiation escape mechanism in that, under the right conditions, they grow faster and are sufficiently abundant that their predators cannot control them. While there were reports from various sources of high densities of *Gymnodinium catenatum*, *Heterosigma akashiwo* and *Karenia* sp. in the south east region of Tasmania we can only confirm high densities of *G. catenatum* from various locations during late summer 2004. We also observed the highest densities of *Polykrikos* during February 2004 and it has been demonstrated that this genus both grazes *G. catenatum* and has a faster intrinsic growth rate (Jeong et al., 2001). It seems likely that predator avoidance, possibly through the diel vertical migration undertaken by *G. catenatum* as observed during HES and in this study (data not shown), represents an important predator escape mechanism.

#### **Management Implications**

As reported for similar ecosystems around the world grazing by microzooplankton consumes a high portion of daily primary production in the Huon Estuary. Significant differential grazing pressure was observed and is likely to contribute to dominance by particular taxa during blooms in the Huon Estuary.

#### *2.2.4. Comparing the Huon Estuary 1996–1998 with 2002–2003.*

The available data set consists of samples collected by:

- CSIRO during the HES from 1996 to 1998 and analysed by high performance liquid chromatography for multiple pigments including chlorophyll *a*.
- Simon Willcox as part of his PhD, Oct 2001 – Feb 2003, TAFI & UTas) and analysed spectrophotometrically for chlorophyll *a*.
- TAFI as part of the Interim Monitoring Program, Aug 2002 - June 2004 and analysed spectrophotometrically for chlorophyll *a*.

Simon Willcox and the TAFI 2002–2004 Interim Monitoring Program conducted sampling in the Huon Estuary to measure chlorophyll *a* at four locations (stations HA1, HA5, HA7, HA12) up the centre of the Estuary (Figure 20). In some cases the exact locations sampled during the 2001–2004 sampling were not sampled during HES (1996–1998) and samples in near proximity were used to make a comparison

(Figure 20). In the situation where more than one station from HES was available to compare to a given station from the 2001–2004 sampling the mean chlorophyll *a* concentration for each season for each station was calculated and then averaged to give a mean value for each season within the vicinity of the four sites sampled during 2001–2004. Thus from the data collected by the HES in 1996–1998 sites A3 and A5 were compared with HA1, sites B1 and B3 with HA5, sites E1, E5, F1, F2 and F3 with HA7 and sites I1 and I3 with HA12 (Table 4).

Given the known variation in chlorophyll *a* with season and depth to make a comparison between samples collected in 1996–1998 and those collected in 2001–2004 the data were sorted into seasons (summer = December, January and February; autumn = March, April, May; winter = June, July, August; spring = September, October, November) and only surface samples were used for the comparison as the Interim Monitoring Program did not have integrated samples and the sub-surface samples were not from comparable depths. Three or more observations were used to calculate the seasonal mean for any of these four sub regions (mouth, lower, mid or upper estuary). Further analysis of the spatial and temporal sampling regimes can be found in the attached Technical Report (Thompson and Parslow 2005).

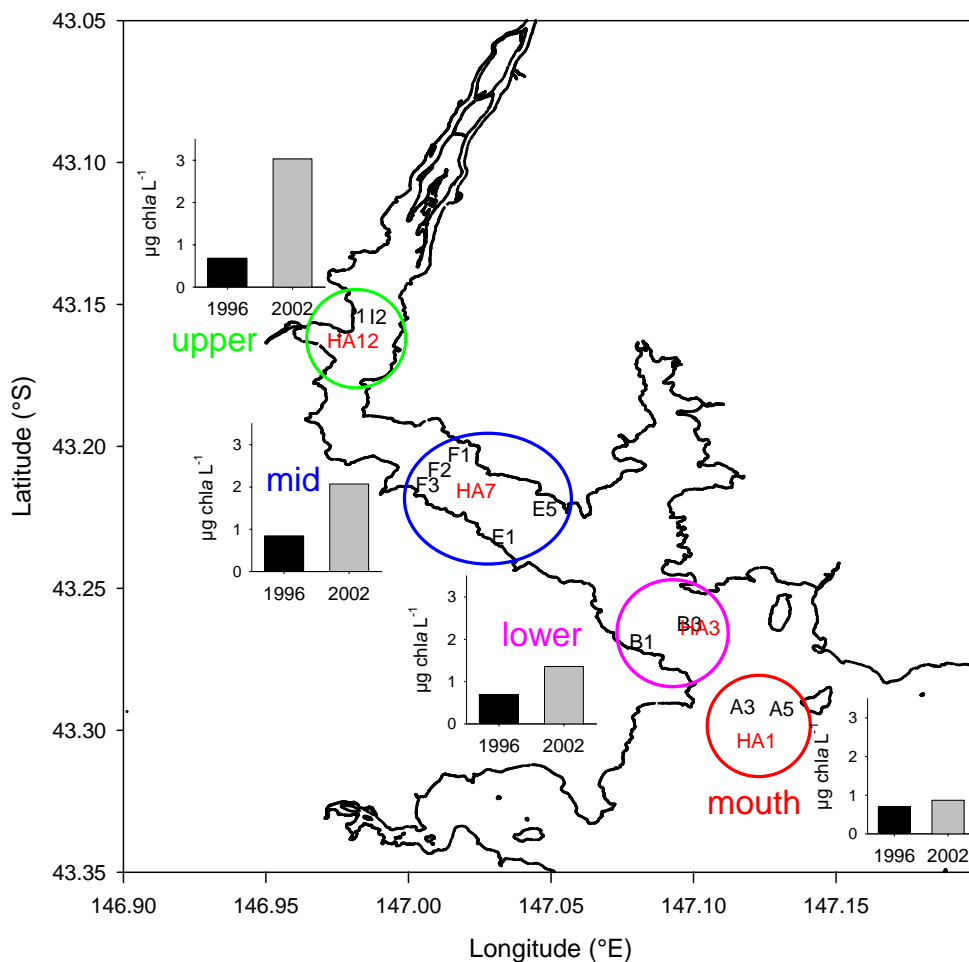


Figure 20. A map showing the sites and subregions (upper, mid, lower and mouth) of the Huon Estuary sampled during HES (1996–1998) and the interim monitoring program (2001–2004). The inset bar graphs show the annual mean for each subregion calculated from season averages where 1996 includes all 1996–1998 data and 2002 includes all 2001–2004 data.

Table 4. Mean chlorophyll *a* concentrations measured in the Huon Estuary at four sites and four seasons during 1996–1998 and at comparable sites during 2001–2004. Sites identified in Figure 20.

Season	1996–1998 (HES data)	2001–2004 (data courtesy of Simon Willcox and TAFI)
	Sub region 1: Mouth of estuary	
	A3 (n=9), A5 (n=9)	HA1 (n=33)
Summer	0.58	0.54
Autumn	0.77	0.95
Winter	0.40	0.65
Spring	1.09	1.33
	Sub region 2: Lower estuary	
	B1 (n=77), B3 (n=9)	HA5 (n=33)
Summer	0.76	1.17
Autumn	0.43	1.08
Winter	0.44	1.52
Spring	0.69	1.65
	Sub region 3: Mid estuary	
	E1 (n=9), E5 (n=9), F1 (n=76), F2 (n=9), F3 (n=77)	HA7 (n=33)
Summer	1.35	1.35
Autumn	0.76	4.40
Winter	0.31	0.60
Spring	0.97	1.92
	Sub region 4: Upper estuary	
	I1 (n=9), I3 (n=5)	HA12 (n=30)
Summer	0.71	2.91
Autumn	0.79	7.45
Winter	0.16	0.70
Spring	1.08	1.08

Using this simple stratified approach a three way ANOVA (season, “year” and region) indicates the mean chlorophyll *a* concentration in 2001–2004 was  $1.831 \mu\text{g L}^{-1}$ , and 60% less in 1996–1998 with a mean of  $0.735 \mu\text{g L}^{-1}$ . The differences for season and “year” were statistically significant ( $P = 0.006$  and  $0.001$ , respectively; [using a three way test and  $\log_{10}$  transformed data]). As chlorophyll *a* concentrations often have a heavily skewed distribution that tends to be more log normal than normal a more appropriate descriptor of the central tendency is medians. In this case the median value in 2001–2004 was 1.25 and it was 40% lower in 1996–1998 at  $0.76 \mu\text{g chlorophyll } a \text{ L}^{-1}$ .

Noting that seasonal variation was significant in the Huon there are several methods that can be used to remove the effect of seasonal variation from data to allow other comparisons. These include time series analysis and multiway ANOVA (as above). Once the data have been stratified by subregion and season a simple approach to the statistical test of whether there is a difference between the two periods 1996–1998 and 2001–2004 is to execute a comparison paired by season and subregion that is between the two columns of data in Table 4. Because the data are not normally distributed a signed rank test can be used with the raw chlorophyll *a* concentrations or a paired Students’ t-test upon the  $\log_{10}$  transformed data (passed a Kolmogorov-Smirnov test for normality). Both tests indicate a statistically significant difference between 1996–1998 and 2001–2004 ( $P = 0.007$  or  $P < 0.001$ , respectively). We caution that neither the HES

study nor the Interim Monitoring Program was designed to facilitate this analysis of change over time and this conclusion should be considered preliminary. Of particular concern is the conclusion that surface samples for chlorophyll *a* underestimate integrated samples by an average of 82% (for details please see Technical Report, Thompson and Parslow 2005) indicating they are not suitable as measure of chlorophyll *a* biomass in this ecosystem.

Although the statistical analysis indicates no significant differences between subregions the data (Table 4, Figure 20) suggest that the changes from 1996–1998 to 2001–2004 were not uniform across the estuary but most evident towards the mid and upper estuary.

#### **Management Implications**

After stratifying by locality and season there is evidence that chlorophyll *a* concentrations increased between 1996–1998 and 2001–2004 in the Huon Estuary with most of this increase occurring in the upper estuary. Surface sampling should be replaced with integrated sampling as the former badly underestimates the integrated chlorophyll *a* concentrations.

### **2.3. Sediment Biogeochemistry**

Research on the role of sediments in carbon remineralisation and nutrient release form the basis for the PhD project undertaken by Dean Thomson at the University of Tasmania. This work was still on-going at the time this report was prepared (see attached progress report: Thomson et al. (2005) and so only a brief account is provided here. Full details can be seen in the PhD thesis which is due for completion in 2006.

Sediments play a vital role in the ecological functioning of an estuary by retaining much of the organic matter and minerals supplied naturally by rivers, catchment run-off and inputs from the overlying water column. Surface sediments provide an integrated picture of inputs over relatively short time frames of a few years. Hence, they can give an indication of local inputs in the context of an estuary-wide baseline and provide a better view of longer term average inputs, in contrast with the snapshots revealed by water column studies. Sediment cores provide a record of estuarine conditions over years to decades and longer depending on the sedimentation rate. Gradients of nutrients and oxygen in porewaters with depth can provide estimates of the fluxes of solutes into or out of the sediment.

The organic matter in sediments is remineralised by the microbial and faunal populations present thus liberating nutrients and consuming oxygen. Sediment organic matter shows varying degrees of resistance to degradation. It is common practice to define a refractory component (i.e. that part of the organic matter that is not degradable over a defined time frame usually months to years) and a labile component that is degraded over hours to days.

The quality of organic matter is a prime determinant of the rates and recycling pathways of carbon and nitrogen in sediments (Herbert, 1999). Where organic matter undergoing decomposition has a high C:N ratio (values of 20–30 such as those from terrestrial plant sources; (Bordovskiy, 1965), much of the nitrogen remineralised may

be reassimilated into microbial biomass (Schlesinger, 1997). Organic matter that is more labile and has a lower C:N ratio (close to that of the Redfield ratio (6.7), such as that derived from algal material) will stimulate rapid remineralisation rates and a release of nitrogen from the sediment (Hansen and Blackburn, 1992). Identifying these sources of organic matter in sediments provides an insight as to how the organic matter is likely to be processed.

Ratios of  $^{12}\text{C}/^{13}\text{C}$  isotopes provide a good estimate of the relative contribution of terrestrial and marine sources to sedimentary OM (Fry and Sherr, 1984). Terrestrial OM (largely of higher plant origin) will generally have a  $\delta^{13}\text{C}$  value of -26 to -30‰ and organic matter with a marine origin will generally have a  $\delta^{13}\text{C}$  of -19‰ to -23‰ depending on the particular organisms present (Heip et al., 1995). The relative proportion of marine and terrestrial carbon in a sample can then be estimated by linear additions of these end-members. While this approach is relatively simple and gives an integrated estimate of sources for the total carbon in the sample, it will only provide useful information when there are well-defined end-members. Furthermore, this technique gives little information about the type of marine or terrestrial organic matter in question.

Sediment can also be remobilised by tidal currents or during high energy events such as floods thus changing the benthic characteristics of a particular region. Cycles of resuspension and deposition can lead to enhanced remineralisation as the particle surfaces are repeatedly exposed to oxidising conditions (e.g. Abril et al., 1999).

### *2.3.1. Sources of organic matter*

The high content of organic matter in the sediments from the Huon Estuary was previously noted in the HES (Butler et al., 2000). From lipid and stable isotope analyses, it was determined that much of it is derived from freshwater inputs of terrestrial sub-alpine moorland and other peaty soils, with additional inputs from autochthonous phytoplankton and localised inputs from salmon fish farms, sewage treatment plants and stormwater drains. Organic matter from these diverse sources has very different compositions and different susceptibilities to biodegradation. Much of the terrestrial material consists of high molecular weight tannin-like material, which seems to be degraded very slowly and thus its remineralisation probably does not contribute greatly to nutrient loads. In contrast, organic nitrogen in sediments over much of the middle and lower estuary is derived from marine sources (mainly phytoplankton) as indicated by its  $\delta^{15}\text{N}$  signature (Butler et al., 2000).

During our studies, we analysed several sediments from the Huon Estuary and some from more marine sites at Port Esperance (D'Entrecasteaux Channel) and Tasman Peninsula (Figure 21). Sites LE, LM and LW correspond to sites A6, A4 and A2 in the HES (Butler et al., 2000), while MW and MM correspond to the H1 and H2 in the HES.

These limited analyses show that organic matter contents in sediments from more exposed marine conditions at transect L are much lower than those in the Huon or in silt-dominated sites close to land. Lipid biomarker analyses of sediments from close inshore and offshore of Dover Bay illustrate this very well (work in progress). The inshore sediments have higher contents of organic matter, but this is mostly of

terrestrial origin as shown by the high contents of long-chain alcohols and plant-derived sterols such as sitosterol and stigmasterol. In contrast, the organic matter in the sandy off-shore sediment is dominated by marine sources.

### 2.3.2. Sediment respiration and nutrient fluxes

Three field trips during 2004, including March, July and November were carried out to measure benthic nutrient fluxes and sites in the Huon Estuary.

The aims of this work were to:

- measure diffusive and total oxygen fluxes at the sediment-water interface;
- compare flux rates in sediments dominated by marine organic carbon with sediments dominated by terrestrial organic carbon; and
- elucidate spatial and temporal variability of sediment oxygen profiles within and between cores.

Sediment cores were obtained from the mouth of the Huon Estuary (sites LW, LM and LE) and from sediments near Port Huon (only in March; sites MW, MM, and ME) as shown in Figure 21.

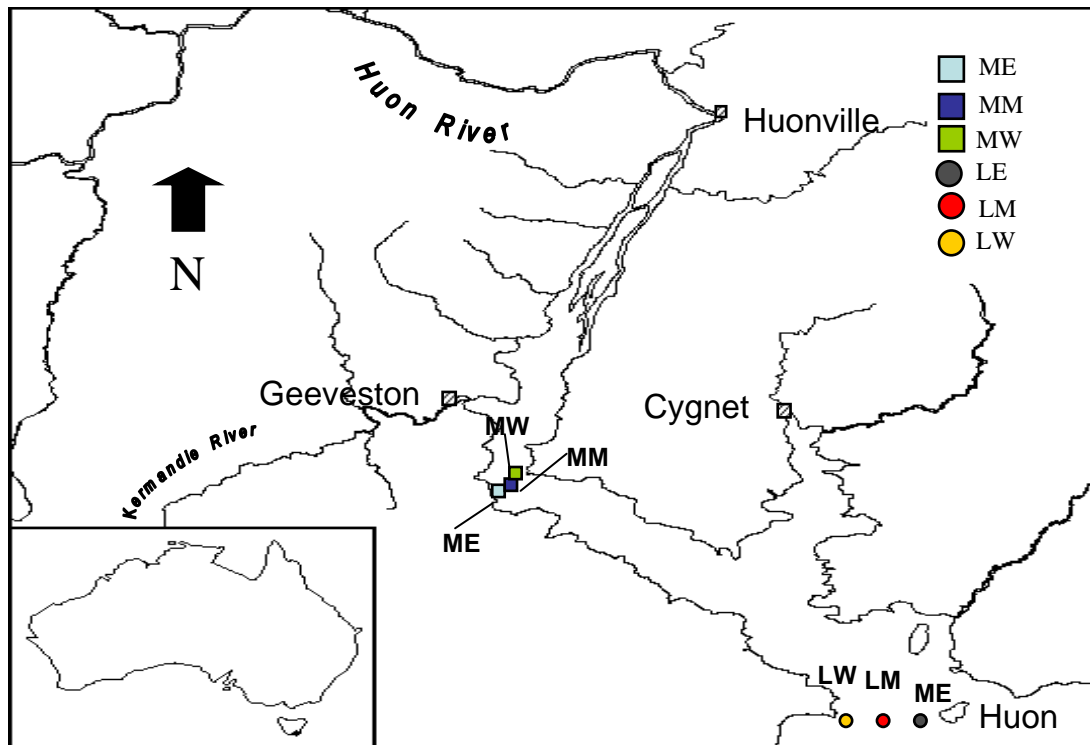


Figure 21. Locations of sediments collected for benthic flux measurements.

The sediment grain sizes at both transects (upper and lower) show that the fine sand (125 – 63  $\mu\text{m}$ ) and silt (<63  $\mu\text{m}$ ) fractions dominant the sediment structure. The organic carbon content of the sediments ranged between 4.1 and 7% at the lower sites during March and July and between 11.8 and 13.1% at the upper estuary sites. There was very

little variation in organic carbon contents between March and July except at LE where it increased from 4.1 to 5.3%. The stable isotope  $\delta^{13}\text{C}$  values ranged between -23.6 and -24.6‰ at the lower estuary and assuming a simple 2-component mixing system (Cook et al., 2004), the terrigenous organic carbon accounted for between 25–40% of the total organic carbon. At the upper estuary sites the stable isotope  $\delta^{13}\text{C}$  ranged between -26 and -27.3‰ and the terrigenous organic carbon accounted for between 62–82% of the total organic carbon.

The organic nitrogen content of the sediments ranged between 0.29 and 0.53% at the lower sites during March and July and between 0.53 and 0.59% at the upper estuary sites. There was very little variation in organic carbon contents between March and July. The stable isotope  $\delta^{15}\text{N}$  ranged between 7.4 and 7.7‰ at the lower estuary and assuming a simple 2-component mixing system (Cook et al., 2004) the terrigenous organic nitrogen accounted for between 0–2% of the total organic nitrogen. At the upper estuary sites the stable isotope  $\delta^{15}\text{N}$  ranged between 4.1 and 5.3 and the terrigenous organic nitrogen accounted for between 37–57% of the total organic nitrogen.

### 2.3.3. Sediment oxygen profiles and diffusive fluxes

Oxygen penetration depths were measured using microelectrodes introduced stepwise (100  $\mu\text{m}$  increments) into the sediment core with the aid of an auto-micromanipulator. The diffusive flux was calculated both from the diffusive boundary layer (DBL) from Fick's first law of diffusion and modelled from sediment gradients just below the surface.

The  $\text{O}_2$  penetration depth at the lower estuary transect varied seasonally. The smallest  $\text{O}_2$  penetration depth was recorded at LM measuring 3.7 mm during March while the biggest  $\text{O}_2$  penetration depth was recorded at LE measuring 9.0 mm in July (Table 5). The  $\text{O}_2$  penetration depths also followed a seasonal trend at the upper estuary transect and were generally shallower than at the lower estuary. The lowest  $\text{O}_2$  penetration depth was recorded during March at MM measuring 3.1 mm and the highest recorded at MW during July measuring 7.4 (Table 5).

The molecular oxygen diffusive fluxes ( $J_{\text{DBL}}$ ) at the lower estuary transect had a low of 134 ( $\pm 7.2$ )  $\mu\text{mol m}^{-2} \text{h}^{-1}$  at LE during July and a high of 435 ( $\pm 162.2$ )  $\mu\text{mol m}^{-2} \text{h}^{-1}$  at LM during March (Table 5). In comparison, the upper estuary transect had a range between 175 ( $\pm 35.4$ )  $\mu\text{mol m}^{-2} \text{h}^{-1}$  at MW in July and 489 ( $\pm 77.7$ ) at MM during March (Table 5). In general there was good agreement between  $J_{\text{DBL}}$  and  $J_{\text{SED}}$  and no significant statistical difference was found ( $p=0.05$ ). Generally the difference was less than 3%.

Table 5. Measured oxygen penetration depths and molecular diffusive fluxes. The fluxes were calculated from the diffusive boundary layer ( $J_{DBL}$ ) and compared with fluxes modelled from the oxygen gradient within the sediment ( $J_{SED}$ )

Site		Oxygen Penetration Depth (mm)	Molecular Diffusive Flux Rates ( $\mu\text{mol m}^{-2} \text{h}^{-1}$ )	
			$J_{DBL}$	$J_{SED}$
LW	March	5.2 ( $\pm 0.5$ )	264 ( $\pm 16.5$ )	259 ( $\pm 15.9$ )
	July	8.3 ( $\pm 0.3$ )	157 ( $\pm 18.5$ )	155 ( $\pm 17.9$ )
	November	7.2 ( $\pm 1.1$ )	181 ( $\pm 33.1$ )	176 ( $\pm 31.3$ )
LM	March	3.7 ( $\pm 0.9$ )	435 ( $\pm 162.2$ )	422 ( $\pm 150.4$ )
	July	8.2 ( $\pm 2.2$ )	144 ( $\pm 29.3$ )	142 ( $\pm 142$ )
	November	4.7 ( $\pm 1.1$ )	264 ( $\pm 48.0$ )	258 ( $\pm 46.4$ )
LE	March	4.6 ( $\pm 0.7$ )	233 ( $\pm 36.2$ )	227 ( $\pm 36.3$ )
	July	9.0 ( $\pm 0.4$ )	134 ( $\pm 7.2$ )	132 ( $\pm 7.2$ )
	November	6.9 ( $\pm 1.1$ )	178 ( $\pm 34.6$ )	173 ( $\pm 32.5$ )
MW	March	3.7 ( $\pm 0.4$ )	347 ( $\pm 60.6$ )	334 ( $\pm 57.1$ )
	July	7.4 ( $\pm 0.6$ )	175 ( $\pm 35.4$ )	171 ( $\pm 34.3$ )
	November	5.1 ( $\pm 0.4$ )	297 ( $\pm 50.4$ )	286 ( $\pm 47.9$ )
MM	March	3.1 ( $\pm 0.5$ )	489 ( $\pm 77.7$ )	468 ( $\pm 78.5$ )
	July	5.5 ( $\pm 1.1$ )	244 ( $\pm 78.8$ )	237 ( $\pm 75.9$ )
	November	4.9 ( $\pm 0.6$ )	314 ( $\pm 34.9$ )	301 ( $\pm 33.7$ )
ME	March	nm	nm	nm
	July	6.2 ( $\pm 0.4$ )	186 ( $\pm 41.5$ )	182 ( $\pm 40.2$ )
	November	4.0 ( $\pm 0.5$ )	320 ( $\pm 53.2$ )	310 ( $\pm 50.8$ )

The oxygen consumption profiles modelled from the curvature of the  $\text{O}_2$  concentration profiles using PROFILE (Berg et al., 1998) exhibited intense activity at the sediment surface and at the oxic-anoxic interface below during all three sampling periods. However oxygen consumption rates during March were approximately three times the rate during July and November indicating the presence of higher concentrations of labile carbon and warmer temperatures. The intense activity at the sediment surface is due presumably to aerobic degradation of labile organic carbon deposited onto the sediment surface and the oxidation of reduced solutes (e.g.  $\text{NH}_4^+$ ,  $\text{H}_2\text{S}$ ) diffusing up from the anaerobic zone below is probably the reason for the increased  $\text{O}_2$  consumption rates at the oxic-anoxic interface. It is plausible that ammonium is one of the reduced solutes diffusing out of the anaerobic zone since the ammonium porewater profiles indicate that ammonium production occurs down to approximately 3 cm.

#### 2.3.4. Total oxygen uptake rates

These were determined using sediment reactors. Sediment cores (9.7 cm diam) were placed in a water bath at the *in-situ* bottom water temperature. These were for the lower estuary: 15.6 °C (March), 10.2 °C (July) and 13.0 °C (November). For the mid-estuary these were 16.0 °C (March), 7.9 °C (July) and 13.0 °C (November). The sediment had a depth of ~ 8–10 cm and there was ~ 18–20 cm of overlying water. Oxygen was measured with a unisense oxygen electrode through a sampling port in the cap. Fluxes were calculated by monitoring the concentration change in oxygen over time.

Sediment respiration rates (measured as TCO<sub>2</sub> fluxes) at the lower estuary site ranged between 228 μmol m<sup>-2</sup> h<sup>-1</sup> TCO<sub>2</sub> at LE and LM stations during July and 644 μmol m<sup>-2</sup> h<sup>-1</sup> TCO<sub>2</sub> at LE during March (Figure 22). The sediment respiration rates at the upper estuary location in the mixed zone had a higher range and varied between 267 μmol m<sup>-2</sup> h<sup>-1</sup> TCO<sub>2</sub> at ME station in November and 839 μmol m<sup>-2</sup> h<sup>-1</sup> TCO<sub>2</sub> at station MM in March (Figure 22). Community respiration quotients (CRQ = TCO<sub>2</sub>/O<sub>2</sub> flux ratio) across the lower estuary stations averaged 1.4 and ranged between 1.1 to 1.8. In comparison, the CRQ across the upper stations averaged 1.2 and ranged between 0.6 and 2.7. The highest CRQ was measured at MM at the upper estuary site during July when oxygen consumption rates were lowest. The CRQ can be used to infer the aerobic/anaerobic status of sediment metabolism. A CRQ of 1 implies that aerobic respiration is the dominant process. Therefore the results from this study suggest aerobic respiration is the dominant form of metabolism however anaerobic respiration accounted for over 50% of metabolism on some occasions. Alkalinity fluxes were always directed out of the sediment and generally lower than CO<sub>2</sub> fluxes. The highest efflux was recorded in March at LW (676 μEq m<sup>-2</sup> h<sup>-1</sup>) and the lowest at MM in March (21 μEq m<sup>-2</sup> h<sup>-1</sup>).

In less permeable sediments such as those dominated by high silt contents, oxygen consumption can be attributed mainly to diffusion and processes mediated by fauna. Flow induced advection, the other major oxygen consuming process can generally be ruled out (Glud et al., 2003). The locations in the current study had a high percentage of silt and thus we have made the assumption that advection does not occur to any significant extent. Thus the difference between the diffusive oxygen uptake rate (measured in the DBL and/or sediment oxygen profile) and the total oxygen uptake rate (as measured in the sediment reactors) can be used to infer the faunal activity within the sediments (Glud et al., 2003). Diffusion was generally the dominant process at both locations over the study period however faunal oxygen consumption accounted for over 40% of total oxygen consumption at the east and west lower estuary sites during March and November. A qualitative analysis of the benthic fauna in the sediments found the brittle star *Amphiura elandiformis* to be the most common animal in the sediments. Other animals found included polychaete worms, the heart urchin and small bivalves and gastropods.

Fluxes of silicate were directed out of the sediment at all sites with the exception of sites MM and ME during July. Fluxes of phosphate were also generally directed out of the sediment however rates were <2 μmol m<sup>-2</sup> h<sup>-1</sup>. No phosphate fluxes at the lower estuary sites during summer were reported due to erratic changes in concentration over the incubation period leading to non-significant flux results.

Fluxes of ammonium were generally directed out of the sediment during summer with the exception of site LM. During July all sites except LW had ammonium fluxes directed into the sediment. In November all sites at the lower estuary had small directed out of the sediment in comparison all sites had at the upper estuary sites consumed ammonia.

The highest ammonium efflux rate across all sites during both seasons was found at site LW during summer with a flux of 6.4 μmol m<sup>-2</sup> h<sup>-1</sup> out of the sediment. Nitrate was always directed out of the sediment and was the dominant form of DIN efflux. Nitrate accounted for between 66–100% of the DIN efflux. Nitrite was a small component of

DIN with a flux of  $\leq -1 \mu\text{mol m}^{-2} \text{h}^{-1}$  generally and always directed into the sediment. DIN was always directed out of the sediment and ranged from 5.5 to  $18.1 \mu\text{mol m}^{-2} \text{h}^{-1}$  during summer and 1.7 to  $6.7 \mu\text{mol m}^{-2} \text{h}^{-1}$  in July.

The uptake of ammonium by the sediments and release of nitrate to the water column suggests that the ammonium produced within the sediments is being converted to nitrate via nitrification. The nitrifiers are consuming more ammonium than can be produced in the sediments and are subsequently using ammonium from the water column. The nitrate is then released to the overlying water column or denitrified to dinitrogen gas which is no longer available for biological uptake. In November, ammonium was measured in the porewaters and production rates were then modelled from the curve using PROFILE (Berg et al., 1998). Ammonium production rates ranged between 16 to  $81 \mu\text{mol m}^{-2} \text{h}^{-1}$ . Comparing this to ammonium fluxes at the sediment – water interface (ranged between 1.6 and  $-6.7 \mu\text{mol m}^{-2} \text{h}^{-1}$ ) indicates a large discrepancy between sediment ammonium production and fluxes of ammonium out of the sediments. This would imply that they are efficiently recycling nitrogen liberated during the breakdown of organic matter in the sediments through the coupling of nitrification and denitrification. On a number of occasions ammonium production was in fact rate limiting for nitrification and the nitrifiers had to obtain additional ammonium from the overlying water.

We can use the  $\text{TCO}_2$ :DIN ratio to infer the expected release of DIN to the overlying water column. The ratio of  $\text{TCO}_2$  to DIN flux was always above 6.625, the ratio that would be predicted from the decomposition of organic matter with a “Redfield composition”. The measured ratios ranged from 17.6 to 86.7 at all sites in March and from 34.1 to 2930.5 at all sites during the July. Assuming that the majority of organic matter decomposed was settled phytoplankton with a Redfield composition, and assuming that  $\text{TCO}_2$  flux reflects decomposition, we calculate from the high  $\text{TCO}_2$ :DIN fluxes that 62.3 – 100% of the nitrogen remineralised in sediments at all stations was not released to the overlying water. This supports the above findings that the majority of nitrogen remineralised in the sediments is released as either nitrate or dinitrogen gas.

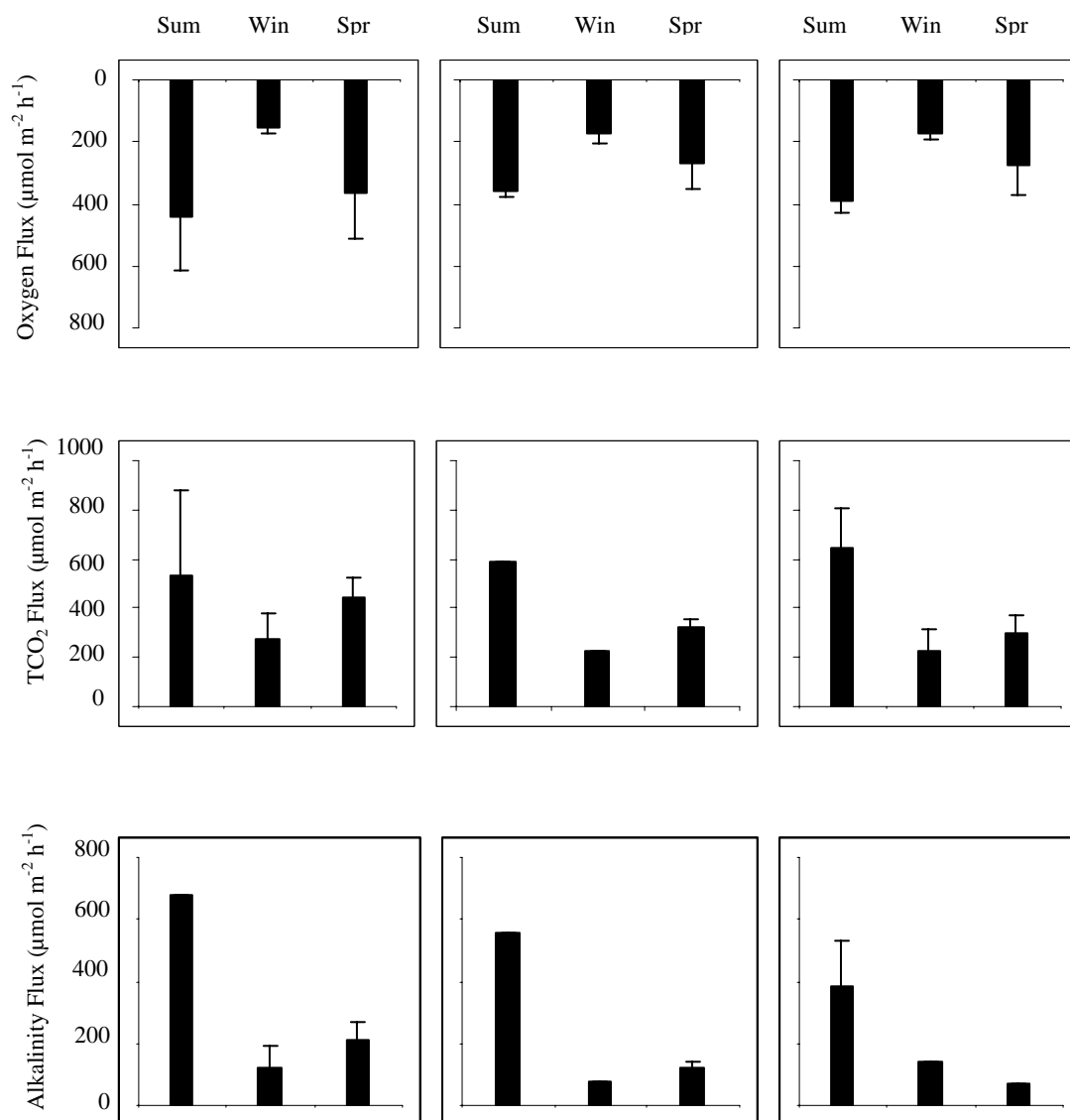


Figure 22. Oxygen,  $\Sigma\text{CO}_2$  and alkalinity fluxes at the lower estuary transect during summer, July and November. Error bars represent the standard error of the mean ( $n = 2$  or  $3$ ). N.B. where no error bars are present, the data represent a single flux. This is due to some fluxes being not significant because of erratic changes over the incubation period.

## 2.4. Biogeochemical Modelling

Information on the phytoplankton and nutrient dynamics of the Huon Estuary during 1996–1998 was reported by Butler et al. (2000). This study found that, on an annual basis, nitrogen fluxes in the Estuary are dominated by (natural) marine inputs of nitrate in winter. However, these are mostly unutilized by phytoplankton, due to low winter temperatures and light intensities. Intense phytoplankton blooms, including harmful algal blooms, occur primarily in summer and autumn, when marine nitrate inputs are low. In these seasons, fish farm loads of nutrients can make a significant contribution to overall system production. Application of simple models suggested that, in 1997, farm loads increased phytoplankton biomass in the Huon Estuary in summer by about 25%, and that a quadrupling of loads could result in approximately a doubling of phytoplankton biomass.

At the end of the Huon Estuary Study, a number of open questions, with potentially important implications for impacts and management of fish farm loads, were identified. In particular, the HES and modelling stopped at the mouth of the estuary, yet it was increasingly clear that the estuary and D'Entrecasteaux Channel are tightly coupled. As fish farm activity in D'Entrecasteaux Channel increased, it was recognized that the two needed to be studied and modelled as a single system. Uncertainty about the depth at which nutrient excreted by farmed fish is released was also shown to have a significant impact on predicted impacts on phytoplankton biomass. The biogeochemical model used to assess and predict impacts in the HES was highly simplified. It could not realistically represent the role of sediments as a temporary or permanent sink for nutrients, a role likely to be important in mediating interactions between winter and summer nutrient loads. It included only one phytoplankton functional group, yet experience elsewhere, and observations in the Huon, suggested it could be important to distinguish different phytoplankton functional groups.

This section describes the development and application of a more complex and realistic biogeochemical model to the combined Huon/D'Entrecasteaux system, to address these questions, and provide an improved basis for understanding and managing nutrient loads into the system. A fuller description can be found in the attached technical report by Wild–Allen et al. (2004).

#### *2.4.1. Biogeochemical model description*

The biogeochemical model applied here evolved through a series of case studies including the Port Phillip Bay Environmental Study (Harris et al., 1996), the National Land and Water Audit Estuaries Theme, the Gippsland Lakes Environmental Study (Webster et al., 2001), and the Ord-Bonaparte Study (Parslow et al., 2003). Each study addressed specific environments and ecological questions resulting in the development, implementation and testing of a diverse range of model components. In these previous studies the biogeochemical model was linked to a box model which represented physical transport with relatively low vertical and horizontal resolution. In the present work, we have restructured the biogeochemical model into a modular form, with a software core linked to a central library of ecological processes. With this structure the code has been incorporated into the CSIRO Environmental Modelling Suite and dynamically linked/coupled to a high resolution 3D hydrodynamic model 'SHOC' (Herzfeld et al., 2005) and a multilayer sediment model (MECOSED; Margvelashvili et al., 2002, 2003). This is the first time the biogeochemical model has been directly coupled to a 3-D hydrodynamic model in an estuarine application, although this was done at continental shelf scales in the Northwest Shelf Environmental Study (2004). Biogeochemical dissolved tracers are advected and diffused in an identical fashion to physical tracers such as temperature and salinity and ecological particulate tracers sink and are resuspended by the same formulation as sediment particles. At each ecological time step, non-conservative ecological rate processes such as growth, nutrient uptake, grazing and mortality are integrated within the ecological module which returns updated tracer concentrations to the hydrodynamic model via an interface routine.

The ecological model water column was organised into three 'zones': pelagic, epibenthic and sediment. Depending on the grid formulation, the pelagic zone may have one or several layers of similar or varying thickness. The epibenthic zone overlaps

with the lowest pelagic layer and shares the same dissolved and suspended particulate material fields. The sediment is modelled in two layers with a thin layer of easily resuspendable material overlying a thicker layer of consolidated sediment.

Ecological processes were organised into the same three zones with pelagic processes including phytoplankton and zooplankton growth and mortality, detritus remineralisation and fluxes of dissolved oxygen, nitrogen and phosphorous. Macroalgal and seagrass growth and mortality are included in the epibenthic zone whilst further phytoplankton mortality, microphytobenthos (benthic diatom) growth, detrital remineralisation and fluxes of dissolved substances were included in the sediment layer.

Four groups of microalgae and two macrophytes are included in the model. For fuller details see Wild-Allen et al. (2005):

- ‘Small phytoplankton’ representing small flagellates, and photoautotrophic pico- and nano-plankton.
- ‘Large phytoplankton’ representing diatoms with opportunistic ecological characteristics and high growth rate.
- ‘Dinoflagellates’ represent large dinoflagellates with much slower growth rates than the large phytoplankton group.
- ‘Microphytobenthos’ are large cells representative of benthic diatoms.
- Seagrass grow in the epibenthic layer where there is sufficient light. They have a fixed carbon to nutrient ratio of 550C:30N:1P (Atkinson Ratio).
- Macroalgae in the model represent both macro- and epiphytic- algal groups that might co-exist with seagrass communities.

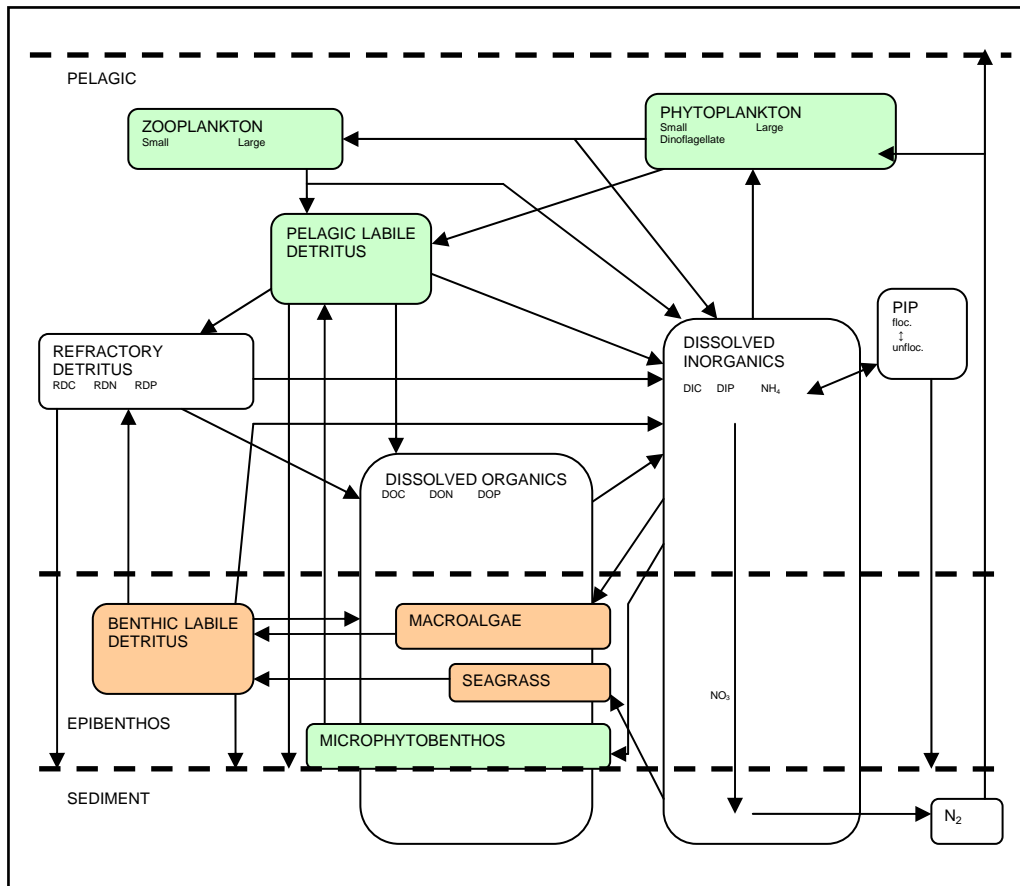


Figure 23. Schematic diagram of the biogeochemical model compartments, links and vertical layers. Green compartments have fixed nutrient content at Redfield ratio (106C:16N:1P); brown compartments are fixed at Atkinson ratio (550C:30N:1P).

Key assumptions of the model include:

- Modelled 24 hour mean autotroph growth rate is determined by access to essential nutrients (nitrogen and phosphate) and photosynthetically active radiation (PAR) by the chemical reaction model of Baird (1999).
- Dissolved nitrogen is present as ammonium and nitrate and autotrophs take up both equally.
- Phosphate and dissolved inorganic carbon are also taken up by phytoplankton at Redfield ratio (106C:16N:1P) and by macrophytes at Atkinson ratio (550C:30N:1P).
- Ambient PAR is calculated from incident surface 24 hour mean PAR attenuated by sea water, coloured dissolved organic substances, organic and inorganic particles.
- Phytoplankton chlorophyll concentration is calculated by assuming a fixed nitrogen to chlorophyll ratio of  $7 \text{ mgN mgChl}^{-1}$ .

Two groups of zooplankton are included in the model:

- ‘Small zooplankton’ representing mobile microzooplankton less than 200  $\mu\text{m}$  in size such as zooflagellates, tintinnids, ciliates, rotifers, small copepod nauplii and polychaeta larvae. These feed on small phytoplankton and have rapid turnover rates.
- ‘Large zooplankton’ represent mesozooplankton such as copepods and small fish larvae. They are mobile, feed on large phytoplankton, microphytobenthos and dinoflagellates.

Three types of particulate detritus and two pools of dissolved substances are included in the model:

- ‘Pelagic labile detritus’ represents fresh detritus with a fixed carbon to nutrient ratio of 106C:16N:1P (Redfield Ratio). It is rapidly broken down by bacteria, viruses and fungi into refractory detritus, dissolved organic and dissolved inorganic substances on the timescale of about a week.
- ‘Benthic labile detritus’ is similar to pelagic labile detritus but has a fixed carbon to nutrient ratio of 550N:30N:1P (Atkinson Ratio). It is generated by mortality of seagrass and macrophytes.
- Refractory detritus represents older detrital material with lower nutrient to carbon content and slower remineralisation time scales of about a year.
- Dissolved organic material is considered to be a pool of very refractory nature with very slow remineralisation time scales of about two years.
- Dissolved inorganic material is modelled as independent carbon, nitrogen and phosphorus pools. It is generated through inefficient feeding and excretion of zooplankton and by remineralisation of pelagic and benthic labile detritus, refractory detritus and dissolved organic material.

The concentration of dissolved oxygen in the model varies with atmospheric exchange at the sea surface, photosynthetic production and respiration of primary producers, respiration of secondary producers and utilization during remineralisation processes. Surface waters are typically oxygen rich, whilst deeper waters and the sediment layer may become depleted in oxygen depending on vertical mixing and flushing of the sediment.

#### *2.4.2. Biogeochemical model implementation*

The biogeochemical model was coupled to the hydrodynamical and sediment models on a coarse curvilinear grid with horizontal resolution which varied between 350 m and 1.3 km and 26 vertical layers. This formulation allowed the runtime ratio to exceed 100:1 so that a one year simulation took less than 3.5 days. Physical surface and boundary fluxes were supplied as for the hydrodynamical model, except for photosynthetically active radiation (PAR) which was supplied as a 24 hour mean.

The biogeochemical model was initialized using data from December 2001 with tracer concentrations derived (where possible) from observations made throughout the region.

Where suitable observations were unavailable historical data and literature values were used. To obtain the initialization fields at the required high vertical resolution, sparse nutrient and biomass observations were interpolated vertically and weighted against profiles of density structure. This gave the initialization field some vertical structure, although at best gave a crude representation of the real depth of any nutricline and/or subsurface biomass feature. Results from the first month of the simulation should therefore be disregarded as during this period the model is adjusting internally to bring the initialization fields into balance.

Nutrient, phytoplankton and oxygen fluxes at the marine boundaries were prescribed as an upstream boundary condition from observations made at monthly intervals at D'Entrecasteaux stations 1 and 12. These data were interpolated vertically against profiles of density to give high resolution vertical structure, and temporally to give a timeseries of concentration for inflowing water.

There are four major rivers draining into the region: the Huon (annual discharge  $3.8 \times 10^9 \text{ m}^3$  in 2002), the Esperance (4% of Huon), the Kermandie (1% of Huon) and the Northwest Bay Rivulet (1% of Huon). Whilst the flow rates of the latter three rivers are comparatively trivial with respect to the Huon and have little impact on the hydrodynamics, the dissolved and particulate nutrient loads from these rivers can be significant and for this reason they have been included. Seasonal variations in river loads of key biogeochemical tracers are poorly known and there is a paucity of data for all rivers in the region. Where possible data for 2002 are used but in general values have been estimated from literature and observations in other years. It was not possible to resolve seasonal fluctuations in tracer concentrations and annual mean values were estimated for all rivers. The limitations in current monitoring of catchment loads represent a significant handicap for attempts to assess or predict the response of the Huon/D'Entrecasteaux system to changing terrestrial and marine loads.

Anthropogenic inputs to the Huon Estuary and D'Entrecasteaux Channel include sewerage and wastewater. Although the region is sparsely populated, there are several small towns of note including Margate, Huonville and Dover with local STP facilities. During the HES sewerage discharge at Ranelagh Treatment Plant corresponded to  $\sim 10 \text{ gN person}^{-1} \text{ d}^{-1}$  for about 2000 people and totalled  $\sim 7 \text{ tN y}^{-1}$ . This input is two orders of magnitude smaller than annual river nitrogen input and a similarly small fraction of fin-fish farm nutrient discharge (see Table 6). In the context of regional nutrient input sewerage and wastewater discharge is generally small and diffuse along the coast and for this reason it was not included in the model.

Fin-fish farm discharges for 2002 were calculated for the 20 salmonid farms operating in the region (DPIWE). Each farm supplied various concentrations of pelleted food to their caged fish and discharged waste material in the form of uneaten feed pellets, fish urea and faeces. We thank Tassal Limited, Huon Aquaculture Limited, Aquatas, Nortas Salmonid Products and Seafarms, who all operate farms in the region and supplied feed data, and Skretting who supplied information on feed composition.

Assuming that all feed pellets are consumed by the fish and that no overfeeding occurs then 5% and 0.8% of the total feed is discharged by the fish as waste nitrogen and phosphorous respectively. For nitrogen, 85% was assumed to be dissolved in the form of ammonia and 15% as particulate labile detritus. Phosphorus was partitioned between

particulate labile detritus (at a fixed Redfield ratio of 16N:1P) and dissolved inorganic phosphorus. Waste material was discharged at the farm sites as a point source discharge evenly distributed between 0.5 m and 12 m and diffused spatially throughout the grid cell in which the farm is located.

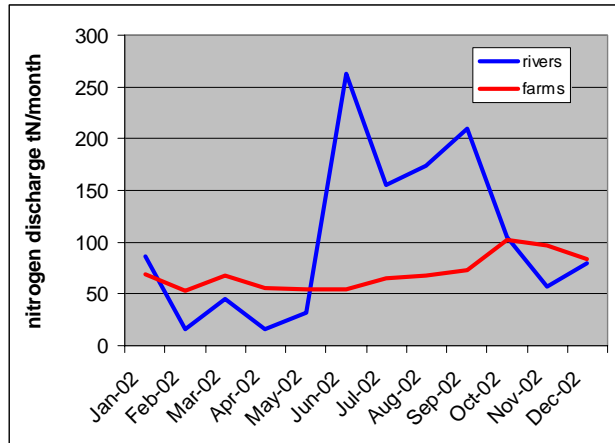


Figure 24. Monthly nitrogen input into the model domain for the sum of all farm sites and the sum of the Huon, Kermandie, Esperance and Northwest Bay rivers in 2002.

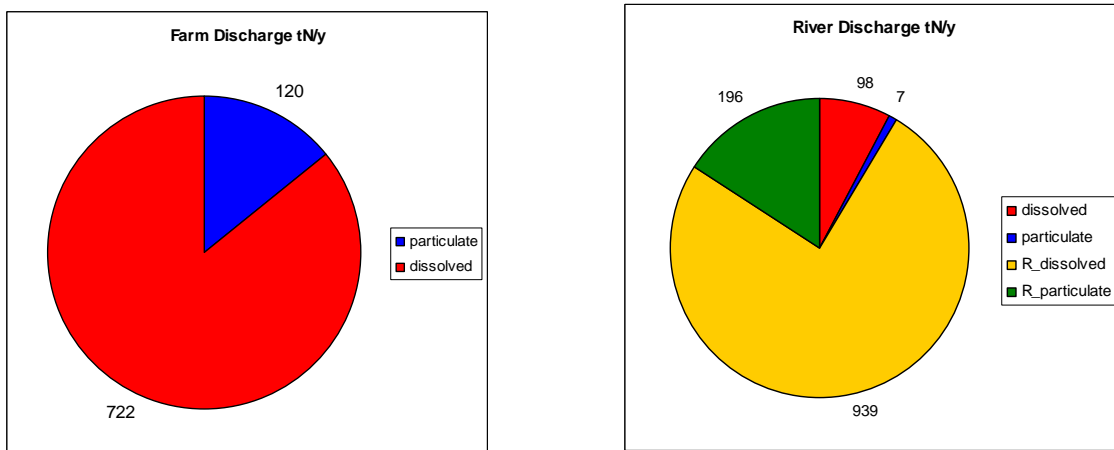


Figure 25. Composition of nitrogen component of (a) the farm discharge and (b) the river discharge. Values indicate tones nitrogen per year.

The maximum monthly farm discharge occurred in October and nitrogen discharged from farms exceeded river inputs through summer and autumn (Figure 24). During this period near surface flux of nutrients into the region across the marine boundary is small due to seasonal stratification and so farm discharges dominate the surface nutrient flux throughout the region.

Waste material discharged from the farm sites enters the biogeochemical model as ammonium and labile detrital particles which can be rapidly remineralised to dissolved inorganic nutrient. The flux of nutrients entering the model from the river discharge is dominated by refractory dissolved and particulate material which is remineralised very slowly to inorganic nutrient. Farm loads of DIN exceed the river loads by more than seven times, and labile particulate detrital farm loads exceed river loads by more than 17 times (Figure 25).

### 2.4.3. Biogeochemical model calibration

The model output was compared with data collected during the Broad Scale Monitoring program (Thompson et al., 2005). Broadly this consisted of monthly data collected at 12 stations in the D'Entrecasteaux Channel and four stations in the Huon Estuary for nutrients (ammonia, nitrate and phosphate), dissolved oxygen, chlorophyll and phytoplankton species. Additionally, bottom water temperature, salinity and oxygen were recorded continuously at three sites in the Huon Estuary for the latter part of 2002. It was not possible to verify the model predictions of seagrass, macroalgae or zooplankton due to absence of observed data. Simulated biomass of these components, whilst consistent with our understanding of the model system, should be treated with extreme caution until verification against observations is demonstrated.

#### 2.4.3.1. Nutrients

Nutrient concentrations in the D'Entrecasteaux Channel have a distinct seasonal cycle with elevated surface concentrations in winter and reduced (frequently to near zero nitrogen), concentrations at other times of the year. A similar cycle is evident in bottom waters particularly in the shallower northern end of the channel. In the deeper southern part of the channel elevated winter concentrations prevail for longer as they are isolated from the surface waters by stratification. Variations in deep water nutrient concentration at the southern boundary appears to relate to fluctuations in the nutrient concentration of shelf waters advected into the channel.

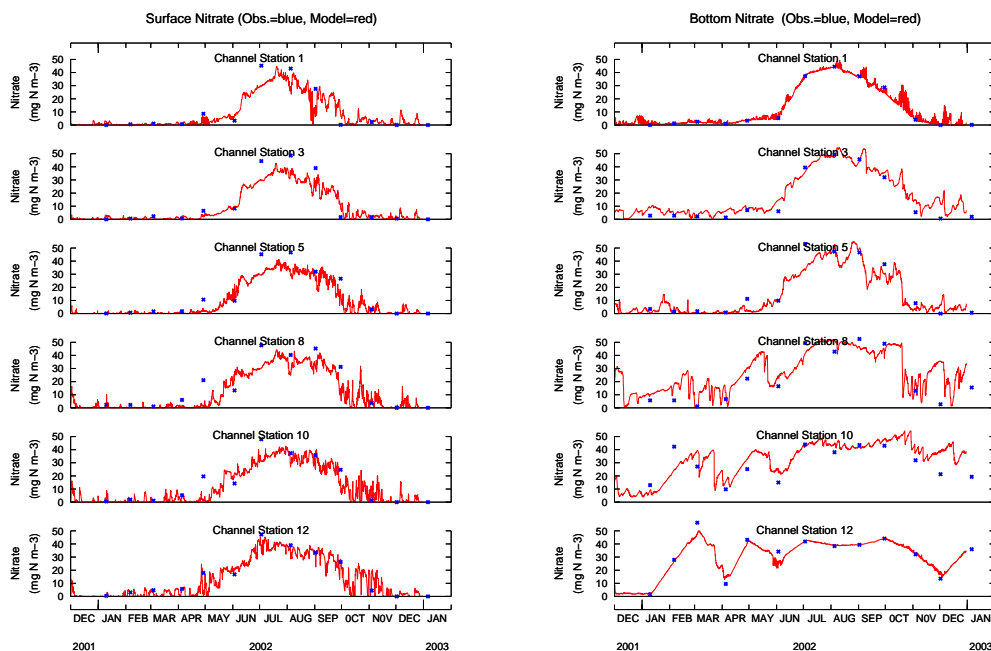


Figure 26. Time series of observed and simulated surface and bottom inorganic nitrate concentration at stations throughout the D'Entrecasteaux Channel (station 1 is at the northern end of the channel)

The model reproduces the observed seasonal cycle of nitrate in the Channel well although modelled winter concentrations in surface waters are slightly lower than observed in the northern end of the channel (Figure 26). This could be due to an over-estimation of modelled phytoplankton uptake and growth in winter, which in turn may

result from inaccuracies in the simulated *in-situ* PAR. Alternatively this discrepancy may result from the under-representation of a surface nitrate source in the model for example nitrification of ammonia. The observed variability in bottom water nitrate at stations eight and ten is reproduced by the model, however the exact timing of this variation is not always achieved, possibly due to inaccuracies in simulating the exact flux of nitrate crossing the southern boundary and discharging from the Huon Estuary.

The seasonal cycle in dissolved inorganic phosphate is similarly reproduced by the model, although concentrations in the northern part of the Channel are lower than observed in autumn and early winter. This discrepancy may result from over-estimation of modelled phytoplankton uptake and growth and/or inefficient simulation of phosphate recycling through dissolved and particulate phases and/or omission of a local discharge. In the southern part of the channel at station 10 there is slight overestimation of modelled dissolved inorganic phosphate in September and October.

The model reproduces a realistic range of surface and bottom water ammonia concentrations in the D'Entrecasteaux Channel, although winter concentrations are typically greater than observed (particularly evident in surface waters). This surplus of ammonia may simply reflect the underestimation of nitrification processes in the modelled water column or it may result from underutilization by phytoplankton. In separate experiments we have observed that some groups of phytoplankton preferentially uptake nitrogen in the form of ammonia over nitrate as it is metabolically easier to process. In the current version of the model, phytoplankton utilize ammonia and nitrate equally which could lead to overestimation of nitrate uptake, and under-representation of ammonia assimilation.

In the Huon Estuary the seasonal variation in nutrient concentration is modified by the nutrient loads discharged by the Huon and Kermantie rivers. Whilst the Huon River contributes the largest volume of water, the smaller Kermantie River (which discharges mid-estuary) has higher nutrient concentrations. Both flows are greater in winter and spring although episodic high flow events, lasting just a few days, occur throughout the year. Modelled nitrate concentrations are in the range of observed values. At the lower end of the estuary the model reproduces the observed surface nitrate well, although deep-water values are overestimated and similar in concentration to the southern basin of the D'Entrecasteaux Channel. Elevated values at Station 1 at the mouth of the estuary may reflect the relatively coarse grid representation of the narrow deep water channel linking the D'Entrecasteaux Channel and lower Huon Estuary resulting in an overestimation of bottom water exchange and deep water nitrate flux between the Channel and estuary.

The model reproduces the observed concentrations of ammonia in the Estuary reasonably well, although winter concentrations in surface waters are under estimated in the upper estuary. The comparison between modelled and observed dissolved inorganic phosphate is similar to that of nitrate (Wild-Allen et al., 2005). Modelled values are greater than observed in the lower estuary, but reproduce the observations fairly well in the upper estuary. The over-estimation of dissolved inorganic phosphate by the model probably results from under-estimation of phytoplankton uptake and growth in the estuary.

### 2.4.3.2. Chlorophyll and phytoplankton biomass

The D'Entrecasteaux Channel has fairly low concentrations of surface chlorophyll ( $\sim 1 \text{ mg m}^{-3}$ ) for most of the year, except during spring when concentrations increase up to fourfold. In deep water, concentrations are much lower as there is insufficient light for *in-situ* growth. Observations of phytoplankton biomass show distinct seasonal variation with large phytoplankton prominent in spring, small phytoplankton evident throughout the year, but especially in winter and small amounts of dinoflagellates present during autumn and also briefly in spring. This type of succession is not unusual in temperate waters with fast growing 'opportunistic' species such as diatoms (represented in the model as large phytoplankton) utilizing spring nutrient, slower growing dinoflagellates prevailing in nutrient-limited summer/autumn conditions and small picoplankton ubiquitous throughout the year.

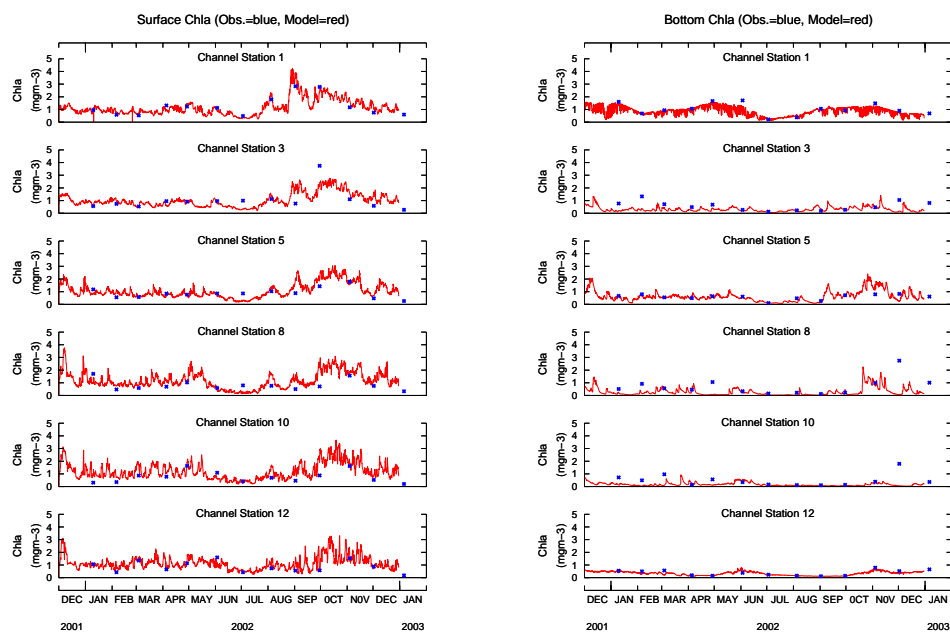


Figure 27. Time series of observed and simulated surface and bottom chlorophyll concentration at stations throughout the D'Entrecasteaux Channel (station 1 is at the northern end of the channel).

The model simulated the observed temporal evolution of surface and bottom water chlorophyll concentration in the D'Entrecasteaux Channel very well (Figure 27). The magnitude and timing of the spring increase in surface chlorophyll concentration was well reproduced, although the model slightly under-estimated spring chlorophyll concentration in bottom waters of the southern basin. A possible explanation for this could be poor resolution of a mixing event which transferred enhanced surface concentrations into deep water and/or coherent sinking of the surface phytoplankton bloom.

Good representations were also observed for each of the algal groups considered separately (Wild-Allen et al., 2005). Modelled dinoflagellates are in the range of observed values, however for much of the year observed and modelled concentrations are very low. An exception to this is in late autumn in the southern basin when an influx of dinoflagellates enters the model domain across the southern boundary. This injection of dinoflagellate biomass propagates northward and diminishes. Earlier

autumn increases in dinoflagellate biomass in the channel are not reproduced. The dinoflagellate functional group comprises of a diverse assemblage of species with distinct life strategies including vertical migration, prey avoidance and cyst resting stages. Any one of these life strategies may facilitate access to resources and avoidance of prey and give rise to an episodic bloom. Modelled dinoflagellates are necessarily parameterized with group mean characteristics which may be insufficient to capture species-specific bloom events.

To verify the simulated vertical structure in the biogeochemical model, cross sections of observed fluorescence were compared with modelled chlorophyll through the D'Entrecasteaux Channel. [Fluorescence is often used as a proxy for chlorophyll concentration; however without reliable calibration against local phytoplankton populations, which vary spatially and temporally, chlorophyll concentration cannot be inferred.] Vertical chlorophyll structure simulated by the model generally agreed well with the observed fluorescence structure in particular the onset and evolution of the spring bloom from August to November (Figure 28).

The model also reproduced the observed seasonal variation in surface chlorophyll concentration in the side bays off the D'Entrecasteaux Channel quite well (Wild-Allen et al., 2005). The timing of the spring bloom was generally well simulated although the modelled bloom occurred a little early in Great Bay and the magnitude was slightly over predicted in North West Bay, Little Taylors Bay and Great Taylors Bay.

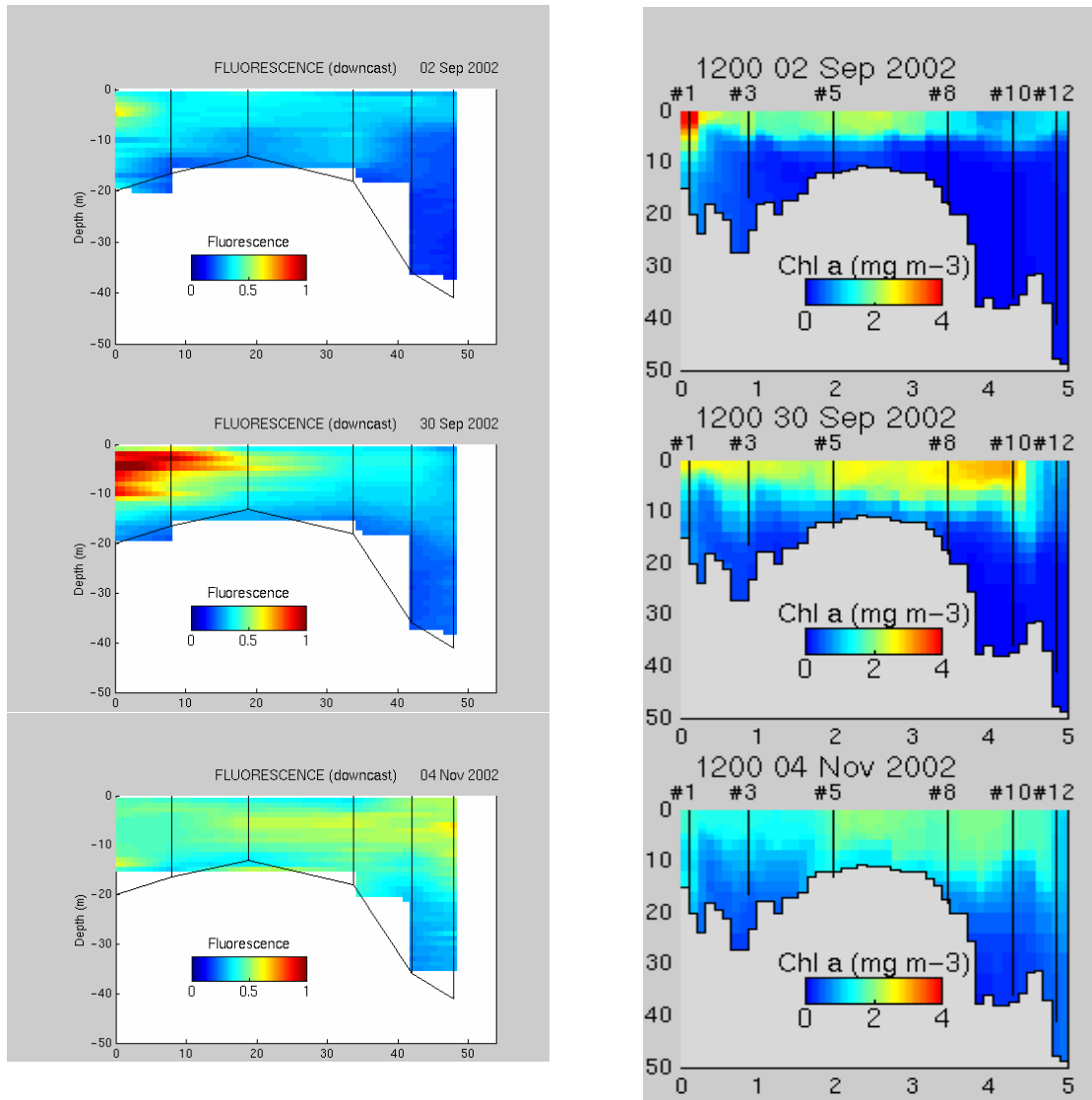


Figure 28. Observed fluorescence and modelled chlorophyll a north-south transect through the D'Entrecasteaux Channel between August and November 2002.

In the Huon Estuary the model simulated realistic chlorophyll concentrations at the mouth, although deep water concentrations were lower than observed. In the mid-estuary observed autumn blooms of significant concentration (up to  $24 \text{ mg m}^{-3}$ ) were not reproduced by the model although background concentrations throughout the rest of the year were of the right magnitude.

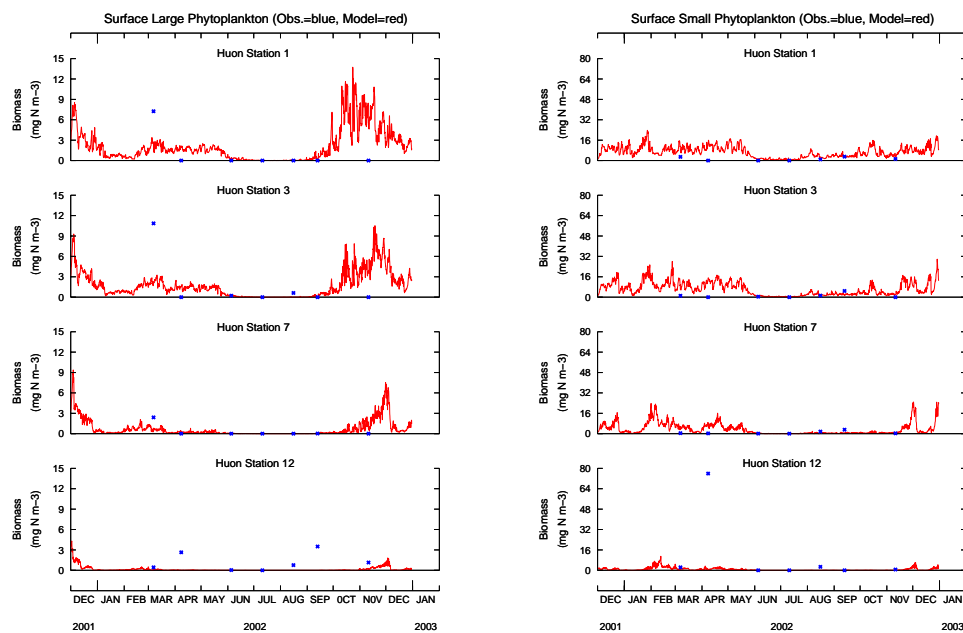


Figure 29. Timeseries of observed and simulated large (left) and small (right) phytoplankton biomass in surface waters at stations in the Huon Estuary (station 1 is at the mouth, and station 12, in the middle of the Estuary).

The model failed to reproduce realistic seasonal variation in biomass concentrations in the three modelled phytoplankton groups in the Huon Estuary. Large and small phytoplankton were simulated at approximately the observed magnitudes however the large phytoplankton autumn bloom period was not reproduced and a spurious spring increase was simulated. [In 2003, and in the HES study 1996–98, a spring bloom dominated by diatoms was observed, and 2002 might be anomalous in this respect.] The observed huge biomass of dinoflagellates in autumn was not simulated, and modelled dinoflagellates were in general absent from the estuary.

These discrepancies between model and observations may result from inaccuracies in both the model flow field and attenuation of light. Retention of phytoplankton in the estuary depends on the estuarine circulation drawing water into the estuary at depth, whilst surface waters are continuously discharged. Modelled fast growing small and large phytoplankton were able to survive in this environment, however dinoflagellates with slower growth rate were advected out of the estuary and did not accumulate. This situation was compounded by high attenuation of PAR in the near surface layer due to humic substances in the river water. For dinoflagellates to accumulate to the observed high concentrations they need to both spend time in the deep water, for upstream advection into the estuary, and in the surface waters to access sufficient PAR for growth. In the Huon the most successful species of dinoflagellate are those that migrate vertically in the water column, e.g. *Gymnodinium catenatum*. The model has provided a clear demonstration that in the absence of vertical migration dinoflagellates do not prevail in the estuary.

### 2.4.3.3. Summary

The model reproduces the observed spatial and temporal dynamics of dissolved nutrients, chlorophyll, phytoplankton biomass and oxygen in the Huon Estuary and D'Entrecasteaux Channel. Observed nitrogen, chlorophyll and large phytoplankton biomass concentrations are particularly well reproduced in the D'Entrecasteaux Channel and side Bays. The phosphorus cycle, which has a greater number of dissolved and particulate phases, is adequately simulated. Modelled small phytoplankton biomass throughout the region lacks the observed seasonal winter maxima, and dinoflagellate biomass is poorly represented, particularly in the Huon where observed autumn blooms are absent. Modelled oxygen concentrations suggest possible over-estimation of horizontal exchange of bottom waters between D'Entrecasteaux Channel and the mouth of the Huon Estuary.

### 2.4.4. Testing model sensitivity

A number of variables were changed to examine the sensitivity of the model outputs to changes in ecological and environmental conditions. Full results can be found in Wild-Allen et al. (2005).

- Micro- and meso-zooplankton grazing exert 'top-down' control on phytoplankton populations in the model. Grazing plays an important role in curtailing the spring bloom and recycling nutrient through waste products and detritus, but the magnitudes of grazing rates are poorly known in this system. Annual phytoplankton primary production was reduced by approximately 50% in model runs with enhanced zooplankton swimming and associated grazing. This impacted the zooplankton production which was similarly reduced over much of the region. Under intense zooplankton grazing the productivity of the whole ecosystem was reduced as grazing limited the biomass of primary producers in the system.
- The model was run with reduced denitrification (the process in sediments where ammonium is oxidized/nitrified to nitrate and subsequently denitrified to nitrogen gas) where the half saturation coefficient for denitrification was reduced by an order of magnitude. This reduced the maximum denitrification efficiency by ~50% compared to the original model run and significantly reduced denitrification (>70%) at elevated oxygen concentrations. Comparisons with field observations demonstrated that this simulation over-estimated bottom water nitrate concentrations in the D'Entrecasteaux Channel and several of the Bays. In Great Bay and Isthmus Bay however the model with reduced denitrification appeared to produce a better fit to the observations suggesting that sediment denitrification may indeed be less in these Bays, possibly due to variations in sediment type and infauna. In surface waters the enhanced nitrate values better fit the observations in winter, however model over-estimation of algal uptake and production and/or under estimation of ammonium nitrification are thought to be more likely causes of the deficit in the original model. Halving the denitrification efficiency had a relatively minor effect on the water column biogeochemistry despite increasing the net flux of nitrogen into the region by 65%. This suggests that the modelled ecosystem is robust to increased nitrogen load, probably due to the relatively short flushing time of the D'Entrecasteaux/Huon system. Further

analysis of the model results are required to calculate a definitive nitrogen budget for the region and clarify the fate of nutrient loads.

- Absorption of PAR by microalgae determines their growth rate under nutrient replete and light-limited conditions. The absorption cross section is evaluated from the size and shape of the algae and its pigment content (absorption coefficient). The model was run with doubled phytoplankton light absorption, but the overall impact was relatively small. There was a small increase in chlorophyll concentration throughout the year, and the spring bloom, dominated by large phytoplankton, occurred about one month earlier. As expected, doubling phytoplankton absorption enhanced phytoplankton production and biomass at depth where ambient PAR is strongly limiting and nutrient concentrations are typically higher. For much of the year, the phytoplankton in the surface layer are nutrient and not light limited, and respond weakly to changes in light absorption efficiency. The exception to this situation is in spring when winter nutrients and increasing day length provide optimal conditions for growth. Nutrient concentrations in surface waters were consistently less than in the original model run, due to the additional phytoplankton uptake. The model already tended to underestimate observed surface nitrate values, and doubling phytoplankton absorption exacerbated this disagreement.
- Vertical migration is thought to give some species of dinoflagellate a competitive advantage by allowing them access to both deep water nutrient and high near surface PAR levels. In particular the species *Gymnodinium catenatum* has been observed vertically migrating in concentrated blooms in the Huon Estuary during the HES study. A formulation for dinoflagellate migration capped with downward swimming above 4 m (and with large zooplankton grazing preference reduced to 0.8) simulated realistic distributions of dinoflagellates in the Huon Estuary throughout the year. Capping the upward swimming of dinoflagellates at 4 m effectively retained them in the estuarine circulation through all seasons. However the simulated autumn biomass was still considerably lower than that observed in autumn blooms. This could be because the migration cap of 4 m was at times too deep, therefore limiting dinoflagellate exposure to light, or too shallow causing too much biomass to be swept out of the estuary in the surface river plume. In addition, implementing vertical migration in the current model effectively halves dinoflagellate exposure to PAR, which is applied in the model at a constant daily mean intensity, as migrating biomass accumulates at the bottom or beyond the euphotic layer for ~10 hours per day. This can only be remedied by modifying the phytoplankton growth model to incorporate a realistic light-dark cycle. Finally there remains the possibility that some other aspect of the dinoflagellate (in particular *Gymnodinium catenatum*) lifecycle, neglected by the model, is playing a fundamental role in the development and maintenance of intense blooms in the estuary. Such a characteristic might be a requirement for a riverine micronutrient(s), the avoidance of a marine predator or successful cycles of encystment and excystment which in turn might depend on spatially variable sediment type and benthic fauna. To examine the occurrence of dinoflagellates in the Huon further a more rigorous model is required which simulates diurnal cycles in ambient PAR, nutrient uptake, and resulting growth and respiration.

#### 2.4.4.1. Summary

The model was sensitive to the level of zooplankton grazing which impacted simulated productivity of the region. Modelled grazing is currently inferred from ancillary data, however proposed observations of zooplankton in the region will allow more direct calibration of zooplankton parameters. The simulated biogeochemistry of the region is less sensitive to changes in denitrification than e.g. Port Phillip Bay, due to the relatively short flushing time of the Huon–D’Entrecasteaux system. Varying phytoplankton light absorption efficiency had small impact on phytoplankton biomass throughout the region as for much of the year and phytoplankton are nutrient and not light limited. Implementing dinoflagellate migration in the model simulated realistic distributions of dinoflagellates throughout the region, although autumn bloom events in the Huon were still not reproduced. A more rigorous model including diurnal cycles in PAR and phytoplankton growth might do better.

The model in its current formulation is adequate to simulate the seasonal evolution of biogeochemical cycles in the D’Entrecasteaux Channel and side Bays, however model results in the Huon are more uncertain due to the unresolved complexities of dinoflagellate dynamics in the estuary.

#### 2.4.5. Model results: annual regional biogeochemistry

Model output is presented as annual median, 10 and 90 percentile concentrations of chlorophyll, nutrients and dissolved oxygen in the Huon and D’Entrecasteaux Channel.

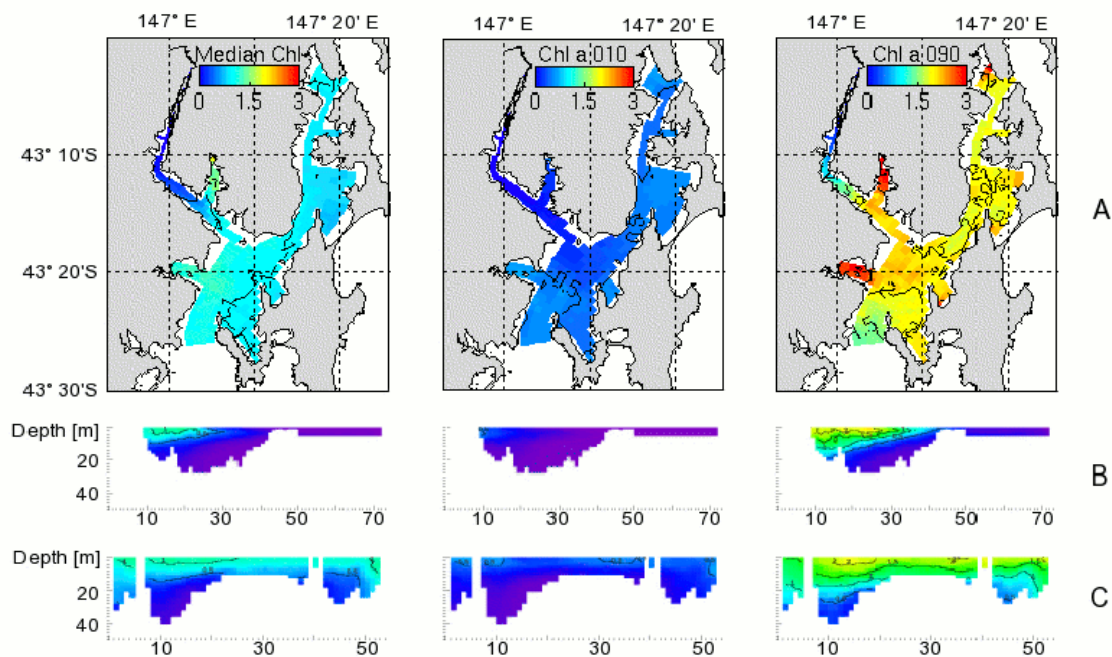


Figure 30 A) Surface concentration of annual median, 10 and 90 percentile chlorophyll concentration with (B) vertical cross sections through the Huon Estuary [from D’Entrecasteaux Channel (left) to Huon river (right)] and (C) the D’Entrecasteaux Channel [from south (left) to north (right)].

Modelled annual median chlorophyll concentrations are  $\sim 1 \text{ mgChl m}^{-3}$  in surface waters throughout the D’Entrecasteaux Channel with slightly higher values in the

southern basin compared to the northern end of the Channel (Figure 30). Comparable data for the summer median are shown in Figure 34. In the Huon Estuary modelled chlorophyll concentrations were lower contrary to observations, because dinoflagellates blooms were not simulated. There was significant variation between the 10 and 90 percentile concentrations with consistently higher chlorophyll concentrations simulated off Cygnet and Port Esperance.

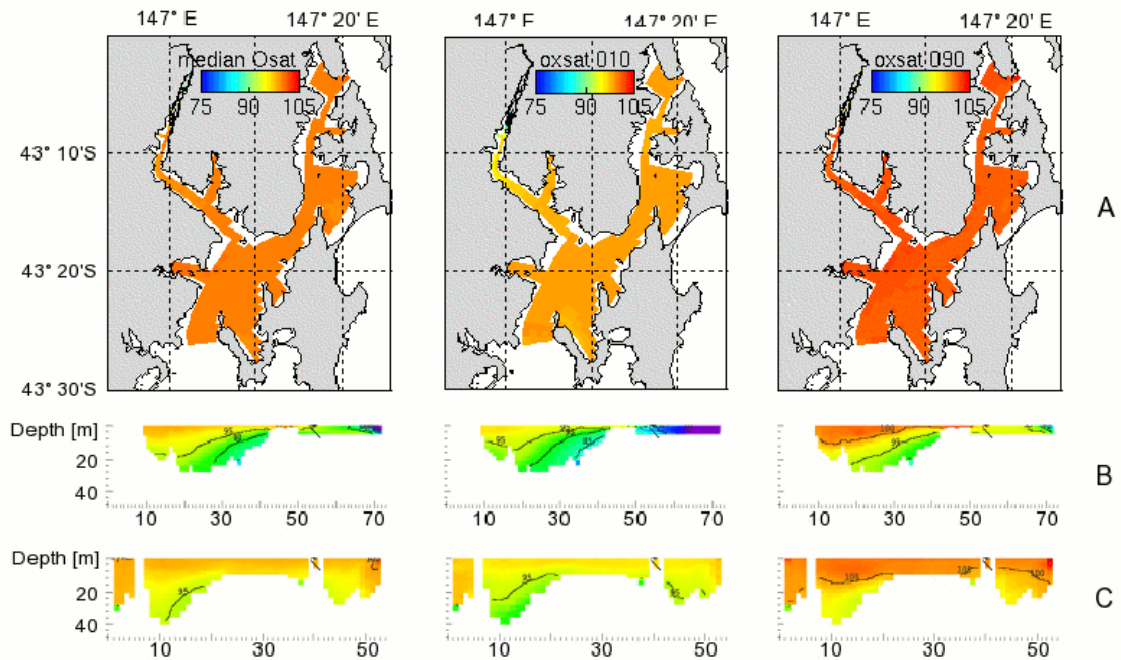


Figure 31. A) Surface concentration of annual median, 10 and 90 percentile oxygen saturation with (B) vertical cross sections through the Huon Estuary [from D'Entrecasteaux Channel (left) to Huon river (right)] and (C) the D'Entrecasteaux Channel [from south (left) to north (right)].

Modelled annual median oxygen saturation dropped from ~100% in surface waters to ~80% in bottom waters of the lower Huon Estuary. The most oxygen depleted waters were simulated in the upper Huon attributed to the influx of fresh river water. Values in bottom waters of the D'Entrecasteaux Channel were generally higher than in the Huon Estuary.

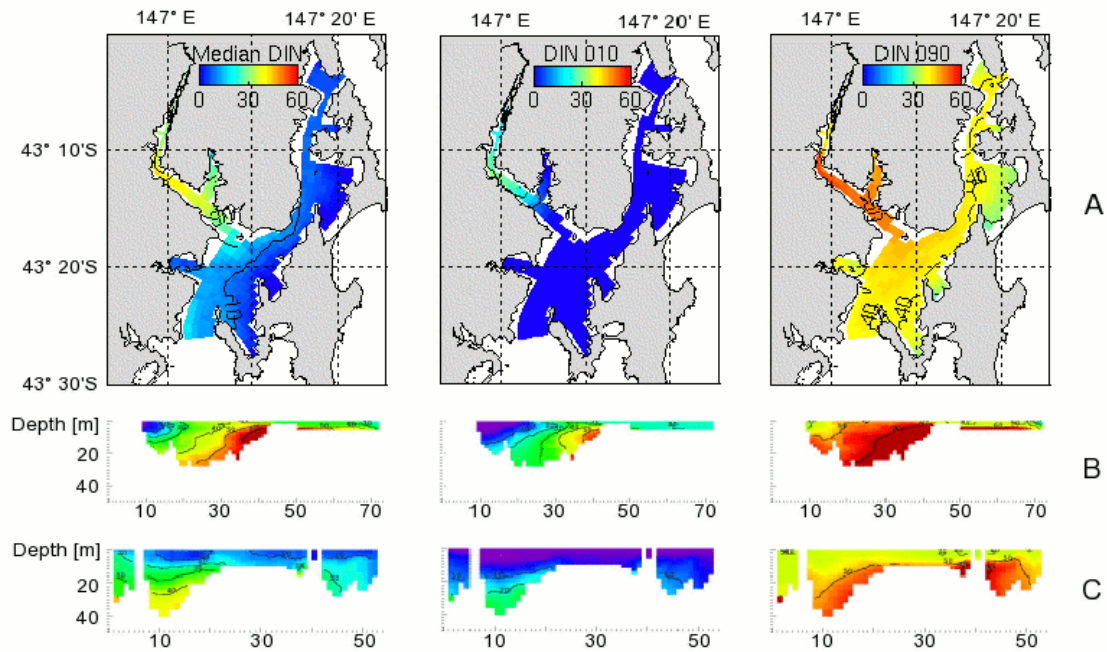


Figure 32. A) Surface concentration of annual median, 10 and 90 percentile DIN with (B) vertical cross sections through the Huon Estuary [from D'Entrecasteaux Channel (left) to Huon river (right)] and (C) the D'Entrecasteaux Channel [from south (left) to north (right)].

Median annual DIN was  $\sim 10 \text{ mgN m}^{-3}$  in surface waters of the D'Entrecasteaux Channel and about four times that in the Huon Estuary. Bottom water concentrations were highest in the mid Huon Estuary and in relatively shallow water, where the opaque river water limited phytoplankton growth and uptake. The considerable range in concentration between the 10 and 90 percentile concentrations results from utilization of nutrients by phytoplankton over an annual cycle.

The spatial distribution and concentration of phosphorus varied in a similar way to nitrogen with the larger concentrations simulated in the Huon Estuary and at depth. The 10 percentile surface concentrations were elevated compared to nitrogen indicating that the latter controls phytoplankton production in the region.

#### 2.4.6. Model results: seasonal regional biogeochemistry

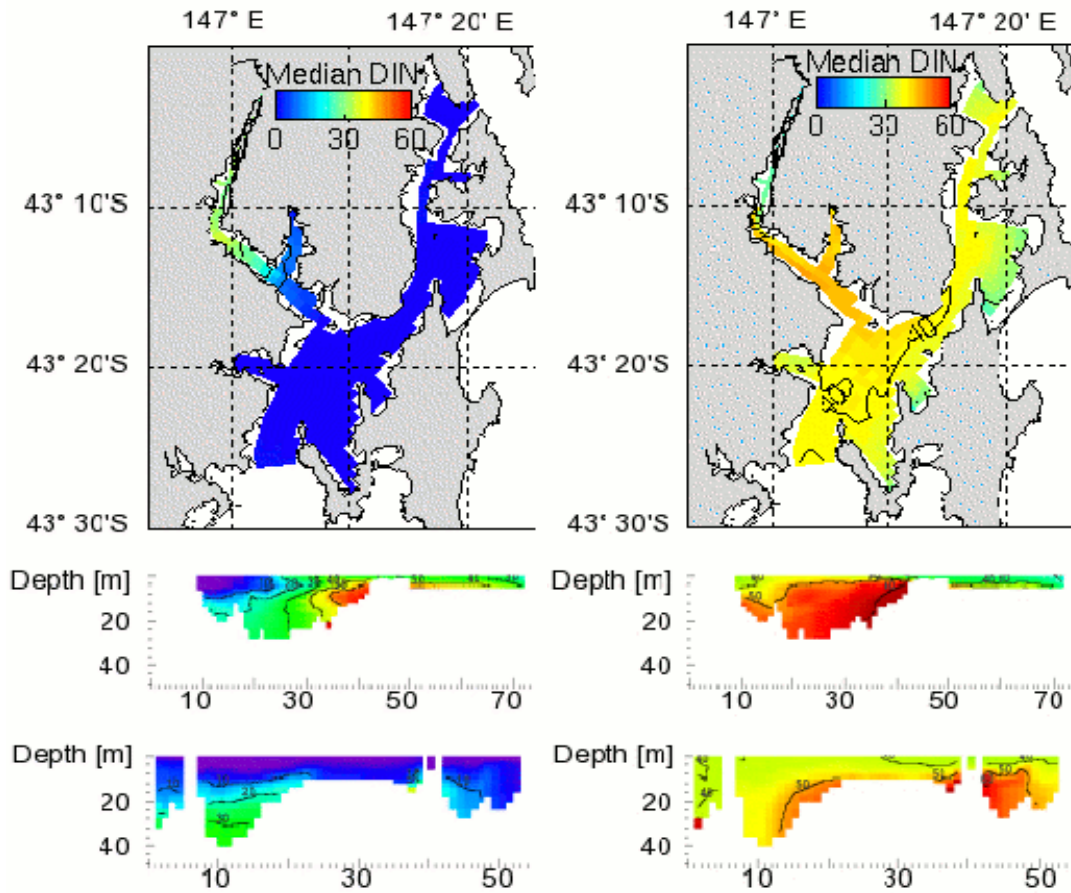


Figure 33. Surface concentration of median summer (left) and winter (right) DIN with vertical cross sections through the Huon Estuary [from D'Entrecasteaux Channel (left) to Huon river (right)] and the D'Entrecasteaux Channel [from south (left) to north (right)].

In summer surface DIN concentrations are depleted throughout the D'Entrecasteaux Channel and lower Huon Estuary due to phytoplankton assimilation and thermal stratification limiting vertical mixing. In the mid and upper Huon Estuary shallow water nutrients remain in summer as phytoplankton assimilation in the opaque river water is low [and probably under predicted by the model] and local nutrient influx from the river water and fish farm discharge exceeds algal uptake.

In winter the seasonal weather mixes river, farm and marine nutrient into surface waters and as phytoplankton growth is limited (by low incident irradiance and vertical mixing) surface concentrations are elevated. Maximum nutrient concentrations are found in the mid and lower Huon Estuary and at the northern end of the D'Entrecasteaux Channel.

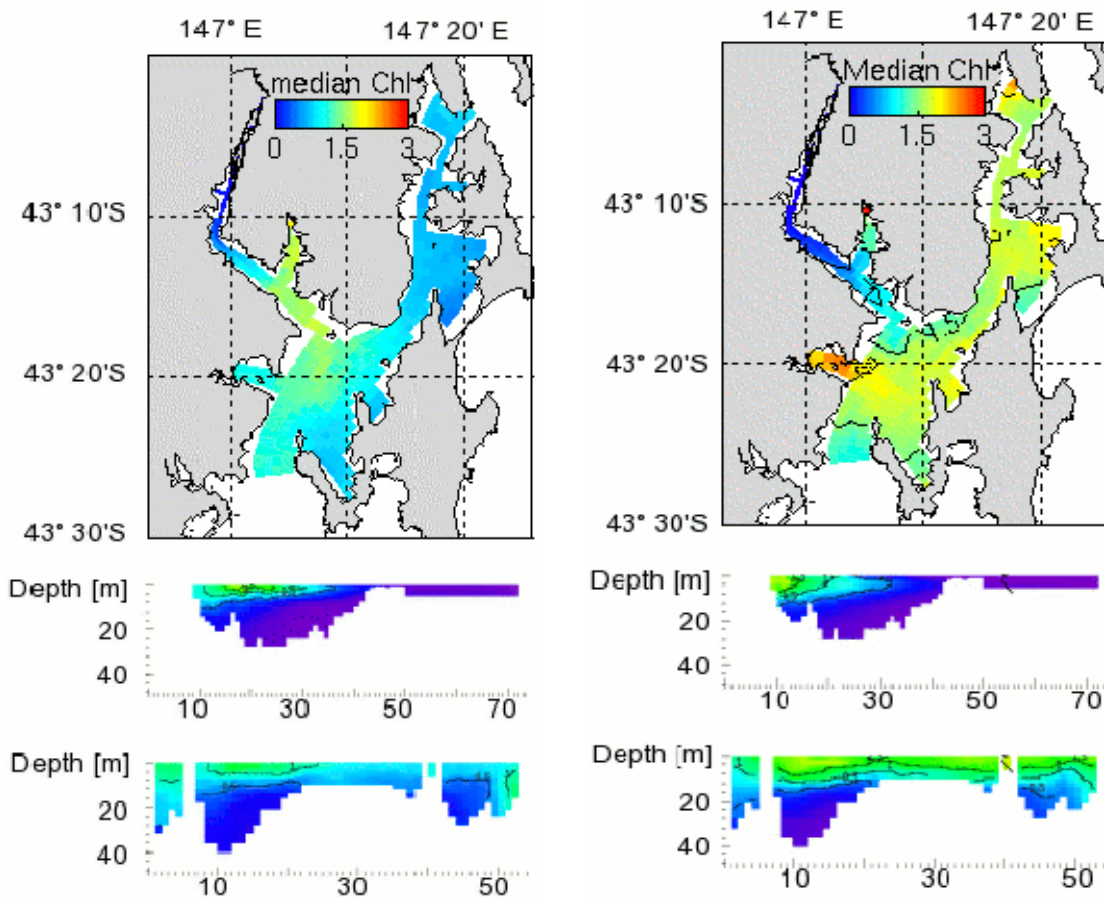


Figure 34. Surface concentration of median autumn (left) and spring (right) chlorophyll concentration with vertical cross sections through the Huon Estuary [from D'Entrecasteaux Channel (left) to Huon river (right)] and the D'Entrecasteaux Channel [from south (left) to north (right)].

Chlorophyll concentrations are elevated in surface waters with highest median concentrations of  $1.5 \text{ mg m}^{-3}$  found in autumn in the lower Huon Estuary and southern basin of the D'Entrecasteaux Channel. In autumn phytoplankton growth is limited by surface nutrient supply and diminishing incident irradiance as winter approaches. [Simulated chlorophyll concentrations in the Huon Estuary are lower than observed as the model fails to capture the complexities of dinoflagellate growth which can be significant in autumn.]

In spring median chlorophyll concentrations are higher throughout the D'Entrecasteaux Channel and side bays reaching  $\sim 2 \text{ mg m}^{-3}$  with maximum concentrations simulated in Port Esperance. Spring chlorophyll concentrations in the Huon Estuary are lower due to the highly attenuating river water limiting available PAR for phytoplankton growth.

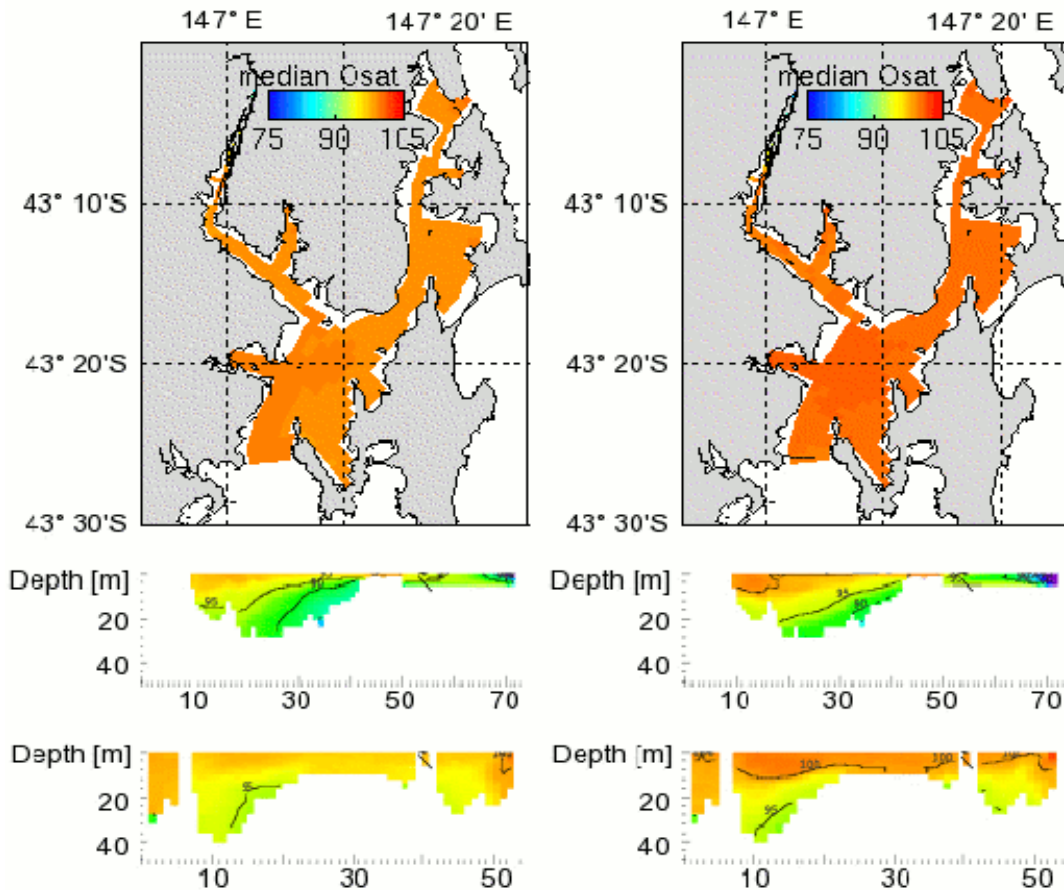


Figure 35. Surface concentration of median autumn (left) and spring (right) oxygen saturation with vertical cross sections through the Huon Estuary [from D'Entrecasteaux Channel (left) to Huon river (right)] and the D'Entrecasteaux Channel [from south (left) to north (right)].

Oxygen saturation is generally high throughout the region and in all seasons the model system is well flushed [possibly excessively due to the necessarily coarse resolution of the bottom bathymetry]. Example sections show some draw-down of oxygen saturation at depth associated with benthic oxygen demand for remineralisation of organic detritus. In autumn stratification limits surface oxygen exchange with bottom waters and maximal draw-down of ~20% occurs in the lower Huon Estuary. In spring the vertical structure is similar although surface waters are supersaturated with oxygen as a by-product of phytoplankton photosynthesis.

#### 2.4.7. Scenario simulations: impact of farm discharges

To demonstrate the impact in the model of fish farm discharges on the biogeochemical cycling and water quality of the Huon Estuary and D'Entrecasteaux Channel, a simulation was made with fish farm discharges omitted. By comparing this simulation with the original model run the impacts of fish farm discharges throughout the region are clearly shown. In general farm discharges had greatest impact on the nutrient fields in summer and on the phytoplankton in autumn.

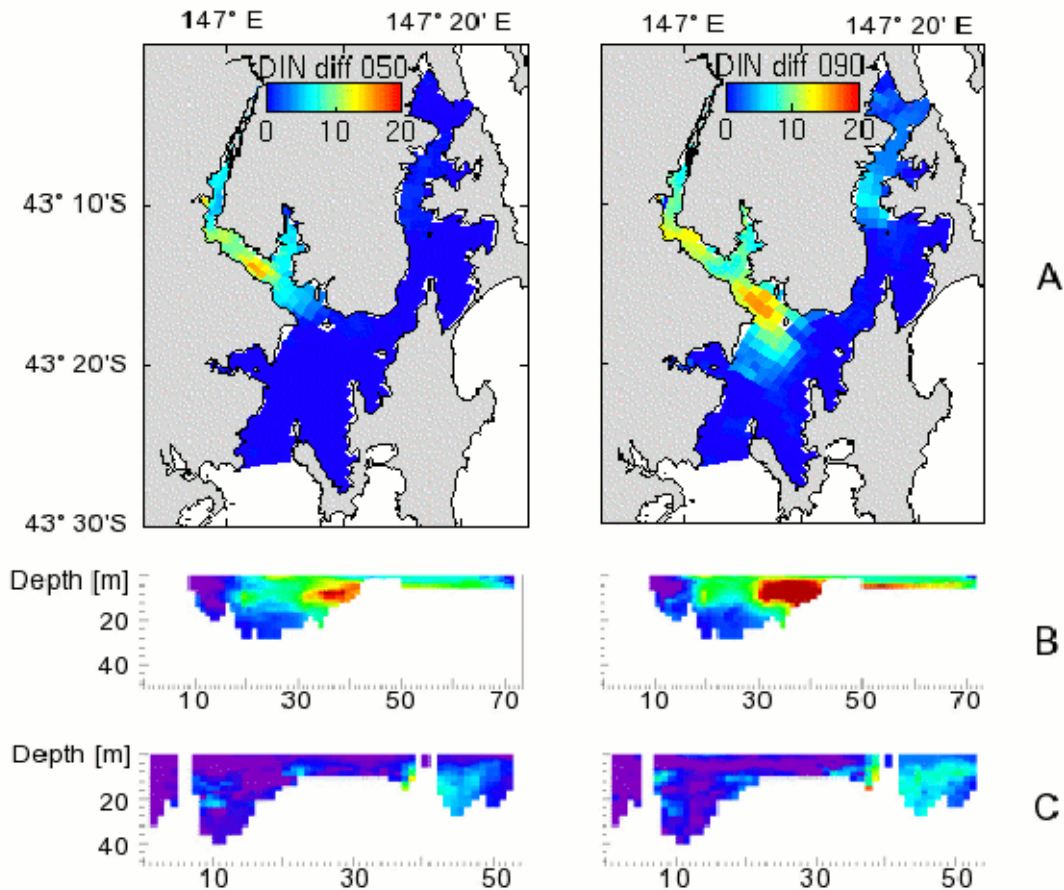


Figure 36. Difference in summer median and 90 percentile DIN concentration in  $\text{mg m}^{-3}$  between the model runs without and with farm discharges [0 = no difference; +ve value indicates enhanced concentration with farm discharges; -ve value indicates reduced concentration with farm discharges]. (A) surface distribution, (B) vertical cross section through the Huon Estuary [from D'Entrecasteaux Channel (left) to Huon river (right)] and (C) vertical cross section through the D'Entrecasteaux Channel [from south (left) to north (right)].

In summer seasonal stratification restricts vertical mixing and DIN and phosphate discharged from farms tends to accumulate in the upper water column, at least to the extent allowed by phytoplankton uptake. Riverine and marine fluxes of nutrient into surface waters are comparatively small during this period and the farm discharges enhance the ambient surface nitrogen concentration by  $>3$  times in the lower Huon Estuary, and mid- and northern ends of the D'Entrecasteaux Channel. This corresponds to significant absolute increases of  $\sim 10 \text{ mgN m}^{-3}$  in the Huon, but to negligible absolute increases ( $< 1 \text{ mgN m}^{-3}$ ) in the D'Entrecasteaux Channel where surface nutrients are seasonally depleted to near zero concentration by phytoplankton uptake. At depth DIN concentrations are elevated by up to  $20 \text{ mgN m}^{-3}$  in the lower Huon and  $8 \text{ mgN m}^{-3}$  at the northern end of the D'Entrecasteaux Channel suggesting that vertical exchanges of DIN, and/or remineralization of sinking particulate matter, are significant at these locations.

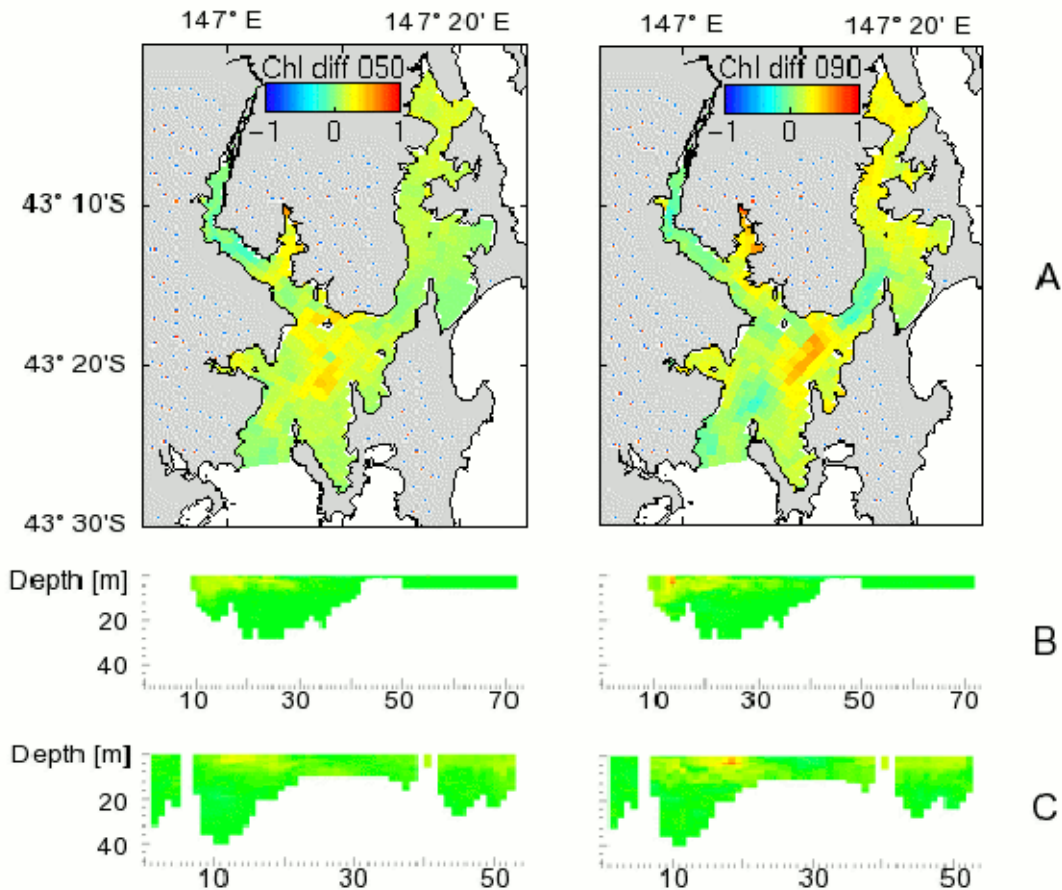


Figure 37. Difference in autumn median and 90 percentile chlorophyll concentration in  $\text{mg m}^{-3}$  between the model runs without and with farm discharges [0 = no difference; +ve value indicates enhanced concentration with farm discharges; -ve value indicates reduced concentration with farm discharges]. (A) surface distribution, (B) vertical cross section through the Huon Estuary [from D'Entrecasteaux Channel (left) to Huon river (right)] and (C) vertical cross section through the D'Entrecasteaux Channel [from south (left) to north (right)].

Autumn chlorophyll concentrations were enhanced by the farm discharges throughout most of the D'Entrecasteaux Channel, the lower Huon and in Northwest Bay. At this time seasonal river and marine nutrient fluxes into surface waters were small, although farm discharges were comparatively high. Median chlorophyll was enhanced by ~50% or  $0.4 \text{ mg Chl m}^{-3}$  in the central and northern end of the Channel and the 90 percentile concentrations indicate an increase in bloom events.

Farm discharges had little impact on simulated dissolved oxygen concentrations throughout the year in the D'Entrecasteaux Channel. In the upper Huon Estuary farm discharge resulted in some variation in absolute concentration within the range of  $\pm 200 \text{ mgO m}^{-3}$  or  $< 2\%$  of the ambient concentration. This likely resulted from spatial differences in phytoplankton production and degradation of organic material between the two model runs. Whilst dissolved oxygen concentrations were depleted at depth, the drawdown was similar in both simulations indicating that farm discharges do not significantly affect the modelled oxygen field which is well ventilated throughout the year.

To summarise the impacts of farm discharges throughout the Huon Estuary and D'Entrecasteaux Channel statistics were prepared for sub-regions of the model domain from the two model runs with and without farm discharges.

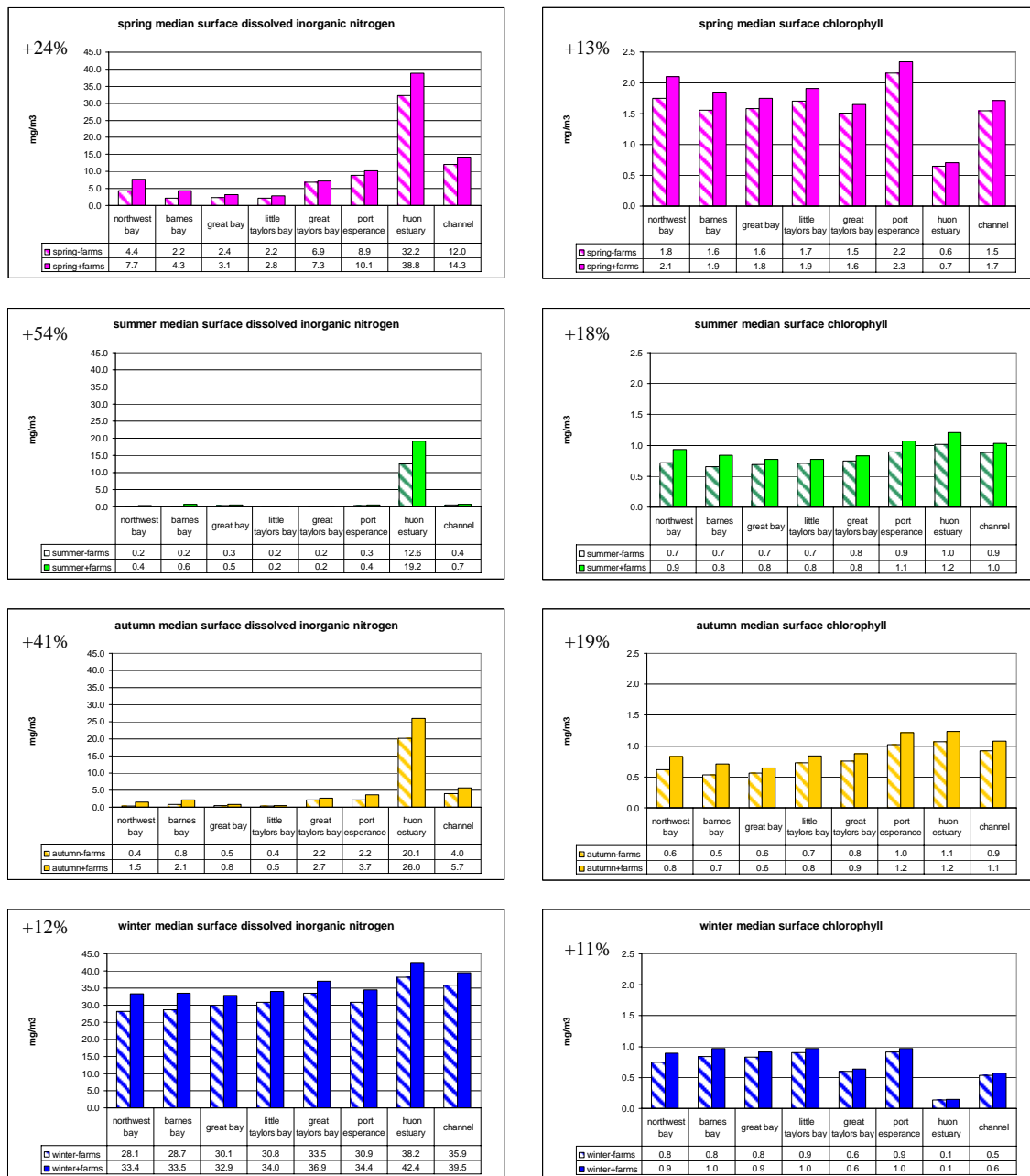


Figure 38. Seasonal surface median DIN (left) and chlorophyll (right) concentration for sub-regions of the model. Summary statistics for average increase in concentration (with simulation of farm discharges) across all sites are inset.

Seasonal statistics for each sub-region show a consistent increase in modelled surface DIN and surface chlorophyll concentration across the whole region resulting from the farm discharge. The Huon Estuary had the greatest increase in surface DIN, followed by Northwest Bay and Barnes Bay. These two Bays also showed the largest response in enhanced chlorophyll concentration, followed by Port Esperance. The maximum increase in seasonal median surface DIN occurred in summer (+54%) when surface

concentrations were seasonally depleted to near zero concentration. Surface chlorophyll concentrations were most enhanced in autumn and summer when surface nutrient concentrations were augmented with the farm discharge.

On an annual basis regional denitrification in tN/yr exceeded nitrogen discharged from the fish farms in 2002. Regional denitrification was compared for the simulations with and without farm discharges to evaluate what fraction of the farm waste was being denitrified.

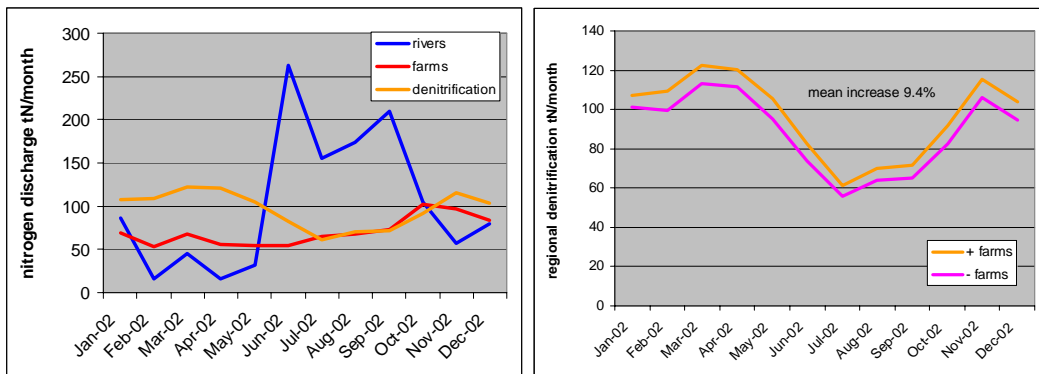


Figure 39. Regional denitrification compared to river and farm loads (left) and for the model runs with and without farm loads (right).

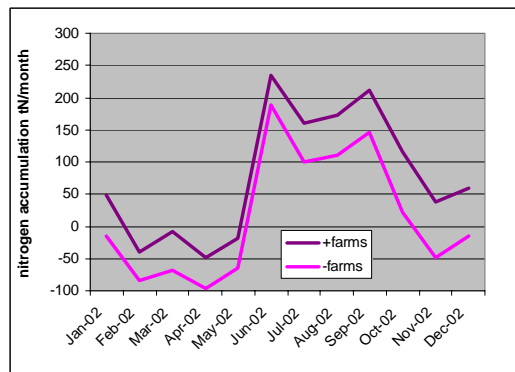


Figure 40. Seasonal nitrogen accumulation

Table 6. Relative fluxes of nitrogen into and out of the model region.

	tN yr <sup>-1</sup>
River discharge into region	1239.6
Fish farm discharge into region	838.7
Modelled denitrification with farm discharge	1161.5
Modelled denitrification without farm discharge	1062.9
Net load with farm discharge	920.5
Net load without farm discharge	176.8

Seasonal denitrification throughout the region exceeded the nitrogen discharge from fish farms by 323 tN y<sup>-1</sup> however the impact of the farm discharge on the denitrification flux was comparatively small. Comparing denitrification between the two simulations indicated a mean increase in denitrification flux of 9.4% with farm discharges. This increase indicates that 98 tN y<sup>-1</sup> or 11.8% of the 838.7 tN discharged from the farms in 2002 was denitrified.

Further scenario simulations have been run to examine the impact of secondary river loads on the region (Wild-Allen et al., 2005) and the impact of contrasting farm discharge loads.

## **2.5. Adaptive Management of Salmon Aquaculture in the Huon and D'Entrecasteaux Channel**

The overall objective of our project was to “acquire the necessary system understanding, and apply it in collaboration with industry and regulators, to support development of an adaptive management program which addresses system-wide impacts and production capacity for, and allows sustainable development of, salmon farms in the Huon Estuary and D'Entrecasteaux Channel”. The adaptive management subproject was designed to support that overall objective by “providing a vehicle for advice and exchange among researchers, regulators and industry, and a focal point for ensuring project outputs are taken up and incorporated in the development and refinement of an adaptive management strategy”.

Thus the adaptive management subproject has been effectively a forum for discussion, and a key part of the delivery pathway for the project. The research to acquire system knowledge, understanding and predictive capability was housed in other subprojects, and is reported in other chapters. The interim monitoring program agreed as an early outcome of the subproject (see below), together with additional field research and analysis to provide an environmental baseline for D'Entrecasteaux Channel and to assess options for additional broadscale ecological indicators, were conducted as part of the separate joint TAFI-CSIRO “Broadscale Monitoring Project”, which is the subject of a separate report.

It should be noted that the commitment of both the salmon industry and the Tasmanian state regulators to an adaptive approach to managing environmental effects of salmon farming is long-standing, and predates this project. In the early development of the industry, attention focused on the potential for adverse benthic impacts on the seafloor in the local vicinity of fish farms. The regulators and industry have run a very successful adaptive management program for local benthic impacts since the mid-1990s, based on benthic monitoring strategies designed with input from TAFI researchers. Following the HES (Butler et al., 2000), it became clear that non-local or system-wide effects of nutrient loads from fish farms also deserved attention, and this led to the inception of this project. The adaptive management subproject discussed here has been responsible only for discussion and exchange with industry and regulators on adaptive management of non-local or system-wide effects.

The Aquafin CRC study of system-wide environmental effects was planned from the start as a seven year study, with a review and revision stage after three years that is at the end of this project. This process has already led to the development and acceptance of a follow-on four year project. The adaptive management sub-project has provided an important forum for discussion with regulators and industry of both the research strategy, and its relationship to the management strategy, over the 2004–2008 period. It should be noted that this chapter effectively represents an interim report of progress towards the design and development of an adaptive management strategy for salmon farming in the Huon/D'Entrecasteaux region.

### 2.5.1. Conceptual framework for adaptive management

The development and application of formal adaptive approaches to environmental and natural resource management has been well-established since the 1970s (Holling, 1978), and the importance and value of an adaptive approach to dealing with uncertainty is now widely recognized and accepted. However, the term “adaptive management” is now used very broadly, and in some cases indiscriminately. Care was therefore taken in early discussions with industry and regulators to establish a shared conceptual framework for adaptive management to be applied to managing system-wide environmental impacts of fish farms.

At the core of any adaptive management approach is a feedback cycle, in which the system to be managed is monitored, the results are assessed against management objectives, appropriate management actions are chosen in response to this assessment, and these actions are implemented and applied to the system (Figure 41). A feedback cycle of this kind can be identified in almost any situation of natural resource or environmental management. Yet not all such situations have successful outcomes. Research over a number of decades has identified important attributes which increase the likelihood of success.

It is important to clearly define the management problem, and a standard terminology has been developed to aid in this process. We use here the standard SCFA definitions (<http://www.fisheries-esd.com/c/glossary/index.cfm>) for Ecologically Sustainable Development. Managers are generally working towards broad *environmental objectives*, often framed in relevant legislation. However, these may be so broadly stated as to provide only limited practical guidance. For example, one sees terms such as “maintaining environmental health”, or, as is the case in the Tasmanian aquaculture legislation, “avoiding unacceptable environmental impact”. For practical management, it is important to translate these broad objectives into *operational objectives*, which have a direct and practical interpretation, against which performance can be evaluated. An *indicator* is a quantity that can be measured as part of a monitoring program, and used to track changes with respect to an operational objective. A *performance measure* is a function which converts the value of an indicator to a measure of performance with respect to an operational objective. A *reference point* or *target* is a value of an indicator that can be used as a benchmark of performance against an operational objective.

Where there is a failure to adequately define operational objectives, and/or to choose appropriate indicators, there is a risk that there will only be the illusion of adaptive management, and the system will in fact be allowed to drift far from the intended state, until some kind of catastrophic failure occurs. It is important to define objectives, indicators and performance measures in initially setting up an adaptive management program. However, it is unrealistic to expect that these elements will necessarily be static and fixed for all time. It is realistic to recognize that objectives and target or reference points may change over time, as system understanding improves, and to explicitly build a longer cycle of review of these and other components of the management strategy into the process (Figure 41).

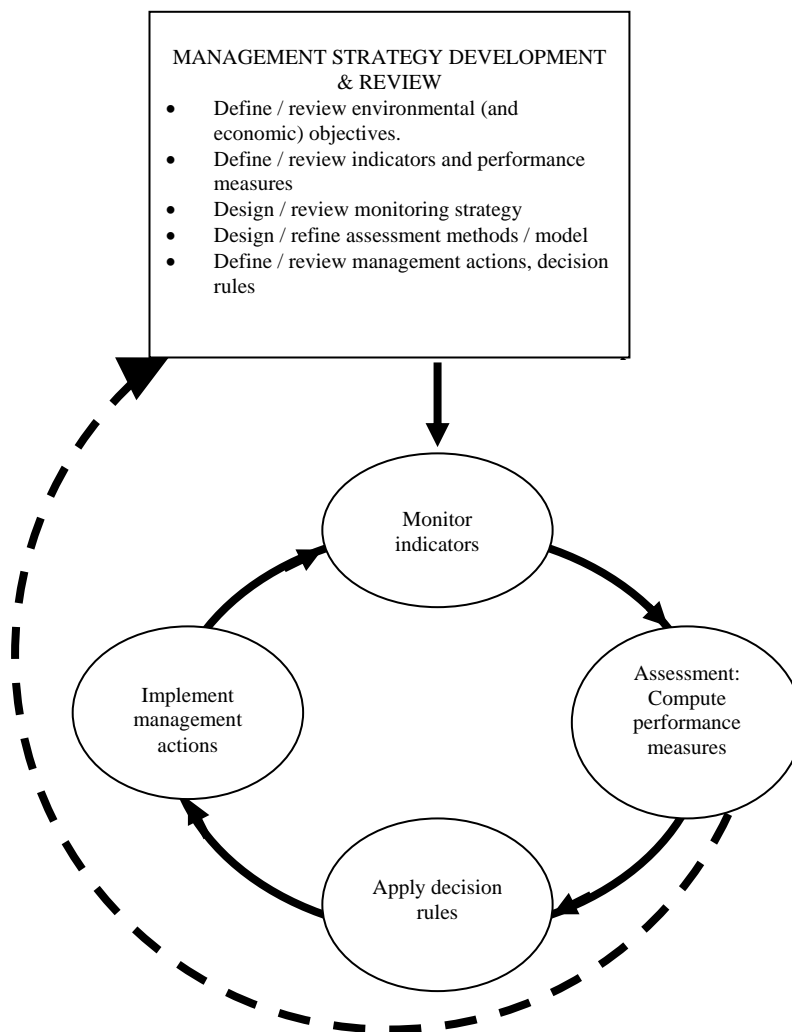


Figure 41. The adaptive management feedback cycle, showing both the core management cycle of monitoring, assessment, decision and action, and a longer-term cycle for review and refinement of the objectives, performance measures and management strategy.

Other elements of the management strategy are also critical to its success. We can think of a management strategy as consisting of a monitoring strategy, an assessment process, and a decision process. Even if there are clear operational objectives, indicators and reference points, we may still fail to achieve these objectives. A principal cause of failure is uncertainty, either about the current state of the system, or about its future response to management actions.

Our ability to monitor natural systems is typically constrained by technical capacity and/or available resources. It is often impractical to directly observe indicators that might be of most relevance to objectives, and thus it is often necessary to monitor surrogate indicators, which may bear an uncertain relationship to objectives. Many environmental variables vary strongly on a range of space and time scales, and observational technologies typically provide only limited spatial and temporal coverage, with the risk of both noise and bias. Depending on the variable of interest,

there may be measurement or instrument error, although this is often outweighed by the effects of spatial and temporal patchiness.

Even if the uncertainty around the estimate of current state is low, if there is high uncertainty about the response of the system to management actions, there is no guarantee that the chosen management actions will lead to a convergence of system state to the target state over time. This is particularly likely to be true if there are multiple potential causes or explanations of observed changes in system state, and/or if management actions are constrained, either in kind, or are subject to time lags in response and implementation. Where there are multiple potential causes, the problem of attribution or diagnosis arises. The capacity for correct attribution of cause will depend both on underlying system understanding, and on the choice of indicators.

Given these complications, it is clear that the selection of indicators for environmental management is both critical and potentially difficult. There are several criteria which need to be considered in choosing indicators:

- The intrinsic variability, and the extent to which that variability is “natural”, or driven by one or more anthropogenic pressures related or unrelated to available management intervention points.
- The technical feasibility and cost of measurements, and the implications for achievable spatial and temporal resolution in relation to the intrinsic scales of variation.
- The direct or indirect relationship of the indicator to operational objectives.
- The time lags involved in measurement and assessment, including whether the indicator is a leading or lagging indicator of critical dynamical system shifts.

It is often the case in marine environmental systems that the indicators of most direct interest to stakeholders’ values are ecological indicators. These “value” indicators can be expensive to measure, and typically respond to a range of natural and anthropogenic stresses, so that interpretation and attribution of change can be difficult. The more traditional water quality indicators, such as nutrients, dissolved oxygen, turbidity and chlorophyll, may be easier and less expensive to measure, and more directly related to particular pressures, but more variable in time. If interpreted correctly, these “system” indicators may be useful leading indicators of system change, and may be used as surrogates for ecological indicators. Particularly in cases such as management of diffuse loads from catchments, but potentially in some cases of point source loads, it may be unclear whether management actions will actually bring about the anticipated change in loads or pressures on the system. Directly monitoring these loads and other “pressure” indicators removes an important source of uncertainty in assessment and prediction. Distinguishing “value”, “system” and “pressure” indicators can help to structure the design of monitoring strategies for complex environmental systems.

The formal adaptive management process is intended to be a learning process, in which uncertainty about system state and likely system response to management actions is reduced over time. Without learning, adaptive management effectively becomes reactive management, and unless uncertainty is low and the system response is

relatively simple, there is a much higher risk of management failure. Formal learning can require an assessment model, which explicitly treats uncertainty about system state and system response, and assimilates observations over time to reduce this uncertainty.

A formal adaptive management strategy comprises a monitoring strategy, an assessment model, and a set of decision rules. The overall management performance depends in a highly interlinked way on all three of these components. This means that management strategy design is a non-trivial task. Trial and error testing of management strategies in the real world is likely to take many years, and involve unacceptable costs. Fisheries scientists have developed a short-cut procedure for *management strategy evaluation*, which avoids these costs by applying a range of candidate strategies to a simulated system, the so-called operating model. This model simulates not only the system to be managed, but also the application of all three elements of the management strategy to this system, and assesses the performance of the strategy (in the simulated world of the operating model) against operational objectives. The technique is generally used to identify robust management strategies, which deliver acceptable performance over a range of plausible assumptions about the (uncertain) underlying system. While the technique was developed primarily for single-species fisheries management, it has recently been tested in applications to multiple-use environmental management, and ecosystem-based fisheries management.

## *2.5.2. Implementing adaptive management strategies in the Huon and D'Entrecasteaux Channel region*

### *2.5.2.1. Huon Estuary*

The design and implementation of this project followed soon after the release of the final report of the HES (Butler et al., 2000). That study involved a comprehensive assessment of the physical and biogeochemical status of the Huon Estuary, which was then the primary site for salmon farm production in the region. The study involved intensive field sampling of physical, chemical and biological variables, and the development of annual and seasonal nutrient budgets for the estuary, incorporating marine, catchment and fish farm loads. While the study was primarily a field study, it did entail the implementation and calibration of simple eutrophication models linking nutrient loads to algal biomass.

A key finding of the HES study was that, while annual and winter nutrient budgets are completely dominated by high (natural) marine inputs, these are much reduced in summer, and fish farms, along with catchments, could make a significant contribution to estuarine nutrient loads and algal production in summer. Simulations using the simple eutrophication model suggested that fish farm inputs in 1997 could be responsible for as much as 25% of algal biomass in the middle and lower estuary, and that increasing fish farm loads four-fold could lead to a doubling of algal biomass.

A number of uncertainties were identified in the HES model assumptions. One issue concerned the proportion of fish farm loads directed to surface and bottom layers in the estuary. Because of the stratification and salt-wedge circulation in the Huon Estuary, one would expect the estuary to be more sensitive to loads discharged into bottom waters. In the model results presented in Butler et al. (2000), it was assumed that all fish farm loads were directed into the bottom layer. A subsequent contracted study for

industry, undertaken to look at the effects of varying the vertical distribution of fish farm loads, found that the impact was substantially reduced as the fraction released into surface waters increased (Parslow et al., 2000).

Other key uncertainties identified in the HES model included the limited spatial domain, and the highly simplified treatment of benthic-pelagic interactions. The model was restricted to the Huon Estuary, and assumed fixed boundary conditions at the estuary mouth. It was consequently unable to deal with any interaction between the Huon Estuary and D'Entrecasteaux Channel, although in practice these are strongly coupled through the estuarine circulation, and the southern D'Entrecasteaux Channel might be thought of as an extension of the Huon estuary. The model did not include an explicit sediment layer and sediment biogeochemistry, and consequently was not able to represent the role of the sediment as a seasonal sink or source for nutrients.

The additional process studies and model development in the system-wide project were designed explicitly to address these uncertainties. However, at the commencement of the project in 2001, managers and industry had to plan based on the information and understanding developed through HES. The period between the HES field season in 1997 and 2001 had seen rapid expansion in salmon production, with fish farm loads into the estuary increasing approximately three-fold. This led to considerable discussion among industry, regulators and researchers both about the likely impact of such an increase in loads, and whether such impacts would be consistent with the environmental objectives for the industry laid down under the relevant state legislation.

As noted above, the legislation requires that there be no unacceptable environmental impact, but translating this broad objective or principle into an operational objective for system-wide impacts has not proved straightforward. In the management of local benthic impacts, the regulators have required that there be no severe benthic impacts (e.g. high organic matter loads) outside lease boundaries, and no irreversible environmental impacts inside lease boundaries. The requirement of reversibility also applies to system-wide impacts. However, for system-wide scales, the impacts being considered are more subtle, there is greater natural variability, and attribution is more difficult.

In these early discussions, attention was focused on the importance of avoiding severe eutrophication at system-wide scales. Other estuaries in Australia have become severely eutrophied as a result of diffuse or point source loads. In stratified estuaries such as the Huon, this typically leads to accumulation of very high concentrations of nutrients in bottom waters, frequent, intense (and often toxic) algal blooms, and hypoxia or anoxia in bottom waters leading to extensive mortality of fish and benthic invertebrates. An account of these phenomena in Gippsland Lakes, including quantitative modelling, can be found in Webster et al. (2001). Researchers, industry and regulators all agreed that such a state would be regarded as “unacceptable” for the Huon Estuary. Aside from the environmental values placed on the estuary by other stakeholders, it would in fact make the estuary unviable as a site for salmon aquaculture.

The Huon Estuary is much better flushed than systems such as Gippsland Lakes (Webster et al., 2001), and should be less vulnerable to severe eutrophication. However, the HES did find instances of dissolved oxygen values as low as 70%

saturation in bottom waters in the lower estuary, suggesting that more severe oxygen sags under increased loads could not be ruled out. The HES simple eutrophication model did not represent oxygen dynamics or the positive feedbacks involved in interactions between water column and sediments under eutrophic conditions, and so could not be used to assess how increased nutrient loads might translate into reductions in bottom oxygen.

Aside from severe eutrophication, it was agreed that, as a precautionary measure, it would be desirable to avoid loads sufficient to double summer phytoplankton biomass, predicted by the HES model under 4-fold loads. The Huon Estuary is already subject to intense algal blooms in summer and autumn, including the toxic dinoflagellates *Gymnodinium catenatum* (which require intermittent closures of shellfish harvesting), and other species (e.g. *Chaetoceros* spp. which could cause salmon losses through gill damage). The precise dynamics underlying these blooms were not well understood, and it was not clear how a doubling in mean chlorophyll levels might translate into changes in bloom frequency and intensity. However, it was agreed that increases in summer nutrient loads sufficient to double mean chlorophyll levels would result in increased risk of harmful algal blooms.

Industry and regulators agreed on a number of management responses to the assessed risk of system-wide impacts provided by HES:

- It was agreed that an adaptive management approach would be used to manage system-wide environmental impacts. While farm leases are granted for 30 years and reviewed at approximately decadal intervals, regulators retain the capability if required to control the stocking density and consequently nutrient load from these leases on an annual basis through licence conditions.
- A voluntary and interim ceiling on further increases in nutrient load into the Huon Estuary was adopted by industry.
- An interim monitoring strategy was developed and implemented in the estuary, to ensure that current loads did not cause unacceptable damage.

The interim monitoring strategy was developed in close consultation among researchers, industry and regulators. The selected indicators were bottom water dissolved oxygen, bottom water ammonium concentration, phytoplankton biomass (chlorophyll concentration) and composition (cell counts for dominant species). Of these indicators, dissolved oxygen and phytoplankton biomass and composition have a direct link to the operational objectives just discussed, and are of direct concern to industry and other stakeholders, so they might be seen as value indicators. Bottom water ammonium concentrations might be expected to increase under conditions of increasing eutrophication, and can be regarded as a system indicator.

As noted earlier, the Interim Monitoring Program was conducted by TAFI researchers as part of the Broadscale Monitoring Project. The detailed sampling design is presented in the final report from that project. The sampling design was guided by field results from the HES, which conducted extensive spatial surveys quarterly, and obtained intensive weekly time series of observations at selected sites. However, the design was also strongly constrained by available resources and logistics.

It was decided that bottom and surface samples would be collected for analysis of nutrients and chlorophyll and Winkler oxygen, and depth-integrated samples for phytoplankton species, monthly at four sites in the middle and lower estuary. Monthly sampling is arguably marginal for detecting algal blooms, which may last only days to weeks. Monthly sampling was seen as a particular risk for dissolved oxygen, as even short-lived but extreme oxygen sags could in principle result in severe environmental or economic losses. The typical time scales of oxygen sags were not clear from the HES data. It was therefore decided to install continuously recording DO sensors located just above the bottom at three sites in the lower estuary, both to assess these time scales, and to provide a more robust assessment of oxygen status. At one of these sites, a telemetering capability was installed to continuously relay oxygen data back to shore.

Explicit reference points and performance measures for these indicators have not been agreed to. It was agreed that a trigger value of  $6 \text{ mg L}^{-1}$  for bottom water DO would be useful in an operational sense for both industry and researchers. Industry agreed that they might want to react when DO fell below  $6 \text{ mg L}^{-1}$ , by moving stock or changing feeding regimes. The researchers were interested in understanding the spatial extent as well as temporal duration of oxygen sags, and so it was agreed that detection of values below  $6 \text{ mg/L}$  would trigger an extensive spatial survey of bottom water DO. However, the telemetering system failed, and so bottom water DO was not available in real-time for operational use. DO values below  $6 \text{ mg L}^{-1}$  were detected at a monthly survey in early February 2003, and a spatial survey was conducted on 13 February 2003.

Detailed results and analyses for the Interim Monitoring Program are presented in the final report of the BROADSCALE Monitoring Project. The Program identified a number of technical difficulties, particularly in the operation of autonomous dissolved oxygen probes in bottom waters, but also issues associated with collection and analysis of ammonia samples. At a broad brush level, the interim monitoring program has provided industry and regulators with reassurance that there has been no dramatic deterioration in water quality in the Huon Estuary since HES, of the kind that might be expected in the onset of severe eutrophication. Dissolved oxygen values did decline in summer, but generally remained above  $5 \text{ mg L}^{-1}$ . Bottom water ammonia values were generally less than  $2 \text{ }\mu\text{M}$ , with some evidence for an increase in late summer. Median chlorophyll values were around  $3 \text{ }\mu\text{g L}^{-1}$ , with bloom values up to  $16 \text{ }\mu\text{g L}^{-1}$ .

The statistical power of the interim monitoring program to detect more subtle changes in these indicators since the HES in 1997, or to resolve trends over time, is not yet clear. These variables are subject to high levels of variability on a range of space and time scales. It would not be feasible to reproduce the intensive spatial and temporal coverage obtained in research mode in HES in a routine monitoring program. Failure of monthly sampling to resolve the typical temporal scales of variation of nutrients and chlorophyll can be expected to result in high levels of uncertainty in seasonal means. In the case of phytoplankton biomass in particular, these effects of short-term “noise” may be outweighed by the high natural interannual variability in bloom densities. In HES, there was an order of magnitude difference in bloom intensities in two successive years, due to the respective absence and presence of *Gymnodinium catenatum*.

A careful and sophisticated statistical analysis of spatial and temporal variation in these indicators is currently being undertaken, using the information collected in HES. It is

anticipated that, as part of the follow-on project, a statistically-rigorous assessment model will be developed. Preliminary attempts to estimate changes in mean summer chlorophyll in the Huon Estuary between 1996–1998 and 2002–2003 have yielded increases of about 25%. These are roughly consistent with those predicted by the biogeochemical model developed in this project as discussed previously.

#### 2.5.2.2. D'Entrecasteaux Channel

As noted above, a voluntary moratorium on further expansion of fish farm loads in the Huon Estuary was adopted by industry in 2001. Industry expansion since then has in practice been constrained by international economic conditions rather than constraints arising from observed or projected environmental impacts. Recent and planned expansion in the region is expected to occur primarily through release of new leases, and increased utilization of existing leases, in D'Entrecasteaux Channel.

The HES separation of the Huon Estuary from D'Entrecasteaux Channel was recognized as arbitrary, as the water bodies are strongly interconnected. Moreover, D'Entrecasteaux Channel itself includes a number of other side bays (North-West Bay, Port Esperance, Barnes Bay, etc) and certainly can't be treated as homogeneous. In the long run, an adaptive management program is required which treats the Huon/D'Entrecasteaux system as an integrated whole, while recognizing the spatial inhomogeneity associated with estuaries, side bays and the north and south channel. This need for a unified approach was recognized in the design of the system-wide project, and in particular the development of integrated physical and biogeochemical models for the Huon/D'Entrecasteaux Channel.

The Broadscale Monitoring Project included a baseline study of the D'Entrecasteaux Channel, which sampled 12 stations distributed along the main channel and through the side bays monthly. This baseline study was partly designed to provide calibration for the hydrodynamic and biogeochemical models, and comparisons between observations and model predictions are provided elsewhere in this report. The study has also provided a picture of the spatial and seasonal variation in environmental water quality in the 2002–2003 period, and a benchmark against which subsequent changes can be compared.

The design of an interim monitoring program for the integrated Huon/D'Entrecasteaux system was actively considered by researchers, industry and regulators in 2004, along with the design of the follow-on research project. It was agreed that we are not in a position to prescribe a routine monitoring program to be conducted by industry at this time, and that, as an interim measure, the baseline sampling should be continued, albeit with a reduced number of stations, and used both for management and research purposes.

The biogeochemical model results (Section 2.4) suggest that the relative effects of current fish farm loads may be comparable in the Huon Estuary and southern D'Entrecasteaux Channel, and that relative effects may be more pronounced in the side bays off the northern D'Entrecasteaux Channel.

### 2.5.3. Ecological indicators

There is an ongoing debate about the relative value of water quality and ecological variables as indicators for coastal environmental management. It is argued that some ecological indicators integrate over time, and therefore show less short-term variability than water quality indicators. On the other hand, ecological indicators may be several steps removed from direct pressures, so that attribution is more difficult. As noted in the conceptual framework, ideally one would use both, using ecological indicators as value indicators, even if assessment or attribution is difficult.

The BROADSCALE Monitoring Project included a specific subproject undertaken by TAFI researchers to investigate the feasibility of a number of potential ecological indicators. These included intertidal flora and fauna, seagrass communities and epiphyte cover, and community structure of macroalgae on subtidal reefs in marine reserves. Again, the detailed design, results and conclusions of this study can be found in the final report of the BROADSCALE Monitoring Project. Repeat sampling showed high variability in the structure of seagrass beds at a range of spatial scales, but little temporal variation. Associated epiphytes showed high spatial and temporal variability. Studies of long-term changes in subtidal macroalgal communities, over the period of expanding aquaculture from 1992 to 2002, showed inconsistent temporal patterns across sites, and no evidence of any consistent trend associated with increased farm activity.

One might expect nutrient loads from fish farms to increase the nutrient available to intertidal macroalgae in an extended mixing zone around lease sites. Sample sites were collected in areas containing fish farms, at contrasting distances from farms, and in control areas with no fish farms. No consistent near-field or far-field effect of farms was detected.

There is qualitative evidence for changes in zooplankton community structure in the regions. Intense jellyfish swarms have occurred in some years, and over the last few years, intense blooms of *Noctiluca*, a zooflagellate, have been reported from waters in south east Tasmania. Both these tend to be reported as they can cause mortality of farmed fish. There is no identified causal link between changes in zooplankton communities and aquaculture activities, and it is possible that these changes are part of long-term changes in pelagic ecosystems. There will be an increased emphasis on zooplankton communities and their ecological role in the follow-on project (CRC 4.2(2); FRDC 2004-074).

Benthic surveys conducted as part of the aquaculture benthic monitoring program have identified a number of introduced marine organisms in benthic fauna. The Aquafin CRC following project (MacLeod et al., 2004) found that some introduced species appear to occur disproportionately as successional stages in recovery of sediments and benthic communities in the near vicinity of cages. Again, it is unclear whether there is any interaction between aquaculture and benthic faunal communities, including introduced pests, at system-wide scales.

#### *2.5.4. Need for further development*

The adaptive management subproject has been successful in its primary role of providing a vehicle for discussion among regulators, industry and researchers to ensure that research findings are translated into management, and that management needs are taken into account in planning research. These discussions have led to the design and implementation of interim monitoring strategies, to the adoption by industry and regulators of an adaptive approach to managing system-wide impacts, and to precautionary management actions by industry in the Huon Estuary. The results suggest that the development of the industry to date is environmentally sustainable and responsible.

That said, we are still some way from the design and adoption of a formal adaptive management strategy by industry and regulators. The conceptual framework describes a number of key steps that have yet to be completed:

- While interim indicators have been identified, performance measures linked explicitly to operational objectives have yet to be defined.
- There are interim monitoring strategies, but no agreed sustained, operational monitoring strategy.
- There is no explicit assessment model, which deals in a statistically rigorous way both with observation error and prediction error, and allows reduction in uncertainty through assimilation of observations over time.
- There are no agreed explicit feedback decision rules for management actions based on output of the assessment.

It is worth noting that there are very few, if any, comparable coastal environmental management case studies where one can argue that all of these components are complete. Completing these steps requires an increased maturity and sophistication in scientific understanding and an increased confidence in the approach on the part of industry and managers, which one can only expect to emerge over time. The scientific understanding of the Huon/D'Entrecasteaux system, and its response to nutrient loads, is now at least as advanced as for any other water body in Australia. An important goal of the follow-on project (CRC 4.2(2); FRDC 2004-074) is to translate this understanding into an effective adaptive management strategy.

One promising avenue for pursuing this goal is the adoption of Management Strategy Evaluation, discussed above at the end of the section on Conceptual Framework for Adaptive Management. To recap, a management strategy consists of a monitoring strategy, an assessment model, and a set of decision rules. Alternative management strategies can be tested by simulating their application over time to an operating model of the system to be managed, and assessing the outcomes in relation to agreed operational objectives and performance measures. The sophisticated integrated biophysical models of the Huon/D'Entrecasteaux developed to date represent an ideal foundation for operating models. However, they are arguably too complex and computationally expensive to be used as assessment models.

An assessment model needs to capture the essentials of our understanding of the relationship between aquaculture loads and indicators, yet be sufficiently simple and fast to allow a rigorous statistical treatment of error and uncertainty in both observation and prediction. An assessment model could be as simple as a hypothesized function relating aquaculture loads to a spatial and seasonal summary statistic of indicators such as chlorophyll, nutrients or dissolved oxygen, or could be a highly spatially aggregated, simplified, dynamical model. An assessment model which works well for aquaculture loads is likely to find much wider use in managing coastal eutrophication from many sources.

The Management Strategy Evaluation approach is likely to encourage industry and stakeholders to adopt explicit performance measures and decision rules, because it allows them to test the consequence of adopting specified measures and rules, and convince themselves that strategies are likely to lead to robust and beneficial outcomes under a variety of plausible assumptions.

There are two other considerations for further development of adaptive management strategies for system-wide environmental impacts, and both relate to the scope of the management problem.

First, it is clear that a statistically robust monitoring system is unlikely to be affordable if it is run solely by research institutions or private consultants, and is likely to be most cost-effective if run by industry. Industry already conducts considerable environmental monitoring, primarily for operational purposes. Industry is concerned with the effects of changing environmental conditions on fish farms, and needs to resolve and predict these changes on the time and space scales appropriate for operational farm management. There is potentially huge synergy between observing systems to support local environmental assessment and short-term prediction for farm management, and observing systems to support system-wide environmental assessment and long-term prediction for environmental management. The follow-on project (CRC 4.2(2); FRDC 2004-074) will devote considerable effort to try to realize this synergy.

Second, the salmon aquaculture industry is only one user of the Huon/D'Entrecasteaux ecosystem, and its activities represent only one pressure on that system. It is now generally agreed that sector-based environmental management is ineffective in the long-term, and that regional, multiple-use, ecosystem-based management is required. This would require a broadening of the stakeholder and regulatory involvement well beyond the existing Aquafin project. Until this is achieved, there will be important practical constraints on what can be achieved. For example, the salmon industry can hardly be expected to fund monitoring of catchment loads into the system, when these measure pressures from other (catchment-based) users. Yet without adequate monitoring of these loads, development of robust assessment methods will be extremely difficult. As a second example, there are good arguments that a number of high-level ecological indicators should be included in any monitoring strategy. This would likely be self-evident to any management authority given overall responsibility for the sustainability of the marine ecosystem. Yet it is difficult to argue that a single sector such as aquaculture should fund the monitoring of such indicators alone, especially if attribution is uncertain, and the indicators have no direct link to industry benefit.

### 3. Summary

The Huon Estuary Study, FRDC project 1996-284, provided the first comprehensive baseline environmental data for the Huon Estuary. These data in combination with simple biogeochemical modelling indicated that the nutrients from salmonid fish farming made a significant contribution to phytoplankton abundance in the estuary. Nutrients are a particular environmental issue here since concentrations drop to near-zero in summer months and thus phytoplankton become nutrient limited. Any additional nutrients during this time, whether from fish farming or other sources, have the potential to add to phytoplankton loads. Various scenarios were run with different farm loads which indicated that the finfish industry could not continue to expand within the Huon Estuary without significant risk of increased frequency or magnitude of phytoplankton blooms. This led to a voluntary moratorium and investigation of sites outside of the Huon, including the D'Entrecasteaux Channel.

The Aquafin CRC project 2001-097 has built on this research in several key ways.

- It has supported the establishment of an adaptive management framework for system-wide impacts of salmon aquaculture in the Huon estuary, including an interim monitoring program which has provided managers and fish farmers reassurance that the cap on fish farming in the Huon has prevented any major wide-scale environmental problem. Measurements of dissolved oxygen, chlorophyll and bottom water ammonia have been trialled as potential monitoring tools for system-wide effects.
- Also, it has provided the first detailed monthly data for environmental conditions in the D'Entrecasteaux Channel. These data establish that the Channel and Huon Estuary are linked, but the dynamics of the phytoplankton blooms in each have distinctive features of timing, species composition and magnitude. These data confirm the generally high environmental quality of the Channel waters.
- The hydrodynamic modelling has been substantially refined, calibrated and validated. This has enabled a range of outputs including the fate of releases at particular farm sites, the role of off-shore forcing, flushing times (and hence sensitivity to environmental effects) and most recently fine-scale modelling of proposed chloramine-T releases. These model outputs clearly show the interconnected nature of the system and have revealed to farmers and managers that environmental effects must be examined on a system-wide basis. Farms cannot be considered as single units unconnected to other farm units. There are potential applications of these results for understanding movement of parasites or disease as well as nutrients between sites.
- The biogeochemical modelling has advanced considerably and now provides a very good simulation of spring and summer phytoplankton blooms. Further refinement is needed to properly represent the autumnal dinoflagellate blooms. A comparison of model outputs with and without farm loads confirms the earlier HES study conclusion that nutrients from fish farming do make a significant contribution to phytoplankton abundance. Moreover, the models allow industry and managers to disentangle the effects of oceanic and terrestrial nutrient loads from those of aquaculture. This provides the industry with a scientific basis for

attribution of environmental impacts, and for management of catchment loads where these adversely impact on aquaculture.

Thus, the work has reduced uncertainty by providing a quantitative measure of environmental effects due to fish farming. Thus far, these effects have not led to any major environmental concern, and the models have provided a means for testing scenarios in which the amount and location of fish farms loads are varied.

The research undertaken has been comprehensive and once the follow-on project (CRC 4.2(2); FRDC 2004/074) has been completed, it is not envisaged that there will be a need for any major research in this region although clearly there will be a need for on-going monitoring. The tools developed are readily translocated to other regions although their implementation will only be as good as the environmental data available to calibrate and validate the models.

Environmental monitoring costs are a fact of life for any major industry that is known to have effect on the environment. Our work and previous monitoring has clearly demonstrated that effects on the benthos are limited to sediments within the farm lease. While these effects can be quite dramatic it is possible through suitable management such as fallowing regimes, attention to stocking densities etc to maintain environmental conditions suitable for finfish farming for many years. Monitoring for system-wide effects is a more difficult issue and the Australian approach is seen as sophisticated and world-leading (comments at Seattle workshop, 2005). By the end of the follow-on project (CRC 4.2(2); FRDC 2004/074) we expect to have in place a cost-effective monitoring scheme that will not only provide managers with confidence that the ecosystem remains healthy, but will also provide farmers with information about environmental conditions that could affect their farm operations.

Our research is designed to estimate the assimilative capacity of the Huon estuary-D'Entrecasteaux Channel region. Monitoring to date indicates that this is not being exceeded with current industry practices. Our ability to run scenarios will provide useful guidelines as to whether there is scope for additional farming in the system. We expect that some expansion of salmon farming will be possible, but it will be necessary to monitor its effects to ensure that healthy environmental conditions are maintained.

Our work to date has established the value of several parameters for long-term monitoring of environmental health. These include chlorophyll, dissolved oxygen and bottom-water ammonia. We will be recommending that a monitoring system be put in place that involves farmers taking some of the samples, and possibly many of the measurements as well, so that monitoring becomes part of an adaptive management framework for the industry going forward.

## References

- Abril G., Etcheber H., Lehir P., Bassoullet P., Boutier B., Frankignoulle M. (1999). Oxidic/anoxic oscillations and organic carbon mineralization in an estuarine maximum turbidity zone (The Gironde, France). *Limnology and Oceanography* 44, 1304-1315.
- ANZECC/ARMCANZ (2000). Australian and New Zealand Guidelines for Fresh and Marine Water Quality. ([www.ea.gov.au/water/quality/nwqms/#quality](http://www.ea.gov.au/water/quality/nwqms/#quality)).
- Baird, M.E., Emsley, S. M. (1999). Towards a mechanistic model of plankton population dynamics. *Journal of Plankton Research* 21, 85-126.
- Berg, P., Risgaard-Petersen, N., Rysgaard, S. (1998). Interpretations of measured concentration profiles in sediment porewater. *Limnology and Oceanography* 81, 289-303.
- Bordovskiy O.K. (1965). Accumulation and transformation of organic in marine substances in marine sediments. *Marine Geology* 3, 3-114.
- Butler E.C.V., Parslow J.P., Volkman J.K., Blackburn S.I., Morgan P., Hunter J., Clementson L.A., Parker N.S., Bailey R., Berry K., Bonham P., Featherstone A., Griffin D., Higgins H.W., Holdsworth D., Latham V., Leeming R., McGhie T.K., McKenzie D., Plaschke R., Revill A., Sherlock M., Trenerry L., Turnbull A., Watson R., Wilkes L. (2000). Huon Estuary Study - environmental research for integrated catchment management and aquaculture. Final report to the Fisheries Research and Development Corporation project number 96/284. CSIRO Division of Marine Research, Hobart.
- Calbet, A., Landry, M.R. (2004). Phytoplankton growth, microzooplankton grazing, and carbon cycling in marine ecosystems. *Limnology and Oceanography* 49, 51-57.
- Cook P.L.M., Revill A.T., Clementson L.A., Volkman J.K. (2004). Carbon and nitrogen cycling on intertidal mudflats of a temperate Australian estuary. III. Sources of organic matter. *Marine Ecology Progress Series* 280, 55-72.
- Eppley, R.W. (1972). Temperature and phytoplankton growth in the sea. *Fisheries Bulletin* 70, 1063-1085.
- Fileman, E., Burkhill, P. (2001). The herbivorous impact of microzooplankton during two short-term lagrangian experiments off the NW coast of Galicia in summer 1998. *Progress in Oceanography* 51, 361-383.
- Froneman, P.W., McQuaid, C.D. (1997). Preliminary investigations of the ecological role of microzooplankton in the Kariega Estuary, South Africa. *Estuarine and Coastal Shelf Science* 45, 689-695.
- Fry B., Sherr E. (1984).  $\delta^{13}\text{C}$  measurements as indicators of carbon flow in marine and freshwater ecosystems. *Contributions in Marine Science* 27, 15-47.
- Gifford, D.J. (1988). Impact of grazing by microzooplankton in the Northwest Arm of Halifax Harbour, Nova Scotia. *Marine Ecology Progress Series* 47, 249-258.
- Glud, R.N., Gundersen, J. K., Roy, H., Jorgensen, B.B. (2003). Seasonal dynamics of benthic  $\text{O}_2$  uptake in a semienclosed bay: Importance of diffusion and faunal activity. *Limnology and Oceanography* 48, 1265-1276.
- Gray, J.S., McIntyre, A.D., Stirn, J. (1992). Manual Methods in Aquatic Environmental Research: Part II – Biological Assessment of Marine Pollution, Food and Agriculture Organization of the United Nations, Fisheries Technical paper 324.
- Hall, J.A., Safi, K., Cumming, A. (2004). Role of microzooplankton grazers in the subtropical and subantarctic waters to the east of New Zealand. *New Zealand Journal of Marine and Freshwater Research* 38, 91-101.

- Hansen, F.C., Reckerman, M., Klein Breteler, W.C.M., Riegman, R. (1993). *Phaeocystis* blooming by enhanced copepod predation on protozoa: Evidence from incubation experiments. *Marine Ecology Progress Series* 102, 51-57.
- Hansen L.S., Blackburn, T.H. (1992). Effect of algal bloom deposition on sediment respiration and fluxes. *Marine Biology* 112, 147-152.
- Harris, G., Batley, G., Fox, D., Hall, D., Jernakoff, J., Molloy, R., Murray, A., Newell, B., Parslow, J., Skyring, G., Walker, S. (1996). Port Phillip Bay Environmental Study. Final Report. CSIRO, Canberra, Australia.
- Heip, C.H.R., Goosen, N.K., Herman, P.M.J., Kromkamp, J., Middelburg, J.J., Soetaert, K. (1995). Production and consumption of biological particles in temperate tidal estuaries. *Oceanography and Marine Biology - an Annual Review* 33, 1-149.
- Herbert, R.A. (1999). Nitrogen cycling in coastal marine ecosystems. *FEMS Microbiology Reviews* 23, 563-590.
- Herzfeld, M., Parslow, J., Sakov, P., Andrewartha, J.R. (2005) Numerical hydrodynamic modelling of the D'Entrecasteaux Channel and Huon Estuary. Aquafin CRC Technical report (on accompanying CD)
- Holling, C.S. (1978). Adaptive Environmental Assessment and Management. John Wiley and Sons, New York.
- James, M.R., Hall, J.A., Barrett, D.P. (1996). Grazing by protozoa in marine coastal and oceanic ecosystems off New Zealand. *New Zealand Journal of Marine and Freshwater Research* 30, 313-324.
- Jeong, H.E., Kim, S.K., Kim, J.S., Kim, S.T., Yoo, Y.D., Yoon, J.Y. (2001). Growth and grazing rates of the heterotrophic dinoflagellate *Polykrikos kofoidii* on red-tide and toxic dinoflagellates. *Journal of Eukaryotic Microbiology* 48, 298-308.
- Landry, M.R., Hassett, R.P. (1982). Estimating the grazing impact of marine microzooplankton. *Marine Biology* 67, 283-288.
- Macleod, C., Bissett, A., Burke, C., Forbes, S., Holdsworth, D., Nichols, P., Revill, A., Volkman, J. (2004). Development of novel methods for the assessment of sediment condition and determination of management protocols for sustainable finfish cage aquaculture operations. Final Report for Aquafin CRC Project 4.1.
- Margvelashvili, N., Andrewartha, J., Herzfeld M., Parslow, J., Sakov, P., Waring, J. (2002) "MECOSED – Model for Estuarine and Coastal Sediment Transport". Scientific Manual, CSIRO Marine Research.
- Margvelashvili, N., Robson, B., Sakov, P., Webster, I.T., Parslow, J., Herzfeld, M., Andrewartha, J. (2003). *Numerical modelling of hydrodynamics, sediment transport and biogeochemistry in the Fitzroy Estuary*. Cooperative Research Centre for Coastal Zone, Estuary and Waterway Management, Technical Report 9.
- McCarthy, J.J., Taylor, W.R., Taft, J.L. (1977). Nitrogenous nutrition of the plankton in Chesapeake Bay, 1. Nutrient availability and phytoplankton preferences. *Limnology and Oceanography* 22, 996-1011.
- Parslow, J. et al. (2000). Huon Estuary Fish Farm Load Scenarios Final Report. CSIRO Marine Research, Hobart.
- Parslow, J., Margvelashvili, N., Palmer, D., Revill, A.T., Robson, B., Sakov, P., Volkman, J.K., Watson, R., Webster, I. (2003). The Response of the Lower Ord River and Estuary to Management of Catchment Flows and Sediment and Nutrient Loads. Final Report to Land and Water Australia.
- Schlesinger, W.H. (1997). Biogeochemistry. An Analysis of Global Change. Academic Press, San Diego.

- Smayda, T.J. (1997). What is a bloom? A commentary. *Limnology and Oceanography*, 42, 1132-1136.
- Stelfox-Widdicombe, C.E., Edwards, E.S., Burkill, P.H., Sleigh, M.A. (2000). Microzooplankton grazing activity in the temperate and sub-tropical NE Atlantic: summer 1996. *Marine Ecology Progress Series* 208, 1-12.
- Thomson, D., Volkman, J., Burke, C., Purser, J. (2005). Sediment biogeochemistry of the Huon Estuary. Status report for Aquafin CRC Project 4.2 (on enclosed CD).
- Thompson P.A., Bonham, P. (2005). Effects of grazing by microzooplankton on phytoplankton in the Huon Estuary. Aquafin CRC Technical report (on accompanying CD).
- Thompson, P.A., Parslow, J.P. (2005). Measuring ecological health: A preliminary assessment of phytoplankton sampling strategies for the Huon Estuary and D'Entrecasteaux Channel including an initial comparison of the Huon interim monitoring (2001–2004) with HES (1996–1998) chlorophyll *a* data. Aquafin CRC Technical report (on accompanying CD).
- Thompson, P.A., Bonham, P., Willcox, S., Crawford, C. (2005). Baseline environmental data for the D'Entrecasteaux Channel. Aquafin CRC Technical report (on accompanying CD).
- Verity, P.G., Smetacek, V. (1996). Organism life cycles, predation, and the structure of marine pelagic ecosystems. *Marine Ecology Progress Series* 130, 277-293.
- Verity, P.G., Stoecker, D.K., Sieracki, M.E., Nelson, J. (1996). Microzooplankton grazing of primary production at 140°W in the equatorial Pacific. *Deep Sea Research II*. 43, 1227-1256.
- Walker, S.J., Waring, J.R. (1998). A multiple grid, 3-dimensional, non-linear, variable-density hydrodynamic model with curvilinear horizontal coordinates and level (*z*) vertical coordinates, CSIRO Marine Research, Report OMR-118/120.
- Webster, I.T., Parslow, J.S., Grayson, R.B., Molloy, R.P., Andrewartha, J., Sakov, P., Tan, K.S., Walker S.J., Wallace, B.B. (2001). Gippsland Lakes Environmental Study Final Report: Assessing Options for Improving Water Quality and Ecological Function. CSIRO.
- Wild-Allen, K., Parslow, J., Herzfeld, M., Sakov, P., Andrewartha, J., Rosebrock, U. (2005). Biogeochemical Modelling of the D'Entrecasteaux Channel and Huon Estuary. Aquafin CRC Technical report (on accompanying CD).
- Wood, E.J.F. (1954). Dinoflagellates in the Australian region. *Australian Journal of Marine and Freshwater Research* 5, 171-351.

## Appendix 1

### Intellectual Property

The nature of the project is such that results are generally not commercially sensitive and have limited or no potential for commercial exploitation. The IP for original model formulations resides with CSIRO Marine Research (now CSIRO Marine and Atmospheric Research), and advances made since then are available for use within the Aquafin CRC. An example of this is the intention to make the models available for use in the “Risk and Response” project which will include training of SARDI-employed personnel in their use. It is intended that much of the information produced will be made publicly available through this report, PhD theses and publications in the open scientific literature after due consideration by the Aquafin CRC publications committee.

## Appendix 2

### Staff employed on the project

Staff Member	Role	Organisation
Dr John Volkman	Project Leader	CSIRO Marine Research
Dr John Parslow	Modeller	CSIRO Marine Research
Dr Peter Thompson	Phytoplankton Ecologist	CSIRO Marine Research
Dr Andrew Revill	Biogeochemist	CSIRO Marine Research
Dr Susan Blackburn	Phytoplankton Ecologist	CSIRO Marine Research
Dr Michael Herzfeld	Modeller	CSIRO Marine Research
Dr Karen Wild-Allen	Biogeochemical Modeller	CSIRO Marine Research
Ms Rebecca Esmay	Organic analysis	CSIRO Marine Research
Ms Pru Bonham	Phytoplankton/zooplankton	CSIRO Marine Research
Dr John Andrewartha	Modelling	CSIRO Marine Research
Dr Pavel Sakov	Modelling	CSIRO Marine Research
Ms Ros Watson	Nutrients	CSIRO Marine Research
Mr Daniel Holdsworth	Organic analysis	CSIRO Marine Research
Ms Val Latham	Nutrient analysis	CSIRO Marine Research
Ms Kate Berry	Nutrient analysis	CSIRO Marine Research
Dr Christine Crawford	Marine biologist	University of Tasmania
Dr Chris Burke	PhD supervisor	University of Tasmania
Dr Chris Bolch	PhD supervisor	University of Tasmania
Dr John Purser	PhD supervisor	University of Tasmania
Mr Dean Thomson	PhD student	University of Tasmania
Mr Paul Armstrong	PhD student	University of Tasmania
Mr Colin Shepherd	Tasmanian State Government	DPIWE
Dr Dom O'Brien	Salmon Industry	TSGA

## Appendix 3

### Communications

The First Scientific Meeting of the Aquafin CRC Environment Program was held at CSIRO Marine Research in Hobart from April 4-5<sup>th</sup>, 2002. About 30 scientists attended from CSIRO Marine Research, Flinders University, SARDI and TAFI representing all of the projects in the Environment program. Staff of the Department of Primary Industries, Water and Environment (DPIWE: Wes Ford and Gwen Fenton), TAFI (Colin Buxton) and the Tasmanian Salmonid Growers Association (TSGA: Vicki Wadley and Dom O'Brien) were also in attendance for all or parts of the meeting.

The meeting provided the first opportunity for many of those involved to meet face-to-face and to learn in detail of the past, present and future aquaculture-related environmental research and monitoring associated with the tuna industry in South Australia and salmon industry in Tasmania. The initial morning session of the first day provided a brief outline of the Aquafin CRC Environment Program and the objectives of the meeting (John Volkman), an overview of the TAFI (Christine Crawford) and SARDI and Flinders University (Anthony Cheshire) projects, and the Tasmanian regulatory environment and its environmental R&D needs (Gwen Fenton). This was followed by talks from each of the projects. On the second morning, a workshop was held to discuss approaches to regional environmental assessment and adaptive management.

#### List of talks presented at the First Scientific Meeting of the Environment Program

#### Thursday, April 4<sup>th</sup> (CSIRO Marine Research Auditorium)

Time	Presenter	Title
<b>Setting the Scene</b>		
1000-1015	John Volkman	General overview of the Aquafin CRC and Environment program
1015-1025	Christine Crawford	Overview of finfish projects at TAFI
1025-1035	Anthony Cheshire	Overview of finfish projects at SARDI/Flinders University
1035-1055	Gwen Fenton	The regulatory environment in Tasmania
1055-1110		<i>Coffee Break</i>
<b>On-Farm Studies (Salmon)</b>		
1110-1120	Susie Forbes	Outline of the salmon fallowing project
1120-1135	Susie Forbes	Benthic fauna
1135-1155	Chris Burke/Andrew Bissett	Sediment microbiology
1155-1210	Andy Revill	Sediment geochemistry
1210-1220	Perran Cook	Sediment reactors
1220-1240	David Wildish	Towards a functional geochemical organic enrichment index
1240-1250		General discussion of projects
1250-1400		<i>Lunch</i>

### **On-Farm Studies (Tuna)**

1400-1420	Anthony Cheshire	Benthic fauna and sediment PCR
1420-1440	Ib Svane	Waste minimisation and characterisation
1440-1500	Stephen Madigan	Tuna environmental monitoring program (TEMP)

### **System Characterisation**

1500-1520	Christine Crawford	TAFI environmental monitoring projects
1520-1540	Peter Thompson	D'Entrecasteaux Channel monitoring
1540-1555		<i>Coffee Break</i>
1555-1615	John Parslow	System scale modelling
1615-1635	Mike Herzfeld	Physical modelling of Huon and D'Entrecasteaux

### **Processes Studies (Phytoplankton)**

1635-1655	Sue Blackburn	HES – Phytoplankton in the Huon
1655-1715	Peter Thompson/Paul Armstrong	Proposed studies on phytoplankton dynamics
1715-1730		General Discussion
1930-2200		<i>Dinner at Blue Skies restaurant</i>

---

## **Friday April 5<sup>th</sup> (Conference Rooms A and B)**

---

<b>Time</b>	<b>Presenter</b>	<b>Title</b>
0900-0930	Anthony Cheshire	RESA & risk assessment
0930-1000	Steve Madigan	System-wide ecological studies for tuna
1000-1030		Discussion
1030-1050		<i>Coffee Break</i>
1050-1120	Christine Crawford/Richard Mount	System-wide ecological studies for salmon
1120-1140	John Parslow	Adaptive management
1140-1220		General Discussion
1220-1230	John Volkman	Closing remarks – future directions

---

## Other Conference Presentations

- Armstrong, P., Bolch, C., Thompson, P. and Blackburn, S. (2003) *Understanding phytoplankton bloom in the Huon Estuary*. Second Annual Conference of the Aquafin CRC.
- Armstrong, P., Thompson, P. and Bolch, C. (2002). *Nutrient dynamics and phytoplankton blooms in the Huon Estuary*. First Aquafin CRC Conference, Hobart, September 24.
- Crawford, C., Foster, S., Jordan, A., Thompson, P., Bonham, P., Parslow, J., Herzfeld, M. and Volkman, J. (2002). *Progress towards the development of a monitoring program for broad-scale effects of salmon aquaculture*. First Aquafin CRC Conference, Hobart, September 24.
- Herzfeld, M. (2003). *Numerical modelling explained*. Second Annual Conference of the Aquafin CRC.
- Herzfeld, M., Parslow, J., Andrewartha, J. and Sakov, P. (2002). *Physical modelling of the Huon and D'Entrecasteaux Channel*. First Aquafin CRC Conference, Hobart, September 24.
- Parslow, J. (2003). *Adaptive management of coastal environments*. Second Annual conference of the Aquafin CRC.
- Parslow, J.P., Herzfeld, M., Andrewartha, J. and Sakov, P. (2003). *Environmental modelling to support salmon aquaculture in Huon-D'Entrecasteaux*. In Battaglene, S.C. and Cobcroft, J.M. (Eds). The Third Scientific Conference of the Atlantic Salmon Aquaculture Subprogram, May 21<sup>st</sup>, 2003, CSIRO Marine Research Marine Laboratories, Hobart.
- Revill, A.T., Cook, P. and Volkman, J. K. (2004) *Carbon flow between bacteria and micro-phytobenthos on a temperate mudflat – insights from bulk and compound-specific isotope analysis*. IsoEcol: Isotopes in Ecological Studies conference, Wellington, NZ.
- Revill, A.T., Cook, P. and Volkman, J. K. (2004) *Carbon flow interactions between bacteria and microphytobenthos on a temperate mudflat – insights from bulk and compound-specific isotope analysis*. Estuaries and Change Conference, Ballina, NSW.
- Thompson, P. and Bonham, P. (2003). *Contrasting phytoplankton ecology in adjacent coastal water bodies: Huon Estuary and D'Entrecasteaux Channel*. In Battaglene, S.C. and Cobcroft, J.M. (Eds). The Third Scientific Conference of the Atlantic Salmon Aquaculture Subprogram, May 21<sup>st</sup>, 2003, CSIRO Marine Research Marine Laboratories, Hobart.
- Thomson, D., Volkman, J., Burke, C. and Purser, J. (2003) *Sediment biogeochemistry – benthic-pelagic coupling of nutrients in the Huon estuary*. Second Annual Conference of the Aquafin CRC.
- Thomson, D., Volkman, J., Burke, C., and Purser, J. (2004). *Sedimentary biogeochemistry of the Huon estuary*. Estuaries and Change Conference, Ballina, NSW.
- Volkman, J.K. (2002) *Environmental research for Aquaculture ESD*. Sustainable Australian Aquaculture: Practical Solutions to Achieving ESD. Melbourne, July 14-18.
- Volkman, J.K. (2002) *Environmental research for the salmonid industry within the Aquafin CRC Environment Program*. The Second Scientific Conference of the Atlantic Salmon Aquaculture Subprogram, Hobart, July 8.

- Volkman, J.K. (2002) *Finfish aquaculture and the Australian environment*. Aquafest Conference, Hobart, Tasmania, September 19-22.
- Volkman, J.K. (2003). *The Aquafin CRC Environment program: highlights of salmon-related research*. In Battaglene, S.C. and Cobcroft, J.M. (Eds). The Third Scientific Conference of the Atlantic Salmon Aquaculture Subprogram, May 21<sup>st</sup>, 2003, CSIRO Marine Research Marine Laboratories, Hobart.
- Volkman, J.K., Parslow, J.P., Butler, E.C.V., Blackburn, S., and Reville, A.T. (2002) *Environmental issues for salmonid farming in southern Tasmania*. American Society of Limnology and Oceanography Summer Meeting “Interdisciplinary Linkages in Aquatic Sciences and Beyond”, Victoria, British Columbia, Canada. June 10-14.

### **Related Presentations**

- Volkman, J.K., Holdsworth, D.G., Reville, A.T., Macleod, C. and Forbes, S (2004). *The organic geochemistry of sediments under salmon sea cages*. Australian Organic Geochemistry Conference. Leura, NSW.
- Volkman, J.K., Holdsworth, D.G., Reville, A.T., Cook, P., Macleod, C. and Forbes, S (2004). *Organic matter degradation in sediments under salmon sea cages*. Estuaries and Change Conference, Ballina, NSW.

### **PhD Thesis**

- Armstrong, P.A. 2005. Physiology of phytoplankton in the Huon Estuary. PhD Thesis. University of Tasmania. In preparation.

### **Technical Reports**

See Appendix 4 for details.

## Appendix 4

### Associated technical reports enclosed on CD

Herzfeld, M., Parslow, J., Sakov, P. Andrewartha, J.R. (2005). Numerical hydrodynamic modelling of the D'Entrecasteaux Channel and Huon Estuary. Aquafin CRC Technical report.

Thompson P.A., Bonham, P. (2005). Effects of grazing by microzooplankton on phytoplankton in the Huon Estuary. Aquafin CRC Technical report

Thompson, P.A., Parslow, J.P. (2005). Measuring ecological health: A preliminary assessment of phytoplankton sampling strategies for the Huon Estuary and D'Entrecasteaux Channel including an initial comparison of the Huon interim monitoring (2001-2004) with HES (1996-1998) chlorophyll *a* data. Aquafin CRC Technical report

Thompson, P.A., Bonham, P., Willcox, S., Crawford, C. (2005). Baseline environmental data for the D'Entrecasteaux Channel. Aquafin CRC Technical report

Thomson, D., Volkman, J., Burke, C., Purser, J. (2005). Sediment biogeochemistry of the Huon Estuary. Status report for Aquafin CRC Project 4.2

Wild-Allen, K., Parslow, J., Herzfeld, M., Sakov, P., Andrewartha, J., Rosebrock, U. (2005). Biogeochemical Modelling of the D'Entrecasteaux Channel and Huon Estuary. Aquafin CRC Technical report

### Associated model animations enclosed on CD (as PowerPoint files).

Herzfeld et al. (Huon Estuary and D'Entrecasteaux Channel Hydrodynamic Model Results).

Hydrodynamic model outputs showing water movements in the Huon Estuary and D'Entrecasteaux Channel in 2002.

Wild-Allen et al. (Huon Estuary and D'Entrecasteaux Channel Biogeochemical Model Results)

Biogeochemical model outputs for the Huon Estuary and D'Entrecasteaux Channel in 2002.

# Technical Report

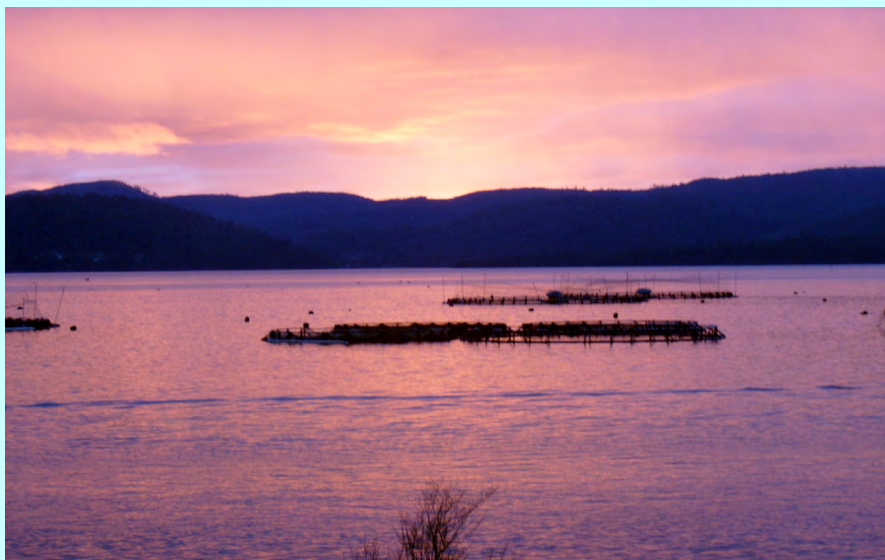


## Numerical Hydrodynamic Modelling of the D'Entrecasteaux Channel and Huon Estuary

Mike Herzfeld, John Parslow, Pavel Sakov and John Andrewartha  
CSIRO Marine and Atmospheric Research

*July 2005*

*Aquafin CRC Project 4.2  
(FRDC Project No. 2001/097)*



© Copyright Aquafin Cooperative Research Centre, Fisheries Research and Development Corporation,  
Commonwealth Scientific and Industrial Research Organisation

**This work is copyright. Except as permitted under the Copyright Act 1968 (Cth), no part of this publication may be reproduced by any process, electronic or otherwise, without the specific written permission of the copyright owners. Neither may information be stored electronically in any form whatsoever without such permission.**

**Every attempt has been made to provide accurate information in this document. However, no liability attaches to Aquafin CRC, its participant organisations or any other organisation or individual concerned with the supply of information or preparation of this document for any consequences of using the information contained in the document.**

*Published by CSIRO Marine and Atmospheric Research*



## Numerical Hydrodynamic Modelling of the D'Entrecasteaux Channel and Huon Estuary

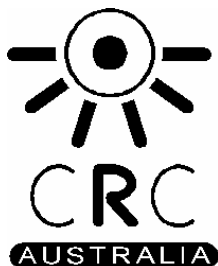
Mike Herzfeld, John Parslow, Pavel Sakov and John Andrewartha  
CSIRO Marine and Atmospheric Research

*July 2005*

*Aquafin CRC Project 4.2  
(FRDC Project No. 2001/097)*



**Australian Government**  
**Fisheries Research and  
Development Corporation**



## Contents

<b>1 Introduction.</b>	<b>5</b>
<b>2 The Hydrodynamic Model.</b>	<b>6</b>
<b>3 Model Domain.</b>	<b>8</b>
<b>4 Field Measurements</b>	<b>9</b>
<b>5 Input Data.</b>	<b>15</b>
<b>5.1 Wind Forcing.</b>	<b>15</b>
<b>5.2 Surface Elevation.</b>	<b>17</b>
<b>5.3 Temperature and Salinity.</b>	<b>19</b>
<b>5.4 River Flow.</b>	<b>21</b>
5.4.1 Huon River Flow	21
5.4.2 Derwent River Flow	21
<b>6 Modelling Strategy.</b>	<b>22</b>
<b>6.1 Local Domain Grid</b>	<b>22</b>
<b>6.2 Thermodynamic Effects</b>	<b>24</b>
<b>6.3 Nesting Procedure</b>	<b>30</b>
<b>7 Model Output.</b>	<b>34</b>
<b>7.1 Model Calibration</b>	<b>34</b>
<b>7.2 Sensitivity</b>	<b>367</b>
<b>7.3 General Model Solutions</b>	<b>41</b>
<b>7.4 Momentum Balance</b>	<b>44</b>
<b>7.5 Flushing Times</b>	<b>578</b>
<b>7.6 Residual Flow</b>	<b>76</b>
<b>7.7 Point Source Releases</b>	<b>80</b>
<b>7.8 Particle Tracking</b>	<b>88</b>
<b>7.9 Coarse Model</b>	<b>96</b>
<b>8. Conclusions</b>	<b>978</b>
<b>9. References</b>	<b>100</b>

## 1 Introduction

The D'Entrecasteaux Channel comprises the water body between the Tasmanian mainland and Bruny Island. The Huon Estuary joins the D'Entrecasteaux Channel near the southern limit of the channel, having fresh water input from the Huon River some 60 km upstream from the mouth of the estuary (Fig. 1). The Huon River is a significant source of fresh water where it enters the head of the Huon Estuary at Huonville. Saline water enters the Channel from the open ocean and propagates up the estuary as a salt wedge creating a classic salt wedge type estuary. These estuaries are characterised by high stratification and a stable water column; the water column only becoming well mixed during times of high flow when the salt wedge is pushed back downstream. The Huon/D'Entrecasteaux region is also characterised by complex geography, making modelling of the region challenging.

The Huon Estuary and D'Entrecasteaux Channel support a growing salmon aquaculture industry. Over the last decade there have been significant increases in aquaculture activity in the Estuary and Channel, raising concerns about the impact of these activities on the health of the ecosystem and ultimately the ecological sustainability of the industry. Specifically, information is needed regarding the number of farm sites that the estuary and channel can accommodate. The potential impact on the ecosystem is primarily that of eutrophication and low oxygen concentrations (which may ultimately lead to anoxia). Nutrients from fish farming enter the environment through direct release from the fish or degradation of detritus and uneaten feed pellets on the sea floor directly below aquaculture cages.

At the start of our project there was uncertainty as to whether the cumulative effect of nutrient sources due to aquaculture cages has an impact on the ecosystem overall. Furthermore, the stable water column, or relative lack of mixing, in the upper estuary means that bottom waters have no contact with overlying water and hence may become anoxic. This may have implications on nutrient release from the sediment and thus the nutrient cycling in the whole system. The presence of additional nutrient sources in bottom waters may complicate nutrient cycling in these regions.

In order to project trends in ecosystem health a series of numerical models were implemented to provide predictive capacity. These consisted of a hydrodynamic model to predict water transports, mixing regimes and temperature/salinity distributions and a biogeochemical model to predict primary productivity and nutrient cycling. This chapter outlines the development of the hydrodynamic model.

Long period simulations are required (>1 year) to assess the impact of aquaculture on the aquatic environment, and these simulations required acceptable run time ratios of greater than 100:1 (i.e. 100 model days in 1 day real time). The model was forced with river flow from various sources (the largest being the head of the Huon Estuary) wind stress and surface elevations, temperature & salinity on the northern and southern limits of the channel. These northern and southern boundary conditions were derived from a larger scale model of the region. The hydrodynamic model is introduced in 2 and the model grid

used described in 3. Data collected for calibration purposes is presented in 4 followed by presentation of data used to force the model in 5. Finally the modeling approach is described in 6, followed by presentation and analysis of model output in 7.

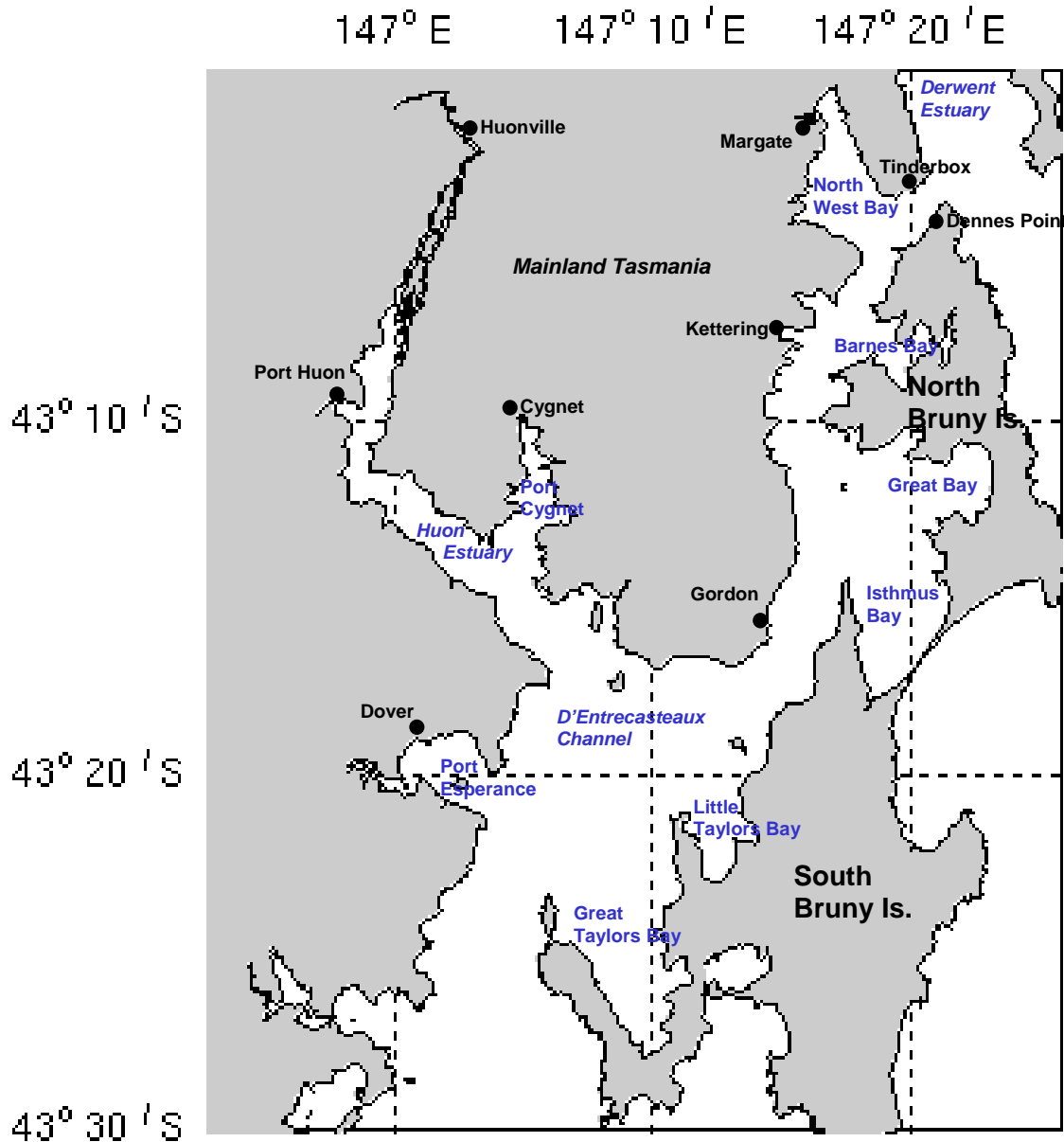


**Fig. 1. Geography of the D'Entrecasteaux Channel / Huon Estuary Region**

## **2 The Hydrodynamic Model**

We used the MECO (Model for Estuaries and Coastal Ocean; Walker and Waring, 1998) hydrodynamic model to simulate the physics of the D'Entrecasteaux Channel and Huon Estuary. This model was developed by the Environmental Modelling group at CSIRO

Marine Research over the last decade. MECO is intended to be a general purpose model applicable to scales ranging from estuaries to regional ocean domains, and has been successfully applied to a variety of applications encompassing these scales to date. MECO is a three-dimensional finite difference hydrodynamic model based on the primitive equations. Outputs from the model include three-dimensional distributions of velocity, temperature, salinity, density, passive tracers, mixing coefficients and sea level. Inputs required by the model include forcing due to wind, atmospheric pressure gradients, surface heat and water fluxes and open boundary conditions (e.g. tides). MECO is based on the three dimensional equations of momentum, continuity and conservation of heat and salt, employing the hydrostatic and Boussinesq assumptions. The equations of motion are discretised on a finite difference stencil corresponding to the Arakawa C grid.

The model uses a curvilinear orthogonal grid in the horizontal and a choice of fixed 'z' coordinates or terrain-following  $\sigma$  coordinates in the vertical. The curvilinear horizontal grid was particularly useful in this application since it enabled high resolution to be specified in areas of the study region where small scale motions were present and larger resolution where they were not. The 'z' vertical system allows for wetting and drying of surface cells, which is useful for resolving the surface layer in the presence of moderate tides. MECO has a free surface and uses mode splitting to separate the two dimensional (2D) mode from the three dimensional (3D) mode. This allows fast moving gravity waves to be solved independently from the slower moving internal waves allowing the 2D and 3D modes to operate on different time-steps, resulting in a considerable contribution to computational efficiency. Computation efficiency was an important issue in this study into which considerable effort was devoted, since long period simulations were to be attempted (greater than one year). The model uses explicit time-stepping throughout except for the vertical diffusion scheme which is implicit. This implicit scheme guarantees unconditional stability in regions of high vertical resolution. A Laplacian diffusion scheme is employed in the horizontal on geopotential surfaces. Smagorinsky mixing coefficients may be utilised in the horizontal.

MECO can invoke several turbulence closure schemes, including k- $\epsilon$ , Mellor-Yamada 2.0 and Csanady type parameterisations. A variety of advection schemes may be used on tracers and 1<sup>st</sup> or 2<sup>nd</sup> order can be used for momentum. This study used the QUICKEST advection scheme for tracers (Leonard, 1979) in conjunction with the ULTIMATE limiter (Leonard, 1991). This scheme is characterised by very low numerical diffusion and dispersion, and yielded excellent performance when resolving frontal features, which often occurred in the salinity distribution during times of high flow of the Huon River. MECO also contains a suite of radiation, extrapolation, sponge and direct data forcing open boundary conditions. Input and output is handled through netCDF data formatted files, with the option of submitting ascii text files for simple time-series forcing. The netCDF format allows input of spatially and temporally varying forcing and initialization data in a grid and time-step independent manner. MECO is capable of performing particle tracking and may be directly coupled to ecological and sediment transport models.

### 3 Model Domain

A common problem encountered when modelling water bodies is the accurate prescription of data along any open boundaries. Open boundaries are the limits of the domain beyond which no information is available for the model, and hence for which data must be explicitly supplied. In the absence of field-derived temperature, salinity and surface elevation measurements to apply to the open boundaries, a common solution to this problem is the practice of successive nesting, where small scale models are nested within larger scale models until the region of interest can be adequately resolved. The simulation of the physics of the D'Entrecasteaux Channel and Huon Estuary required the construction of three nested model grids. A large scale regional grid was made which acted to supply the initial and open boundary conditions for an intermediate scale grid, which in turn supplied boundary forcing for the local grid of the study region. The regional domain is illustrated in Fig. 2 and the nested domain in Fig. 3. The nesting procedure is discussed in more detail in 6.3.

Note that the bathymetries are included in these Figures, which show that the channel domain is relatively shallow, with maximum depths less than 60 m. The Huon Estuary is generally less than half this depth, with a narrow channel creating a connection between the estuary mouth and the main body of the channel. Also, the regional domain includes three open boundaries; two cross-shore and one offshore beyond the shelf break. The channel domain only uses two open boundaries at the northern and southern limits of Bruny Island.

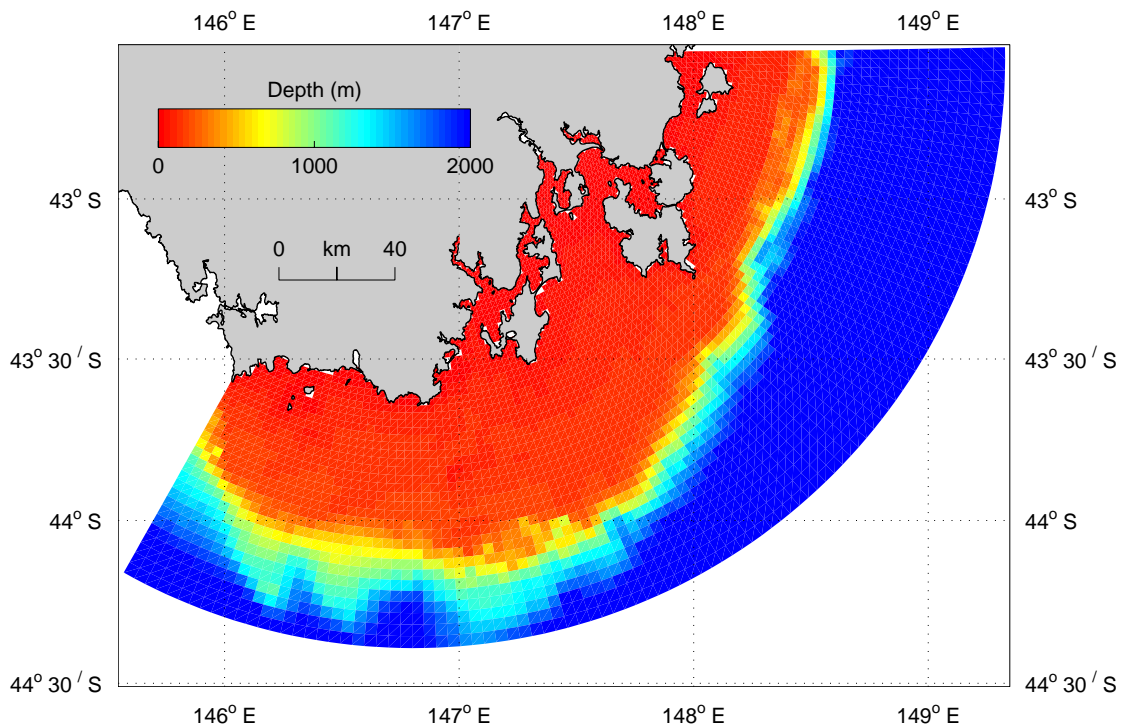


**Fig. 2. Regional Model Domain**

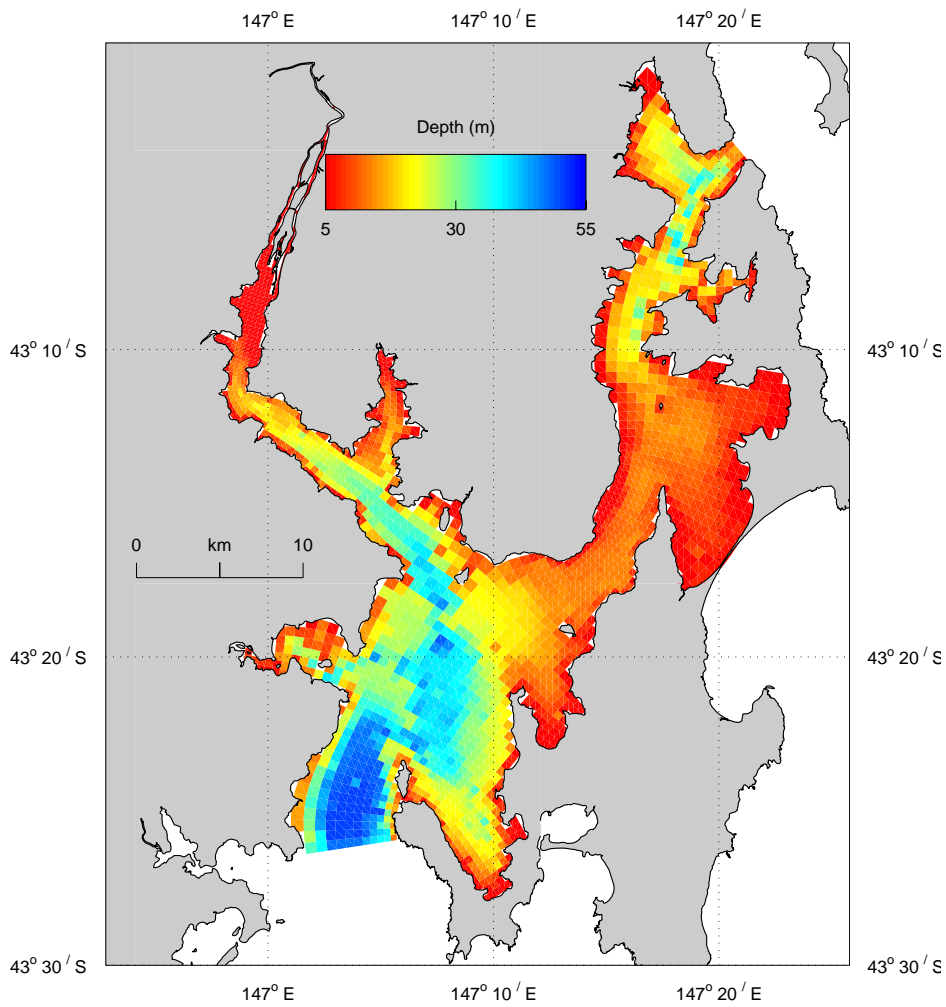


**Fig. 3. The Huon/D'Entrecasteaux Domain**

## 4 Field Measurements

Included in the Environment Program of the Aquafin CRC was a Broad-Scale Monitoring Program. This program collected temperature, salinity, nutrients and phytoplankton samples on a monthly basis from throughout 2002 along a transect down the D'Entrecasteaux Channel and at specific sites in the side bays. Numbered CTD sampling sites in the D'Entrecasteaux Channel relevant to this study are depicted in Fig. 4. Temperature and salinity sections interpolated from data collected at these sites are displayed in Figs 5 to 13. Both the downcast and upcast of the CTD cast were measured, but only the downcast is displayed since it is more reliable due to the steady sinking rate and undisturbed surrounding water.

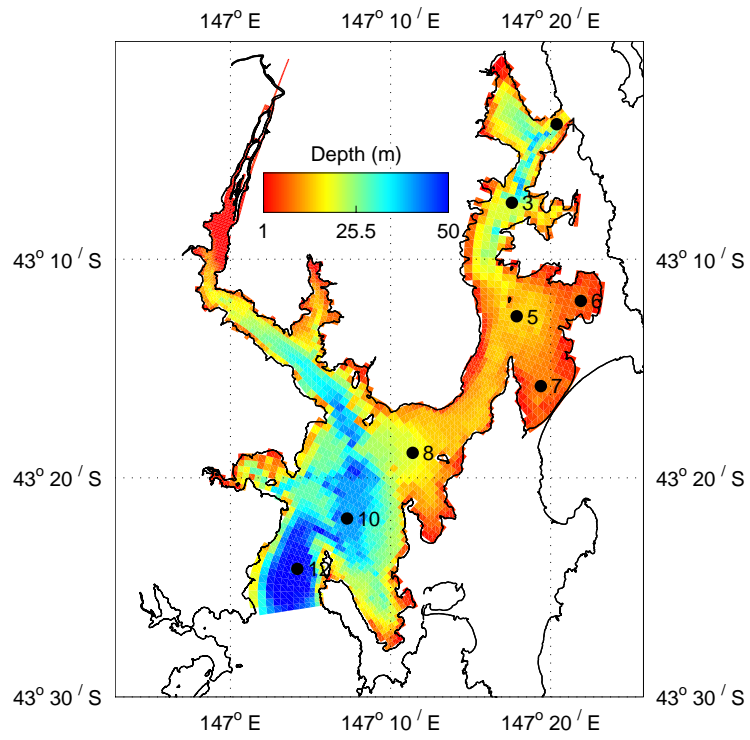


**Fig. 4. D'Entrecasteaux Channel station locations.**

**Fig. 2.5: OBSERVED (downcast) 10 Jan 2002**

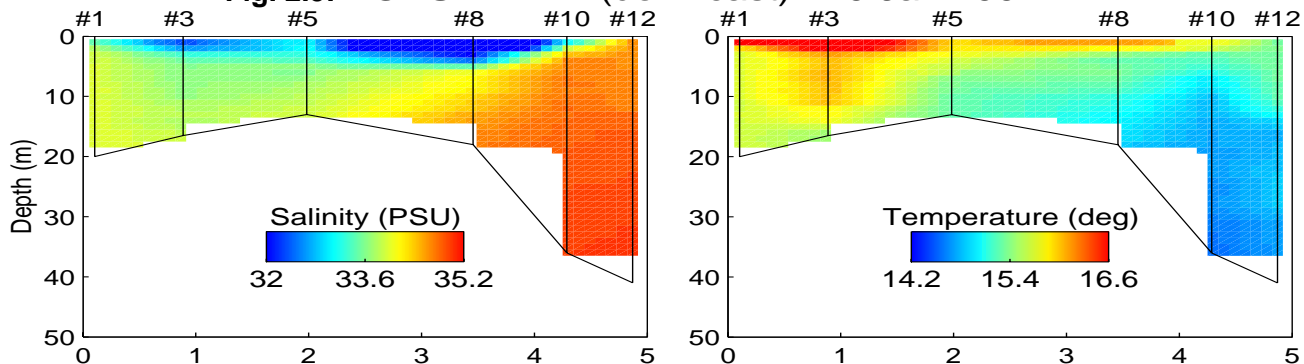


**Fig. 4.6: OBSERVED (downcast) 06 Feb 2002**

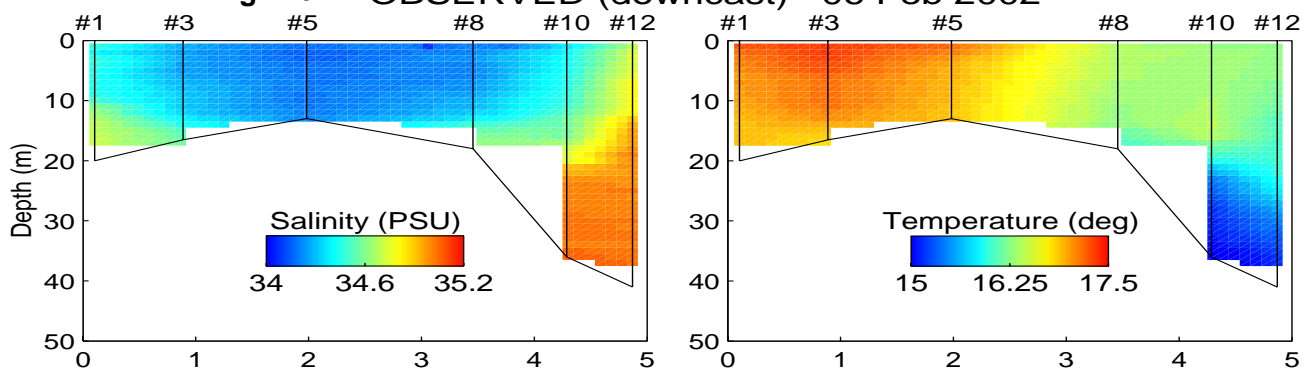


**Fig. 2.7: OBSERVED (downcast) 04 Mar 2002**

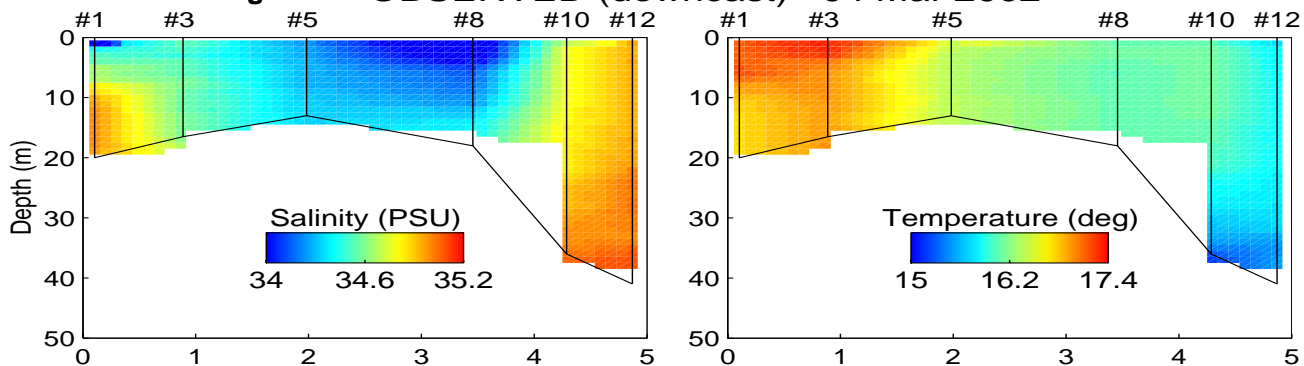


**Fig. 2.8: OBSERVED (downcast) 05 Apr 2002**

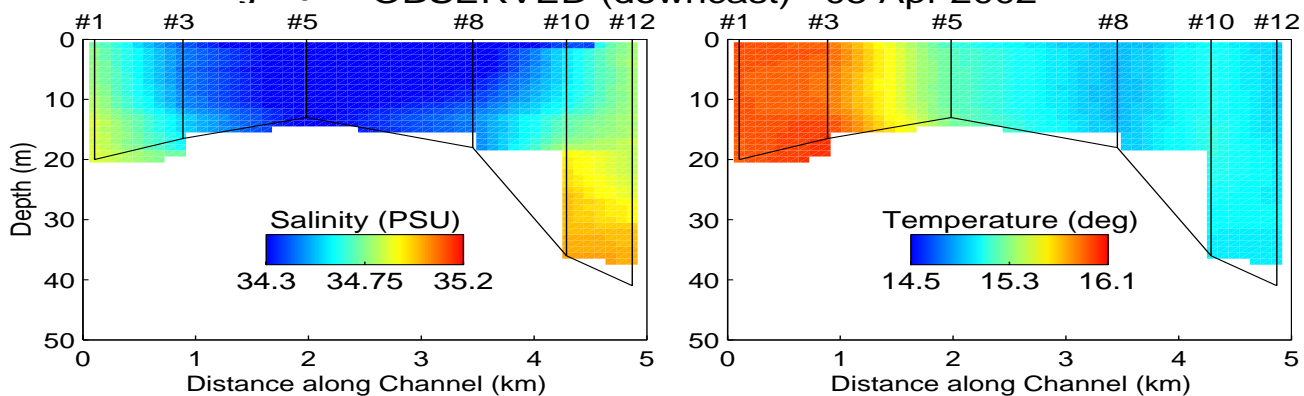


**Fig. 2.9: OBSERVED (downcast) 29 Apr 2002**

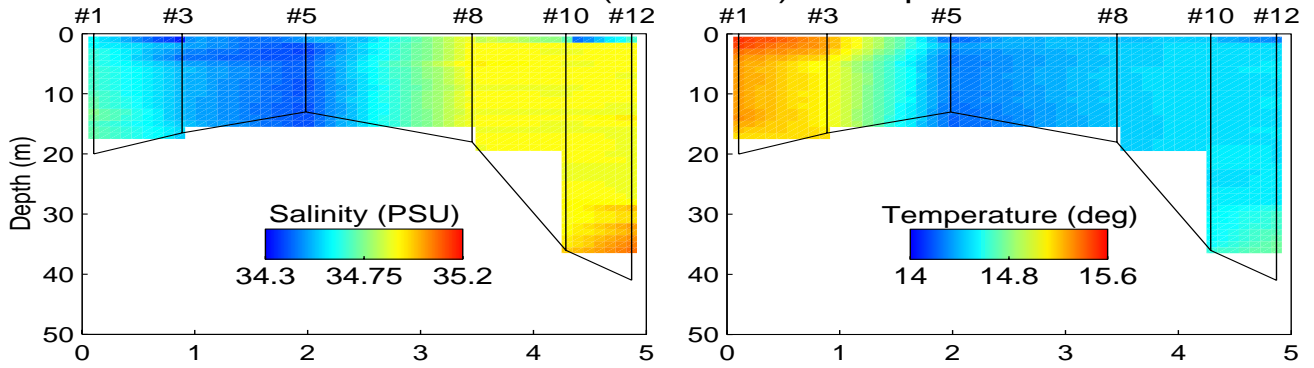


**Fig. 2.10: OBSERVED (downcast) 03 Jun 2002**

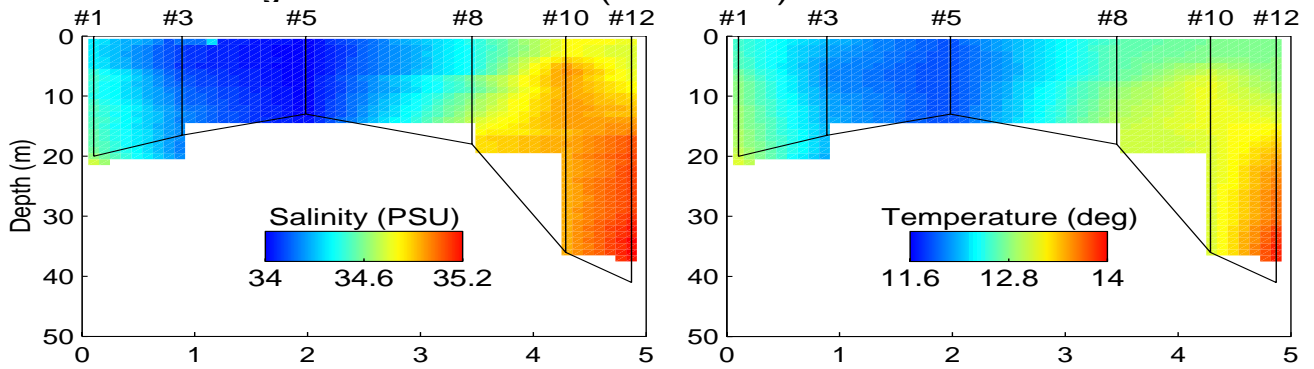


**Fig. 2.11: OBSERVED (downcast) 03 Jul 2002**

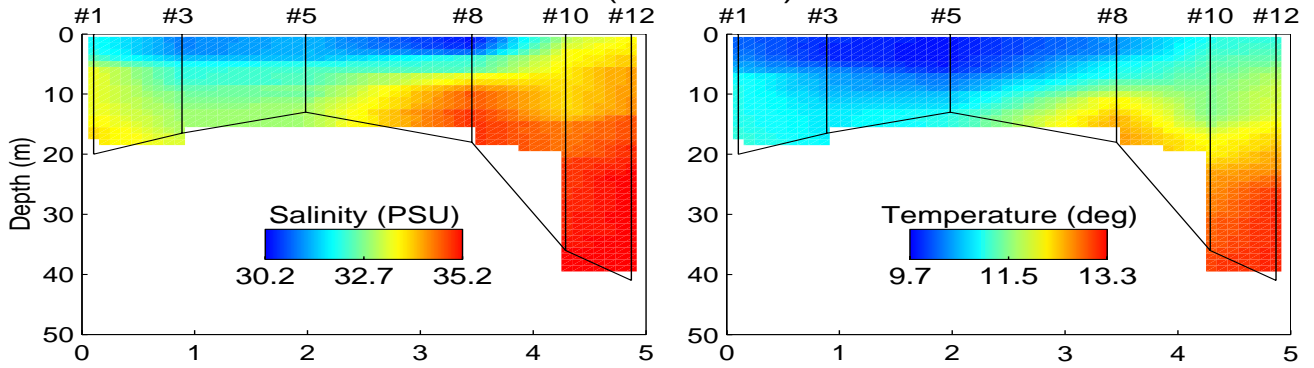


**Fig. 2.12: OBSERVED (downcast) 05 Aug 2002**

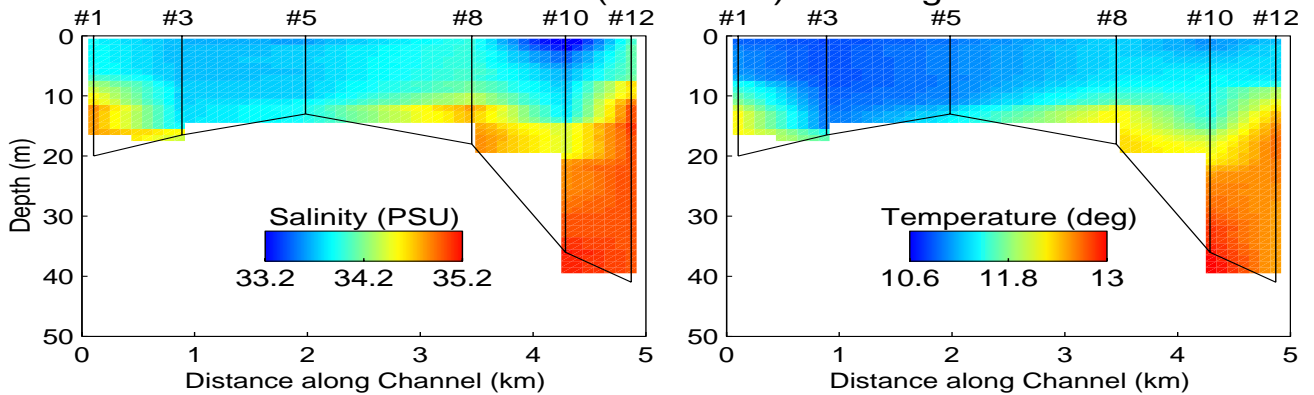


**Fig. 2.13: OBSERVED (downcast) 02 Sep 2002**

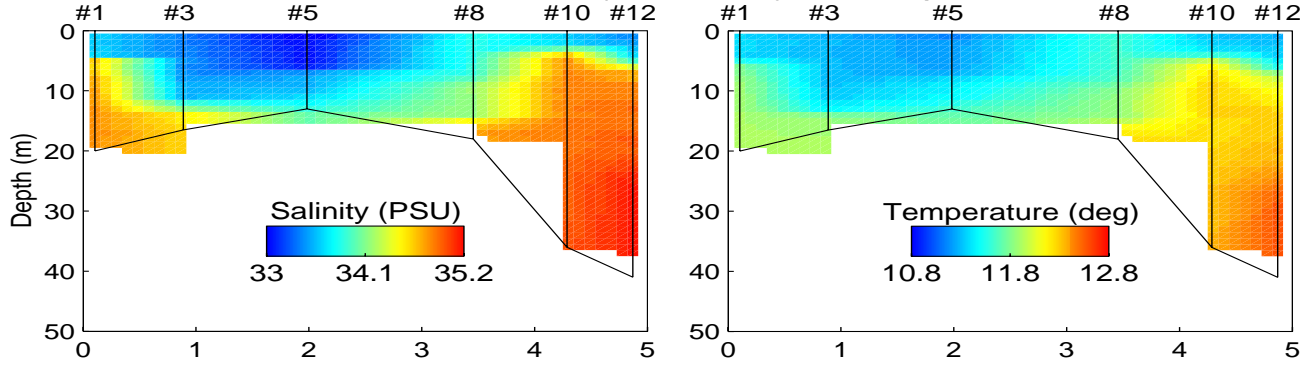


**Fig. 2.14: OBSERVED (downcast) 30 Sep 2002**

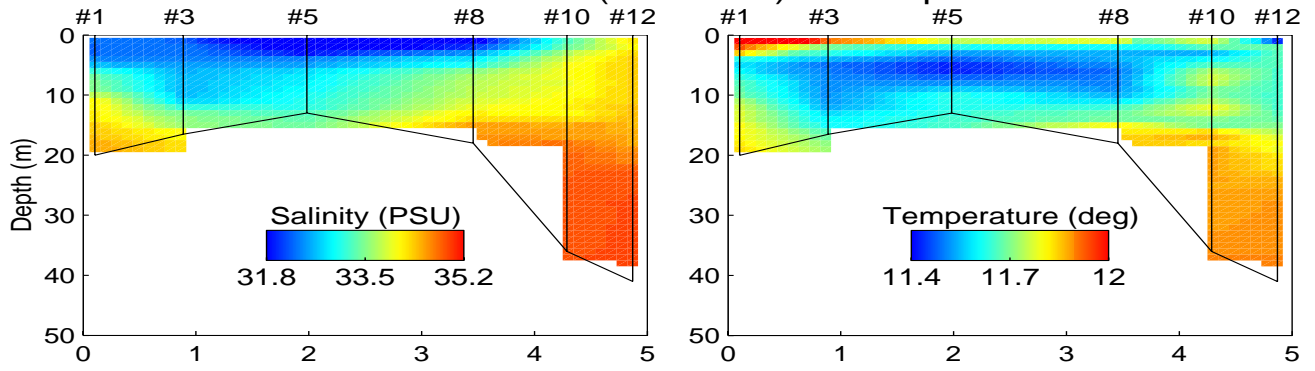


**Fig. 2.15: OBSERVED (downcast) 04 Nov 2002**

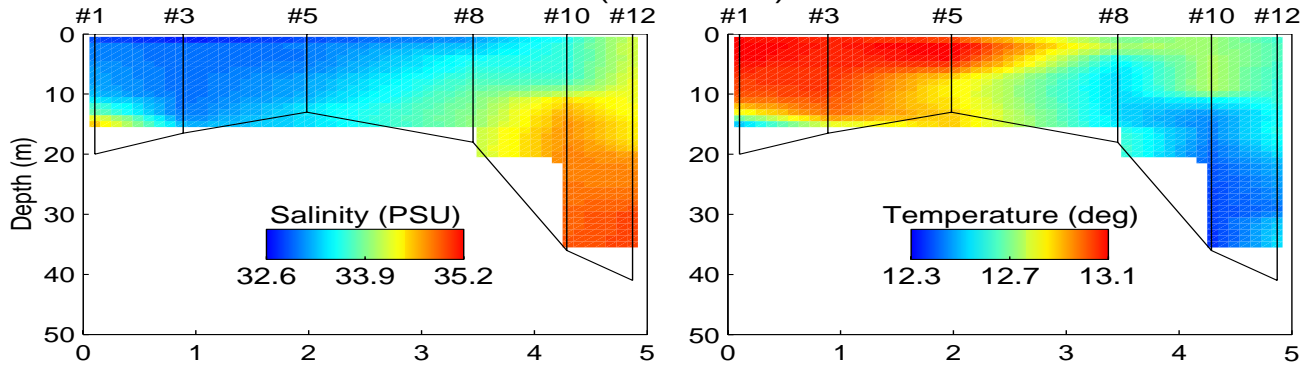
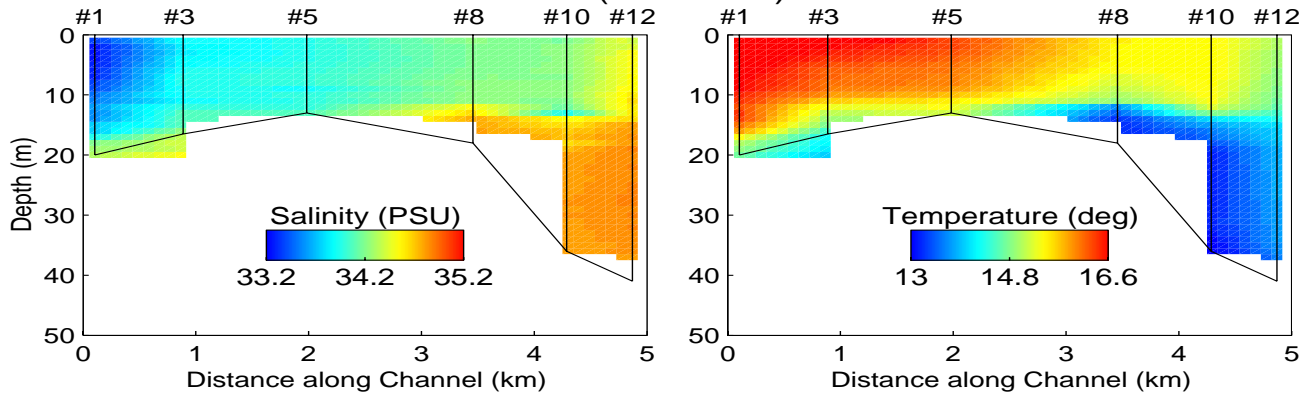


**Fig. 2.16: OBSERVED (downcast) 02 Dec 2002**



These data show that a gradient in temperature (up to 1°C) exists down the D'Entrecasteaux Channel during summer and autumn, with the northern end associated with higher temperature. The deeper waters at the southern end have the lowest temperature in the channel, presumably due to the sub-thermocline oceanic influence. Towards autumn this vertical gradient at the southern end is less pronounced as surface cooling decreases surface temperature heading into winter. In winter bottom waters become warmer than surface waters, but still several degrees cooler than the summer bottom temperature. This bottom temperature increase in winter is also observed at the northern end of the channel. On 10 January 2001, a warm surface layer was particularly pronounced and shallow, and is associated with a thin layer of fresher water attributed to the influence of Huon River outflow. The flow data indicates that a large flow of 883 m<sup>3</sup>s<sup>-1</sup> occurred on 8 Jan 2001, thus the measurements taken on 10 Jan 2001 certainly captures this event. Generally, salinity is lower in the mid-channel region and attains the highest values in bottom waters at the ends of the channel throughout the year, thus density compensating the temperature distribution. Thin fresh water layers can also be observed mid-channel during times of high Huon River flow.

Additional data was collected in the North West Bay region independently by TAFI (Tasmanian Aquaculture and Fisheries Institute). These data consisted of CTD and nutrient samples collected at specific sites and ADCP data from specific sites (courtesy of Dr Alan Jordan, TAFI) and covered the period Nov 2001 to Feb 2002. The North West Bay sampling are displayed in Fig. 17.

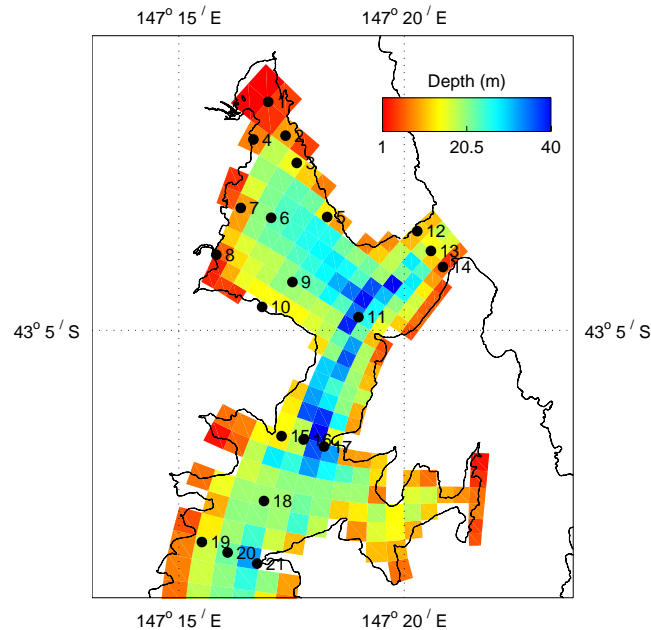


**Fig. 17. North West Bay Sites as sampled by TAFI**

The temperature and salinity data collected from field programs can be used for both model initialisation and forcing through the open boundaries as well as model calibration.

Additionally, these data provide useful insight into the thermodynamics and exchange processes occurring in the Huon / D'Entrecasteaux, which are discussed in Section 6.

## 5 Input Data

The model was forced with wind, river flow from the Huon River and elevation, temperature and salinity at the two oceanic open boundaries. The sources of these forcings are detailed below.

### 5.1 Wind Forcing

Wind speed and direction data were obtained from the Bureau of Meteorology (BOM, except for \* = CSIRO) at the following locations and interpolated onto the regional and D'Entrecasteaux / Huon domains to provide a temporally and spatially varying wind-field. Wind measurement sites are summarised in Table 1 and Fig. 18.

**Table 1. Wind Measurement Sites**

Site	Latitude (deg S)	Longitude (deg E)
Hobart Airport	42.8389	147.4992
Palmer's Lookout	43.1650	147.8317
Cape Bruny	43.4903	147.1447
Maatsuyker Island	43.6578	146.2711
Droughty Hill*	42.9256	147.4206

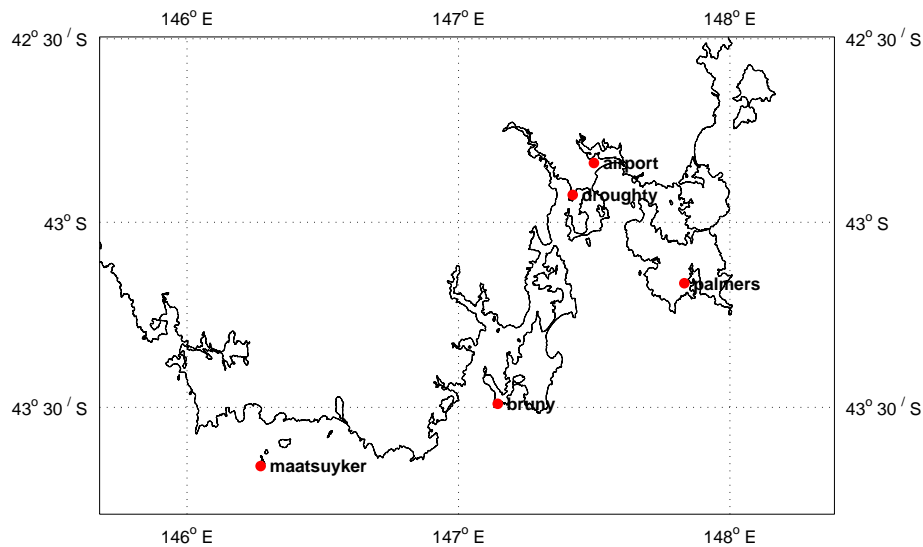


**Fig. 18. Wind measurement sites**

A sample of the wind-field at these sites is shown in Fig. 19 (a) and (b) for the year 2002. The mean for this period is a southerly with speed of  $4.3 \text{ ms}^{-1}$ .

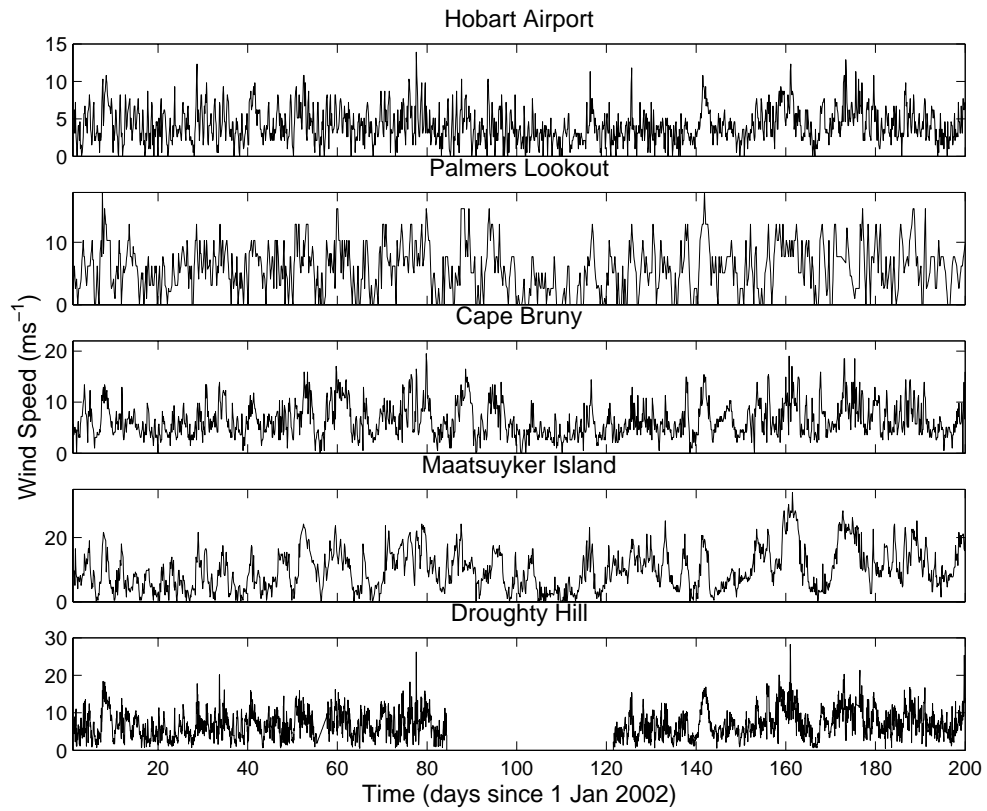


**Fig. 19 (a). Wind Speed at Measurement Sites**

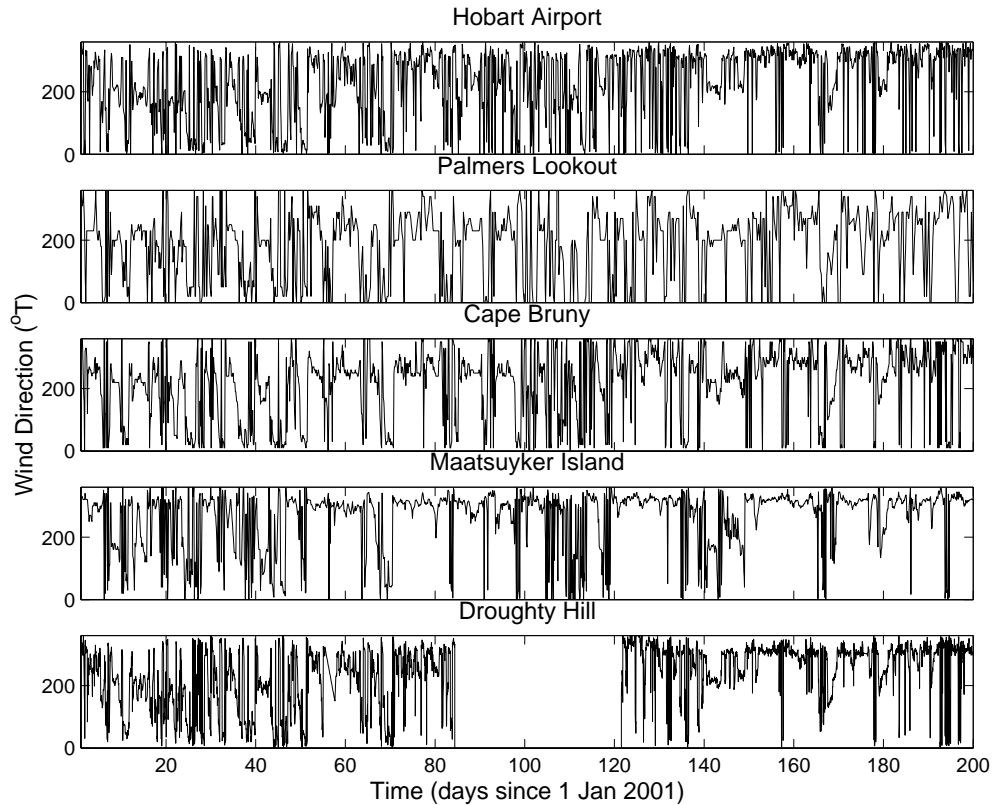


**Fig. 19 (b): Wind Direction at Measurement Sites**

## 5.2 Surface Elevation

The surface elevation for the Huon/D'Entrecasteaux domain was supplied from output of the regional model. The elevations used in the region model consist of a high frequency component (tidal component with frequencies  $< 1$  day) and a long period component with frequencies of days to weeks. The tidal component applicable to the regional domain was constructed from a global tidal model (Cartwright and Ray, 1990). This global model did not perform well in the vicinity of the north-eastern cross-shelf boundary, so a yet larger domain was created to encompass the regional grid upon which the model was run in barotropic (2-D) mode only to yield time series of surface elevation on this boundary. These time series were then decomposed into the tidal constituents, which were subsequently used to force the tidal component in the regional model. This approach provided better results than directly imposing the global tidal model constituents on the north-eastern boundary. The tidal constituents are presented in Table 5.2 with the ranges of amplitude encountered. Note that these constituent's amplitude and phase vary spatially around the open boundary perimeter.

The long period component was extracted from low passed elevation records collected at Port Arthur on the Tasman Peninsula (courtesy of Dr John Hunter, University of

Tasmania) and Spring Bay on the east coast (from National Tidal Facility). The Port Arthur signal was lead by 0.5 days and applied at the western open boundary of the regional model with no change in amplitude. The Spring Bay long period component was applied directly to north-eastern boundary. These long period components are applicable to the coast only, and an offshore profile was imposed on the amplitude to correctly specify the long period wave over the shelf. The resulting modelled surface elevations were compared to those measured at Hobart to validate the forcing, as illustrated in Fig. 20.

**Table 2. Tidal Harmonics for the Regional Model**

Name	Western Boundary Amplitude (m)	Offshore Boundary Amplitude (m)	NE Boundary Amplitude (m)
Q1	0.028 - 0.029	0.022 – 0.028	0.022
O1	0.119 - 0.125	0.099 – 0.119	0.099 - .113
P1	0.054 - 0.058	0.049 – 0.054	0.049 – 0.058
S1	0.001	0.001	0.001 – 0.002
K1	0.165 - 0.176	0.150 – 0.165	0.151 – 0.172
2N2	0.008 - 0.010	0.008 - 0.014	0.014
MU2	0.009 - 0.011	0.009 - 0.016	0.017
N2	0.031 - 0.034	0.031 - 0.083	0.085
NU2	0.005 - 0.006	0.005 - 0.015	0.016
M2	0.119 - 0.120	0.119 - 0.325	0.330 – 0.332
L2	0.003 - 0.004	0.003 - 0.006	0.006
T2	0.004 - 0.005	0.003 – 0.004	0.002 – 0.003
S2	0.074 - 0.087	0.038 – 0.074	0.035 – 0.039
K2	0.022 - 0.026	0.008 – 0.022	0.008

The elevations provided by the regional model were then used in the higher resolution nested grids. Obviously these elevation signals contained both the diurnal and long period fluctuations.

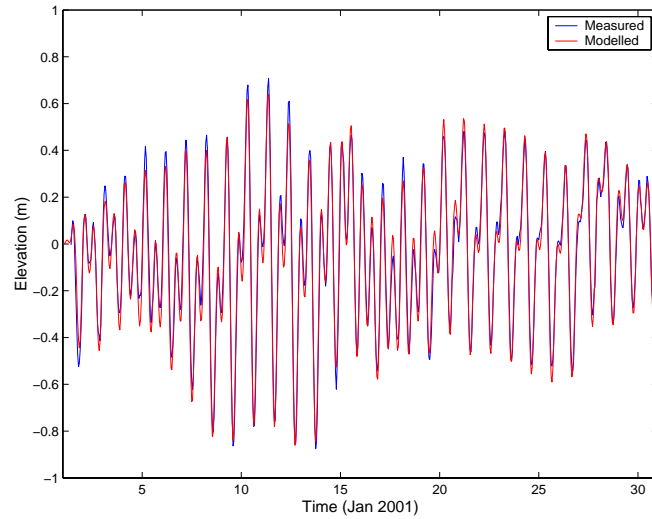


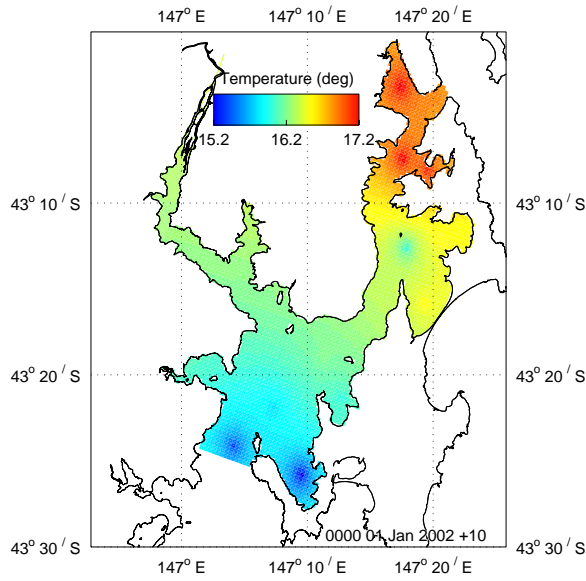
**Fig. 20. Segment of Surface Elevation at Hobart.**

### 5.3 Temperature and Salinity

The temperature and salinity distribution in the regional model was initialised with annual mean distributions provided by the CARS atlas (Climatological Atlas of Regional Seas, Ridgway et al 2002). These data provide a mean annual cycle of temperature and salinity output at 10 day intervals on a 1/8 degree grid. The open boundaries of the regional domain were also forced with the CARS climatology. The CARS data did not perform well in the inshore regions, presumably due to lack of data in the assimilation procedure. Temperature was too low in these regions, and salinity was typically too high. The lack of data in the compilation of CARS in the inshore region probably omitted signatures of important sources of heat (e.g. local atmospheric heat fluxes) and fresh water (river flows) which contributed to these inconsistencies. For this reason it was decided not to use output from the regional model to initialise and force the local Huon / D'Entrecasteaux domain on the open boundaries.

Although the data collected from the broad-scale field program is temporally and spatially coarse, these data could be interpolated onto the grid to provide initial conditions and interpolated temporally to provide open boundary conditions that were better than output from the regional model. The temperature and salinity distribution in the local domain on 10 January 2002 as derived from the field program and output from the regional model are presented in Figs 21 and 22. The regional model is relaxed to CARS on a time scale of 10 days so as to provide a pseudo seasonal forcing. It can be seen that the regional model is significantly cooler and saltier than the field derived measurements. Again, there exist no local heat and salt sources in the CARS relaxed solutions, leading to these inaccuracies

(a) Field Interpolation (°C)



(b) Regional Model with Relaxation to CARS

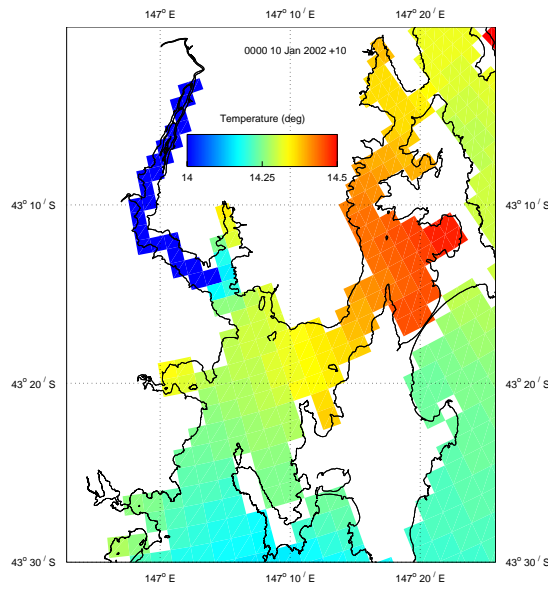
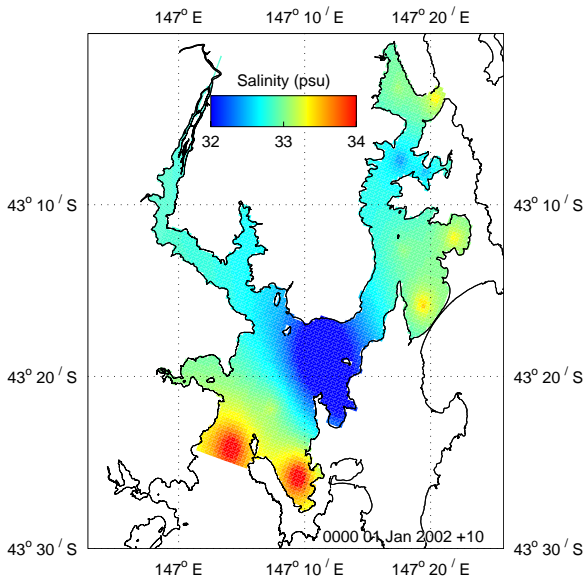


**Fig. 21. Temperature Distribution at 10 Jan 2002**

(a) Field Interpolation (°C)



(b) Regional Model with Relaxation to CARS

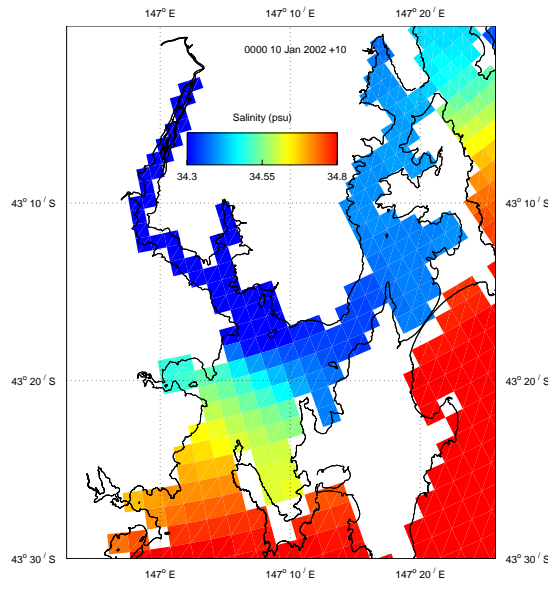


**Fig. 22. Salinity Distribution at 10 Jan 2002**

## 5.4 River Flow

### 5.4.1 Huon River Flow

Flow from the Huon River was input directly into the model as an open boundary condition. River flow records were obtained at Frying Pan Creek, upstream from the riverine input open boundary in the Huon/D'Entrecasteaux domain (courtesy of DPIWE). This flow record was multiplied by a scaling factor of 1.2 to allow for catchment area contributing to flow below Frying Pan Creek, resulting in flow applicable to Huonville. Time series of this flow is presented in Fig. 23, from which it is observed that several large flood events occurred in 2002, primarily in the winter and spring months. The largest flow of close to 1000 cumecs occurred on 13 Aug. The salinity of the Huon inflow is assumed to be fresh (i.e. 0 psu) and the temperature was obtained from measurement (DPIWE). River temperature is illustrated in Fig. 23.

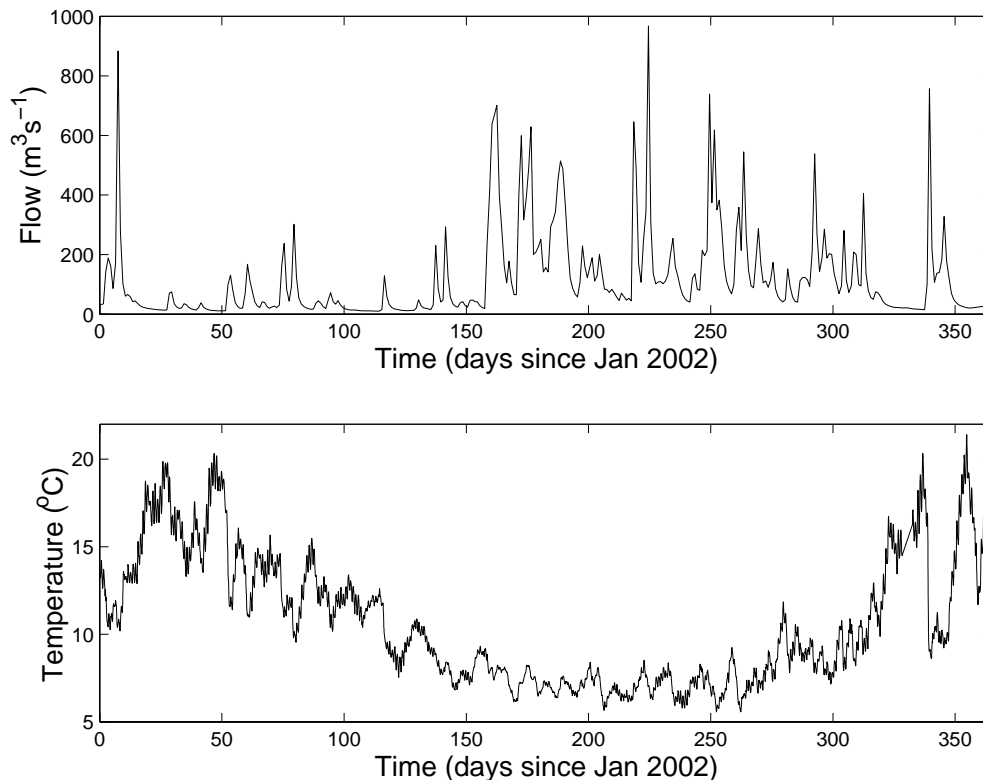


**Fig. 23. River Characteristics at Huonville**

### 5.4.2 Derwent River Flow

Derwent River flow was input as boundary conditions to the larger scale models within which the local domain was nested. Daily flow was obtained from the Tasmanian Hydro below Meadowbank and hourly data from DPIWE of the Tyenna flow. These flows were combined and used as the river flow at New Norfolk. River temperature was unavailable and the low passed air temperature at Hobart airport was assumed to be representative of

the river temperature at New Norfolk. River flow and temperature are displayed in Fig. 24.

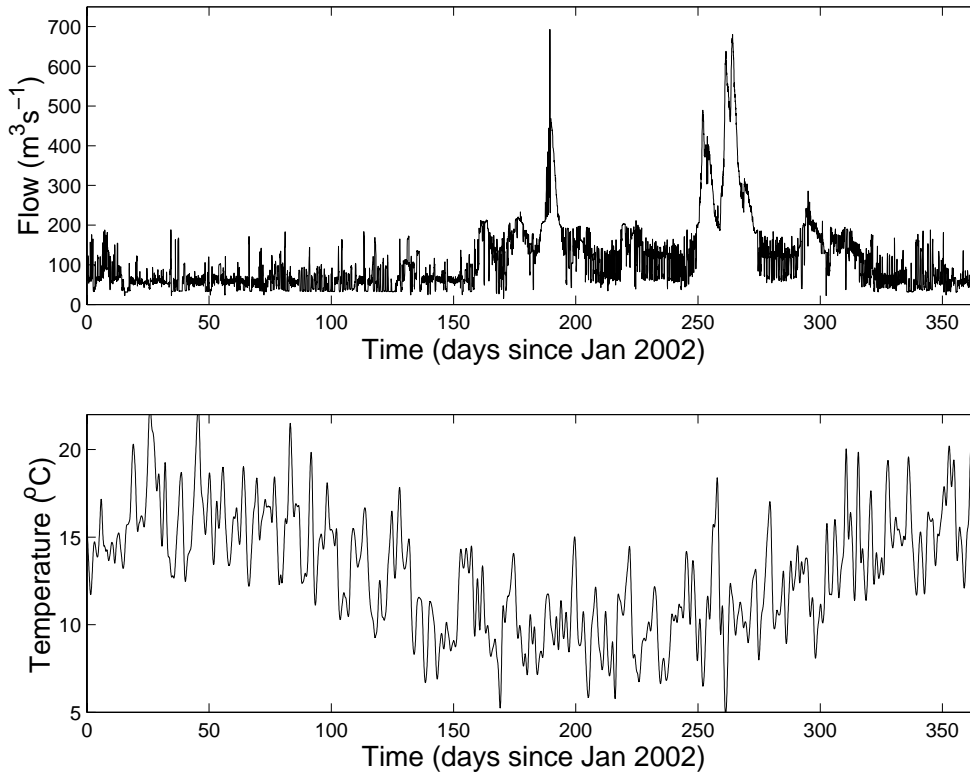


**Fig. 24. River Characteristics at New Norfolk**

## 6 Modelling Strategy

The objective of running the hydrodynamic model is to provide insight into the physics governing the Huon Estuary/D'Entrecasteaux Channel system and provide transports and the mixing regime for the biogeochemical model. Output is generated for the period Jan 2002 to Aug 2002 using the forcing data described in Section 5, which may then be calibrated and validated against data collected during the field programs from Dec 2001 to May 2002.

### 6.1 Local Domain Grid

A common challenge faced in developing a hydrodynamic grid is to maintain sufficient spatial resolution in the domain without sacrificing accuracy by under-resolving certain scales of motion. Basically, the greater the resolution the longer the model takes to execute, which often places prohibitive restrictions on the length of a simulation. The objective is to create a model that executes at a run-time ratio of at least 100:1 (i.e. 100 model days for each day of real time) allowing one year of simulation in under 4 days real time. There exists stability criterion the model is subject to which place restrictions on the time-stepping used, e.g. basically any wave or current in the model cannot traverse more than one grid cell in one time-step. Among other things this is dependent on the

water depth, degree of stratification and the grid cell size. Obviously it is only the latter that control may be exerted over when building a grid, and an iterative process is usually employed to obtain an optimum grid that balances resolution with computational pressures.

This iterative process involves performing simulations on a given grid with a conservative time-step. The theoretical upper limit for the time-step is then computed at every grid node and at every time-step, allowing the minimum over the simulation to be obtained and areas in the grid susceptible to restrictive time-steps identified. The resolution in these areas could then be increased, and the process repeated. The optimized grid resulting from this process is displayed in Fig. 25.

The grid resolution in this domain ranged from a minimum of 150 m in the Huon Estuary to a maximum of 700 m near the southern boundary. The model uses 26 layers in the vertical. There exist 13000 surface cells total in this grid, only 1800 (13%) of which are wet; i.e. the majority of this grid is associated with dry land which can also lead to computational inefficiencies. Using this grid, time steps of 60 and 5 seconds were used for the 3D and 2D components of the model respectively, yielding a run time ratio of greater than 100:1 which allowed long term simulations to be performed (e.g. 1 year simulations in approximately 3 days real time) .

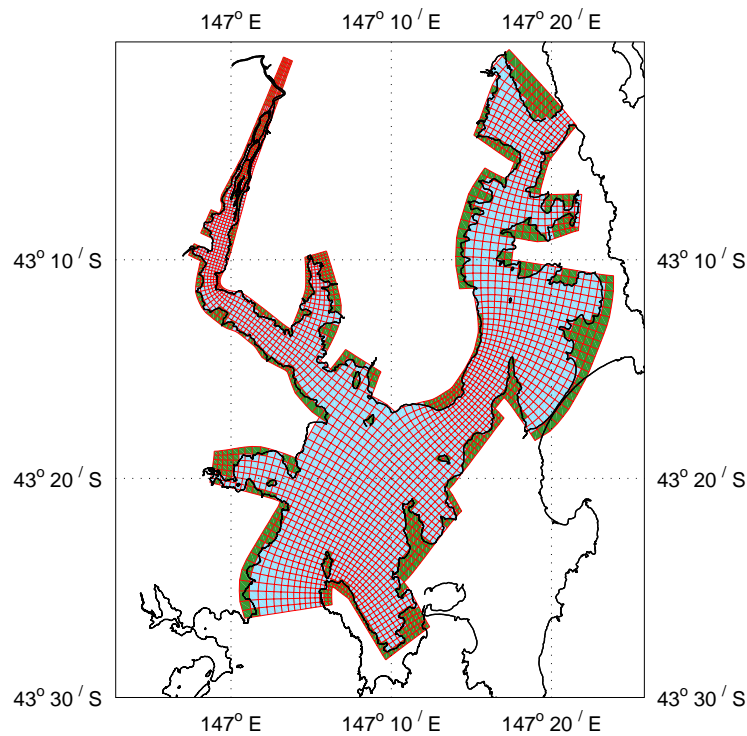


**Fig. 25. Model Discretization**

## 6.2 Thermodynamic Effects

The sea surface temperature and salinity at the sites in Fig. 4 and 10 are displayed in Table 3 and 4 respectively.

**Table 3. Sea Surface Temperature (°C) and Salinity (psu) in the D'Entrecasteaux Channel. Measurements are quoted from the downcast at depths <1 m.**

Date	Station 1		Station 3		Station 5		Station 8		Station 10		Station 12	
	T	S	T	S	T	S	T	S	T	S	T	S
10/01	16.9	33.43	17.3	32.27	15.9	33.04	16.2	29.13	15.8	33.14	15.3	34.63
06/02	17.3	34.47	17.3	34.26	17.2	34.10	16.4	34.17	16.3	34.40	16.3	34.65
04/03	17.1	34.27	17.2	34.63	16.6	34.29	16.0	33.84	16.1	34.78	15.8	34.92
05/04	15.9	34.73	15.9	34.46	15.2	34.19	14.9	34.13	15.1	34.56	14.9	34.76
29/04	15.3	34.70	15.2	34.43	14.4	34.39	14.4	34.89	14.4	34.27	14.1	34.69
03/06	12.6	34.37	12.1	34.10	11.9	34.06	12.7	34.43	12.8	34.77	12.8	34.73
03/07	10.2	31.87	9.9	31.03	9.8	31.42	10.4	30.38	11.1	33.10	11.1	33.56
05/08	11.0	33.84	10.8	33.69	11.0	33.69	11.2	34.00	11.1	33.10	9.6	33.24

**Table 4. Sea Surface Temperature (°C) and Salinity (psu) in the northern D'Entrecasteaux Channel. Measurements are quoted from the upcast at depths < 1m.**

Date	Station 13		Station 11		Station 16		Station 18		Station 20	
	T	S	T	S	T	S	T	S	T	S
13/11/01	14.3	41.40	14.3	41.64	14.3	41.17	14.4	35.65	14.5	
05/12/01	15.6	32.59							15.3	32.46
17/12/01	15.4	32.68			15.8	32.36	15.6	32.72	15.7	32.75
10/01/02	16.7	32.91	16.6	31.29	16.9	32.26	16.9	32.01	16.8	32.25
23/01/02	18.5	32.93	19.1	33.06					18.7	33.11
15/02/02	17.8	34.07								

These data indicate that the Channel generally becomes warmer and slightly saltier over summer, and then tends to a cooler, fresher state in autumn. The temperature solutions resulting from the model forcing and initialisation described in Section 5 indicate that boundary forcing alone cannot input sufficient heat to raise temperatures to those observed in summer. Fig. 26 shows the measured and modelled temperature at all

stations. It is observed that the SST at all stations is underestimated in summer when the observed temperature increases, and warmer in autumn when the system cools and observed temperature decreases. The discrepancy in temperature between modelled and measured can be over 1°C.

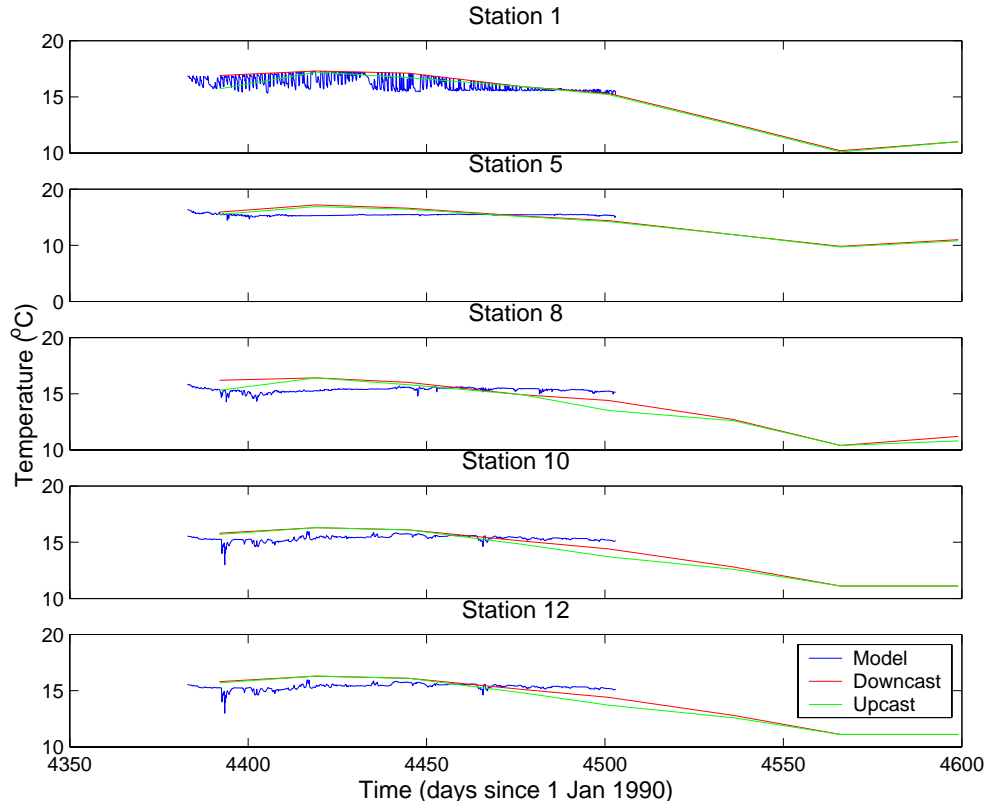


**Fig. 26. Modelled and Observed Temperature at Station 8**

Note that cooler input from the Huon River may contribute to temperature changes in the cooler months, however, these calculations suggest that boundary driven advection cannot be solely responsible for temperature changes in the mid-channel regions away from the open boundaries. The only possible alternate heat source is a heat flux through the surface, which should be accounted for in the model. This was calculated from standard meteorological measurements collected at Hobart airport (wet and dry bulb temperature, air pressure, wind speed and cloud amount) using short and longwave calculations outlined in Zillman (1972) and the bulk method for sensible and latent heat using bulk coefficients of Large and Pond (1981). The heatflux for the period 2002 is displayed in Fig. 27.

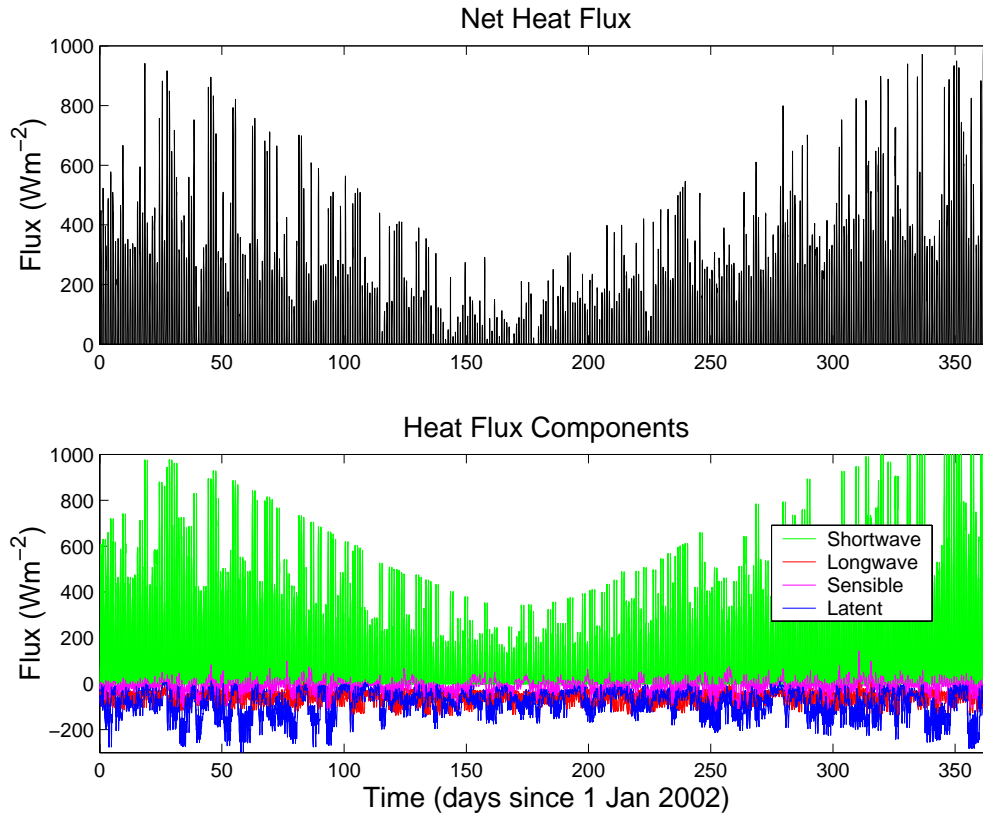


**Fig. 27. Heat Flux Characteristics for 2002**

The largest input of heat into the region is due to the short wave radiation component. During the winter months this decreases by approximately one-third in comparison to summer. The latent heat flux constitutes the largest heat loss term, with larger losses observed during summer. Long wave radiation is predominantly a loss although occasionally diffuse sky input results in net longwave input. The sensible heat flux can act as a source or sink of heat and remains relatively invariant throughout the year.

This heat flux was applied as the surface boundary condition for vertical diffusion of heat; the resulting temperature at the field station locations are displayed in Fig. 28. The annual cycle of SST is well captured by the model. The temperature distribution along the measurement section on March 2 is displayed in Fig. 29. This section is directly comparable to Fig. 7, and it is observed that the inclusion of heatflux terms greatly improved the temperature solutions.

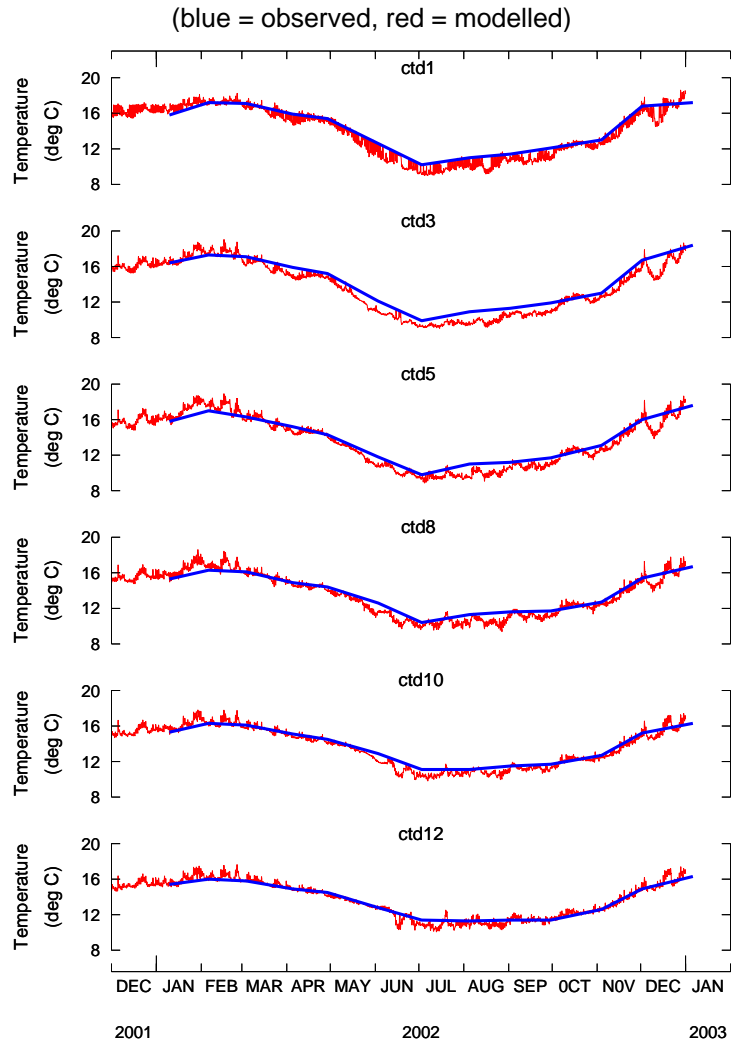


**Fig. 28. Surface Temperature with Heat Flux Included**

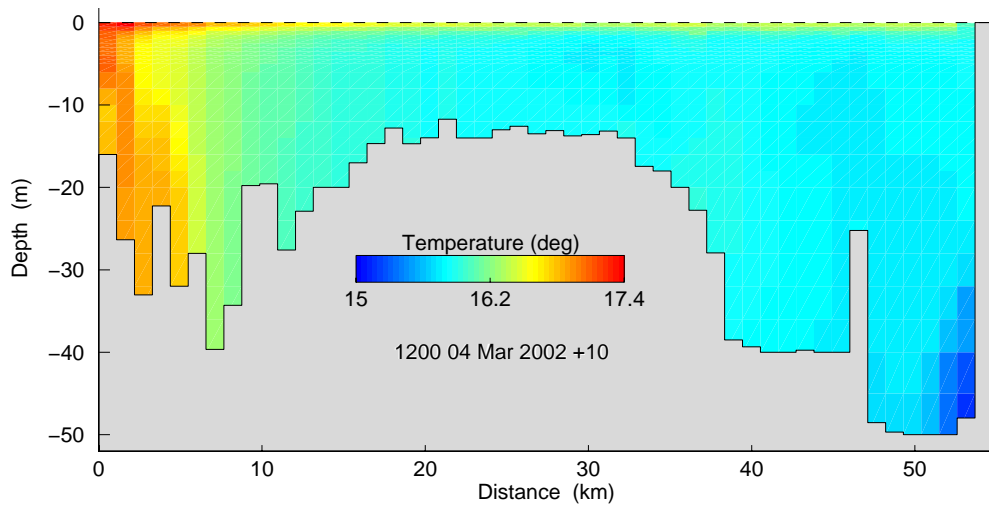


**Fig. 29. Modelled Temperature Section with Heat Flux Included**

The SST along a transect from the head of North West Bay (Station 1) into the channel (Station 11) is displayed in Table 5. It is observed that temperature is significantly higher at the head of the bay than the channel during summer, presumably due to differential heating associated with the gradient of bathymetry. This suggests that the shallow side bays adjacent to the main channel may play an important role in acting as a heat source for the main channel during summer, subject to exchange processes.

**Table 5. Sea Surface Temperature (SST) in North West Bay**

Date	Site 1 T (°C)	Site 4 T (°C)	Site 6 T (°C)	Site 9 T (°C)	Site 11 T (°C)
13/11/01	14.4	13.5	14.6	14.7	14.3
05/12/01	16.3				
17/12/01	17.1	16.7	15.8	15.6	
10/01/02	20.8	17.2	17.2	16.8	16.6
23/01/02	20.9	20.7	19.8	19.2	19.1
15/02/02	19.1	18.6	18.4	18.4	

Certainly from the data in Table 5 it appears that differential heating of North West Bay generated a strong SST gradient across the bay around 10 Jan 2001 (over 4°C temperature change). In order for this gradient to be maintained it can be assumed that the Bay remained in a relatively quiescent state for this period. The bay/channel appears to be subsequently exposed to exchange/mixing processes thus reducing the temperature gradient across the bay and elevating the temperature in the main channel around 23 Jan 2001. The temperatures at Stations 6, 7 and 8 from the broad-scale field program also indicate slight warming of Isthmus and Great Bays in summer (Table 6), whereas on 10 Jan the shallow side bay is 0.7 °C warmer than the main channel. When a strong net gain of heat at the sea surface is absent in ensuing months the side bay is consistently slightly cooler than the channel. The temperature solution for February with heat flux applied is displayed in Fig. 30, showing the above-mentioned temperature increase in the side bays due to differential heating.

**Table 6. SST in Isthmus and Great Bays**

Date	Station 5 T (°C)	Station 6 T (°C)	Station 7 T (°C)
10/01	15.9	16.6	16.6
06/02	17.2	14.8	17.1
04/03	16.6	16.7	16.4
05/04	15.2	14.9	15.0
29/04	14.4	14.2	14.3
03/06	11.9	11.8	11.5
03/07	9.8	9.8	9.8
05/08	11.0	10.5	10.2

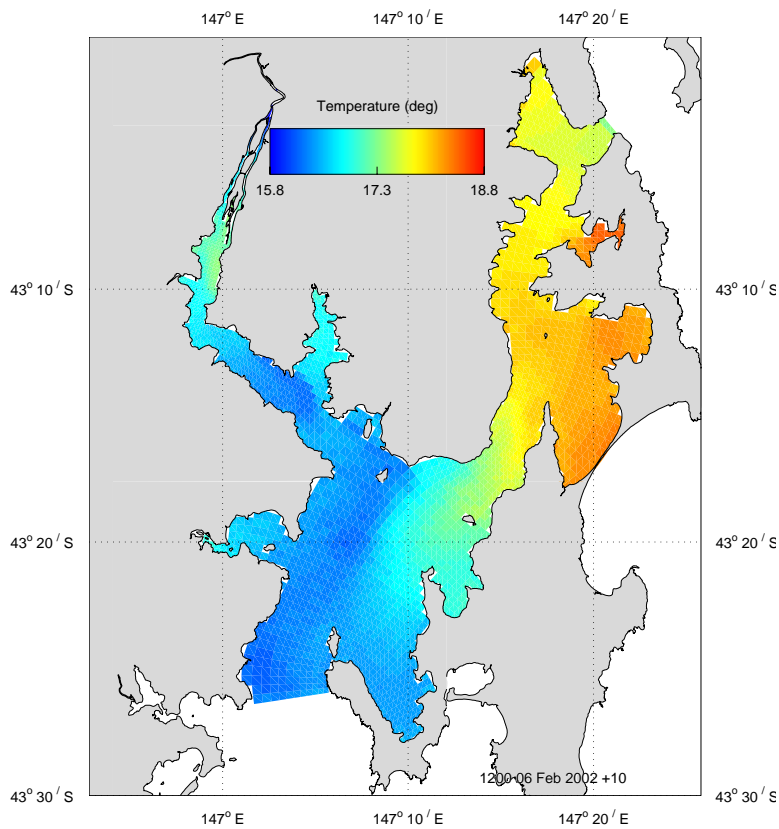


**Fig. 30. SST Solution for February 6 2002**

### 6.3 Nesting Procedure

Successively nesting local scale models inside larger regional models is a common practice that has two main advantages: (a) Regional models are capable of resolving large scale phenomena (e.g. boundary currents, mesoscale eddies, large scale upwelling, coastally trapped waves) that are not captured by local models. Motion resulting from these phenomena can be communicated into the local model through the open boundaries. (b) Open boundaries are notorious sources of error due to reflection and over-specification<sup>1</sup> problems. By prescribing measured data on regional open boundaries and using output of the regional model to drive the local model these problems are minimized.

The open boundaries of the model may be forced with either sea level or vertical profiles of velocity. The latter is the preferred method since all motion described by the momentum equations is represented, rather than just motion due to the pressure term as is the case with elevation forcing (i.e. non-linear effects are excluded in the elevation forced case). Velocity forcing is more problematic since velocity measurements are rarely available at the resolution required to force a model. Also, if velocity is available from a nesting process, this method is prone to over-specification which is difficult to alleviate using partially passive boundaries as is common with elevation forcing (e.g. Blumberg and Kantha, 1985).

It was observed that solutions of the local model compared more favourably to observation using a velocity forced northern boundary than the elevation-forced case (e.g. Fig. 31). This suggests that non-linear effects may be important in the Storm Bay area that contributes towards driving flow through the north entrance of D'Entrecasteaux Channel, probably through inertial effects of gyral activity or perhaps the influence of Derwent River flow. To avoid instabilities due to over-specification the southern boundary was partially passive by using a radiation condition (Miller and Thorpe, 1981) that was relaxed to prescribed elevation on a time-scale of 15 minutes.

The non-linearity of the boundary forcing was investigated further by examining the components contributing to the momentum balance (obtained from an intermediate scale model – see below) at Station 1 (Fig. 32). The  $u_1$  velocity component is oriented normal to the northern boundary (i.e. along-channel) in the local domain, and it is observed that the largest contributor to the velocity is the barotropic pressure gradient, i.e. the tide. However, the non-linear terms (advection and horizontal diffusion) are also dominant contributors to the balance; the horizontal diffusion tendency acting to always oppose the barotropic pressure gradient and non-linear advection acting to induce flow into the channel. If these non-linear terms were absent, the flow would be over-estimated on the flood tide and under-estimated on the ebb (e.g. difference between black and yellow curves). For the  $u_2$  velocity component (across-channel) the non-linear terms are the dominant contributors to the momentum balance and oppose each other. It is clear that

---

<sup>1</sup> Over-specification occurs when the data the model is being forced with is not compatible with the solutions provided by the equations in the domain interior (see Marchesiello et al., 2001).

non-linearity is important in this region, and as stated above, the flow cannot be represented accurately in the northern local domain by only prescribing the pressure gradient at the boundary.

The regional model resolves the northern open boundary of the local model quite poorly; hence an intermediate model was constructed with the aim of generating more accurate velocities with which to force the local model. A three level nesting process was therefore used; a regional model which forced the open boundary of an intermediate model with sea level, and the local model which was forced on the northern boundary with velocity and the southern boundary with elevation derived from the intermediate model (Fig. 33).

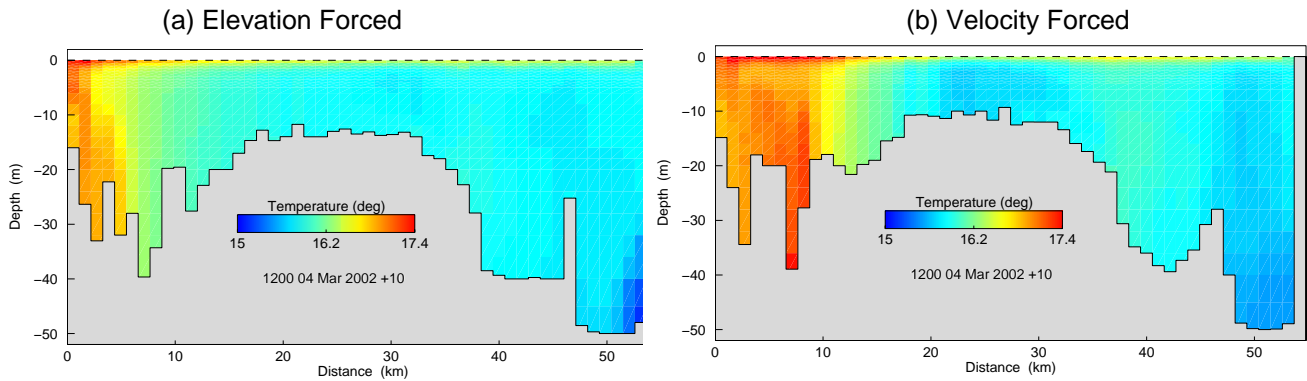


**Fig. 31. SST for 04 March 2002 using elevation and velocity forcing. These sections are comparable with Fig. 7.**

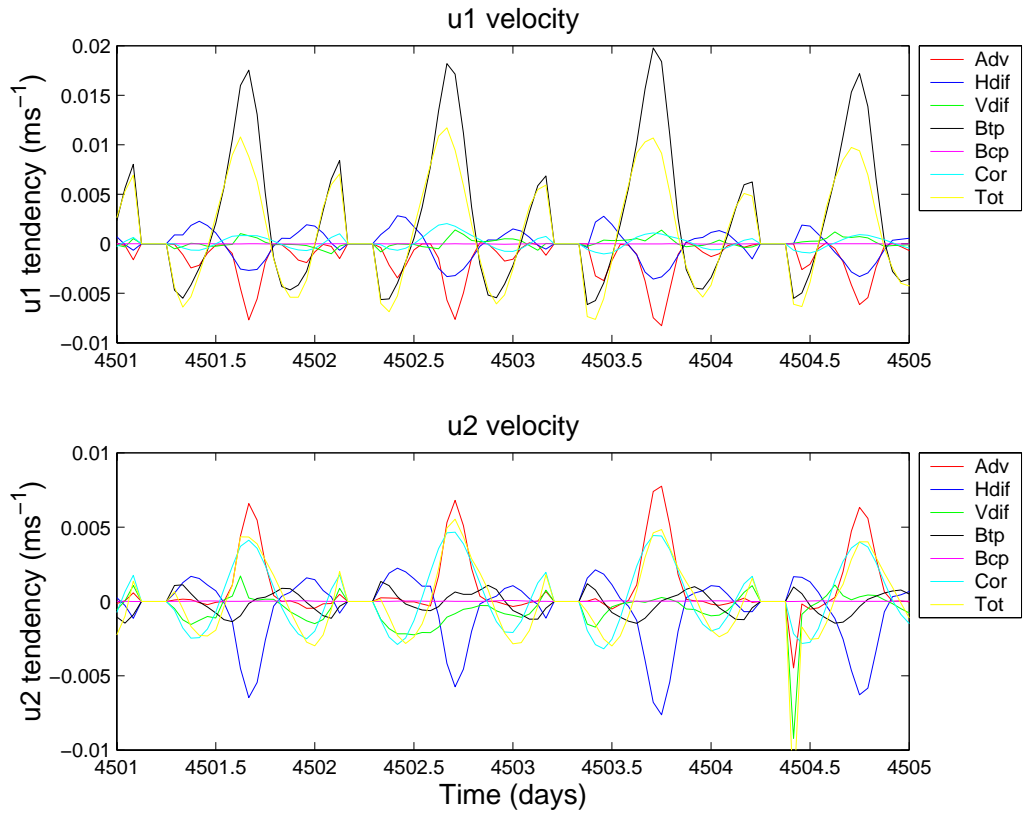


**Fig. 32. Momentum balance components for Station 1, intermediate grid.** Adv = advective terms, Hdif = horizontal diffusion terms, Vdif = vertical diffusion terms, Btp = barotropic pressure gradient, Bcp = baroclinic pressure gradient, Cor = Coriolis term and Tot = total tendency.

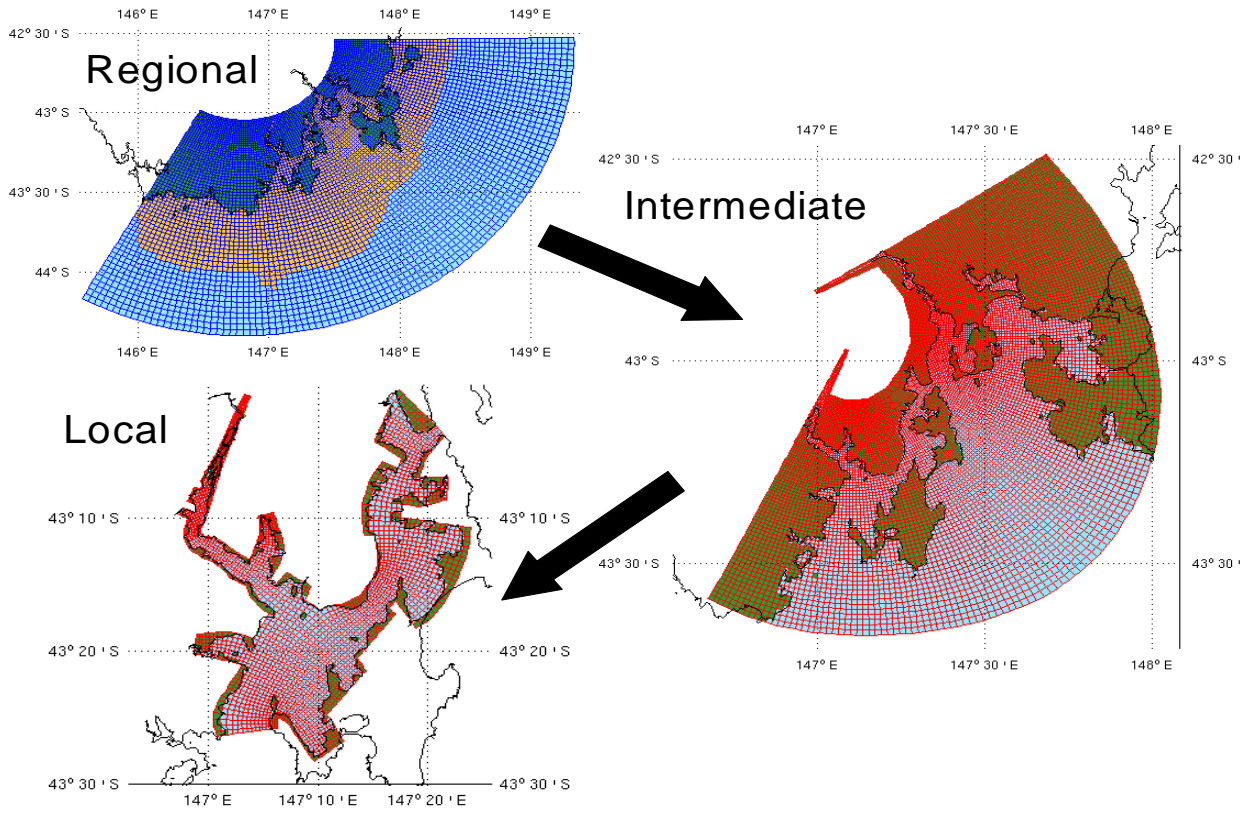
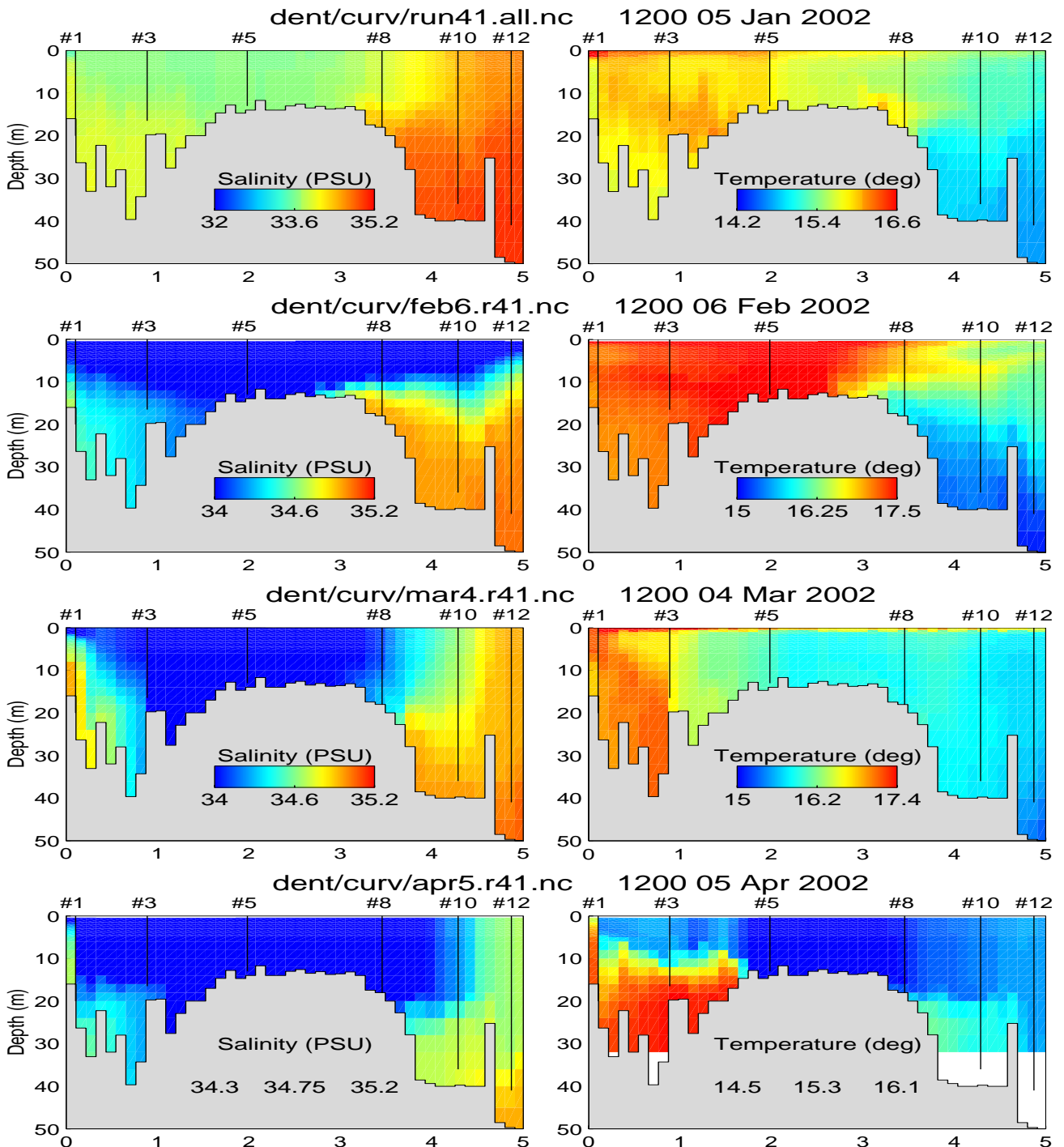


**Fig. 33. Nesting procedure**

## 7 Model Output

### 7.1 Model Calibration

The simulation period for all models was Jan 2001 to Jan 2002. Data from the broad-scale monitoring program along the main channel (Fig. 4) was used for calibration and validation for the model. The first 3 months of 2002 were used to obtain an acceptable calibration, and the remainder of the year was used to validate this calibration. The sections along the main channel, directly comparable to Figs 5 to 16, are displayed in Fig. 34 and time series at the broad-scale sampling sites are displayed in Fig. 35.



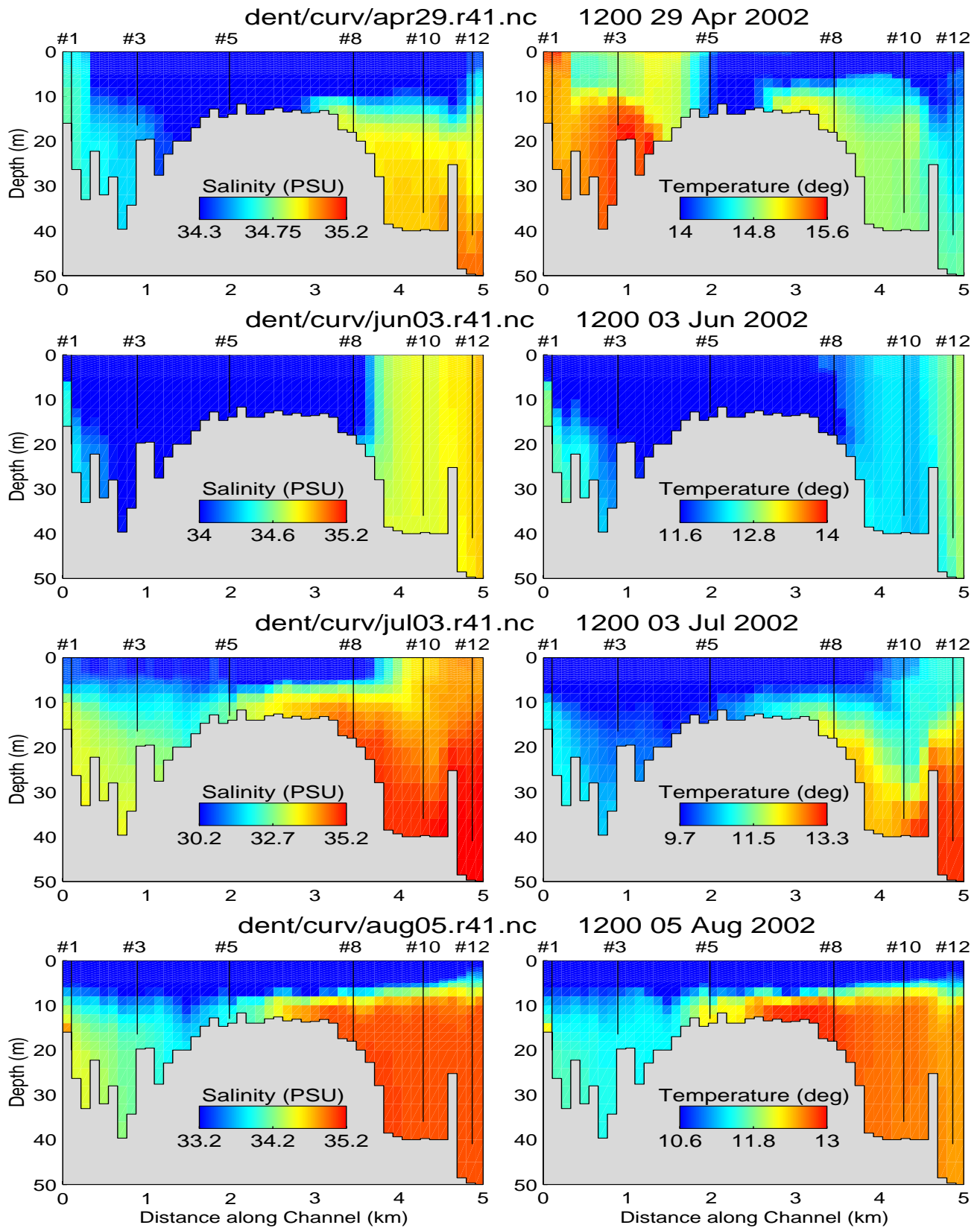


**Fig. 34. Modelled temperature and salinity sections**

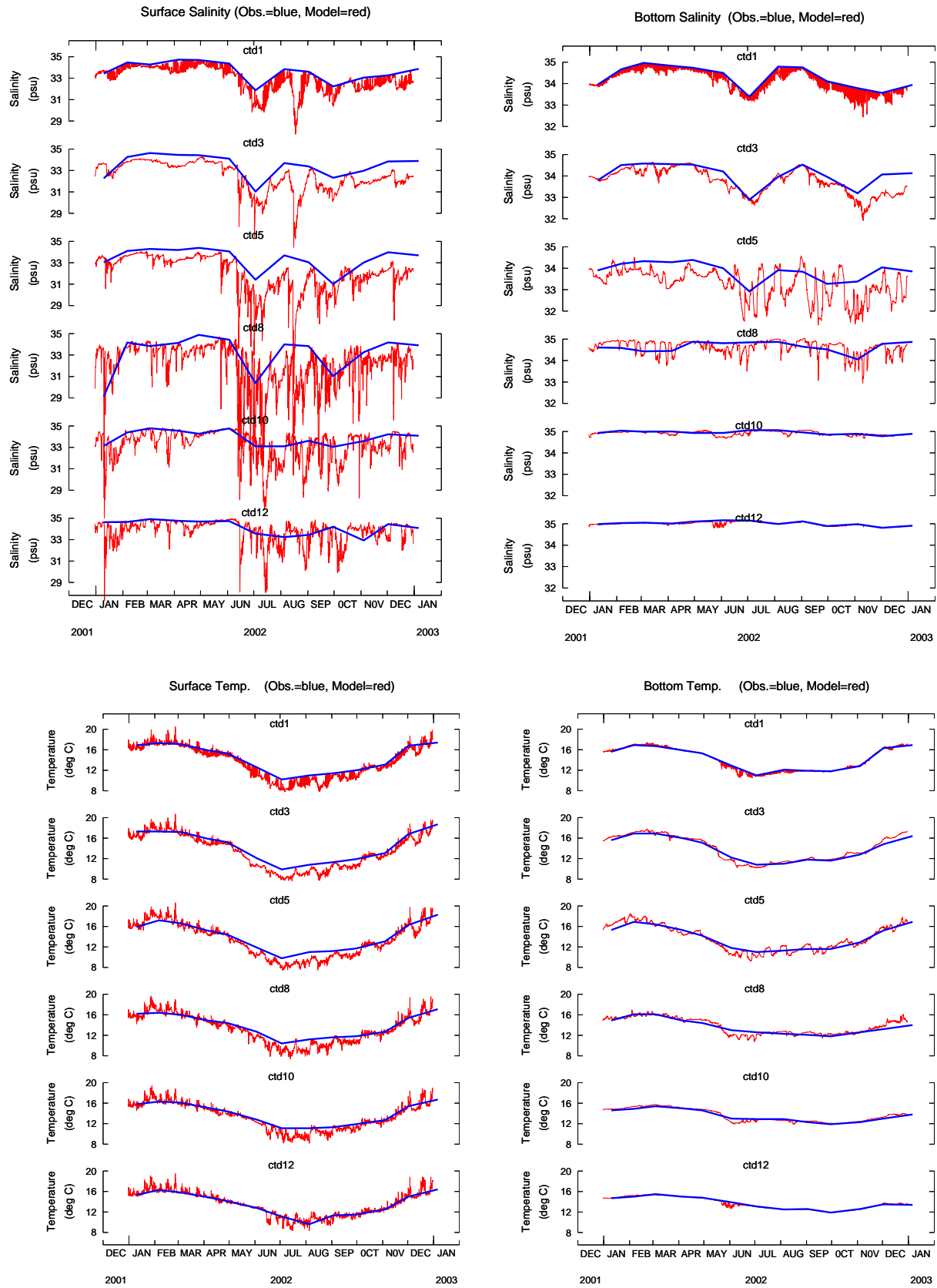


**Fig. 35. T/S time series comparison of observation and model results at monitoring stations.**

## 7.2 Sensitivity

During the calibration procedure an assessment of the sensitivity of model parameters and processes was made. As noted in section 6.2, the temperature solutions are very sensitive to surface heat flux parameterisations; particularly requiring short wave radiation to be depth distributed and being sensitive to the type of bulk scheme employed for sensible and latent heat fluxes. Examples of this sensitivity are displayed in Figs 36 and 37 which show salinity and temperature sections for March 2002 resulting from using two different bulk schemes for the latent and sensible heat fluxes. These Figures may be directly compared with measured data, Fig. 7. It can be seen that the temperature solutions show significant difference at the northern end of the channel (Stations 1 and 3), where the scheme of Kondo (1975) overestimates latent heat loss and excessively cools the channel in comparison to the scheme of Large and Pond (1982). The Large and Pond scheme was used in the verification simulations.

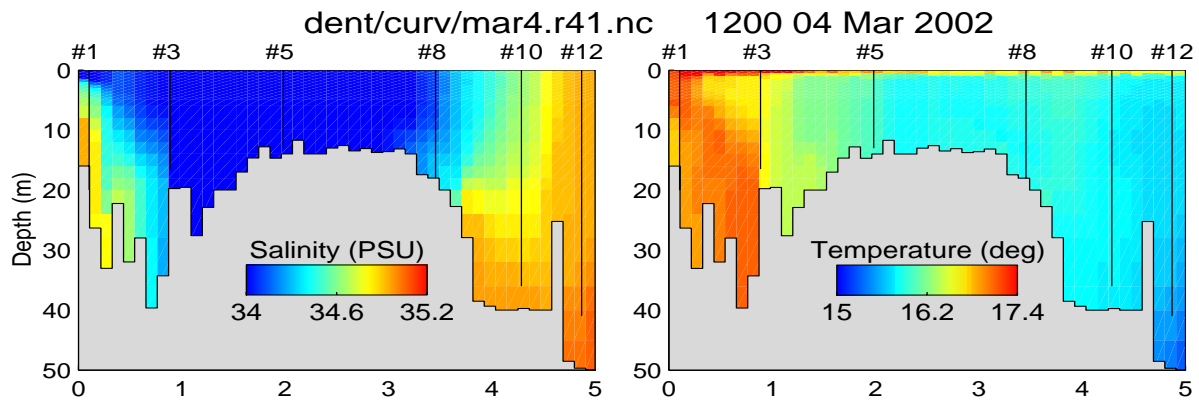


**Fig. 36. March sections using the bulk scheme of Kondo (1975)**

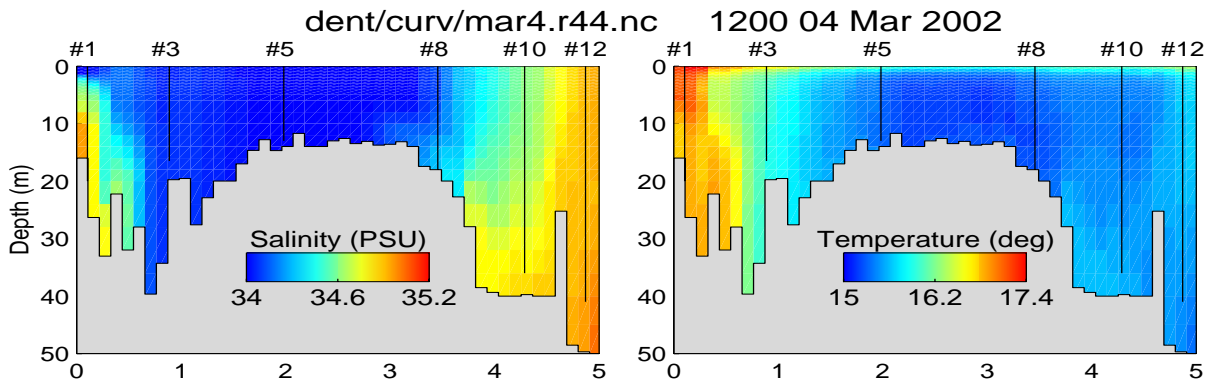


**Fig. 37. March sections using the bulk scheme of Large and Pond (1982)**

Solutions exhibited slight variability in response to the type of mixing scheme employed and the background diffusion coefficients prescribed for those schemes. Increasing background mixing tended towards a more well mixed solution which particularly impacted on the development of salt-wedge circulation in the Huon Estuary by pushing the equilibrium position of the salt-wedge downstream. Bottom salinity also became too low in the northern and mid-channel regions due to excessive mixing with fresher surface water. Too little background mixing resulted in the development of a stable surface skin due to short wave radiation input, which consequently further reduced surface mixing and led to too small mixed layers in the main channel. A vertical diffusivity of around  $1 \times 10^{-5} \text{ m}^2 \text{ s}^{-1}$  was found to be optimum. The effect of background diffusion coefficients is illustrated in Fig. 38, where comparisons mid-year at Station 5 represents the most dramatic difference in the solutions.

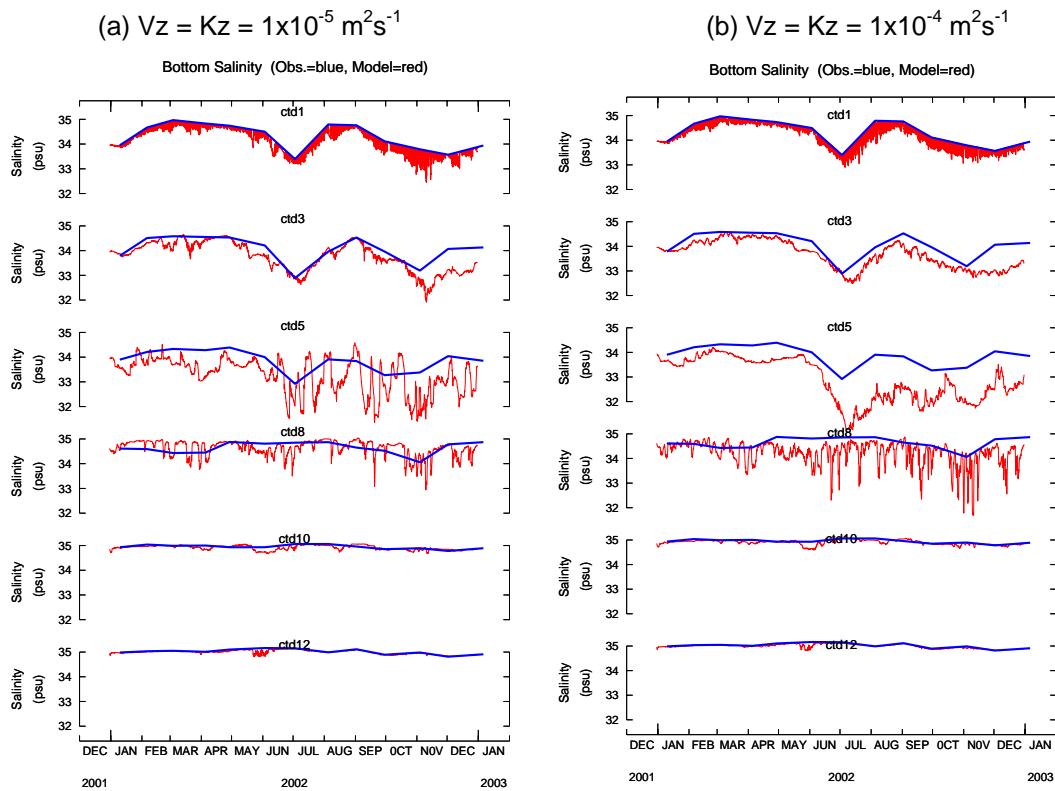


**Fig. 38. Bottom salinity resulting from different background mixing**

Bottom salinity exhibited the largest variation due to the choice of mixing scheme (Fig. 29) where the Mellor-Yamada 2.0 (Mellor and Yamada, 1982) scheme showed the best performance. The improved Mellor-Yamada 2.0 scheme features alternate turbulence length scale parameterization (Burchard et al, 1999) and is based on a three layer system where surface and bottom mixed layers are intersected by a stably stratified interior layer. This scheme generally delivers better performance in highly stratified regions such as the head of the Huon Estuary, but was generally not as stable as the Mellor-Yamada 2.0 scheme. The k-ε scheme (Burchard et al, 1998) generally provides too much mixing in

the highly stratified salt-wedge regions. The Mellor-Yamada 2.0 was considered optimum due to the better performance in the Huon Estuary mouth and main channel.

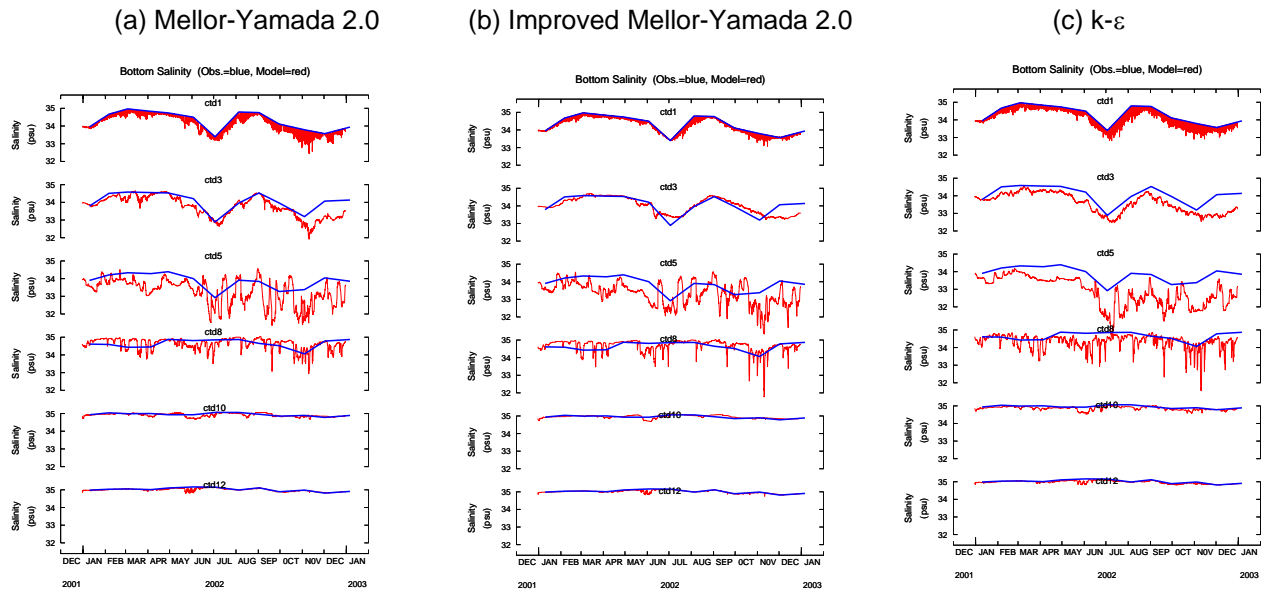


**Fig. 39. Bottom salinity resulting from 3 different mixing schemes**

The magnitude of the Huon River flow also impacted on the solutions; the less Huon flow the saltier and cooler the waters in the channel became. Reducing the flow by a factor of 1.2 (this was the scaling factor applied to allow for catchment area contributing to flow below Frying Pan Creek; section 5.4) resulted in negligible difference in solutions, whereas a distinct cooling in the channel was observed when the Huon flow was set to zero, especially in bottom water (Fig. 40). Also, as expected, the channel remained considerably saltier with little deviation below 34 psu. This suggests that the Huon River is also an important contributor of heat to the main channel. Increasing the salinity of the Huon River from 0 to 3 psu resulted in negligible changes to the salinity solutions in the channel.

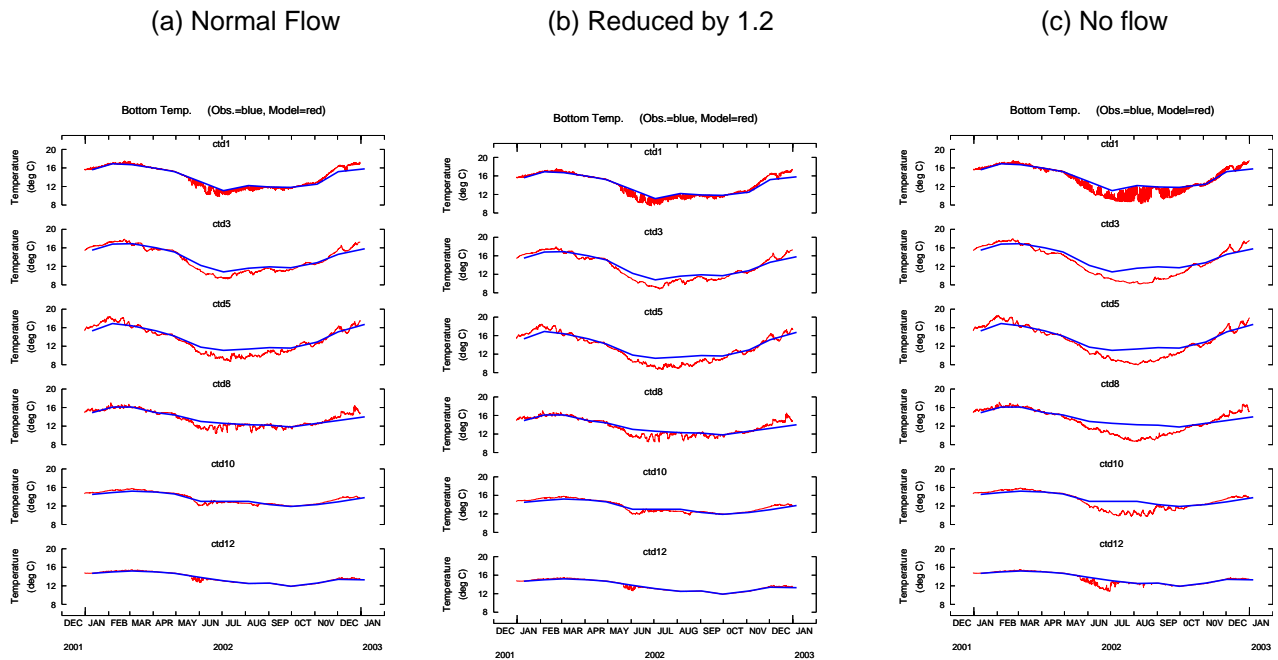


**Fig. 40. Bottom temperature resulting from 3 different flow regimes.** These simulations were performed with the improved Mellor-Yamada mixing.

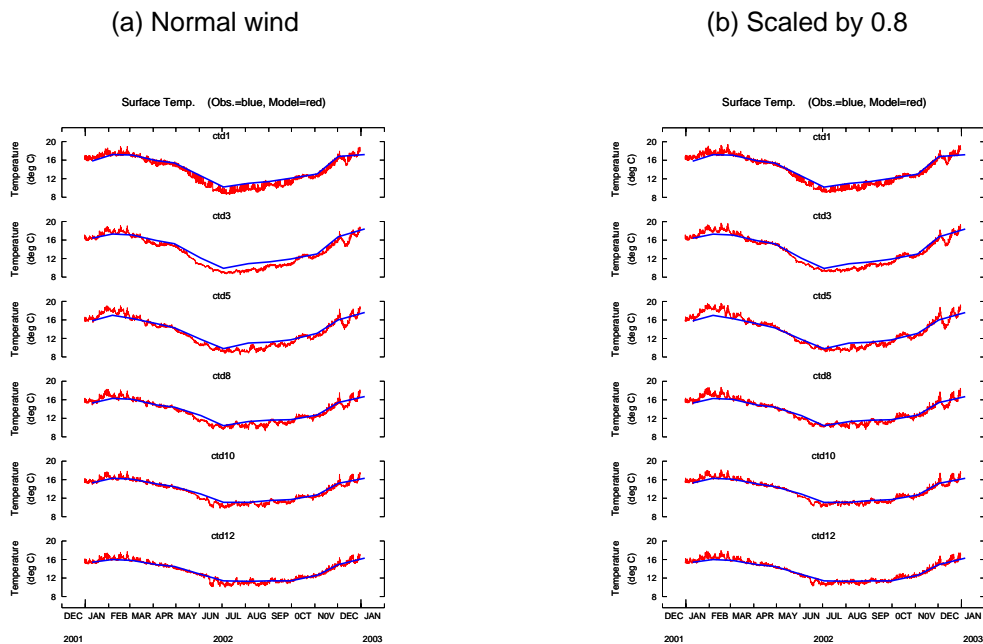


**Fig. 41. Surface temperature resulting from 2 different wind regimes.** These simulations were performed with the improved Mellor-Yamada mixing.

The applied wind stress has a two fold impact on the model solutions. Firstly the wind stress magnitude and direction affects the wind driven transport in the domain. Although the broad-scale wind characteristics are well represented using the interpolated wind from measurement sites (Fig. 18), local fluctuations, particularly due to topographic steering, may alter the wind and thus local circulation at certain points. A more intensive local sampling strategy is required to be implemented to address this issue. The wind stress also supplies energy for vertical mixing and is therefore important for regulating mixed layer depths. The model was run with a scaling of 0.8 applied to the wind. This resulted in little overall change in the temperature or salinity solutions. Surface temperatures at the northern end of the channel (Stations 3 and 5) during summer were slightly elevated, but winter temperatures were comparable (Fig. 41).

In this case the reduction in wind appears to decrease the mixed layer depth in summer resulting in warmer surface temperatures as the surface heat flux is distributed throughout a smaller volume. The absence of any significant difference in surface temperature in winter suggests that mixing is dominated by convective mixing due to surface cooling during this time. It is expected that dramatic changes in wind speed are required to alter the mixing regime to such an extent where manifestations are apparent in the temperature and salinity solutions.

Solutions did not alter to any great degree in response to the choice of bottom roughness, layer thickness, minimum coastal depth or horizontal mixing coefficients.

### 7.3 General Model Solutions

The annual cycle of temperature and salinity in the Huon-D'Entrecasteaux region is displayed in Figs 33 and 34. Generally the model tends to be slightly fresh and cool mid-channel in the winter months. The warmer winter southern bottom water and associated seasonal variability described in Section 4 is also evident. The Huon-D'Entrecasteaux system is micro-tidal with spring tide ranges up to 1 m. The diurnal tide has a range that is slightly larger than the semi-diurnal tide, and sea level in the region varies between periods of pure diurnal to pure semi-diurnal character (e.g. Fig. 42, semi-diurnal character around 18 July, diurnal character around 26 July). This is quantified by the form factor  $F = \text{ratio of diurnal to semi-diurnal amplitudes} (F = K_1 + O_1 / M_2 + S_2)$ , which in the case of the D'Entrecasteaux  $\sim 1.5$  verifying that the tide is of predominantly diurnal mixed character. The Huon Estuary is a salt-wedge estuary characterized by a freshwater layer overlying a saline wedge that intrudes up estuary. Fig. 43 shows this fresh layer overlying the salt wedge which propagates up to the river boundary at Huonville under low flow conditions. During periods of high flow a distinct fresh water plume is seen to emanate from the Huon Estuary and propagate up the D'Entrecasteaux Channel towards the northern boundary (Fig. 44a). This fresh water plume appears to favour the northern side of the estuary within the Huon, consistent with observation. Little fresh water makes its way to the southern boundary, and this occurs only under the influence of north-easterly winds (Section 7.5). Under high flow the salt wedge in the Huon Estuary is pushed downstream (Fig. 44b). Maximum current velocities are observed midway up the D'Entrecasteaux channel at the narrowest point near Gordon, and may reach more than

0.5ms<sup>-1</sup> at times (evidence exists in sediment composition at this location to suggest there are persistent strong currents in the region). These currents are predominately tidal in nature, exhibiting a distinct oscillation at the tidal frequency (Fig. 7.3.4). Motion is generally directed up-channel and up-river during the flood tide and down-channel and down-river during the ebb (see Section 7.5). Sea level gradients are low throughout the domain.

The general net flow through the system is inflow in bottom waters at the southern boundary following a route up the Huon Estuary in the salt wedge. Entrainment into the fresh river flow then carries water down-river into the channel where net flow up-channel out of the northern boundary occurs (Section 7.5).

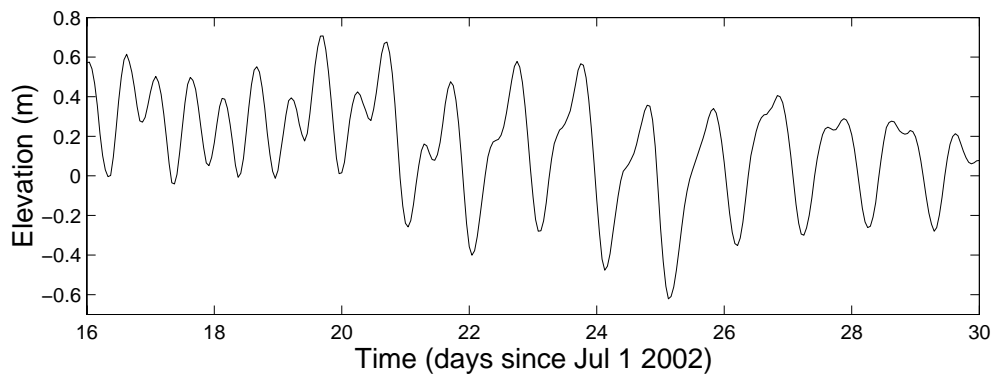


**Fig. 42. Tidal height at Station 10, July 2002**

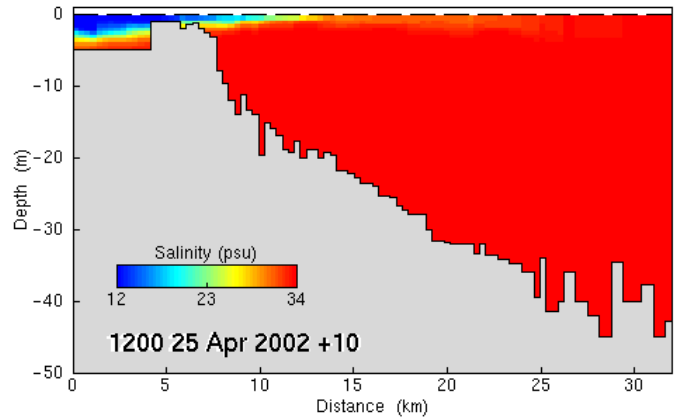
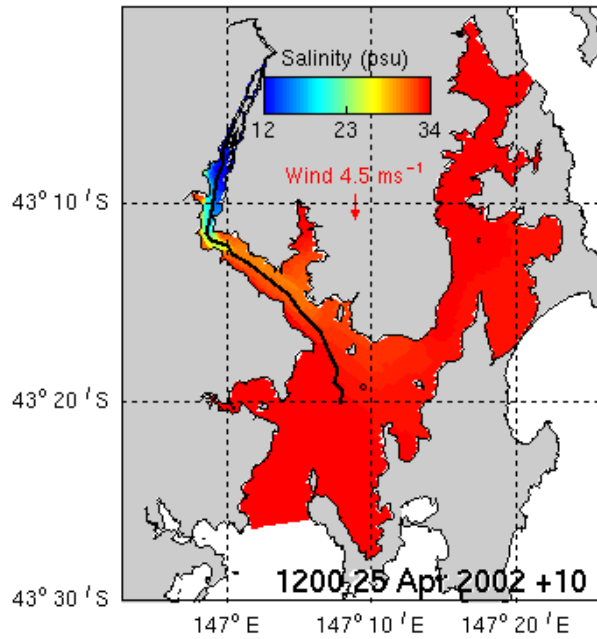
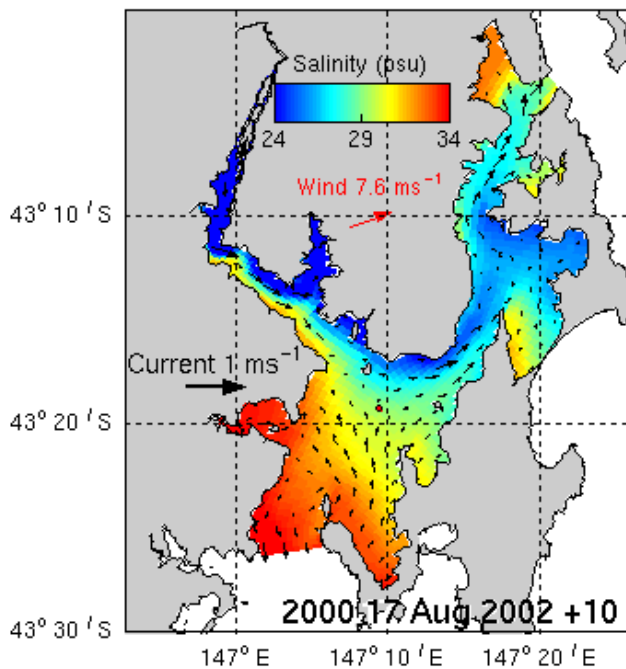


**Fig. 43. Plan view of surface salinity distribution and Huon Estuary section on 15 Apr 2002.** River flow is  $\sim 10 \text{ m}^3 \text{ s}^{-1}$ . The section location is marked on Fig. (a).

(a) Plan 17 Aug



(b) Section 18 Aug

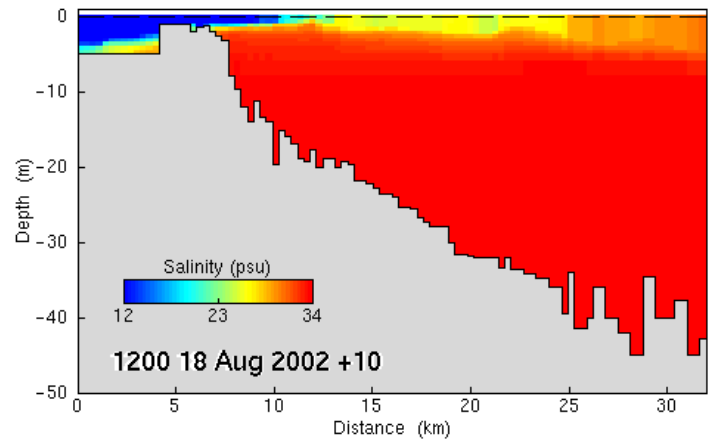


**Fig. 44. Surface salinity and surface currents during  $\sim 1000 \text{ m}^3 \text{ s}^{-1}$  flood.** Tide is ebbing with a range of 0.83 m.

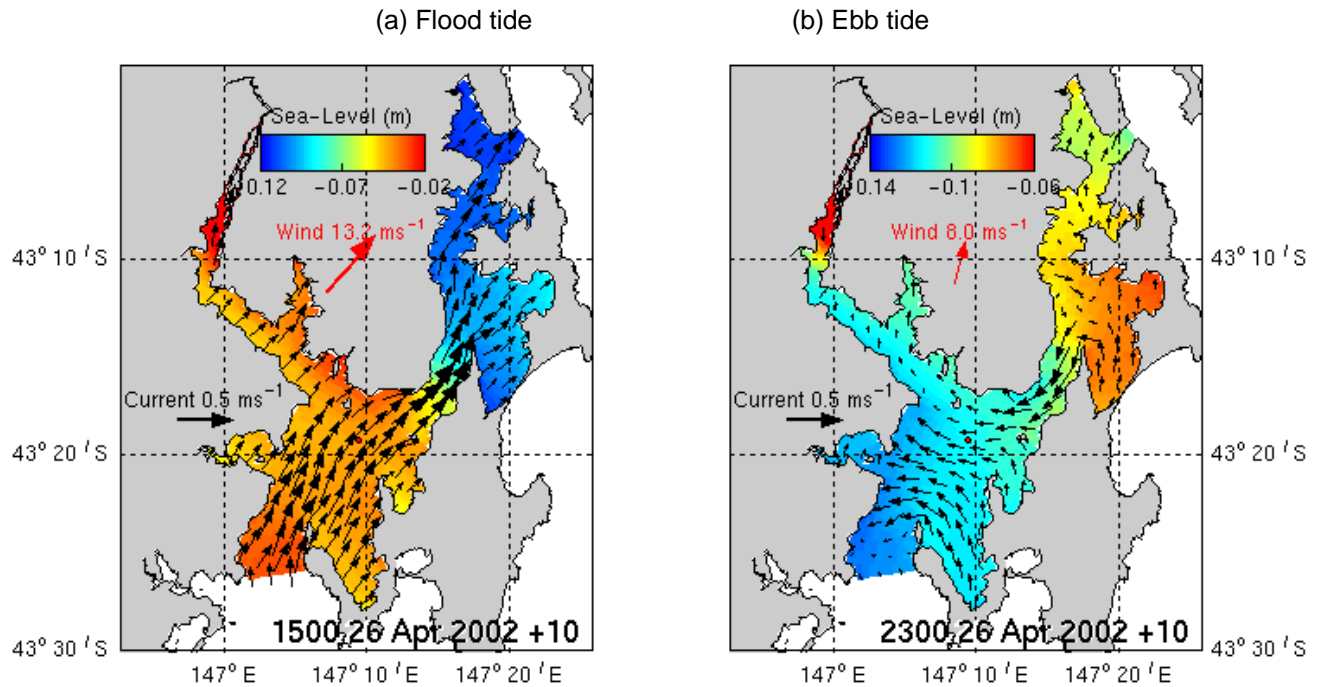


**Fig. 45. Surface currents and sea level on 26 Apr 2002.**  
Tidal range is  $\sim 0.7 \text{ m}$  and river flow is  $\sim 10 \text{ m}^3 \text{ s}^{-1}$ .

## 7.4 Momentum Balance

The model is capable of diagnosing the contribution from each term in the momentum balance to the change in velocity. This is in the form of a velocity tendency in  $\text{ms}^{-1}$  for each term in the momentum balance; i.e. momentum advection, horizontal diffusion (mixing), Coriolis (rotation), vertical diffusion (vertical mixing), barotropic pressure gradient forces (sea level gradients) and baroclinic pressure gradient forces (density gradients). Generally near the surface vertical diffusion represents the contribution due to the wind, which acts to accelerate the flow. Near the bottom vertical diffusion represents bottom drag which acts to retard the flow. The sum of all tendencies is equal to the total change in velocity over one time step. Note that the sum of tendencies is *not* equal to the actual velocity at any particular time, and must be added to the velocity at the previous time-step in order to obtain this actual velocity. Under steady state conditions the total tendency is zero and all momentum tendencies must balance. For non-steady motion one or several tendencies may dominate resulting in non-zero total tendency and acceleration of flow. Momentum tendencies are useful in evaluating the relative contributions of each

forcing mechanism and diagnosing the dominant forcing mechanisms that drive motion in the domain.

The local momentum balance varies markedly in time and space throughout the domain depending on wind strength and direction, river flow and the phase of the diurnal tide and neap-spring tidal cycle. A snapshot at Station 8 (approximately the middle of the domain) is presented in Fig. 42 for the surface and 43 for the bottom. During this time river flow varies from  $\sim 10 - 70 \text{ m}^3\text{s}^{-1}$  (low flow) and the tide was passing through a neap phase with minimum tidal range of 0.25 m occurring on 13 Apr and maximum range of 0.68 occurring on 19 Apr. Wind was generally low, coming from the south-western quadrant with speeds of around  $3 \text{ ms}^{-1}$  and an easterly maximum of  $\sim 7 \text{ ms}^{-1}$ . The along-channel direction corresponds to the  $u_1$  velocity and cross-channel direction by the  $u_2$  velocity. Fig. 42 shows that generally the barotropic pressure gradient (i.e. tidal forcing, black line in Fig. 42) and vertical diffusion (green line) dominates the solutions. This time series is taken at the surface, hence vertical diffusion represents acceleration on the flow due to the wind. The tide and wind are opposed by the Coriolis force (aqua line). The contributions from baroclinic pressure gradient forcing, momentum advection and horizontal diffusion are small in comparison. Therefore, a first order analysis is that surface motion in the domain is driven predominantly by wind and tide and balanced by Coriolis during this period. The bottom momentum balance (Fig. 43) is considerably different, with the frictional terms (horizontal and vertical diffusion) playing a more dominant role. All terms except the momentum advection contribute to the balance at this location. The momentum balance varies spatially and temporally throughout the domain, as mentioned above, hence while tendency snapshots are useful for diagnosing the momentum balance for a particular place and time, the characterisation of the system as a whole is difficult to capture. A mean momentum balance is of more use to infer the net motion in the domain.

The momentum tendencies are produced as a seasonal (90 day) mean in Figures 44 – 50 at Stations 1, 3, 5, 8, 10 and 12 (see Fig. 4), and the spatial distribution at the surface in Figures 51 – 66. The averaging process removes all contribution from the barotropic pressure, i.e. the tidal forcing has negligible contribution to the net flow. The relative contribution to the surface balance varies down the channel, as observed in Figs 44 to 49. At Station 1 for the  $u_1$  velocity (along-channel component) the baroclinic pressure is opposed by the advective forces. This was noted in Section 6.3 and prompted the use of velocity forcing at the northern boundary. The  $u_2$  velocity (cross-channel) component exhibits a balance between Coriolis and vertical diffusion, i.e. wind forcing. At Station 3 the along-channel component balance changes such that baroclinic pressure and Coriolis are opposed by the frictional terms. The cross-channel component remains similar to Station 1, except that the baroclinic pressure combines with Coriolis in the winter and spring. Coriolis is opposed by wind at Station 5 for the  $u_1$  component, with the baroclinic pressure contributing to Coriolis in the winter. A small up-channel momentum advection contribution exists throughout the year. The  $u_2$  component exhibits a balance between baroclinic pressure + Coriolis and vertical diffusion. During winter and spring the Coriolis influence lessens. At Station 8 the  $u_1$  component exhibits opposing baroclinic pressure and Coriolis forces. Wind contributes to Coriolis in the spring.

All the above stations exhibit a positive total tendency in the along-channel direction, indicating flow up-channel towards the north. This means that the baroclinic pressure and Coriolis forces are predominantly driving flow up-channel in the northern part of the channel. The cross channel total tendency is close to zero.

The balance at Station 10 for the  $u_1$  component is similar to Station 8, except the total tendency is close to zero at this location. The  $u_2$  component exhibits a balance between baroclinic pressure and vertical diffusion. At Station 12 Coriolis opposes the baroclinic pressure for the  $u_1$  component with an advective contribution to Coriolis in winter and spring. The total tendency is now negative, indicating down-channel flow. For the  $u_2$  component baroclinic pressure + advection opposes vertical diffusion + Coriolis. Again the total tendency is negative, indicating flow to the south-east.

The momentum balance mid-domain at the bottom (Station 8, Fig. 50) is again different to the surface. Baroclinic pressure dominates in the along-channel direction with horizontal friction predominantly providing the balancing force. Cross-channel horizontal friction balances vertical friction and the baroclinic pressure gradient. Horizontal friction generally plays a larger role in the bottom waters.

Care needs to be applied when interpreting the vertical diffusion tendency as a contribution by the wind, since if the drag on the sea floor is 'felt' at the surface (e.g. the bottom boundary layer extends to near the surface) then the vertical diffusion tendency may represent frictional effects retarding the flow rather than wind accelerating the flow. If the total tendency is zero (i.e. the tendencies balance) or vertical diffusion is of opposite sign to the total tendency then when vertical diffusion opposes baroclinic pressure (the pressure gradient is balanced by friction) this is a more likely scenario, whereas if vertical diffusion opposes Coriolis a more likely scenario is wind is balanced by Coriolis.

The spatial distributions for these seasonal means are shown in Figs 51 – 66. These Figures show the largest tendencies are due to the baroclinic pressure, vertical diffusion and Coriolis. The barotropic pressure tendency is negligible (Fig. 64). The Coriolis force tends to drive flow up-channel and cross-river towards the northern bank in the Huon (Fig. 65). In the Huon this is opposed by the baroclinic pressure gradient, which tends to drive flow towards the southern bank. Baroclinic flow in the D'Entrecasteaux is up-channel in the northern channel and towards the mainland in the southern channel (Fig. 65). The vertical diffusion tendency directs flow in the opposite direction in the channel, towards Bruny Island. In the Huon Estuary this tendency drives flow in a down-river direction (Fig. 63). These tendencies are generally strongest during winter and spring. The advective and horizontal diffusive tendencies show no coherent pattern and have maximum contributions in the upper Huon Estuary and the narrowest point of the channel near Gordon. Some boundary effects are also visible.

This analysis indicates that locally the tide and wind are dominant drivers of surface flow, opposed by the Coriolis force. The mean surface flow in the Huon Estuary is a balance between density forcing and Coriolis (as expected in a salt wedge estuary) with

wind contributing to down-river flow. In the northern channel density driven flow combines with rotation forces to produce seasonal up-channel residual flow. Cross channel forces balance in this area, with Coriolis opposing wind driven flow with some contribution of density effects to Coriolis. The southern channel exhibits both along and cross-channel net flow. Coriolis forcing opposes density forces in the along-channel direction while the wind driven flow opposes density driven flow in the cross-channel direction. Coriolis forcing is directed up-channel throughout the channel, whereas density effects are directed up-channel in the northern channel and down-channel in the southern channel. Horizontal friction becomes more important in bottom waters.

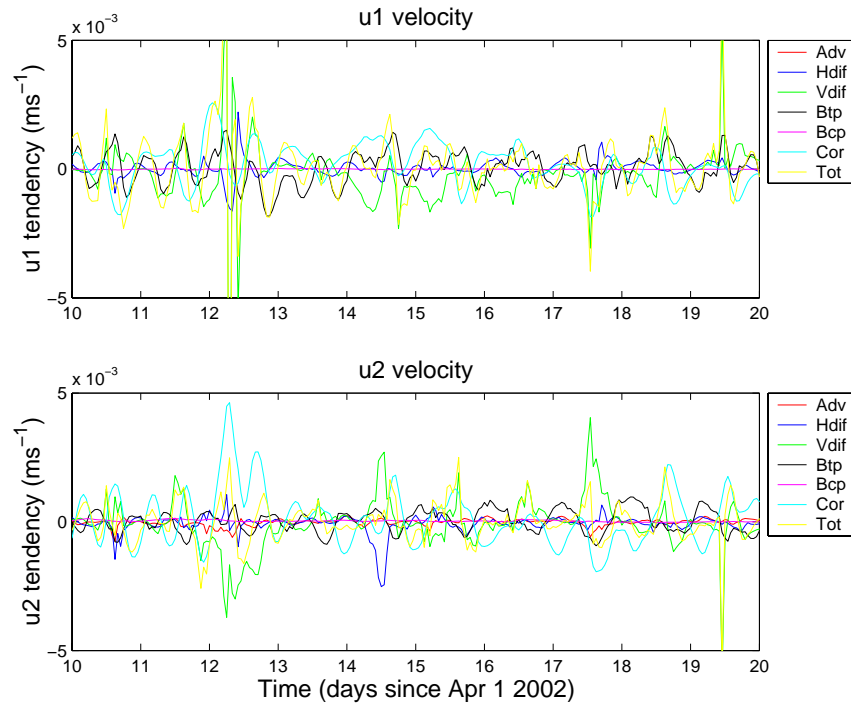


**Fig 42. Local surface momentum balance at station 8, 10 – 20 Apr 2002**  
 Adv = advective terms, Hdif = horizontal diffusion terms, Vdif = vertical diffusion terms, Btp = barotropic pressure gradient, Bcp = baroclinic pressure gradient, Cor = Coriolis term and Tot = total tendency.

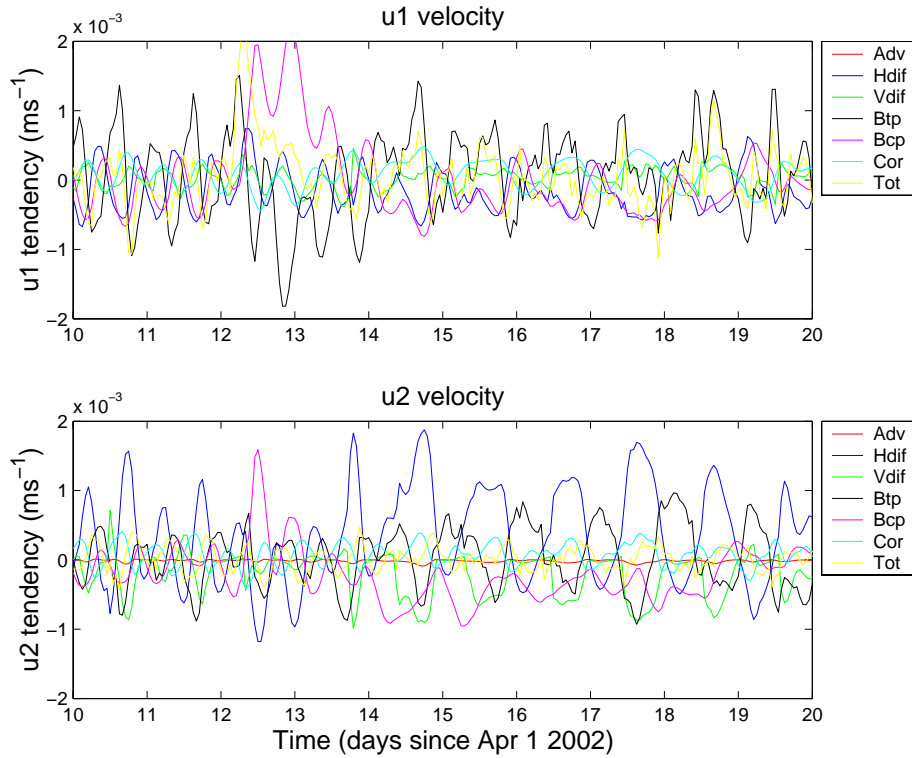


**Fig. 43. Local bottom momentum balance at station 8, 10 – 20 Apr 2002**

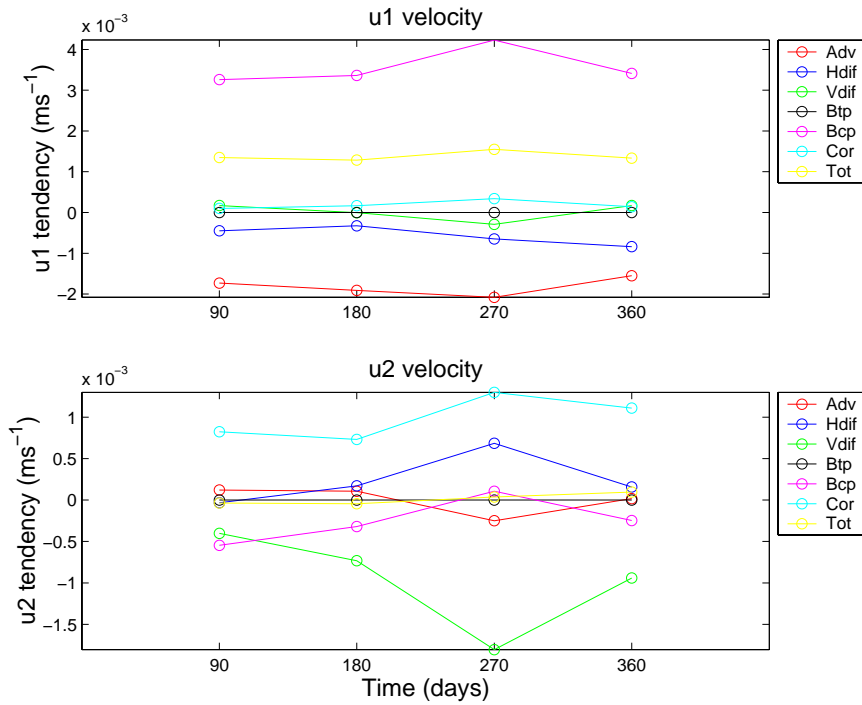


**Fig. 44. Surface momentum balance at Station 1.** Note: Day 90 corresponds to the mean from Jan to Mar (approximately summer), day 180 to autumn, day 270 to winter and day 360 to spring.

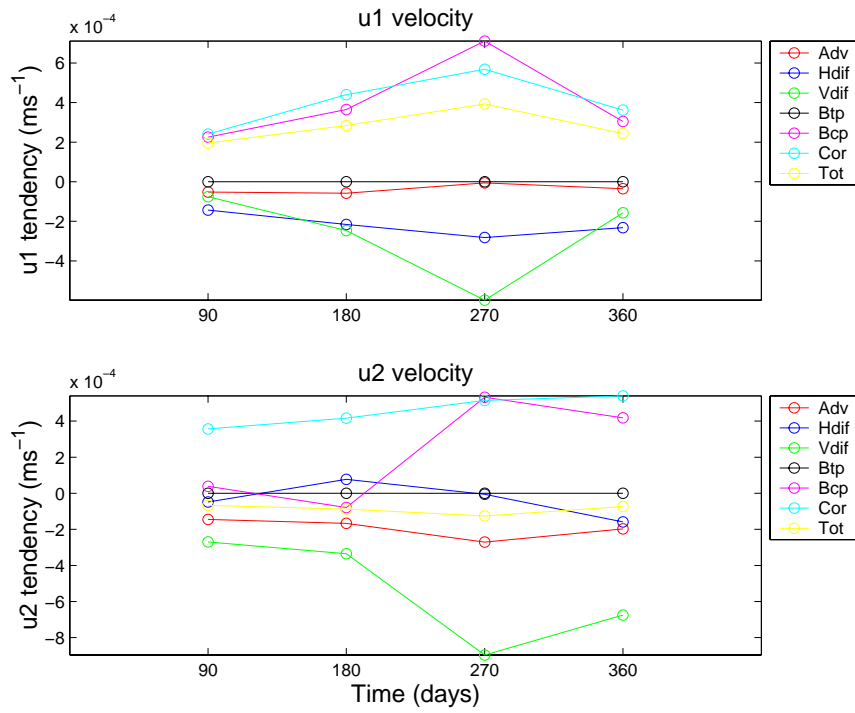


**Fig. 45. Surface momentum balance at Station 3**

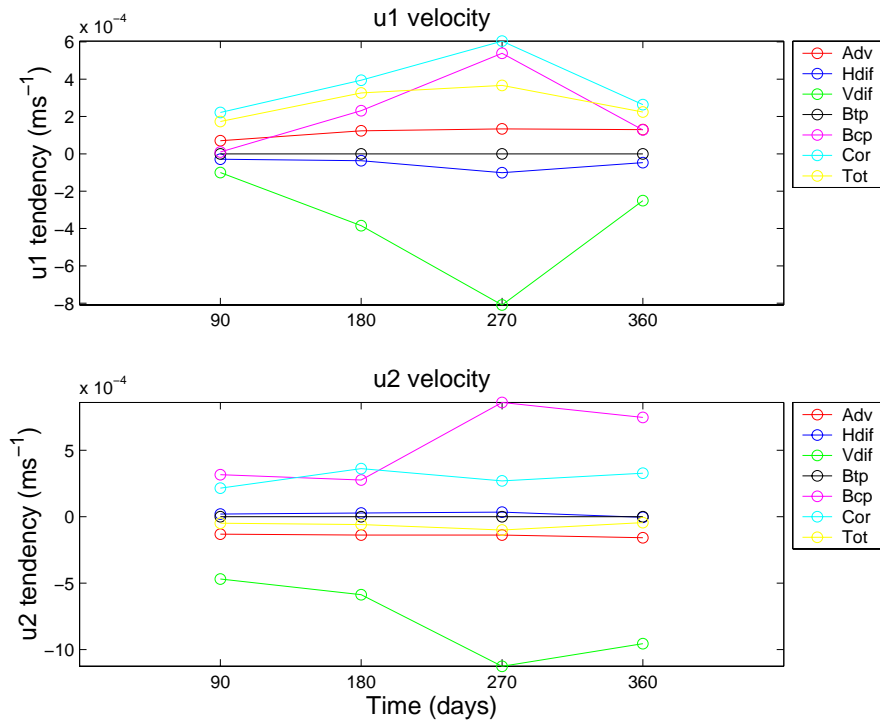


**Fig. 46. Surface momentum balance at Station 5**

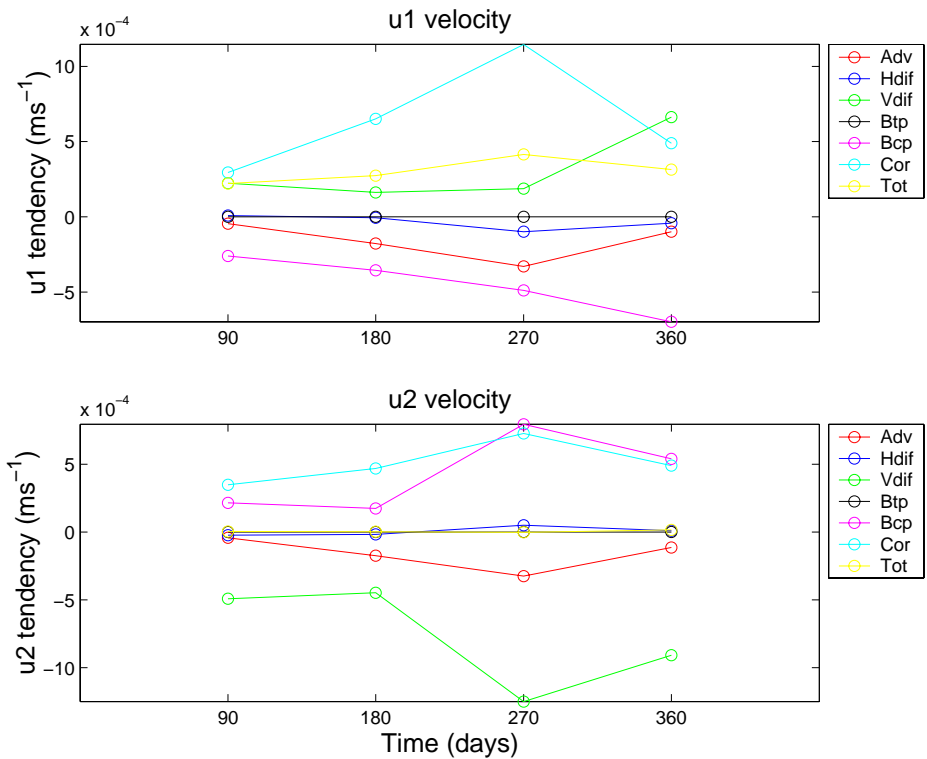


**Fig. 47. Surface momentum balance at Station 8**

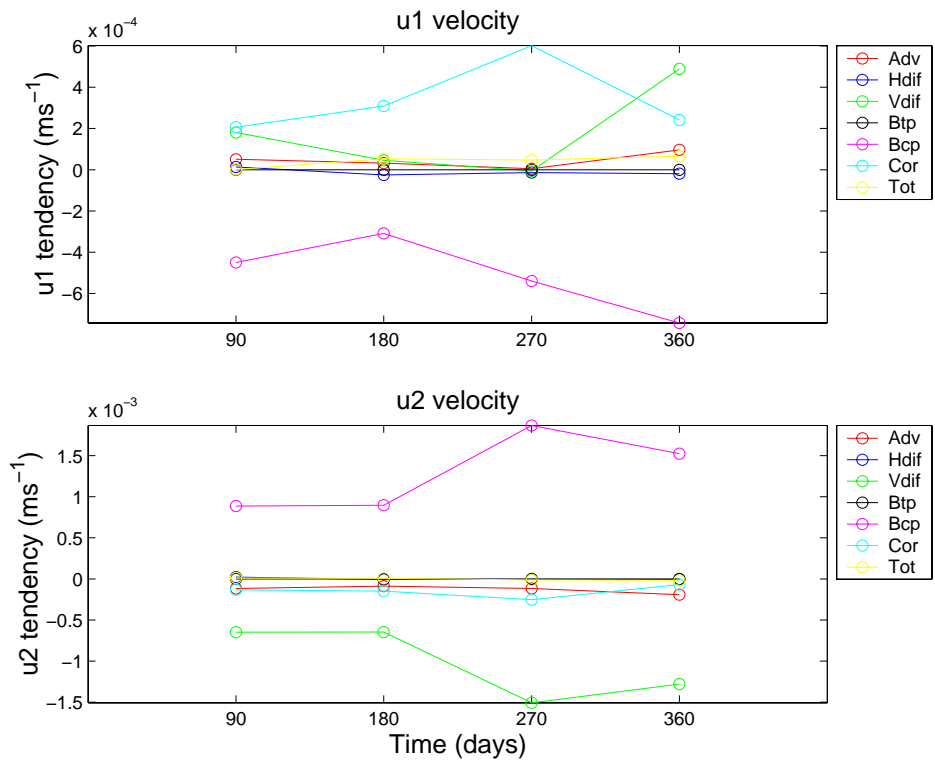


**Fig. 48: Surface momentum balance at Station 10**

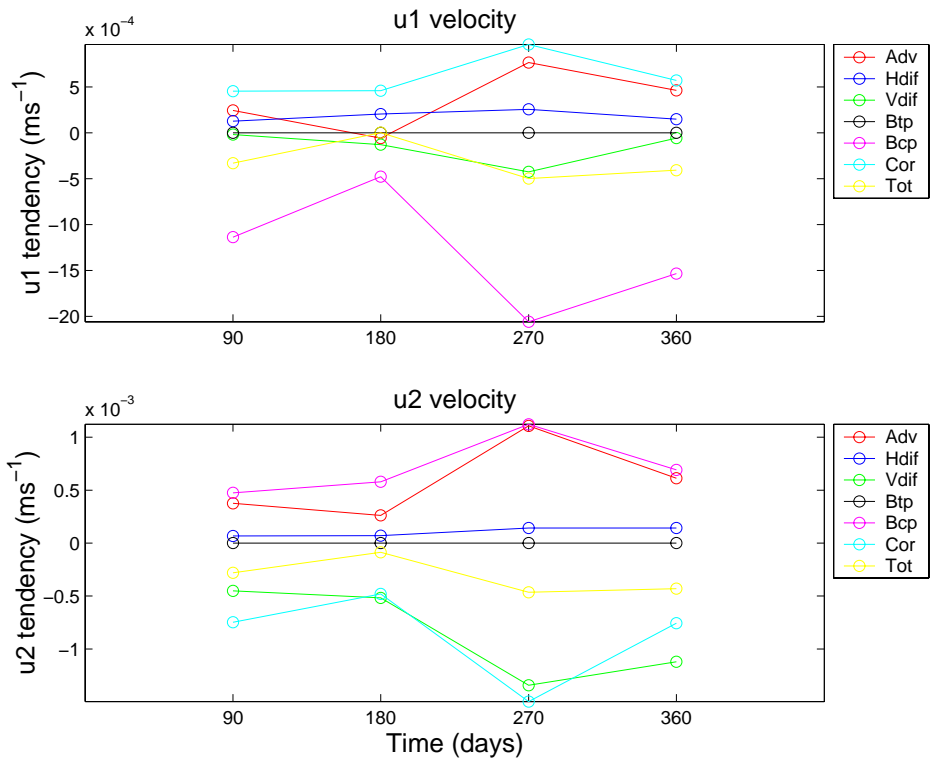


**Fig. 49. Surface momentum balance at Station 12**

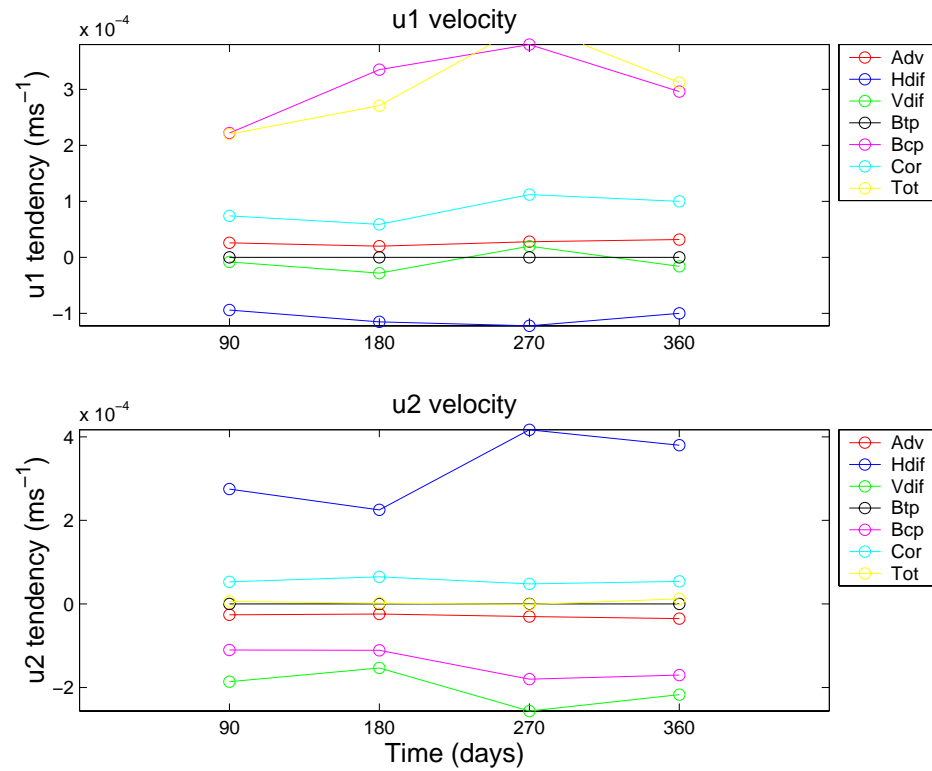


**Fig. 50. Bottom momentum balance at Station 8**

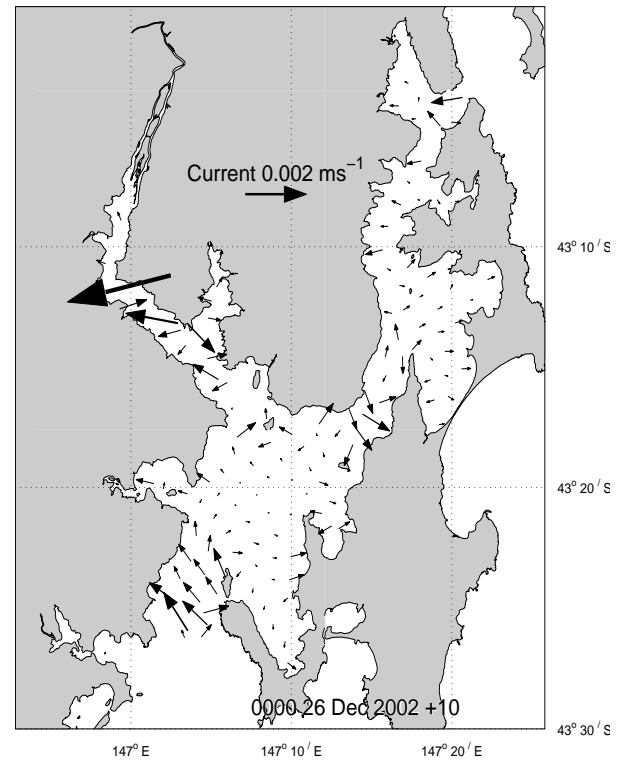
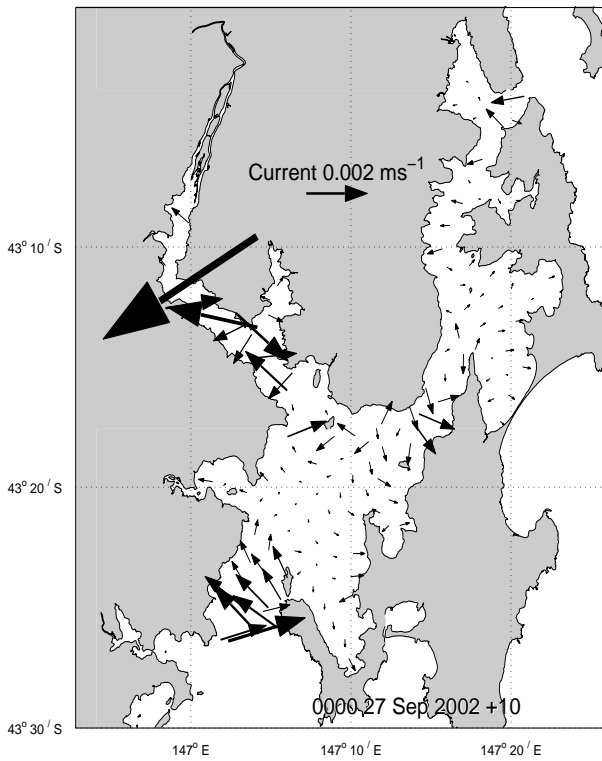
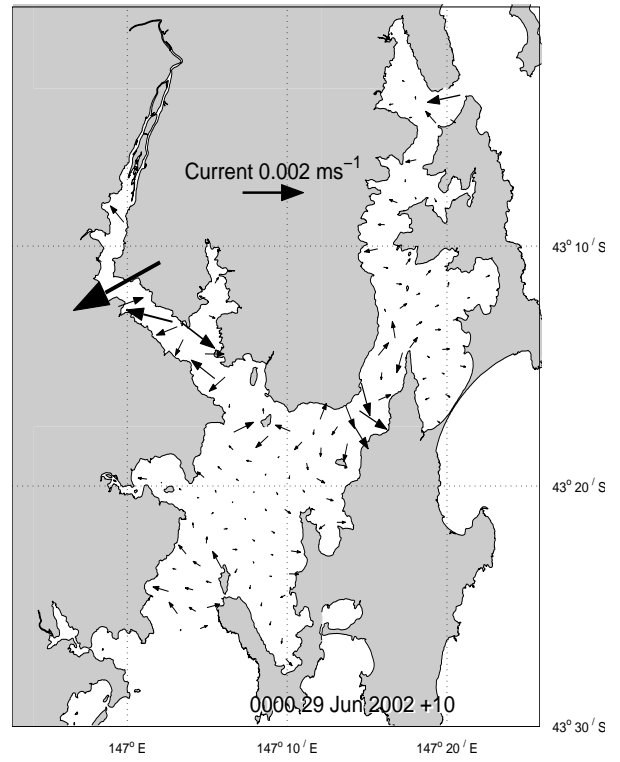
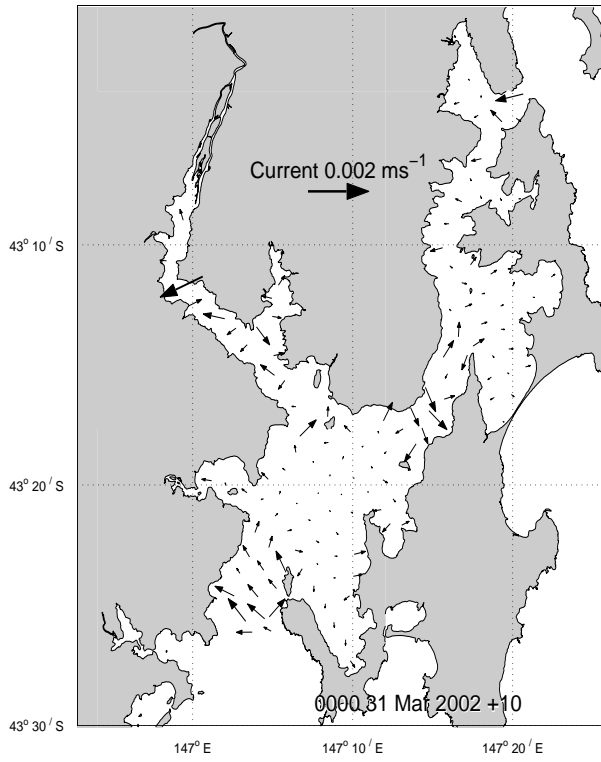


**Fig. 51. Mean Surface Advective Momentum Tendency**

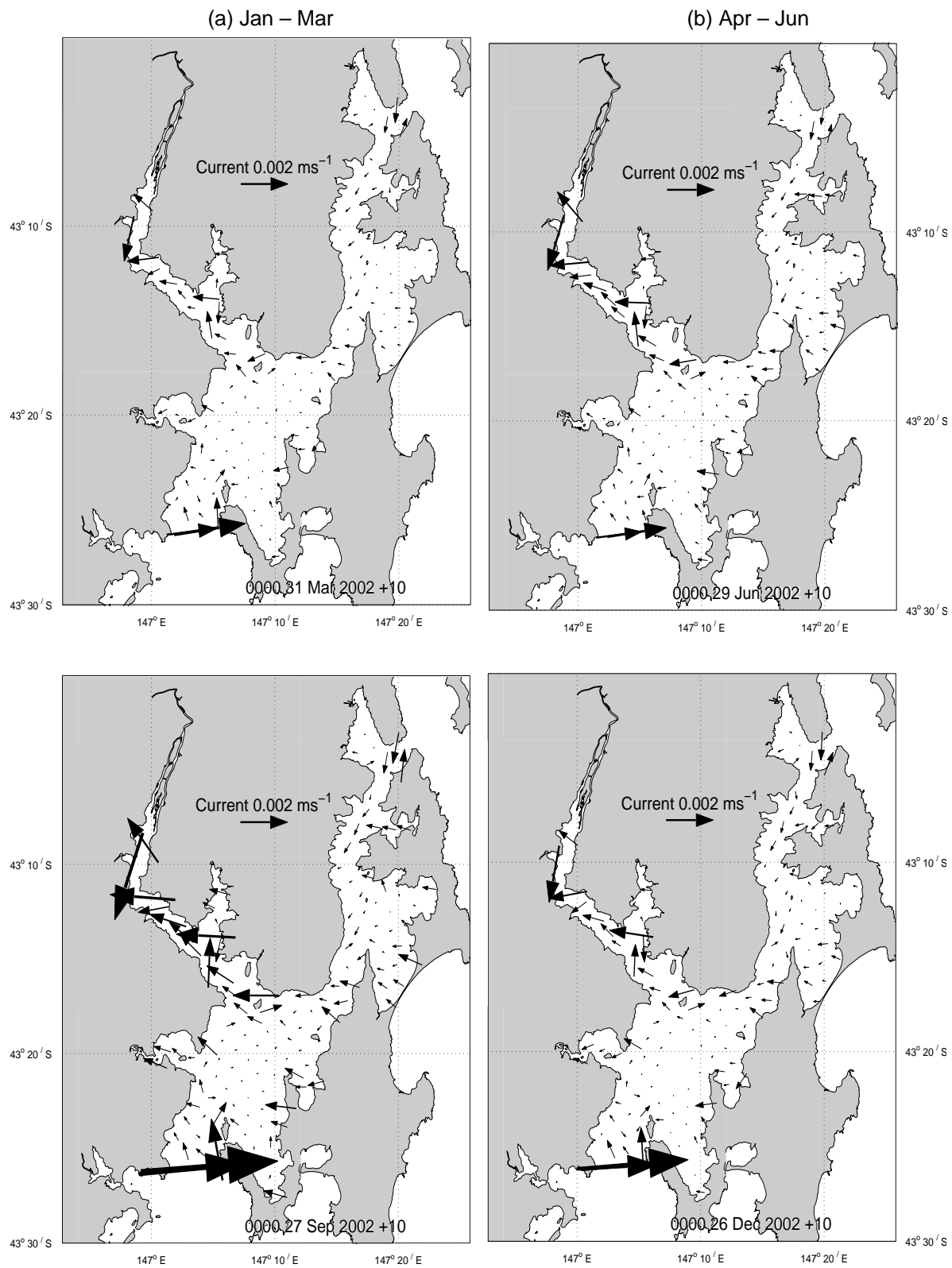


**Fig. 52. Mean Surface Horizontal Diffusion Tendency**

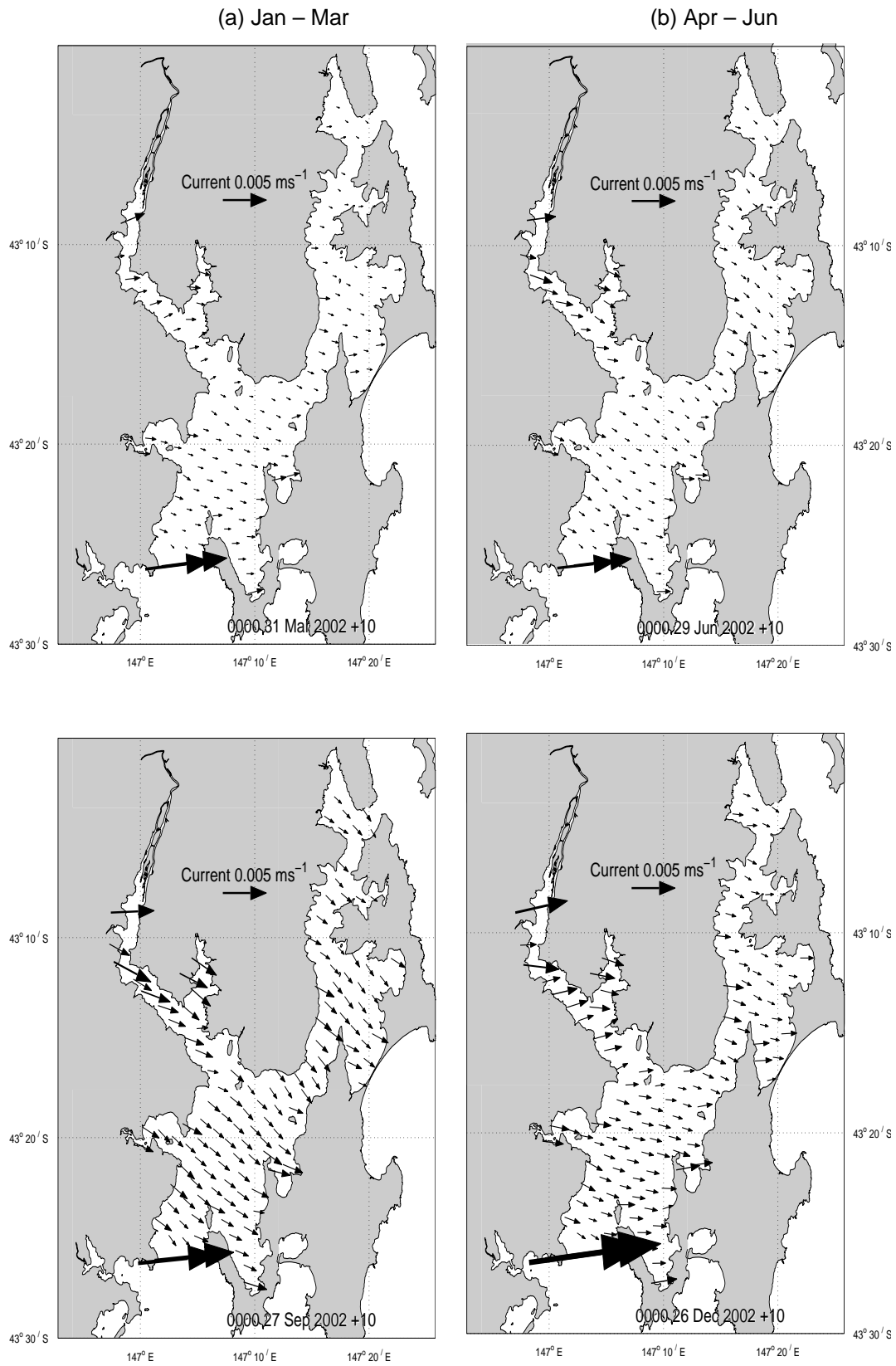


**Fig. 53. Mean Surface Vertical Diffusion Tendency**

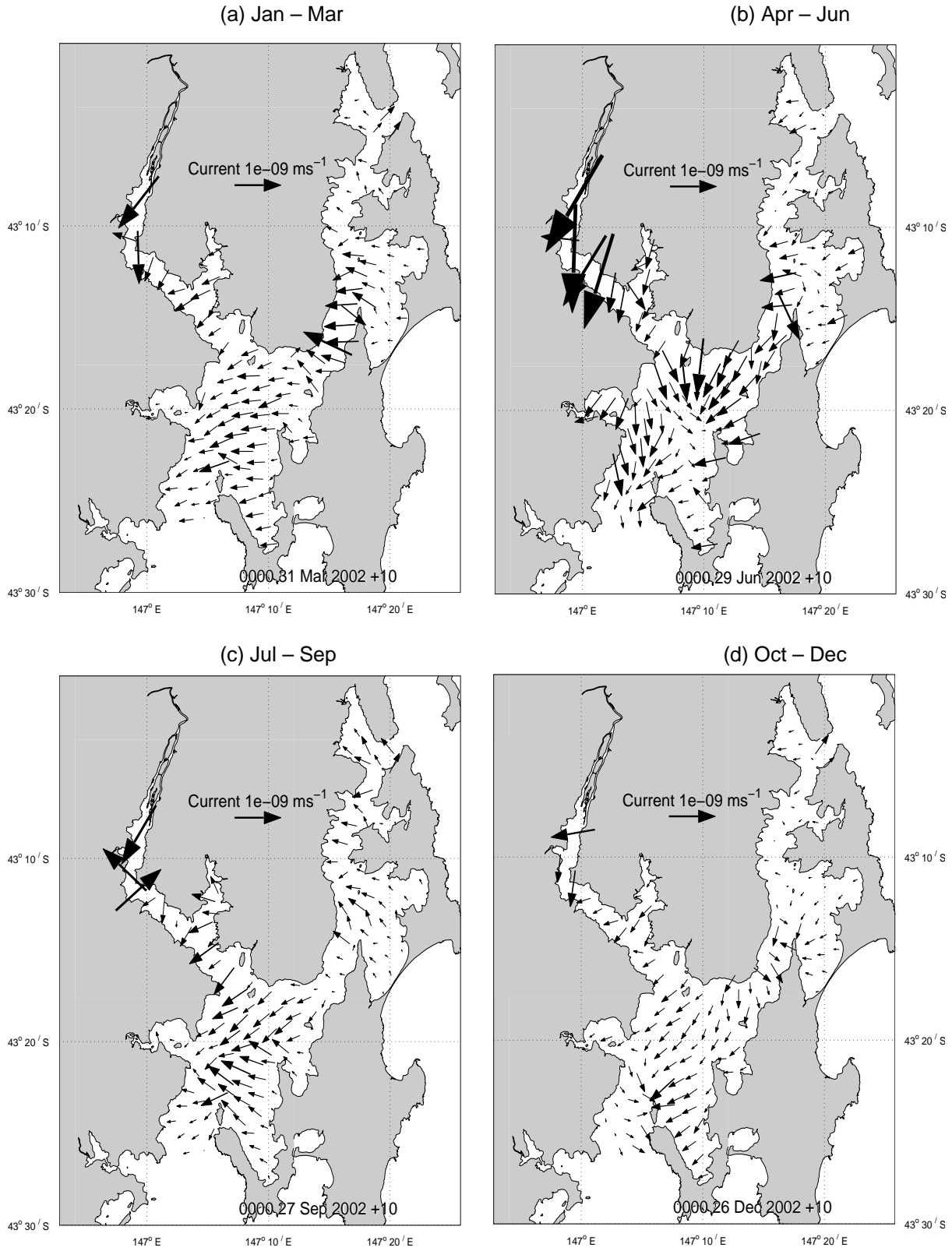


**Fig. 54. Mean Surface Barotropic Pressure Gradient Tendency**

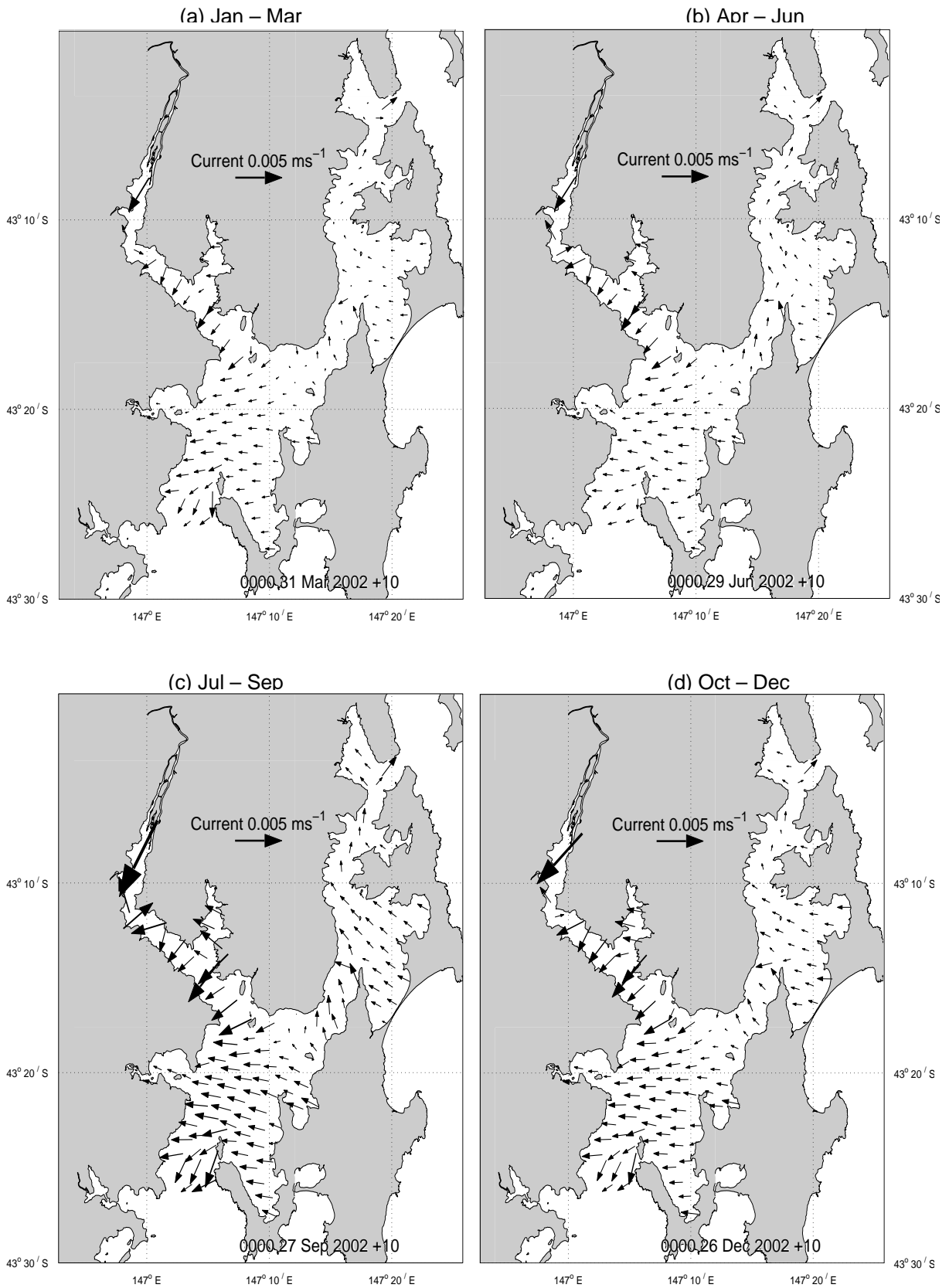


**Fig. 55. Mean Surface Baroclinic Pressure Gradient Tendency**

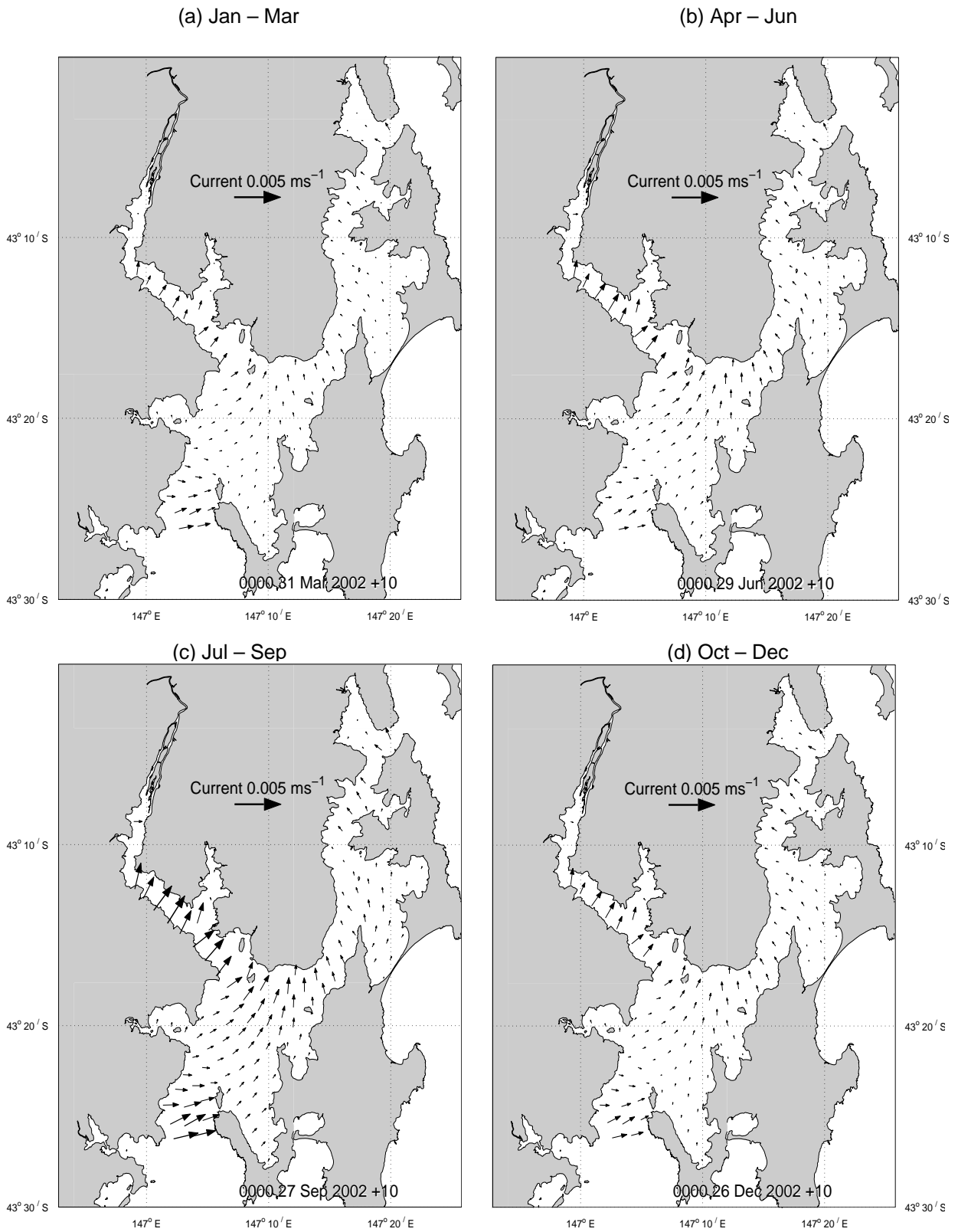


**Fig. 56. Mean Surface Coriolis Tendency**

## 7.5 Flushing Times

Passive tracers were used to obtain an estimate of the flushing characteristics of the estuary. A passive tracer was initialized in a sub-region of the estuary (Fig. 57) with a concentration of 1 and zero elsewhere, and the total mass in this sub-region was calculated throughout the simulation. Full forcing was applied to the domain (i.e. wind, tide, low frequency sea level and temperature / salinity effects) and the tracer distribution was simulated for a fixed period (14 days in this case). The e-folding time for flushing this sub-region is encountered when the total mass was reduced to  $1/e$  ( $\sim 38\%$ ) of the initial mass.

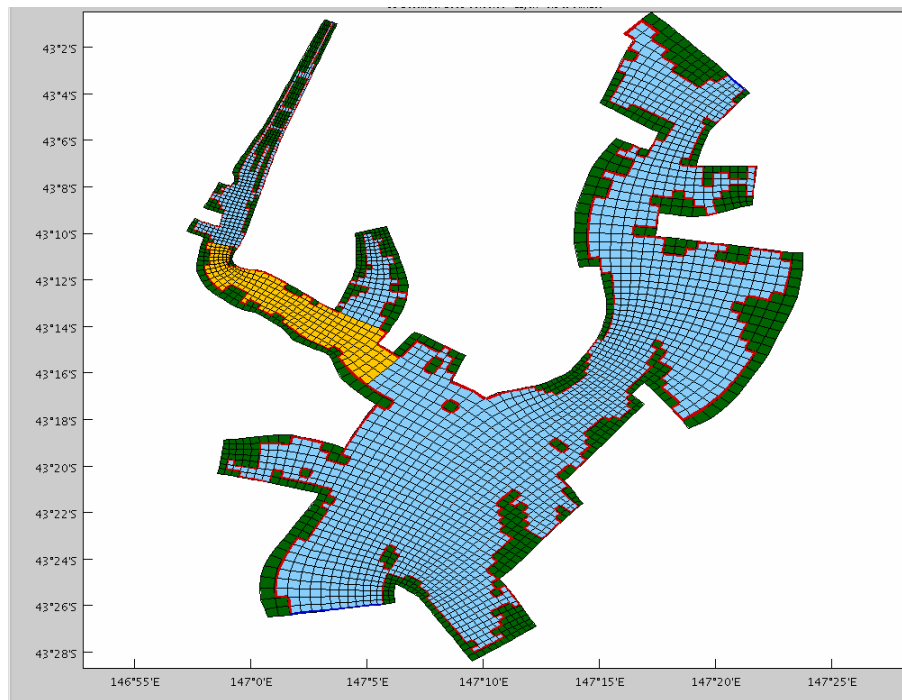


**Fig. 57. Huon flushing region**

Flushing times were calculated for the dates 14 Feb, 15 Apr, 14 Jul and 17 Oct. Time series of the normalized total mass in the sub-region for these times is displayed in Figs 58 to 61 respectively. The general trend of tracer decrease is obtained by fitting a curve to the total mass, from which it can be seen that the e-folding time for this sub-region varies from approximately 3.5 to 9.5 days depending on the magnitude of the Huon River flow, with faster flushing rates for higher flows. The passive tracer distribution in the surface layer at the end of the simulation is shown in Fig. 62 to 65. Maximum surface tracer concentration is found at the head of the estuary after 14 days, with significant concentrations ( $> 0.7$ , i.e. 70% of the original concentration) for low flows. The large flows in October deliver some tracer to the northern end of D'Entrecasteaux Channel.

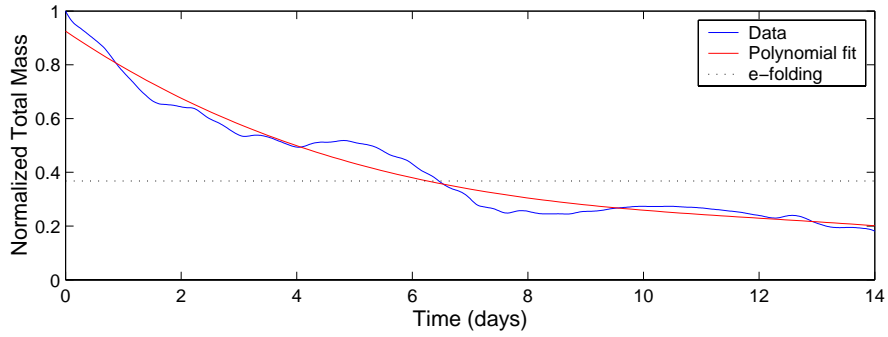


**Fig. 58. Flushing time initiated on 14 Feb 2002; max flow =  $131 \text{ m}^3\text{s}^{-1}$**

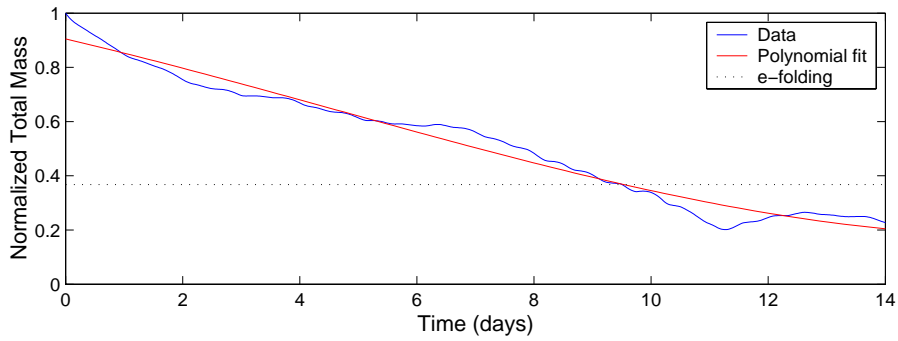


**Fig. 59. Flushing time initiated on 15 Apr 2002; max flow =  $128 \text{ m}^3\text{s}^{-1}$**

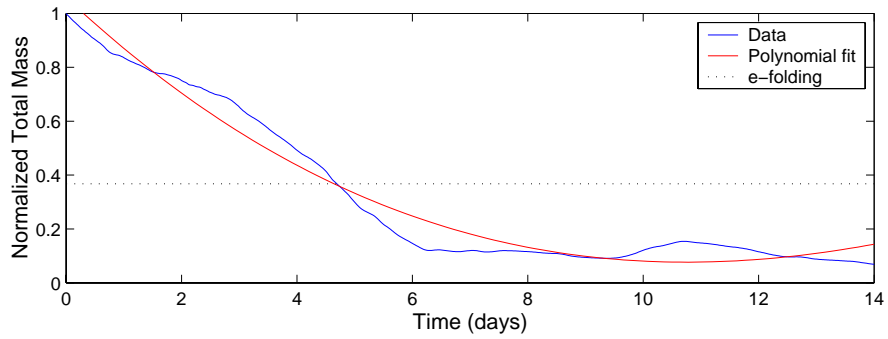


**Fig. 60. Flushing time initiated on 14 Jul 2002; max flow =  $229 \text{ m}^3\text{s}^{-1}$**

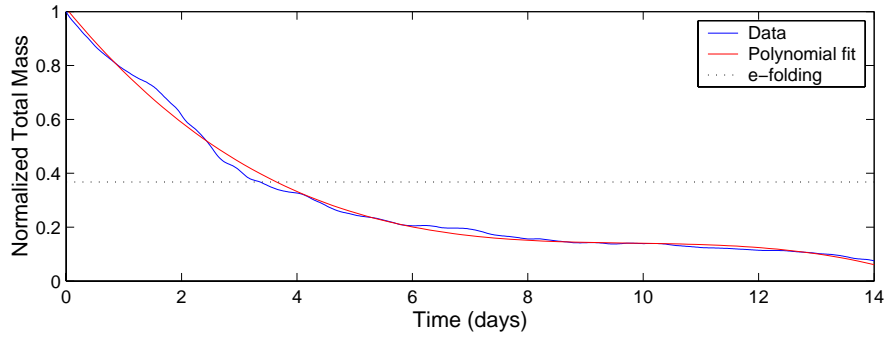


**Fig. 61. Flushing time initiated on 17 Oct 2002; max flow = 537 m<sup>3</sup>s<sup>-1</sup>**

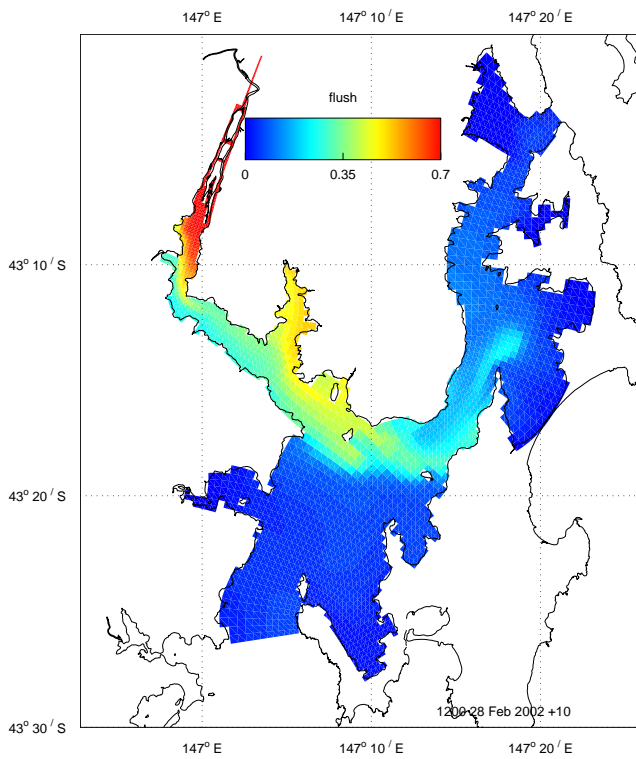


**Fig. 62. Flushing tracer distribution: Feb**

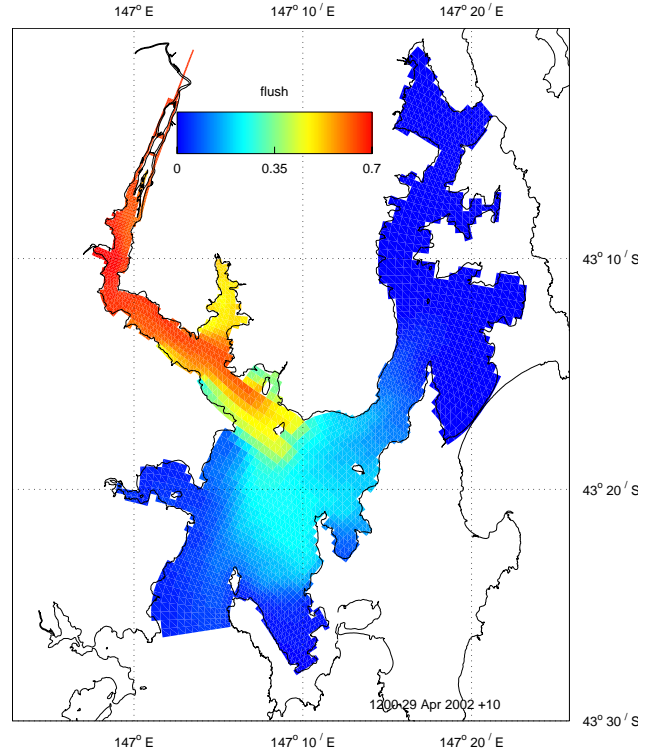


**Fig. 63. Flushing tracer distribution: Apr**

Flushing of the D'Entrecasteaux Channel was estimated by initializing tracer in the sub-region depicted in Fig. 66. Note that this flushing estimate is for the main channel only, excluding the side bays, therefore mass in the flushing region is reduced by advection and mixing through the open boundaries, into the Huon Estuary and into the side bays. Time series for tracer initialization on 14 Feb, 15 Apr, 14 Jul and 17 Oct are displayed in Figs 67 to 70.

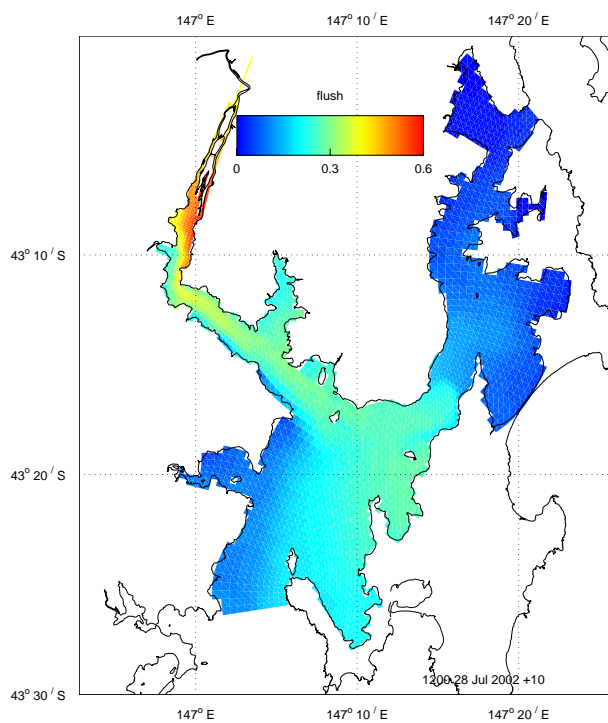


**Fig. 64. Flushing tracer distribution: Jul**

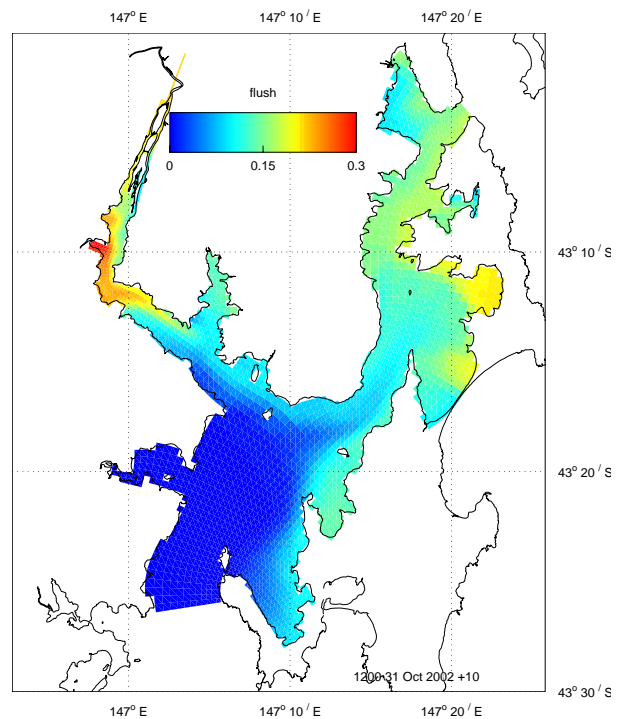


**Fig. 65. Flushing tracer distribution: Oct**

Flushing times for the main channel range from 7.5 days in February to 8.8 in October. Surface concentrations after 14 days of simulation are displayed in Figs 71 to 74. Surface concentration generally is higher (up to 0.7 in April) in the northern end of the channel and remains low in the southern end and upper Huon Estuary. The high flow case (October) results in highest concentrations in the lower Huon.

The open boundary conditions used on the flushing tracer were such that if flow is directed out of the domain, then boundary concentrations are set reflecting advection of tracer having interior values onto the boundary. If flow is directed into the domain, then boundary concentrations are set assuming advection of zero concentration into the domain. Hence if flow is into the domain, mass is decreased since new water (having zero tracer concentration) is brought into the flushing region. Two scenarios were

explored where each open boundary was separately given a zero-flux boundary condition; i.e. no new water is brought into the domain. This allows assessment as to which boundary is responsible for bringing the majority of new water into the flushing region. Time series of normalized total mass during July for the cases when southern and northern boundaries only can bring in new water are displayed in Fig. 75 and 76 respectively. It can be seen that the northern boundary is responsible for little import of new water, with total mass never reaching the e-folding fraction after 14 days. In fact total mass is approaching steady state, indicating that after an initial decrease while tracer is mixed into the side bays and Huon, there is negligible import of new water and this boundary must be associated with mass export. The southern boundary is almost exclusively responsible for bringing in new water with zero concentration tracer, since the flushing time in this case is 8.2 days, only marginally longer than the 8.0 days when both boundaries were open.

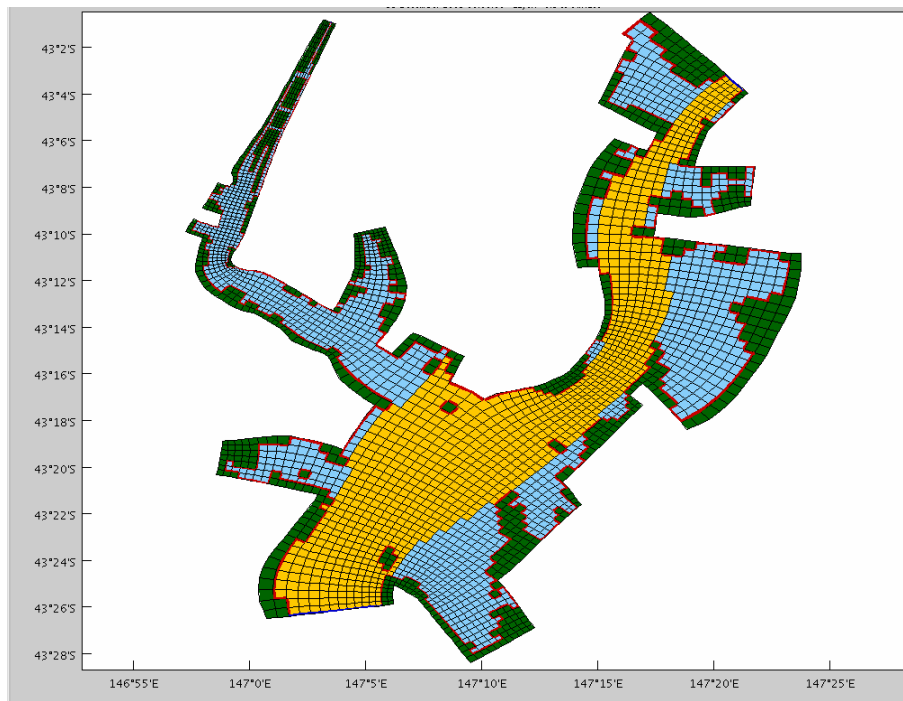


**Fig. 66. D'Entrecasteaux flushing region**

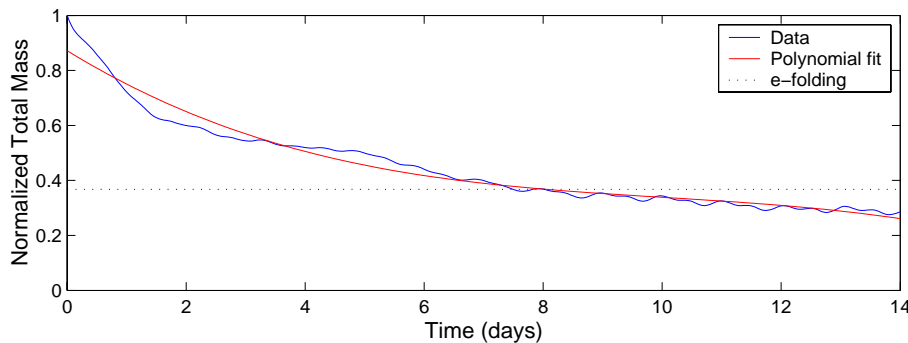


**Fig. 67. Flushing time initiated on 14 Feb 2002; max flow = 131 m<sup>3</sup>s<sup>-1</sup>**

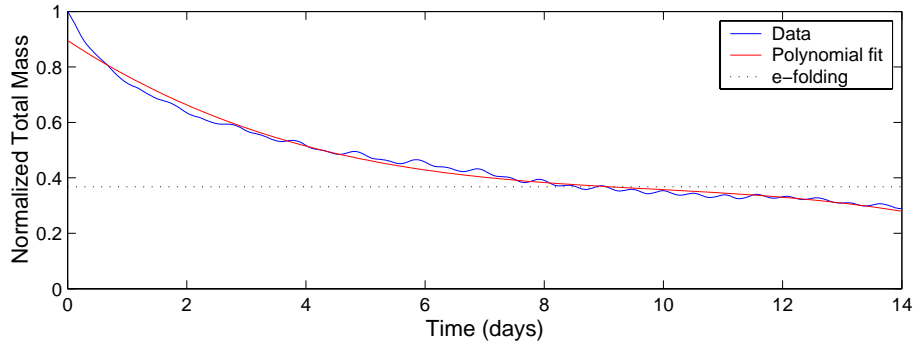


**Fig. 68. Flushing time initiated on 15 Apr 2002; max flow = 128 m<sup>3</sup>s<sup>-1</sup>**

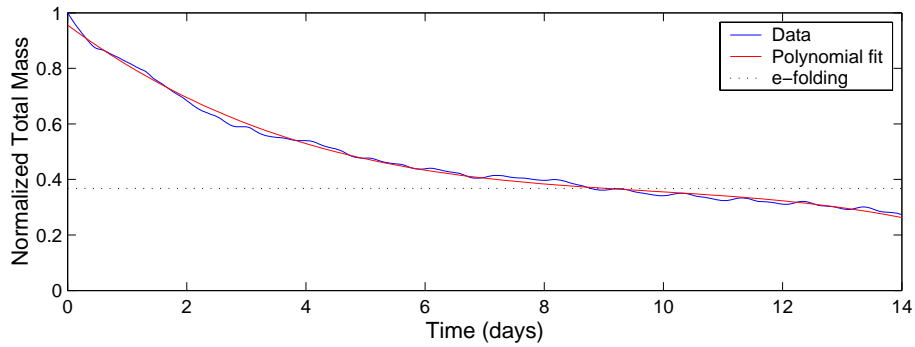


**Fig. 69. Flushing time initiated on 14 Jul 2002; max flow = 229 m<sup>3</sup>s<sup>-1</sup>**

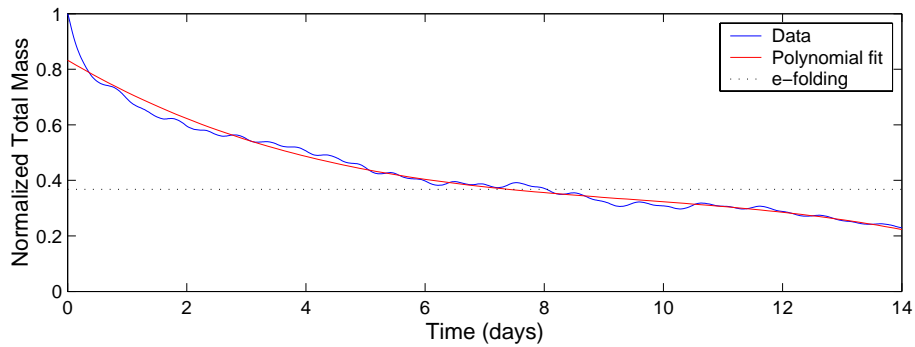


**Fig. 70. Flushing time initiated on 17 Oct 2002; max flow = 537 m<sup>3</sup>s<sup>-1</sup>**

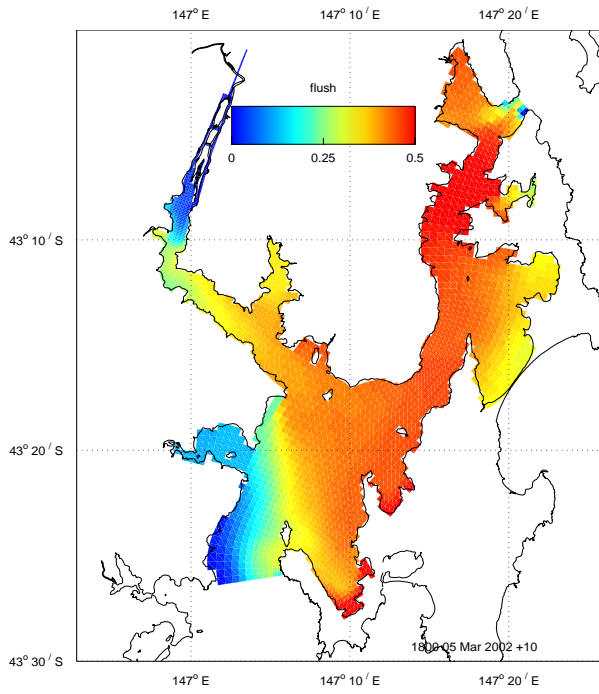


**Fig. 71. Flushing tracer distribution: Feb**

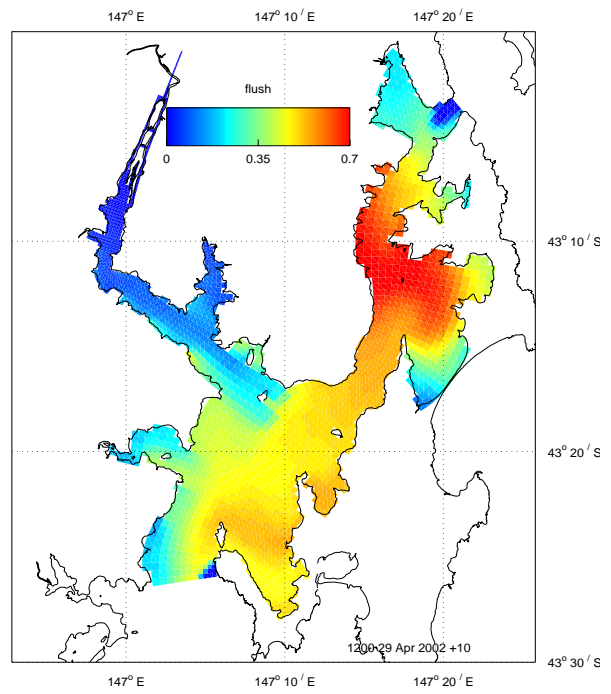


**Fig. 72. Flushing tracer distribution: Apr**

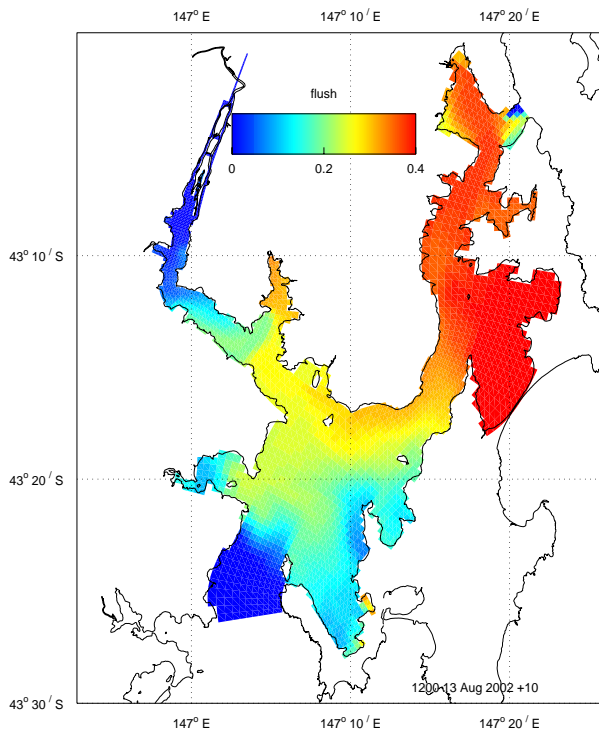


**Fig. 73: Flushing tracer distribution: Jul**

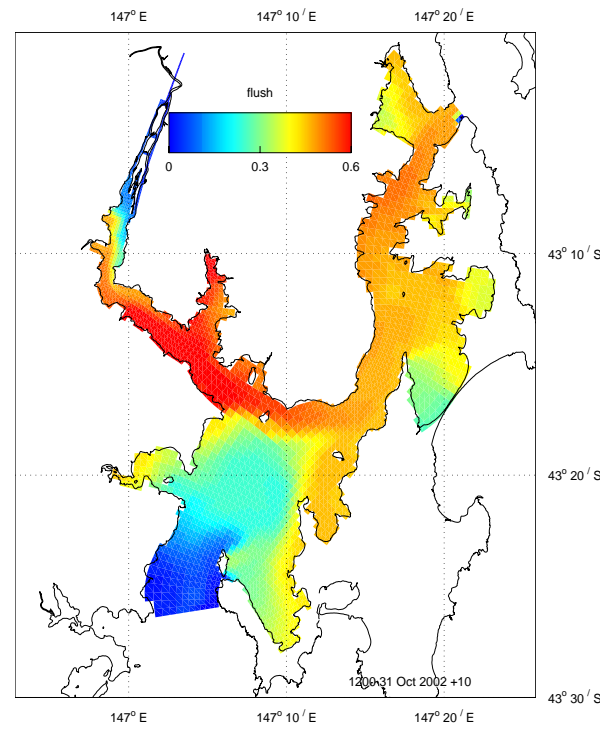


**Fig. 74: Flushing tracer distribution: Oct**

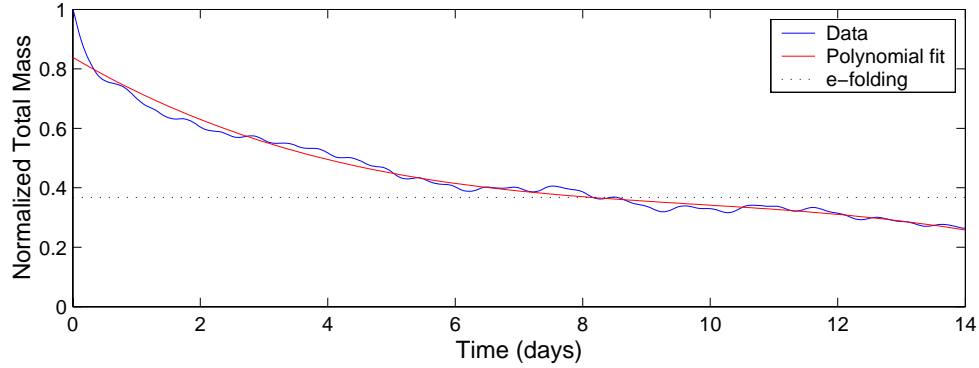


**Fig 75. D’Entrecasteaux flushing through southern boundary only**

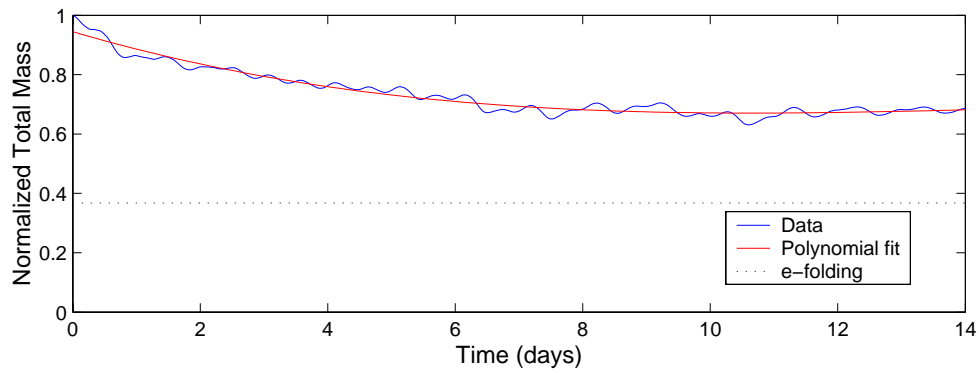


**Fig 76. D’Entrecasteaux flushing through northern boundary only**

The flushing region was set to the complete domain, excluding the upper reaches of the Huon Estuary (Fig. 77a). Time series of normalized total mass during July is displayed in Fig. 77b, and the surface concentration after 30 days in Fig. 77c. Flushing time in this case is 19.8 days. Maximum surface concentrations are approximately 0.8 in Great Bay after 30 days. Minimum concentrations are in the lower D’Entrecasteaux Channel and Huon Estuary. The northern Channel generally contains tracer with higher concentration than the lower, due to the southern boundary being the major supplier of new water.

Similar flushing experiments were conducted from all major side bays in the D’Entrecasteaux for July 2002 only. Although flushing times are expected to vary at other times of the year, this provides a relative comparison of various regions in the D’Entrecasteaux. Results are presented in Figs 78 to 85 and summarized in Table 6. North West Bay resulted in the shortest flushing time of 5 days for this time period, and Barnes Bay the longest with 10.3 days.

**Table 6. Summary of flushing times for major side bays**

Region	Date	River Flow (m <sup>3</sup> s <sup>-1</sup> )	Flushing Time (days)
Lower Huon Estuary	Feb 2002	131	6.5
Lower Huon Estuary	Apr 2002	128	9.5
Lower Huon Estuary	Jul 2002	229	4.7
Lower Huon Estuary	Oct 2002	537	3.4
Main D'Ent Channel	Feb 2002	131	7.5
Main D'Ent Channel	Apr 2002	128	8.5
Main D'Ent Channel	Jul 2002	229	8.0
Main D'Ent Channel	Oct 2002	537	8.8
Whole domain	Jul 2002	229	19.8
NWB	Jul 2002	229	5.0
Port Esperance	Jul 2002	229	5.1
Barnes Bay	Jul 2002	229	10.3
Great Bay	Jul 2002	229	7.4
Isthmus Bay	Jul 2002	229	9.5
Little Taylors Bay	Jul 2002	229	6.3
Great Taylors Bay	Jul 2002	229	6.9
Isthmus + Great Bays	Jul 2002	229	13.6

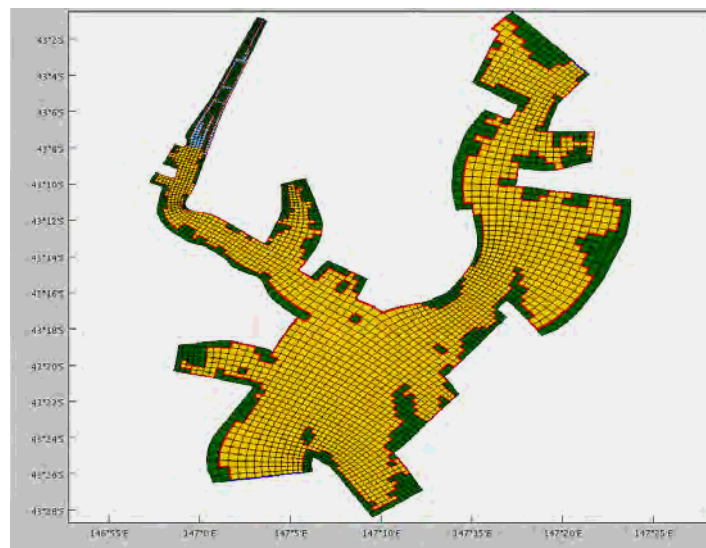


**Fig 77(a). D'Entrecasteaux – Huon flushing region**

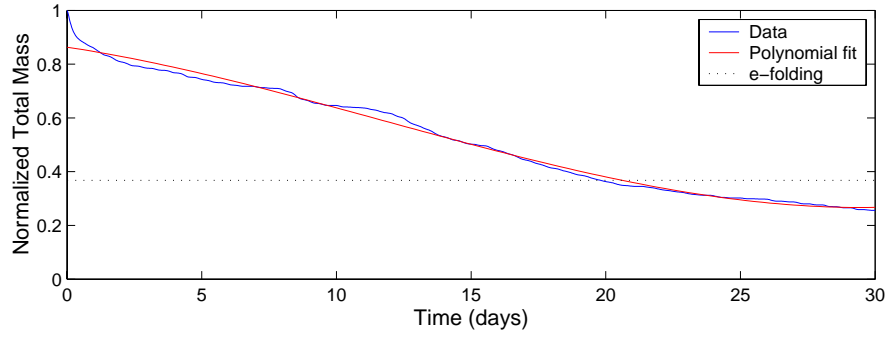


**Fig. 77(b). Flushing time initiated on 14 Jul 2002; max flow =  $229 \text{ m}^3\text{s}^{-1}$**

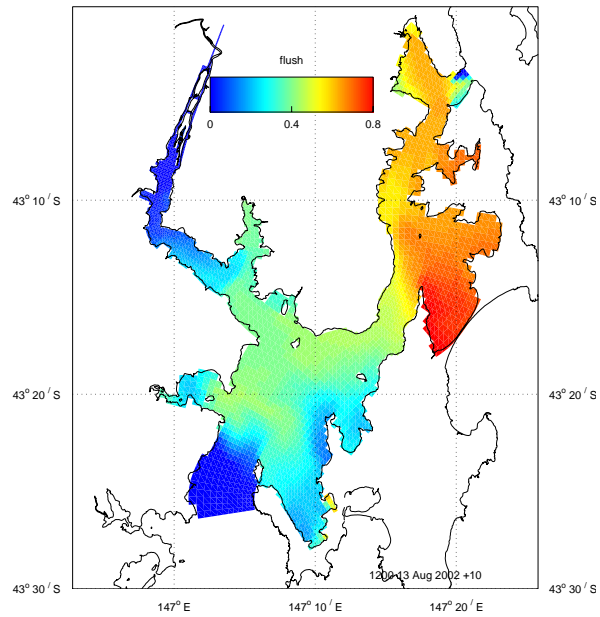


**Fig. 77(c). D'Entrecasteaux Channel – Huon flushing tracer distribution: Jul**

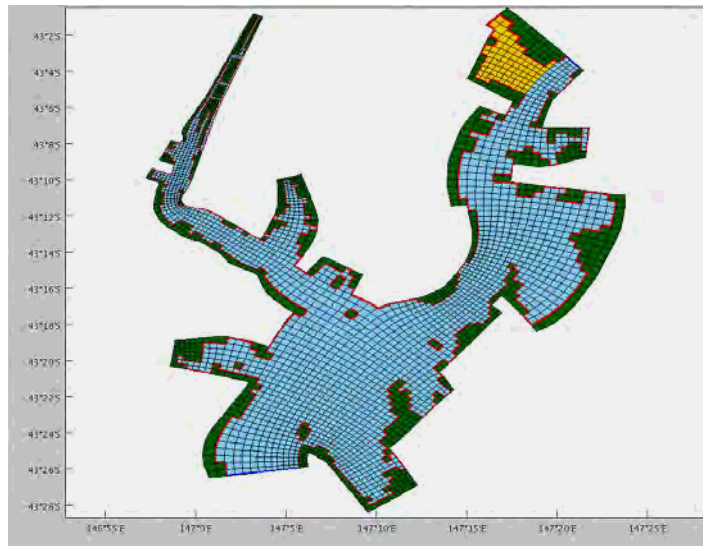


**Fig. 78(a). North West Bay flushing region**

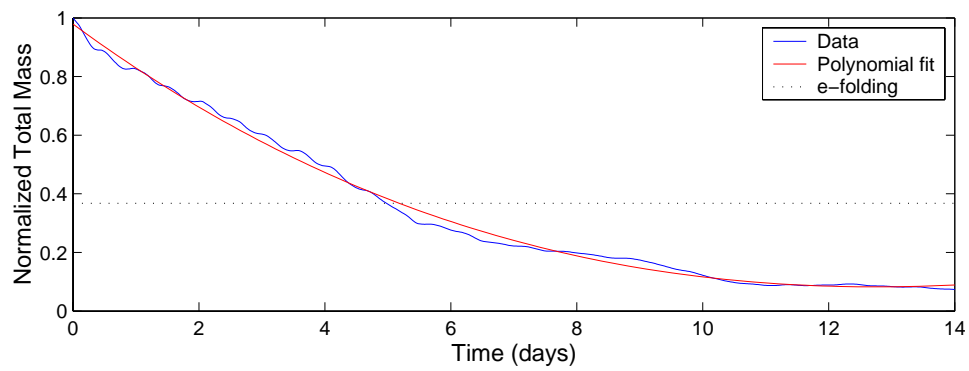


**Fig. 78(b). Flushing time initiated on 14 Jul 2002; ; max flow = 229 m<sup>3</sup>s<sup>-1</sup>**

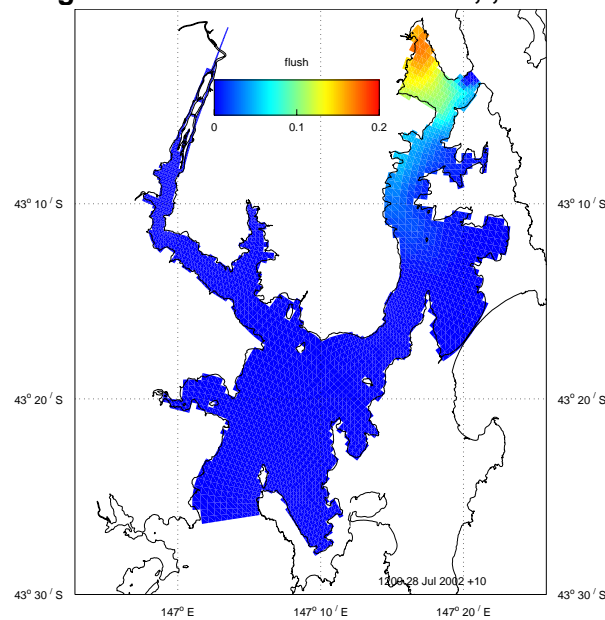


**Fig. 78(c). North West Bay flushing tracer distribution: July**

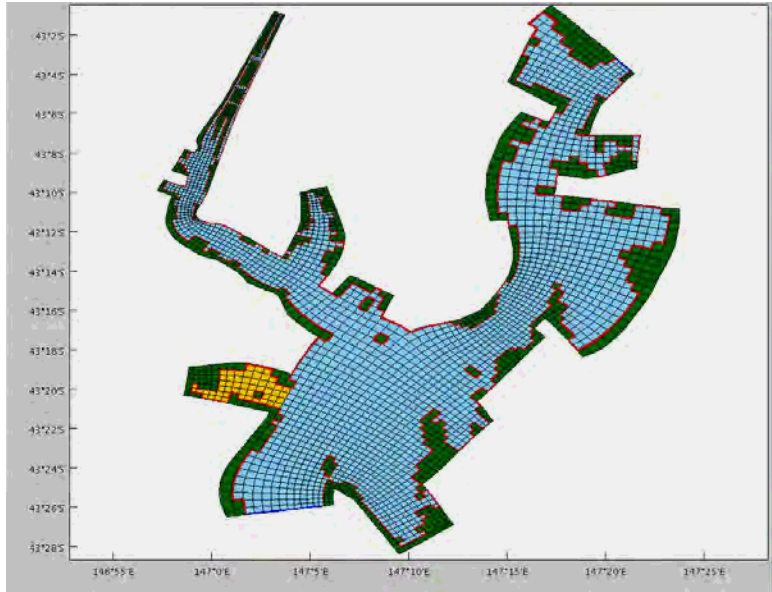


**Fig. 79(a). Port Esperance Bay flushing region**

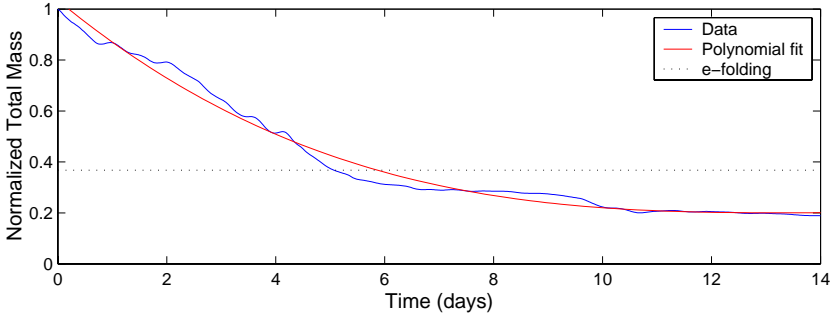


**Fig. 79(b). Flushing time initiated on 14 Jul 2002; max flow = 229 m<sup>3</sup>s<sup>-1</sup>**

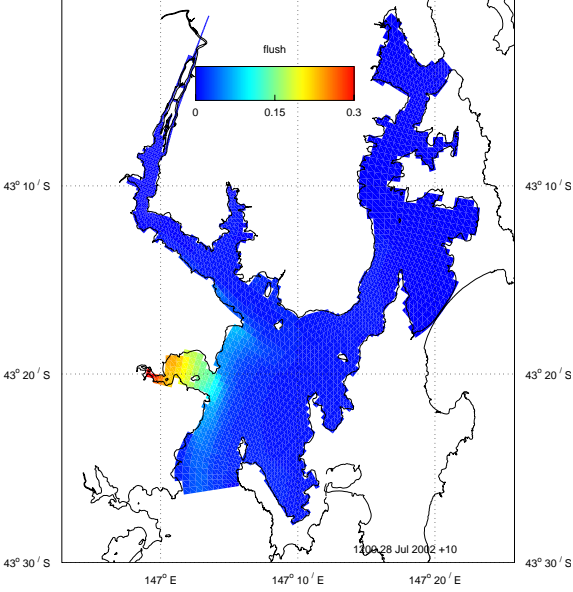


**Fig. 79(c). Port Esperance Bay flushing tracer distribution: Jul**

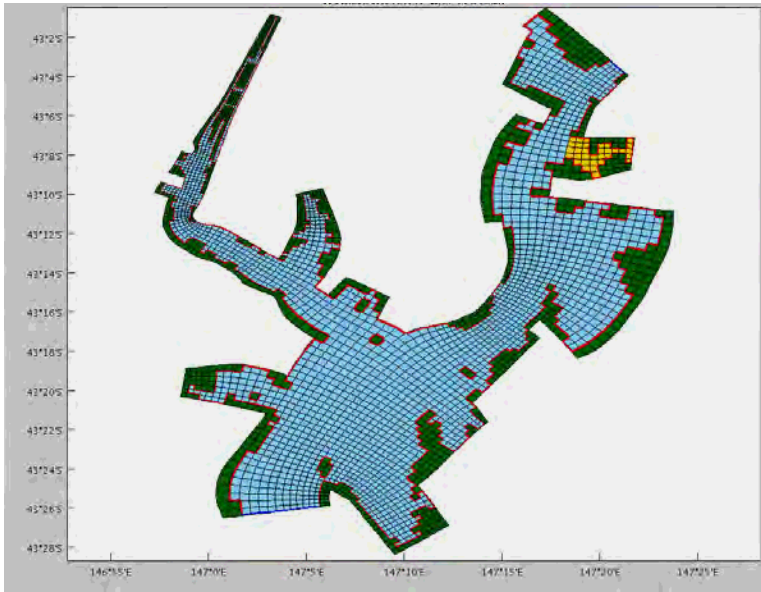


**Fig. 80(a). Barnes Bay flushing region**

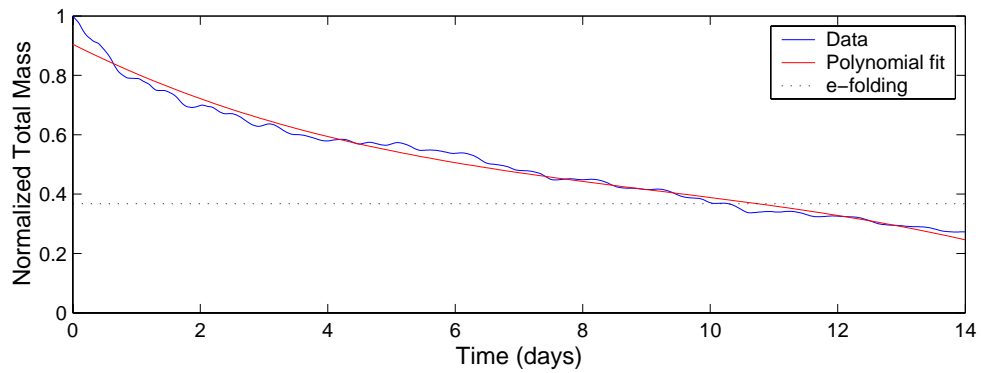


**Fig. 80(b). Flushing time initiated on 14 Jul 2002; max flow = 229 m<sup>3</sup>s<sup>-1</sup>**

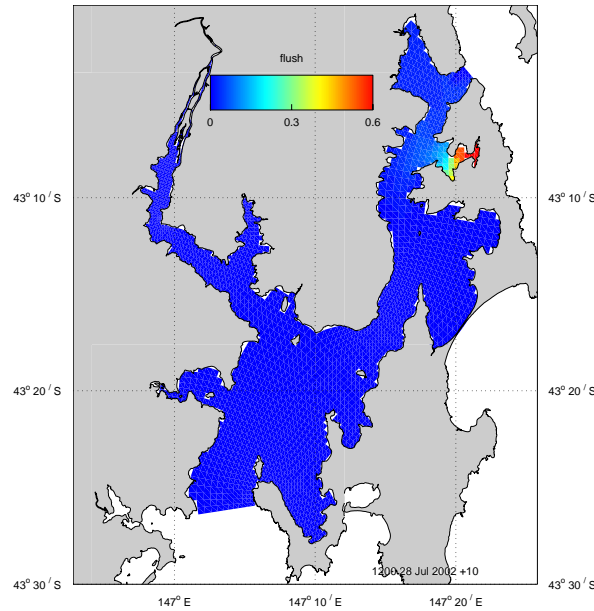


**Fig. 80(c). Barnes Bay flushing tracer distribution: Jul**

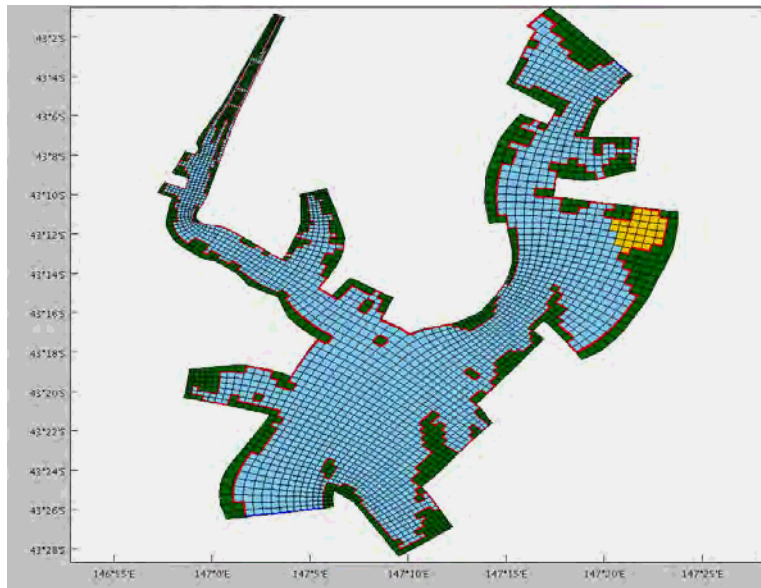


**Fig. 81(a). Great Bay flushing region**

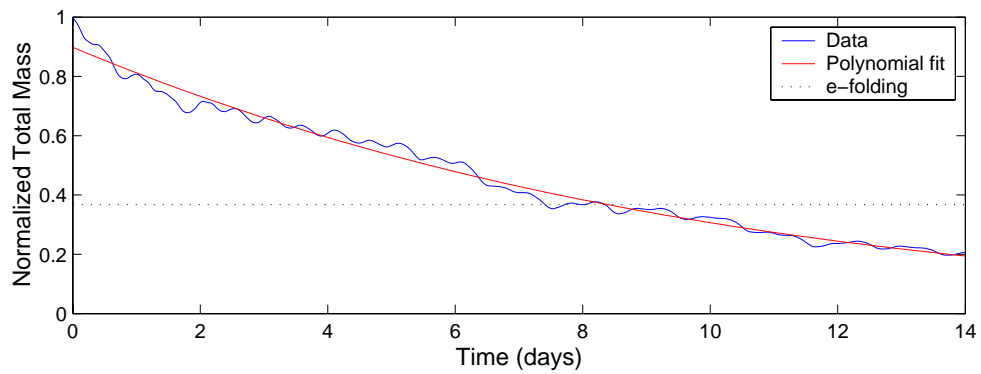


**Fig. 81(b). Flushing time initiated on 14 Jul 2002; max flow =  $229 \text{ m}^3 \text{ s}^{-1}$**

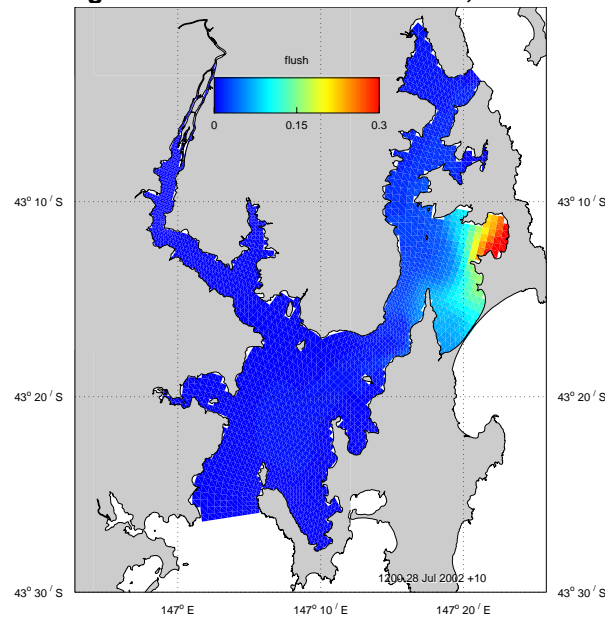


**Fig. 81(c). Great Bay flushing tracer distribution: Jul**

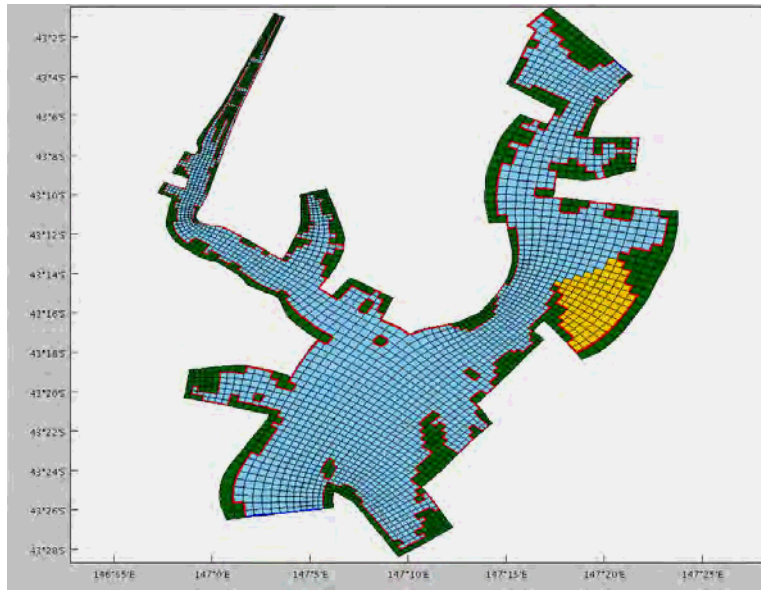


**Fig. 82(a). Isthmus Bay flushing region**

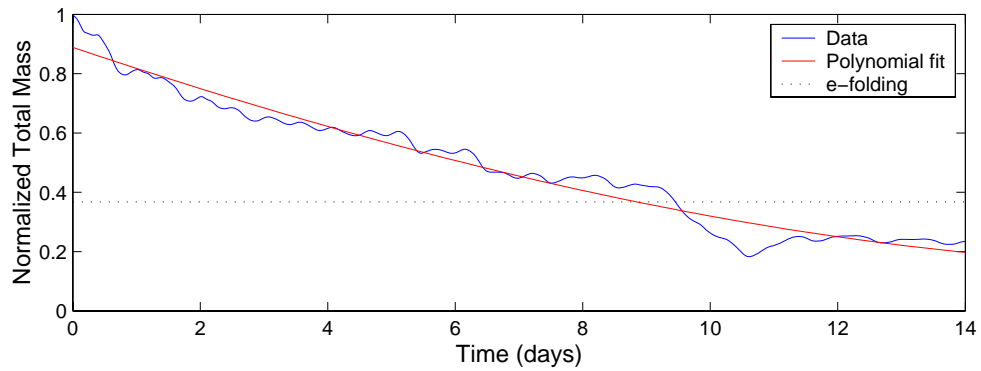


**Fig. 82(b). Flushing time initiated on 14 Jul 2002; max flow = 229 m<sup>3</sup>s<sup>-1</sup>**

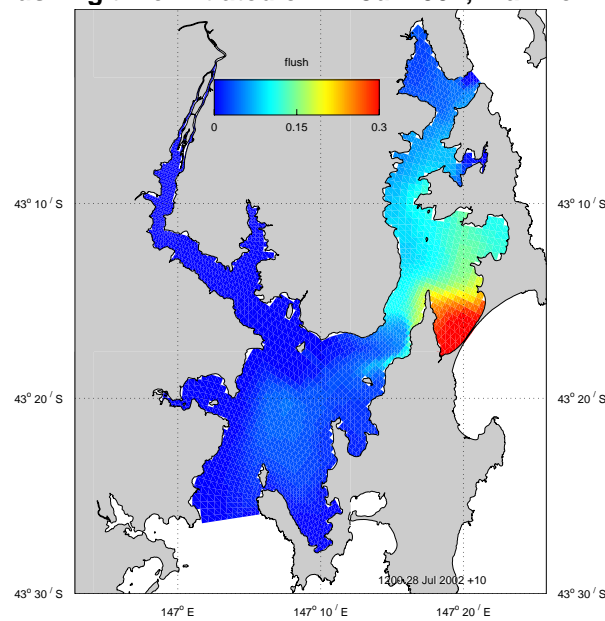


**Fig. 82(c). Isthmus Bay flushing tracer distribution: Jul**

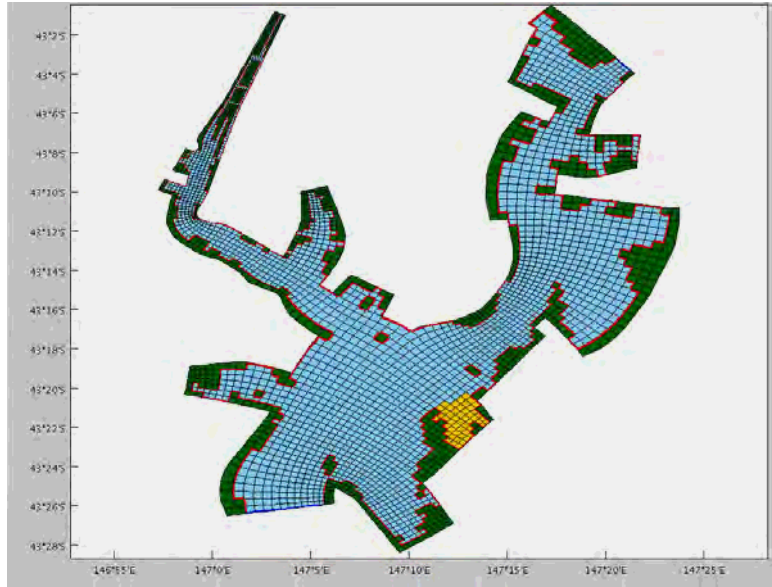


**Fig. 83(a). Little Taylors Bay flushing region**

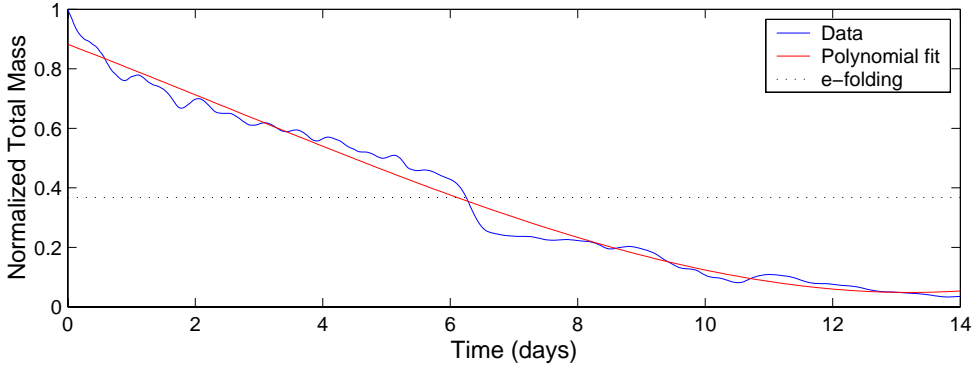


**Fig. 83(b). Flushing time initiated on 14 Jul 2002; max flow = 229 m<sup>3</sup>s<sup>-1</sup>**

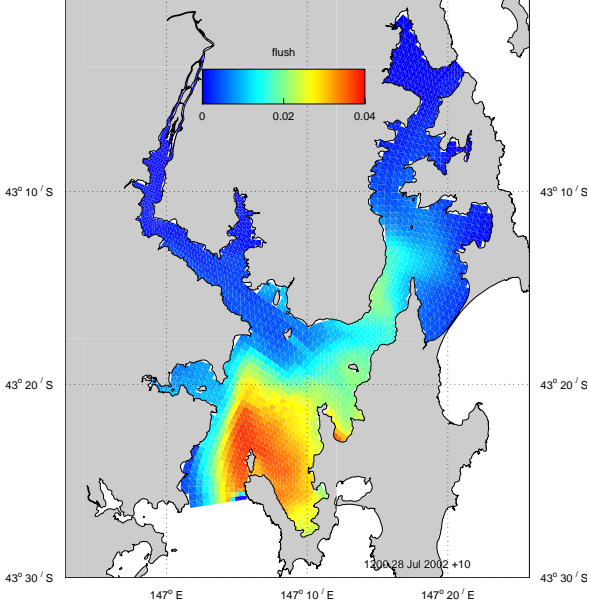


**Fig. 83(c). Little Taylors Bay flushing tracer distribution: Jul**

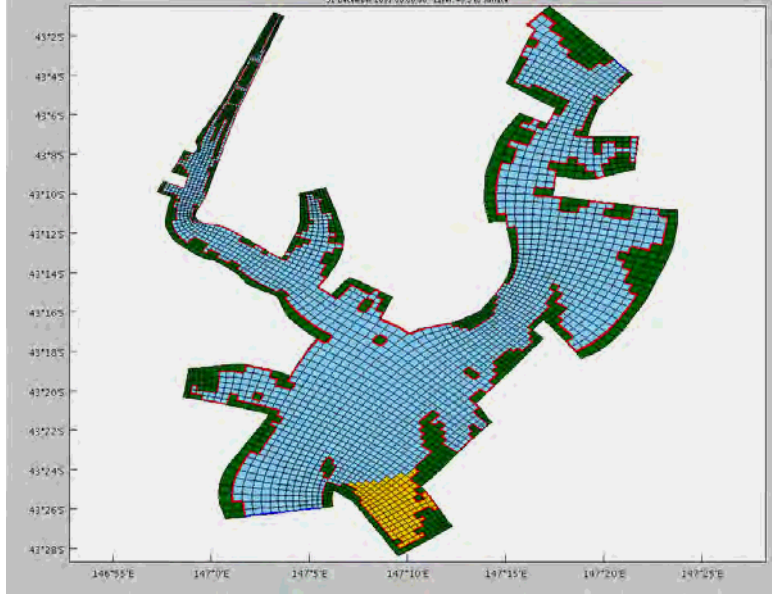


**Fig. 84(a). Great Taylors Bay flushing region**

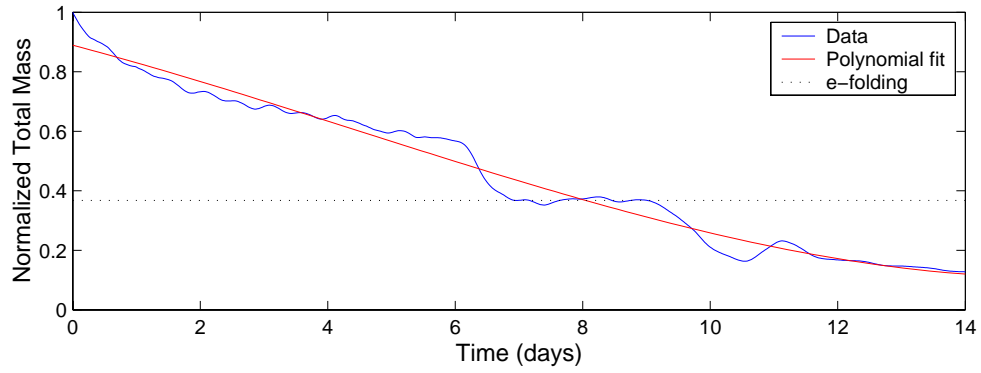


**Fig. 84(b). Flushing time initiated on 14 Jul 2002; max flow =  $229 \text{ m}^3 \text{ s}^{-1}$**

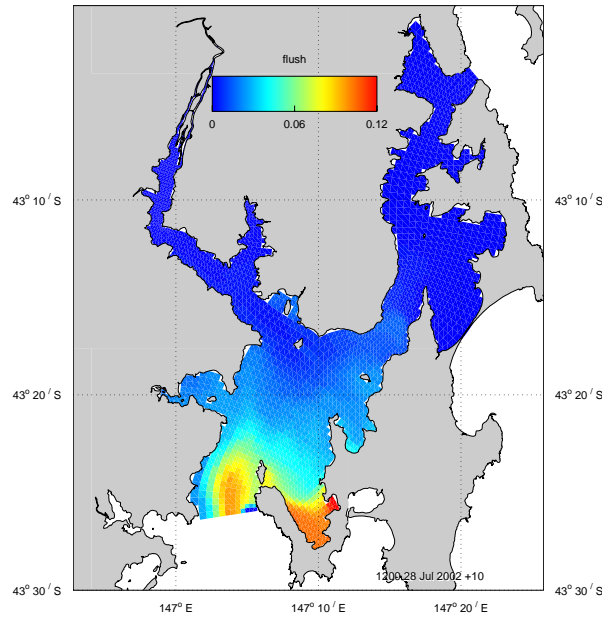


**Fig. 84(c). Great Taylors Bay flushing tracer distribution: Jul**

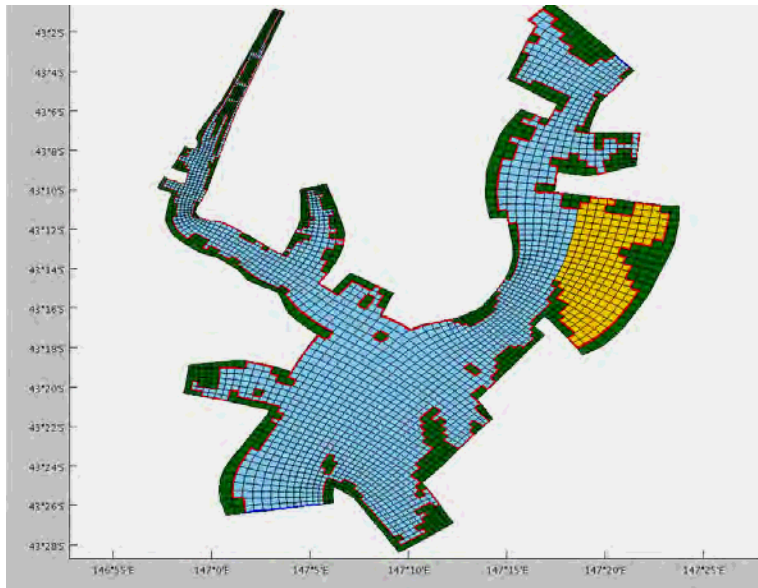


**Fig. 85(a). Isthmus + Great Bay flushing region**

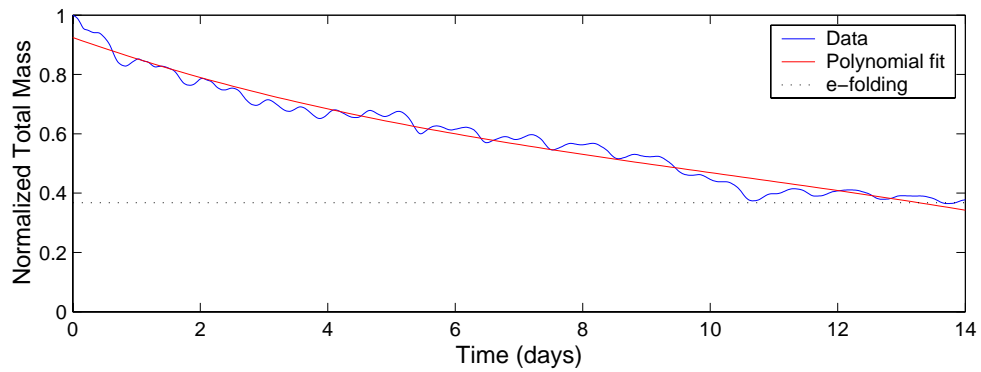


**Fig. 85(b). Flushing time initiated on 14 Jul 2002; max flow =  $229 \text{ m}^3 \text{ s}^{-1}$**

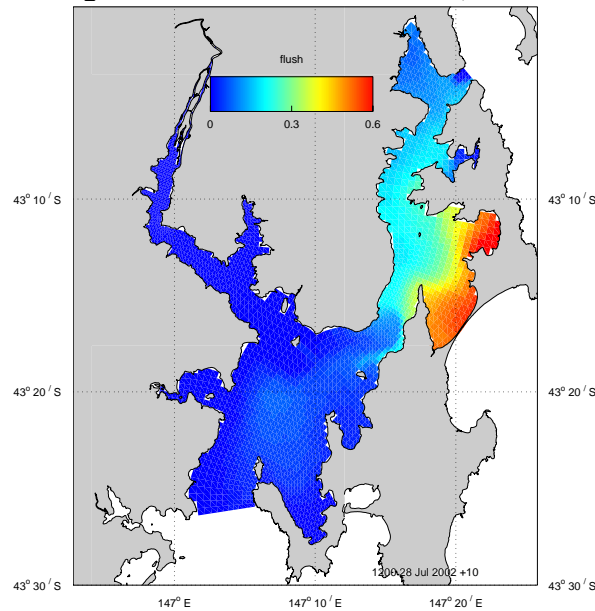


**Fig. 85(c). Isthmus + Great Bay flushing tracer distribution: Jul**

## 7.6 Residual Flow

Residual, or mean/net, flow is the long term circulation the system experiences, and contributes towards flushing the region and distributing tracers input from the open ocean throughout the system. In this case the seasonal residual was calculated by averaging the velocities from every time-step over a 90 day period. Surface and bottom mean flow for each season are displayed in Figs 86 to 89 and 90 to 93 respectively.

Surface residual currents are directed down-river in the Huon Estuary during all seasons, with maximum speeds of up to approximately  $0.2 \text{ ms}^{-1}$  in the winter and spring when rainfall (hence river flow) is greatest. This river flow enters the channel and flows predominantly up-channel towards the north. Some flow is observed down-channel to the southern boundary.

The bottom flow is strongly directed into the domain at the southern boundary and continues northward towards the Huon Estuary mouth. Here the flow splits with the majority of water continuing upstream into the Huon Estuary along the southern bank, a smaller secondary bottom flow continuing through the narrowest point of the channel past Gordon into Isthmus Bay and a smaller still recirculation heading south into Great Taylor Bay (Fig. 94). Further up the Huon Estuary bottom flow is directed down-river. At the northern end of the D'Entrecasteaux Channel bottom flow is directed down-channel and into North West Bay. Away from the southern boundary bottom velocities are generally quite weak throughout the domain, of the order of  $1 \text{ cms}^{-1}$ .

The conceptual model of residual flow for the D'Entrecasteaux – Huon Estuary system is as follows: flow enters the region in bottom water at the southern end of the channel and continues along the bottom and upstream into the Huon Estuary in the salt wedge, favouring the southern bank. Entrainment occurs from the salt wedge into the downstream freshwater flow, the majority of which then turns north upon entering the channel and exits into Storm Bay at the northern end of the channel. A smaller proportion of Huon flow exits the southern channel.

The momentum balance analysis of Section 7.4 concluded that the surface residual flow is predominantly the result of density gradient forces, wind and effects of rotation. Horizontal and vertical friction becomes important in the bottom waters. A schematic of the residual flow is presented in Fig. 95.

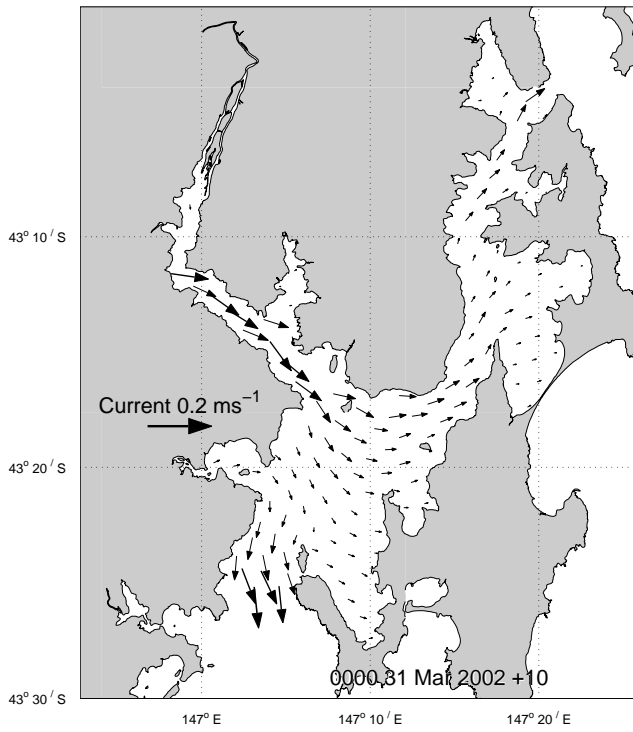


**Fig. 86: Surface mean flow, summer**

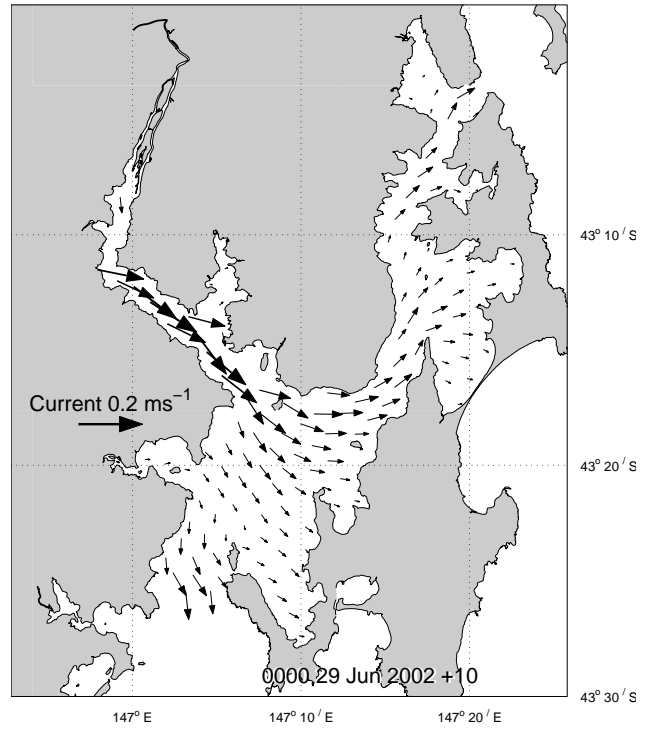


**Fig. 87: Surface mean flow, autumn**

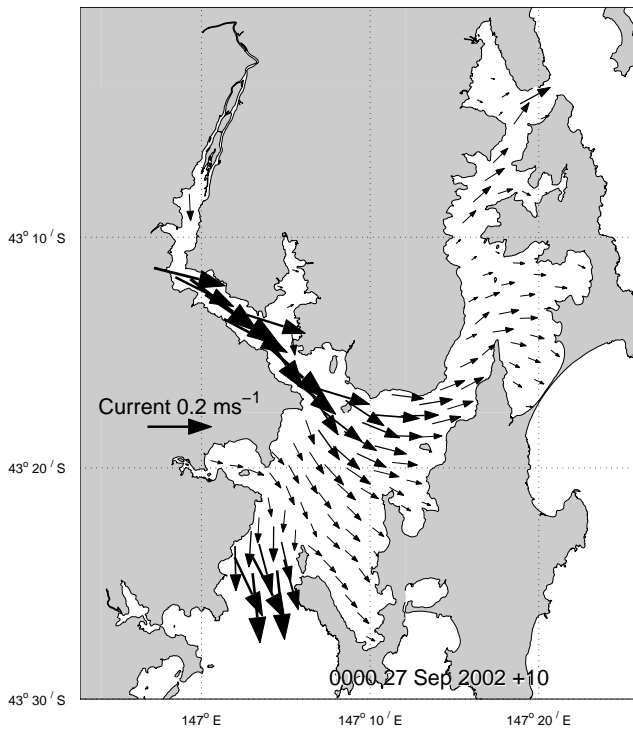


**Fig. 88: Surface mean flow, winter**

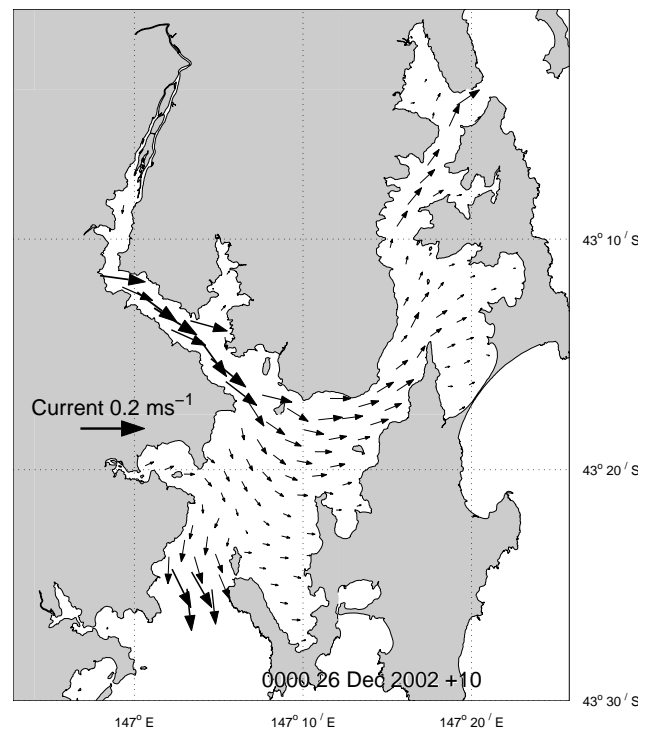


**Fig. 89: Surface mean flow, spring**

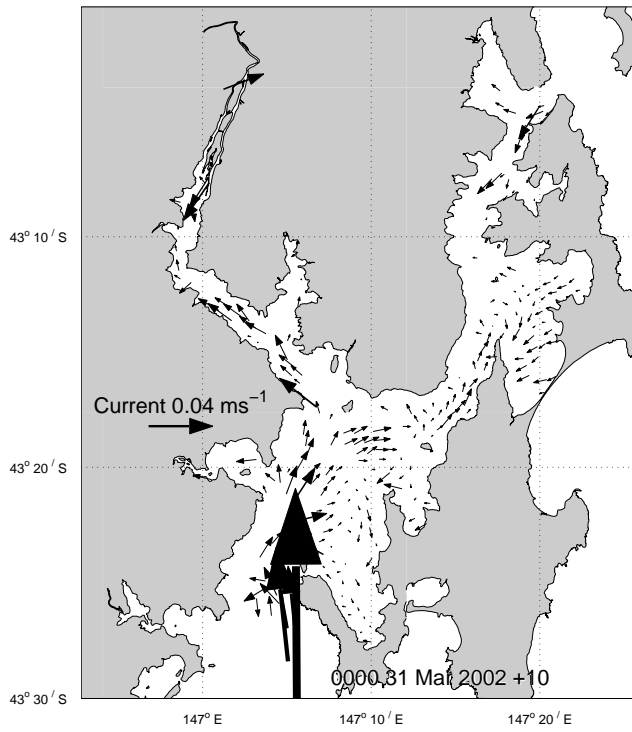


**Fig. 90: Bottom mean flow, summer**

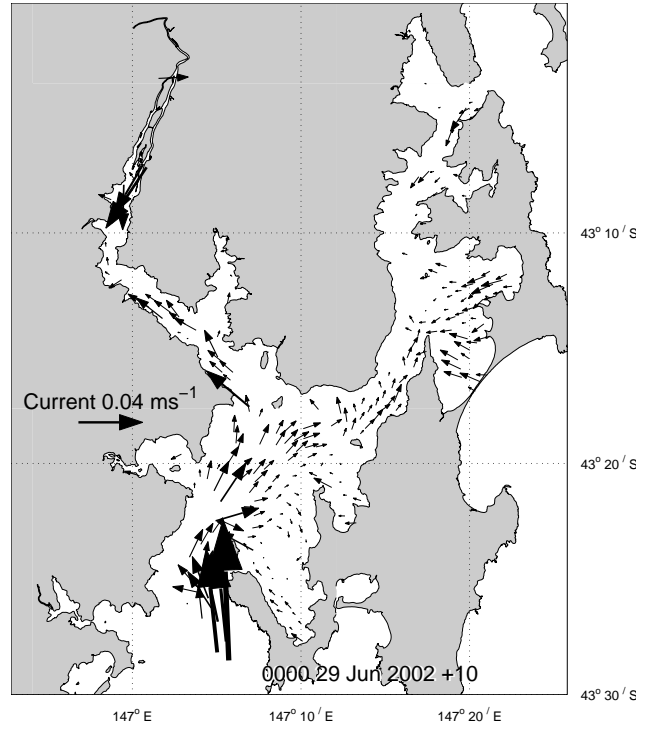


**Fig. 91: Bottom mean flow, autumn**

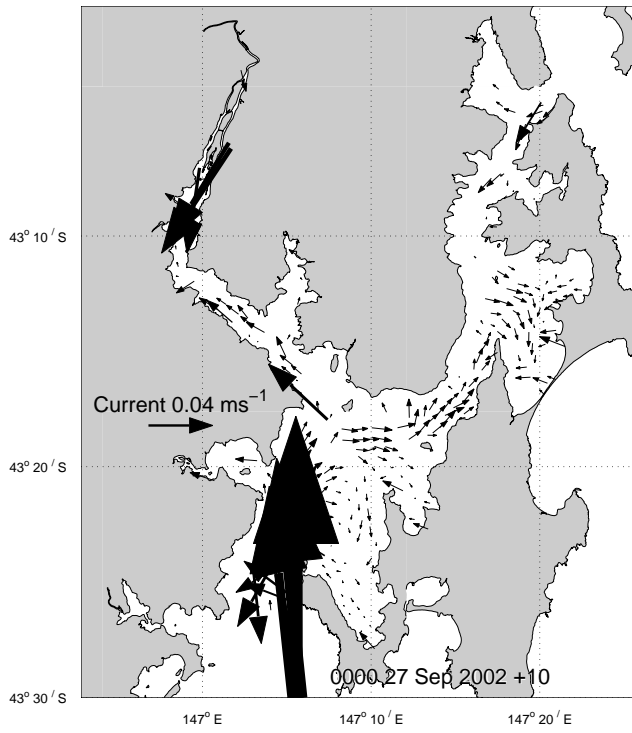


**Fig. 92: Bottom mean flow, winter**

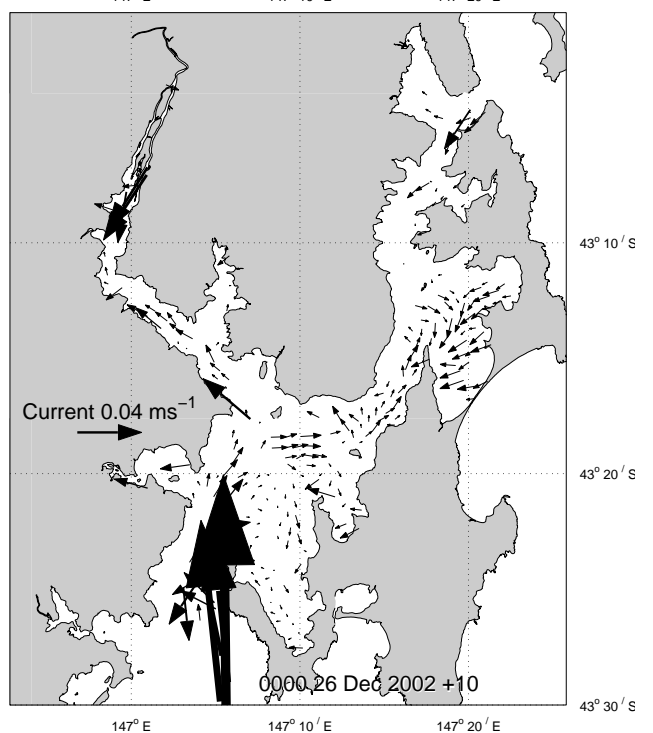


**Fig. 93: Bottom mean flow, spring**

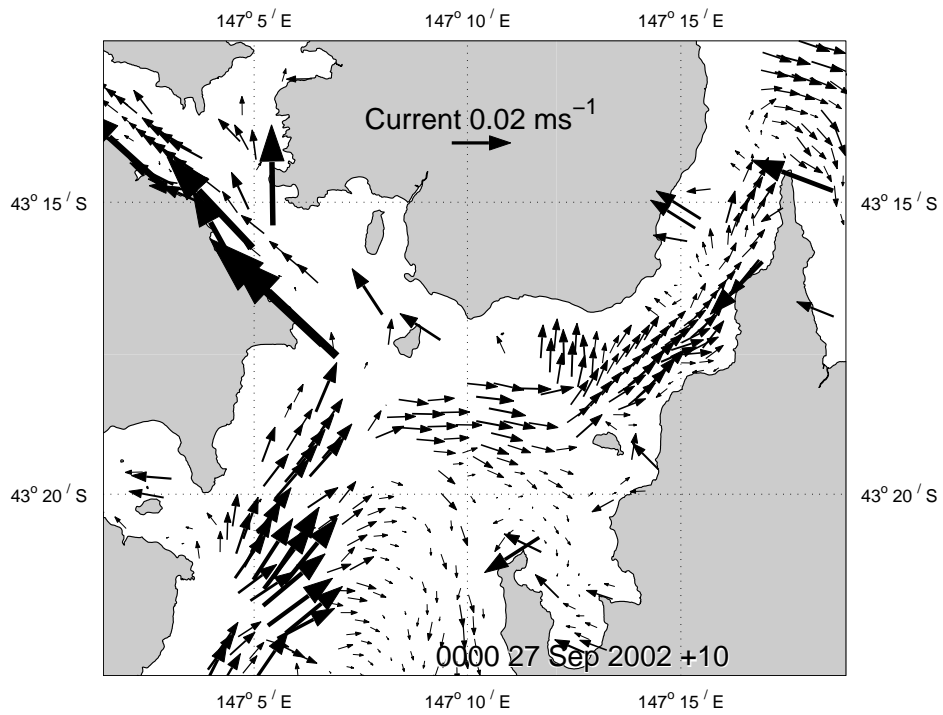


**Fig. 94. Bottom Flow near the Huon Mouth, Winter**

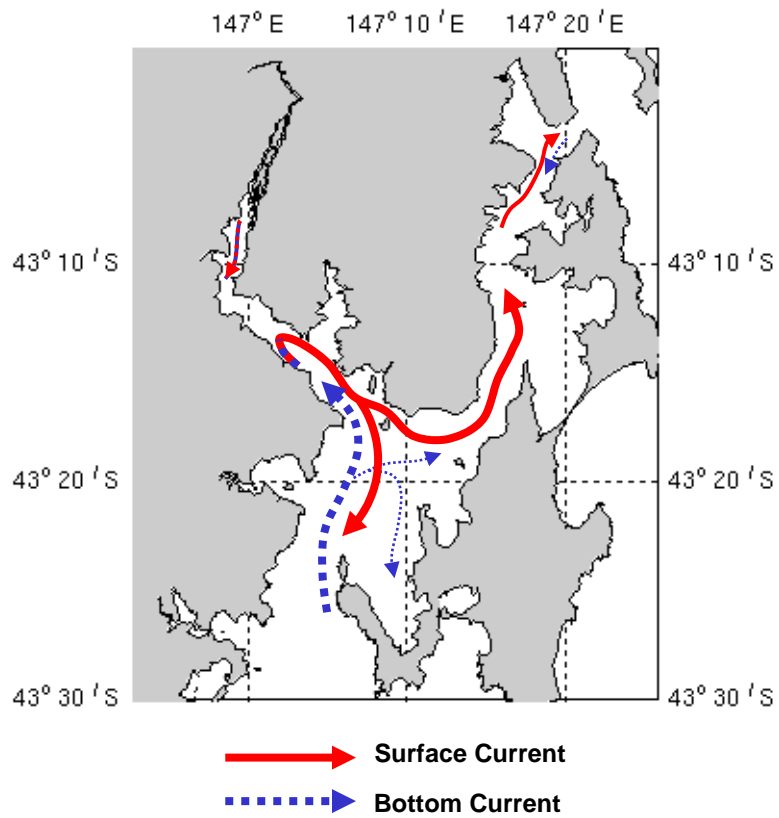


**Fig. 95. Residual Flow Schematic**

## 7.7 Point Source Releases

Point sources of tracers were continuously input into the water column at locations corresponding to a number of fish farm sites (Fig. 96 and Table 7) with unit loads (assumed to be  $1 \text{ gs}^{-1} \sim 31,500 \text{ kg/year}$ , giving output concentrations in units of  $\text{gm}^{-3}$ , or  $\text{mgL}^{-1}$ ) for the 12 month simulation period of 2002. Tracers were released over a depth range of 0 m to the shallower of 14 m depth (assumed to be the maximum depth of a farm cage) or the bottom. Surface tracer concentrations were output at 2 hour intervals and post-processed to compute the 5th, 50th (median) and 95th percentile distributions for the whole simulation, providing a statistical description of the distributions resulting from tracer transport over this period. Note that the response of the tracers to the interaction of the point source input with the system dynamics is linear, so that if the load were increased by some arbitrary factor then the corresponding concentrations can be scaled accordingly.

Results are displayed as Fig. 97 to 104. Results are interpreted thus: given that a continuous unit load is input at the Northwest farm site and its distribution throughout the domain allowed to reach quasi-steady state, at any given location in the domain one would expect to find the concentrations less than those shown in Fig. 97 (a) for 5% of the time, less than those in Fig. 97 (b) for 50% of the time and less than those in Fig. 97 (c) for 95% of the time. Note that the concentration scales in the Figures for the three percentiles differ from one another.

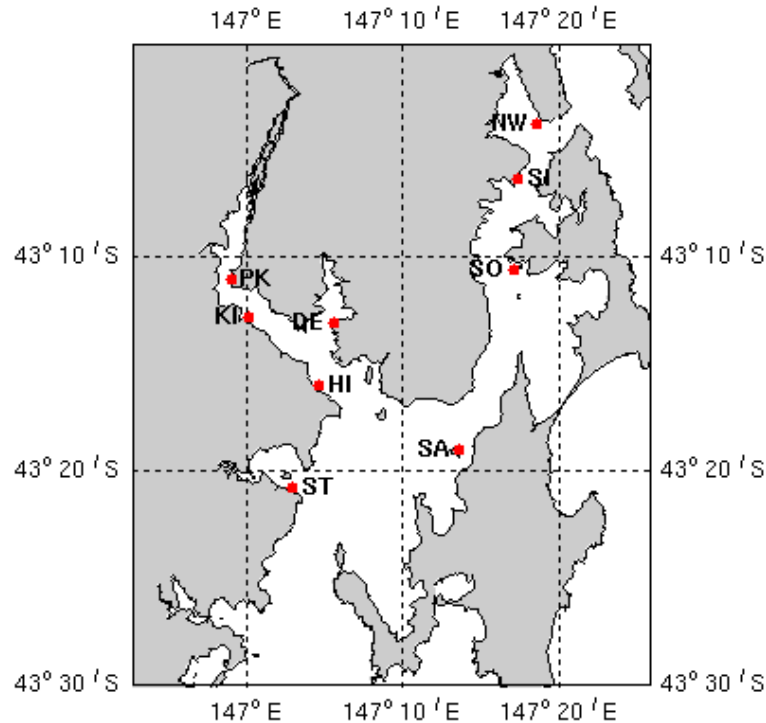


**Fig. 96. Fish Farm Locations**

**Table 7. Fish Farm Locations**

Name	Abbreviation	Latitude South	Longitude East	Release Depth (m)
NorthWest	NW	43.063020	147.309240	0 to 14
Simmonds	SI	43.105797	147.289587	0 to 10.9
Soldiers	SO	43.177225	147.285018	0 to 11.6
Satellite	SA	43.316706	147.226917	0 to 11.1
Stringers	ST	43.345850	147.049574	0 to 14
Hideaway	HI	43.267059	147.077482	0 to 14
Deep	DE	43.217831	147.093111	0 to 13.2
Killala	KI	43.213835	147.002434	0 to 9.6
Brabazon Park	PK	43.184632	146.983638	0 to 11

Release sites in the northern portion of the domain result in tracer distributions that are confined to the northern channel. Distributions from the Northwest release are mainly confined to the head of North West Bay, with median concentration of  $\sim 0.0005$  found down to Barnes Bay. Once the release moves outside of North West Bay into the channel, concentrations in the channel increase and relatively uniform distributions are observed in North West Bay. The concentrations near the Simmonds release mixing zone can reach  $\sim 0.003$ . Release at Soldiers again distributes tracer throughout the upper channel and North West Bay, although concentrations decrease slightly towards the head of North West Bay. Low concentrations are now encountered in Great Bay (median  $\sim 0.0004$ ).

Distributions resulting from release further south down the channel at Satellite exhibit a dramatic change. Tracer is now found throughout the channel, and a well defined mixing zone of several kilometers exists around the release point with median concentrations of  $\sim 0.001$ . Low concentrations are now observed in the Huon Estuary. The Stringers release site also results in tracers distributions throughout the domain, with relatively uniform distributions found outside the mixing zone region of Port Esperance. Again tracer is found within the Huon Estuary, having median concentrations of  $\sim 0.0005$  and maximums of  $\sim 0.001$ . The Hideaway release again shows relatively uniform distributions throughout the domain outside a reasonably well defined mixing zone. Median concentration in the northern channel due to release at this site are  $\sim 0.0007$ , surprisingly slightly more than median concentrations in the upper Huon of  $\sim 0.0005$ . This general distribution is repeated for the Deep release site, with the mixing zone confined to Port Cygnet and

quite uniform concentrations elsewhere, having a channel median of  $\sim 0.0007$  and 95 percentile of 0.001.

The Killala release site results in distributions that are larger in the Huon Estuary than the D'Entrecasteaux Channel. Median concentrations are 0.001 in the upper and lower Huon while channel concentrations are  $\sim 0.0007$ . Elevated concentrations are observed in the channel near the Huon mouth. Finally release at Brabazon Park results in highest concentrations in the upper Huon, which decrease down-river and into the channel. Median concentrations are  $\sim 0.006$  at Huonville and  $\sim 0.001$  throughout the channel.

The tracer distributions therefore exhibit significant variability depending on the release location. Generally those sites in the northern channel result in distributions confined to the northern D'Entrecasteaux. Releases in the channel below Gordon and in the lower Huon result in relatively uniform concentrations throughout the domain outside a well defined mixing zone having high concentration. For release sites further up the Huon Estuary, the largest concentrations are confined to the upper Huon and uniform concentrations of lower magnitude are found throughout the rest of the domain. Surprisingly, median concentrations in North West Bay resulting from the furthest upstream release site in the Huon Estuary, Brabazon Park, were the largest of all release sites in the lower channel and Huon Estuary, and comparable to that of the Simmonds release site. This is probably because the Brabazon Park site bears the full brunt of any Huon flow, while since the river favours the northern bank the Killala site is not exposed to as much advection and can establish a local mixing zone.

(a) 5 Percentile

(b) Median

(c) 95 Percentile

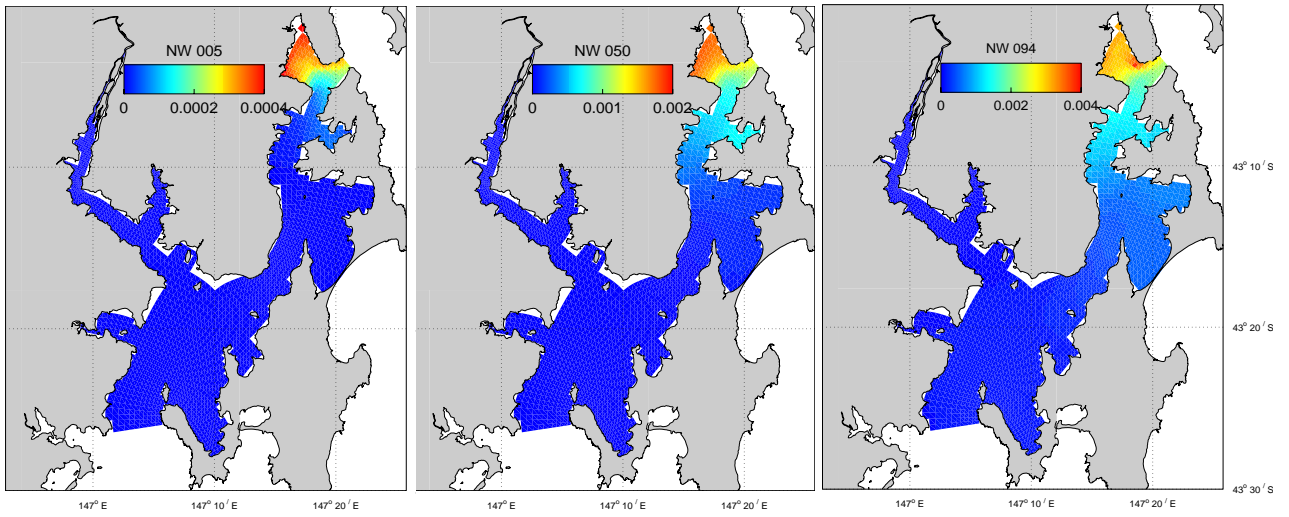


**Fig. 97. Norwest Surface Percentile Distributions**

(a) 5 Percentile

(b) Median

(c) 95 Percentile

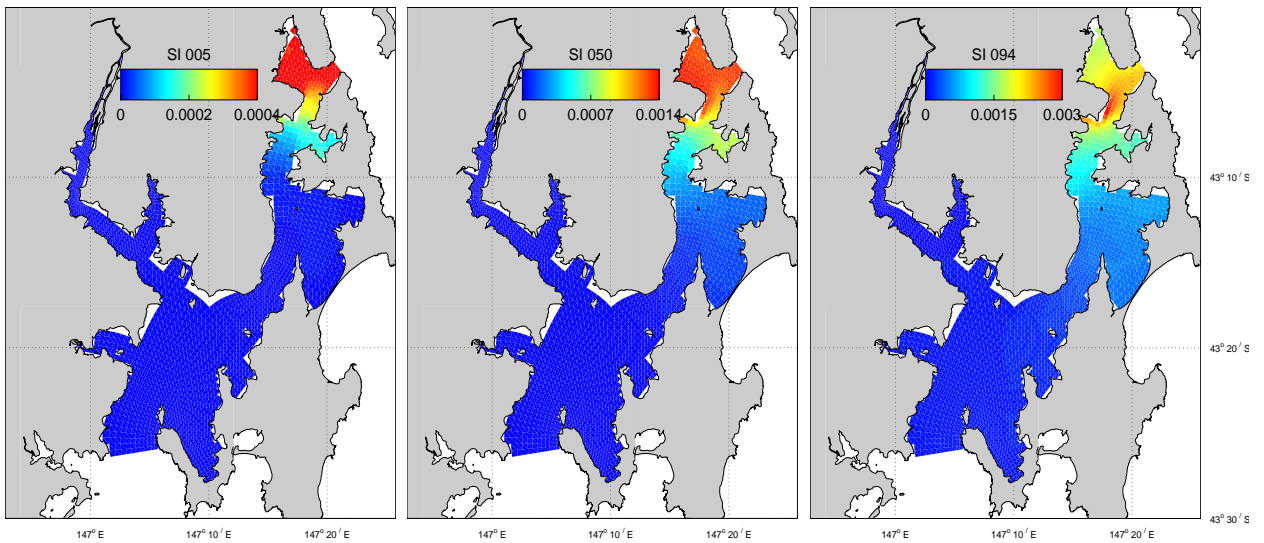


**Fig. 98. Simmonds Surface Percentile Distributions**

(a) 5 Percentile

(b) Median

(c) 95 Percentile

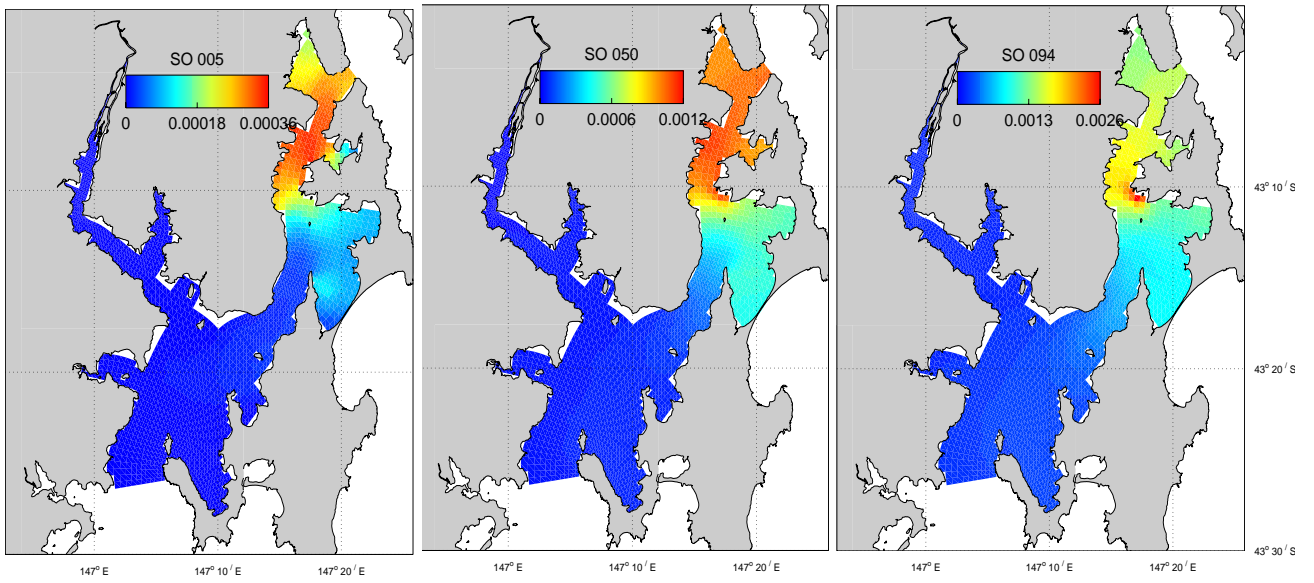


**Fig. 99. Soldiers Surface Percentile Distributions**

(a) 5 Percentile

(b) Median

(c) 95 Percentile

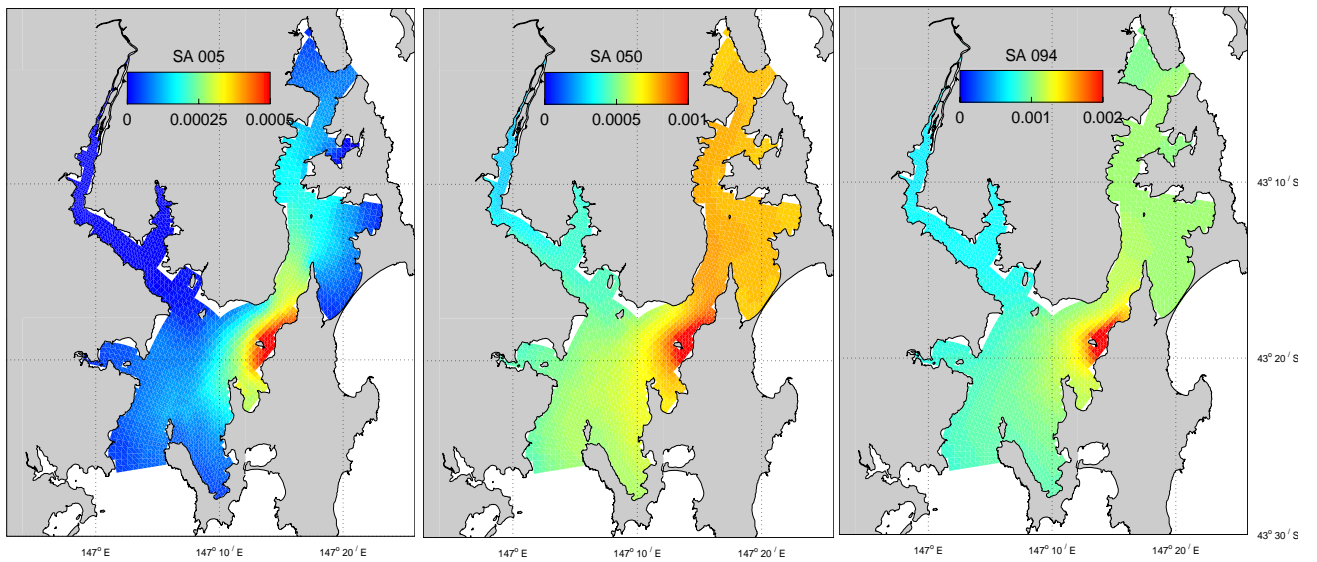


**Fig. 100. Satellite Surface Percentile Distributions**

(a) 5 Percentile

(b) Median

(c) 95 Percentile

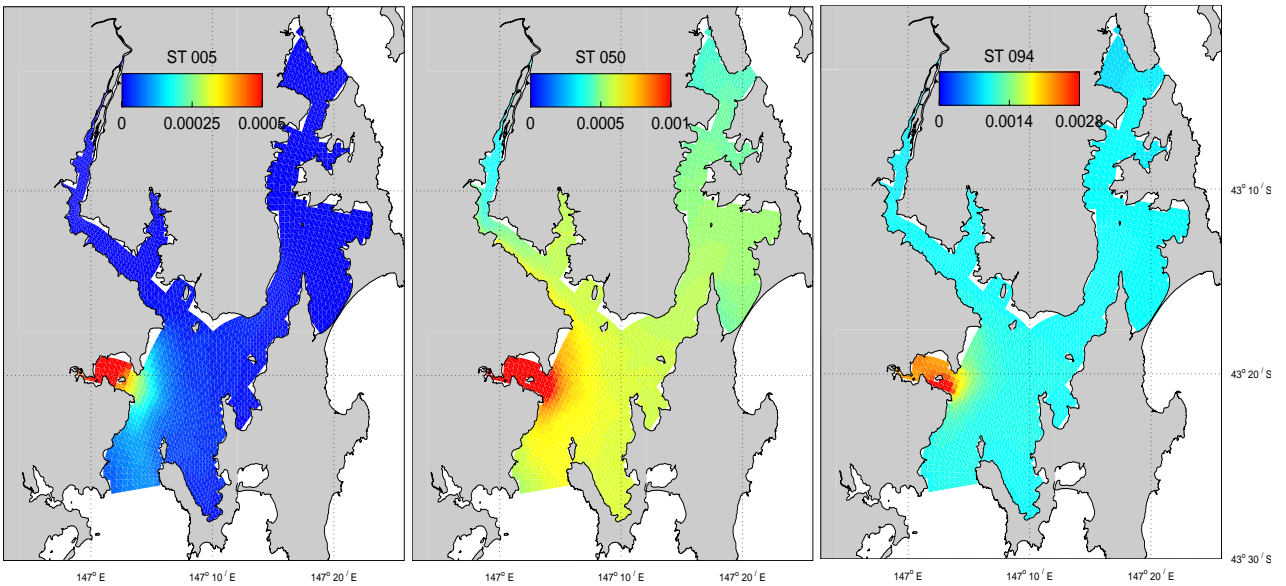


**Fig. 101. Stringers Surface Percentile Distributions**

(a) 5 Percentile

(b) Median

(c) 95 Percentile

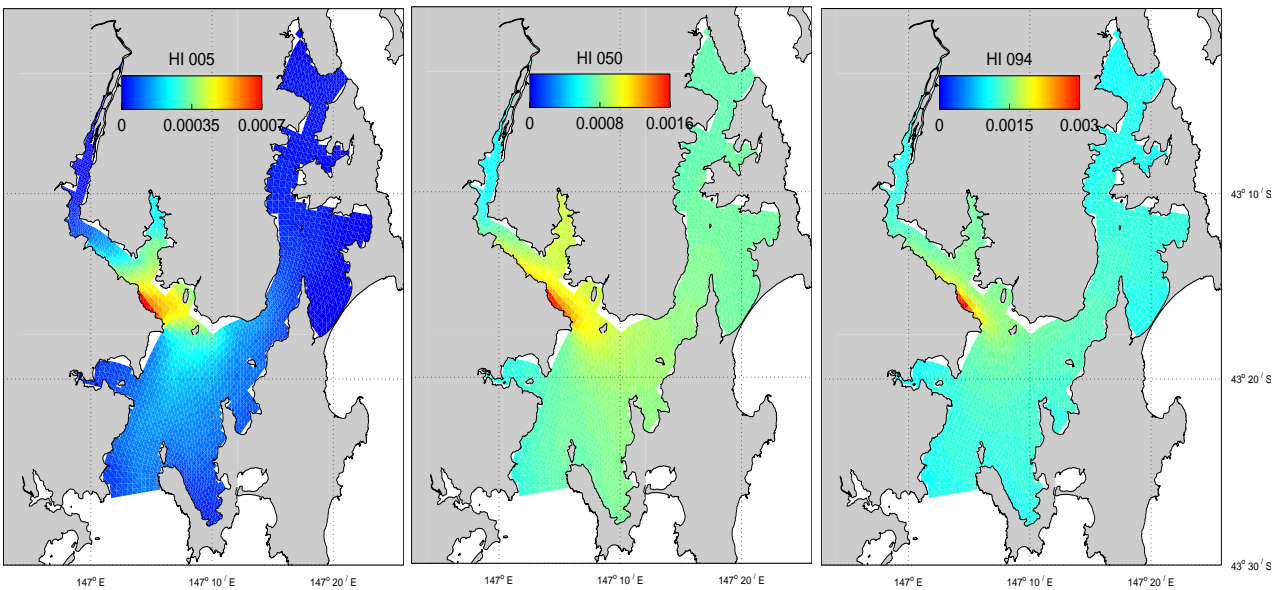


**Fig. 102. Hideaway Surface Percentile Distributions**

(a) 5 Percentile

(b) Median

(c) 95 Percentile

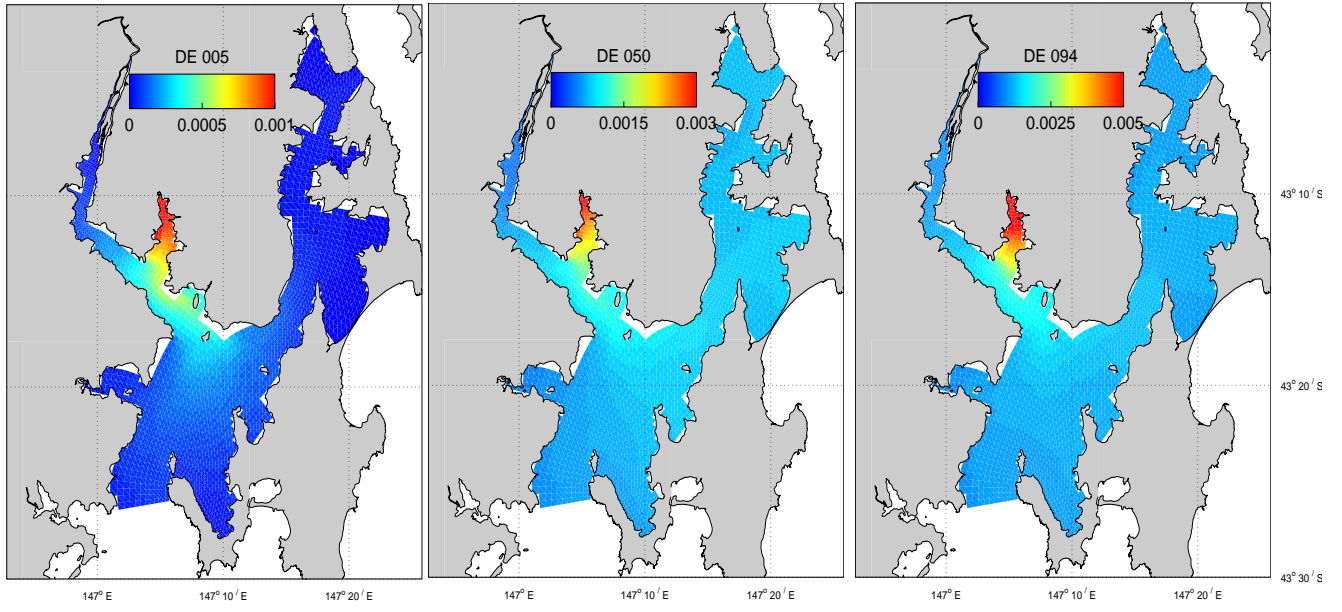


**Fig. 103. Deep Surface Percentile Distributions**

(a) 5 Percentile

(b) Median

(c) 95 Percentile

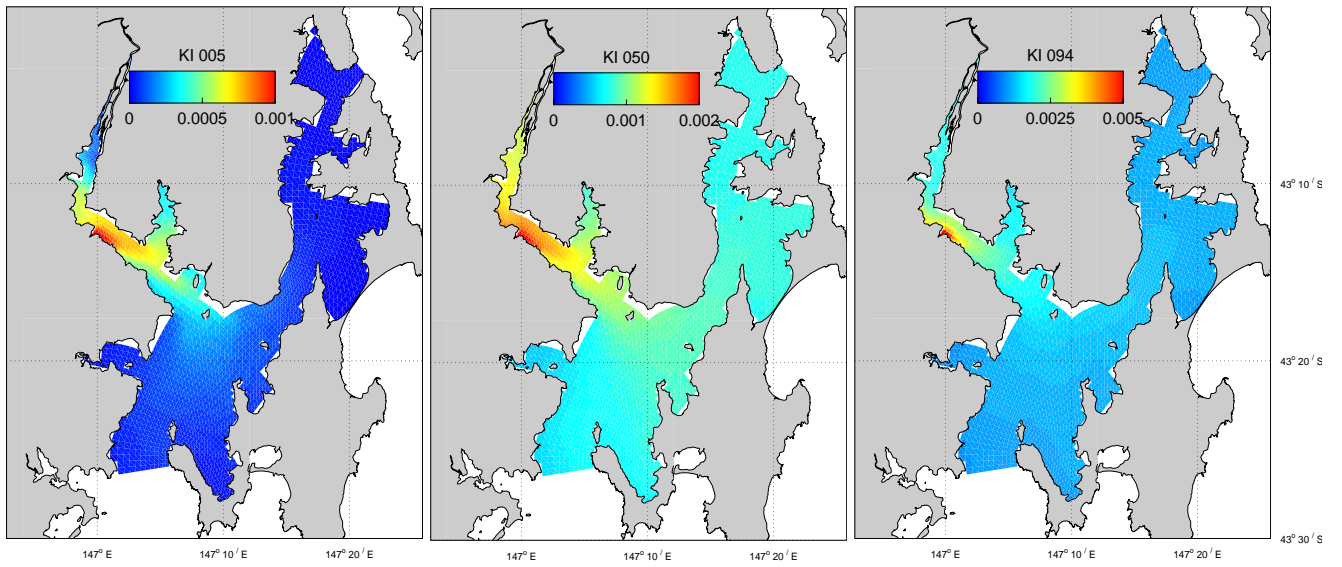
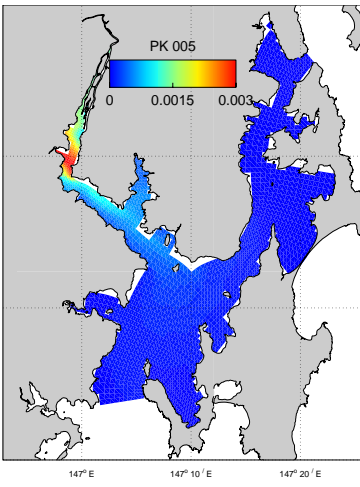
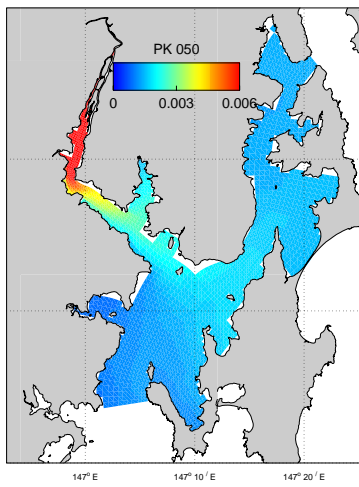


**Fig 104. Killala Surface Percentile Distributions**

(a) 5 Percentile



(b) Median



(c) 95 Percentile

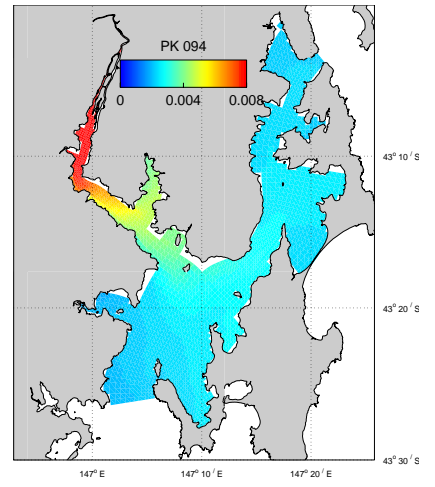


**Fig. 104b. Brabazon Park Surface Percentile Distributions**

## 7.8 Particle Tracking

The connectivity of the domain can be examined by observing the behaviour of neutrally buoyant particles released at the same locations as the point source releases in Section 7.6 and over the same depth range. The particles were released from random locations over the depth range at a rate of 2 particles/hour from an initial pool of 10,000 particles. These particles were subsequently advected with the circulation to provide insight into how various regions of the domain are connected. The particles are also subjected to random motion representing the effect of diffusion (i.e. sub-grid scale effects). Therefore, any two particles released from the same place at the same time are expected to undergo different trajectories due to this random motion. When a particle crosses the open boundaries at the northern and southern end of the model domain it is placed in the initial pool for subsequent re-release. The particle distributions after 6 months of simulation (corresponding to mid-winter) are displayed in Figs 105 to 113. This distribution is the projection of particles at all depths onto the surface. Particles are colour coded according to their age since being released over the range 0 – 20 days (i.e. blue particles are 0 days old, red particles are > 20 days old).

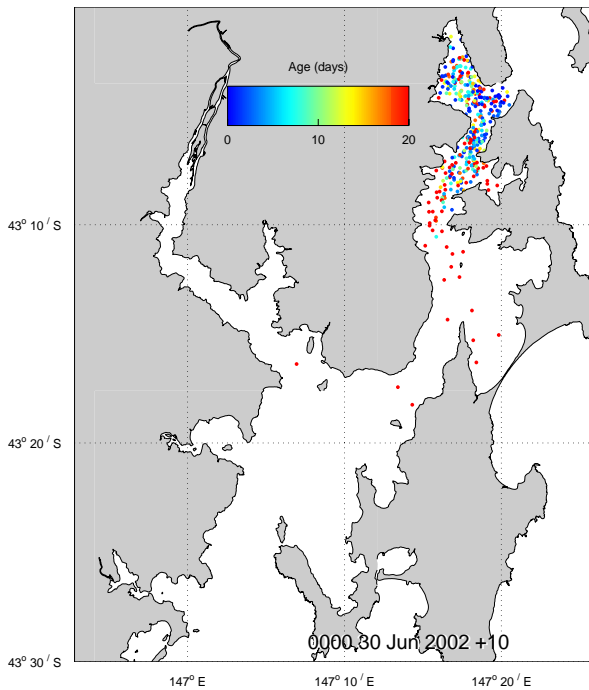


**Fig. 105. Northwest**

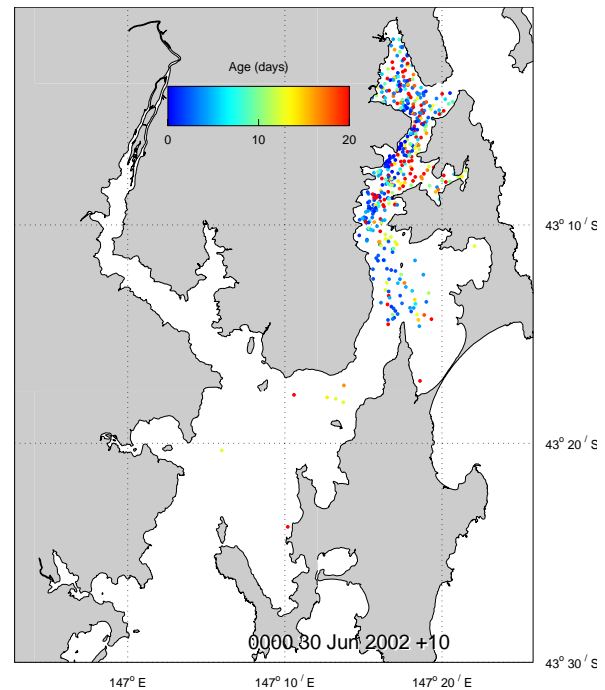


**Fig. 106. Simmonds**

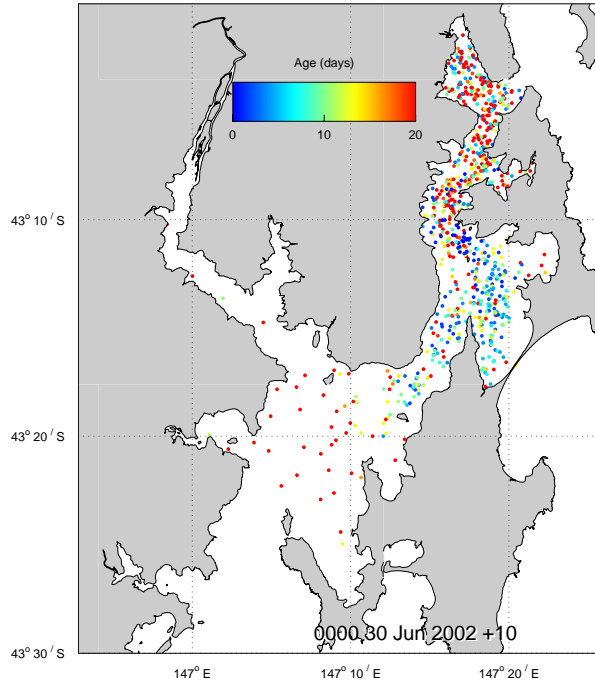


**Fig. 107. Soldiers**

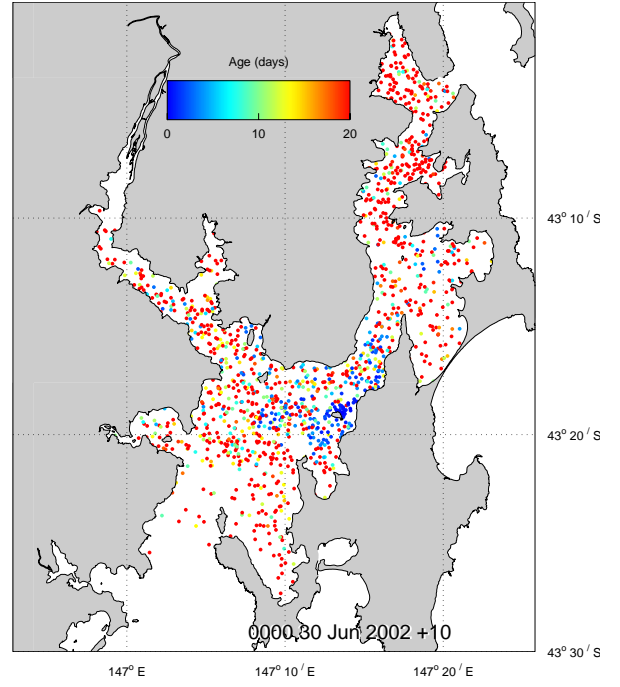


**Fig. 108. Satellite**

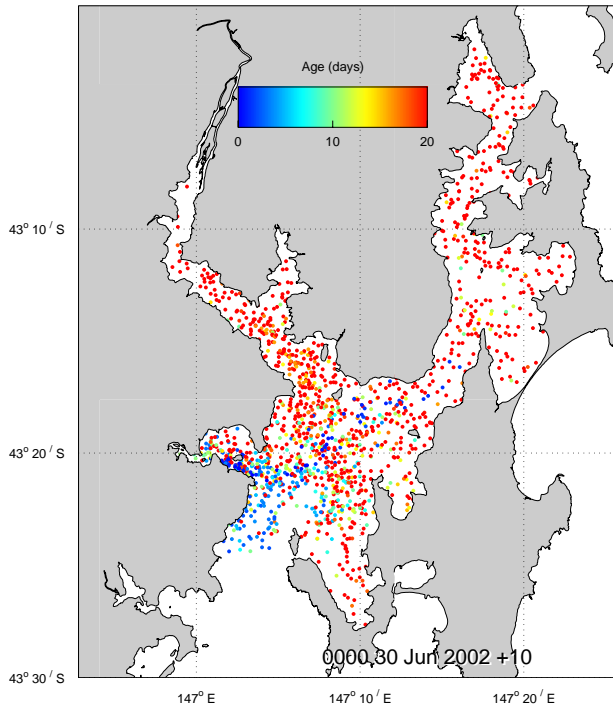


**Fig. 109. Stringers**

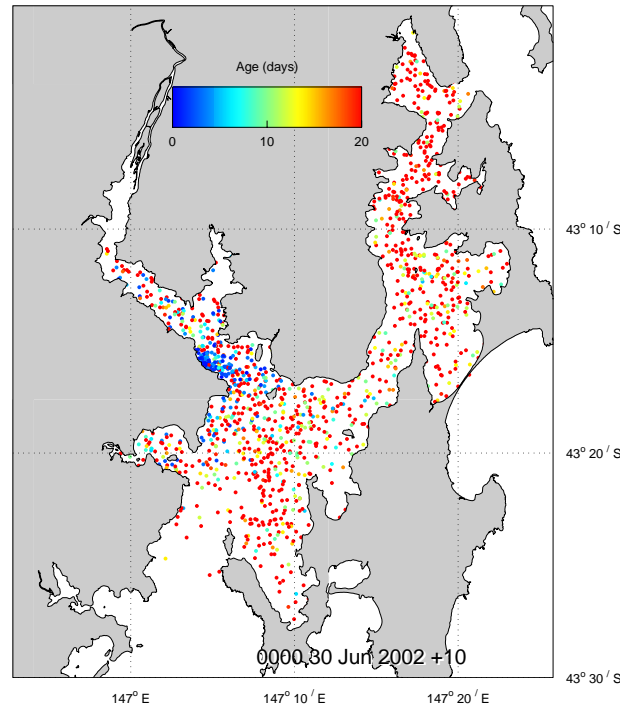


**Fig. 110. Hideaway**

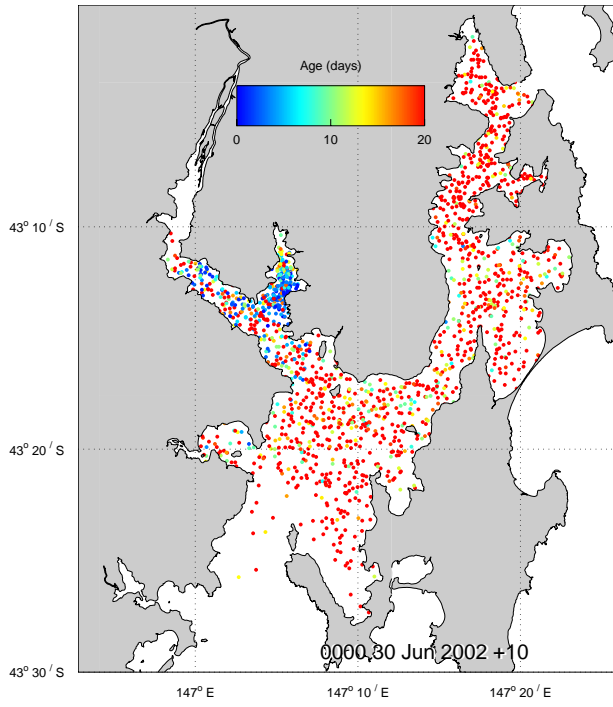


**Fig. 111. Deep**

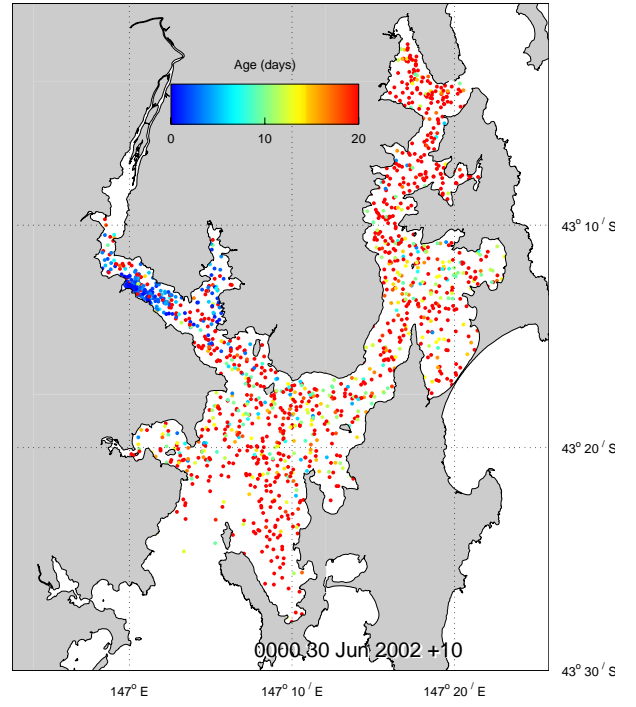


**Fig. 112. Killala**

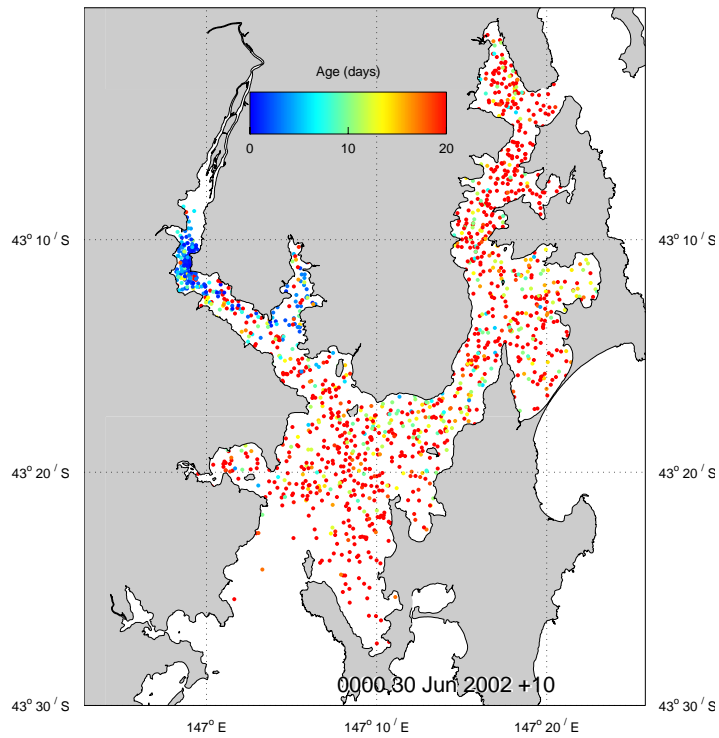


**Fig. 113. Brabazon Park**

These Figures show that particles released in the southern channel and Huon Estuary exhibit relatively uniform distribution throughout the whole domain whereas those released at sites in the northern channel result in distributions confined to the northern domain. Therefore the southern channel and Huon Estuary are well connected to the whole domain, whereas the northern channel has relatively poor connectivity with the southern channel. This is consistent with the residual flow analyses which suggest a net flow up-channel exiting through the northern boundary. In the long term particles are expected to follow trajectories corresponding to this mean flow. Also, it can be seen that many of the particles have ages greater than 20 days, suggesting the e-folding flushing time of the whole estuary estimated in Section 7.4 may actually be an underestimation of the time it takes neutrally buoyant particles to be transported out of the domain. Of particles released from all sites, there existed 47162 particles that were lost through the open boundaries, and the mean age of these particles was 26 days. Figs 111 - 113 also show that particles released in the Huon Estuary are capable of reaching the northern channel and North West Bay in around 10 days.

Due to the large number of particles in the domain, an animation of the particle trajectories best conveys the connectivity of the region, although observation of isolated particle trajectories does supply insight into the dynamics of the system. The trajectories of particles were traced during the flood and ebb of a spring tide during 17 – 20 May 2002 (Fig. 114) and displayed in Figs 115 and 116 respectively.

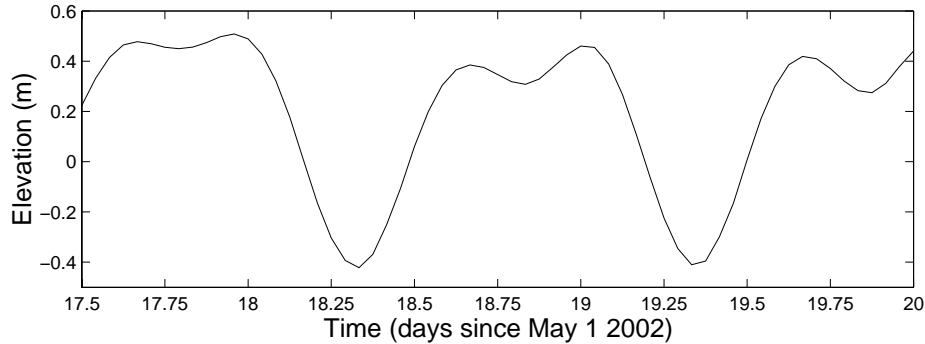


**Fig. 114. Spring tide during 17 – 20 May 2002**

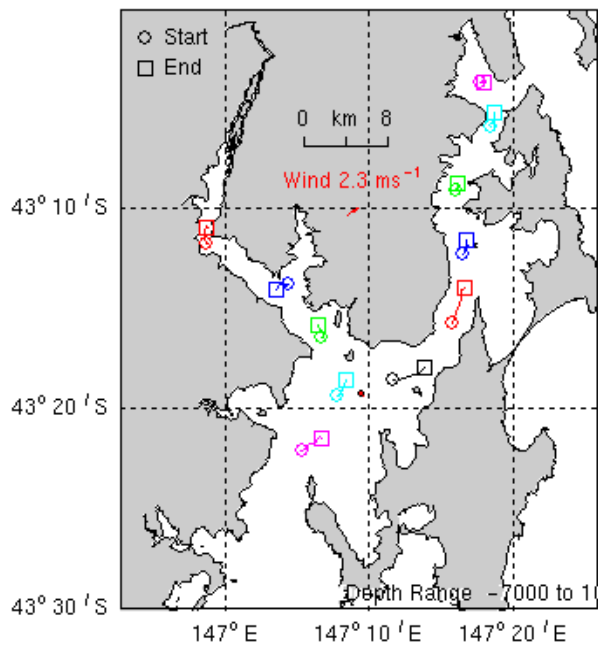


**Fig. 115. Flood Tide, 19 May 0800**

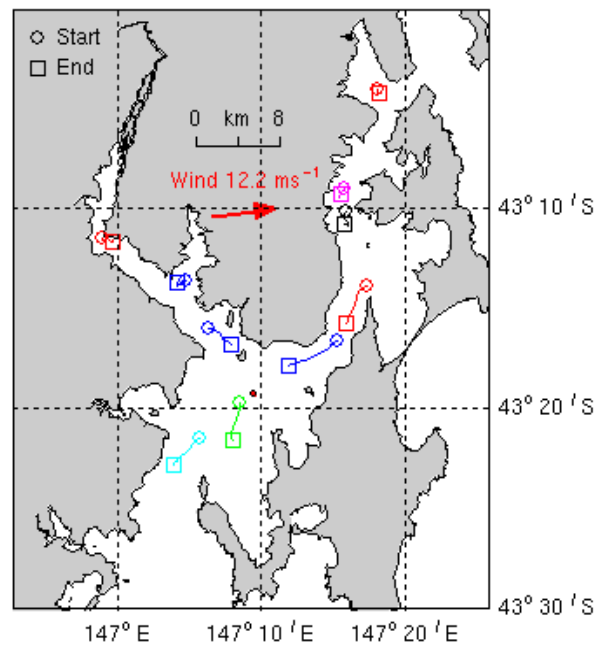


**Fig. 116. Ebb Tide, 18 May 0000**

The flood tide in this instance had a tidal range of 0.83 m and the ebb of 0.95 m. Low to moderate south-westerly winds of  $\sim 0.5 - 12 \text{ ms}^{-1}$  were in effect during this period. During the flood tide, particles are transported up-channel towards the north (and up-river in the Huon; north-west) and during the ebb transported down-channel towards the south (and down-river south-eastwards) as expected. Maximum tidal excursions are found mid-channel at the narrowest location near Gordon, where excursions are of the order of 4 km. Further south the excursion decreases and in the northern channel and Huon Estuary the excursions are less than 1 km.

A large flow event occurred on 15 August with a flow of close to  $1000 \text{ m}^3\text{s}^{-1}$  (day 227 Fig. 23) under the influence of moderate south-westerly winds ranging from  $\sim 5-10 \text{ ms}^{-1}$ . Tidal ranges were of the order 0.88 m. In this case the flood plume charged up-channel to as far as North West Bay (Fig. 117). Particle trajectories also reflect this up-channel motion (Fig. 118) where particles traced for 57 hours from 14 Aug 1200 to 17 Aug 2100 show displacement of greater than 24km, in some cases from near Cygnet to Barnes Bay (green trajectory).

Similar strength north-easterly winds occurred during a flood event centered on 15 June with a flow of  $\sim 700 \text{ m}^3\text{s}^{-1}$  (day 160 Fig. 23). These winds pushed the flood plume southwards into Great Taylor Bay and out of the southern boundary (Fig. 119). During this time the tide underwent a cycle with range 0.89 m. Corresponding trajectories for the 20 hour period from 0900 14 June to 0500 15 June are displayed in Fig. 120. Trajectories are oriented down-channel during this event with displacements up to  $\sim 16 \text{ km}$ . This

demonstrates the strong impact of north-easterly winds on the freshwater plume during flood events.

The up-channel direction for the freshwater plume transport is the preferred direction, since under the influence of cross-channel north-westerly winds the plume favours the up-channel direction (Fig. 121). Flow was  $\sim 550 \text{ m}^3\text{s}^{-1}$  with a tidal range of 0.64m. Particles were tracked for 38 hours from 30 Jun 0800 to 01 Jul 2200. The favoured up-channel motion is the result of Coriolis balancing the baroclinic pressure gradients, where the Coriolis force deflects the surface flow towards the left (i.e. up-channel) of the down-river pressure gradient.

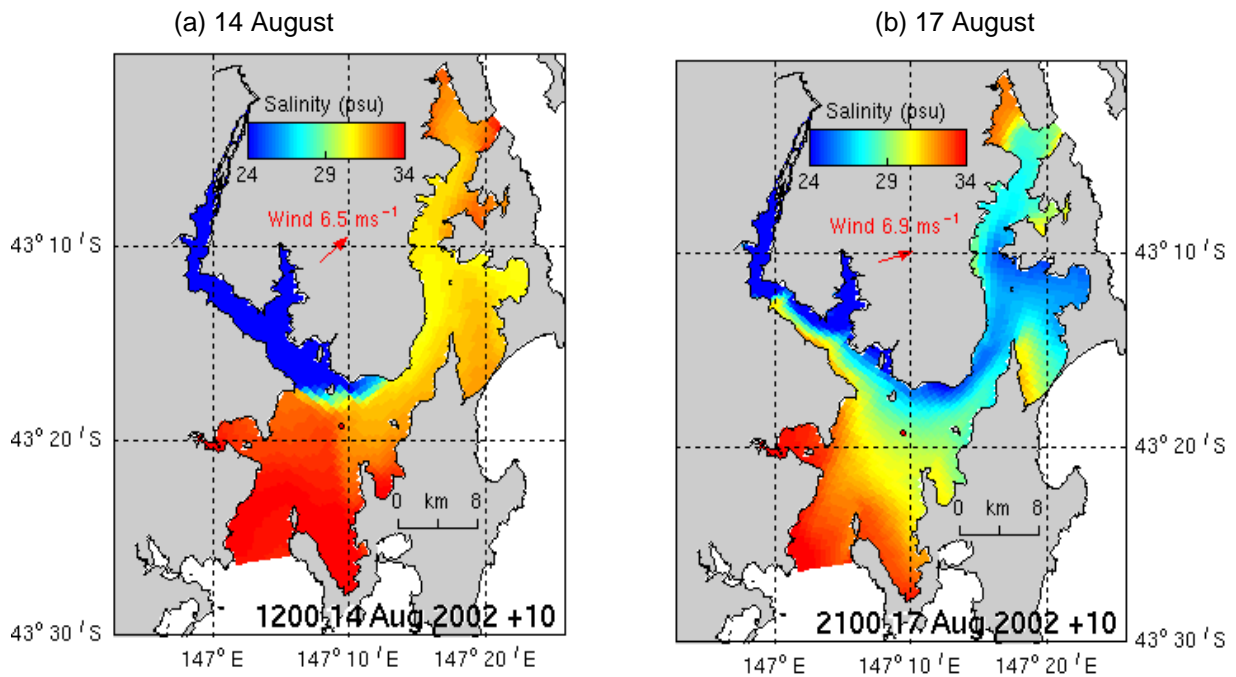


**Fig. 117: Surface salinity during 15 August flood event**

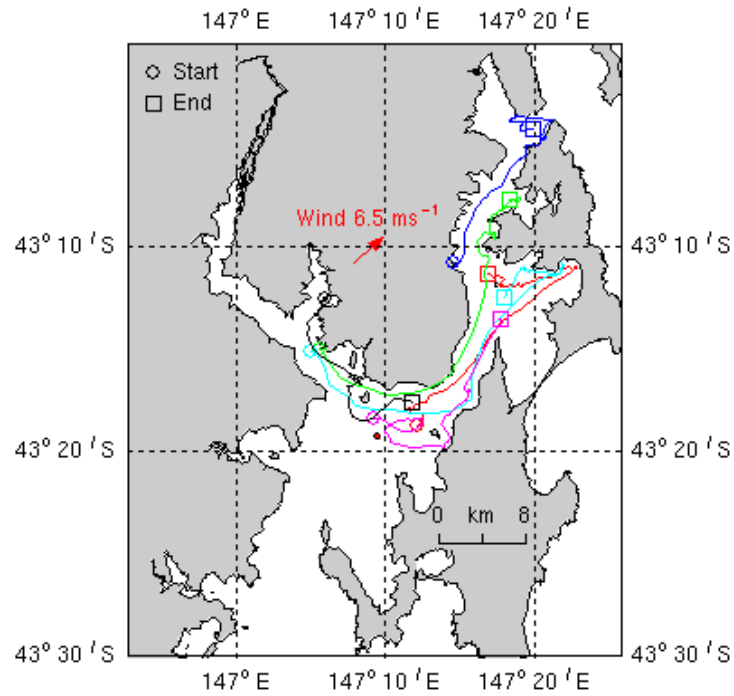


**Fig. 118. Trajectories during 15 August flood event**

(a) 14 June

(b) 15 June

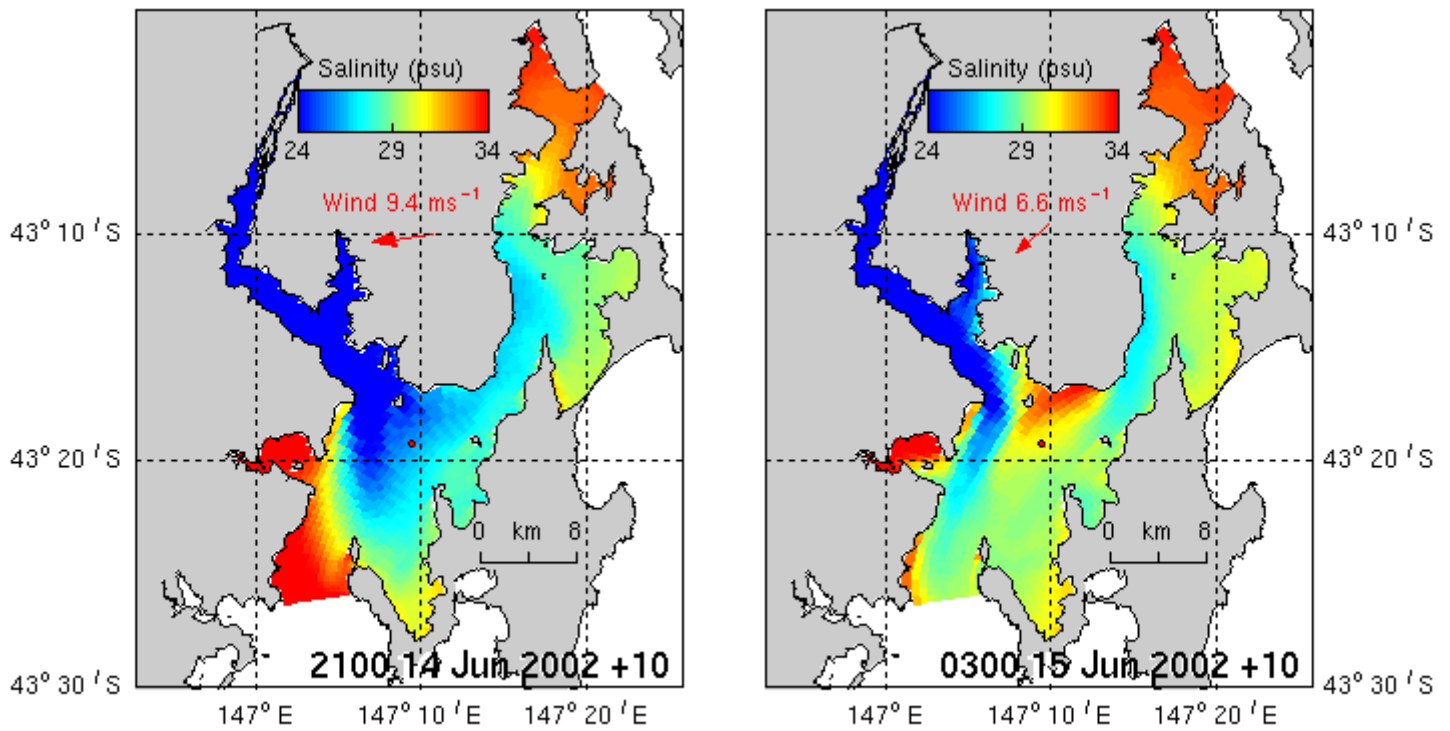


**Fig. 119. Surface salinity during 15 June flood event**

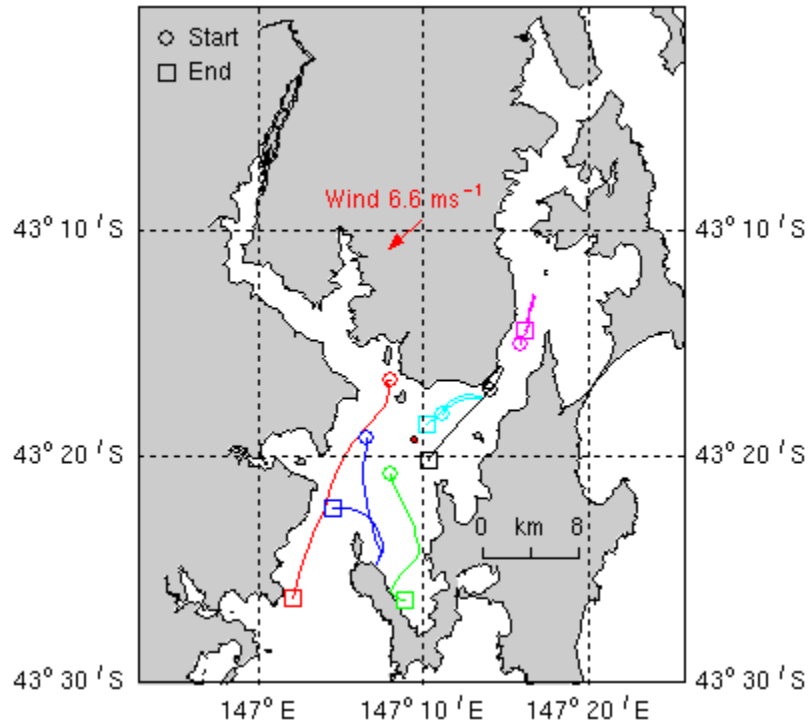


**Fig. 120. Trajectories during 15 June flood event**

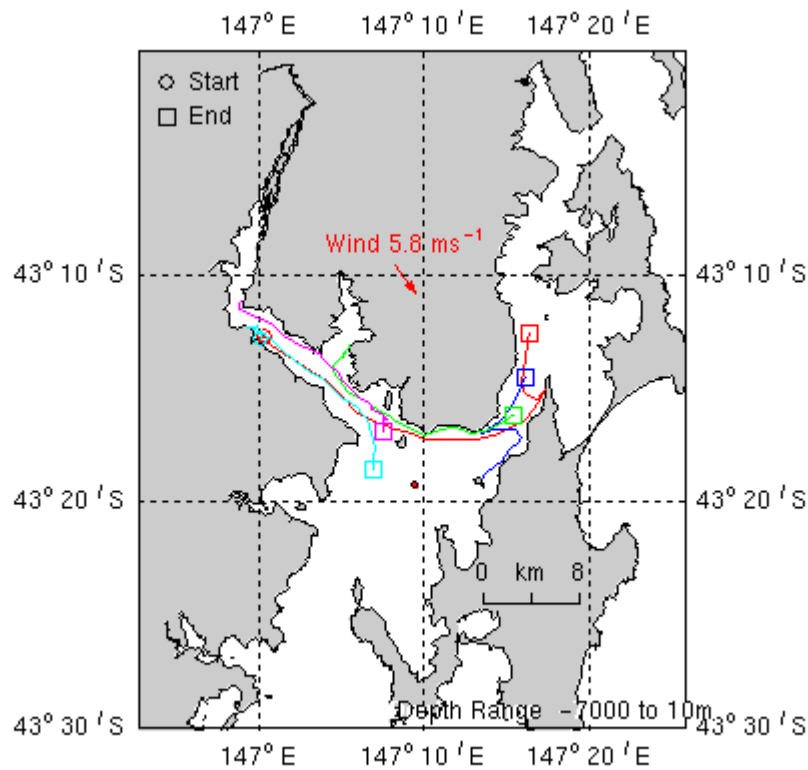


**Fig. 121. Trajectories during 1 July flood event**

## 7.9 Coarse Model

The model presented above proved unsuitable for coupling with ecology and sediment transport models since the high resolution of the model in conjunction with the large number of tracers required by the ecology and sediment models resulted in run-time ratios becoming unreasonably low. A model grid with reduced horizontal resolution was constructed to rectify this problem (coarse model). The coarse model grid is depicted in Fig. 122. Resolution ranged from ~350 m cross-river in the upper Huon to 1.3 km in the upper channel, lower Huon and near the southern boundary. This grid coupled to ecology and sediments resulted in acceptable run-time ratios of  $> 100:1$ . The calibration for this model is displayed in Fig. 123. It can be seen that the calibration is not as good as the high resolution model owing to the decrease in resolution, but is still nonetheless acceptable.

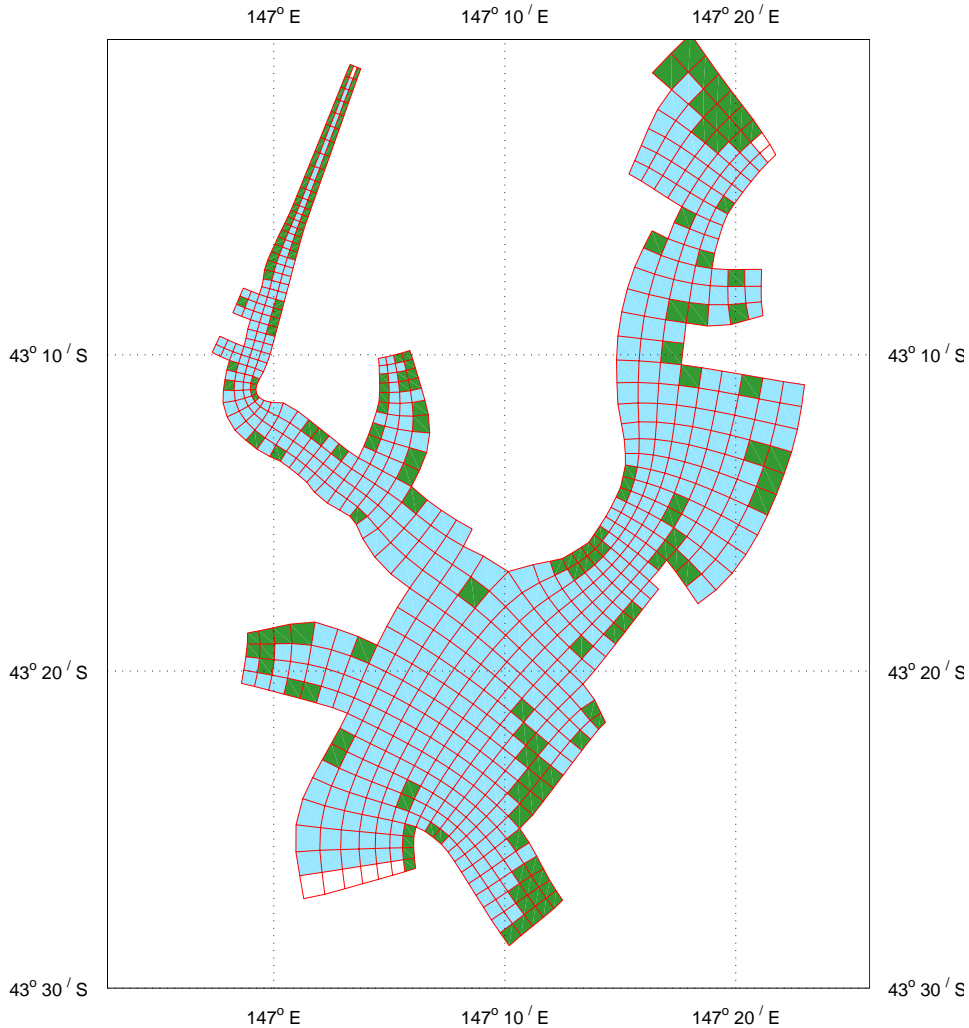


**Fig. 122. Coarse Model Domain**

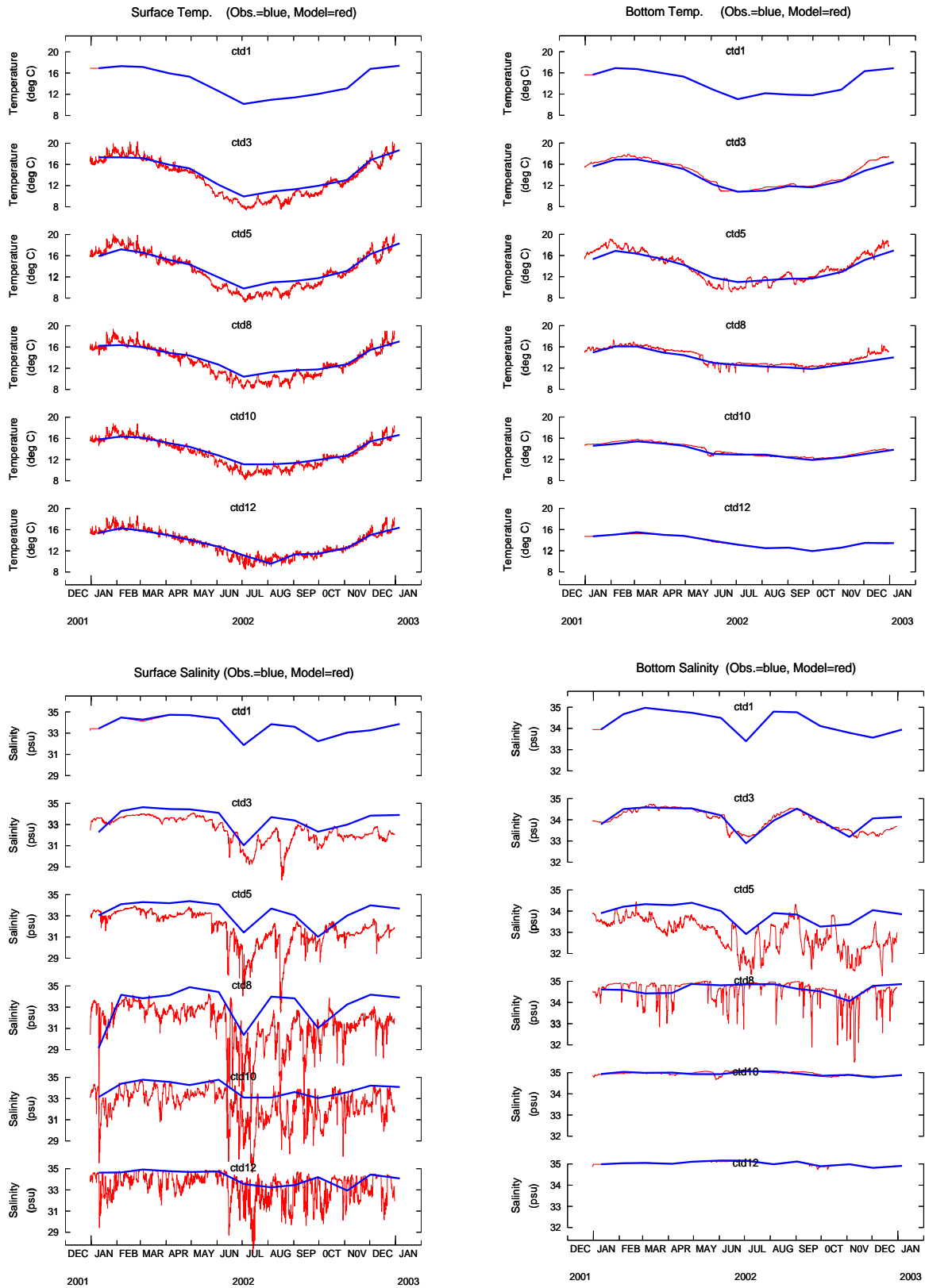


**Fig. 123. Coarse Model Calibration**

## 8 Conclusions

A 3D primitive equation model was applied to Huon Estuary/D'Entrecasteaux to examine the hydrodynamics of the region. Using a nesting process the region was represented with high resolution while incorporating forcing due to wind stress, tides, low frequency sea level oscillations and pressure gradients due to temperature and salinity distributions. Major forcing consists of river flow, which may be as large as  $1000 \text{ m}^3\text{s}^{-1}$ , wind which has an annual average speed of speed of  $4.3 \text{ ms}^{-1}$  from the south and tide which has a range of  $\sim 1\text{m}$  during the spring tide. The full year of 2002 was simulated and calibrated to data collected within the Broad Scale Monitoring Program.

Several physical processes proved important in obtaining an acceptable calibration. Surface heat fluxes play a crucial role in regulating temperature in the region. The model proved sensitive to the type of bulk formulation used for surface sensible and latent heat fluxes, and to a lesser extent the depth to which short wave radiation is allowed to penetrate. Differential heating is apparent in the side bays, both in measured data and in the model and this may contribute towards heating of the main channel.

Non-linear effects were important near the northern boundary of the domain. This prompted the construction of an intermediate scale model which better resolved velocity in this region and was suitable for nesting the local model in using boundary velocity forcing. The local model also proved sensitive to the background vertical diffusion coefficient, type of mixing scheme used and magnitude of the imposed Huon River flow.

Data collected within the Broad Scale Monitoring Program revealed that a temperature gradient (up to  $1^\circ\text{C}$ ) exists along the D'Entrecasteaux Channel during summer and autumn, with the northern end associated with higher temperature. The deeper waters at the southern end have the lowest temperature in the channel, presumably due to the sub-thermocline oceanic influence. Towards autumn the vertical temperature gradient at the southern end is less pronounced, as surface cooling decreases surface temperature heading into winter. In winter bottom waters become warmer than surface waters, but still several degrees cooler than the summer bottom temperature. This bottom temperature increase in winter is also observed at the northern end of the channel. Salinity is lower in the mid-channel region and attains the highest values in bottom waters at the ends of the channel throughout the year, thus density compensating the temperature distribution. Thin fresh water layers can be observed mid-channel during times of high Huon River flow.

The model results confirm these trends and validate that the Huon Estuary behaves as a salt wedge estuary with marine flow in bottom waters directed upstream in the estuary and a fresh water surface flow heading downstream. The head of the salt wedge is located near Huonville under low flow and is pushed downstream under high flow conditions. The downstream surface flow generally favours the northern bank of the river, heading northwards up-channel upon entering the D'Entrecasteaux. Under high flow conditions fresher water may be found as far north as North West Bay, and may be advected north as much as 24km in just over 2 days.

On diurnal timescales the tidal flow dominates the region, with flow directed up-river and up-channel during the flood tide, and vice versa during the ebb. Strongest currents exist in the narrowest point in the channel near Gordon, where they approach  $0.5 \text{ ms}^{-1}$ . The tide undergoes a neap-spring cycle of the order of 14 days, with maximum tidal ranges approaching 1m. The tide is predominantly of diurnal (daily) mixed character with a form factor  $F \sim 1.5$ . Maximum tidal excursions are of the order of 4km mid-channel. In the southern channel the excursion decreases and in the northern channel and Huon Estuary the excursions are less than 1km. The momentum balance of surface flow on these timescales is dominated by the tide and wind, opposed by the Coriolis force. In bottom water vertical and lateral friction becomes important.

The mean seasonal flow for the D'Entrecasteaux–Huon Estuary system consists of bottom water entering the region at the southern end of the channel and moving up into the Huon Estuary in the salt wedge, favouring the southern bank. Entrainment occurs from the salt wedge into the downstream freshwater flow, the majority of which then turns north upon entering the channel and exits into Storm Bay at the northern end of the channel. A smaller proportion of Huon flow exits the channel through the southern boundary. The momentum balance indicates that the mean surface flow in the Huon Estuary consists of a balance between density forcing and Coriolis, with wind contributing to down-river flow. In the northern channel density driven flow combines with rotation forces to produce seasonal up-channel residual flow. Cross channel forces balance in this area, with Coriolis opposing wind driven flow with some contribution of density effects to Coriolis. The southern channel exhibits both along and cross-channel mean flow. Coriolis forcing opposes density forces in the along-channel direction while the wind driven flow opposes density driven flow in the cross-channel direction. Coriolis forcing is directed up-channel throughout the channel, whereas density effects are directed up-channel in the northern channel and down-channel in the southern channel. Horizontal friction becomes more important in bottom waters.

The calculation of flushing times can be subjective depending on the method used to compute the flushing. Using an e-folding rate based on depletion of total mass in a region the flushing times varied from around 3 days for the lower Huon Estuary under high flow conditions to ~20 days for the whole domain in winter. A flushing estimate for the whole domain based on the average time for neutrally buoyant particles to exit the domain was computed as ~26 days.

Distributions of passive tracers resulting from release in the top 14m of the water column at locations corresponding to selected farm sites showed significant variability with release location. Generally those sites in the northern channel result in distributions confined to the northern D'Entrecasteaux. Release sites in the channel below Gordon and in the lower Huon Estuary resulted in relatively uniform concentrations throughout the domain outside a well defined mixing zone of high concentration. For release sites further up the Huon the largest concentrations are confined to the upper Huon and uniform concentrations of lower magnitude are found throughout the rest of the domain. These general distributions were also observed in results obtained via particle tracking of

neutrally buoyant particles released from the respective farm sites. The southern channel and Huon Estuary can be characterized as well connected to the whole domain, whereas the northern channel has relatively poor connectivity with the southern channel.

Particle tracking results also confirmed the diurnal dominance of tidal forcing, with particles exhibiting up-channel and up-river movement on the flood tide, and down-channel / river on the ebb. During flood events the favoured trajectory out of the Huon was up-channel. The freshwater plume also favoured the northern bank of the Huon due to the influence of Coriolis forces. The location of the freshwater plume was, however, sensitive to wind direction, with north-easterly winds pushing the freshwater plume southwards.

The hydrodynamic model has provided useful insight into the physics of the D'Entrecasteaux and Huon Estuary system. Due to computational pressures the model was unsuitable for coupling to ecological models, and a coarser resolution model was developed to fulfill this role.

## 9 References

- Blumberg, A.F., Kantha, L.H. (1985) Open boundary condition for circulation models, *J. Hydraulic Eng.*, 111, 237-255.
- Burchard, H., Peterson, K.O., Rippeth, T.P. (1998) Comparing the performance of the Mellor Yamada and the k- $\epsilon$  turbulence models. *J. Geophys. Res.*, 103, 10,543-10,554.
- Burchard, H., Bolding, K., Villarreal, M.R. (1999) GOTM, a general ocean turbulence model. Theory implementation and test cases. Technical Report EUR 18745EN, European Commission, 103 pp.
- Cartwright, D.E., Ray, R.D. (1990) Oceanic tides from Geosat altimetry. *J. Geophys. Res.*, 95 C3, 3069-3090.
- Kondo, J. (1975) Air-sea bulk transfer coefficients in diabatic conditions. *Boundary-Layer Meteorology*, 9, 91-112.
- Large, W.G., Pond, S. (1981) Open ocean momentum flux measurements in moderate to strong winds, *J. Phys. Oceanogr.*, 11, 324-336.
- Leonard, B.P. (1979) A stable and accurate convective modelling procedure based on quadratic upstream interpolation. *Comp. Meth. Appl. Mech. Eng.*, 19, 59-98.
- Leonard, B.P. (1991) The ULTIMATE conservative difference scheme applied to unsteady one-dimensional advection. *Comp. Meth. Appl. Mech. Eng.*, 19, 17-74.
- Marchesiello, P., McWilliams, J.C., Shchepetkin, A. (2001) Open boundary conditions for long term integration of regional oceanic models. *Ocean Modelling*, 3, 1-20.
- Mellor, G.L., Yamada, T. (1982) development of a turbulence closure model for geophysical fluid problems. *Rev. Geophys.*, 20, 851-875.
- Miller, M.J., Thorpe, A.J. (1981) Radiation conditions for the lateral boundaries of limited-area numerical models. *Q. J. R. Meteorol. Soc.*, 107, 615-628.

- Ridgway, K.R., Dunn, J.R., Wilkin, J.L. (2002) Ocean interpolation by four-dimensional least squares -Application to the waters around Australia, *J. Atmos. Ocean. Tech.*, 19, 1357-1375.
- Walker, S.J., Waring, J.R., (1998) A multiple grid, 3-dimensional, non-linear, variable-density hydrodynamic model with curvilinear horizontal coordinates and level ( $z$ ) vertical coordinates, CSIRO Marine Research, Report OMR-118/120.
- Zillman, J.W. (1972) A study of some aspects of the radiation and heat budgets of the southern hemisphere oceans. Bureau of Meteorology, Meteorological Study No. 26, Australian Govt. Pub. Service, Canberra.

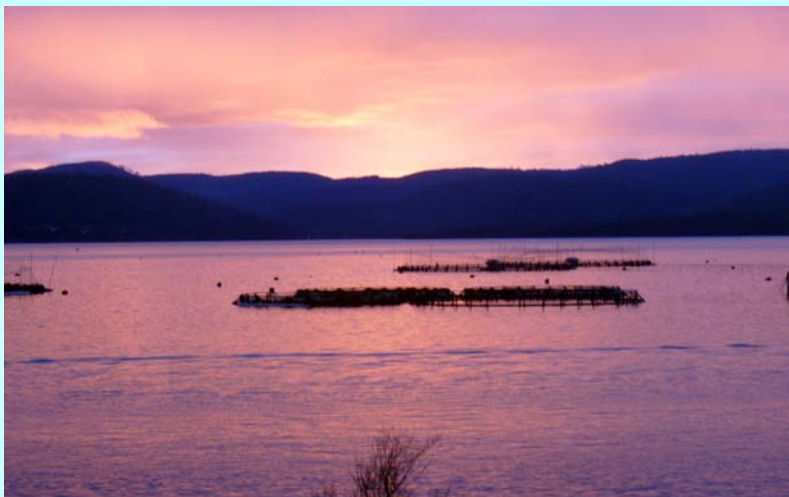
# Technical Report



## Effects of grazing by microzooplankton on phytoplankton in the Huon Estuary

*Peter Thompson and Pru Bonham  
CSIRO Marine and Atmospheric Research  
July 2005*

*Aquafin CRC Project 4.2  
(FRDC Project No. 2001/097)*



© Copyright Aquafin Cooperative Research Centre, Fisheries Research and Development Corporation, Commonwealth Scientific and Industrial Research Organisation

**This work is copyright. Except as permitted under the Copyright Act 1968 (Cth), no part of this publication may be reproduced by any process, electronic or otherwise, without the specific written permission of the copyright owners. Neither may information be stored electronically in any form whatsoever without such permission.**

**Every attempt has been made to provide accurate information in this document. However, no liability attaches to Aquafin CRC, its participant organisations or any other organisation or individual concerned with the supply of information or preparation of this document for any consequences of using the information contained in the document.**

*Published by CSIRO Marine and Atmospheric Research*



## Effects of grazing by microzooplankton on phytoplankton in the Huon Estuary

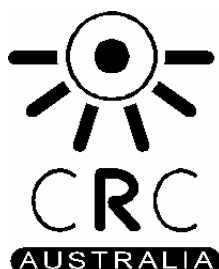
*Peter Thompson and Pru Bonham*  
*CSIRO Marine and Atmospheric Research*

*July 2005*

*Aquafin CRC Project 4.2*  
*(FRDC Project No. 2001/097)*



**Australian Government**  
**Fisheries Research and  
Development Corporation**



Tasmanian Aquaculture  
& Fisheries Institute  
University of Tasmania

# 1. Introduction

One of the key issues for management of the Huon Estuary is better quantification of the processes that cycle nutrients. More frequent algal blooms or greater algal biomass are typical responses to nutrient loading and have been predicted for the Huon Estuary if inputs of nitrogen were to rise (HES 2000). There are well documented seasonal cycles of algal biomass in the Huon and quantifying the various processes of “loss” such as consumption, sedimentation to the bottom or transportation out of the ecosystem is fundamental to our capacity to predict the response of this ecosystem to nutrient loading. For example, if most of the nitrogen input to the ecosystem is quickly buried deep into sediments or advected out to sea then local nitrogen inputs may have little impact on Huon Estuary ecology. Conversely if the inputs of nitrogen are largely captured by phytoplankton, grazed and recycled within the water column then the local ecosystem is much more susceptible to the deleterious effects of increased nutrient loading. In this report we present our preliminary efforts to quantify grazing, in this case grazing by microheterotrophs on phytoplankton. Recent research has shown that the majority of phytoplankton may be grazed by microheterotrophs in some ecosystems. Experiments to measure microheterotroph grazing rate are considerably more difficult than classical zooplankton grazing experiments because the size of the grazers is very similar to the size of the prey. Ideally these experiments would be conducted in parallel with experiments to measure grazing by zooplankton so that fluxes through both size categories of grazers could be directly comparable.

## 1.1 Introduction to the technique

The technique developed to measure grazing rates on phytoplankton by microheterotrophs uses a serial dilution of field samples (Landry and Hassett 1982) and is referred to as the “grazing dilution technique”. The grazing dilution technique and calculations used in these experiments were adapted by Brian Griffiths (CSIRO Marine Research) from the method of Landry and Hassett (1982). Landry and Hassett made three assumptions regarding the interactions of nutrients, phytoplankton (prey) and microzooplankton (herbivore):

1. The growth of individual phytoplankton is not directly affected by the presence or absence of other phytoplankton *per se*. The implication of this is that a reduction in the density of cells in natural sea water will not directly cause a change in the growth rate of the remaining cells.
2. The probability of a phytoplankton cell being consumed is a direct function of the rate of encounter of microzooplankton grazers with prey
3. The change in density of phytoplankton,  $P$ , over some time  $t$ , can be represented appropriately by the exponential equation, where  $k$  and  $g$  are the instantaneous coefficients of population growth and grazing mortality of the cells. This implies that grazers are not food satiated at natural prey densities and that the number of prey ingested by a given grazer is linearly related to prey density; i.e.

$$P_t = P_0 e^{(k-g)t}$$

A constant growth coefficient  $k$  follows from assumption 1 if the concentrations of nutrients and other growth factors remain approximately constant (and/or non-limiting). According to the second assumption, the mortality coefficient  $g$  varies directly with the density of grazers but is not affected by changes in phytoplankton concentrations. The third assumption states that although the coefficients of  $k$  and  $g$  may vary with time of day, this

does not affect the comparisons of growth rates of natural phytoplankton in different dilutions over a fixed period of incubation. Landry and Hassett (1982) note that the instantaneous rate of phytoplankton mortality should decline in direct proportion to the dilution effect on grazer density.

The rates of phytoplankton growth and mortality due to grazing can be inferred from the observed changes in phytoplankton population density following incubations of different dilutions of populations in natural seawater.

Given a dilution series of unfiltered to filtered seawater of 1:0 (100% unfiltered sea water), 3:1 (75%), 1:1 (50%), and 1:3 (25%), the equations describing the changes in phytoplankton over time are exponential change over time with parameters of phytoplankton growth rates ( $k$  or  $\mu$ ) and zooplankton grazing rates ( $g$ ) for the dilution series (Table 1).

**Table 1. Equations for the change in phytoplankton biomass ( $P_t$ ) at some time ( $t$ ) from initial biomass ( $P_o$ ) with a growth rate ( $k$ ) and a grazing rate ( $g$ ) at various dilutions.**

Ratio	Or	
100%	$P_t = P_o e^{(k-g)t}$	$1/t \ln(P_t/P_o) = k-1.0g$
75%	$P_t = P_o e^{(k-.75g)t}$	$1/t \ln(P_t/P_o) = k-0.75g$
50%	$P_t = P_o e^{(k-.50g)t}$	$1/t \ln(P_t/P_o) = k-0.50g$
25%	$P_t = P_o e^{(k-.25g)t}$	$1/t \ln(P_t/P_o) = k-0.25g$

If the assumptions of the technique are valid then over all dilution treatments the observed rate of change in phytoplankton density is linearly related to dilution factor (decimal fraction of undiluted seawater) due consumption by microzooplankton. The negative slope of this relationship is the grazing coefficient  $g$ ; the Y axis intercept is the phytoplankton growth rate,  $k$ .

Landry and Hassett argue that the observed rates of change of phytoplankton density at any two dilution levels will yield two equations with two unknowns that can be solved explicitly for  $g$  and  $k$ . Linear regression analysis will provide estimates of the confidence limits for the coefficients.



**Table 2. A summary of the sample volumes required for various purposes in the grazing dilution experiments (modified after Landry and Hassett 1982).**

<b>Bottles required</b>	<b>Contents</b>	<b>Sample for</b>	<b>Seawater volume (L)</b>	<b>Diluent volume (L)</b>
<b>Time zero</b>				
1	100% D	T <sub>0</sub> 100% diluent chla T <sub>0</sub> (nuts + NH <sub>3</sub> )		2.6
3	100% SW	T <sub>0</sub> 100% SW chla	7.8	
2 * 1L	1L, 100% SW	T <sub>0</sub> microzooplankton / phytoplankton	2.5	
1*100 mL nutrient tubes	100 mL, 100% SW 200 mL 100% SW	T <sub>0</sub> picoplankton T <sub>0</sub> SW (nuts + NH <sub>3</sub> )	0.1 0.2	
<b>Post incubation</b>				
3	100% SW	T <sub>24</sub> 100% SW chla T <sub>24</sub> microzooplankton / phytoplankton 500mL	7.8	
3	70% SW + 30% D	70% T <sub>24</sub> SW chla	5.7	3.0
3	40% SW + 60% D	40% T <sub>24</sub> SW chla	3.6	5.1
3	10% SW + 90% D	10% T <sub>24</sub> SW chla	1.5	7.2
1	100% D	T <sub>24</sub> 100% diluent T <sub>24</sub> (nuts + NH <sub>3</sub> )		2.6
1 100 mL	100% SW	T <sub>24</sub> (nuts + NH <sub>3</sub> ) T <sub>24</sub> picoplankton	2.6	
	Totals (nearest litre)		32 L	21 L
Niskins			4	3

**Notes:**

1. Bottle volumes are about 2.4 L; in water calculations a rinse volume of 0.2 L was allowed, giving a total water requirement of 2.6 litres per bottle
2. SW = seawater filtered through 200 µm mesh to remove meso and macrozooplankton
3. D = diluent water, filtered through 0.2 µm Supor filter
4. "T<sub>0</sub> (nuts + NH<sub>4</sub>)" means that nutrients and ammonium were measured in these samples

### Calculations

Unfiltered water (SW)  
70%:  $2.4 \times 0.7 = 1.68 + 0.2 = 1.9\text{L} / \text{bottle} \times 3 \text{ bottles} = 5.7 \text{ L}$   
 $0.92\text{L} / \text{bottle} \times 3 = 3.0 \text{ L}$   
40%:  $2.4 \times 0.4 = 0.96 + 0.2 = 1.2\text{L} / \text{bottle} \times 3 \text{ bottles} = 3.6 \text{ L}$   
 $1.7\text{L} / \text{bottle} \times 3 = 5.1 \text{ L}$   
10%:  $2.4 \times 0.1 = 0.24 + 0.2 = 0.5\text{L} / \text{bottle} \times 3 \text{ bottles} = 1.5 \text{ L}$   
 $2.4\text{L} / \text{bottle} \times 3 = 7.2 \text{ L}$   
(+ 0.2 = RINSE)

Filtered water (D)  
30%:  $2.4 \times 3 = 0.72 + 0.2 =$   
60%:  $2.4 \times 6 = 1.44 + 0.2 =$   
90%:  $2.4 \times 9 = 2.16 + 0.2 =$

### 2.3. Sampling site

The location for these experiments was close to the mouth of the Huon Estuary, at the Hideaway Bay aquaculture facility of Huon Aquaculture Company Pty Ltd. (Fig 1.) Three experiments were carried out, one in September, one in November 2003, and third one in February 2004.

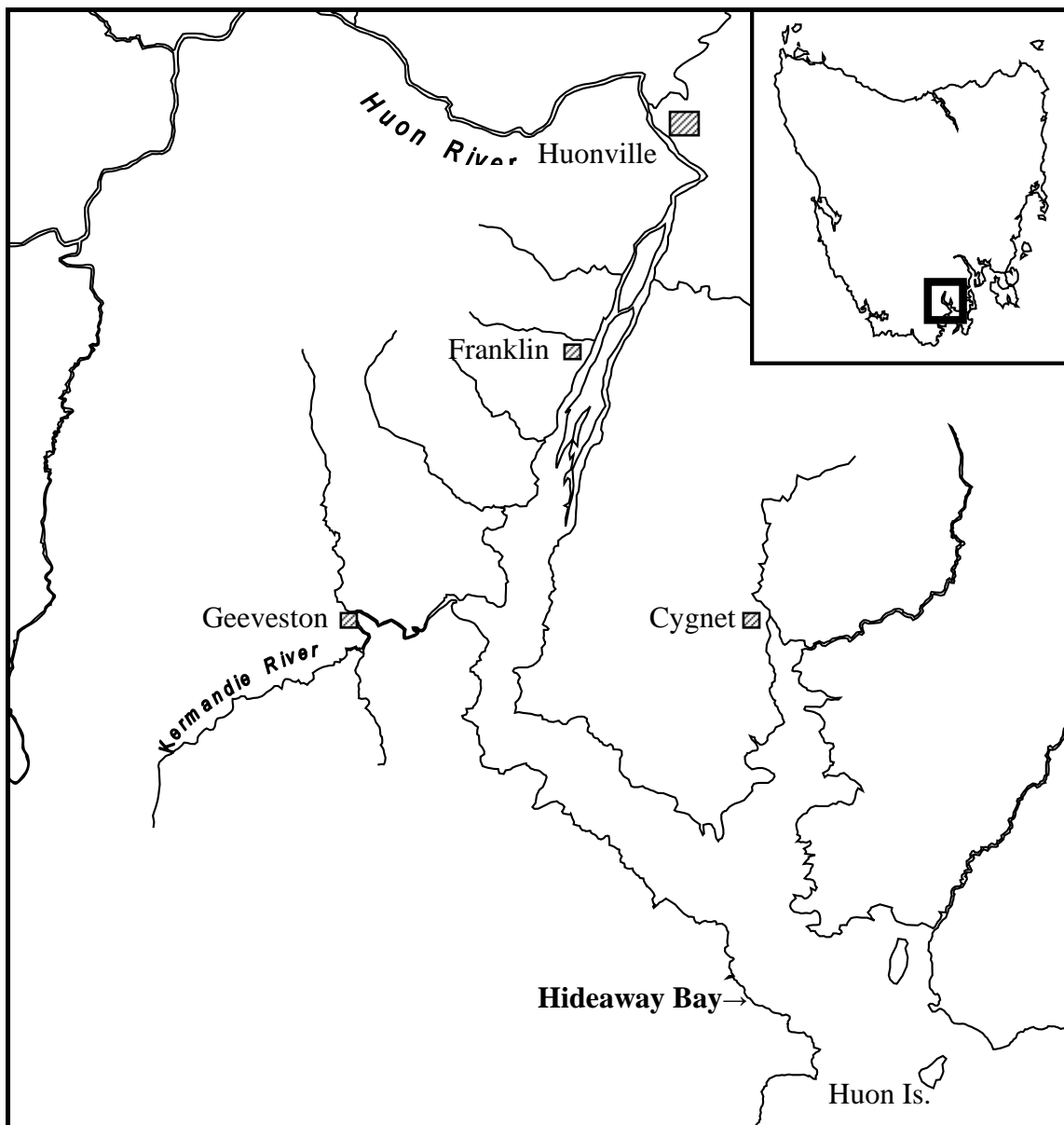


Fig 1. Location for grazing dilution experiments in Hideaway Bay, 2003-2004.

## 2.4. Sample Collection

Two sampling trips were made to collect seawater for each set of experiments. On the first trip at about 09:30, approximately 40 L seawater for the diluent was collected in 8 L Niskin bottles closed at 5–7m, i.e. at about 50% of surface light level and below any surface freshwater runoff layer. The Niskin bottle samples were gently decanted through a 200  $\mu\text{m}$  mesh insert in a large funnel into four 10 L carboys to take back to the field lab.

In the field lab, the seawater in the 10 L carboys was gently decanted into a 50 L carboy (C1). Approximately 35 L of this seawater was filtered under minimal vacuum through a 0.2  $\mu\text{m}$  Supor filter (12992 SuporCap 100 Sterile Capsule), and stored in a second 50 L carboy (C2). Samples were taken for nutrients from both the initial seawater and the filtered diluent. The incubation bottles were gently filled up with diluent (Supor-filtered water) through silicon tubing until the water reached the tape-mark. The filled bottles were stored in cotton “sleeves” in Eskies.

In oceanic waters, nutrients approximately equal to those in the water mass, plus  $\text{NH}_3$  to a final concentration of 2  $\mu\text{M}$ , would be added to each bottle, to ensure that nutrients were equally available to phytoplankton at all dilutions. Nutrient addition at this site in the Huon Estuary was deemed unnecessary. Seasonal variation in N:P ratios suggest there may be nitrate limitation at some sites in the Huon in the summer months, particularly in times of dense microalgal blooms, (CSIRO Huon Estuary Study Team, 2000). However, the Huon Aquaculture site is near the mouth of the estuary, water at the site is generally well-mixed and a residual store of nitrate is available in bottom waters at the marine end of the estuary (CSIRO Huon Estuary Study Team, 2000).

On the second sampling trip, around noon, seawater was collected from the same location and depth sampled as on the earlier trip. Water from the Niskins was gently transferred through a 200  $\mu\text{m}$  mesh insert in a large funnel into a 50 L carboy (C1), which had been rinsed with a small amount of the sample. Using silicon tubing, the polycarbonate bottles were gently filled to just overflowing with unfiltered seawater from the 50 L carboy C1. The bottles were sealed and stored in cotton “sleeves” in Eskies until all were filled. The bottles for incubation were transferred to wire-mesh cages, suspended at the same depth as sample collection (usually 5 m) and incubated for 24 hours.

In the field lab, the seawater carboy C1 and the diluent were sampled for  $T_0$  nutrients. Two one-litre samples of the seawater from carboy C1 were preserved for  $T_0$  microzooplankton / phytoplankton with Lugols iodine fixative solution (100 g potassium iodide, 50 g iodine, 1 L distilled water, 100 mL glacial acetic acid) to approximately 2% final concentration. 100 mL of the sample from C1 was also preserved with 25% glutaraldehyde (to about 0.3% final concentration) for  $T_0$  picoplankton samples. The contents of the three,  $T_0$  100% seawater bottles and the  $T_0$  100% diluent bottle were filtered, using less than 5 in Hg vacuum, through 47 mm GF/F filters, and the filters were stored in labelled cryotubes, immersed in liquid nitrogen until extraction of pigments.

## 2.5 End of Experiment

After approximately 24 hours, the cages and bottles were retrieved and the bottles placed in cotton “sleeves” in Eskies until filtration commenced. 500 mL was collected for  $T_{24}$  microzooplankton and phytoplankton from each of the three 100%  $T_{24}$  seawater samples and preserved with acid Lugol’s solution as detailed above. One 100%  $T_{24}$  seawater bottle

and the T<sub>24</sub> diluent bottle were sampled for nutrients. 100 mL from one 100% seawater bottle was sub-sampled for picoplankton and preserved with glutaraldehyde.

All the T<sub>24</sub> seawater and diluent samples were filtered, using less than 5 in Hg vacuum, through 47 mm GF/F filters, one dilution at a time, starting with all the 100% seawater samples, then the 70% seawater/ 30% diluent, and so on. The filters were stored in labelled cryotubes, immersed in liquid nitrogen until extraction of pigments. At the end of the experiment, all the 2-litre bottles were rinsed with dilute hydrochloric acid, then three rinses of MilliQ water, and stored dry in cotton sleeves for the next experiment.

For the November and February experiments, both fresh (refrigerated only) and frozen nutrient samples were analysed to determine whether the silicates were affected by freezing, because it is generally recognised that silicates, particularly in fresh water samples, are polymerised by freezing (Val Latham, pers. comm.). Silicate, nitrate / nitrite and phosphate samples were analysed on a Technicon AutoAnalyser 11 using methods described in Cowley (1999).

## **2.6. Microzooplankton and phytoplankton counting**

The Lugol's preserved samples were transferred to 1-litre measuring cylinders (volume recorded as V<sub>1</sub>) and allowed to settle for at least 24 hours. After this time, approximately 90% of the volume was siphoned off and the remaining sample was transferred to a 100 mL measuring cylinder and again allowed to settle for at least 24 hours. Then approximately 90% of the volume was siphoned off, the final volume recorded (V<sub>2</sub>) and thoroughly mixed before a 1 mL aliquot was taken, placed in a Sedgwick Rafter counting chamber and examined under an inverted microscope.

## **2.7. Microzooplankton and phytoplankton identification**

A Sedgwick Rafter counting chamber with a grid of 1000 squares, each of 1 µl, was used. For microzooplankton and larger phytoplankton species such as *Gymnodinium catenatum*, the entire slide was counted on a 10\* scale and a second 1 mL sample was also counted. Results for the two counts were averaged. For microplankton (cells generally larger than 20 µm diameter) at least 100 squares or 10% of the counting chamber was scanned on the 10\* scale (except in cases where there were dense blooms of one or more microplankton species, when at least one column of 20 squares was scanned). For nanoplankton, (2–20 µm in diameter) the chamber was examined under the highest possible magnification until at least 200 cells of the dominant nanoplankton “species” had been counted. Flagellates in the nanoplankton were grouped, as time constraints did not allow fuller identification.

$$\text{Cells per litre} = \text{cell “species” count} * (1000 / \text{number squares counted}) * (V_2 / V_1)$$

## **2.8. Pigment Samples**

All glassware was cleaned in dilute Extran solution, rinsed three times with MilliQ water and once with acetone (AR). Frozen filters were cut into halves and placed in a clean 10 mL glass centrifuge tube. Three mL of 100% acetone was added to each tube. The tube was covered with Parafilm and vortexed for ≈ 30 seconds before placing the tube in an ice-water bath and sonicating the filter and acetone for 15 minutes. The filters and acetone were then stored for at least 18 hours at 4°C. After this time, 0.2 mL MilliQ water was added to each tube (to bring solvent to ≈ 90:10 acetone:water) and the filter and solvent

sonicated for another 15 minutes. Solvent and filter were then transferred to a Biorad column containing a small GF/F filter acting as a plug.

The sample tubes were rinsed with 2 x 0.5 mL of acetone/water (90:10) which was added to the Biorad column. Each Biorad column was fitted into a centrifuge tube and the tubes were centrifuged for 5 minutes at 5000 rpm. The filtrate was stored on ice and darkness until just prior to analysis.

Pigment samples were analysed for pigment concentration and composition by high performance liquid chromatography (HPLC) with Waters instrumentation (Waters 996 Photodiode Array Detector, Waters 600 Controller, and Waters 717plus Autosampler) and processed for pigment identification and composition with Millennium software. Samples from February 2004 were analysed using Empower Pro software.

Before HPLC analysis, the extract was filtered through a 25 mm PTFE syringe filter, pore size 0.20  $\mu\text{m}$  (Advantec MFS Inc.) The HPLC system used an SGE 250\*4.6 mm SS Exsil ODS (octodecyl silica) 5  $\mu\text{m}$  column.

Pigments were eluted over a 30 minute period with a flow rate of 1 mL min<sup>-1</sup> using the following solvents:

- A. 80:20 (v/v) methanol:ammonium acetate buffer (0.5M, pH of 7.2)
- B. 90:10 (v/v) acetonitrile:MilliQ water
- C. 100% ethyl acetate

Each solvent was pre-filtered through a Millipore HVLP 0.45  $\mu\text{m}$  filter and degassed by sonication.

## 2.9. Calculations

The apparent growth rates for phytoplankton in individual bottles were calculated from the following equation, using total chlorophyll *a*, calculated from HPLC results, as the measure of standing stock:

$$P_t = P_0 e^{(k-g)t}$$

**Equation #1**

where  $P_t$  and  $P_0$  are the initial and final concentrations of chlorophyll *a* respectively.

Instantaneous coefficients of phytoplankton growth (*k*) and mortality through microzooplankton grazing (*g*) were determined from a least-squares and linear regression analysis of the relationship between the rate of change of chlorophyll and the fraction of undiluted seawater in the various bottles. The negative slope of this relationship is the grazing coefficient *g*; the Y axis intercept is the phytoplankton growth rate, *k*.

If a single grazer is present, clearance rate estimates, expressed as mL animal<sup>-1</sup> day<sup>-1</sup> could be calculated by dividing the estimate of the microzooplankton grazing impact by the density of microzooplankton determined from microscope counts (Landry and Hassett, 1982). In a mixed phyla grazing community with a variety of taxa present, average grazer numbers are calculated to provide a check on the status of the community (Brian Griffiths, pers. comm.).

Three other production parameters were calculated (Table 3); these formulae were adapted from Stelfox-Widdicombe et al. (2000) and Hall et al. (2004). The proportion of initial

standing stock ( $P_i$ ) turned over, as %  $d^{-1}$ , by the microzooplankton, was calculated according to:

$$P_i = 1 - e^{(-g)} * 100$$

**Equation #2**

Total microzooplankton ingestion rates (IR), expressed as  $\mu g \text{ Chl } L^{-1} d^{-1}$ , were estimated from:

$$IR = P_i * P_0$$

**Equation #3**

Stelfox-Widdicombe et al. (2000) use the calculation  $IR = P_i * P_0 * (C: \text{chl } a)$  but utilised image-analysis to measure cell-size and calculated biovolumes, then converted these biovolumes to carbon using conversion factors of  $0.14 \text{ pg C } \mu m^{-3}$  for dinoflagellates and  $0.19 \text{ pg C } \mu m^{-3}$  for other species. These techniques were outside the scope of the current experiments.

Potential percentage of the primary production grazed was calculated using:

$$100 * (1 - e^{(-g)}) / (1 - e^{(-\mu)})$$

**Equation #4**

where  $g$  is the grazing rate measured using the dilution method and  $\mu$  ( $\equiv k$  in Equation #1) is the specific growth rate (Hall et al., 2004).

### 3. Results

#### 3.1. General grazing on chlorophyll *a*, a temporal review

The first grazing dilution experiment was conducted in spring 2003. At this time the spring phytoplankton bloom had not yet occurred and the phytoplankton biomass in the water was relatively low,  $0.36 \mu\text{g L}^{-1}$ . The experiment did not yield very good results with quite variable data being obtained for the replicates at the lowest proportion (10%) of seawater (Fig. 2) and the slope of the line used to estimate grazing being very low  $0.031 \text{ d}^{-1}$  which was statistically indistinguishable from zero. Phytoplankton growth was also estimated to be low at  $0.044 \text{ d}^{-1}$  and not statistically different from zero. The estimated grazing pressure on the standing stock was 3% per day and 70% of new production was estimated to be grazed. The high degree of variability suggests a technical problem with the procedure and relatively little weight should be given to this first set of results.

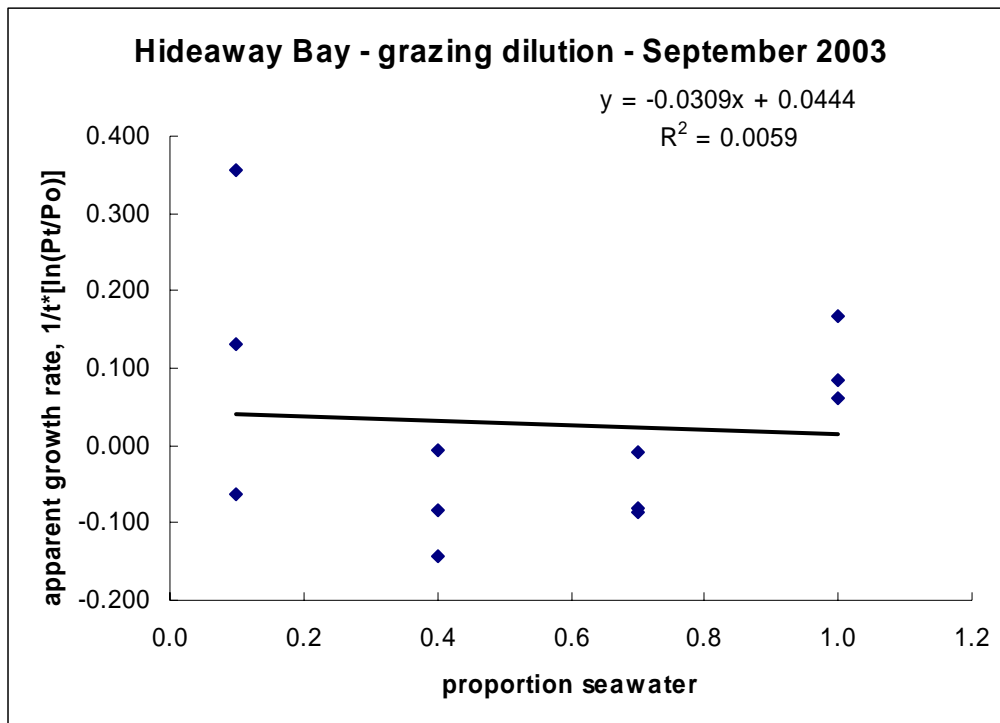


Fig. 2. Results from the first grazing dilution experiment conducted at Hideaway Bay in the Huon Estuary during Sept, 2003. Sample was collected from 5 m.

The second grazing dilution experiment was conducted in late spring 2003. At this time the spring phytoplankton bloom had commenced and the phytoplankton biomass in the water was relatively high, three times the September biomass, at  $1.18 \mu\text{g L}^{-1}$ . The experiment yielded better results with quite good agreement between the replicates at all dilutions (Fig. 3) and the slope of the line used to estimate grazing was  $0.66 \text{ d}^{-1}$  which was statistically greater than the rate measured in September 2003. Phytoplankton growth was also estimated to be greater than in September at  $1.03 \text{ d}^{-1}$ . The estimated grazing pressure on the standing stock was 48% per day and 76% of new production was estimated to be grazed.

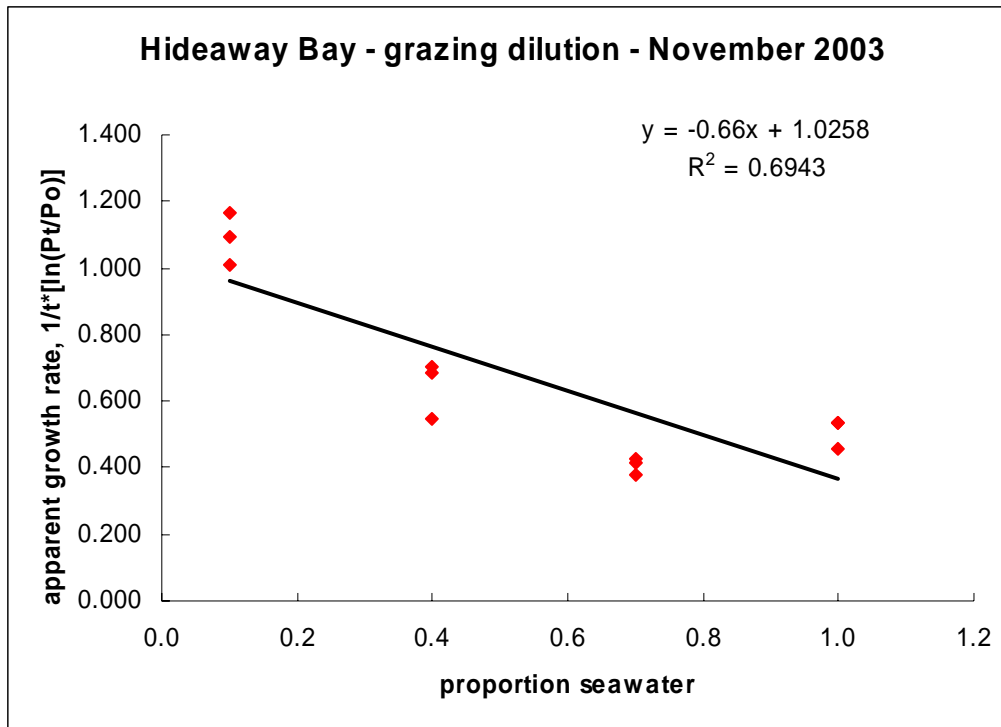


Fig. 3. Results from the second grazing dilution experiment conducted at Hideaway Bay in the Huon Estuary during November 2003. Sample was collected from 5 m.

The third grazing dilution experiment was conducted in late Summer 2003-2004. At this time another phytoplankton bloom was occurring and the phytoplankton biomass in the water was relatively high, more than five times the September biomass, at  $1.97 \mu\text{g L}^{-1}$ . The experiment yielded good results with very good agreement between the replicates at all the various dilutions (Fig. 4). The slope of the line used to estimate grazing was  $0.81 \text{ d}^{-1}$  which was the highest absolute grazing rate measured during these experiments. Phytoplankton growth was also estimated to be the highest observed during the study at  $1.32 \text{ d}^{-1}$ . The estimated grazing pressure on the standing stock was 56% per day and 76% of new production was estimated to be grazed each day.

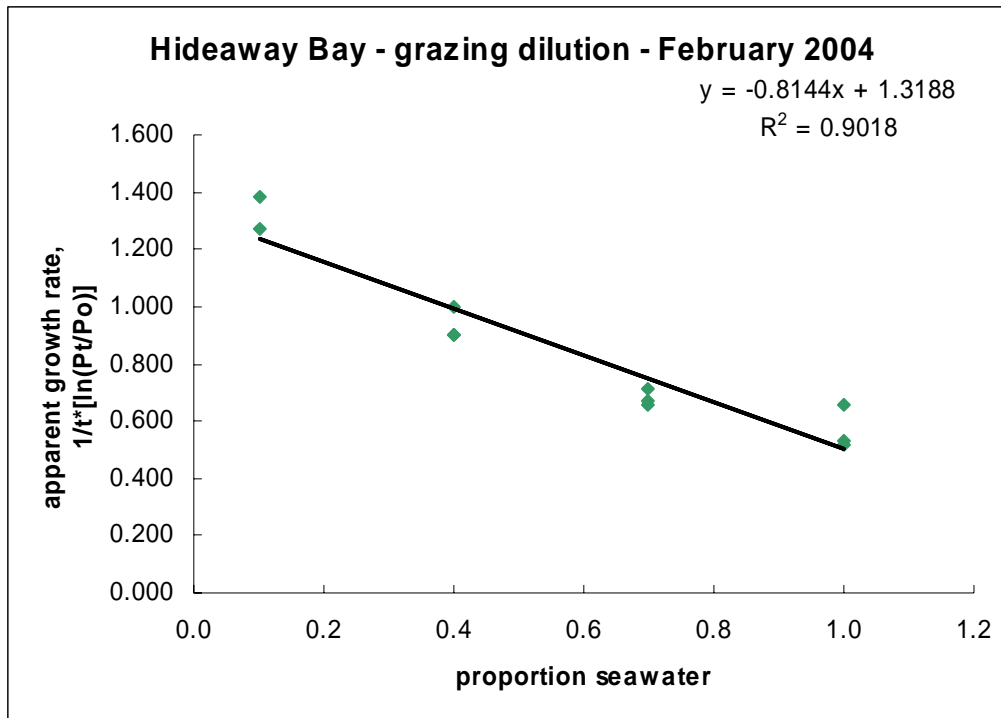


Fig. 4. Results from the third grazing dilution experiment conducted at Hideaway Bay in the Huon Estuary during February 2004. Sample was collected from 5 m.

The fourth grazing dilution experiment was conducted in winter 2004. At this time the phytoplankton biomass in the water was at its annual low with only  $0.25 \mu\text{g L}^{-1}$  or about  $1/8^{\text{th}}$  the biomass observed during summer. The experimental results were a bit more variable than those experiments conducted with more phytoplankton present with some greater variability between replicates at most of the various dilutions (Fig. 5). The slope of the line used to estimate grazing was  $0.51 \text{ d}^{-1}$  which was still quite a high grazing rate considering the small biomass of available phytoplankton. Phytoplankton growth was lower than late spring or Summer at  $0.54 \text{ d}^{-1}$ . The estimated grazing pressure on the standing stock was 40% per day and 96% of new production was estimated to be grazed on this day. This grazing rate (96%) on new production was the highest observed throughout the year.

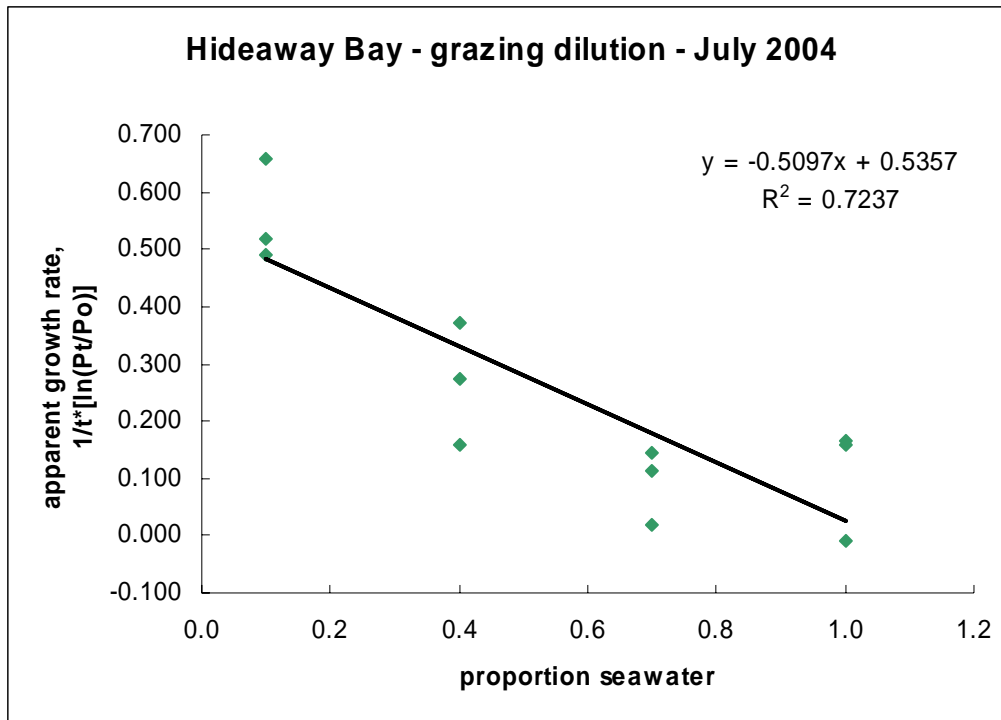


Fig. 5. Results from the forth grazing dilution experiment conducted at Hideaway Bay in the Huon Estuary during July 2004. Sample was collected from 5 m.

The net growth of phytoplankton can be estimated from the difference between  $\mu$  and  $g$ . Based on these results net growth rates of the whole phytoplankton community (using the ubiquitous chlorophyll *a* as the measure of phytoplankton) were very low in early spring (September 2003) and winter (June 2004). The highest net growth rates occurred during the spring and late summer algal blooms (Table 3, Fig. 6).

**Table 3. Summary of the grazing rates and gross phytoplankton growth rates (based upon chlorophyll *a*) in the Huon Estuary during 2003-2004. Means, ( $\pm$  standard errors) are reported.**

Date	Standing stock chlorophyll <i>a</i> $\mu\text{g L}^{-1}$	Slope = grazing coefficient: <i>g</i> $\text{d}^{-1}$	Y axis intercept = phytoplankton growth rate: $\mu$ or <i>k</i> $\text{d}^{-1}$	$R^2$	Net growth rate ( $\mu - g$ ) $\text{d}^{-1}$
September 2003	0.36	-0.03 ( $\pm 0.13$ )	0.04 ( $\pm 0.08$ )	0.006	0.01 ( $\pm 0.15$ )
November 2003	1.18	-0.66 ( $\pm 0.14$ )	1.03 ( $\pm 0.09$ )	0.694	0.37 ( $\pm 0.16$ )
February 2004	1.98	-0.81 ( $\pm 0.09$ )	1.32 ( $\pm 0.06$ )	0.902	0.504 ( $\pm 0.11$ )
July 2004	0.25	-0.51 ( $\pm 0.10$ )	0.54 ( $\pm 0.06$ )	0.724	0.0260 ( $\pm 0.12$ )

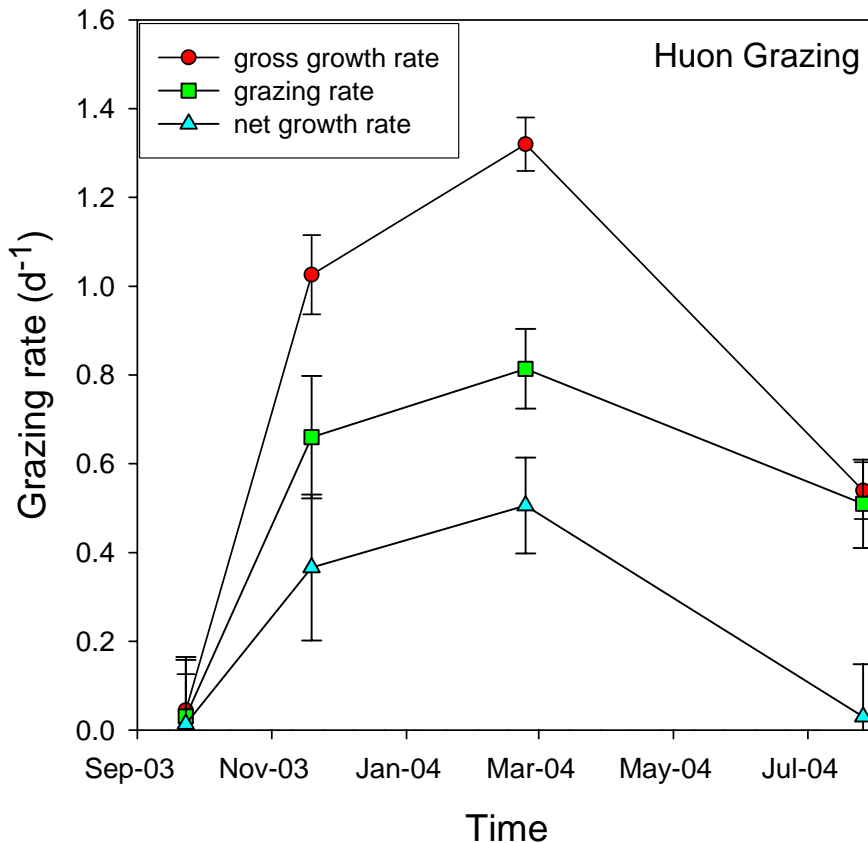


Figure 6. Measurements of gross phytoplankton growth, grazing by microheterotrophs and net phytoplankton growth rates measured approximately seasonally from September 2003 to June 2004.

### 3.2. Differential grazing rates, examples from February 2004

When sufficient biomass was present some of the taxon specific marker pigments were present above detection limits in even the most highly diluted samples (a full set of pigment data can be found in Appendix 1). These marker pigments can also be used to calculate growth and grazing rates in a manner similar to that for chlorophyll *a*. During such an experiment in February 2004 some pigments were clearly grazed more than others (Fig. 7).

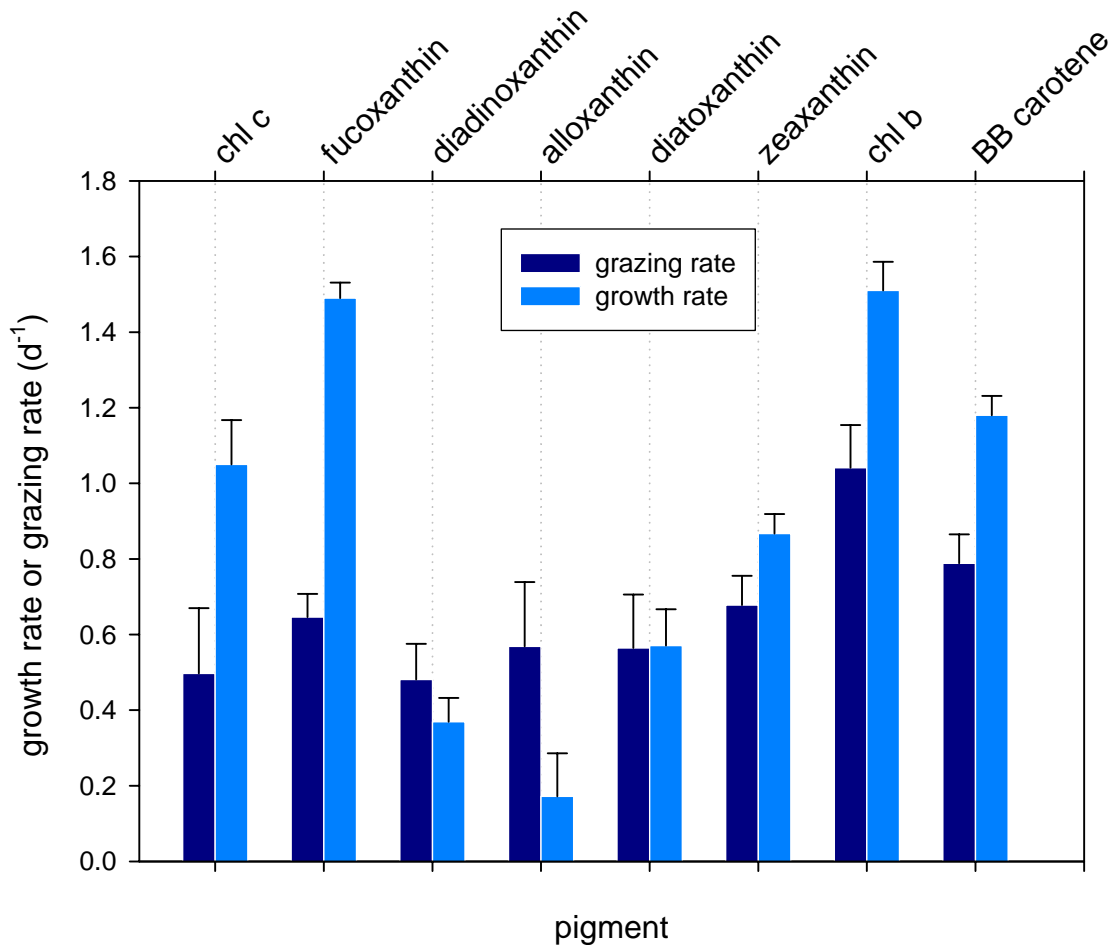


Fig. 7. Growth and grazing rates determined for specific pigments from the grazing-dilution experiment conducted in the Huon Estuary, February 2004.

For example, the grazing rate on alloxanthin exceeded its growth rate by a factor of ~3 while grazing was only ½ the growth rate of pigments such as chlorophyll *c* and fucoxanthin. Grazing was approximately equal to or greater than gross growth rates for alloxanthin, diadinoxanthin, diatoxanthin and zeaxanthin, while for chlorophyll *b*, chlorophyll *c*, fucoxanthin and  $\beta,\beta$ -carotene the growth rates were substantially greater than the grazing rates. The calculated net growth rates ( $\mu - g$ ) were greatest for fucoxanthin ( $0.84 \text{ d}^{-1}$ ) and about 33% greater than for the most generic pigment, chlorophyll *a*. The results clearly indicate that differential grazing was sufficient to shift phytoplankton community composition relatively quickly reducing Cyanophyta and

Cryptophyta relative to taxa such as Bacillariophyta, Dinophyta, Prymnesiophyceae, Chrysophyceae and Raphidophyceae.

Cell counts by light microscopy provide another data set that can be used to estimate grazing upon particular taxa. This approach of estimating growth for individual species is only feasible for the more dominant species and even then the precision of the estimated net growth rates can be relatively poor due to the uncertainty associated with the technique. For the experiments reported here only the initial and final 100% seawater samples were enumerated providing a species-specific estimate of net growth rather than separate estimates of grazing and growth. The complete list and mean densities found in the initial and final 100% seawater samples demonstrate some of the dramatic changes in species density that occur over a seasonal cycle in the Huon Estuary (Table 4). Where sufficient data are available the densities of common diatoms such as *Skeletonema costatum*, *Nitzschia closterium* and small (< 10  $\mu\text{m}$ ) *Chaetoceros* vary in abundance by ~200x during the transition from winter to summer. Positive net growth rates were calculated for all of the 8 most dominant diatoms and the 3 most dominant dinoflagellates observed during the summer (Feb 2004) bloom event (Fig. 8).

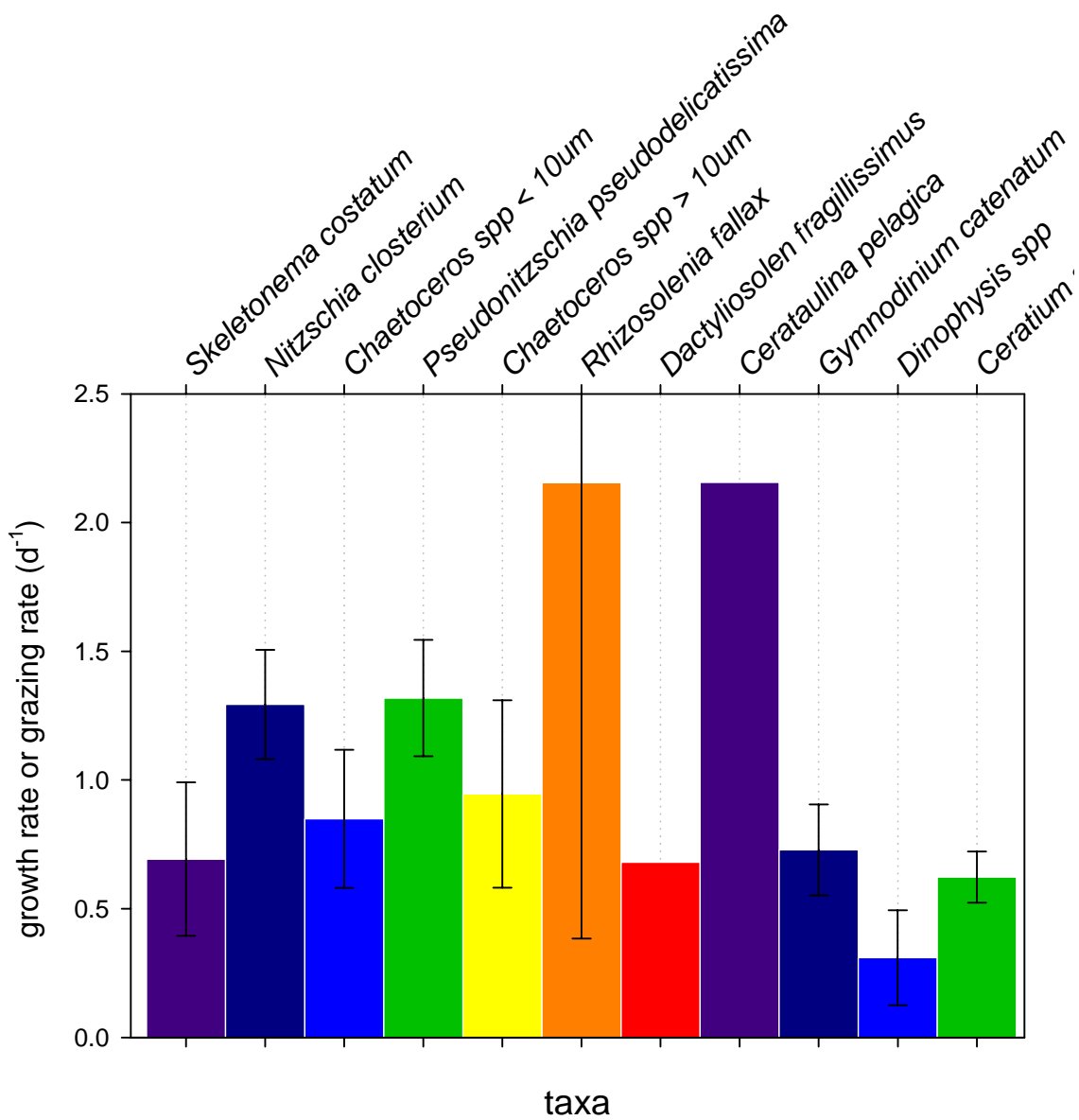


Figure 8. Estimated net growth rates for various species or functional groups (e.g. *Chaetoceros* > 10 microns) observed within a late summer bloom in the Huon Estuary during February 2004. Means  $\pm$  1 standard error are indicated (with the exception of no SE for *Dactyliosolen fragillissimus* and *Cerataulina pelagica*).

**Table 4. Phytoplankton species densities in the Huon Estuary from Sept 23, 2003 to July 26, 2004. Numbers per litre.**

	HG01 23 Sept- 2003	HG01 24 Sept- 2003	HG02 18 Nov- 2003	HG02 19 Nov- 2003	HG03 24 Feb- 2004	HG03 25 Feb 2004	HG04 26 Jul 2004	HG04 27 Jul 2004
	T <sub>0</sub> SW	T <sub>24</sub> SW	T <sub>0</sub> SW	T <sub>24</sub> SW	T <sub>0</sub> SW	T <sub>24</sub> SW	T <sub>0</sub> SW	T <sub>24</sub> SW
<b>1. Diatoms</b>								
<i>Amphora</i>	54						29	39
<i>Cerataulina pelagica</i>			682	5366	519	4482		
<i>Coscinodiscus sp</i>	21	155	319	938	871	2648	10	
<i>Lauderia annulata</i>	86	425	82	173				
<i>Licmophora</i>			429				31	17
<i>Melosira</i>	352	512						78
<i>Nitzschia closterium</i>	793	2110	2385	5237	49499	183482	161	278
<i>Nitzschia spp.</i>	91							235
<i>Pleurosigma</i>	18	196	171				8	24
<i>Pseudo-nitzschia pseudodelicatissima</i>	1248	732	2136	7195	19234	73413	451	435
<i>Guinardia striata</i>			569	972	56	2367		
<i>Rhizosolenia setigera</i>								20
<i>Skeletonema costatum</i>	521	1540	1602	12182	938150	1835305	124	335
<i>Thalassiosira sp.</i>							77	157
<i>Thalassionema sp.</i>							16	
<i>Leptocylindrus mediterraneus</i>				438		10385		
<i>Eucampia</i>			360	748				
<i>Striatella</i>				18			10	
<i>Grammatophora</i>	311							
<i>Paralia</i>					280			
<i>Guinardia delicatula</i>	227		936	4160				
<i>Corethron criophilum</i>	77							
<i>Odontella</i>		95						
<i>Chaetoceros spp &gt; 10um</i>	401	488	1988	5115	6630	15855	26	130
<i>Chaetoceros spp &lt; 10um</i>		480	1681	4074	29695	66584		131
<i>Leptocylindrus danicus</i>	91		341	4393	104			
<i>Guinardia flaccida</i>	9		41223	50312	61	2939		
<i>Dactyliosolen fragillissimus</i>			4607	8704	1608	3175		

	HG01 23 Sept- 2003	HG01 24 Sept- 2003	HG02 18 Nov- 2003	HG02 19 Nov- 2003	HG03 24 Feb- 2004	HG03 25 Feb 2004	HG04 26 Jul 2004	HG04 27 Jul 2004
<i>Rhizosolenia fallax</i>	58	148	557	36	787	1761		20
<b>2. Dinoflagellates and nanoflagellates</b>								
small dinoflagellates	273	1760						
<i>Prorocentrum</i>					15	47		
<i>Ceratium spp</i>	27	10	1024	2451	226	423	365	479
<i>Dissodinium lunula</i>			13	30				
<i>Dinophysis spp</i>	36	17	228	304	344	478		15
<i>Gymnodinium catenatum</i>	132	278	33	235	2657	5576	501	191
<i>Mesodinium rubrum</i>	1450							
flagellates ('000)	863	2262	1355	2333	1067	2457	629	1326

N.B. Blank cells represent densities below detection limits. (approximately 10 cells per litre for larger taxa, 25–50 per litre for nanoplankton).

### 3.3. Microzooplankton counts

Microzooplankton grazers included copepod nauplii, tintinnids, heterotrophic dinoflagellates such as *Polykrikos*, and naked (oligotrich) ciliates. Oligotrich ciliates, tintinnids and heterotrophic dinoflagellates dominated the microzooplankton in all samples counted (Table 5). All ciliated protozoans were classed as potential grazers, except for the ciliate *Mesodinium* spp which contains cryptophyte symbionts and was regarded as photosynthetic. There are several possible sources of error in counting and identifying microzooplankton grazers to determine community structure. For example, results from the November 2003 experiment appear to indicate a reduction in grazer numbers. Possible explanations may include: larger grazers consuming smaller microzooplankton, or possible mis-identification of autotrophic taxa as heterotrophic, or vice versa.

Heterotrophic nanoflagellates cannot be distinguished from autotrophic forms using ordinary light microscopy, and separate methods such as fixation with glutaraldehyde, staining with DAPI and epifluorescent microscopy would be needed to quantify these nanoflagellates. Picoplankton samples from the current experiments have been collected and fixed with glutaraldehyde, but have not been examined or counted pending commissioning of the epifluorescent Olympus microscope. Similarly, heterotrophic dinoflagellates could be more accurately distinguished from autotrophic forms by examining chlorophyll fluorescence in fresh specimens. Finally, species counts are based on total counts, when not all individuals may have been acting as heterotrophic grazers at any one time during the experiment. Grazer counts have been averaged over the 24 hour period but a more accurate calculation may be relative geometric mean predator density (GMPD) as described by Hall et al. (2004).

The dominant microheterotroph grazers were ciliates (43%), followed by heterotrophic dinoflagellates (30%) and tintinnids (18%). Small numbers of most other grazers were observed with radiolarians, copepod nauplii, bivalve larvae, Appendicularians (larval tunicates), and rotifers each averaging less than 1% of the total (Fig. 9). Numbers of

*Polykrikos schwartzii* peaked (combined T<sub>0</sub> and T<sub>24</sub> 100% seawater samples) at  $510 \pm 361$  L<sup>-1</sup> in February 2004. Temporal variability was not as pronounced as in the phytoplankton community but overall the total number of grazers was maximal during November 2003, and significantly greater ( $P < 0.001$ ) than the numbers observed in February or July 2004 (Fig.10). The rise in grazers during November 2003 was primarily due to an increase in ciliates and was accompanied by a significant ( $P < 0.05$ ) decline in grazer diversity (Fig. 10).

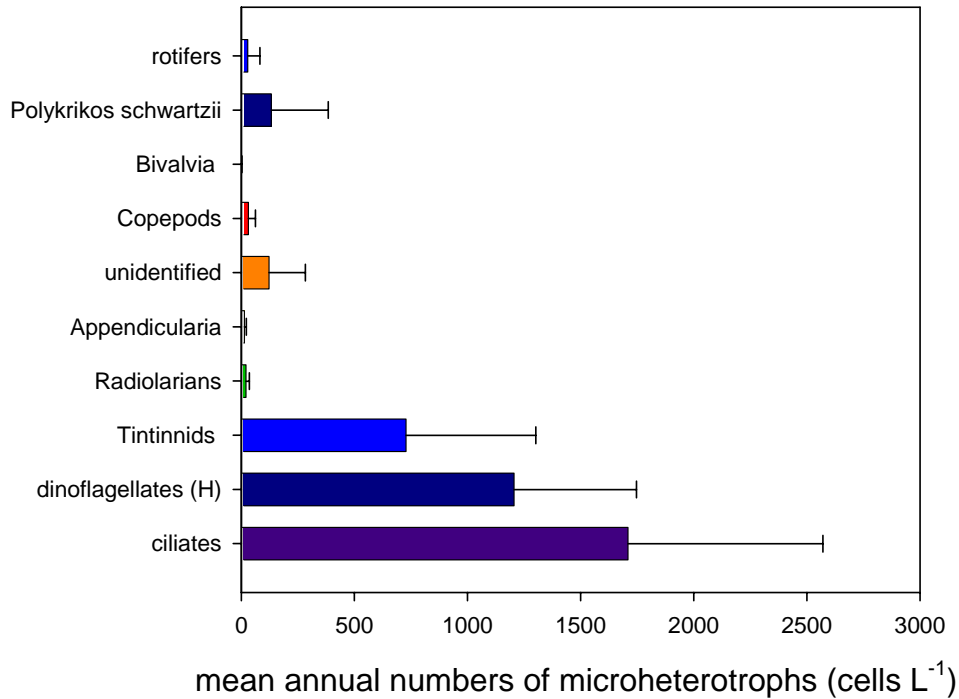


Figure 9. The mean (+ 1 std. error) abundances of dominant groups of microheterotroph grazers (microzooplankton) in the Huon Estuary, sampled four times during 2003-2004

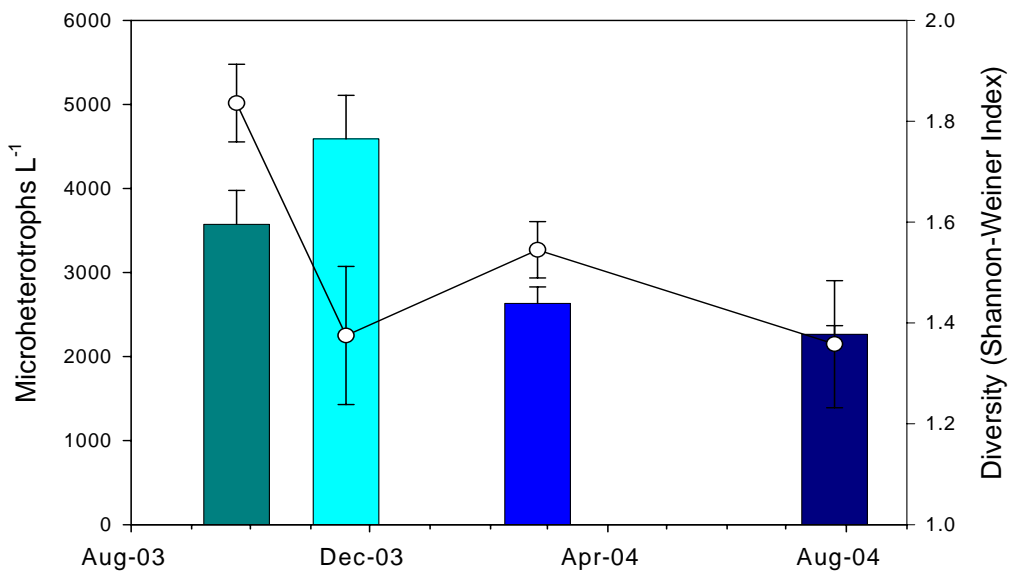


Figure 10. The mean (+ 1 std error) abundance of all microheterotrophs at the four sample periods and the diversity (○) of the community.

**Table 5. Microzooplankton densities in the Huon Estuary from Sept 23, 2003 to July 26, 2004. Numbers per litre.**

	<b>HG01 23-Sep- 2003</b>	<b>HG01 24-Sep- 2003</b>	<b>HG02 18-Nov- 2003</b>	<b>HG02 19-Nov- 2003</b>	<b>HG03 24-Feb- 2004</b>	<b>HG03 25-Feb- 2004</b>	<b>HG04 26-Jul- 2004</b>	<b>HG04 27-Jul- 2004</b>
	T <sub>0</sub> SW	T <sub>24</sub> SW						
<i>Polykrikos schwartzii</i>		22	14	17	124	767	4	8
Tintinnids	708	658	393	454	1076	1862	397	166
Bivalvia	5	10	4					
Copepods	12	16	64	68	34	57		
Cnidaria					10	18		
Appendicularia	14	13	9	21	9	36	4	
Radiolarians	28	14	5		45	21	21	39
Rotifers			4	17	5			
Dinoflagellates (heterotrophic)	1053	1649	716	1303	1128	2446	582	500
Ciliates	760	1007	4594	1898	821	1781	1070	1647
Other grazers	64	116	28	26	55	48	18	18

N.B. a blank cell indicates the taxon was not seen during counting and indicates a density below our detection limit (approximately 10 cells per litre).

### 3.4. Nutrient concentrations

A comparison of the T<sub>0</sub> and T<sub>24</sub> nutrient samples indicates that during the experiments phosphate and silicate limitation did not occur and errors caused by the incubations “running out” of phosphate or silicate were not observed (Table 6). The results further indicate that nitrogen limitation was probable during the November 2003 experiment (Table 6). However this condition was present in the natural environment, it was not an artefact of the experimental conditions thus the experimental results can be considered to reflect the ambient conditions.

**Table 6. Nutrient concentrations**

Date	Treatment	Nitrate/Nitrite μM-N	Phosphate μM-P	Nitrite μM-N	Silicate μM-Si
23-Sep-03	T <sub>0</sub> Diluent	4.00	0.42	0.31	4.54
23-Sep-03	T <sub>0</sub> Seawater	3.87	0.44	0.33	3.21
24-Sep-03	T <sub>24</sub> Seawater	3.87	0.42	0.32	3.37
18-Nov-03	T <sub>0</sub> Seawater for Diluent	0.02	0.21	0.00	2.10
18-Nov-03	T <sub>0</sub> Diluent	0.02	0.17	0.00	2.10
18-Nov-03	T <sub>0</sub> SW	0.02	0.21	0.01	1.90
19-Nov-03	T <sub>24</sub> Seawater	0.02	0.14	0.01	1.72
19-Nov-03	T <sub>24</sub> Diluent	0.07	0.18	0.01	2.11
24-Feb-04	T <sub>0</sub> Seawater for Diluent	0.25	0.25	0.03	4.17
24-Feb-04	T <sub>0</sub> Diluent	0.22	0.25	0.03	4.52
24-Feb-04	T <sub>0</sub> SW	0.12	0.22	0.01	3.76
25-Feb-04	T <sub>24</sub> Seawater	0.02	0.19	0.00	2.52
25-Feb-04	T <sub>24</sub> Diluent	0.22	0.25	0.03	4.41
26-Jul-04	T <sub>0</sub> Seawater for Diluent	4.35	0.50	0.30	2.49
26-Jul-04	T <sub>0</sub> Diluent	5.72	0.55	0.29	2.79
26-Jul-04	T <sub>0</sub> SW	3.54	0.41	0.32	10.30
27-Jul-04	T <sub>24</sub> Seawater	4.37	0.45	0.35	2.30
27-Jul-04	T <sub>24</sub> Diluent	5.56	0.59	0.29	2.73
<i>Limits of detection (uM):</i>		<i>0.03</i>	<i>0.03</i>	<i>0.01</i>	<i>0.04</i>

## 4. Discussion

Gross phytoplankton growth rates ( $\mu$ ) varied over the annual cycle from about zero to 1.3 d<sup>-1</sup>. The upper gross growth rate (1.3 d<sup>-1</sup>) is approximately the maximum that can be expected for temperate phytoplankton species under the prevailing temperature conditions (Eppley 1972). Net phytoplankton growth rates based on chlorophyll *a* were sometimes small, but increased sharply during the blooms both during spring and in the late summer bloom reaching 0.37 to 0.5 d<sup>-1</sup> (~40% of gross growth rates) during November 2003 and February 2004. That net growth rates may be small at certain times of the year is perfectly consistent with the observations of changes in widespread chlorophyll *a* concentrations in

the Huon Estuary and nearby D'Entrecasteaux Channel. For example, averaged over 12 sites in D'Entrecasteaux Channel the observed increase in chlorophyll *a* concentration represented a net growth rate of  $0.005 \text{ d}^{-1}$  during the annual transition from winter minimum to spring maximum.

Given that our experiments measured gross growth rates that are consistent with the demonstrated capability of the species present in this ecosystem and that net growth rates observed from local sampling and estimated by the grazing dilution technique were generally lower, and sometimes considerably lower, we can conclude that microheterotroph grazing was always capable of consuming a substantial portion of the daily primary production. In other ecosystems around the world reported grazing rates were often lower but range from  $\sim 40\%$  to  $100+\%$  of primary production (see review by Calbet and Landry 2004). As our observations indicate grazing rates in the Huon were always greater than 69% of gross production and reached 96% in winter they are at the upper end of those observed elsewhere. This comparison suggests that the Huon Estuary is characterized by a high degree of top-down control on phytoplankton.

Using individual pigments to calculate pigment specific growth and grazing rates suggested that grazing pressure was not uniform across a range of phytoplankton classes. Diatoms (based on cell counts and fucoxanthin) and some dinoflagellates had quite high net growth rates, a result consistent with the observed concurrent late summer bloom. Zeaxanthin was present (as in 1997, CSIRO Huon Estuary Study Team. 2000) and was also grazed efficiently. Possible sources of zeaxanthin are cyanobacteria, although these were seldom observed during phytoplankton counts, or some species of the Chlorophyta. Chlorophyll *b* was also present and grazed although at this time we cannot resolve whether this is divinyl chlorophyll *b* from prochlorophytes or monovinyl chlorophyll *b* from chlorophytes, prasinophytes or euglenophytes such as *Eutreptiella*; however monovinyl is considered more likely. The results of net growth rate estimates for particular pigments or species make it clear that the overall grazing rate estimated for the entire community (based on chlorophyll *a*) can considerably overestimate the grazing on some species.

It is clear that the nutrient concentration in the surface layer was not sufficient to support the development of a phytoplankton bloom from November to May. Ignoring physical concentration as a mechanism to achieve bloom densities, phytoplankton must access nutrients from recycling a local source or from deeper in the water column. Given the dual controls on phytoplankton biomass (bottom-up by nutrients or top-down by predators) it would only seem possible for the blooms to occur when phytoplankton escape grazing and access sufficient nutrients. It is possible that vertical migration by dinoflagellates achieves both these objectives while allowing the cells to remain within the estuary in spite of the relatively strong estuarine circulation.

The microzooplankton community was similar in composition to those observed in coastal water bodies from Nova Scotia, Canada (Gifford 1988) to South Africa (Froneman and McQuaid 1997) with dominance by ciliates (aloricate) followed by tintinnids. Densities of both types of ciliates (aloricate + tintinnids) were  $\sim 2400 \text{ L}^{-1}$ , which is very similar to the value of  $2100 \text{ L}^{-1}$  reported for waters around New Zealand (James et al., 1996, Hall et al., 2004). The major difference between microheterotrophs in the Huon Estuary and other coastal locations in the world seems to be the greater importance of heterotrophic dinoflagellates. Heterotrophic dinoflagellates have been reported to be dominant grazers in some pelagic ecosystems but not in oligotrophic ones where the picoplankton are considered too small for efficient grazing by some dinoflagellates (Stelfox-Widdicombe et al. 2000). Large numbers of heterotrophic dinoflagellates are characteristic of the Australasian region north of the subtropical convergence (Wood

1954). Although *Noctiluca scintillans* was present during February 2004 (P. Thompson, pers. obs.) its large size meant that it was considered a component of the macrozooplankton (> 200 µm) and it was excluded from these experiments.

The available data indicate that grazing pressure was always high in the Huon Estuary with microheterotrophs capable of consuming ~ 80% of primary production. Although this conclusion should be tempered by the lack of resolution in time and space it indicates that top down control is an important component of the pelagic ecology in this ecosystem. For a phytoplankton bloom to occur a species or community must escape this strong grazing pressure for sufficient time to bloom. At the phytoplankton community level there are only a few mechanisms that would allow a general escape from microheterotroph predation. For example there is often a lag between the increasing growth rate of phytoplankton relative to zooplankton in early spring, the net result is a spring bloom. Spring blooms occur most years in the Huon Estuary and D'Entrecasteaux Channel indicating this uncoupling does occur. During summer it is possible that grazing pressure is reduced as a result of a trophic cascade. Grazing by macrozooplankton on microzooplankton has been shown to reduce grazing on phytoplankton by 50% (Hansen et al. 1993). We have observed episodic high densities of salps (tunicates) that appear to remove most of the particles from the water column. Subsequent to these salp "blooms" there may be an opportunity for phytoplankton growth to escape top down control. It is also possible that *Noctiluca scintillans* may act in the same manner. In general the published accounts of trophic cascades involve nonvisual feeders such as ctenophores or medusae (Table 1 in Verity and Smetacek 1996).

Species-specific mechanisms used to escape predation are much better studied in terrestrial ecosystems and include: satiation, spatial separation, size, physical defences, chemical defences, colouration or behaviour, and symbiosis. Routine monitoring of the Huon Estuary and D'Entrecasteaux Channel found mostly diatom blooms. As a group diatoms often use the satiation escape mechanism in that, under the right conditions, they grow faster and are sufficiently abundant that their predators cannot control them. While there were reports from various sources of high densities of *Gymnodinium catenatum*, *Heterosigma akashiwo* and *Karenia* sp. in the south east region of Tasmania we can only confirm high densities of *G. catenatum* from various locations during late summer 2004. We also observed the highest densities of *Polykrikos* during February 2004 and it has been demonstrated that this genus both grazes *G. catenatum* and has a faster intrinsic growth rate (Jeong et al., 2001). It seems likely that predator avoidance, possibly through the diel vertical migration undertaken by *G. catenatum* as observed during HES and in this study (data not shown), represents an important predator escape mechanism.

## **Acknowledgements**

These experiments were carried out through the Environment program in the Aquafin CRC with considerable assistance from: Huon Aquaculture Company Pty Ltd and their staff, particularly Dominic O'Brien. Funding was provided by the Aquafin CRC, CSIRO, and FRDC. Additional support was provided by CSIRO Marine Research staff: Brian Griffiths, Paul Armstrong, Val Latham, Kate Berry, Ros Watson, Lesley Clementson, Matt Sherlock, & Lindsay Macdonald.

## References

- Calbet, A., M.R. Landry (2004). Phytoplankton growth, microzooplankton grazing, and carbon cycling in marine ecosystems. *Limnology and Oceanography* 49:51-57.
- Cowley, R (ed.) (1999). Hydrochemistry Operations Manual, CSIRO Marine Research. CSIRO Marine Laboratories Report 236, 1999.
- CSIRO Huon Estuary Study Team (2000). Huon Estuary Study: Environmental Research for Integrated Catchment Management and Aquaculture. *CSIRO Marine Research and FRDC Project no 96/284*.
- Eppley, R.W. (1972). Temperature and phytoplankton growth in the sea. *Fish. Bull.* 70, 1063-1085.
- Froneman, P.W., McQuaid, C.D. (1997). Preliminary investigations of the ecological role of microzooplankton in the Kariega Estuary, South Africa. *Estuarine and Coastal Shelf Science* 45, 689-695.
- Fileman, E., Burkhill, P. (2001). The herbivorous impact of microzooplankton during two short-term lagrangian experiments off the NW coast of Galicia in summer 1998. *Progress in Oceanography* 51, 361-383.
- Hall, J.A., Safi, K., and Cumming, A. (2004) Role of microzooplankton grazers in the subtropical and subantarctic waters to the east of New Zealand. *New Zealand Journal of Marine and Freshwater Research* 38: 91-101.
- Jeong, H.E., Kim, S.K., Kim, J.S., Kim, S.T., Yoo, Y.D., Yoon, J.Y. (2001). Growth and grazing rates of the heterotrophic dinoflagellate *Polykrikos kofoidii* on red-tide and toxic dinoflagellates. *J. Eukaryotic Microbiology* 48, 298-308.
- Landry, M.R. and Hassett, R.P. (1982). Estimating the grazing impact of marine microzooplankton. *Marine Biology* 67: 283-288.
- Stelfox-Widdicombe, C.E., Edwards, E.S., Burkill, P.H., and Sleight, M.A. (2000). Microzooplankton grazing activity in the temperate and sub-tropical NE Atlantic: summer 1996. *Marine Ecology Progress Series* 208: 1-12.
- Verity P.G., Smetacek, V. (1996). Organism life cycles, predation, and the structure of marine pelagic ecosystems. *Marine Ecology Progress Series* 130, 277-293.
- Wood, E.J.F. (1954). Dinoflagellates in the Australian region. *Australian Journal of Marine and Freshwater Research* 5, 171-351.

Appendix 1: Huon grazing dilution experiments – HPLC pigments - Hideaway Bay site

HG01 - September 2003

Date	% unfiltered seawater	Chl c1+c2	Peri	19'-but	Fuco	19'-hex	cis-fuco	Pras	Viola	Dino	cis-pras	Diadino	Allo	Diat	Lut	Zea	Chl b	β-car	ββ-car	Total Chl a-like
23-Sep-03	100% T <sub>0</sub>	0.084	0.015	---	0.070	0.018	---	0.007	---	---	---	0.021	0.025	---	0.004	0.007	0.050	0.004	0.008	0.366
23-Sep-03	100% T <sub>0</sub>	0.069	0.013	---	0.068	0.016	---	0.010	---	---	---	0.020	0.024	---	0.004	0.007	0.052	0.004	0.009	0.357
23-Sep-03	100% T <sub>0</sub>	0.072	0.014	---	0.066	0.017	---	0.010	0.003	0.003	---	0.019	0.023	---	---	0.007	0.050	0.004	0.009	0.350
23-Sep-03	0% T <sub>0</sub>	---	---	---	---	---	---	---	---	---	---	---	---	---	---	---	---	---	---	---
24-Sep-03	100% T <sub>24</sub>	0.079	0.013	---	0.087	0.017	---	0.008	0.005	---	---	0.022	0.024	---	---	0.009	0.060	---	0.009	0.388
24-Sep-03	100% T <sub>24</sub>	0.076	0.015	---	0.085	0.022	---	0.009	0.004	---	---	0.023	0.023	---	---	0.009	0.052	---	0.011	0.379
24-Sep-03	100% T <sub>24</sub>	0.073	0.013	---	0.084	0.018	---	0.009	---	---	---	0.024	0.027	---	---	0.009	0.060	0.005	0.010	0.420
24-Sep-03	70% T <sub>24</sub>	0.026	---	---	0.045	0.009	---	0.004	---	---	---	0.012	0.016	---	---	0.005	0.031	---	0.005	0.232
24-Sep-03	70% T <sub>24</sub>	0.038	---	---	0.053	0.010	---	---	---	---	---	0.014	0.016	---	---	0.005	0.036	0.003	0.006	0.248
24-Sep-03	70% T <sub>24</sub>	0.037	0.010	---	0.049	0.005	---	0.004	---	---	---	0.014	0.016	---	---	0.005	0.031	---	0.005	0.231
24-Sep-03	40% T <sub>24</sub>	0.014	---	---	0.025	---	---	---	---	---	---	0.008	0.009	---	---	---	0.018	---	---	0.132
24-Sep-03	40% T <sub>24</sub>	0.011	---	---	0.024	---	---	---	---	---	---	0.007	0.009	---	---	---	0.017	---	---	0.125
24-Sep-03	40% T <sub>24</sub>	0.015	---	---	0.029	---	---	---	---	---	---	0.007	0.010	---	---	---	0.020	---	---	0.142
24-Sep-03	10% T <sub>24</sub>	---	---	---	0.007	---	---	---	---	---	---	---	0.004	---	---	---	---	---	---	0.051
24-Sep-03	10% T <sub>24</sub>	---	---	---	0.007	---	---	---	---	---	---	---	---	---	---	---	---	---	---	0.034
24-Sep-03	10% T <sub>24</sub>	---	---	---	0.006	---	---	---	---	---	---	---	---	---	---	---	---	---	---	0.041
24-Sep-03	0% T <sub>24</sub>	---	---	---	---	---	---	---	---	---	---	---	---	---	---	---	---	---	---	---
24-Sep-03	100% T <sub>24</sub>	0.074	0.007	---	0.081	0.013	---	0.010	---	---	---	0.027	0.028	---	---	0.009	0.064	0.005	0.011	0.456

**HG02 - November 2003**

Date	% unfiltered seawater	Chl c1+c2	Peri	19'-but	Fuco	19'-hex	cis-fuco	Pras	Viola	Dino	cis-pras	Diadino	Allo	Diat	Lut	Zea	Chl b	β-car	ββ-car	Total Chl a-like
18-Nov-03	100% T <sub>0</sub>	0.297	0.082	---	0.398	0.078	0.022	0.023	0.017	---	---	0.164	0.025	0.028	0.008	0.019	0.086	---	0.033	1.229
18-Nov-03	100% T <sub>0</sub>	0.270	0.065	---	0.330	0.070	0.015	0.019	0.014	---	---	0.132	0.012	0.022	0.006	0.015	0.083	---	0.027	1.095
18-Nov-03	100% T <sub>0</sub>	0.268	0.072	---	0.388	0.072	0.019	0.018	0.014	---	---	0.164	0.023	0.025	0.007	0.017	0.085	---	0.034	1.226
18-Nov-03	0% T <sub>0</sub>	---	---	---	---	---	---	---	---	---	---	---	---	---	---	---	---	---	---	---
19-Nov-03	100% T <sub>24</sub>	0.363	0.073	---	0.596	0.078	0.032	0.022	0.024	---	0.012	0.156	0.020	0.040	0.007	0.022	0.150	0.004	0.049	2.026
19-Nov-03	100% T <sub>24</sub>	0.471	0.080	---	0.572	0.071	0.031	0.027	0.025	---	0.012	0.153	0.020	0.036	0.006	0.018	0.150	---	0.049	1.877
19-Nov-03	100% T <sub>24</sub>	0.449	0.089	---	0.639	0.103	0.044	0.037	0.029	---	0.015	0.170	0.023	0.041	0.008	0.023	0.150	---	0.051	2.027
19-Nov-03	70% T <sub>24</sub>	0.300	0.050	---	0.379	0.074	0.026	0.024	0.019	---	0.009	0.097	0.014	0.022	0.004	0.015	0.097	0.003	0.031	1.270
19-Nov-03	70% T <sub>24</sub>	0.328	0.051	---	0.389	0.075	0.022	0.021	0.016	---	0.007	0.085	0.010	0.022	0.005	0.015	0.099	---	0.031	1.256
19-Nov-03	70% T <sub>24</sub>	0.302	0.050	---	0.346	0.084	0.020	0.022	0.016	---	0.006	0.088	0.011	0.020	0.004	0.015	0.107	---	0.028	1.215
19-Nov-03	40% T <sub>24</sub>	0.213	0.038	---	0.284	0.060	0.015	0.016	0.013	---	0.005	0.070	0.008	0.015	---	0.010	0.073	---	0.021	0.961
19-Nov-03	40% T <sub>24</sub>	0.153	0.035	---	0.250	0.055	0.013	0.014	0.011	---	---	0.069	0.008	0.012	---	0.010	0.067	---	0.022	0.830
19-Nov-03	40% T <sub>24</sub>	0.190	0.039	---	0.293	0.048	0.012	0.014	0.012	---	0.004	0.078	0.011	0.018	---	0.009	0.070	---	0.025	0.951
19-Nov-03	10% T <sub>24</sub>	0.031	0.014	---	0.093	0.015	0.013	---	---	---	---	0.022	---	---	---	---	0.023	---	0.006	0.330
19-Nov-03	10% T <sub>24</sub>	0.043	0.013	---	0.108	0.014	0.016	---	0.004	---	---	0.025	---	0.006	---	---	0.028	---	0.006	0.388
19-Nov-03	10% T <sub>24</sub>	0.053	0.016	---	0.105	0.018	0.013	---	0.004	---	---	0.026	---	0.006	---	---	0.024	---	0.007	0.362
19-Nov-03	0% T <sub>24</sub>	---	---	---	---	---	---	---	---	---	---	---	---	---	---	---	---	---	---	---
19-Nov-03	100% T <sub>0</sub>	0.283	0.072	---	0.487	0.045	0.084	0.017	0.017	---	---	0.136	0.013	0.042	0.009	0.025	0.139	---	0.035	1.910

HG03 - February 2004

Date	% unfiltered seawater	Chl c1+c2	Peri	19'-but	Fuco	19'-hex	cis-fuco	Pras	Viola	Dino	cis-pras	Diadi no	Allo	Diat	Lut	Zea	Chl b	Be-car	ββ-car	Total Chl a-like
24-Feb-04	100% T <sub>0</sub>	0.391	0.103	0.013	0.481	0.032	0.077	---	0.028	0.026	0.010	0.260	0.058	0.045	0.009	0.029	0.138	0.007	0.054	1.909
24-Feb-04	100% T <sub>0</sub>	0.413	0.105	0.013	0.475	0.030	0.079	---	0.028	0.024	0.010	0.264	0.059	0.051	0.010	0.030	0.137	0.006	0.051	1.940
24-Feb-04	100% T <sub>0</sub>	0.336	0.107	0.012	0.504	0.035	0.079	---	0.029	0.027	0.010	0.273	0.062	0.050	0.012	0.034	0.153	0.007	0.057	2.078
24-Feb-04	0% T <sub>0</sub>	---	---	---	---	---	---	---	---	---	---	---	---	---	---	---	---	---	---	---
25-Feb-04	100% T <sub>24</sub>	0.633	0.123	---	1.081	0.050	0.167	---	0.036	0.040	0.022	0.245	0.046	0.049	0.010	0.041	0.244	0.007	0.083	3.283
25-Feb-04	100% T <sub>24</sub>	0.753	0.132	0.010	1.167	0.052	0.180	---	0.037	0.042	0.024	0.254	0.040	0.064	0.011	0.041	0.274	0.007	0.088	3.718
25-Feb-04	100% T <sub>24</sub>	0.736	0.137	---	1.139	0.050	0.176	---	0.036	0.043	0.022	0.263	0.047	0.049	0.008	0.035	0.203	0.007	0.075	3.247
25-Feb-04	70% T <sub>24</sub>	0.584	0.086	---	0.871	0.032	0.136	---	0.030	0.027	0.017	0.183	0.029	0.035	0.006	0.027	0.187	0.005	0.062	2.624
25-Feb-04	70% T <sub>24</sub>	0.469	0.083	---	0.918	0.025	0.122	---	0.027	0.023	0.015	0.184	0.035	0.037	0.007	0.031	0.196	0.006	0.070	2.747
25-Feb-04	70% T <sub>24</sub>	0.353	0.078	---	0.859	0.017	0.125	---	0.028	0.023	0.014	0.173	0.028	0.035	0.006	0.030	0.201	0.005	0.068	2.597
25-Feb-04	40% T <sub>24</sub>	0.280	0.050	---	0.587	---	0.080	---	0.018	0.013	0.009	0.106	0.018	0.022	0.004	0.021	0.153	0.004	0.046	1.881
25-Feb-04	40% T <sub>24</sub>	0.363	0.055	---	0.638	---	0.094	---	0.021	0.016	0.011	0.119	0.018	0.026	0.005	0.023	0.152	0.004	0.048	1.878
25-Feb-04	40% T <sub>24</sub>	0.359	0.061	---	0.679	---	0.103	---	0.023	0.018	0.011	0.133	0.027	0.031	0.005	0.022	0.164	0.005	0.053	2.062
25-Feb-04	10% T <sub>24</sub>	0.112	0.005	---	0.215	---	0.038	---	0.002	---	---	0.041	0.008	0.009	---	0.007	0.066	---	0.018	0.763
25-Feb-04	10% T <sub>24</sub>	0.109	0.005	---	0.188	---	0.036	---	---	---	---	0.039	0.007	0.008	---	0.007	0.055	---	0.016	0.684
25-Feb-04	10% T <sub>24</sub>	lost	lost	lost	lost	lost	lost	lost	lost	lost	lost	lost	lost	lost	lost	lost	lost	lost	lost	lost
25-Feb-04	0% T <sub>24</sub>	---	---	---	---	---	---	---	---	---	---	---	---	---	---	---	---	---	---	---
25-Feb-04	100% T <sub>0</sub>	lost	lost	lost	lost	lost	lost	lost	lost	lost	lost	lost	lost	lost	lost	lost	lost	lost	lost	lost

HG04 - July 2004

Date	% unfiltered seawater	Chl c1+c2	Peri	19'-but	Fuco	19'-hex	cis-fuco	Pras	Viola	Dino	cis-pras	Diadino	Allo	Diat	Lut	Zea	Chl b	β-car	ββ-car	Total Chl a-like
24-Feb-04	100% T <sub>0</sub>	0.081	0.056	---	0.027	---	---	---	---	0.007	---	0.027	0.015	---	---	0.005	0.016	---	0.006	0.248
24-Feb-04	100% T <sub>0</sub>	0.074	0.055	---	0.025	---	---	---	---	0.008	---	0.026	0.017	---	---	0.006	0.017	---	0.006	0.255
24-Feb-04	100% T <sub>0</sub>	0.077	0.052	---	0.028	---	---	---	---	0.007	---	0.028	0.016	---	---	---	0.019	---	0.005	0.257
24-Feb-04	0% T <sub>0</sub>	---	---	---	---	---	---	---	---	---	---	---	---	---	---	---	---	---	---	---
25-Feb-04	100% T <sub>24</sub>	0.078	0.053	---	0.038	---	---	---	---	0.009	---	0.029	0.014	---	---	0.008	0.026	---	0.008	0.296
25-Feb-04	100% T <sub>24</sub>	0.060	0.058	---	0.039	---	---	---	---	0.005	---	0.030	0.013	---	---	0.008	0.024	---	0.008	0.298
25-Feb-04	100% T <sub>24</sub>	0.071	0.049	---	0.035	---	---	---	---	0.008	---	0.024	0.012	---	---	0.006	0.020	---	0.007	0.251
25-Feb-04	70% T <sub>24</sub>	0.067	0.038	---	0.028	0.008	---	---	---	0.007	---	0.019	0.011	---	---	0.005	0.018	---	0.004	0.204
25-Feb-04	70% T <sub>24</sub>	0.054	0.035	---	0.021	---	---	---	---	0.004	---	0.018	0.009	---	---	0.005	0.016	---	0.005	0.198
25-Feb-04	70% T <sub>24</sub>	0.042	0.033	---	0.028	---	---	---	---	0.004	---	0.017	0.008	---	---	0.004	0.014	---	0.004	0.181
25-Feb-04	40% T <sub>24</sub>	0.024	0.016	---	0.017	---	---	---	---	0.000	---	0.010	0.006	---	---	---	---	---	---	0.119
25-Feb-04	40% T <sub>24</sub>	0.021	0.021	---	0.018	---	---	---	---	0.003	---	0.012	0.008	---	---	---	---	---	---	0.133
25-Feb-04	40% T <sub>24</sub>	0.021	0.016	---	0.014	---	---	---	---	0.000	---	0.012	0.007	---	---	---	---	---	0.004	0.146
25-Feb-04	10% T <sub>24</sub>	0.009	---	---	---	---	---	---	---	0.000	---	0.005	---	---	---	---	---	---	---	0.043
25-Feb-04	10% T <sub>24</sub>	---	---	---	---	---	---	---	---	0.000	---	0.004	---	---	---	---	---	---	---	0.049
25-Feb-04	10% T <sub>24</sub>	---	---	---	---	---	---	---	---	0.000	---	0.004	---	---	---	---	---	---	---	0.041
25-Feb-04	0% T <sub>24</sub>	---	---	---	---	---	---	---	---	0.000	---	0.000	---	---	---	---	---	---	---	---
25-Feb-04	100% T <sub>0</sub>	0.059	0.051	---	0.034	---	---	---	---	0.007	---	0.025	0.013	---	---	0.005	0.023	---	0.006	0.271

Key: Chl c1+c2 = Chlorophyll c1+c2, Peri = Peridinin, 19'-but = 19'-butanoyloxyfucoxanthin, Fuco = Fucoxanthin, 19'-hex = 19'-hexanoyloxyfucoxanthin, cis-fuco = cis-fucoxanthin, Pras = Prasincoxanthin, Viola = Violaxanthin, Dino = Dincoxanthin, Cis-pras = cis-prasincoxanthin, Diadino = Diadinoxanthin, Allo = Alloxanthin, Diato = Diatoxanthin, Lut = Lutein, Zeax = Zeaxanthin, Chl b = Chlorophyll b, β-car = β-carotene, ββ-car = ββ-carotene, Total Chl a-like = Total Chlorophyll a-like (total results of all chlorophyll a like compounds and derivatives)

# Technical Report

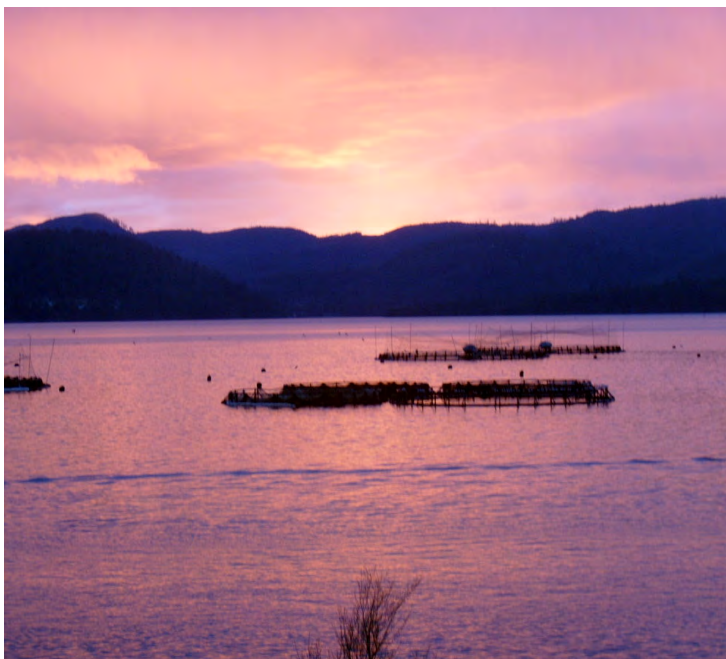


Measuring ecological health: A preliminary assessment of phytoplankton sampling strategies for the Huon Estuary and D'Entrecasteaux Channel including an initial comparison of the Huon interim monitoring (2001-2004) with HES (1996-1998) data for chlorophyll a concentration.

*Peter Thompson and John Parslow*

*July 2005*

*Aquafin CRC Project 4.2  
(FRDC Project No. 2001/097)*



© Copyright Aquafin Cooperative Research Centre, Fisheries Research and Development Corporation, Commonwealth Scientific and Industrial Research Organisation

**This work is copyright. Except as permitted under the Copyright Act 1968 (Cth), no part of this publication may be reproduced by any process, electronic or otherwise, without the specific written permission of the copyright owners. Neither may information be stored electronically in any form whatsoever without such permission.**

**Every attempt has been made to provide accurate information in this document. However, no liability attaches to Aquafin CRC, its participant organisations or any other organisation or individual concerned with the supply of information or preparation of this document for any consequences of using the information contained in the document.**

*Published by CSIRO Marine and Atmospheric Research*



Measuring ecological health: A preliminary assessment of phytoplankton sampling strategies for the Huon Estuary and D'Entrecasteaux Channel including an initial comparison of the Huon interim monitoring (2001-2004) with HES (1996-1998) data for chlorophyll *a* concentration

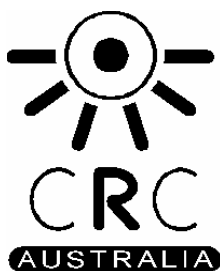
**Peter Thompson and John Parslow**  
CSIRO Marine and Atmospheric Research

*July 2005*

*Aquafin CRC Project 4.2  
(FRDC Project No. 2001/097)*



**Australian Government**  
**Fisheries Research and  
Development Corporation**



Tasmanian Aquaculture  
& Fisheries Institute  
*University of Tasmania*

## General Introduction

Two major issues are addressed in this appendix to the report. They include (1) assessing the existing data to make preliminary recommendations on improvements to the sampling strategy and (2) comparing the HES (1996-1998) data on chlorophyll *a* concentrations in the Huon with those from 2001-2004. The primary issues with regard to sampling regime were: whether integrated or surface samples should be used; and at what time and space scales do data become suitably independent so they may be used as statistical replicates? Once these issues were resolved then we began the assessment of whether the existing sampling design could be improved by applying the following principles:

### ***1. Formulate a clear, concise hypothesis\****

*The success of a sampling program often hinges on clear, explicit hypotheses. Imprecise thinking at this stage frequently leads to wasteful data collection without enough planning as to how, to what end, and at what cost the information can be subsequently handled. The hypotheses to be tested have implications for what and how data are to be collected.*

### ***2. Stratify in time and space to reduce heterogeneity\****

*If the area to be sampled is large and heterogeneous (highly variable), then sampling from the entire area, ignoring the known heterogeneity, reduces the precision of the estimate. By stratifying ( $\equiv$  blocking) the survey area in advance this extra variability can be accounted for.*

*\*adapted from Roger Green 1979*

# Part I: Assessment of existing data

## Introduction

Phytoplankton biomass, measured as chlorophyll *a*, is one of the few national (ANZECC/ARMCANZ 2000) and internationally accepted criteria as an indicator of ecological health for aquatic ecosystems. Increases in phytoplankton biomass or an increased frequency of algal blooms are considered indicators of an increase in nutrient loading to aquatic ecosystems. In the case of the region of interest, SE Tasmania, the D'Entrecasteaux Channel and Huon Estuary there are both natural and anthropogenic sources of variation in the nutrient loading.

The 2000 HES report predicted that “at four times current loads...the predicted phytoplankton biomass...is about twice current levels” and “a substantial risk of prolonged algal blooms would arise”. We understand nutrient loads into the Huon Estuary from fish farming have risen (Colin Shepard, pers. com.). There has been an “interim monitoring program” in the Huon since 2002, however, it is important to note that this interim monitoring program was never designed to assess changes in chlorophyll *a* concentration over time or to detect the number, size or magnitude of algal blooms but simply to determine whether the Huon Estuary was in danger of ecosystem failure. In this context “ecosystem failure” was considered to be hypoxia leading to failure of the aerobic component of the natural nitrogen cycle resulting in a build up of ammonia in subsurface waters that might fuel algal blooms. The results of the interim monitoring are reported elsewhere (Crawford et al. 2004) but the general conclusion is the aquatic ecosystem remains in relatively good health. Furthermore based on what we already know about interannual variability in chlorophyll *a* concentrations within the Huon Estuary a simple comparison of the 1996-1998 data with that from 2002-2003 may not be a reliable indicator of change.

## Sampling considerations.

By undertaking a statistical analysis of data collected as part of the baseline monitoring of the D'Entrecasteaux Channel, the Huon Estuary Study (HES) or the interim monitoring of the Huon we are accepting that the input data comply with the assumptions of sampling theory and therefore that the statistical analyses will yield valid conclusions regarding the state of the environment(s) being sampled. Most statistical analyses assume that

1. the sampling technique adequately reflects reality
2. all sampling is random or appropriately stratified
3. the samples are independent.

The first section of this chapter addresses these assumptions in the geographical context of the Huon Estuary and D'Entrecasteaux Channel and for chlorophyll *a*.

In situations where the variability in the parameter of interest is distributed randomly then random sampling is an appropriate and cost effective sampling strategy. Where the variation is not distributed at random then detecting a difference in time or space

by using a random sampling approach may be impossible and/or can waste an enormous amount of time and effort (=money). Where a significant fraction of the variation is due to identifiable causes the sampling effort should be stratified (= blocked) to capture this variation and then random within the stratification. The following sections provide a preliminary review of the information in the existing data that is relevant to efficient sampling design. At the onset it is worth noting that the existing data on chlorophyll *a* concentrations was collected by several programs where sampling was not random in time or space although in some instances sampling was explicitly designed around hypothesized patterns that, if demonstrated to be real, would justify stratification of the sampling effort.

A properly designed monitoring program should be capable of detecting an agreed change in time or space. In the case of the Huon Estuary and D'Entrecasteaux Channel the objectives of the final monitoring program may be to detect change over time in the ecosystem as a whole or change over time at specific locations. As with many monitoring programs minimizing the cost is often an additional and important design consideration. In most cases minimizing the cost involves reducing the number of samples collected or analysed. One method of reducing cost is to ensure that each sample provides the maximum amount of new information or has a high value. In situations where samples are collected too close together in time or space their value is low and they may invalidate the underlying assumptions of statistical procedures designed to test for differences. Only through intelligent sampling design can the sampling regime and the detection of change (statistical power) be appropriately balanced against cost.

## Temporal variability

The temporal frequency of sampling can invalidate any statistical comparison if the samples are taken at inappropriate intervals and thus were not independent. For example, samples taken a few seconds apart at one site are likely to be similar. It may even be possible to compare them to samples collected in rapid succession at another site, however, if the samples were not really independent then the statistical comparison is not valid. The statistical test relies on each observation being independent. A cursory examination of the integrated chlorophyll *a* concentrations for the weekly samples collected as part of the HES indicate a strong degree of concordance in time across stations (Fig 1).

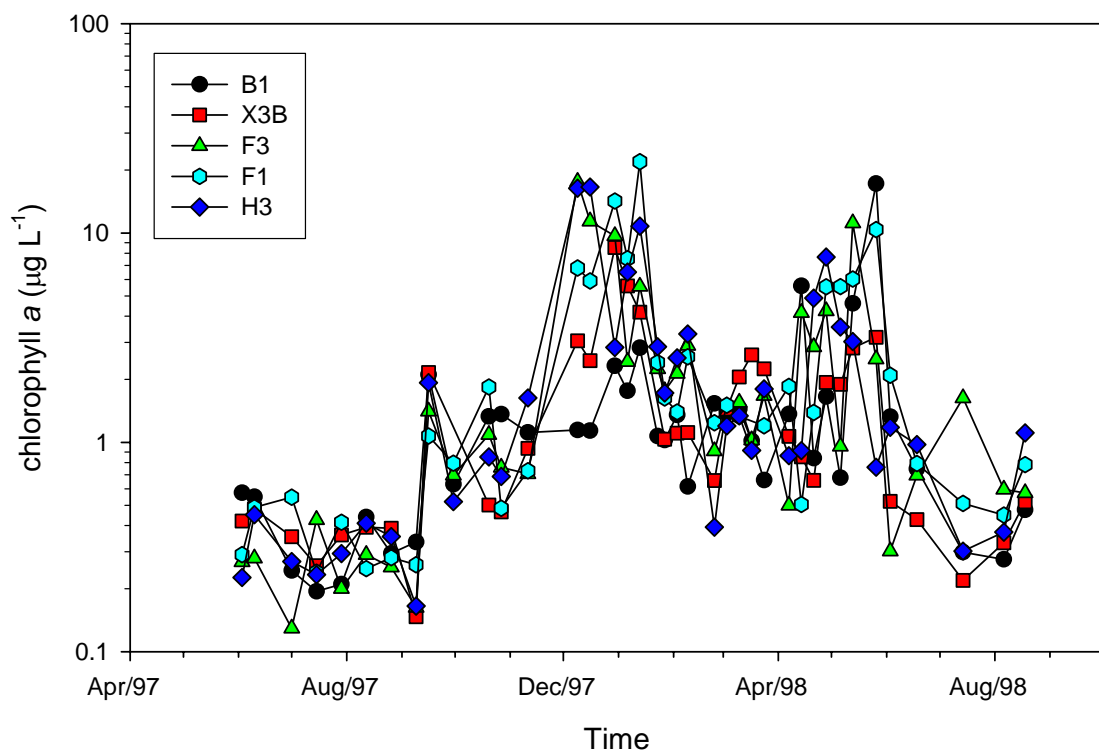


Figure 1. Integrated chlorophyll *a* concentrations from five weekly monitored stations in the Huon Estuary.

A simple test for dependence is to see if the data collected at different time intervals are correlated. High degrees of autocorrelation indicate both inefficient sampling design (less information gained per sample) and data that violate the assumption of independence required so that any statistical comparison may be valid.

In the Huon Estuary Study five sites (B1, F1, F3, H3 and X3B) were sampled weekly for ~ 70 weeks from November 5, 1996 to August 18 1998. For each site the surface and integrated chlorophyll *a* concentrations were tested for a correlation with the chlorophyll *a* concentrations lagged by 1, 2, 3.... to 12 weeks. Higher correlations were found for the shorter lags in the integrated chlorophyll *a* concentrations relative to the surface concentrations (data not shown). The time lag of correlations was also tested on log transformed integrated chlorophyll *a* data. Short term correlations were greatest in the log transformed integrated chlorophyll *a* concentrations. The site F3 from the Huon Estuary showed the highest degree of autocorrelation in its integrated chlorophyll *a* measurements (Fig. 2). Fifty three percent of the variability in samples taken one week later was “explained” by the chlorophyll *a* concentration measured the preceding week ( $r^2= 0.527$ ). Significant autocorrelation was also present after two weeks, but a three week lag was sufficient to reduce temporal autocorrelation to insignificance (Fig. 2).

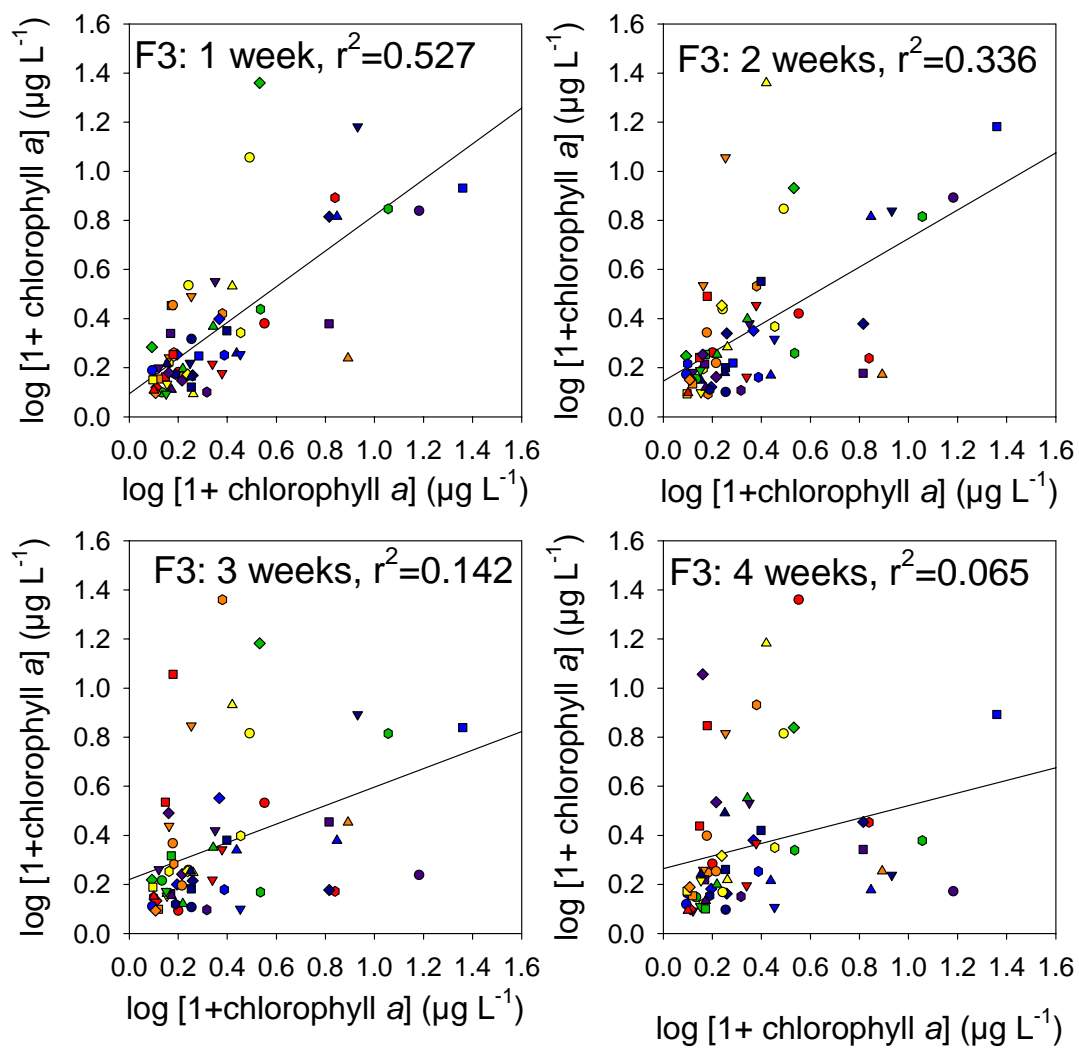


Fig. 2. Autocorrelation of integrated chlorophyll *a* concentrations from HES site F3 lagged by one, two, three and four weeks.

It can be argued that applying this test for temporal autocorrelation to all five stations with 12 lagged time steps requires some adjustment to the probability of rejecting the null hypothesis of no significant correlation (type I error or alpha). Normally alpha is set at 0.05 or a one in twenty chance of rejecting the null hypothesis when, in fact, it is true and the data are NOT correlated. The most rigorous, well tested and conservative adjustment of alpha ( $\alpha$ ) is via the Dunn-Sidak procedure that defines a new alpha ( $\alpha'$ ):

$$\alpha' = 1 - (1 - \alpha)^{1/r}$$

where  $r$  = number of comparisons from a single data set. Where the number of comparisons is 60 (5 sites and 12 time steps each) then it might be appropriate to set  $\alpha'$  at 0.000855. For this analysis of temporal autocorrelation we are, however, leaving alpha at 0.05. We view this as a more conservative assessment of autocorrelation. It is also true that the significance of a given correlation coefficient ( $R$ ) is dependent upon the number of observations. In these time lagged correlations the initial correlation (1 week time lag) has a mean of 68 observations but this falls as the lag is made longer to about 42 observations at 12 weeks of lag. For this reason the correlation coefficient that is significant at any given probability should rise as the time lag is extended. In the case of our data this consideration is also ignored as largely irrelevant since none of the longer time lags even approach statistical significance.

Across the five sites the maximum degree of autocorrelation was found at one week at site F3 ( $r^2 = 0.527$ ) in the integrated chlorophyll  $a$  after log transformation (Fig. 2). This degree of autocorrelation was highly significant ( $P < 0.001$ ). At one week the mean degree of autocorrelation ( $r^2 = 0.203$ ) across the five sites was significant with the probability less than 0.000855. The mean degree of autocorrelation dropped steadily with increasing lag time reaching a low point at six weeks (Fig. 3).

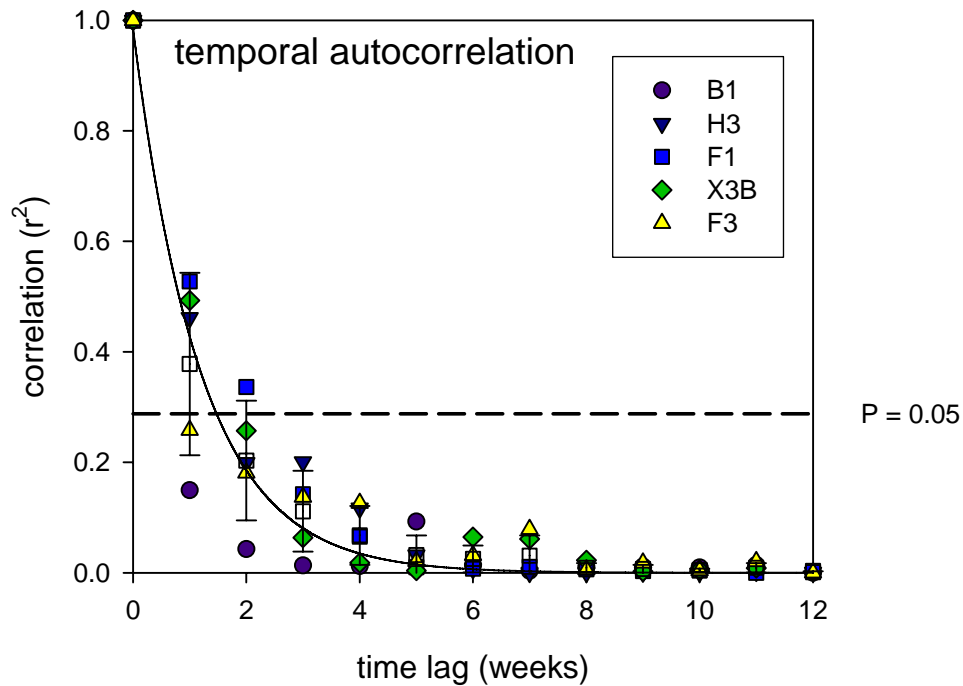


Figure 3. Autocorrelation for repeated measures of log transformed integrated chlorophyll *a* concentrations lagged by one to twelve weeks from five sites (B1, F1, F3, H3, X3B) in the Huon Estuary. Large open squares are means for the five sites, error bars are  $\pm 1$  standard deviation. Near horizontal lines represent correlation coefficients with different probabilities of significance at the number of observations used (bottom line,  $P = 0.05$ ; next line up,  $P = 0.01$ , indistinguishable top lines  $P = 0.001$  or  $0.000855$ ).

In general the degree of autocorrelation was significant at one or more sites until the time lag exceeded two weeks and did not fall below  $P = 0.05$  for all sites until the time lag was three weeks. Sites F3 and B1 did not have any significant autocorrelation at any time lag suggesting that the degree of autocorrelation may be site specific.

#### Conclusions:

1. at some sites in the Huon sampling intervals of 2 weeks or less have significant autocorrelation and are therefore not independent.
2. none of the sites sampled showed any significant autocorrelation at time intervals of 3 weeks (or longer).
3. seasonal means are highly likely to be temporally independent

Given these conclusions it seems reasonable to progress to the next step, how many samples are required to accurately estimate the seasonal mean?

As the first step to assess the relative performance of different temporal sampling regimes designed to estimate the seasonal mean the existing  $\sim 70$  weeks of HES data

for stations B1, F1, F3, H3, and X3B were repeated subsampled once, twice, three..... to ten times through a series of arbitrary 12 week periods. The means from these subsampling efforts with one to ten samples were converted to a percentage of the mean obtained by averaging over the 12 weeks ( $=\bar{x}_{12}$ ). Using this approach generated some 1008 to 755 subsampled estimates of the mean with from 1 to 10 (respectively) samples which were then compared to  $\bar{x}_{12}$  (Fig. 4). The results suggest that in order to be 95% confident that the mean will be within  $\pm 20\%$  of  $\bar{x}_{12}$  would require 9 samples in a 12 week period.

There are problems with this approach, we note that these weekly samples are not independent due to autocorrelated at some sites. Also that the variability about the real mean could be substantially greater than suggested by this exercise which subsamples repeatedly from 12 possible values rather than from the  $\sim 90$  daily samples that would be available in any one season. Regardless it is a characteristic of statistics that the observed mean will be closer to the true mean as the sampling frequency increases and in the case of chlorophyll *a* concentrations in the Huon Estuary it appears that frequent sampling is likely to be required to get the seasonal means close their true values (Fig. 4).

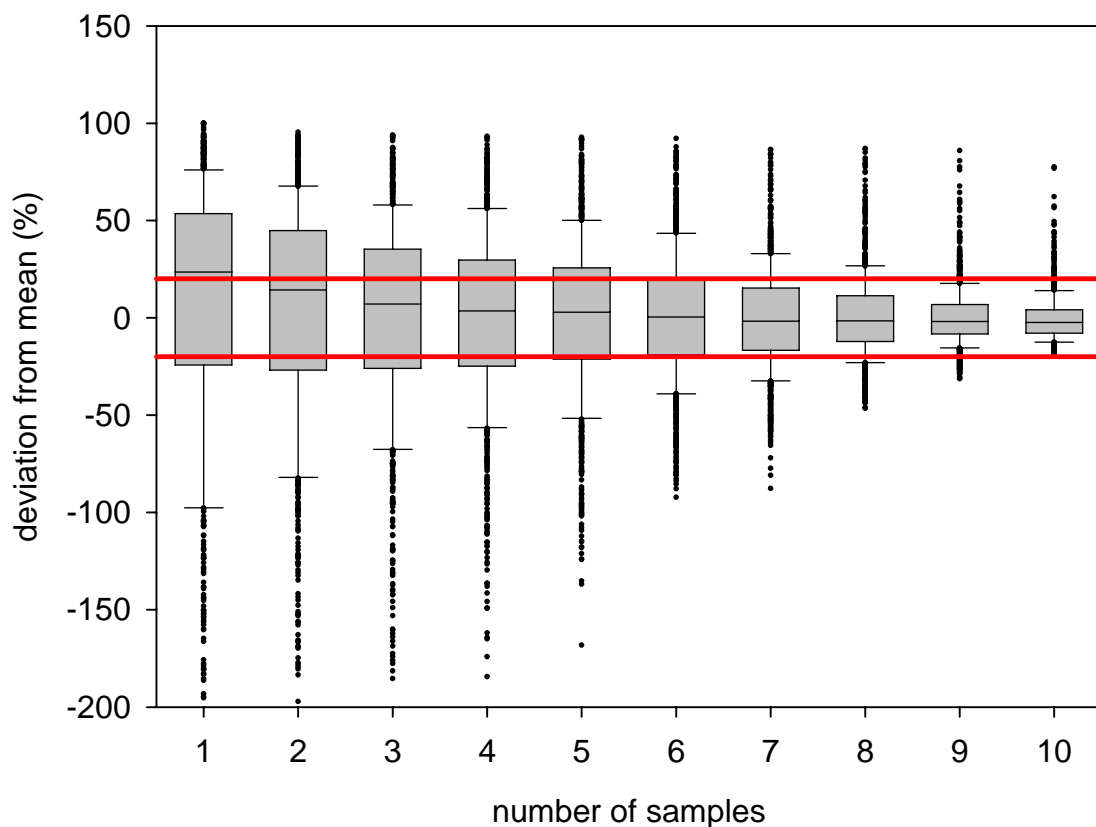


Figure 4. Percentage deviations from the mean for chlorophyll *a* concentrations from the Huon Estuary re-sampled at frequencies of 1 to 10 times in any 12 week period. Boxes are 25 to 75 percentiles, error bars are 95 percentiles and points are outliers. Red horizontal lines are  $\pm 20\%$  of the 12 week average.

An alternative approach that overcomes some of the subsampling problems noted above is to calculate the error that would occur in an estimate of the mean annual [chlorophyll *a*] from sampling the Huon at various temporal frequencies. Sampling frequencies investigated were 1, 4 and 12 times per year using the integrated samples of  $\log(1 + [\text{chlorophyll } a])$  data from sites F1, B1 and H3 from 1997 and 1998. The value reported is the percentage error relative to the mean ( $\bar{x}_{52}$ ) obtained from  $\sim 52$  samples per year. Using one sample per year the estimated annual mean would tend to average  $\pm 44\%$  of  $\bar{x}_{52}$  and 95% of the values would be  $\pm 80\%$  (Fig 5). The largest single error was 224%, which when corrected for logarithmic transformation is 14 times the mean. Increasing sampling effort to 12 times per year reduces mean error to  $\pm 12\%$  and the 95% confidence interval for the errors to  $\pm 20\%$  relative to  $\bar{x}_{52}$ .

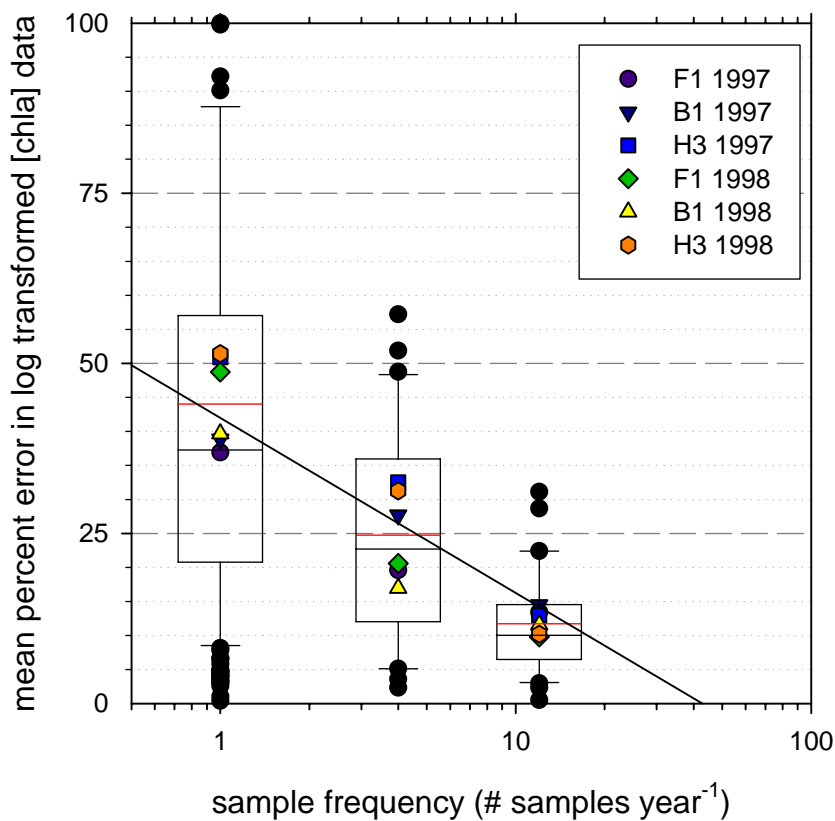


Figure 5. Percentage errors obtained by sampling log transformed chlorophyll *a* concentrations from three sites and two years at frequencies from 1 to 12 times per year and comparing with the mean obtained from weekly sampling. Boxes have a black line at the median, a red line at the mean, ends at 75<sup>th</sup> percentiles, caps at 95<sup>th</sup> percentiles and outliers. Means for various HES sites in both 1997 and 1998 are also shown.

## Spatial variation

### Vertical variation

In a highly mixed and homogenous environment a sample from any one point may be representative of a relatively large area. This is not true for the Huon Estuary or D'Entrecasteaux Channel. In both there was significant variation in chlorophyll *a* concentration with depth. In D'Entrecasteaux Channel surface chlorophyll *a* concentrations were 27% greater than those near the bottom ( $P < 0.001$ ). In HES significant differences in the vertical distribution of chlorophyll *a* were also noted (HES pg 111) with mid depth samples being greater than surface ( $P < 0.05$ ) during eight of nine surveys. For any monitoring strategy in a stratified water body such as the Huon Estuary and D'Entrecasteaux Channel there is a need to decide how to sample the vertical variation in chlorophyll *a* concentrations. Traditionally multiple samples are taken over the depth range and numerically integrated post analysis but this is an expensive sampling strategy. A single depth-integrated sample is much less expensive in terms of sample processing and will give an integrated areal value for chlorophyll *a* concentration. Calibrated vertical fluorescence traces can be used in some ecosystems, especially those without much interference from humics. Fluorescence measurements are inexpensive in terms of processing time. The most commonly adopted, most rapid and relatively low cost approach is to measure at only one depth (typically surface). Even this can be reasonably accurate if there is no change with depth or the surface concentration is a known and constant fraction of depth integrated chlorophyll *a*.

Where there is significant variation in chlorophyll *a* concentration with depth a vertically integrated sample represents a superior measure for the purpose of quantifying the ecological health of a water body. Unfortunately where previous sampling has not used depth integrated samples the change can complicate the analysis of long term temporal trends or comparisons across ecosystems. The choice of the best vertical sampling strategy depends upon the magnitude of the error associated with single depth sampling. For the Huon Estuary the magnitude of this error can be assessed by comparing the surface chlorophyll *a* concentrations from the 5 biological stations (sampled weekly) in HES with the simultaneously collected and vertically integrated samples (using a tube that could extend to 12 m depth).

For the purpose of the statistical analysis data from the five HES biological stations (B1, F1, F3, X3B and H3) for surface and vertically integrated samples were paired in time. Details of the sampling, sites, temporal period, sample extraction and processing are in the HES report. If one sample was missing the matching sample was also eliminated from the analysis. Each station was analysed separately using 65 to 67 matched pairs of data. Chlorophyll *a* concentrations are not normally distributed so the data were transformed using  $\log_{10}([\text{chlorophyll } a] + 1)$  but these data also failed the Kolmogorov Smirnov test for normality. The statistical comparisons of data from the same site but collected from either the surface or via an integrating tube was undertaken using a paired (by time) *t-test* on the transformed data and a nonparametric *sign rank test* on both the nontransformed and transformed data.

The results from this analysis indicate that surface sampling for chlorophyll *a* underestimates the vertically integrated concentrations at every Huon Estuary station by an average of 82% (Fig. 6). The smallest error was in Port Cygnet where the means

varied by 29% but this difference was not statistically significant. At all other Huon Estuary stations the difference between surface and integrated chlorophyll *a* concentrations were statistically significant regardless of whether a parametric or nonparametric statistical test was used.

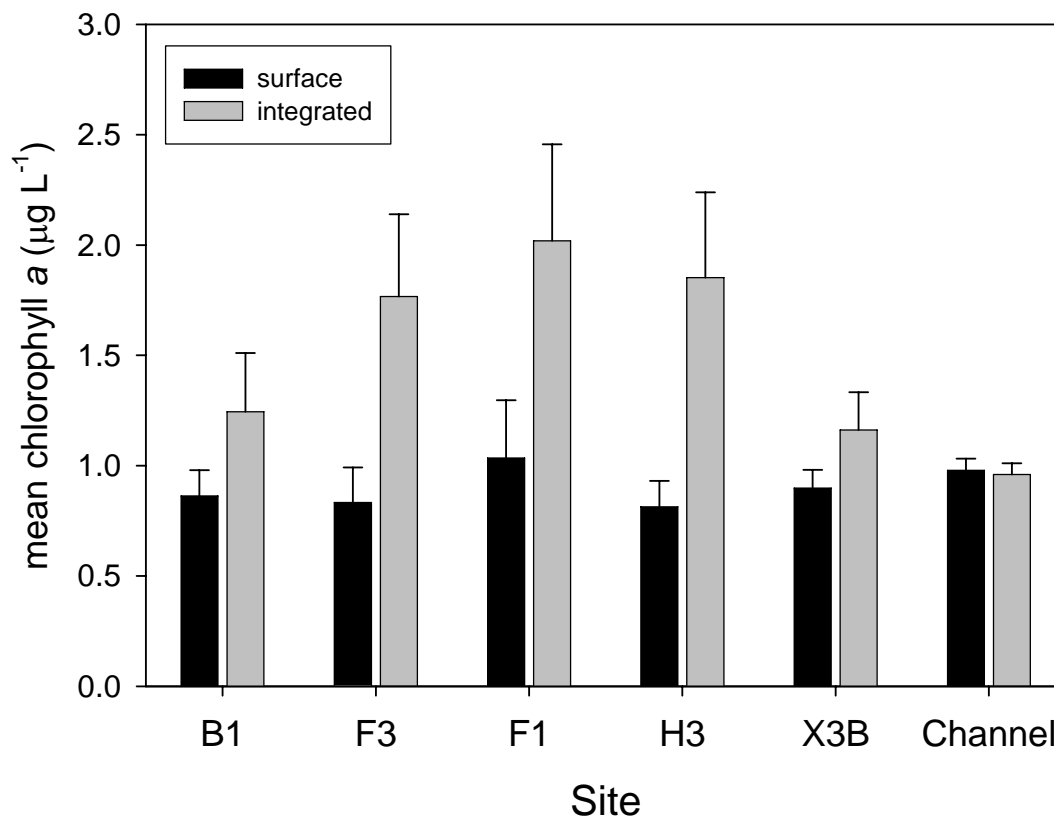


**Figure 6. Mean chlorophyll *a* concentrations for surface and integrated samples from five stations in the Huon Estuary sampled weekly during 1996-1998.**

If the underestimation of integrated chlorophyll *a* was consistent then it might be possible to use surface chlorophyll *a* as a reliable indicator of ecosystem concentration with an appropriate correction. To investigate this possibility the surface and integrated chlorophyll *a* concentrations at the 5 weekly sampled HES sites were correlated. Correlations ( $r^2$ ) were 0.111, 0.130, 0.399, 0.472, 0.682 for sites X3B, F1, B1, F3 and H3, respectively (Fig. 7). All correlations were statistically significant but the capability to accurately predict integrated chlorophyll *a* from surface concentrations ranged substantially across sites.

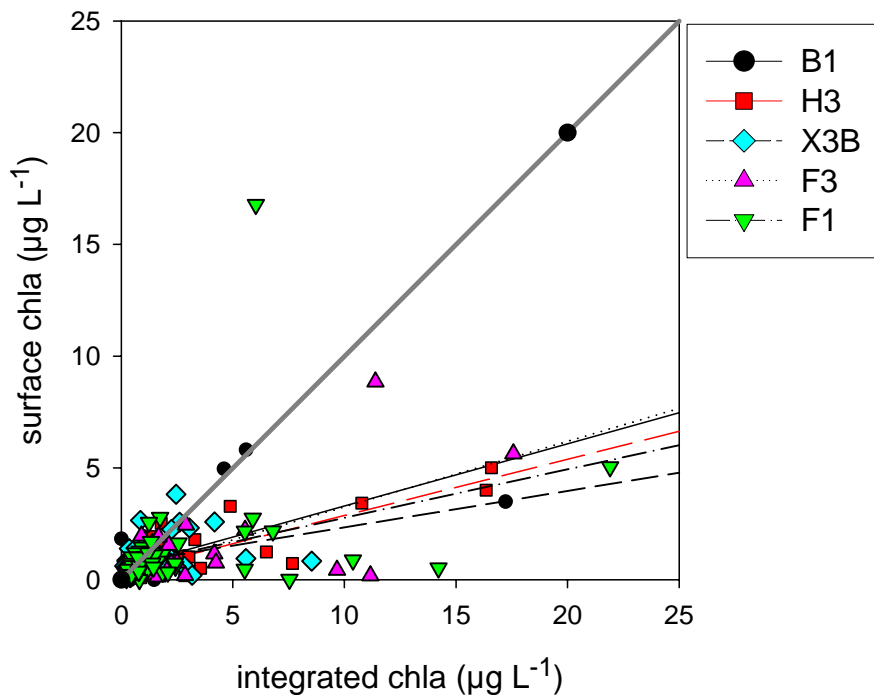


Figure 7. Correlations between chlorophyll *a* concentrations from bottle collected surface samples and those from hose collected integrated samples. Dark grey line is 1:1.

The largest single error was a surface sample that underestimated the integrated chlorophyll *a* by 670 times during January 1998 at station F1. The fact that the vertical differences in mean surface versus mean integrated chlorophyll *a* concentrations are three times greater at H3 relative to B1 suggests that there is a significant spatial component to this bias. The spatial sampling (B1, F1, F3, H3 & X3B) is too sparse to resolve any trends although the data are suggestive of greater differences associated with distance up or across the Estuary. The ranking of sites based on mean chlorophyll *a* concentrations changes quite dramatically depending whether it is done on surface or integrated concentrations (Fig. 5). Lowest to highest mean surface concentrations were: H3, F3, B1, X3B, & F1. In contrast the sites with lowest to highest mean integrated concentrations were: X3B, B1, F3, H3 & F1. All sites except F1 changed rank.

In conclusion it is very clear that surface sampling in the Huon significantly underestimates the real chlorophyll *a* concentration and that this error is not consistent in time or space.

During all of 2002 and across all twelve sites in D'Entrecasteaux Channel the mean chlorophyll *a* concentration at the surface was 1.9% greater (not statistically significant) than the mean integrated chlorophyll *a* concentration (Fig. 6). The median surface concentrations, however, were 12% greater and this difference was statistically significant ( $P = 0.015$ ). In contrast to the Huon, surface sampling in the Channel overestimates chlorophyll *a* although the error is relatively modest.

## Horizontal variation

Similar to temporal autocorrelation there is an issue with spatial autocorrelation and the independence of data to be used in statistical analysis. For many parameters the samples in close proximity to each other are more likely to be similar than those far apart. Where this is true the samples in close proximity are not independent and will bias statistical comparisons. Conversely there is a need to sample with sufficient spatial coverage such that the true mean for the region can be estimated with some precision if the region is to be monitored for change. Consider two extreme examples, in situations where the parameter is uniform over large areas then a single sample may adequately represent the mean condition, alternatively where the spatial pattern is heterogenous it may be necessary to sample many locations to accurately estimate the mean condition.

Traditional sampling schemes usually grid the area of interest and all points, or a random, subsample of points would be sampled. A major advancement was to recognize that more statistical power to detect differences in time or space could be obtained by identifying times or subregions of less variability and stratifying sampling within these. Thus for spatial monitoring design in the Huon we want to know:

1. the proportion of samples that should be collected from any subregion, or are there subregions with less variability that can be identified?
2. does this sampling density provide independent data?
3. how many samples within each subregion will need to be sampled to adequately reflect the mean condition?

A strategy to achieve an improved sampling design was adopted from Grey et al. (1992) where the grouping of stations (= subregion) is adjusted by trial and error until the variance between subregions is equal. The following steps were undertaken:

1. for HES surveys 2 to 9 the variance for the four putative HES subregions
  - i) upper estuary = HES stations: I1, I3, J1, K1, L1, N1, N2, R1, R2, R3, R5, & R6.
  - ii) middle estuary = HES stations: E1, E5, F1, F2, F3, H1, H2, & H3.
  - iii) Port Cygnet = HES stations: V1, V3, X3, Y1.
  - iv) lower estuary = A1, A3, A5, A7, B1, B3, B5.
2. for each survey the variance from the four groups was summed for a total variance
3. for each survey the variance for each subregion was converted into a percentage of the total variance to obtain the proportion of the variance in each subregion
4. the value obtained in step 3 is considered as a factor in the allocation of stations.

The results of this analysis indicated that the spatial and temporal variability of chlorophyll *a* was very high with no statistically significant difference ( $P = 0.067$ , although the test had low power = 0.37) in variance between subregions. The mean proportions of variance across these putative subregions were 6.1% in the lower estuary, 19.5% in Port Cygnet, 27.2% in the middle estuary, and 46.2% in the upper estuary. The high variability in surface chlorophyll *a* concentrations reflects the sporadic spatial and temporal nature of the high biomass blooms. Most of the high biomass blooms that were detected occurred at spatial scales smaller than subregional and greatly increased the spatial variability between stations within a subregion. The

lower estuary did not experience any very dense or subregional scale surface blooms while Port Cygnet did on one occasion giving it a single outlier with a high degree of the overall variance during HES survey 8. The upper estuary had the greatest average variability but also a very large range in variability was observed in this subregion. Some of this variation was caused by the inclusion of stations I and J within the upper estuary subregion (as noted in HES report) but by no means was this always the case, although on several occasions just the two adjacent stations I and J showed more variability than the other putative subregions. Although these differences in variability were not statistically significant a sampling strategy that assigns sample density based on variance will improve accuracy in terms of estimating the regional mean chlorophyll *a* concentration which might be used to assess long term trends in ecosystem performance. To reduce the effect of spatial heterogeneity a sampling program would benefit from collecting more data from the upper estuary relative to the lower estuary.

### Achieving density independent samples

There are several techniques that can be used to determine the minimum distance between samples such that the degree of spatial autocorrelation is insignificant and the samples can be considered sufficiently independent to be used as replicates in a statistical comparison. Although there were only five stations sampled weekly in HES the integrated chlorophyll *a* data (as shown in Fig. 1) provide a high quality data set that, when analysed, showed the strength of the temporal correlation in chlorophyll *a* concentrations between stations was a significant negative, linear function of the distance between stations (Fig 8). The fact that all of the station pairings that fall below the line are 'across' the estuary (stations 1 - 3) while all but one pairing above the line is along the estuary (stations 1-1 or 3-3) implies more spatial coherence in phytoplankton along the SE to NW axis of the estuary relative to across the estuary.

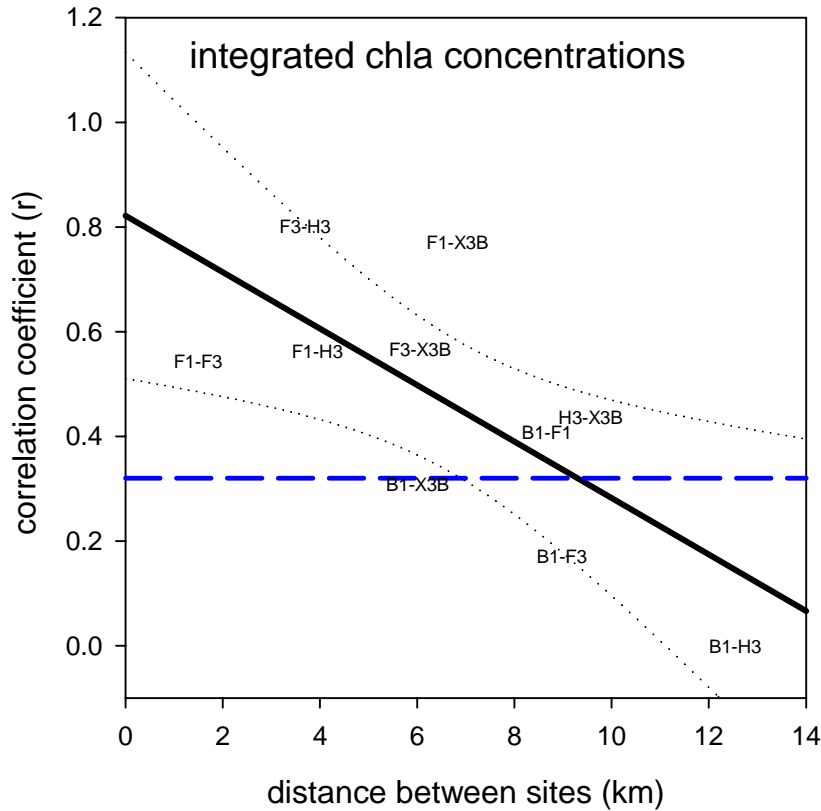


Figure 8. The strength of the temporal correlation in chlorophyll *a* concentrations between stations plotted as a function of distance. Given the number of comparisons between any two stations an *r* value of 0.319 or greater would be significant for any individual correlation. The heavy solid line is the overall regression between *r* and distance ( $r^2 = 0.50$ ,  $P = 0.023$ ).

The quarterly sampling from HES offers more stations than the weekly sampling thus sufficient spatial coverage and temporally independent samples (time period between samples ~ 3 months) to allow semi variograms to be constructed. On the negative side there are only fixed depth chlorophyll *a* data available. The semi variogram plots the calculated relationship between a variable (in this case chlorophyll *a*) lagged by increasing distance or time (Lam 1983):

$$\gamma(h) = \frac{1}{2n} \sum_{i=1}^n \{Z(x_i) - z(x_i+h)\}^2$$

where  $Z(x_i)$  is the concentration of chlorophyll *a* at the position  $x_i$ ,  $Z(x_i + h)$  is the concentration of chlorophyll *a* at the position  $x_i + h$  and  $n$  is the number of pairs of samples separated by distance  $h$ . Plots of  $\gamma(h)$  against  $h$  summarize spatial variation, its magnitude and scale (Oliver and Webster 1990). The distances between HES stations A1, A3, A5, A7, B1, B3, B5, E1, E5, F1, F2, F3, H2, H3 & H3 were calculated and “binned by increasing 1 km intervals giving 6, 7, 4, 17, 9, 3, 4, 6, 5, 5, 6, 4, 6, 9, 3, 2, 3, 5 comparisons from 1 to 18 km, respectively. For example, there were 3 stations between 0 and 1 km apart and 17 stations that were between 3 and 4 km apart. The values of  $\gamma h$  for surface chlorophyll *a* were calculated for each survey. The pattern of variation in  $\gamma h$  versus  $h$  changed quite dramatically depending upon the

survey with the occasional bloom detected at a few stations generating quite a few outliers (data not shown). The outliers in the semivariogram from stations a short distance apart (1-5 km) occurred during March 1998 and were caused largely by a bloom at site B1. The outliers at greater distances (9-17 km) arose from Feb 1998 when the chlorophyll *a* concentrations were high at F1, F2 and F3. The parameter  $\gamma h$  was poorly distributed even if calculated using log transformed chlorophyll *a* data, however, values of  $\log \gamma h$  produced from log transformed chl*a* data were more normally distributed (Fig. 9). Over all the sampling periods the mean  $\log \gamma h$  increased as distance increased from 1 to 4 or 5 km and then declined to a lower value between 6-8 km. This dip in variance at 6-8 km is considered to be caused by the difference in variance ‘across’ relative to ‘along’ the estuary. The station spacing meant that more ‘along’ stations would be 6-8 km apart while those ‘across’ the estuary would be mostly 0-5 km apart. The mean  $\gamma h$  rose until > 12 km and then fell to a lower value when stations were > 16 km apart. These results suggest that stations reach their greatest independence when more than 12 km apart.

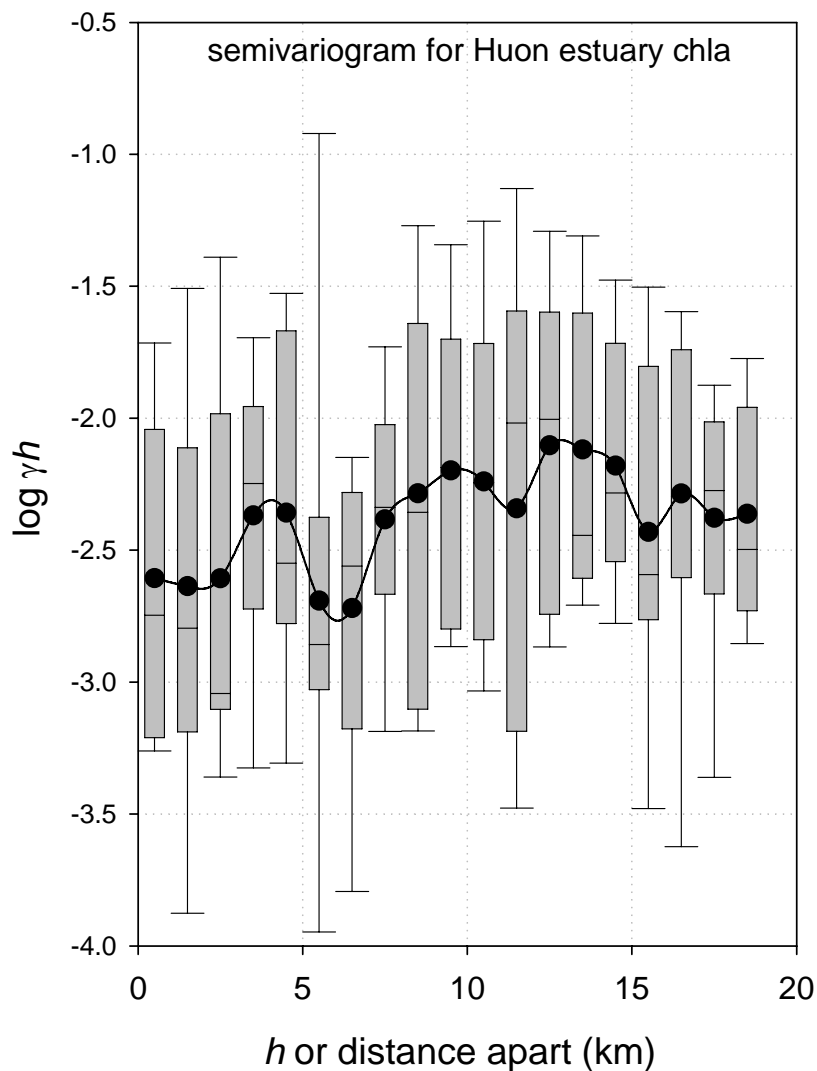


Figure 9. The semivariogram for surface chlorophyll *a* from the quarterly surveys of the Huon Estuary. Boxes encompass the 25-75 percentiles, error bars the 90<sup>th</sup> percentiles and symbols the means of  $\log \gamma h$  calculated using log transformed chlorophyll *a* concentrations.

## Conclusions

In the D'Entrecasteaux Channel and the Huon Estuary there are significant differences in mean chlorophyll *a* concentrations with season. Given the temporal pattern of variation in chlorophyll *a* the sampling and analysis should be stratified by season. It is suggested that sampling within a season could be uniform or random in time and of sufficient frequency to characterize each season. The degree of characterization required is dependent upon the magnitude of the change that needs to be detected (detection limit). As scientists we may be prepared to recommend a detection limit but in reality the issue should be a matter for input by, and consultation with, stakeholders. During the interim monitoring a minimum of three sampling times per season is recommended. Given that the seasonal variation in chlorophyll *a* concentration is large relative to other sources of variability any statistical analysis that is not stratified by season will tend to obscure other patterns in time or space. Furthermore any sampling regime that over or undersamples within seasons and is not stratified during analysis is likely to give biased (incorrect or misleading) indications of variation in time, possibly in space.

Stratifying future sampling into relatively homogenous subregions would improve our capacity to detect change. There are indications that the lower or mouth of the estuary is more homogenous than the middle or upper estuary. The results presented here also suggest that stations should be located a minimum of 4 km apart across the estuary and >10 km apart along the estuary to maximize independence. Further discussion on the issue of spatial location of sampling sites is provided at the end of section #2.

Areas of high chlorophyll *a* (= blooms) were occasionally detected in the HES. The frequency of these blooms is discussed in the next section. The fact that the spatial extent of these blooms has not been characterized complicates the efficient design of spatial sampling. The application of more sophisticated statistical analyses to the existing data is underway and should provide some more guidance as to the number of relatively homogenous sub-regions that could be used to efficiently stratify sampling. Stakeholders may also wish to have some input into any decisions regarding the spatial location of the horizontal sampling effort as sites under anthropogenic pressure, those with relatively slow exchange rates or those of special recreational significance may not otherwise be identified. Integrated chlorophyll *a* samples are strongly recommended as a superior measure of ecosystem performance in the Huon Estuary.

## Part II: Comparing HES with interim monitoring:

The 2001-2004 (hereafter referred to as 2001) chlorophyll *a* data set from the Huon Estuary was collected as part of the Aquafin CRC's interim monitoring program conducted by the University of Tasmania's Tasmanian Aquaculture and Fisheries Institute (TAFI) in combination with sampling by TAFI PhD student Simon Willcox. They reported one hundred and twenty nine surface chlorophyll *a* concentrations from 4 locations (stations HA1, HA5, HA7, HA12) up the centre of the Estuary (Fig. 10). These can be compared with sampling from the Huon Estuary Study and its six hundred and ten reported surface chlorophyll *a* concentrations from a wide range of sample locations over the period 1996-1998 (hereafter referred to as 1996). The simplest comparison is a Mann-Whitney Rank sum test upon the entire data set of  $\log_{10}$  transformed chlorophyll *a* concentrations. The results indicate a statistically significant ( $P < 0.001$ ) rise from a median concentration of 0.54 to 0.80  $\mu\text{g}$  chlorophyll *a*  $\text{L}^{-1}$  over the period from 1996 to 2001. We note this simple comparison could be biased by variation in sampling density in time and, or space. We further acknowledge that some stations and some sampling periods were too close together to be considered statistically independent.

A more complex analysis of the chlorophyll *a* concentrations was undertaken. Intra-annual temporal bias associated with the known seasonal cycle in chlorophyll *a* concentrations was blocked by classifying all data into the four seasons (summer = December, January and February; autumn = March, April, May; winter = June, July, August; spring = September, October, November). The seasonal means were not temporally autocorrelated so this approach has two advantages: it partitions (blocks) a significant portion of the temporal variance and it ensures temporal independence between measurements. A two way ANOVA was conducted upon the  $\log_{10}$  transformed chlorophyll *a* data. The  $\log_{10}$  transformed data still failed tests for homogeneity and normality. The results indicated a statistically significant effect of season ( $P < 0.001$ ) and a statistically significant rise from a mean of 0.66 to 1.1  $\mu\text{g}$  chlorophyll *a*  $\text{L}^{-1}$  over the period from 1996 to 2001. We note that this analysis could still be biased by spatial variation in sampling density and the lack of independence between stations close to each other.

In an effort to remove any bias due to the differences in the density of spatial sampling in the comparison of 1996 versus 2001 the Huon Estuary was divided into 4 sub-regions: upper, middle, lower and mouth of the estuary. In some cases the exact locations sampled during the interim monitoring (2001-2004) were not sampled during HES (1996-1998) and samples in near proximity were included in the comparison (Fig 10). In the situation where more than one station from HES was available to compare to a given station from the interim monitoring program the mean chlorophyll *a* concentration for each season for each station was calculated and then averaged to give a mean value for each season within the vicinity or sub-region of the four sites sampled during the interim monitoring. Thus from the data collected by the HES in 1996-1998 sites A3&A5 were compared with HA1, sites B1&B3 with HA5, sites E1&E5&F1&F2&F3 with HA7 and sites I1&I3 with HA12. Given the known variation in chlorophyll *a* with season and depth to make a comparison between

samples collected in 1996-1998 and those collected in 2001-2004 the data were put into seasons and only surface samples were used for the comparison. A minimum of three observations were used to calculate the seasonal mean for any of these four sub regions (mouth, lower, mid or upper estuary). These data were  $\log_{10}$  transformed and passed tests for homogeneity and normalcy.

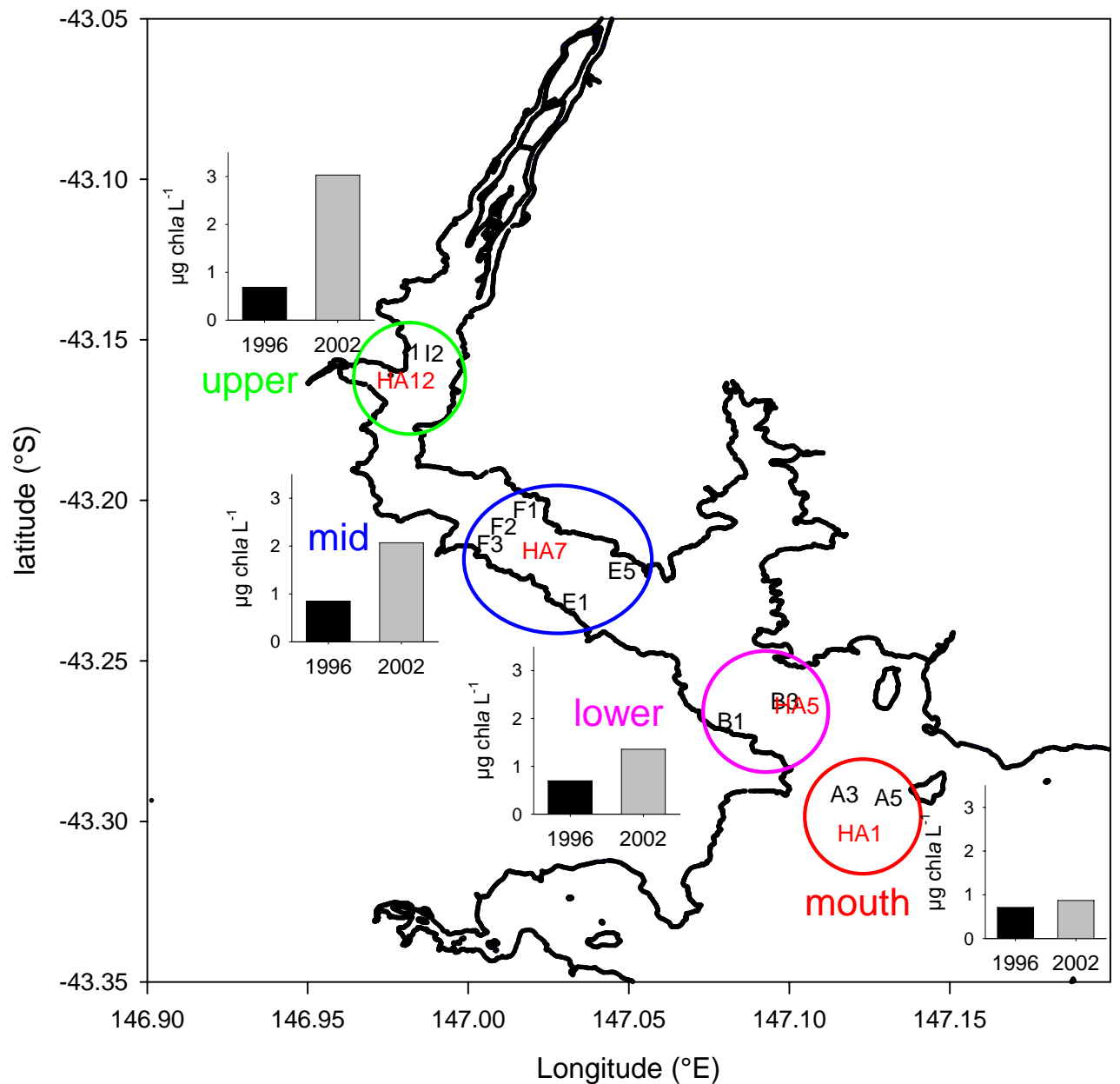


Figure 10. A map showing the sites and subregions (upper, mid, lower and mouth) of the Huon Estuary sampled during HES (1996-1998) and the interim monitoring program (2001-2004). The inset bar graphs show the mean for each subregion calculated from season averages where 1996 includes all 1996-1998 data and 2002 includes all 2001-2004 data.

Table 1. Mean chlorophyll <i>a</i> concentrations measured in the Huon Estuary at four sites and four seasons during 2002-2003 and at comparable sites during 1996-1998. Sites identified in Figure 1.		
Season	1996-1998 (HES data)	2002-2003 (data courtesy of TAFI)
Sub region 1: Mouth of estuary		
	A3 (n=9), A5 (n=9)	HA1 (n=33)
Summer	0.58	0.54
Autumn	0.77	0.95
Winter	0.40	0.65
Spring	1.09	1.33
Sub region 2: Lower estuary		
	B1 (n=77), B3 (n=9)	HA5 (n=33)
summer	0.76	1.17
autumn	0.43	1.08
winter	0.44	1.52
spring	0.69	1.65
Sub region 3: Mid estuary		
	E1 (n=9), E5 (n=9), F1 (n=76), F2 (n=9), F3 (n=77)	HA7 (n=33)
summer	1.35	1.35
autumn	0.76	4.40
winter	0.31	0.60
spring	0.97	1.92
Sub region 4: Upper estuary		
	I1 (n=9), I3 (n=5)	HA12 (n=30)
summer	0.71	2.91
autumn	0.79	7.45
winter	0.16	0.70
spring	1.08	1.08

Using this stratified in time and space approach a three way ANOVA (season, “year” and region) indicates the mean chlorophyll *a* concentration in 2001 was 1.831  $\mu\text{g L}^{-1}$ , and 60% less in 1996 with a mean of 0.735  $\mu\text{g L}^{-1}$ . The differences for season and “year” were statistically significant ( $P = 0.006$  and  $0.001$ , respectively; [using a three way test and  $\log_{10}$  transformed data]). No significant difference ( $P=0.321$ ) was detected between subregions. Although the statistical analysis indicates no significant differences between subregions the data (Fig. 10) suggest that the changes from 1996 to 2001 were not uniform across the estuary but most evident towards the mid and upper estuary. The three way ANOVA reported here gives equal weighting to the four subregions and results in an apparently larger increase in mean chlorophyll *a* from 1996 to 2001 than the two way ANOVA reported above. The mean distance between the 2001 monitoring stations (HA1, HA5, HA7, HA12) which represent the epicentre of putative subregions used in this comparison was 11.1 km although the range was

4.7 to 19.4 km. The stations that are closest together may not be sufficiently independent and this may compromise the statistical results.

Noting that seasonal variation was significant in the Huon there are several methods that can be used to remove the effect of seasonal variation from data to allow other comparisons. These include time series analysis and multiway ANOVA (as above). Once the data have been stratified by subregion and season a simple approach to the statistical test of whether there is a difference between the two periods 1996 and 2001 is to execute a comparison paired by season and subregion, that is between the two columns of data in Table 1. Because the data are not normally distributed both a signed rank test was used with the raw chlorophyll *a* concentrations and a paired Students' t-test upon the log<sub>10</sub> transformed data (data passed a Kolmogorov-Smirnov test for normality). Both tests indicate a statistically significant difference between 1996 and 2001 ( $P = 0.007$  or  $P < 0.001$ , respectively).

### A change in bloom frequency?

To assess whether the increased variation seen during the summers from 1996-97 to 2003-04 was related to an increase in algal blooms the data from these comparable stations was analysed for bloom frequency. Blooms were defined as the number of observations exceeding three times the median concentration. Of the 298 surface samples obtain during 1996-1998 taken from stations A3, A5, B1, B3, E1, E5, F1, F2, F3, I1 and I3 twenty one of them were greater than three times the median concentration (Table 2). Of the 129 samples collected during 2002-2003 and reported by TAFI for the same subregions 23 were greater than three times the median (Table 2). Chi squared analysis of the frequencies indicates a significant change ( $\chi^2 = 7.9$ ,  $P = 0.005$ ).

Table 2. Calculation of some summary statistics from surface chlorophyll *a* samples collected in the Huon Estuary between 1996-1998 or 2002-2003.

	2001-2004	1996-1998
Median chlorophyll <i>a</i> ( $\mu\text{g l}^{-1}$ )	0.80	0.58
3x median ( $\mu\text{g l}^{-1}$ )	2.40	1.74
# observations > 3x median	23	21
total # observations	129	298
% bloom	17.8	7.1

## Discussion

The intervals between sampling for chlorophyll *a* in the HES were highly variable, from 7 to 136 days depending upon the site while the intervals in the interim monitoring program were ~ 30 days. Data collected at short time steps (< 3 weeks) were autocorrelated and thus not fully independent and are unlikely to be cost effective in a monitoring strategy. The approach of stratifying the available data by season makes it possible to statistically compare data collected on shorter time scales. Stratifying by season also accounts for a significant amount of the variation and improves the statistical power available to compare the two longer time periods (1996-1998 versus 2001-2004). The analyses conducted show that the latter period can be distinguished by more chlorophyll *a* and more spatial and short term temporal variation in the chlorophyll *a* concentrations (blooms).

Spatial variability was dramatic in the vertical. Surface samples seriously underestimate the phytoplankton density on an area basis (per m<sup>2</sup>) in this stratified estuary. A monitoring program should use integrated samples. Autocorrelation was present in stations located less than 10 km apart. Variability between stations did not peak until they were > 12 km apart. There is also evidence that variation with distance is greater across the estuary than it is along the estuary. The currently selected monitoring stations range from 4.7 to 19.4 km apart along the centre of the estuary. Along this axis the minimum distance between stations should be greater to maximize their information content. The putative 4 subregions did not show any statistically significant difference in chlorophyll *a* concentrations. The data, however, are suggestive that changes in phytoplankton between 1996 and 2001 were not uniform throughout the estuary but most pronounced at the mid or upper estuary. Although there is no proof, these results suggest the possible impacts of aquaculture are not felt uniformly throughout the estuary, but may be more acute at certain locations, possibly at certain seasons. Until this is better resolved the monitoring should include a minimum of 3 stations more than 10 km apart along the centre of the Huon Estuary. More analysis of the spatial variability is underway and decisions regarding sampling locations still require input from stakeholders.

There is still a need to examine the implications of the natural interannual variability on the design of a monitoring strategy. The data presented here indicate a significant increase in chlorophyll *a* concentrations between 1996 and 2001. Some undetermined fraction of this increase may be associated with natural variation in nutrient inputs or nutrient inputs from sources other than aquaculture. Monitoring design research combined with biogeochemical modeling will be used to address this issue in the second phase of this project.

## References

- ANZECC/ARMCANZ (October 2000) Australian and New Zealand Guidelines for Fresh and Marine Water Quality.  
([www.ea.gov.au/water/quality/nwqms/#quality](http://www.ea.gov.au/water/quality/nwqms/#quality))
- CSIRO Huon Estuary Study Team. 2000. Huon Estuary Study – environmental research for integrated catchment management and aquaculture. Final report to Fisheries Research and Development Corporation. Project number 96/284. June 2000. CSIRO Division of Marine Research, Marine Laboratories, Hobart.
- Gray, J. S., A. D. McIntyre, J. Stirn. 1992. Manual Methods in Aquatic Environmental Research: Part II – Biological Assessment of Marine Pollution, Food and Agriculture Organization of the United Nations, Fisheries Technical paper 324.
- Green, R. H. 1979. Sampling design and statistical methods for environmental biologists. New York, USA, Wiley, 257 pp.
- Krebs, C. J. 1989. Ecological Methodology. Harper and Row Publishers, New York. USA. 654 pp.
- Lam, N. S. N. 1983. Spatial interpolation methods: a review. The American Cartographer 10:129-149.
- Oliver, M. A. and R. Webster. 1990. “Kriging: A method of interpolation for geographical information systems. Inter. J. Geograph. Inform. Sys. 4:313-332.

# Technical Report

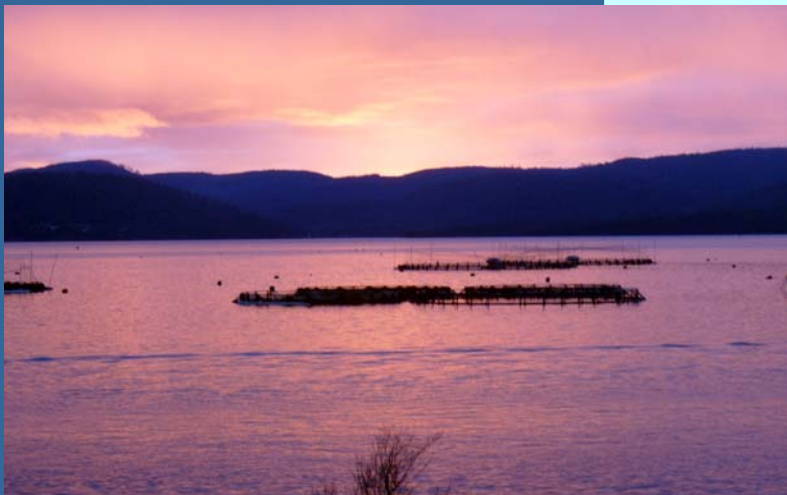


## ***Baseline monitoring in D'Entrecasteaux Channel***

*Peter Thompson and Pru Bonham  
CSIRO Marine and Atmospheric Research*

*Simon Willcox and Christine Crawford  
Tasmanian Aquaculture and Fisheries Institute, University of  
July 2005*

*Aquafin CRC Project 4.2  
(FRDC Project No. 2001/097)*



© Copyright Aquafin Cooperative Research Centre, Fisheries Research and Development Corporation, Commonwealth Scientific and Industrial Research Organisation

**This work is copyright. Except as permitted under the Copyright Act 1968 (Cth), no part of this publication may be reproduced by any process, electronic or otherwise, without the specific written permission of the copyright owners. Neither may information be stored electronically in any form whatsoever without such permission.**

**Every attempt has been made to provide accurate information in this document. However, no liability attaches to Aquafin CRC, its participant organisations or any other organisation or individual concerned with the supply of information or preparation of this document for any consequences of using the information contained in the document.**

*Published by CSIRO Marine and Atmospheric Research*



***Baseline monitoring in D'Entrecasteaux Channel***

*Peter Thompson and Pru Bonham  
CSIRO Marine and Atmospheric Research*

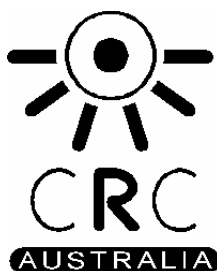
*Simon Willcox and Christine Crawford  
Tasmanian Aquaculture and Fisheries Institute,  
University of Tasmania*

July 2005

*Aquafin CRC Project 4.2  
(FRDC Project No. 2001/097)*



**Australian Government**  
**Fisheries Research and  
Development Corporation**



Tasmanian Aquaculture  
& Fisheries Institute  
University of Tasmania

## **Summary**

None of the stations sampled in D'Entrecasteaux Channel during the sixteen months from January 2002 to March 2003 showed any significant signs that would be considered indications of serious eutrophication or anthropogenic nutrient inputs. The commonly accepted primary symptoms of eutrophication include hypoxia, anoxia, excessive phytoplankton blooms and high ambient nutrient concentrations (Gray 1992). For example, all of the sites sampled had mean annual chlorophyll *a* concentrations less than the  $2 \mu\text{g L}^{-1}$  that is an internationally accepted criterion for oligotrophic waters. Some sites, however, were better or worse than others. The site judged to be in the best environmental health was Little Taylors Bay with a relatively short flushing time, high dissolved oxygen, low ammonium and low chlorophyll *a*. In contrast both NW Bay and Barnes Bay had greater  $\text{NH}_4$  and chlorophyll *a* concentrations than most other sites. NW Bay is showing modest but early symptoms of eutrophication and seems to maintain a reasonably good health primarily due to its short flushing time. Barnes Bay is also reasonably healthy but its relatively slow flushing time suggests this Bay would be more susceptible to eutrophication than most other embayments in D'Entrecasteaux Channel.

## ***Introduction***

The D'Entrecasteaux Channel lies between Tasmania and Bruny Island: at the south end it opens to Storm Bay through a 5 km wide and 50 m deep channel while the north end opens to the River Derwent through ~ 1 km wide and less than 20m deep channel. There are no significant river inputs directly into the Channel although there are significant indirect inputs from the Huon River and North West Bay River. Major nutrient inputs into the euphotic zone are largely seasonal resulting from deep oceanic water pushed into the region during winter and mixed to the surface as stratification decreases. The recent expansion of finfish farming into the region made it desirable to document the current status of various indicators of environmental health with the intention of setting a "baseline" from which it might be possible to compare future measurements. Furthermore the baseline data set was needed to calibrate both the 3D hydrodynamic model and the coupled biogeochemical model under development at CSIRO for this region. Support from DPIWE, CSIRO, TAFI, the Aquafin CRC and FRDC made it possible conduct this baseline research.

Primary production can increase as the result of adding a previously limiting nutrient to an aquatic ecosystem (Smayda 1989). In most marine ecosystems the limiting nutrient is nitrogen (Ryther and Dunstan 1971). Increased rates of eutrophication sometimes result from human activities adjacent to, or in the watershed of, the body of water (Laws 1993) that result in increased loading with reduced carbon, nitrogen or phosphorous. There are sufficient studies of eutrophication that a few common responses to eutrophication, such as shifts in species, changes in standing stock, increases in primary production, changes in relative importance of nutrient cycling pathways have been documented (Gray 1992). In most cases the organisms that can directly use the nutrients, typically photosynthetic autotrophs, are the first to respond to eutrophication (Philippart and Cadee 2000). The magnitude of these responses, however, is determined by the nature of the inputs and by complex interactions between physics, chemistry and biology within the water body and its sediments.

Anthropogenic nutrient inputs can affect biological change in two fundamentally different ways. The simplest form of impact is more biomass as a response to more nutrients (Clark 1989, Vollenweider 1981). A second type of impact results from disruptions to the normal temporal pattern of nutrient inputs. Most temperate ecosystems have cyclic (seasonal) nutrient inputs often associated with rainfall (Mallin *et al.* 1993), turnover or upwelling (Parsons and Takahashi 1973). The timing of anthropogenic nutrient inputs can be quite different from natural cycles, sometimes with very different temporal fluctuations, occasionally peaking during summer when natural inputs are normally small. The frequency and intensity of physical disturbance or nutrient availability (Sommer 1995, Hambright and Zohary 2000) can determine whether communities consist of  $r$  selected species or remain stable long enough to reach a climax of  $k$  selected dominant species (Fong *et al.* 1993, Loreau *et al.* 2001). If the nutrient pulses are very rare relative to the life spans of the organisms then even the  $k$  selected species will not survive between pulses and the ecosystem will be a "desert" with periodic blooms of  $r$  selected species (coinciding with nutrient pulses). If pulses

are at relatively long intervals then  $k$  selected species should proliferate, while intermediate pulses should give a mixture of species and a rise in diversity (Floeder and Sommer 1999). Long periods of high nutrient availability with low N:P ratios are often associated with a loss of diversity and nuisance algal blooms (Birch et al 1981). Large scale finfish aquaculture would be expected to make nutrients available on a more continuous basis. In particular it would be expected to increase the nitrogen loading particularly as  $\text{NH}_4$  and should have its biggest impact on the phytoplankton ecology during summer (Parslow et al. in HES 2000). It is not anticipated that these nutrient inputs would result in an increase in phytoplankton abundance in the immediate vicinity of the aquaculture operations as physical processes, such as dilution, will determine whether a biological response to a nutrient input is local or widespread (Lindenschmidt and Chorus 1998). Under conditions of rapid dilution nutrient concentrations can fall to the point where nutrient uptake by phytoplankton is relatively slow and the resulting growth does not accumulate as a local increase in biomass.

## ***Materials and Methods***

### **Spatial and temporal sampling regime**

Sample stations were selected to be representative of the entire D'Entrecasteaux region. There were twelve stations identified, representing a mix of open channel and embayment locations (Table 1, Fig.1).

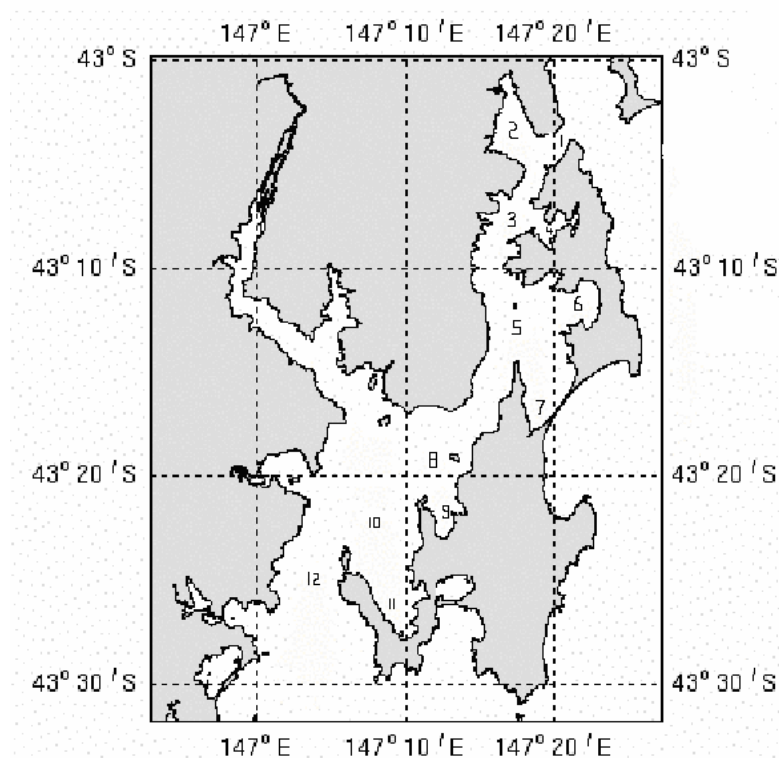


Figure 1. Map showing approximate locations of the stations sampled in D'Entrecasteaux Channel.

**Table 1. Locations of D'Entrecasteaux Channel stations**

Channel station #	latitude (south)		longitude (east)		notes
	Degrees	minutes	degrees	minutes	
1	43	3.90	147	20.30	mid channel off Dennes Pt
2	43	3.30	147	17.35	centre NW Bay
3	43	7.50	147	17.50	midchannel off Oyster Cove Pt
4	43	8.20	147	19.50	centre Barnes Bay
5	43	12.70	147	17.80	mid channel south of Green Is
6	43	12.00	147	21.80	centre of Great Bay
7	43	15.90	147	19.30	centre of Isthmus Bay
8	43	18.95	147	11.30	mid channel west of Satellite Is
9	43	21.44	147	12.64	inside Little Taylors Bay
10	43	21.95	147	7.20	mid channel, half way from Partridge Is and Ventenat Pt
11	43	25.90	147	9.40	inside Great Taylors Bay
12	43	24.25	147	4.10	south boundary condition

Sampling commenced on January 10<sup>th</sup> 2002 and continued monthly concluding in March 2003 (Table 2).

**Table 2. Sample dates for D'Entrecasteaux field work**

---

Survey 1	10-Jan-02
Survey 2	06-Feb-02
Survey 3	04-Mar-02
Survey 4	05-Apr-02
Survey 5	29-Apr-02
Survey 6	03-Jun-02
Survey 7	03-Jul-02
Survey 8	05-Aug-02
Survey 9	02-Sep-02
Survey 10	30-Sep-02
Survey 11	04-Nov-02
Survey 12	02-Dec-02
Survey 13	06-Jan-03
Survey 14	07-Feb-03
Survey 15	04-Mar-03
Survey 16	31-Mar-03

---

## General methods

At each station a vertical profile for temperature, salinity (conductivity), light (PAR), fluorescence, and dissolved oxygen (DO) was measured using a Seabird SBE 19 conductivity, temperature and depth (CTD) unit that included a DO meter, a Wetstar fluorometer and a Biospherical light meter.

Surface and bottom water samples were collected using a Niskin bottle and sampled for chlorophyll *a*, *b*, *c*; nutrients ( $\text{NO}_3+\text{NO}_2$ ,  $\text{SiO}_4$ ,  $\text{PO}_4$ ,  $\text{NH}_4$ ). Commencing in September 2002, at approximately three stations per survey, top and bottom water samples were taken and analyzed chemically for oxygen concentration and salinity. Physical results (temperature and salinity), most DO results were single point determinations selected to be representative of the upper meter or lowest meter sampled during a CTD cast.

A secchi disk depth was also measure and an integrated sample collected for phytoplankton taxonomy and chlorophylls *a*, *b*, *c*. See below for details.

## Nutrients

Samples collected in a 5-litre Niskin bottle subsampled for pigments and nutrients at both the surface and bottom depths at each of the 12 sites.

The following general techniques were used for nutrient analysis:  $\text{NO}_3^- + \text{NO}_2$  (after Wood *et al.* 1967),  $\text{PO}_4$  (after Murphy and Riley 1962),  $\text{SiO}_4$  (after Armstrong 1951). The techniques were modified for use on a Technicon Autoanalyze model II after Crowley *et al.* (1999). Ammonium analysis used a modified version of Jones (1991) recently demonstrated by Kerouel and Aminot (1997) to resolve concentrations as low as 1.5 nM.

## Methods for phytoplankton

### 1. Sample collection

**Preserved samples for cell counts:** Samples for phytoplankton identification were collected using an integrated water column sampler from the surface to a maximum of 12 meters or to within 1 meter of the bottom. The integrated sampler was a 12 m long clear plastic hose, 30 mm in external diameter and graduated at 1 m intervals. A 12 m long rope was attached to its 0 m (“bottom”) end, and a second rope (about 2 m long) to its 12m (“top”) end. To deploy the sampler, two diving weights were attached to a clip on the 0m (bottom) end of the hose, and the hose was lowered through the water column at approximately 1 metre per second. When the required depth was reached a plug was inserted in the 12m (top) end, and the sampler hose hauled to the surface by means of the longer rope.

With the bottom end of the sampler held over a funnel in the mouth of a 10 litre carboy, the plug was removed from the top end, and the sample in the hose was siphoned into the carboy and mixed thoroughly. 1 litre aliquots were taken for phytoplankton identification and pigment analysis. The phytoplankton samples were preserved in the

field with Lugols iodine fixative solution (110 g potassium iodide, 50 g iodine, 1 litre distilled water, 100 ml glacial acetic acid) to approximately 2% final concentration.

The Lugols preserved samples were transferred to 1 litre measuring cylinders (volume recorded –  $V_1$ ) and allowed to settle for at least 24 hours. After this time, approximately 900 ml were siphoned off and the remaining sample was transferred to a 100-ml measuring cylinder and again allowed to settle for at least 24 hours. Then approximately 90 ml were siphoned off, the final volume recorded ( $V_2$ ) and thoroughly mixed before a 1-ml aliquot was taken, placed in a Sedgwick Rafter counting chamber and examined under an inverted microscope.

## Phytoplankton identification

**Preserved samples for cell counts:** A Sedgwick Rafter counting chamber with a grid of 1000 squares, each of 1  $\mu\text{l}$  was used. For microplankton, (cells generally larger than 20  $\mu\text{m}$  diameter) at least 100 squares or 10% of the counting chamber was scanned (except in cases where there were dense blooms of one or more microplankton species, when at least one column of 20 squares was scanned.) For nanoplankton, (2-20  $\mu\text{m}$  in diameter) the chamber was examined under the highest possible magnification until at least 300 cells of the dominant nanoplankton “species” had been counted. Flagellates in the nanoplankton were grouped, as time constraints did not allow fuller identification. In some instances where fixed samples revealed blooms of particular flagellate “species,” unfixed whole water samples were collected on the following field sampling to check for dominant flagellate species.

Cells per litre = cell “species” count \* (1000 / number squares counted) \* ( $V_2$  \* 1000 /  $V_1$ )

## Methods for chlorophyll a

**Sample collection:** A 5 litre Niskin bottle was used to sample from the surface and the bottom at each of the 12 sites. These were subsampled for pigments and nutrients. Additional pigment samples were collected from the integrated phytoplankton sampler during the first twelve months of the survey.

**Sample treatment:** Water samples were filtered under less than 5 mm Hg vacuum through a GF/F filter. The filters were stored in cryovials immersed in liquid nitrogen until extraction.

All glassware was cleaned in dilute Extran solution, rinsed three times with MilliQ water and once with acetone (AR).

Frozen filters were cut into halves and placed in a clean 10 ml centrifuge tube. 3 ml of 100% acetone was added to each tube. The tube was covered with parafilm and vortexed for  $\approx$  30 seconds before placing the tube in an ice-water bath and sonicating the filter and acetone for 15 minutes. The filters and acetone were then stored for at least 18 hours at 4°C. After this time, 0.2 ml MilliQ water was added to each tube (to bring solvent to  $\approx$  90:10 acetone : water) and the filter and solvent sonicated for another

15 minutes. Solvent and filter were then transferred to a Biorad column containing a small GF/F filter acting as a plug.

The sample tubes were rinsed with 2 x 0.5 ml of acetone/water (90:10) which is quantitatively added to the Biorad column. Each Biorad column was fitted into a centrifuge tube and centrifuged for 5 minutes at 5000 rpm. The filtrate was stored in the cool and dark (small foam esky) just prior to analysis.

Samples were analysed for chlorophyll *a*, *b* and *c*, using a GBC UV/VIS 916 spectrophotometer with 40 mm path length optical glass cells.

Absorbance was read at wavelengths of 750, 664, 647 and 630 nm. The absorbance at 750 nm was subtracted from the absorbance at each of the other three wavelengths and substituted into the following equations:

$$[\text{chl. a}]_{\text{extract}} = 11.85A_{664/l} - 1.54A_{647/l} - 0.08A_{630/l}$$

$$[\text{chl. b}]_{\text{extract}} = 21.03A_{647/l} - 5.43A_{664/l} - 2.66A_{630/l}$$

$$[\text{chl. c}]_{\text{extract}} = 24.52A_{630/l} - 1.67A_{664/l} - 7.60A_{647/l}$$

A = corrected absorbance.

l = path length in cm.

The concentration of each chlorophyll in the sample in  $\mu\text{g/L}$  was obtained by the following equation:

$$[\text{chl.x}]_{\text{sample}} = [\text{chl.x}]_{\text{extract}} * (v/V)$$

v = volume of extract in ml.

V = volume of seawater filtered in litres.

The total concentration of chlorophyll in the sample in  $\mu\text{g/L}$  was obtained by the following equation:

$$[\text{chl.}]_{\text{total}} = [\text{chl.a}]_{\text{sample}} + [\text{chl.b}]_{\text{sample}} + [\text{chl.c}]_{\text{sample}}$$

## Statistical analysis

Data are summarized using a variety of simple statistical procedures, such as the calculations of means, standard deviations or standard errors. Comparisons between sites or sampling periods used analysis of variance (ANOVA). If the data were not normally distributed or not homoscedastic then transformations were undertaken. For example, [chlorophyll *a*] data collected for this research were not normally distributed but, as is often the case, were skewed right. Chlorophyll *a* concentration data were transformed by:

$$x' = \text{Log}_{10}(x+1)$$

where x is the original concentration and x' is the transformed value used in the statistical analysis.

If ANOVA indicated a significant difference was present then it was followed by a least significant difference (LSD) test to identify the specific site or sampling periods that were significantly different. The LSD test used here (Bonferroni *t*-test) seeks to reduce type I errors by adjusting alpha for the number of nonorthogonal comparisons as follows:

$$\alpha' = 1 - (1-\alpha)^{1/r}$$

where  $r$  = the number of comparisons to be made and  $\alpha = 0.05$  while  $\alpha'$  is the new probability that  $P$  must be less than to reject the null hypothesis. To reduce the number of possible LSD tests post ANOVA a single site (site 12) was nominated as a “control” for statistical purposes. In most cases the data available were insufficient to permit the interaction terms in the ANOVAs to be estimated and thus they are not presented.

## Results

### Summary of seasonal patterns of chlorophyll distribution

#### Chlorophyll summary data

Summary chlorophyll data were derived from averaged chlorophyll *a* measurements across the twelve D'Entrecasteaux Channel sampling sites. (Fig 1)

Average surface chlorophyll results show chlorophyll concentrations of generally less than  $1.0 \mu\text{g L}^{-1}$ , with a small peak in May 2002, rising to a peak of almost  $2.0 \mu\text{g L}^{-1}$  in September 2002 (Fig. 2). Average concentration then fell to very low levels in summer 2002-03 before a substantial increase in March 2003 when monthly sampling ceased.

There were statistically significant differences associated with depth (Table 3, surface > bottom). Some sites were significantly different in mean chlorophyll *a* concentrations with northern sites tending to have greater concentrations than southern ones (Fig. 3). Fitting the data to a general linear model and using Bonferroni corrected multiple *t*-tests with site 12 as a control: sites 1 through 6 were shown to have statistically different chlorophyll *a* concentrations relative to site 12. There were also statistically significant differences associated with date (Table 3).

Bottom average chlorophyll *a* results are largely similar to the corresponding surface result, but slightly lower (Fig 2.) However the temporal peak in bottom chlorophyll *a* concentration was in November rather than September-October 2002, probably reflecting slowly senescing cells from the earlier surface bloom sinking through the water column.

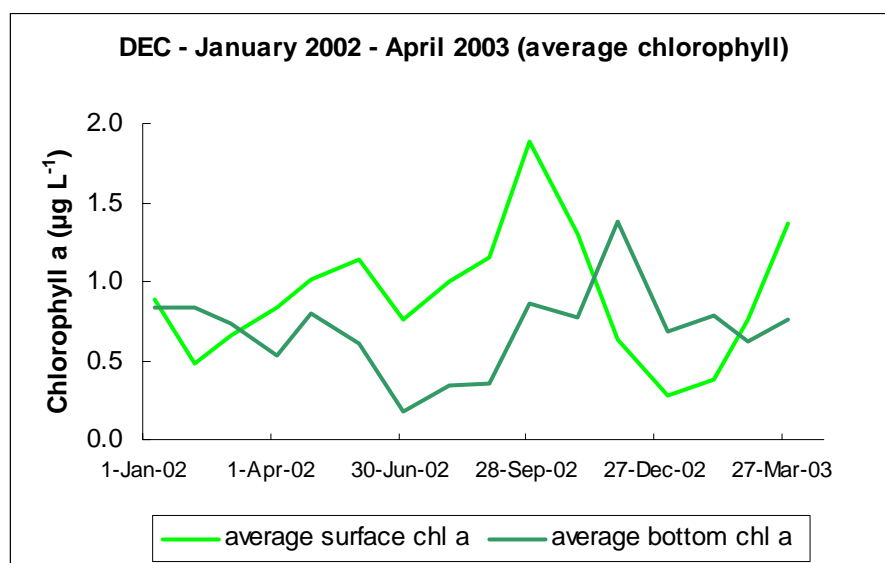


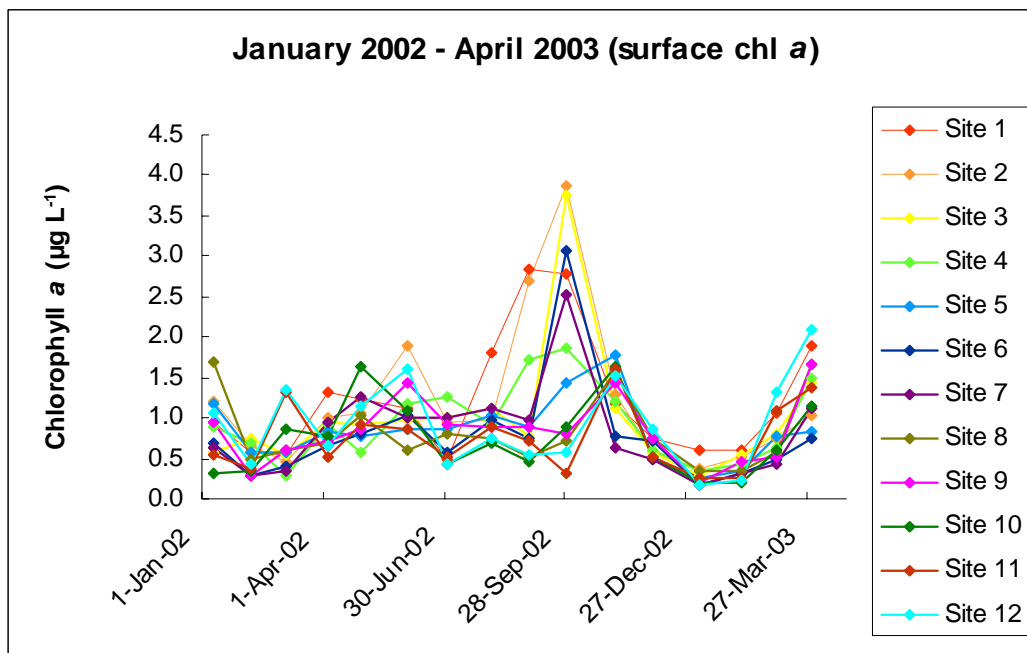
Fig 2. Surface and bottom chlorophyll *a*, averaged across 12 sites in the D'Entrecasteaux Channel.

**Table 3. Statistical analysis of the chlorophyll *a* data (log 10 transformed).**

Source of Variation	DF	SS	MS	F	P
Date	14	5.59	0.399	14.27	<0.001
Site	11	2.76	0.251	8.98	<0.001
Depth	1	1.86	1.865	66.71	<0.001
Residual	154	4.30	0.0280		
Total	359	33.39	0.0930		

*Surface and bottom chlorophyll*

Figures 3 and 4 contrast surface and bottom chlorophyll *a* levels at all sites. At the surface there was a spring peak of up to 4.0  $\mu\text{g L}^{-1}$  in chlorophyll *a*, either at the August-September sampling in the upper Channel (Sites 1, 2, 3, 4, 6 and 7) or at the October sampling in the lower Channel (Sites 5, 8, 9, 10, 11 and 12)



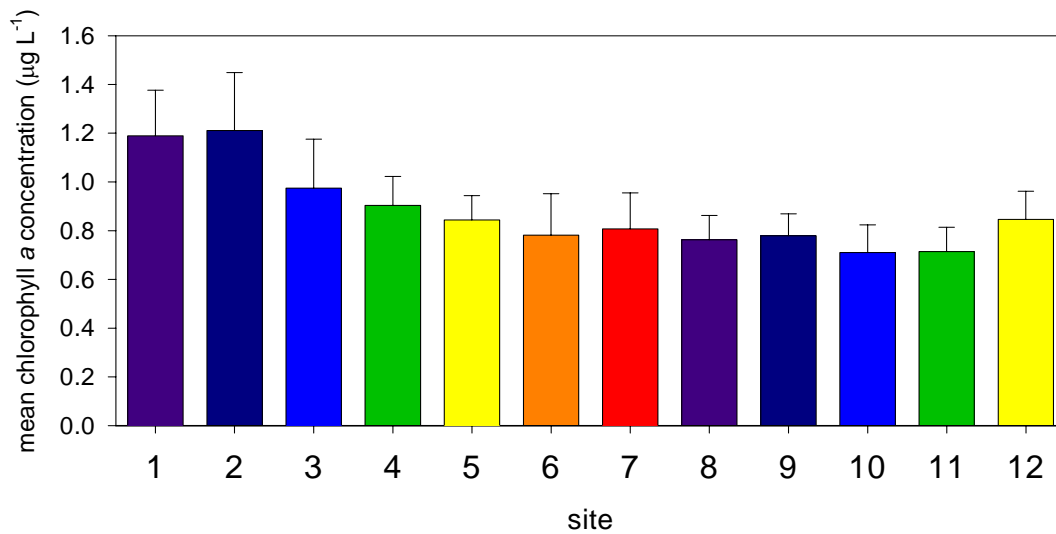


Fig. 3. Surface level chlorophyll *a* concentrations at 12 sites in the D'Entrecasteaux Channel (upper panel), mean surface chlorophyll *a* concentrations by site (lower panel).

The only sites showing a “bottom” September chlorophyll peak were sites 6 and 7 which are shallow bays (Great Bay and Isthmus Bay on Bruny Island) with well-mixed water columns (Fig. 4). Deeper mid channel sites such as #1, 9 and 12 peaked in October, while at all the remaining sites bottom chlorophyll peaked in November.

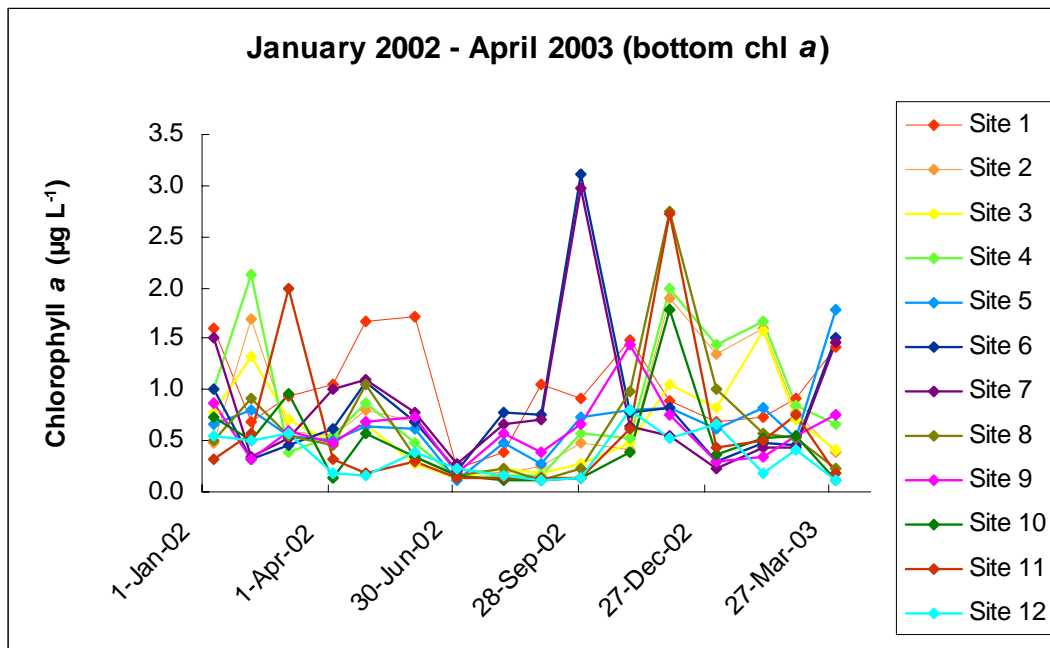


Fig. 4. Near bottom chlorophyll *a* concentrations at 12 sites in the D'Entrecasteaux Channel.

## Summary of seasonal patterns of nutrient distribution

### *Nutrient summary data*

Summary nutrient data were derived from averaged nutrient measurements across the twelve D'Entrecasteaux Channel sampling sites (Figures 5-9).

Average surface and bottom nitrate results initially showed concentrations of generally less than 1.0  $\mu\text{M}$ , rising to a broad peak of approximately 3  $\mu\text{M}$  from July to September 2002 (Fig. 5). Bottom nitrate concentrations remained greater longer than surface concentrations being double surface concentrations on September 30<sup>th</sup> 2002 (mean bottom across all 12 sites was 2.1  $\mu\text{M}$  versus 1.0  $\mu\text{M}$  for the mean surface concentration). Average concentrations then fell to very low levels in summer 2002-03 before a substantial increase in bottom nitrate in March 2003, when monthly sampling ceased.

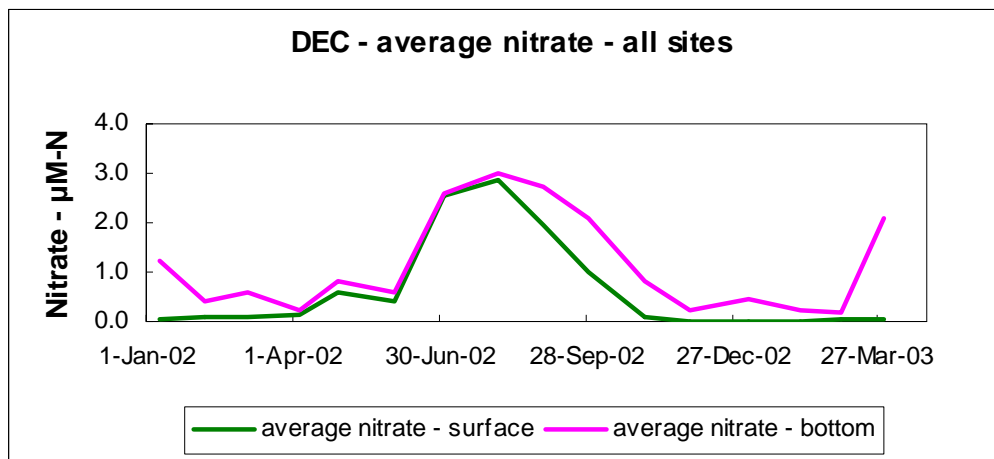


Fig. 5. Surface and bottom nitrate, averaged across 12 sites in the D'Entrecasteaux Channel.

Surface and bottom nitrite concentrations were also elevated throughout the winter and appear to show a double peak in concentration with the highest nitrite concentration measured in June 2002 followed by a smaller peak in spring. (Fig. 6).

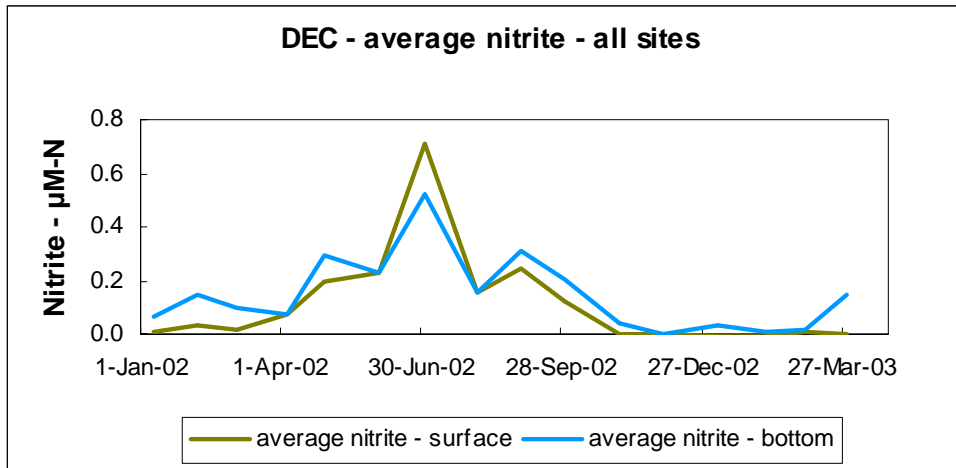


Fig. 6. Surface and bottom nitrite, averaged across 12 sites in the D'Entrecasteaux Channel.

In contrast, there appears no definite temporal pattern in bottom ammonium concentrations; average surface ammonium concentrations were elevated only in April-May 2002 and again in January 2003 (Fig. 7). The data were fit to a general linear model that indicated ammonium concentrations were significantly greater at depth than at the surface (Table 4). There were also significant differences between sites (Table 4) with sites 5, 6, 7 having the lower  $\text{NH}_4^+$  concentrations than either the upper or lower end of the Channel especially near the bottom (Fig. 7). To reduce the possible number of statistical comparisons site 12 was selected as a control and Bonferroni corrected multiple *t*-tests indicated that site 7 was significantly lower in ammonium concentration than the control site.

**Table 4. Results of statistical analyses for [NH<sub>4</sub>].**

Source of Variation	DF	SS	MS	F	P
Site	11	1.91	0.174	2.411	0.008
Depth	1	1.64	1.638	22.721	<0.001
Date	15	2.90	0.193	2.679	0.001
Residual	165	11.89	0.0721		
Total	383	36.68	0.0958		

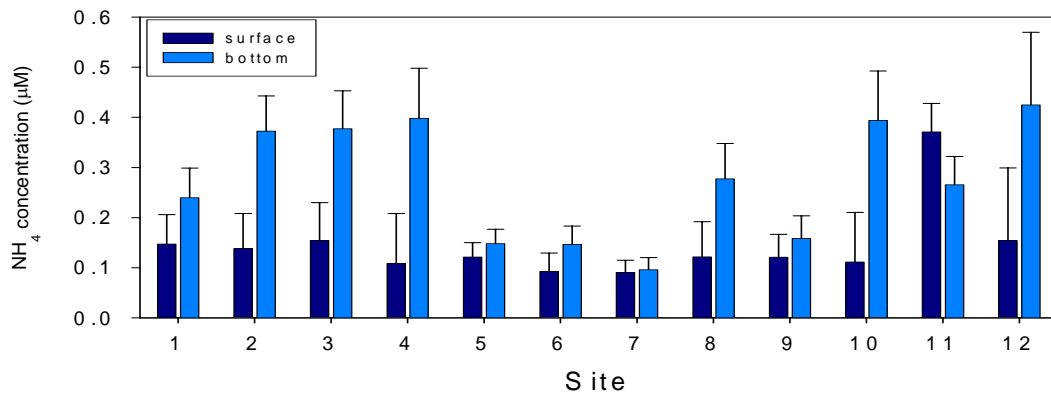
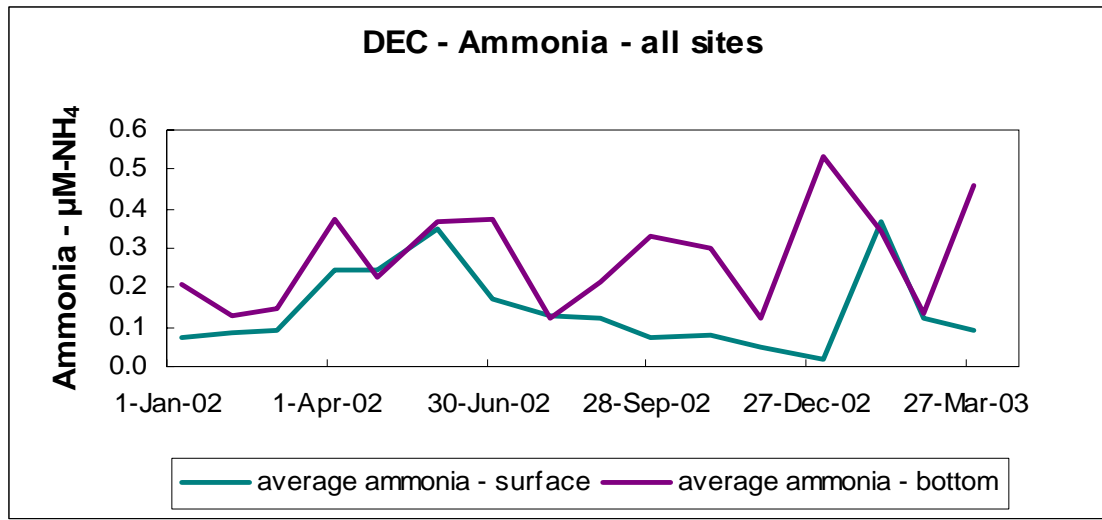


Fig. 7. Surface and bottom ammonium concentrations averaged across 12 sites in the D'Entrecasteaux Channel (upper panel); mean [NH<sub>4</sub>] by site averaged across time (lower panel; error bars are standard errors).

Average phosphate concentrations at both surface and bottom were about 0.2 μM in the summer 2002 at the start of the survey, rising to a sustained level above 0.3 μM throughout autumn and winter 2002 (Fig. 8).

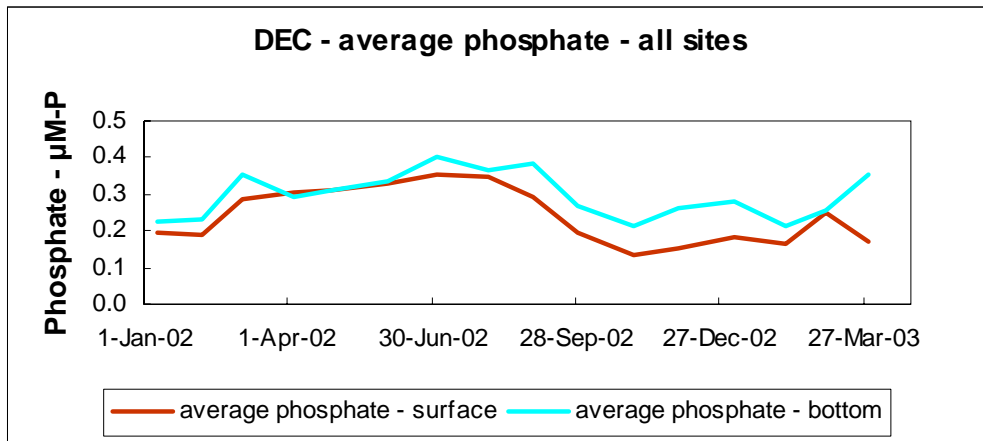


Fig. 8. Surface and bottom phosphate concentrations, averaged across 12 sites in the D'Entrecasteaux Channel.

Silicate concentrations near the bottom did not vary substantially throughout the sampling period, with a broad peak in winter 2002 (Fig. 9). In contrast, surface concentrations showed a sharp peak at almost 10.0 µM in June 2002 with indications another peak would probably occur in winter 2003. Quite low surface concentrations of silicate were observed in November 2002 and January 2003.

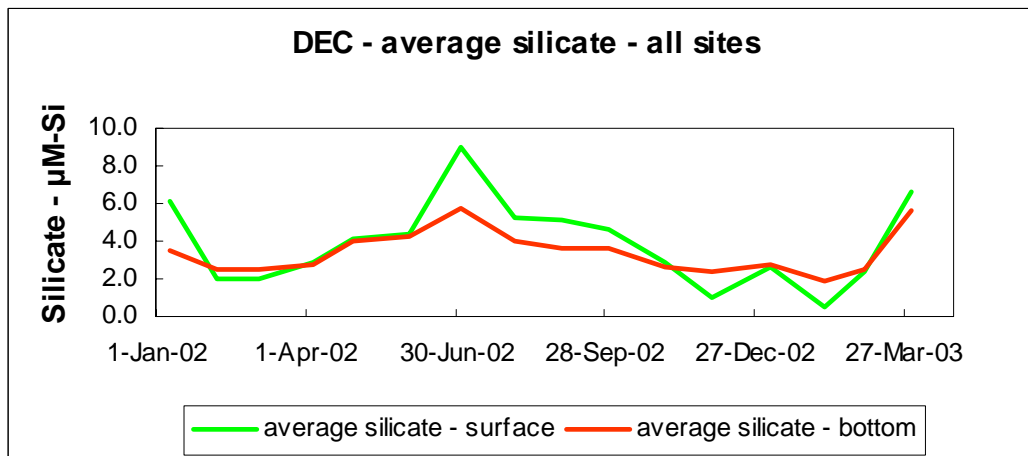


Fig 10. Surface and bottom silicate, averaged across 12 sites in the D'Entrecasteaux Channel.

## Summary of seasonal patterns of phytoplankton distribution

Samples for phytoplankton identification were collected using an integrated water column sampler that collected water from the surface to a maximum of 12 metres. The phytoplankton samples were preserved in the field with Lugols iodine fixative solution to approximately 2% final concentration. Time constraints prevented examination and counting of samples from surface and bottom depths.

Counts of individual "species" were calculated and entered into the project database. Additionally, totals of diatoms, dinoflagellates and small flagellates were calculated.

Flagellates in the nanoplankton were grouped, as time constraints and the resolution of the microscope did not allow fuller identification.

Counts of “species” tabulated individually were the dominant diatoms *Skeletonema costatum* (or other dominant centric diatom), *Pseudo-nitzschia* spp. and *Chaetoceros* spp. and the dinoflagellates *Ceratium* spp. and *Gymnodinium catenatum*. These taxa were chosen for more detailed analysis to facilitate comparison with results from the Huon Estuary Study. Summary phytoplankton data were derived from averaged phytoplankton counts across the twelve D’Entrecasteaux Channel sampling sites.

At all stations high counts of nanoflagellates (around  $1.0$  to  $1.5 \times 10^6$  cells per litre) outnumbered counts of the diatom or dinoflagellate “bloom” species. Generally these small flagellates accounted for up to 90% of cell numbers; with diatoms and dinoflagellates being in very low numbers throughout winter 2002 and in November 2002. (Fig. 10)

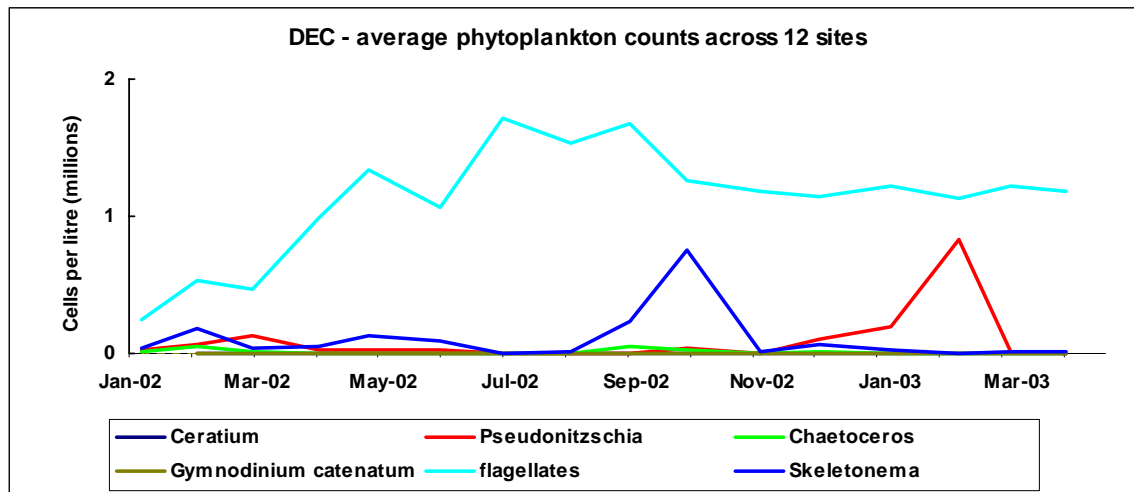


Fig. 10. Average phytoplankton counts across 12 sites in the D’Entrecasteaux Channel.

In the summer and autumn of 2002, there were no significant diatom blooms; the levels of the dominant species *Skeletonema* and *Pseudo-nitzschia* did not exceed  $2 \times 10^5$  cells per litre. However, in spring 2003 (Fig. 11), the average counts showed a significant *Skeletonema costatum* bloom at  $8 \times 10^5$  cells per litre, contrasting in autumn 2003 with a *Pseudo-nitzschia* spp bloom. ( $9 \times 10^5$  cells per litre.) The *Skeletonema* bloom was most prominent at sites north of Site 9; at the southern sites larger centric diatoms such as *Guinardia* or *Leptocylindrus* sometimes yielded slightly higher counts than *Skeletonema*.

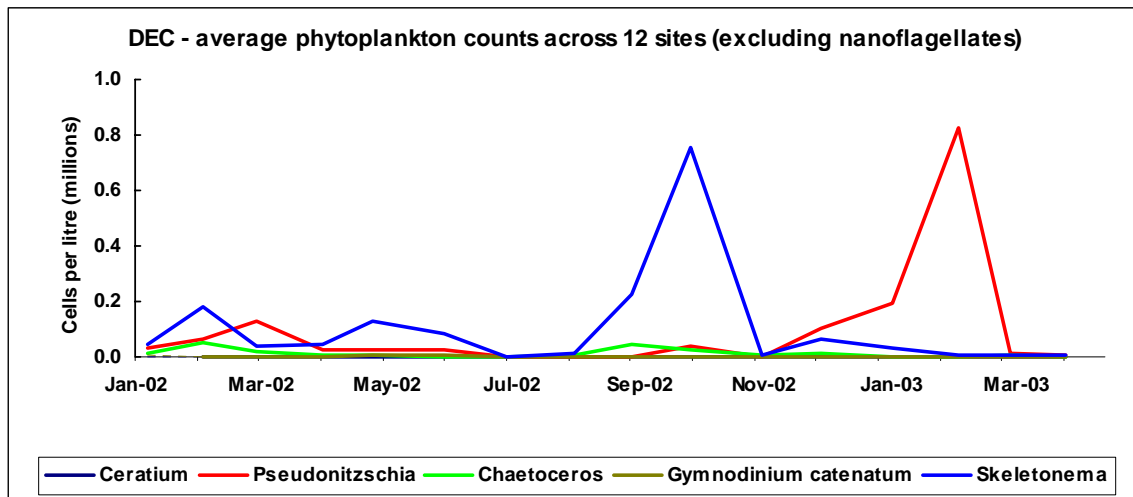


Fig. 11. Average counts across 12 sites in the D'Entrecasteaux Channel (small flagellates excluded.)

The high counts of diatoms in the spring and autumn blooms were also not uniform across all sites, being generally concentrated at sites in the northern end of the Channel. Total diatom numbers were up to  $4 \times 10^6$  cells per litre at site 4 (Barnes Bay) in October 2002, (Fig. 12 upper panel) and up to  $3 \times 10^6$  cells per litre at site 1 (off Dennes Point) in February 2003 (Fig. 12 lower panel).

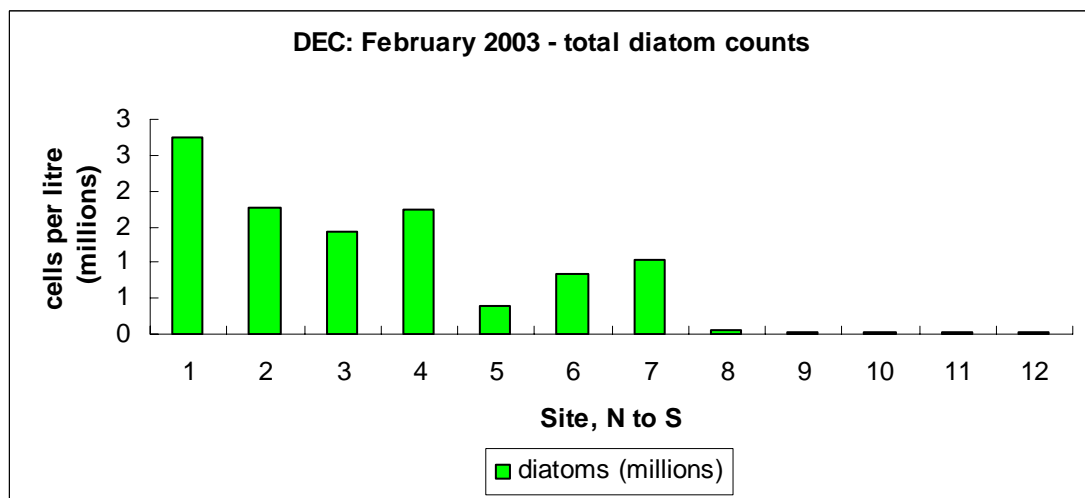
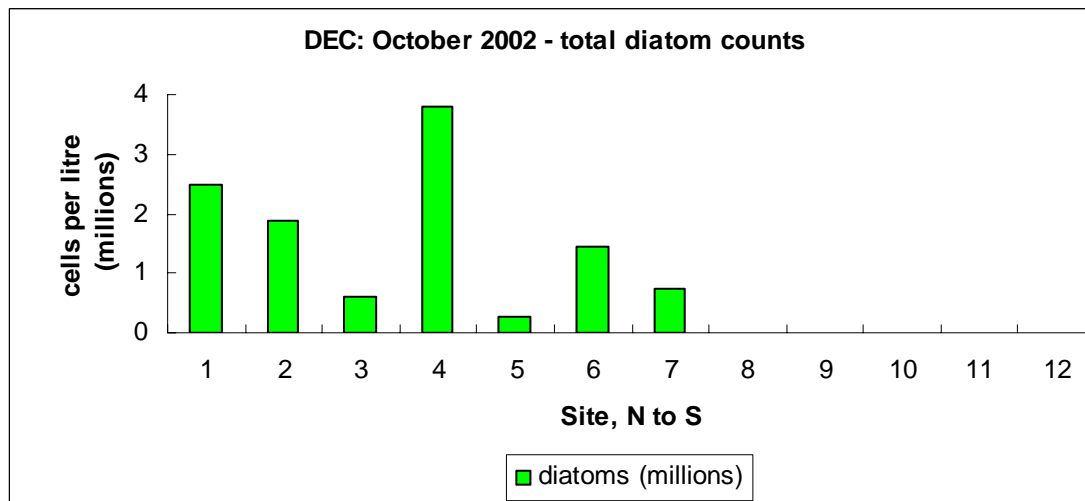


Fig. 12. Total diatom numbers at all sites in the D'Entrecasteaux Channel in spring (October 2002) and late summer (February 2003).

Dinoflagellates outnumbered diatoms at all or most sites in winter (July-August 2003,) in November 2002 and March 2003. Generally the most numerous dinoflagellates were smaller species in the range of 8-10µm in diameter. Again, time constraints did not allow fuller identification of these cells. Larger dinoflagellates such as *Ceratium*, *Dinophysis* and *Prorocentrum* occasionally showed high counts. High numbers of *Dinophysis* and *Prorocentrum* were noted in the lower Channel in November 2002 and March 2003 (Fig. 13).

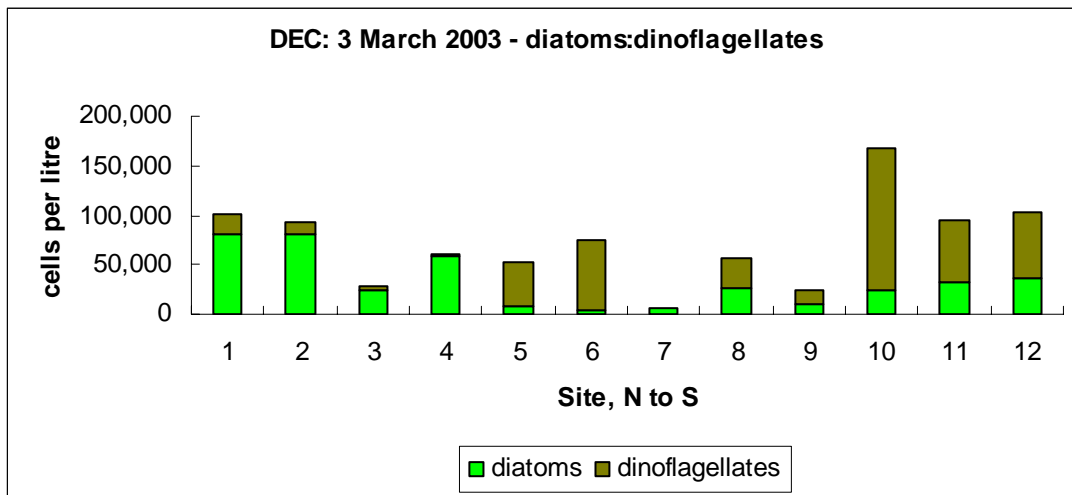


Fig. 13. Comparison of dinoflagellate and diatom numbers at March 3, 2003 sampling

At many sites, *Gymnodinium catenatum* densities peaked in summer and late autumn 2002, and were still at bloom levels, above  $10^4$  cells per litre, at some sites in May and June 2002. Generally *Gymnodinium* was concentrated at the southern or northern ends of the Channel in 2002 and not usually in high numbers in any of the bays, except in the June 2002 sampling at sites 2, 9 and 11 (Fig. 14).

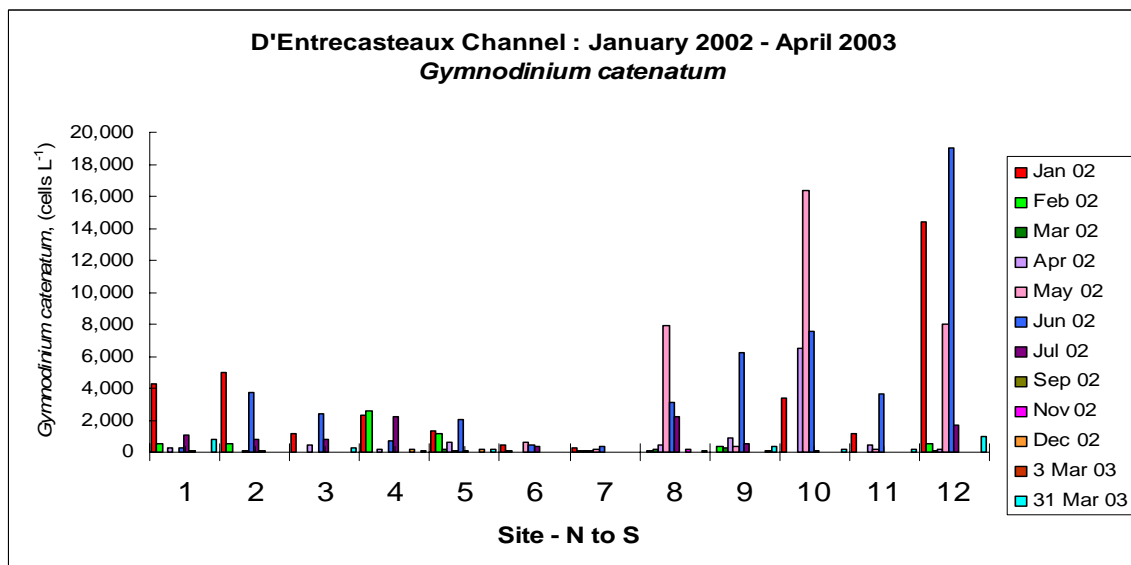


Fig. 14. Concentrations of *Gymnodinium catenatum* at 12 sites in the D'Entrecasteaux Channel

*G. catenatum* did not reach significant levels in the second summer of sampling; however, at the final sampling in March 2003 numbers appeared to be again increasing (Fig. 15). On May 1 2003, two stations in the Channel and one site in the Huon were sampled and *G. catenatum* was found at densities of up to 2500 cell L<sup>-1</sup> at a site approximating to DEC site 8 and at 5500 cells L<sup>-1</sup> at a site at the mouth of Port Cygnet. At this time Tasmanian Shellfish Quality Assurance Program monitoring showed an extensive bloom of *G. catenatum* in the Huon River and Port Esperance, with shellfish beds in Port Esperance remaining closed until mid-June 2003. (A. Turnbull, pers. comm.)

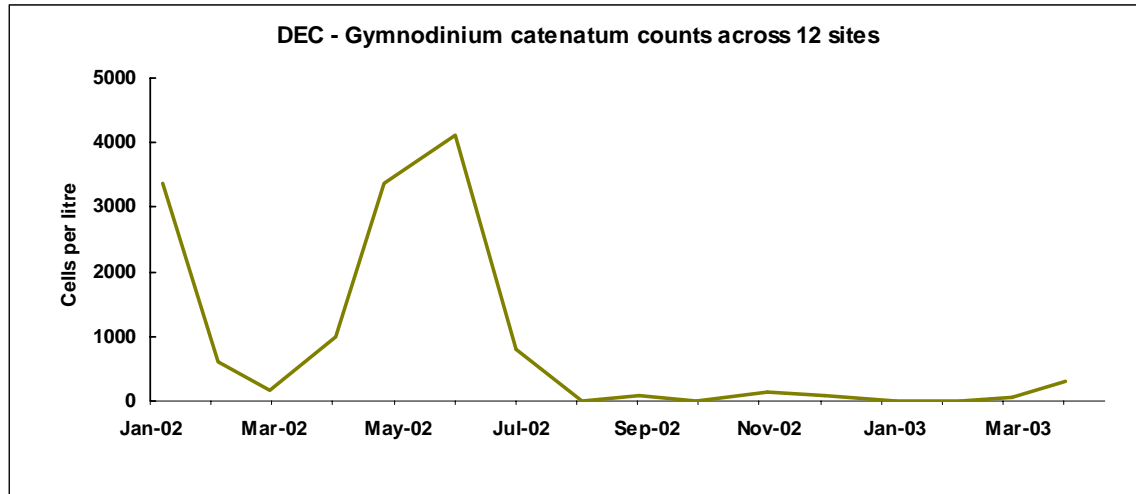


Fig. 15. Average *Gymnodinium catenatum* cell densities across 12 sites in the D'Entrecasteaux Channel.

*Noctiluca scintillans* is an herbivorous or heterotrophic dinoflagellate. During 2002 and the summer of 2003 it appeared in the D'Entrecasteaux Channel in its greatest abundance during December (2002) or January (2002) (Fig. 16). In the summer of 2002-2003 it appears to have been sudden suggesting arrival via advection rather than *in situ* growth.

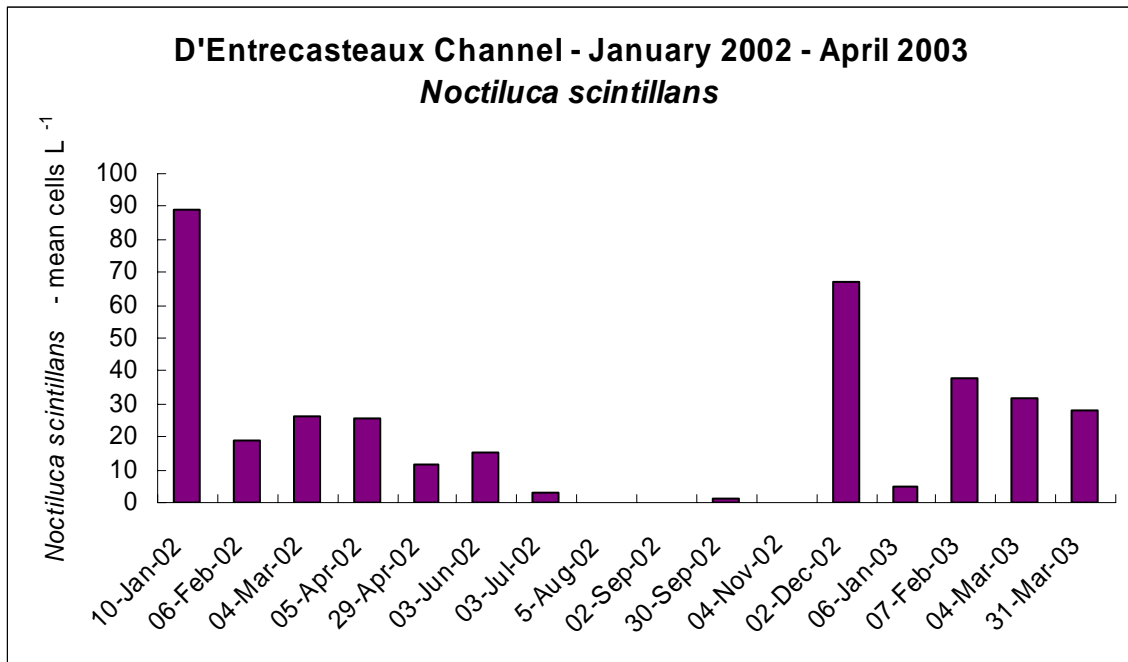


Fig. 16. Average *Noctiluca scintillans* cell densities across twelve sites in the D'Entrecasteaux Channel (error bars were relatively large and removed for clarity).

The *N. scintillans* appear at its highest densities in the north of the D'Entrecasteaux Channel (Fig. 17) at site 1 (off Dennes Point) or site 2 (Northwest Bay).

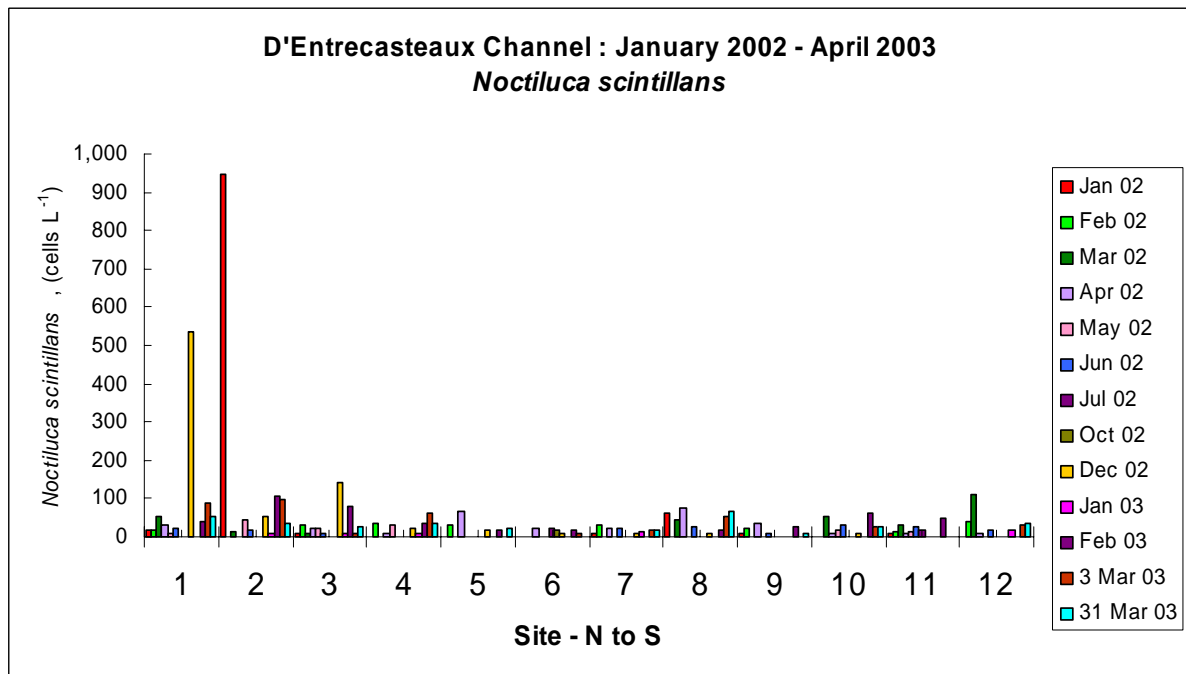


Fig. 17. *Noctiluca scintillans* cell densities at twelve sites in the D'Entrecasteaux Channel.

## Summary of phytoplankton distribution by sites

Counts of individual “species” were calculated and entered into the project database. Additionally, totals of diatoms, dinoflagellates and small flagellates were calculated. Flagellates in the nanoplankton were grouped, as time constraints and the resolution of the microscope did not allow fuller identification.

When counts were averaged across the 15 months of sampling, high counts of nanoflagellates (around  $1.0$  to  $1.5 \times 10^6$  cells per litre) generally outnumbered counts of the diatom or dinoflagellate “bloom” species. These small flagellates accounted for over 80% of cell numbers (on average) at all sites south of Site 4 (Barnes Bay); with diatoms and dinoflagellates being at lower densities in the southern Channel (Fig. 18).

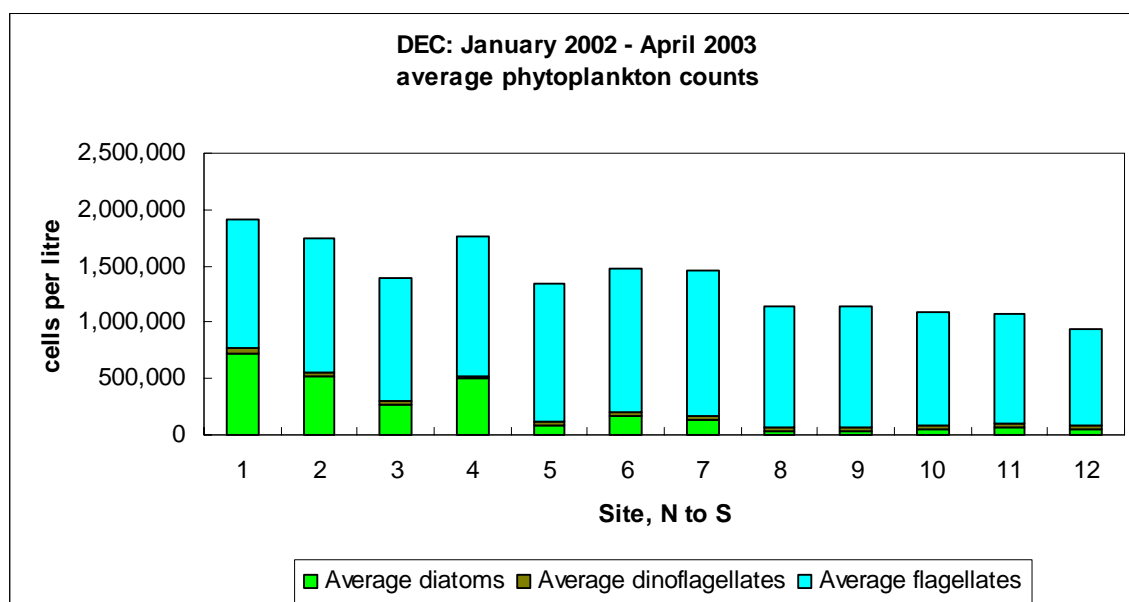


Fig. 18. Phytoplankton counts averaged over 15 months of sampling, at 12 sites in the D'Entrecasteaux Channel.

Diatoms were in greater numbers at the northern sites; over the 15 months of sampling, diatoms accounted for 20-40% of total cell numbers at these sites. The diatom blooms of October 2002 and February-March 2003 produced high numbers of diatoms at all the northern sites, elevating the site averages. Total diatom numbers were up to  $4 \times 10^6$  cells per litre at site 4 (Barnes Bay) in October 2002, and up to  $3 \times 10^6$  cells per litre at site 1 (off Dennes Point) in February 2003. Earlier in the survey period, in summer to autumn of 2002, there were much lower diatom counts at all sites (Fig. 19).

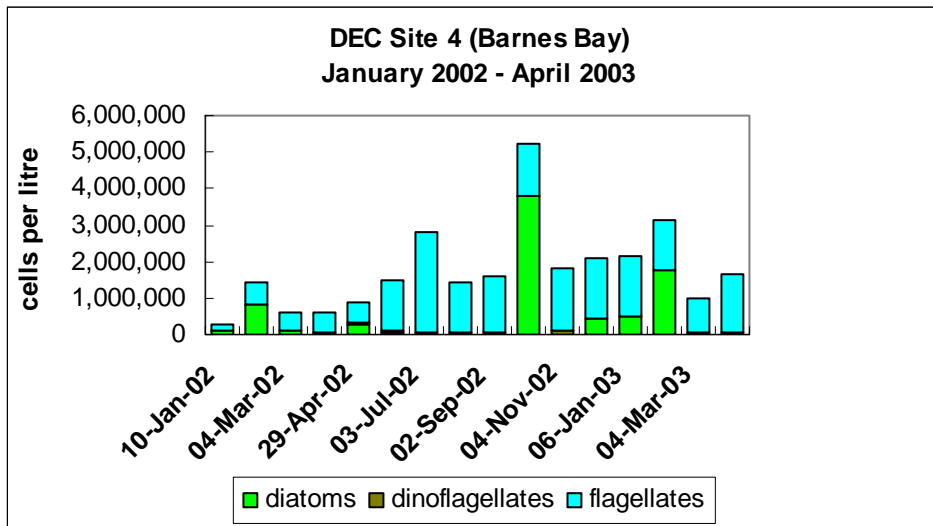


Fig. 19. Cell counts at site 4, Barnes Bay, showing diatom blooms in October 2002 and March 2003.

Dinoflagellates outnumbered diatoms at all or most sites in winter (July-August 2003) again in November 2002 and March 2003. Generally the most numerous dinoflagellates were smaller cells of 8-10µm diameter. Time constraints did not allow fuller identification of these cells. Larger diatoms such as *Ceratium*, *Dinophysis* and *Prorocentrum* were occasionally present at relatively high cell densities.

#### Cell counts at individual sites

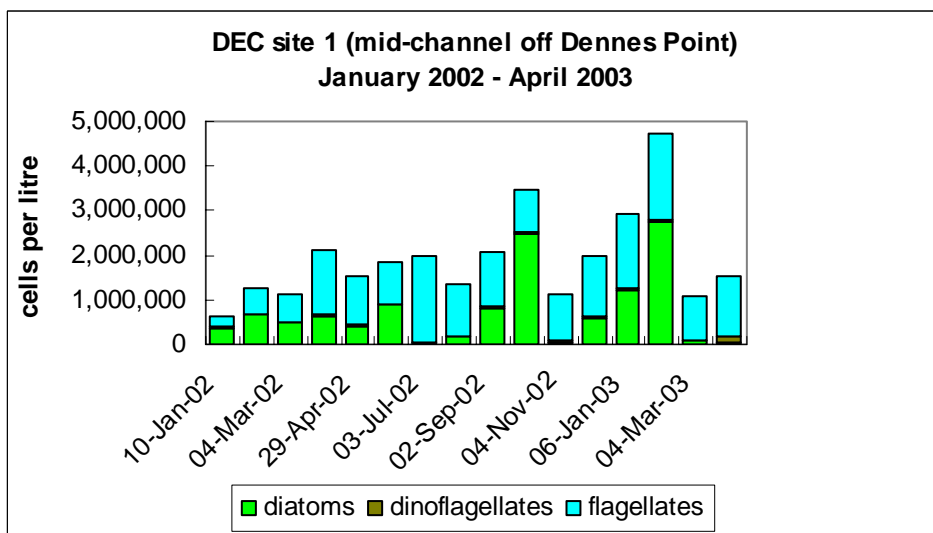


Fig. 20. Site 1 - mid channel off Dennes Point

Diatoms were present all year round, usually in high proportions relevant to other taxa. This site displayed less seasonal fluctuation than other sites.

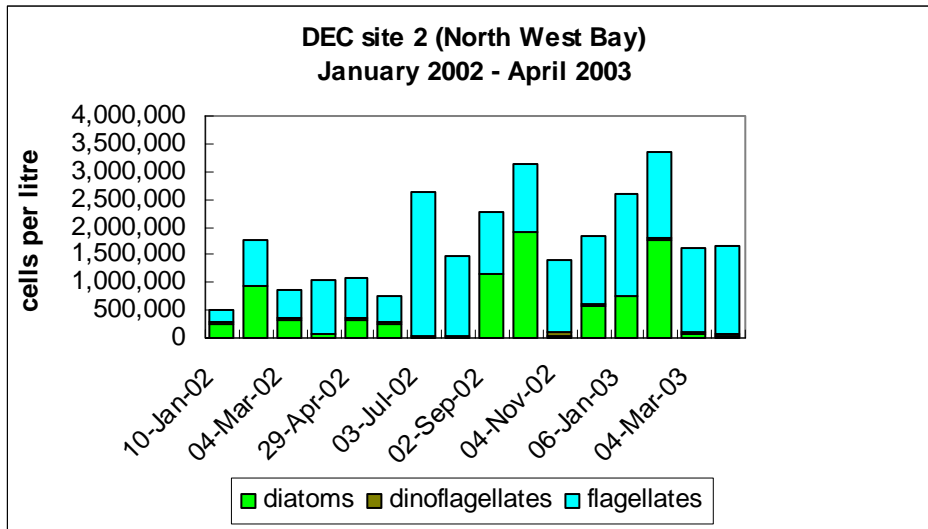


Fig. 21. Site 2 - centre of North West Bay

Diatoms were present in substantial proportions (up to 60% of total cell counts) in most months, except during July and August 2002.

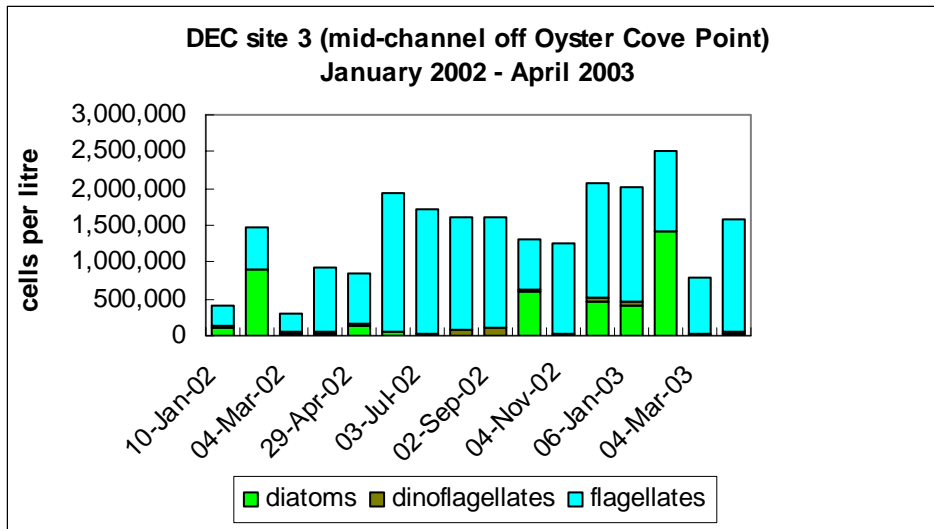


Fig. 22. Site 3 - mid channel off Oyster Cove Point

This site showed lower cell counts than the other northern sites, particularly through autumn 2002. It also had low diatom counts for a substantial part of the year.

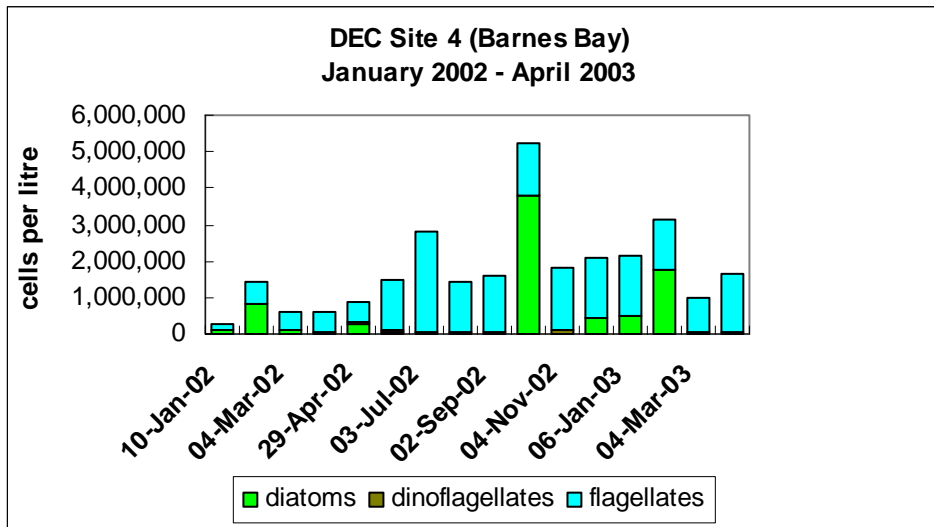


Fig. 23. Site 4 - centre of Barnes Bay

Site 4 had the highest cell counts of any of the 12 sites, with counts up to  $4 \times 10^6$  cells per litre in spring 2002, due to a bloom of diatoms (predominantly *Skeletonema costatum*.)

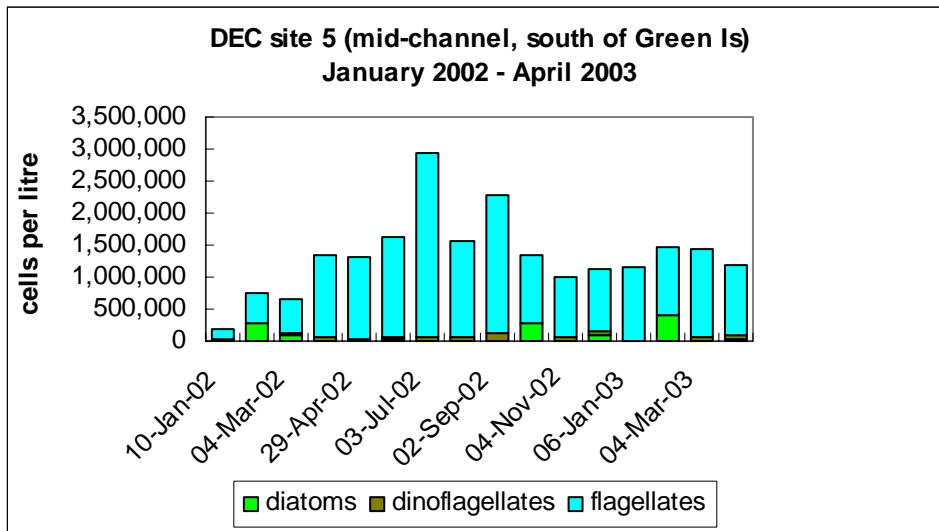


Fig. 24. Site 5 - mid channel, south of Green Is

This site displayed less seasonal fluctuation than most other sites, and generally lower counts of the larger taxa.

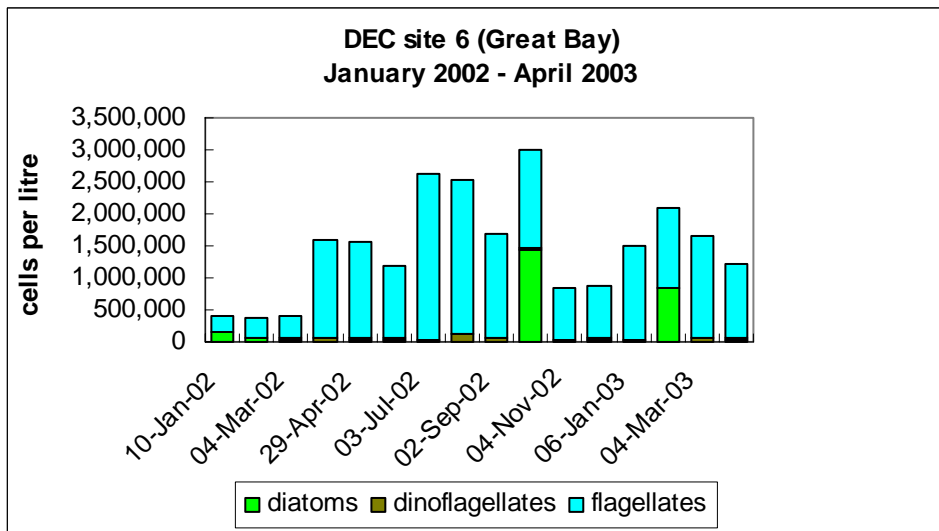


Fig. 25. Site 6 - centre of Great Bay

This was the shallowest site surveyed. Great Bay had relatively high proportions of dinoflagellates for most of the survey period, and high diatom numbers only in spring and autumn 2002-03.

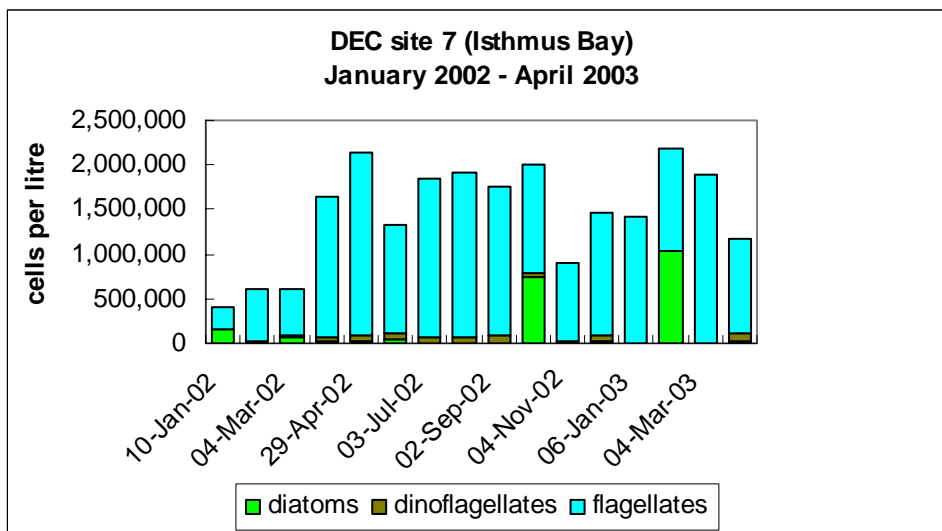


Fig. 26. Site 7 - centre of Isthmus Bay

Similar to Site 6, Isthmus Bay showed relatively high proportions of dinoflagellates for most of the survey period, and high diatom numbers only in October and February 2002-03. High numbers of *Dinophysis* and *Prorocentrum* were noted in the lower Channel in November 2002 and March 2003.

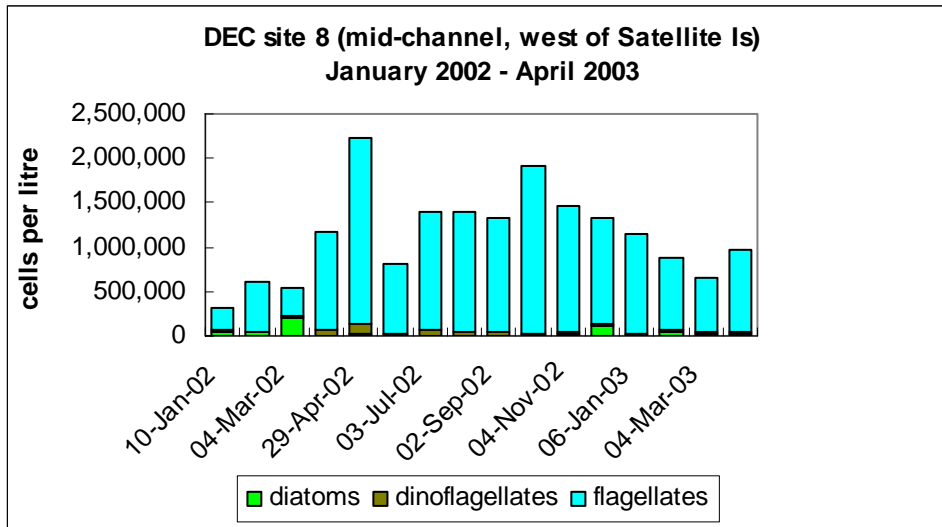


Fig. 27. Site 8 - mid channel, west of Satellite Is (opposite Huon River mouth)

Site 8, which was located in mid-channel opposite the mouth of the Huon River, showed the lowest diatom counts of any of the channel sites.

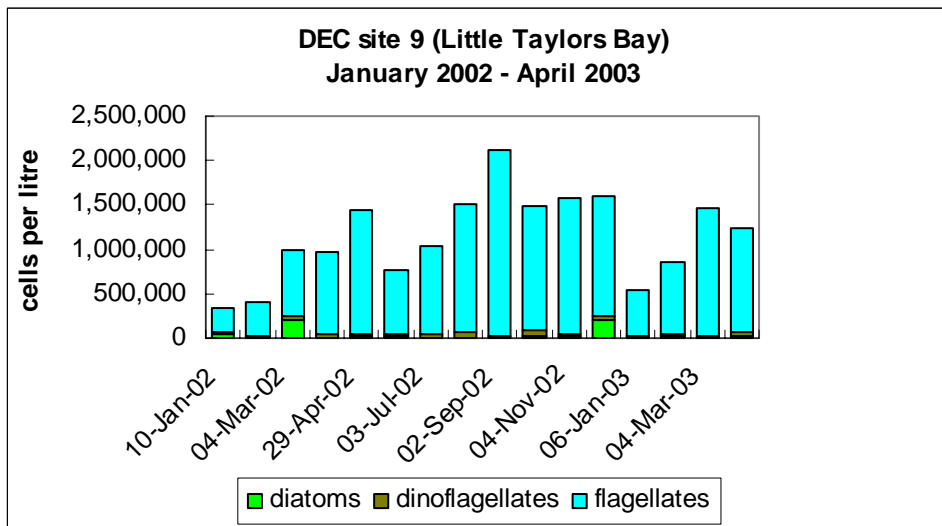


Fig. 28. Site 9 - inside Little Taylors Bay

Site 9 showed the lowest diatom counts of any of the 12 sites, with proportionally higher dinoflagellate counts, particularly *Dinophysis* and *Prorocentrum*. There were also high counts of *Gymnodinium catenatum* in June 2002.

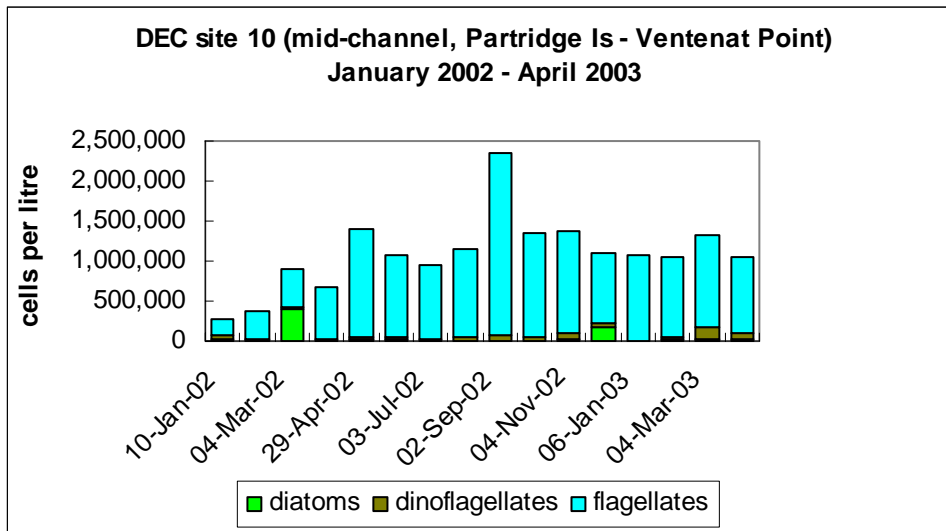


Fig. 29. Site 10 - mid channel, half way between Partridge Is and Ventenat Pt

Apart from a diatom bloom in autumn 2002, diatom numbers were again comparatively low. There were proportionally high numbers of dinoflagellates in most months.

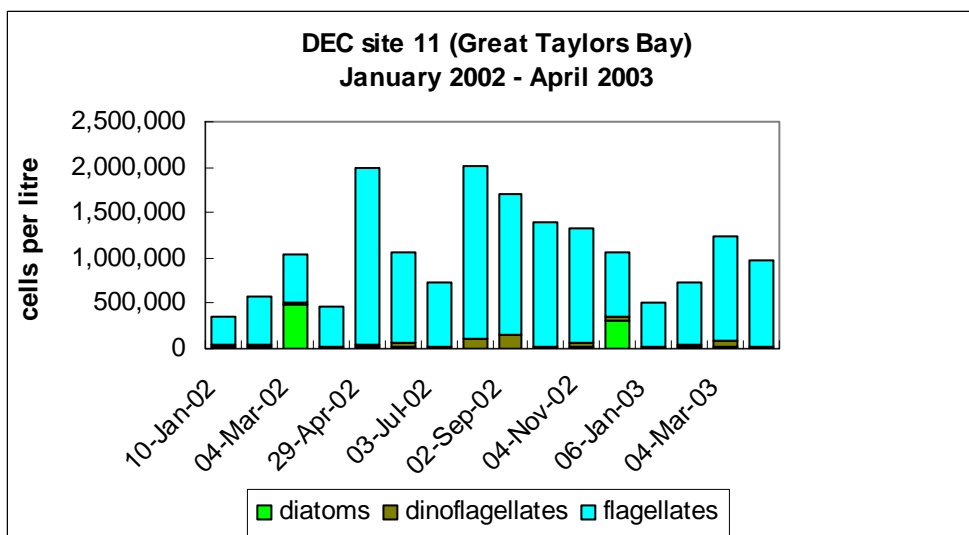


Fig. 30. Site 11 - inside Great Taylors Bay

*Gymnodinium catenatum* had high counts in June 2002. There were proportionally high numbers of dinoflagellates most of the year, with high diatom counts only in March and December 2002.

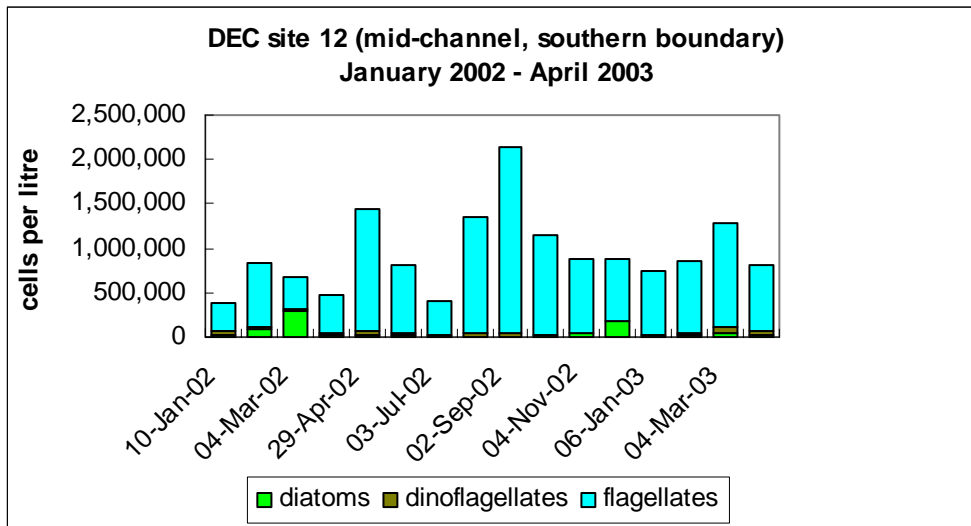


Fig. 31. Site 12 - southern boundary condition

Site 12, at the southern boundary, generally had the lowest total cell counts and lower evidence of seasonal diatom blooms.

*Physics*

The mean surface temperatures were considerably lower and salinities markedly greater throughout the summer of 2001-2002 than during 2002-2003 (Fig. 32). Minimum temperatures ( $\sim 10^\circ\text{C}$ ) and minimum salinities were observed in July 2002.

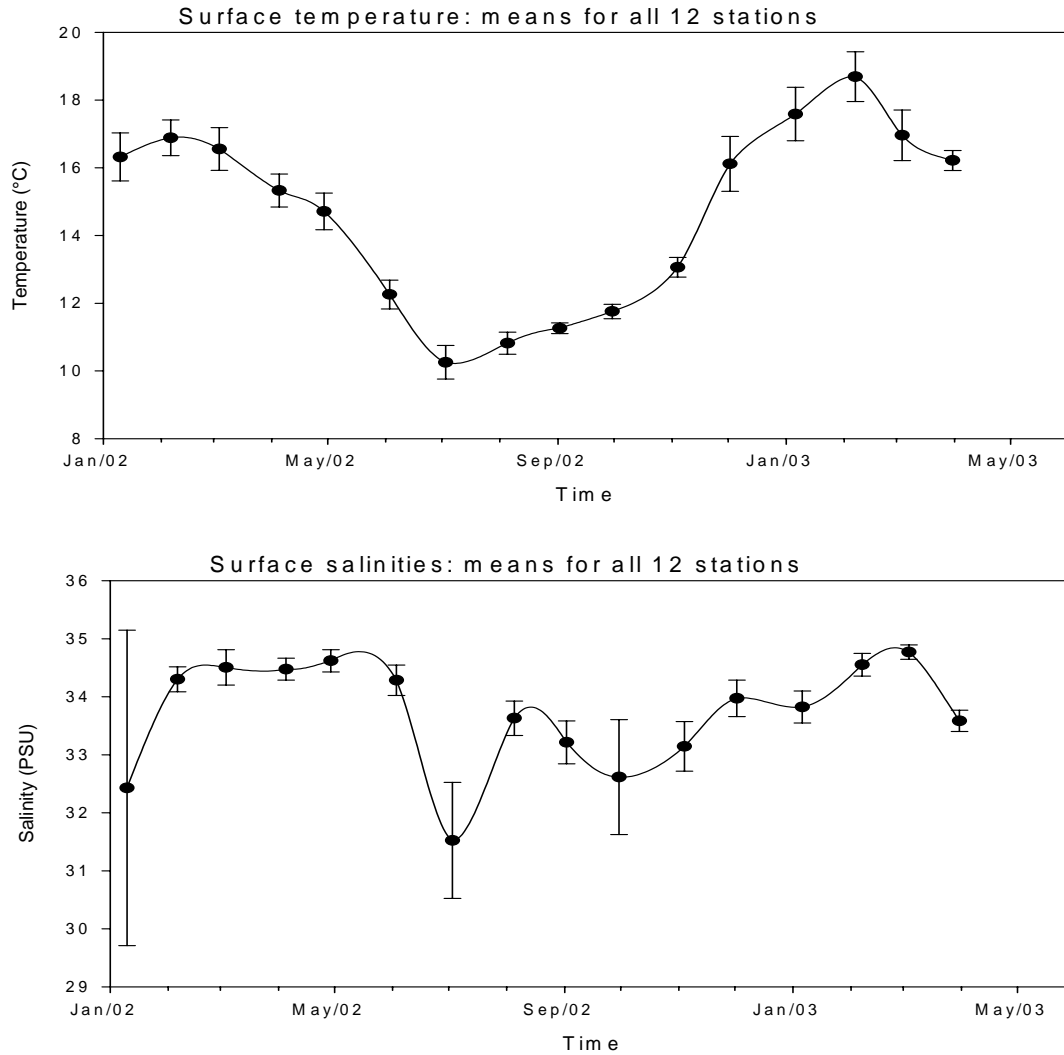


Figure 32. Mean surface temperature (upper panel) and salinity (lower panel) for all twelve sites over the duration of the study. Error bars are standard deviations.

All sites followed a similar seasonal pattern reaching minima in July 2002 and maxima in February 2003. Site 12 tended to be the coldest site during summer and the warmest site during winter reflecting its more intimate connection to the larger thermal mass of the offshore water body (Fig. 33, upper). Over an annual cycle site 2 (Northwest Bay) tended to be warmest (Fig. 33, lower).

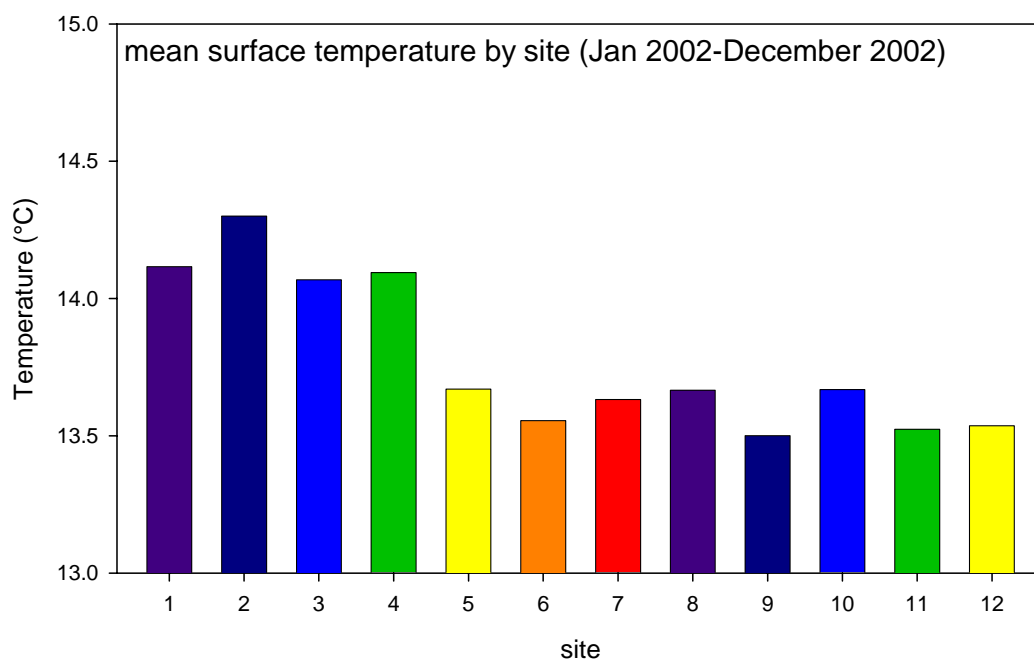
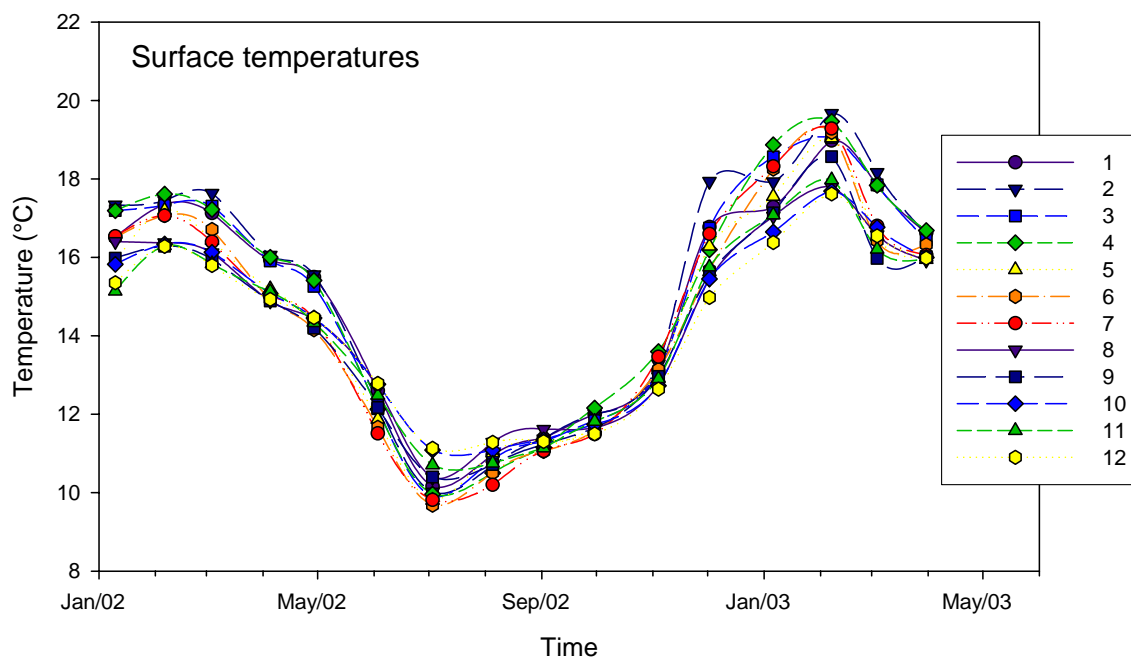


Figure 33. Surface temperature for each site and date (upper panel) and annual mean (2002) for all twelve sites (lower panel).

Salinity was highly dominated by the maritime influence with only one observation below 30 PSU (Fig. 34). Site 8 at the point closest to the entrance to the Huon River had the lowest mean salinity (Fig. 34 lower).

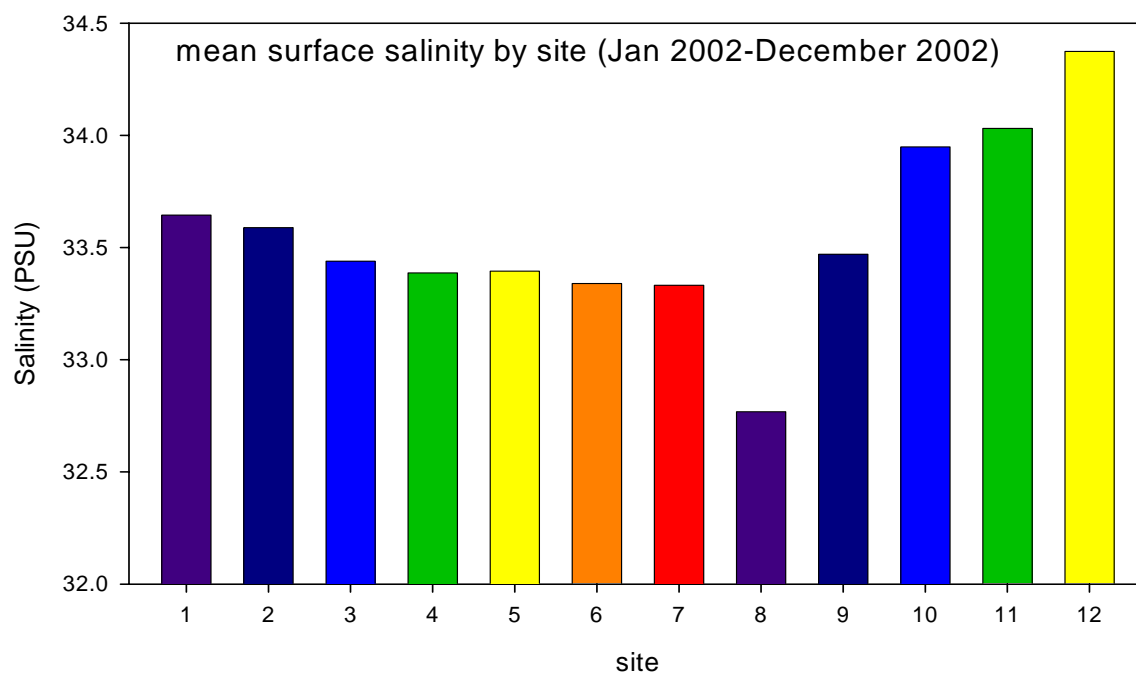
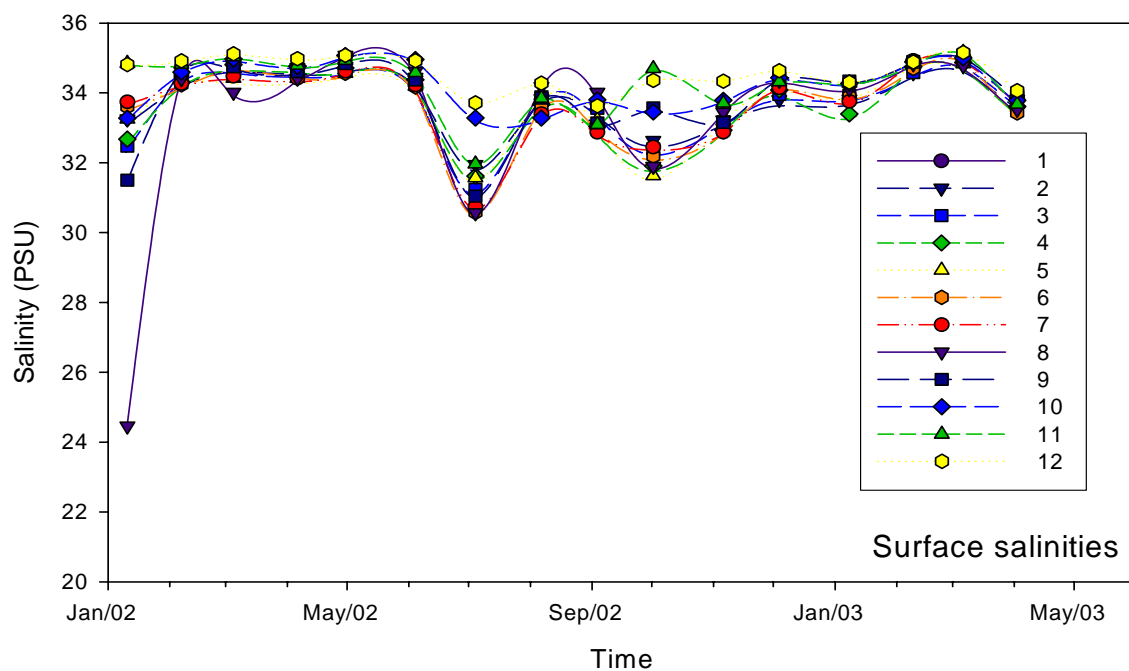


Figure 34. Salinities at all sites (upper panel) and mean annual salinity at each site (lower panel).

### *Dissolved oxygen*

Dissolved oxygen was routinely measured by a Clark polarographic membrane type sensor mounted on the CTD. During a typical vertical profile hundreds of measurements were made by the sensor. For the analysis presented here two “typical” single point measurements were extracted from each vertical profile, one from the top meter and one from the bottom meter of the cast. This provided 384 measurements from 12 sites over 16 months for analysis. Some bottle samples were also collected to assess the accuracy of the sensor data. In comparison with titrated bottle samples the sensor underestimated reality (paired t-test,  $P < 0.001$ ) on average by 6.6%. The magnitude of the error was not, however, randomly distributed but more severe at higher DO concentrations (Fig. 35). Overall the sensor estimated DO concentrations accounted for only 45% of the variation determined from titrated samples ( $r^2$  in Fig. 35 was 0.45). Given the relatively small range of DO concentrations encountered in this study, however, this error is unlikely to bias conclusions regarding environmental health.

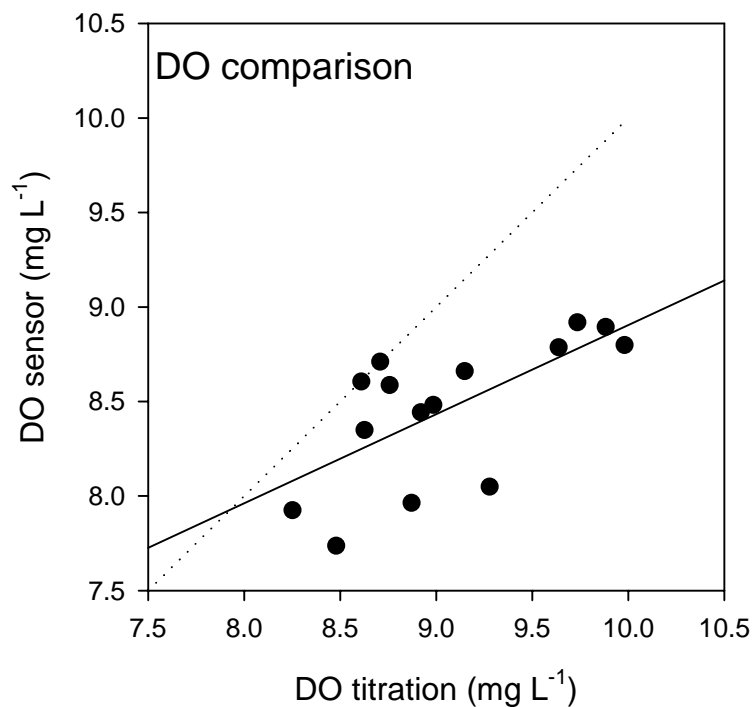


Fig. 35. A comparison of dissolved oxygen measurements made by two different techniques. A linear regression is shown (solid line) as well as the 1:1 line (dotted).

In terms of sensor measured dissolved oxygen concentrations there was a significant impact of site and date (Table 5, Fig. 35). Using general linear model with depth, date and site followed by Bonferroni correct t-tests with site twelve as a control, sites 1, 2, 3 and 4 were significantly lower in dissolved oxygen concentrations. This analysis was rerun with DO converted to percent saturation (using the formula in Benson and Krause 1984) to account for differences associated with temperature with the same results;

sites 1, 2, 3 & 4 > 12. Using percent saturation values rather than concentrations ANOVA also indicated that the surface was statistically ( $F= 20.2$ ,  $P< 0.001$ ) more saturated than the bottom samples. Although these differences between sites and depths were detected in the DO (sensor data) they were very small. Looking for at a “worse case” scenario by concentrating on the summer (December, January and February data) only and data from the bottom at each site the absolute range in average DO concentrations across all twelve sites was 7.85 to 8.23 mg L<sup>-1</sup>. Most of this variation was due to temperature as the saturation only ranged from 99.78 to 99.80%.

Although these statistical differences exist in the DO data, of the > 380 observations extracted from the data set for analysis, the minimum DO value was 99.7% saturation. Clearly none of the sites sampled were showing signs of significant oxygen depletion. The greatest variation detected in the sensor data was the influence of temperature with greater [DO] observed during winter. Concentrations also stayed relatively high through spring (Fig 36), possibly as a result of photosynthesis associated with the Spring phytoplankton bloom.

**Table 5. Statistical analysis of the dissolved oxygen concentrations in D’Entrecasteaux Channel.**

Source of Variation	DF	SS	MS	F	P
Depth	1	0.005	0.005	1.07	0.303
Site	11	0.549	0.050	10.5	<0.001
Date	15	64.24	4.28	902.1	<0.001
Residual	165	0.78	0.0048		
Total	383	71.69	0.187		

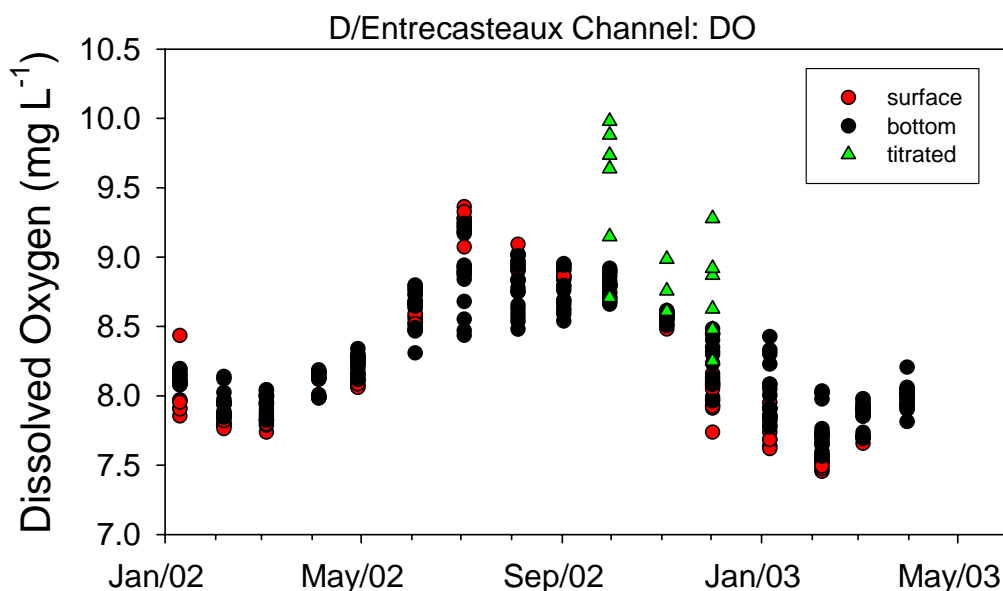


Figure 36. Dissolved oxygen concentrations as determined by Seabird SBE 19+ CTD oxygen sensor for the top and bottom at each of the twelve sites plus several chemically titrated DO measurements made from bottle collected samples at the same time at three sites.

### Comparisons between ecosystems

Phytoplankton community composition was broadly similar between the Huon and D'Entrecasteaux Channel in terms of algal class and seasonal timing of blooms (Fig. 37). In general microflagellates were numerically dominant in both ecosystems. There were spring diatom blooms in both ecosystems. The data suggest that in the period from 1996-1998 (Huon Estuary Study) to 2002-2003 the main genus in the spring bloom changed from *Chaetoceros* spp. to *Skeletonema* spp. In both water bodies there were autumn diatom blooms of *Pseudo-nitzschia*. The major difference was the presence of summer or autumn dinoflagellate blooms, including more *Ceratium* but especially more *Gymnodinium catenatum* in the Huon Estuary.

In comparison with nearby ecosystems the D'Entrecasteaux Channel had a mean chlorophyll *a* concentration of  $0.83 \mu\text{g L}^{-1}$ , lower than that observed in the Huon Estuary Study ( $1.32 \mu\text{g l}^{-1}$ ; CSIRO Huon Estuary Study Team, 2000) and about 30% of the mean value observed in the lower River Derwent ( $2.63 \mu\text{g L}^{-1}$ : data for 14 sites in the lower Derwent over the period from 1996 to 2004 were kindly supplied by the Tasmanian Department of Primary Industries, Water and Environment (DPIWE)).

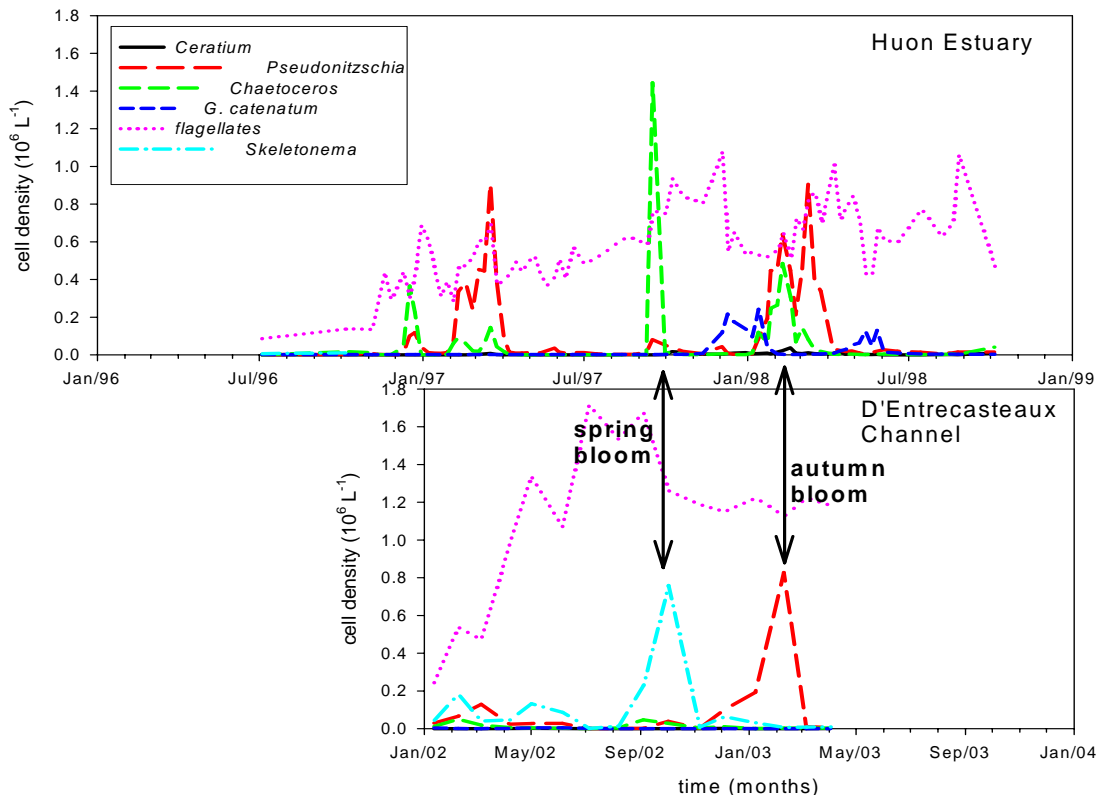


Figure 37. A comparison of dominant phytoplankton genera and their temporal abundance in the Huon Estuary (1996-1998 data from CSIRO Huon Estuary Study Team, 2000) and D'Entrecasteaux Channel 2002-2003. Note panels are aligned by season not year.

The frequency of blooms is often cited as a measure of ecosystem health even though blooms are a poorly defined phenomenon (Smayda 1997). For the purpose of this report we will use the definition that a bloom is a sudden rise in phytoplankton density to three times the median concentration. Assessed on a site by site basis, using chlorophyll *a* as the measure of phytoplankton, across the 12 sites and 16 monthly measurements at the surface (n=192) 4 blooms were observed, one each at site 2, 3, 6 & 7. Alternatively over all sites and depths (all chlorophyll *a* for the Channel; n=504) some 18 observations (3.6%) were greater than three times the overall median value of 0.695  $\mu\text{g L}^{-1}$ . Although an increase in blooms is often cited as a manifestation of eutrophication there few statistical analyses available for a meaning comparison across ecosystems.

Of the southeast Tasmanian ecosystems where we have sufficient data the mean concentrations of chlorophyll rank these three ecosystems: lower Derwent\* > Huon > Channel (i. e. Channel is lowest, = more oligotrophic and least eutrophic). The frequency of bloom events provided a different ranking with the Huon experiencing many more observations of high chlorophyll *a* concentrations (Fig. 38) and observations of much greater peak concentrations. The relative frequencies of blooms was Huon > Derwent >> Channel. There was a significant difference between these ecosystems ( $\chi^2 = 31.3$  with 2 degrees of freedom,  $P < 0.001$ ) in terms of bloom frequency. Together the relatively low mean chlorophyll *a* concentration and high bloom frequency indicates that the Huon Estuary has a low baseline of chlorophyll *a* biomass and yet is beset with more algal blooms than would be expected. By comparison the D'Entrecasteaux Channel had fewer blooms with only 3.6% of all observations exceeding three times the median chlorophyll *a* concentration.

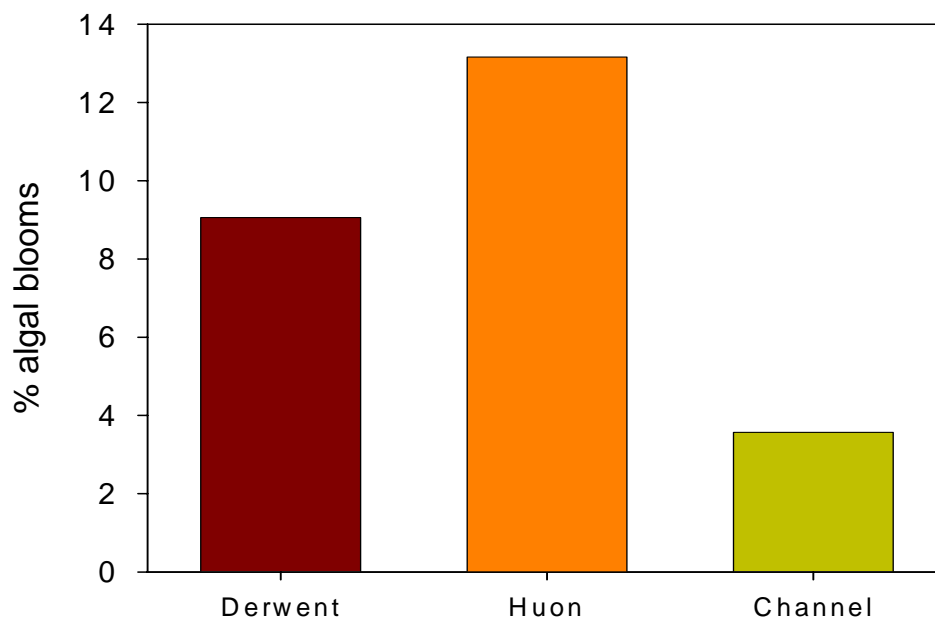


Figure 38. The percentage of algal blooms observed in the lower River Derwent, the D'Entrecasteaux Channel or the Huon River.

*Secchi disk data*

A Secchi disk was lowered at each site and sampling period. The maximum depth of visibility was recorded. Statistically significant differences were found for site and date (Table 6). Secchi disk depths were lowest in July 2002 with a mean depth of only 3.9 meters (Fig. 39). The greatest Secchi depths (clearest water) were observed in February 2003 especially at sites 10, 11 and 12. There was a large difference between Jan 2002 and January 2003 that was probably related to the order of magnitude more Huon River discharge in the 10 days preceding sampling in Jan 2002 relative to Jan 2003 ( $1.8 \times 10^9 \text{ m}^3$  versus  $1.9 \times 10^8 \text{ m}^3$ ). Mean Secchi disk depths for individual sites suggest that sites at the south end of D'Entrecasteaux Channel had more transparent water than those at the northern end of the Channel. Water clarity as measured by Secchi disk was significantly greater at Site 12 relative to sites 1 to 9 (Table 6, 2 way ANOVA followed by Bonferroni *t*-tests). Mean Secchi disk depths for shallow sites (sites 6, 7, and 9) are not reliable indicators of water clarity as the Secchi disk was occasionally visible when resting on the bottom.

**Table 6. Two way ANOVA (without interactions) for Secchi disk depth as a function of date and site.**

Source of Variation	DF	SS	MS	F	P
Date	15	866.9	57.8	17.7	<0.001
Site	11	315.1	28.6	8.79	<0.001
Residual	161	524.7	3.2		
Total	187	1699.1	9.1		

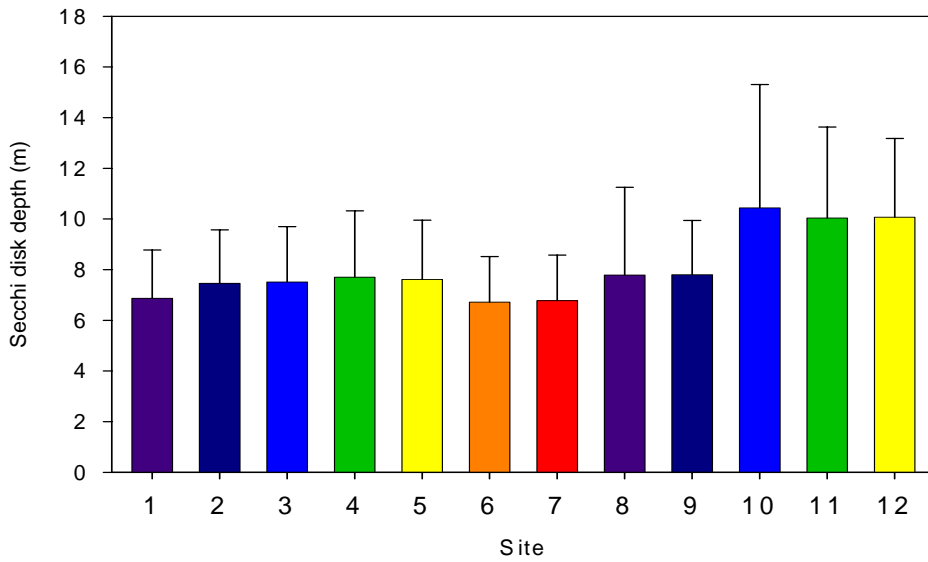
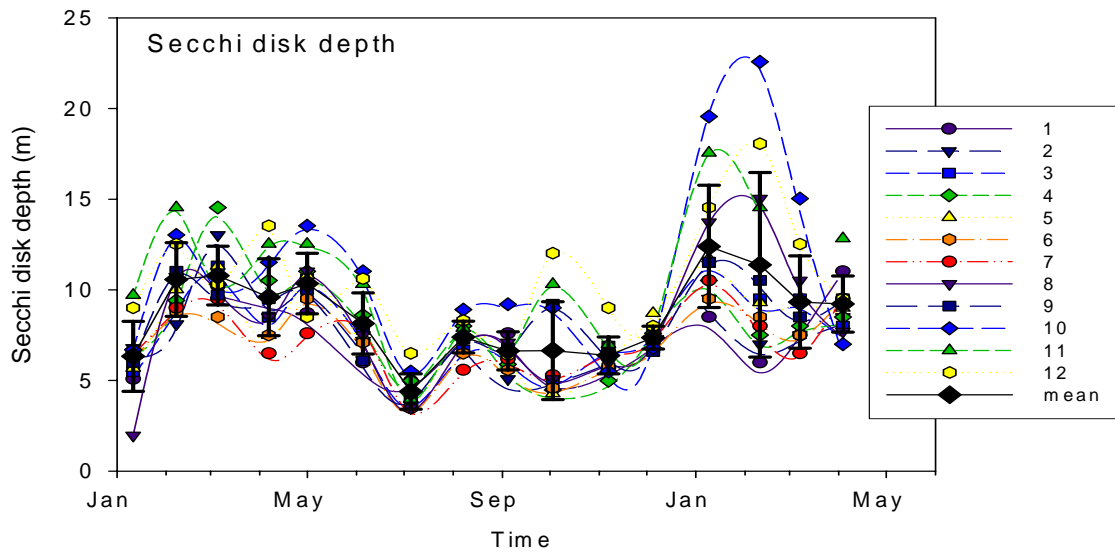


Figure 39. Secchi disk depths measured at each sampling date (upper panel) or averaged over time at each site (lower panel). Error bars are standard deviations.

*Summarizing the observations from the D'Entrecasteaux Channel.*

All of the D'Entrecasteaux Channel sites had mean annual chlorophyll *a* concentrations less than 2 µg L<sup>-1</sup> the internationally accepted criterion for oligotrophic waters. Some sites, however, were better than others. The site judged to be in the best environmental health was Little Taylors Bay with a relatively short flushing time, high dissolved oxygen, low ammonium and low chlorophyll *a* (Fig 40, Table 7) and we assigned it a grade of A+. In an effort to succinctly express these differences a summary statistic was developed consisting of mean annual chlorophyll *a* concentration, mean ammonium concentration and mean dissolved oxygen concentration. These site characteristics were weighted to achieve approximately equal emphasis using a very simple formula:

$$\text{score} = [\text{DO}]/10 + \text{chl}a + [\text{NH}_4^+]$$

Where [DO] is the concentration of dissolved oxygen in mg L<sup>-1</sup>, chl*a* = the concentration of chlorophyll *a* in mg L<sup>-1</sup> and [NH<sub>4</sub><sup>+</sup>] is the concentration of ammonium in µM and all measurements are annual means. The summary statistic was used to estimate the relative environmental health of all the sites but adjusted for flushing times for the various embayments (Table 7). A comparison of more water bodies should be undertaken to determine whether such a simple statistic can be used to rank the environmental health of water bodies around Tasmania. Regionally based intercomparisons are likely to be valid although it is unclear whether all State waters can be assessed using this simple approach, in particular, naturally anoxic water bodies may be problematic.

**Table 7. Environmental characteristics at sites 1-12 in the D'Entrecasteaux Channel sampled in 2002 and 2003. See Fig. 2.2.2 for approximate site locations or Technical Report (Thompson and Bonham 2004) for exact locations.**

Site	Description	DO mg L <sup>-1</sup>	NH <sub>4</sub> μM	Chla (g L <sup>-1</sup> )	score	grade	flushing time (Days)	comment
1	Mid channel off Dennes Pt	8.216	0.193	1.094	2.50	B+		High [chla] suggests frontal zone in this passage Moderate NH <sub>4</sub> , relatively low DO, greater chla suggest this Bay is under stress, probably healthy due to short flushing time.
2	NW Bay	8.216	0.255	1.005	2.48	C+	5.0	
3	Mid channel off Oyster Cove Pt	8.232	0.266	0.811	2.29	B		Relatively high NH <sub>4</sub> is a concern Moderate NH <sub>4</sub> , moderate chla and relatively long flushing time make this Bay one to be watched
4	Barnes Bay	8.229	0.253	0.882	2.35	B-	10.3	
5	Mid channel south of Green Is	8.292	0.135	0.720	2.06	B+		No problems detected Good DO, low NH <sub>4</sub> , low chla and short flushing time
6	Great Bay	8.316	0.120	0.786	2.11	A-	7.4	
7	Isthmus Bay	8.299	0.093	0.808	2.11	B+	9.5	Good, but longer flushing time than site 6
8	Mid channel west of Satellite Is	8.314	0.199	0.727	2.13	B+		No problems detected
9	Little Taylors Bay	8.308	0.140	0.686	2.03	A+	6.3	Best overall site in survey
10	Mid channel, half way from Partridge Is and Ventenat Pt	8.291	0.253	0.602	2.06	B		Moderate NH <sub>4</sub> 1 of 16 [NH <sub>4</sub> ] was very high, potential concern in this Bay
11	Great Taylors Bay	8.298	0.318	0.664	2.19	B+	6.9	
12	Mid channel off Browns Point	8.291	0.290	0.608	2.10	B		Moderate NH <sub>4</sub>

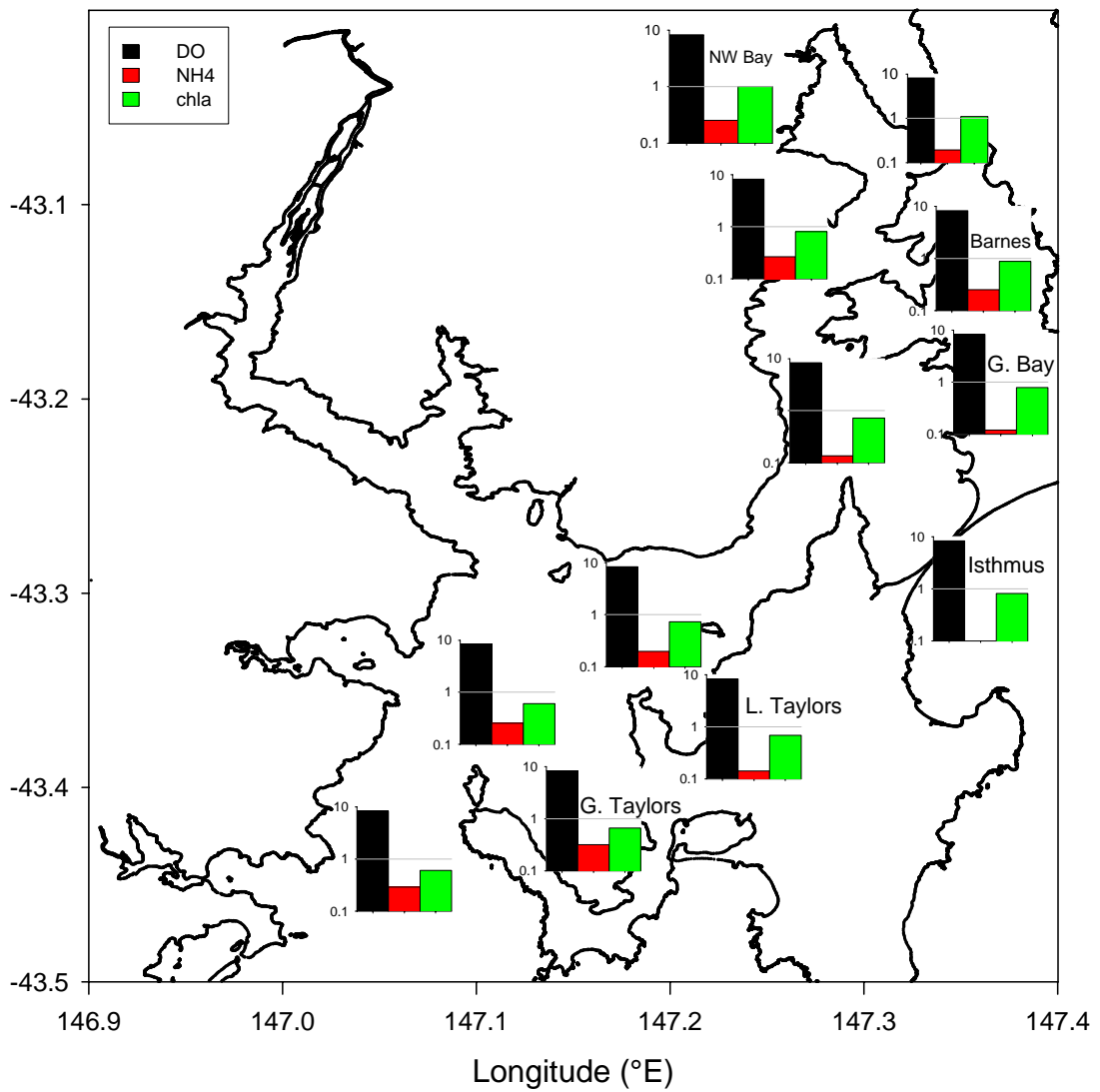


Figure 40. Map showing mean concentrations of dissolved oxygen, chlorophyll *a* and NH<sub>4</sub><sup>+</sup> at twelve locations in D'Entrecasteaux Channel during 2002 and 2003. Note the logarithmic scale on the inserted bar graphs.

## *Discussion*

The baseline data set collected during 2002 and part of 2003 for D'Entrecasteaux Channel demonstrated significant temporal and spatial variability in the key water quality parameters: dissolved oxygen (DO), chlorophyll *a*, and nutrient concentrations. When under stress from eutrophication these parameters are considered the fundamental criteria used to assess environmental health for water bodies that range from lakes to oceans. While every water body will have a concentration of DO, chlorophyll *a*, and nutrients that represents a pristine condition the addition of labile carbon as a result of anthropogenic activities has seen the status of many water bodies deteriorate noticeably over the last 50 years. In lakes and rivers this deterioration has been linked with increased supply of phosphorous (Vollenweider 1981) and in coastal water bodies with increased supply of nitrogen (Ryther and Dunstan 1971). The normal course of events is increased nutrient loading and increased primary production resulting in more reduced carbon to be oxidized (Nixon 1981). Alternatively some ecosystems have deteriorated simply as a result of increased inputs of reduced carbon. The susceptibility of any particular water body to the impacts of nutrient or carbon loading are complex with the net result depending upon many factors such as depth, exchange and trophic transfer.

The range and complexity of possible responses to nutrient loading are substantial. Integrating the ecological responses of a water body to nutrient inputs over appropriate time and space scales to predict the consequences is a daunting task that can be tackled in a rigorous manner by a sophisticated hydrodynamically coupled biogeochemical model. It is also possible that natural processes that integrate biological responses can be used to assess how an ecosystem is coping with eutrophication. In many ecosystems the oversupply of reduced carbon via point and diffuse sources will result in an accumulation of labile carbon in the deeper regions of the water body. The decomposition (oxidation) of this carbon will consume oxygen and the oxygen concentration becomes both a measure of the overall stress and an indicator of environmental health.

There is no debate that hypoxia and anoxia are among the most serious of primary responses to eutrophication. Either can result in an ecosystem that will no longer support the same range of biota as were previously present. Both are associated with many, many well documented cases of eutrophication in lakes, rivers, coastal and open ocean ecosystems. Furthermore there is evidence that normal nutrient cycling is impaired in ecosystems with low DO and if these are moderately shallow the nutrients may be cycled repeatedly through primary production rather than buried or exported. Repeated cycling through primary production will increase reduced carbon loading and exacerbate DO problems. There are, however, some ecosystems where DO is not suitable as a measure of eutrophication. For example, ecosystems where DO is not suitable as a measure of eutrophication include those that are naturally anoxic such as fjords or estuaries with shallow sills or other factors that result in slow, or episodic deep water exchange. Obviously in an ecosystem with a complete lack of DO the ecological impacts associated with increasing carbon loads are less significant. Other ecosystems with more capacity to cope with high carbon loads include those ecosystems:

1. with very rapid exchange
2. that are very deep

Nutrient concentrations are a direct measure of eutrophication. The practical difficulty lies in their use as a monitoring tool for compliance especially when the sources are diffuse and the anthropogenic inputs are a small fraction of the natural inputs. Nutrient inputs exist primarily as dissolved inorganic, dissolved organic or particulate organic forms with biological transformations converting one form to another and back again. The natural inputs of nutrients into coastal water bodies often has significant temporal variability (typically a seasonal dynamic in temperate water bodies) which further complicates the use of nutrient concentrations as a tool to assess eutrophication status. In many temperate zone coastal water bodies dissolved N is primarily input as nitrate during winter and some variable fraction of that is recycled to appear as  $\text{NH}_4$  in summer. This tendency for recycled nitrogen to appear as  $\text{NH}_4$  in summer was evident in the Channel data where relatively high concentrations of  $\text{NH}_4$  appeared in the bottom waters in December 2002 and in the surface waters in January 2003. Typically in oligotrophic, temperate water bodies the summer is characterized by low dissolved nutrient concentrations in the euphotic zone and low chlorophyll *a* biomass. Nutrient inputs during summer are rapidly taken up and converted into organic compounds. If a sufficient quantity of biomass results and ends up on the bottom it is likely to contribute significantly to the biological oxygen demand increasing the likelihood of low dissolved oxygen concentrations. It is believed that low DO favours the release of more nutrients from the sediments potentially making the situation worse. In the case of D'Entrecasteaux Channel the source of the  $\text{NH}_4$  during summer is unknown and should be investigated.

Chlorophyll *a* concentrations in D'Entrecasteaux Channel were low relative to many other coastal ecosystems. Sites in the northern half of the Channel tended to have an earlier and larger spring bloom than those in the southern half. The most probable explanation for this is the more rapid development of a suitable mixed layer depth and evidence to support this hypothesis can be found in the hydrodynamic and ecological modelling. Excluding the nanoflagellates, the spring bloom was numerically dominated by diatoms, a characteristic of spring blooms in coastal ecosystems worldwide. The dominant diatoms *Skeletonema* and *Chaetoceros* species are ubiquitous in the temperate coastal zone especially during spring blooms. *Pseudo-nitzschia* is also a widespread diatom. Only a small number of blooms (defined as 3x the median chlorophyll *a* concentration) occurred in D'Entrecasteaux Channel and none of them were dominated by toxic species and none of them occurred during summer.

For phytoplankton and for nutrients there is a strong tendency by some ecologists to expect the manifestations of eutrophication during summer. This is true for many temperate lakes where elevated chlorophyll *a* or nutrients in the euphotic zone during summer are recognized symptoms of eutrophication. To some extent the same applies to estuaries although a greater range of nutrient sources and sinks are typically possible. There was no evidence in the Channel data of a problem with summer phytoplankton blooms. During summer the highest chlorophyll *a* concentrations were found off Dennes Point and were largely composed of diatoms. An alternative conceptual model of eutrophication symptoms in the temperate zone is that the spring and autumn blooms will increase in magnitude and persist longer. Where this occurs it is often seen in response to increasing catchment loads (not assessed as part of this study). Other sources of nitrogen for the Channel include the nitrate supplied from deep offshore

waters and advected into D'Entrecasteaux Channel. Insufficient data are available to assess interannual variability in nitrate supply from this source.

Many of the phytoplankton genera that were reported to be causing problems to aquaculture in 2003-2004, such as *Gymnodinium*, *Karenia*, *Heterosigma*, *Noctiluca* were observed in the Channel, but never at high densities. From the research presented herein it does not seem likely that any of the sites surveyed have sufficient nutrients available to produce a bloom of these problem species. Cell densities high enough to be considered a problem (e.g. a harmful algal bloom) seem likely to occur only through advection and other physical processes that can result in concentration. Of these species *Noctiluca* is the most susceptible to concentration by physical processes because of its tendency to accumulate near the surface towards the end of a bloom.

*Noctiluca* is heterotrophic and as a herbivore it can only reach bloom densities following an autotrophic bloom of sufficient density and persistence to allow for *Noctiluca* growth. Outside the sampling reported here, in the Huon estuary during autumn 2004, *Noctiluca* was observed at relatively high densities during a diatom bloom (largely *Skeletonema*). Individual *Noctiluca* cells were observed to contain *Gymnodinium catenatum*. Although it has been suggested that *Noctiluca* will not grow below 18°C (Dela Cruz 2002) clearly this is not true in Tasmania where it reached considerable densities in waters that are persistently colder than 18°C. It can be reasonably assumed that limitations to *Noctiluca*'s biomass are determined by the balance between growth and death. Based on current evidence mortality seems low and the supply of prey relatively large. What fraction of the *Noctiluca* problem results from increased phytoplankton abundance associated with eutrophication is not known but that fraction cannot be reduced without control on nutrient inputs leading to a reduction in algal blooms. If, however, the source of *Noctiluca* is offshore with the nutrients supplied via upwelling then localized nutrient management will have little effect. Some research designed to address this question should be considered.

The phytoplankton composition of the Channel is intriguing because of the tendency for the dominant photosynthetic dinoflagellates to be typical offshore species. *Gymnodinium*, *Ceratium*, *Dinophysis*, and *Karenia* are not considered to be near shore species but to be predominately found in deeper coastal or offshore water bodies (Smayda 2002). In other parts of the world the prevailing hypothesis for near shore blooms of these species is that they are advected into the region and then bloom opportunistically or are physically concentrated (or both). The generally accepted hypothesis is that flagellates can dominate over diatoms in environments where swimming allows access to light from the surface and nutrients from depth. In laboratory culture some dinoflagellates fail to grow under moderate or high mixing conditions and this combined with observations of blooms under conditions of relatively low wind stress have led to considerable speculation about the stability of the water column as a contributing factor. It is also well known that most of these dinoflagellates are relatively slow growing so that to achieve community dominance the conditions that favour their growth must persist for a relatively long time. Some targeted research on a few problem species and their particular ecophysiology should be considered. Research into whether the conditions that allow these problem species to grow and achieve bloom densities occurs in specific localities should be considered. The alternative of offshore population development followed by advection into the SE Tasmanian region and localized blooms cannot be ruled out.

All sites surveyed in D'Entrecasteaux Channel and adjacent bays had relatively low concentrations of  $\text{NH}_4$  and chlorophyll *a* and relative high concentrations of DO. These parameters are well accepted indicators of productivity or eutrophication so that this baseline assessment of D'Entrecasteaux Channel and adjacent bays indicates an ecosystem that is fundamentally oligotrophic. Naturally oligotrophic ecosystems are highly susceptible to ecological change induced by increased nutrient loading. Some sites are likely to naturally experience more nutrient loading than others especially those with relatively high terrestrial inputs of nutrients or carbon such as Northwest Bay. Most Bays were observed to be similar in water quality to the adjacent site in the middle of the Channel suggesting relatively little local nutrient input or rapid water exchange or both. Risk factors that are likely to exacerbate a deterioration of water quality for a given nutrient load include stratification intensity and duration plus exchange rate or flushing time. Stratification intensity or duration were not assessed as part of this study and exchange rates were calculated as part of the overall projects hydrodynamic modelling. There were several sites in D'Entrecasteaux Channel that showed elevated (relative to other sites) concentrations of chlorophyll *a* and/or  $\text{NH}_4$ . These sites should be viewed as showing early warning signs of potential problems associated with relatively high nutrient loading. Those sites, such as NW and Barnes Bay, already showing relatively high chlorophyll *a*,  $\text{NH}_4$  and a low exchange rate are particularly vulnerable to additional nutrient loading.

This technical report has been amended from Crawford et al. 2004. Development of broad scale environmental monitoring and baseline surveys in relation to sustainable salmon aquaculture in the D'Entrecasteaux Channel region. Aquafin CRC Project 4.4.

## References

- Armstrong, F.A. J. (1951). The determination of silicate in sea water. *Journal of the Marine Biological Association of the United Kingdom* 30, 149-60.
- Birch, P. B., Gordon, D. M., and McComb, A. J. (1981). Nitrogen and Phosphorus Nutrition of *Cladophora* in the Peel-Harvey Estuarine System, Western Australia. *Botanica Marina* 24, 381-7.
- Benson, B.B. and D. Krause Jr. (1984). The concentration and isotopic fractionation of oxygen dissolved in freshwater and seawater in equilibrium with the atmosphere. *Limnology and Oceanography* 29:620-632.
- Bricker, S. B., Clement, C. G., Pirhalla, D. E., Orlando, S. P., and Farrow, D. R. G. (1999). National estuarine eutrophication assessment: Effects of nutrient enrichment in the Nation's estuaries. National Oceanic and Atmospheric Administration, National Ocean Service, Special Projects Office and the National Centers for Coastal Ocean Science. (Silver Spring: MD, USA).
- Clark, R. B. (1989). 'Marine Pollution'. (Oxford: New York).
- Cloern, J. E. (2001). Our evolving conceptual model of the coastal eutrophication problem. *Marine Ecology Progress Series* 210, 223-53.
- Cowley, R. (1999). Hydrochemistry Operations Manual, CSIRO Marine Research. CSIRO Marine Laboratories Report 236.
- Dela Cruz, Jocelyn. (2002). The biology of *Noctiluca scintillans* – a eutrophication indicator? UNSW PhD Thesis.
- Floeder, S., and Sommer, U. (1999). Diversity in planktonic communities: An experimental test of the intermediate disturbance hypothesis. *Limnology and Oceanography* 44, 1114-9.
- Fong, P., Zedler, J. B., and Donohoe R. M. (1993). Nitrogen vs. phosphorus limitation of algal biomass in shallow coastal lagoons. *Limnology and Oceanography* 38, 906-23.
- Gray, J. S. (1992). Eutrophication in the sea. In 'Marine Eutrophication and Population Dynamics' (Eds. Columbo, G., Ferrari, I., Ceccherelli, V. U., and Rossi, R.) pp 3-15. (25<sup>th</sup> European Marine Biology Symposium: Olsen and Olsen, Fredensborg, Denmark.
- Hambright, K. D., and Zohary, T. (2000). Phytoplankton species diversity control through competitive exclusion and physical disturbances. *Limnology and Oceanography* 45:110-22.
- Jones, R.D. (1991). An improved fluorescence method for the determination of nanomolar concentrations of ammonium in natural waters. *Limnology and Oceanography* 36:814-819.
- Kerouel, R. and A. Aminot. (1997). Fluorometric determination of ammonia in sea and estuarine waters by direct segmented flow analysis. *Marine Chemistry* 57:265-275.
- Laws, E. A. (1993). 'Aquatic Pollution: An introductory text.' (John Wiley and Sons, New York).
- Lindenschmidt, K. E., and Chorus, I. (1998). The effect of water column mixing on phytoplankton succession, diversity and similarity. *Journal of Plankton Research* 20, 1927-51.
- Loreau, M., Naeem, S., Inchausti, P., Bengtsson, J., Grime, J. P., Hector, A., Hooper, D. U., Huston, M. A., Raffaelli, D., Schmid, B., Tilman, D., and Wardle, D. A.

- (2001). Biodiversity and ecosystem functioning: Current knowledge and future challenges. *Science* (Washington.) 294, 804-8.
- Mallin, M. A., Paerl, H. W., Rudek, J., and Bates, P. W. (1993). Regulation of estuarine primary production by watershed rainfall and river flow. *Marine Ecology Progress Series* 93, 199-200.
- Murphy J., and Riley, J. P. (1962). A modified single-solution for the determination of phosphate in natural waters. *Analytica chimica acta* 27, 31-6.
- Nixon, S. (1990). Marine eutrophication: a growing international problem. *Ambio* 19, 101.
- Parsons, T. R., and Takahashi, M. (1973). 'Biological Oceanographic Processes.' (Pergamon: New York).
- Parslow, J. P. (2000). Nutrient budgets and water-quality models. Pages 231-262 in, Huon Estuary Study – environmental research for integrated catchment management and aquaculture. CSIRO Division of Marine Research. 285pp.
- Philippart, C. J. M., and Cadee, G. C. (2000). Was total primary production in the western Wadden Sea stimulated by nitrogen loading? *Helgoland Marine Research* 54, 55-62.
- Smayda, T. (2002). Adaptive ecology, growth strategies and the global bloom expansion of dinoflagellates. *J. Oceanography* 58:281-294.
- Smayda, T. J. (1997). What is a bloom?: A commentary. *Limnology and Oceanography*, 42, 1132-1136.
- Smayda, T. J. (1989). Primary production and the global epidemic of phytoplankton blooms in the sea: A linkage? In, 'Novel Phytoplankton Blooms: Causes and Impacts of recurrent brown tides and other unusual blooms' (Eds. Cosper, E. M., V. M. Bricelj and E. J. Carpenter.) pp. 449-83. (Coastal and Estuarine Studies 35: Springer Verlag, Berlin).
- Sommer, U. (1995). An experimental test of the intermediate disturbance hypothesis using cultures of marine phytoplankton. *Limnology and Oceanography* 40, 1271-7.
- Vollenweider, R. A (1981). Eutrophication - a global problem. *Water Quality Bulletin*. 6, 59-62.
- Wood E. D., Armstrong, F. A. J., and Richards, F. A. (1967). Determination of nitrate in sea water by cadmium-copper reduction to nitrite. *Journal of the Marine Biology Association of the United Kingdom* 47, 23-31.

# Status Report



## Sediment Biogeochemistry of the Huon Estuary

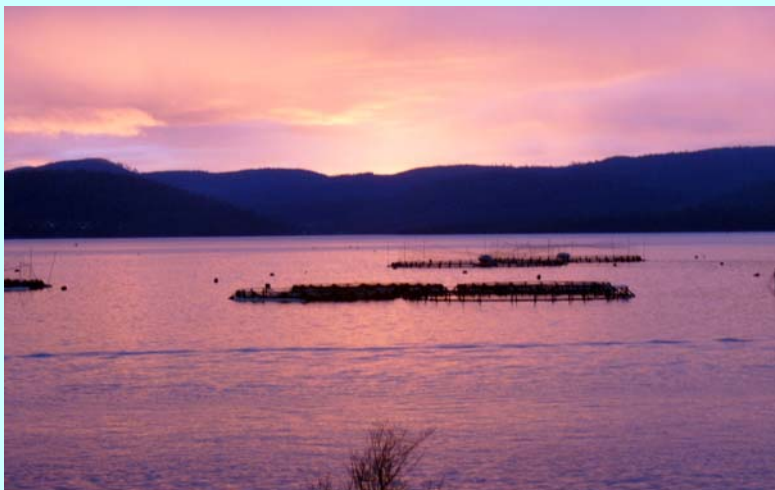
Dean Thomson<sup>1</sup>, John Volkman<sup>2</sup>, Chris Burke<sup>1</sup> and John Purser<sup>1</sup>

<sup>1</sup> Aquafin CRC and University of Tasmania

<sup>2</sup> Aquafin CRC and CSIRO Marine Research, Tasmania

*July 2005*

*Aquafin CRC Project 4.2  
(FRDC Project No. 2001/097)*



© Copyright Aquafin Cooperative Research Centre, Fisheries Research and Development Corporation, Commonwealth Scientific and Industrial Research Organisation

**This work is copyright. Except as permitted under the Copyright Act 1968 (Cth), no part of this publication may be reproduced by any process, electronic or otherwise, without the specific written permission of the copyright owners. Neither may information be stored electronically in any form whatsoever without such permission.**

**Every attempt has been made to provide accurate information in this document. However, no liability attaches to Aquafin CRC, its participant organisations or any other organisation or individual concerned with the supply of information or preparation of this document for any consequences of using the information contained in the document.**

*Published by CSIRO Marine and Atmospheric Research*



## Sediment Biogeochemistry of the Huon Estuary

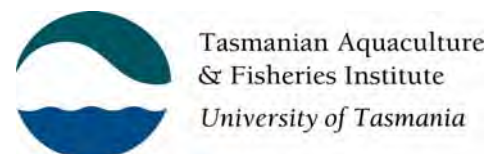
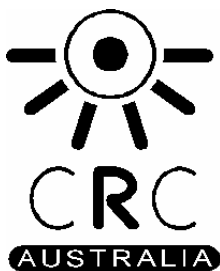
*Dean Thomson<sup>1</sup>, John Volkman<sup>2</sup>, Chris Burke<sup>1</sup> and John Purser<sup>1</sup>*

July 2005

Aquafin CRC Project 4.2  
(FRDC Project No. 2001/097)



**Australian Government**  
**Fisheries Research and  
Development Corporation**



## Introduction

Sediments play a vital role in the ecological functioning of an estuary by retaining much of the organic matter and minerals supplied naturally by rivers, catchment run-off and inputs from the overlying water column. Concentrations of metals and organic compounds are often several orders of magnitude higher in the sediments than in the overlying water column, thus simplifying their analysis. Surface sediments provide an integrated picture of inputs over relatively short time frames of a few years. Hence, they can give an indication of local inputs in the context of an estuary-wide baseline and provide a better view of longer term average inputs, in contrast with the snapshots revealed by water column studies. Sediment cores provide a record of estuarine conditions over years to decades and longer depending on the sedimentation rate. Gradients of nutrients and oxygen in porewaters with depth can provide estimates of the fluxes of solutes into or out of the sediment.

The organic matter in sediments is remineralised by the microbial and faunal populations present thus liberating nutrients and consuming oxygen. Sediment organic matter shows varying degrees of resistance to degradation. It is common practice to define a refractory component (i.e. that part of the organic matter that is not degradable over a defined time frame usually months to years) and a labile component that is degraded over hours to days.

The quality of organic matter (as roughly reflected in the C:N ratio) is a prime determinant of the rates and recycling pathways of carbon and nitrogen (Herbert 1999) in sediments. Where organic matter undergoing decomposition has a high C:N ratio (such as that from terrestrial plant sources), much of the nitrogen remineralised may be reassimilated into microbial biomass (Schlesinger 1997). Organic matter that is more labile and has a lower C:N ratio (such as that derived from algal material) will stimulate rapid remineralisation rates and a release of nitrogen from the sediment (Hansen and Blackburn 1992). Identifying these sources of organic matter in sediments provides an insight as to how the organic matter is likely to be processed. A C:N ratio close to that of the Redfield ratio (6.7) is indicative of organic matter derived from marine microalgae while organic matter derived from terrestrial sources can have a C:N ratio of 20 or more (Bordovskiy 1965). This approach is, however, very approximate as degradation may significantly alter these ratios (Thornton and McManus 1994).

Ratios of  $^{12}\text{C}/^{13}\text{C}$  isotopes provide a good estimate of the relative contribution of terrestrial and marine sources to sedimentary OM (Fry and Sherr, 1984). Terrestrial OM (largely of higher plant origin) will generally have a  $\delta^{13}\text{C}$  value of -26 to -30‰ and organic matter with a marine origin will generally have a  $\delta^{13}\text{C}$  of -19‰ to -23‰ depending on the particular organisms present (Heip et al., 1995). The relative proportion of marine and terrestrial carbon in a sample can then be estimated by linear additions of these end-members. While this approach is relatively simple and gives an integrated estimate of sources for the total carbon in the sample, it will only provide useful information when there are two well-defined end-members. Furthermore, this technique gives little information about the type of marine or terrestrial organic matter in question.

Various proxies have been used to estimate the sources of organic matter in sediments and from this inferences about the amount of labile organic matter present can be made. For example, biochemicals such as carbohydrates, proteins and lipids are rapidly degraded in sediments and so measures of their abundance provide an estimate of the labile organic matter present (e.g. Pusceddu et al, 1999). Alternatively, lipid and pigment biomarkers can allow the various sources of various sub-fractions of organic matter to be identified. Fatty acids provide a range of useful markers for microalgae, macroalgae, bacteria, seagrasses and terrestrial plants (Volkman et al. 1980, Meziane et al. 1997, Volkman et al. 1998, Kharlamenko et al. 2001). Sterols have also been used to identify sources of organic matter including that derived from faeces, diatoms and terrestrial sources (Volkman 1986, Barrett et al. 1995). Triterpenoid alcohols such as  $\alpha$ - and  $\beta$ -amyrins, lupeol, taraxasterol, betulin etc. are widely used as markers for higher plants (e.g. Volkman et al. 1987, 2000), even though some of these have additional minor sources (Volkman 2005). Hopanoid alcohols are excellent markers for cyanobacteria and other prokaryotes (Summons et al. 1999).

While these methods are useful, they are often time consuming and they still only provide an indirect measure of labile organic matter. Accordingly, we attempted to develop a simple procedure based on the biochemical oxygen demand (BOD) incubation technique (see later) for determining labile organic matter in sediments.

Sediment can also be remobilised by tidal currents or during high energy events such as floods thus changing the benthic characteristics of a particular region. Cycles of resuspension and deposition can lead to enhanced remineralisation as the particle surfaces are repeatedly exposed to oxidising conditions (e.g. Abril et al., 1999).

## Results and Discussion

### Sources of Organic Matter

One of the observations noted in the Huon Estuary Study (Butler et al. 2000) was the high content of organic matter in the sediments from the Huon estuary. From lipid and stable isotope analyses, it was determined that much of it is derived from freshwater inputs of terrestrial sub-alpine moorland and other peaty soils, with additional inputs from autochthonous phytoplankton and localised inputs from salmon fish farms, sewage treatment plants and stormwater drains. Organic matter from these diverse sources has very different compositions and different susceptibilities to biodegradation. Much of the terrestrial material consists of high molecular weight tannin-like material, which seems to be degraded very slowly and thus its remineralisation probably does not contribute greatly to nutrient loads. In contrast, organic nitrogen in sediments over much of the middle and lower estuary is derived from marine sources as indicated by its  $\delta^{15}\text{N}$  signature (Butler et al., 2000). It was presumed that the organic nitrogen was mainly derived from sedimenting microalgae, and thus might be remineralised relatively easily to be returned to bottom waters.

During our studies, we analysed several sediments from the Huon estuary and some from more marine sites at Port Esperance (D'Entrecasteaux Channel) and Tasman Peninsula. It was not within the scope of this project to do a full sediment survey, but

these new data do provide some insights into temporal and spatial differences in this region.

Sites LE, LM and LW correspond to sites A6, A4 and A2 in the HES (Butler et al., 2000), while MW and MM correspond to the H1 and H2 in the HES.

These limited analyses show that organic matter contents in sediments from more exposed marine conditions are much lower than those in the Huon or in silt-dominated sites close to land. Biomarker analyses of sediments from close inshore and offshore of Dover Bay illustrate this very well. The inshore sediments have higher contents of organic matter, but this is mostly of terrestrial origin as shown by the high contents of long-chain alcohols and plant-derived sterols such as sitosterol and stigmasterol. In contrast, the organic matter in the sandy off-shore sediment is dominated by marine sources.

### **Sediment respiration and nutrient fluxes**

Three field trips during 2004, including March, July and November were carried out to measure benthic nutrient fluxes and sites in the Huon Estuary.

The aims of this work were:

- To measure diffusive and total oxygen fluxes at the sediment-water interface
- To compare flux rates in sediments dominated by marine organic carbon with sediments dominated by terrestrial organic carbon
- To elucidate spatial and temporal variability of sediment oxygen profiles within and between cores

Sediment cores were obtained from the mouth of the Huon Estuary (sites LW, LM and LE) and from sediments near Port Huon (only in March; sites MW, MM, and ME). The sites are shown in Fig. 1.

Intact sediment was obtained using a box corer and then sub-cored with either 4.5 cm or 9.7 cm clear polypropylene tubes. The cores then had bungs inserted into both ends and placed into an ice bin for transport to the CSIRO Marine Laboratories. The cores were taken back to the lab within 6 hours of sampling and then placed into a tank and left to equilibrate overnight. The sediment cores were then incubated for 8 - 12 hours. The following solutes were measured over time to obtain flux rates ( $\mu\text{mol m}^{-2}\text{h}^{-1}$ ) between the sediment-water interface:

- Oxygen
- Alkalinity
- pH
- $\Sigma\text{CO}_2$
- Nutrients –  $\text{NH}_3$ ,  $\text{NO}_2^-$ ,  $\text{NO}_3^-$ , Si and  $\text{PO}_4^{3-}$

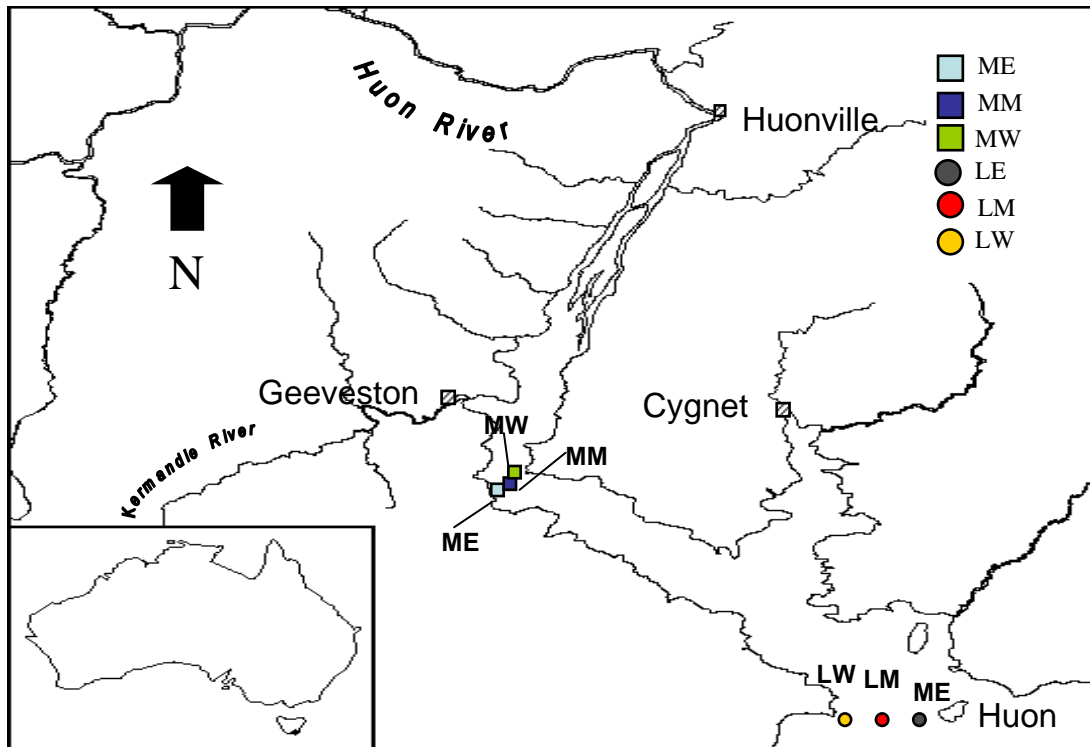


**Figure 1. Locations of sediments collected for benthic flux measurements.**

**Table 1. Physio-chemical conditions of bottom water at sample sites**

	LE	LM	LW	MW	MM	ME
Water Depth(m)	25	37	37	15	19	10
Salinity (‰) - Mar	35	35	35	35	35	35
- July	35	35	35	34	34	28
- Nov	35	35	35	34	34	34
Temp (°C) - Mar	15.5	15.5	15.5	15.7	15.7	15.7
- July	10.3	10.2	10.2	8.1	8.2	8.0
- Nov	13.0	13.0	13.0	12.8	12.8	12.8
Secchi depth (meters) - Mar	nm	nm	nm	nm	nm	nm
- July	1.5	1.5	1.5	<1	<1	<1
- Nov	2.0	2.0	2.0	<1	<1	<1

nm – not measured

**Table 2. Sediment grain size (top 1 cm) at sampling sites during July**

	>500 $\mu\text{m}$	250 – 500 $\mu\text{m}$	125 – 250 $\mu\text{m}$	63 – 125 $\mu\text{m}$	<63 $\mu\text{m}$
LW	1.6	3.8	20.6	42.5	31.5
LM	0.0	9.7	21.1	25.5	43.7
LE	-	-	-	-	-
MW	-	-	-	-	-
MM	-	-	-	-	-
ME	0.6	7.7	14.2	30.5	47.0

The sediment grain sizes at both locations (upper and lower) show that the fine sand (125 – 63  $\mu\text{m}$ ) and silt (<63  $\mu\text{m}$ ) fractions dominant the sediment structure (Table 2). The organic carbon content of the sediments ranged between 4.1 and 7% at the lower sites during March and July and between 11.8 and 13.1% at the upper estuary sites. There was very little variation in organic carbon contents between March and July except at LE where it increased from 4.1 to 5.3%. The stable isotope  $\delta^{13}\text{C}$  ranged between -23.6 and -24.6‰ at the lower estuary and assuming a simple 2-component mixing system (Cook et al. 2004a-c), the terrigenous organic carbon accounted for between 25 – 40% of the total organic carbon. At the upper estuary sites the stable isotope  $\delta^{13}\text{C}$  ranged between -26 and -27.3‰ and the terrigenous organic carbon accounted for between 62 – 82% of the total organic carbon (Table 3).

The organic nitrogen content of the sediments ranged between 0.29 and 0.53% at the lower sites during March and July and between 0.53 and 0.59% at the upper estuary sites. There was very little variation in organic carbon contents between March and July. The stable isotope  $\delta^{15}\text{N}$  ranged between 7.4 and 7.7‰ at the lower estuary and assuming a simple 2-component mixing system (Cook et al. 2004c) the terrigenous organic nitrogen accounted for between 0 – 2% of the total organic nitrogen. At the upper estuary sites the stable isotope  $\delta^{15}\text{N}$  ranged between 4.1 and 5.3 and the terrigenous organic nitrogen accounted for between 37 – 57% of the total organic nitrogen (Table 3)

### **Sediment Oxygen Profiles and Diffusive Fluxes**

Sediment cores (4.5 cm diam) were transferred to a water bath and microelectrodes introduced stepwise (100  $\mu\text{m}$  increments) into the sediment with the aid of a auto-micromanipulator (Fig. 2). A stereomicroscope was used to note when the tip of the oxygen electrode hits the surface. The diffusive flux was calculated both from the diffusive boundary layer (DBL) from Fick's first law of diffusion and modelled from sediment gradients just below the surface.

**Table 3. Organic carbon and nitrogen in sediments as % dry wt. (%C<sub>org</sub> and %N<sub>org</sub>), stable isotope values  $\delta^{13}\text{C}$  and  $\delta^{15}\text{N}$ , carbon:nitrogen ratios in organic matter (C:N) plus estimates of terrestrial and marine organic carbon and nitrogen determined from the stable isotope data**

	%C <sub>org</sub>	%N <sub>org</sub>	C:N	$\delta^{13}\text{C}$	$\delta^{15}\text{N}$	% C <sub>Terr</sub>	% N <sub>Terr</sub>	% C <sub>Mar</sub>	% N <sub>Mar</sub>
<b>LW</b>									
March	5.9	0.47	12.6	-23.6	7.74	25	0	75	100
July	5.3	0.40	13.3	-24.6	7.63	40	0	60	100
<b>LM</b>									
March	7.0	0.52	13.5	-23.6	7.49	25	0	75	100
July	6.9	0.53	13.0	-24.1	7.46	32	0	68	100
<b>LE</b>									
March	4.1	0.29	14.1	-24.3	7.39	35	2	65	98
July	5.3	0.39	13.6	-24.6	7.43	40	2	60	98
<b>MW</b>									
March	12.4	0.59	21.0	-26.4	5.29	68	37	32	63
July	11.8	0.56	21.3	-26.8	5.16	74	38	26	62
<b>MM</b>									
March	12.9	0.55	23.5	-26.0	4.62	62	48	38	52
July	12.7	0.56	22.7	-27.1	4.71	78	47	22	53
<b>ME</b>									
March	13.1	0.53	24.7	-26.4	4.29	68	53	32	47
July	13.0	0.56	23.2	-27.3	4.10	82	57	18	43

The percentage of terrestrial and aquatic organic matter was determined from the  $\delta^{13}\text{C}$  and  $\delta^{15}\text{N}$  values assuming a terrestrial plant end-member having a  $\delta^{13}\text{C}$  value of -28.5‰ and  $\delta^{15}\text{N}$  value of 1.5‰ and a marine sediment end member having a  $\delta^{13}\text{C}$  value of -22.0‰ and  $\delta^{15}\text{N}$  value of 7.5‰. These values were taken from the Huon Estuary Report (Butler et al., 2000).



**Figure 2. Experimental set-up for measurement of oxygen penetration depths.**

The O<sub>2</sub> penetration depth at the lower estuary transect varied seasonally. The smallest O<sub>2</sub> penetration depth was recorded at LM measuring 3.7 mm during March while the biggest O<sub>2</sub> penetration depth was recorded at LE measuring 9.0 mm in July (Table 4). The O<sub>2</sub> penetration depths also followed a seasonal trend at the upper estuary transect and were generally shallower than at the lower estuary. The smallest O<sub>2</sub> penetration depth was recorded during March at MM measuring 3.1 mm and the highest recorded at MW during July measuring 7.4 (Table 4).

The molecular oxygen diffusive fluxes ( $J_{DBL}$ ) at the lower estuary transect had a low of 134 ( $\pm 7.2$ )  $\mu\text{mol m}^{-2} \text{h}^{-1}$  at LE during July and a high of 435 ( $\pm 162.2$ )  $\mu\text{mol m}^{-2} \text{h}^{-1}$  at LM during March (Table 4). In comparison, the upper estuary transect had a range between 175 ( $\pm 35.4$ )  $\mu\text{mol m}^{-2} \text{h}^{-1}$  at MW in July and 489 ( $\pm 77.7$ ) at MM during March (Table 4). In general there was good agreement between  $J_{DBL}$  and  $J_{SED}$  and no significant statistical difference was found ( $p=0.05$ ). Generally the difference was less than 3%.

**Table 4. Measured oxygen penetration depths and molecular diffusive fluxes. The fluxes were calculated from the diffusive boundary layer ( $J_{DBL}$ ) and compared with fluxes modelled from the oxygen gradient within the sediment ( $J_{SED}$ )**

Site		Oxygen Penetration Depth (mm)	Molecular Diffusive Flux Rates ( $\mu\text{mol m}^{-2} \text{h}^{-1}$ )	
			$J_{DBL}$	$J_{SED}$
LW	March	5.2 ( $\pm 0.5$ )	264 ( $\pm 16.5$ )	259 ( $\pm 15.9$ )
	July	8.3 ( $\pm 0.3$ )	157 ( $\pm 18.5$ )	155 ( $\pm 17.9$ )
	November	7.2 ( $\pm 1.1$ )	181 ( $\pm 33.1$ )	176 ( $\pm 31.3$ )
LM	March	3.7 ( $\pm 0.9$ )	435 ( $\pm 162.2$ )	422 ( $\pm 150.4$ )
	July	8.2 ( $\pm 2.2$ )	144 ( $\pm 29.3$ )	142 ( $\pm 142$ )
	November	4.7 ( $\pm 1.1$ )	264 ( $\pm 48.0$ )	258 ( $\pm 46.4$ )
LE	March	4.6 ( $\pm 0.7$ )	233 ( $\pm 36.2$ )	227 ( $\pm 36.3$ )
	July	9.0 ( $\pm 0.4$ )	134 ( $\pm 7.2$ )	132 ( $\pm 7.2$ )
	November	6.9 ( $\pm 1.1$ )	178 ( $\pm 34.6$ )	173 ( $\pm 32.5$ )
MW	March	3.7 ( $\pm 0.4$ )	347 ( $\pm 60.6$ )	334 ( $\pm 57.1$ )
	July	7.4 ( $\pm 0.6$ )	175 ( $\pm 35.4$ )	171 ( $\pm 34.3$ )
	November	5.1 ( $\pm 0.4$ )	297 ( $\pm 50.4$ )	286 ( $\pm 47.9$ )
MM	March	3.1 ( $\pm 0.5$ )	489 ( $\pm 77.7$ )	468 ( $\pm 78.5$ )
	July	5.5 ( $\pm 1.1$ )	244 ( $\pm 78.8$ )	237 ( $\pm 75.9$ )
	November	4.9 ( $\pm 0.6$ )	314 ( $\pm 34.9$ )	301 ( $\pm 33.7$ )
ME	March	nm	nm	nm
	July	6.2 ( $\pm 0.4$ )	186 ( $\pm 41.5$ )	182 ( $\pm 40.2$ )
	November	4.0 ( $\pm 0.5$ )	320 ( $\pm 53.2$ )	310 ( $\pm 50.8$ )

The oxygen microgradient profiles for the most part (Figures 3 and 4) reflected smoothly declining O<sub>2</sub> concentrations with inward curvature within the sediment. On no

occasions were the profiles broken which would have indicated faunal irrigation activity within the sediments. This was also reflected in the microprofiles where the error bars were small suggesting a relatively homogenous sediment microstructure. No large benthic fauna were ever found to be present in the cores used for the oxygen microprofiles although small disturbances, which may have been caused by worms, just beneath the sediment were witnessed on a few occasions. Unfortunately the benthic fauna were not quantitatively recorded in these cores and only qualitative information about the presence of fauna was measured. However given the relative smooth O<sub>2</sub> microprofiles and small standard errors and lack of any large fauna present, the results should reflect reasonably accurately the diffusive oxygen uptake minus fauna within the sediments and will serve as a useful comparison with the total oxygen uptakes (see later) that were measured in sediment reactors and had large fauna such as the brittle star, present on a number of occasions.

The oxygen consumption profiles modelled from the curvature of the O<sub>2</sub> concentration profiles using PROFILE (Berg et al., 1998) exhibited intense activity at the sediment surface and at the oxic-anoxic interface below during all three sampling periods (Figures 3 and 4). However oxygen consumption rates during March were approximately three times the rate during July and November indicating the presence of higher concentrations of labile carbon. The intense activity at the sediment surface is due presumably to aerobic degradation of labile organic carbon deposited onto the sediment surface (need lipid biomarker data for elaboration) and the oxidation of reduced solutes (e.g. NH<sub>4</sub><sup>+</sup>, H<sub>2</sub>S) diffusing up from the anaerobic zone below is probably the reason for the increased O<sub>2</sub> consumption rates at the oxic-anoxic interface. It is plausible that ammonium is one of the reduced solutes diffusing out of the anaerobic zone as the ammonium porewater profiles indicate that ammonium production occurs down to approximately 3 cm.

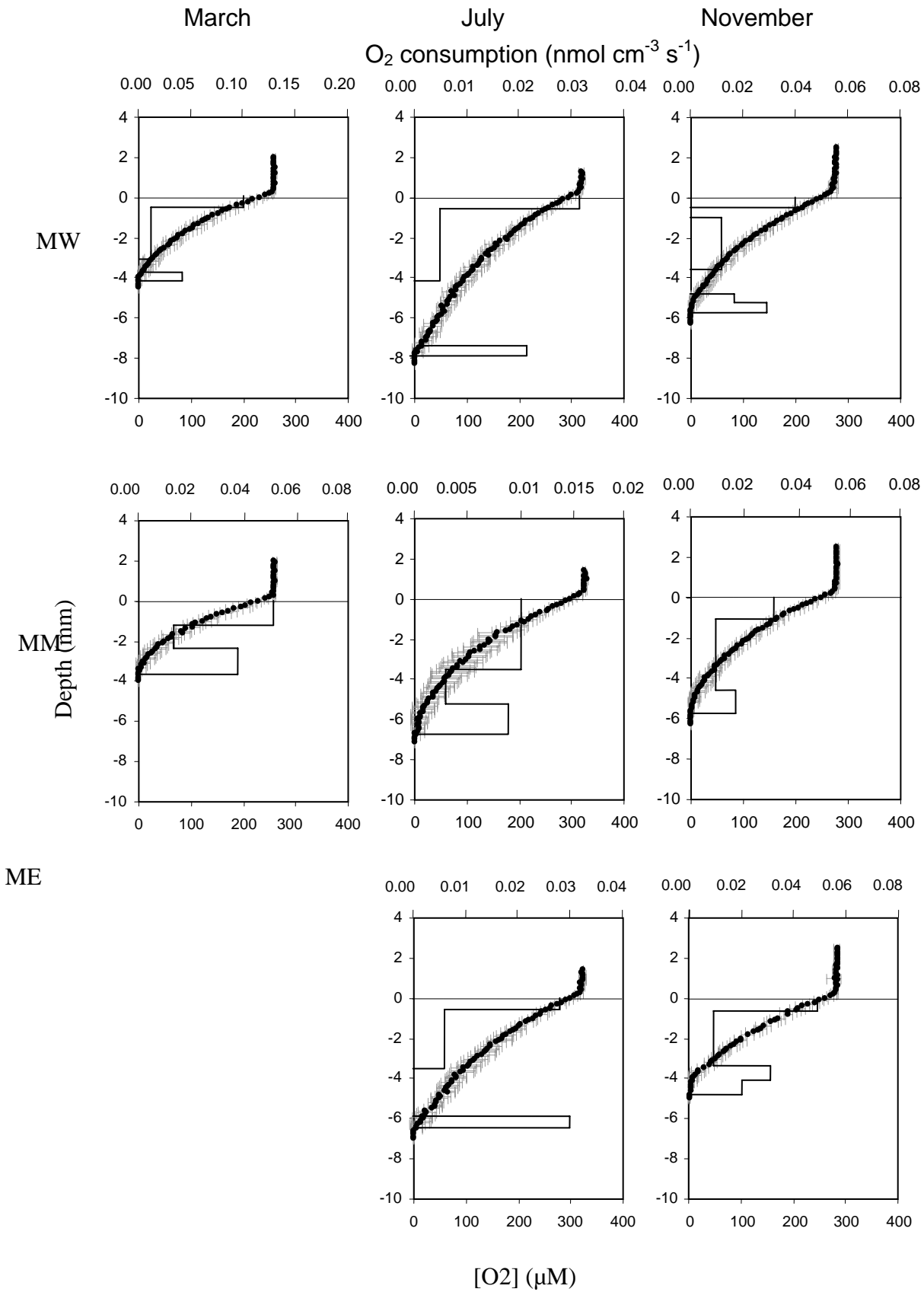


**Figure 3. Measured oxygen microgradients and consumption profiles during March, July and November at the mid estuary station sites: MW, MM and ME. The microgradients and consumption profiles represent the mean profiles from two cores at each site. The error bars on the microgradients represent the standard deviation of the mean.**

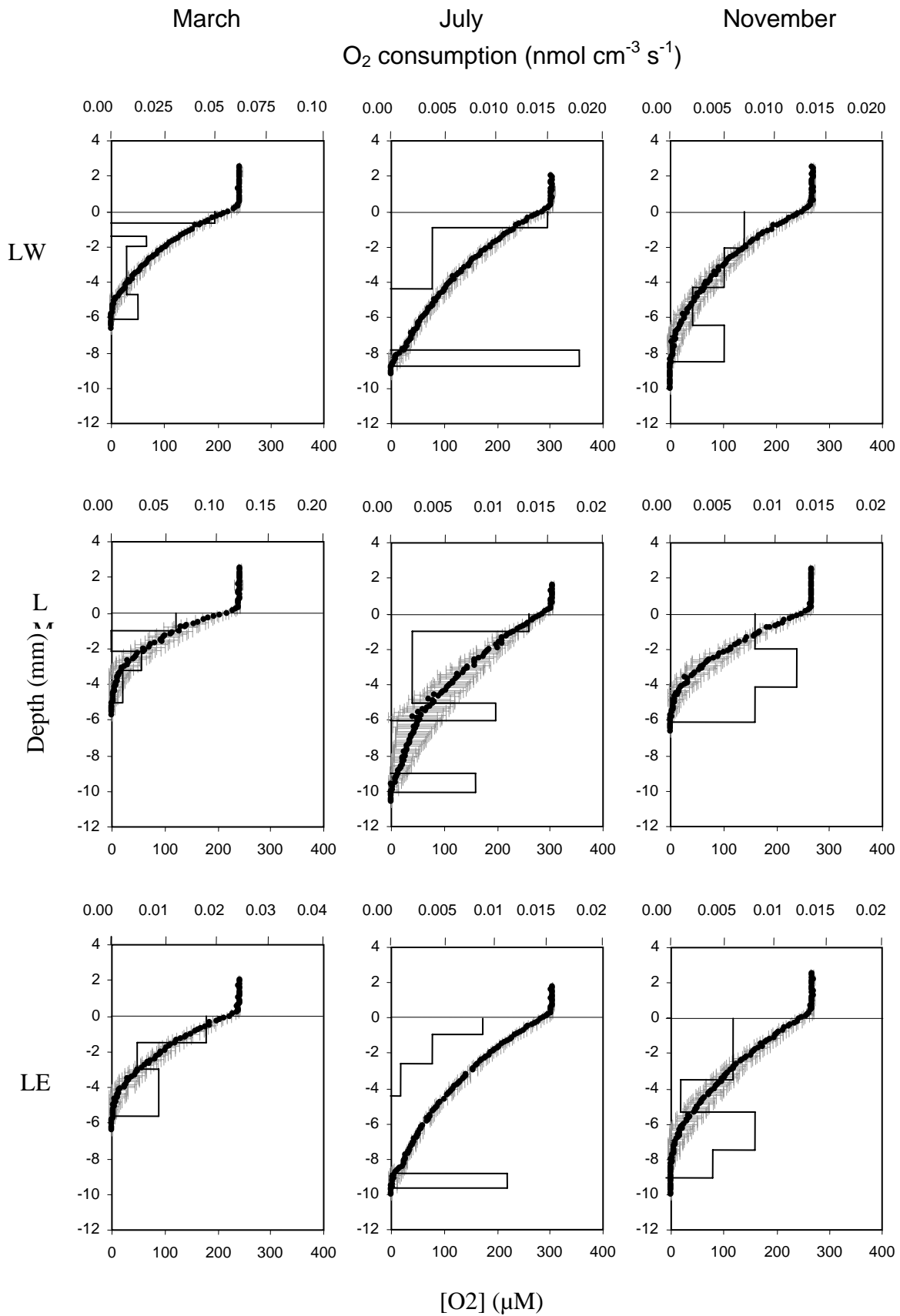


**Figure 4. Measured oxygen microgradients and consumption profiles during March, July and November at the lower estuary station sites: LW, LM, and LE. The microgradients and consumption profiles represent the**

**mean profiles from two cores at each site. The error bars on the microgradients represent the standard deviation of the mean.**

## Total Oxygen Uptake Rates

These were determined using sediment reactors as depicted in Fig 5. Sediment cores (9.7 cm diam) were placed in a water bath at the *in-situ* bottom water temperature. These were for the lower estuary: 15.6 °C (March), 10.2 °C (July) and 13.0 °C (November). For the mid-estuary these were 16.0 °C (March), 7.9 °C (July) and 13.0 °C (November). The sediment had a depth of ~ 8–10 cm and there was ~ 18–20 cm of overlying water. Lids containing a rubber O-ring were used to cap the cores at the start of the incubation and oxygen was measured with a unisense oxygen electrode through a sampling port in the cap.

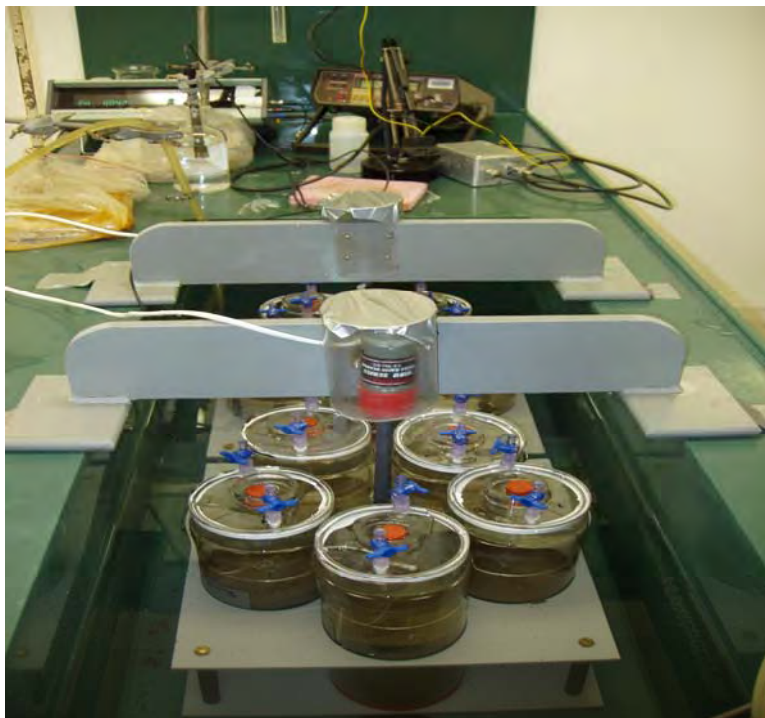


**Figure 5. Sediment reactors used to determine nutrient fluxes and oxygen consumption in sediments from the Huon Estuary.**

Fluxes were calculated by monitoring the concentration change in oxygen over time:

$$\text{Flux} = (\alpha - \alpha_w) V/A$$

Where:

$\alpha$  = linear regression slope of O<sub>2</sub> ( $\mu\text{mol L}^{-1} \text{h}^{-1}$ )

$\alpha_w$  = linear regression slope of O<sub>2</sub> in blank core

V = water column volume (L), and

A = sediment surface area ( $\text{m}^2$ )

Fig. 6 gives examples of oxygen consumption over time and the linear regression fit. The linear regression used 3 – 4 data points. The flux was considered to be significant if the standard error of the slope of the line was less than the magnitude of the flux.

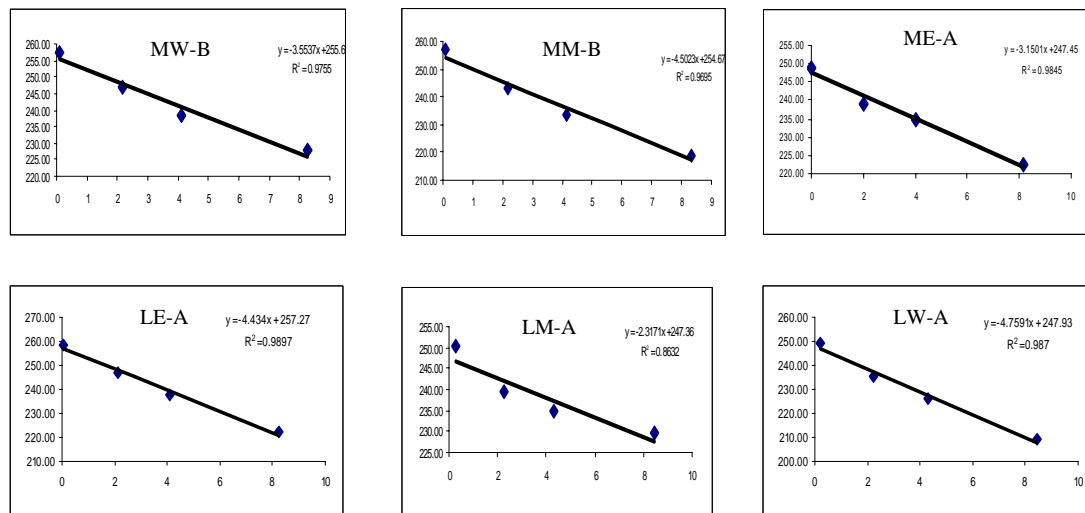


**Figure 6. Representative oxygen flux measurements; Oxygen concentration ( $\mu\text{mol l}^{-1}$ ) was measured over time and fitted to a linear relationship**

Sediment respiration rates (measured as  $\text{TCO}_2$  fluxes) at the lower estuary site ranged between  $228 \mu\text{mol m}^{-2} \text{h}^{-1} \text{TCO}_2$  at LE and LM stations during July and  $644 \mu\text{mol m}^{-2} \text{h}^{-1} \text{TCO}_2$  at LE during March (Fig. 7). The sediment respiration rates at the upper estuary location in the mixed zone had a higher range and varied between  $267 \mu\text{mol m}^{-2} \text{h}^{-1} \text{TCO}_2$  at ME station in November and  $839 \mu\text{mol m}^{-2} \text{h}^{-1} \text{TCO}_2$  at station MM in March (Fig. 8). Community respiration quotients ( $\text{CRQ} = \text{TCO}_2/\text{O}_2$  flux ratio) across the lower estuary stations averaged 1.4 and ranged between 1.1 to 1.8. In comparison, the CRQ across the upper stations averaged 1.2 and ranged between 0.6 and 2.7. The highest CRQ was measured at MM at the upper estuary site during July when oxygen consumption rates were lowest. The CRQ can be used to infer the aerobic/anaerobic status of sediment metabolism. A CRQ of 1 would imply that aerobic respiration is the dominant process. Therefore the results from this study suggest aerobic respiration is the dominant form of metabolism however anaerobic respiration accounted for over 50% of metabolism on occasion. Alkalinity fluxes were always directed out of the sediment and generally lower than  $\text{CO}_2$  fluxes. The highest efflux was recorded in March at LW ( $676 \mu\text{Eq m}^{-2} \text{h}^{-1}$ ) and the lowest at MM in March ( $21 \mu\text{Eq m}^{-2} \text{h}^{-1}$ ).

In less permeable sediments such as those dominated by high silt contents, oxygen consumption can be attributed mainly to diffusive and faunal mediated processes. Flow induced advection, the other major oxygen consuming process can generally be ruled

out (Glud et al. 2003) The locations in the current study had a high percentage of silt and thus we have made the assumption that advection does not occur to any significant extent. Thus the difference between the diffusive oxygen uptake (DOU) rate (measured in the diffusive boundary layer and/or sediment oxygen profile) and the total oxygen uptake (TOU) rate (as measured in the sediment reactors) can be used to infer the faunal activity within the sediments (Glud et al, 2003). Diffusion was generally the dominant process at both locations over the study period however faunal oxygen consumption accounted for over 40% of total oxygen consumption at the east and west lower estuary sites during March and November (Figure 9). A qualitative analysis of the benthic fauna in the sediments found the brittle star *Amphiura elandiformis* to be the most common faunal animal in the sediments. Other animals found included polychaete worms, the heart urchin and small bivalves and gastropods.

Fluxes of silicate were directed out of the sediment at all sites (Figures 10 and 11) with the exception of sites MM and ME during winter. Fluxes of phosphate were also generally directed out of the sediment however rates were  $<2 \mu\text{mol m}^{-2} \text{h}^{-1}$ . No phosphate fluxes at the lower estuary sites during summer were reported due to erratic changes in concentration over the incubation period leading to non-significant flux results.

Fluxes of ammonium were generally directed out of the sediment during March with the exception of site LM. During July all sites except LW had ammonium fluxes directed into the sediment. In November all sites at the lower estuary had small directed out of the sediment in comparison all sites had at the upper estuary sites consumed ammonia.

The highest ammonium efflux rate across all sites during both seasons was found at site LW during March with a flux of  $6.4 \mu\text{mol m}^{-2} \text{h}^{-1}$  out of the sediment. Nitrate was always directed out of the sediment and was the dominant form of DIN efflux. Nitrate accounted for between 66 – 100% of the DIN efflux. Nitrite was a small component of DIN with a flux of  $\leq -1 \mu\text{mol m}^{-2} \text{h}^{-1}$  generally and always directed into the sediment. DIN was always directed out of the sediment and ranged between  $5.5$  and  $18.1 \mu\text{mol m}^{-2} \text{h}^{-1}$  during March and  $1.7$  to  $6.7 \mu\text{mol m}^{-2} \text{h}^{-1}$  in July.

The uptake of ammonium by the sediments and release of nitrate to the water column suggests that the ammonium produced within the sediments is being converted to nitrate *via* nitrification. The nitrifiers are consuming more ammonium than can be produced in the sediments and are subsequently using ammonium from the water column. The nitrate is then released to the overlying water column or denitrified to dinitrogen gas which is no longer available for biological uptake. In November, ammonium was measured in the porewaters and production rates were then modeled from the curve using PROFILE (Berg et al., 1998). Ammonium production rates ranged between  $16$  to  $81 \mu\text{mol m}^{-2} \text{h}^{-1}$  (Figure 12). Comparing this to ammonium fluxes at the sediment – water interface (ranged between  $1.6$  and  $-6.7 \mu\text{mol m}^{-2} \text{h}^{-1}$ ) indicates a large discrepancy between sediment ammonium production and fluxes of ammonium out of the sediments. This implies that the microbial populations are efficiently recycling nitrogen liberated during the breakdown of organic matter in the sediments through the coupling of nitrification and denitrification. On a number of occasions ammonium production was in fact rate limiting for nitrification and the nitrifiers had to obtain more ammonium from the overlying water.

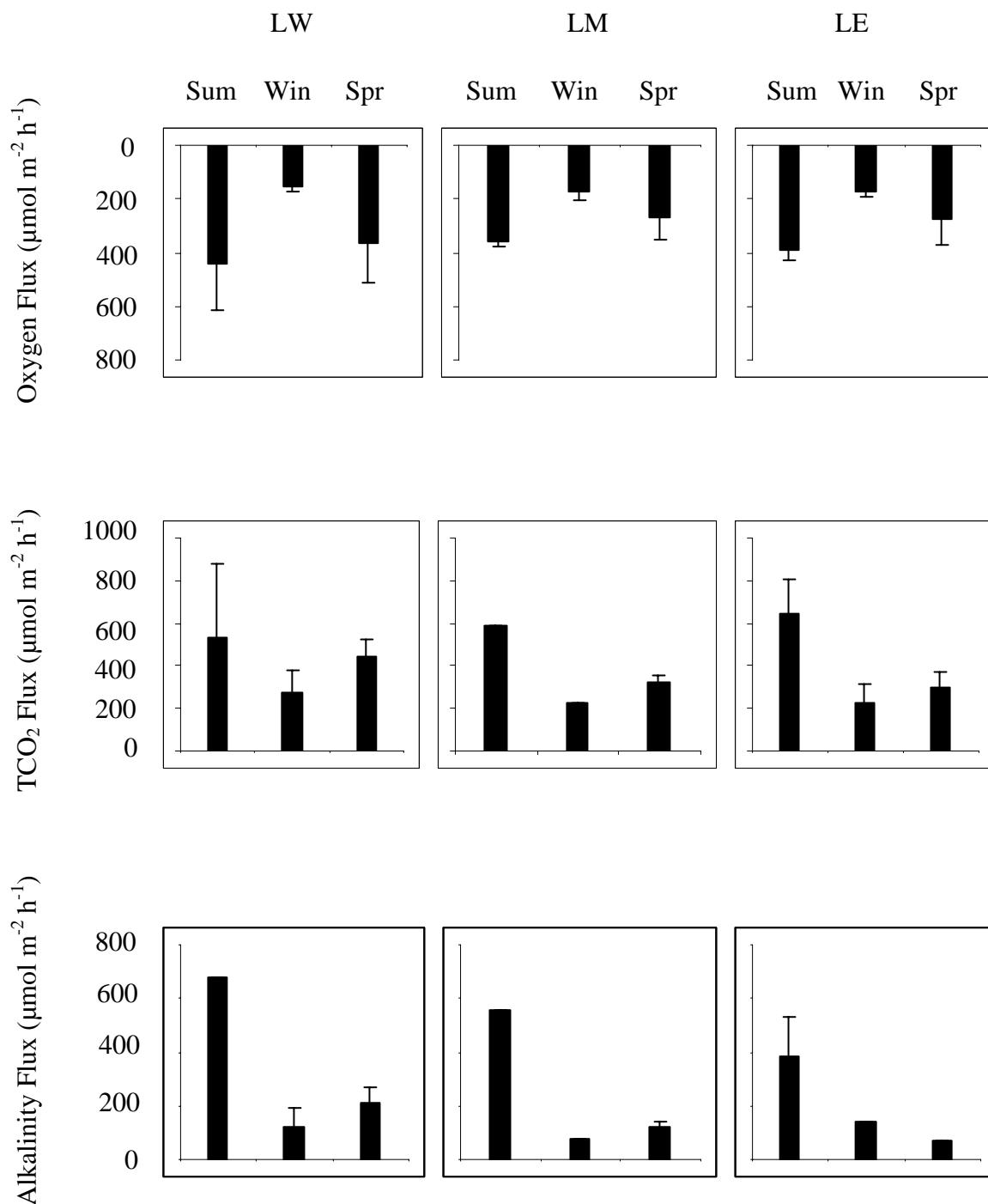


**Figure 7. Oxygen,  $\Sigma\text{CO}_2$  and alkalinity fluxes at the lower estuary transect during March, July and spring. Error bars represent the standard error of the mean ( $n = 2$  or  $3$ ). N.B. where no error bars are present, the data represent a single flux. This is due to some fluxes being not significant because of erratic changes over the incubation period.**

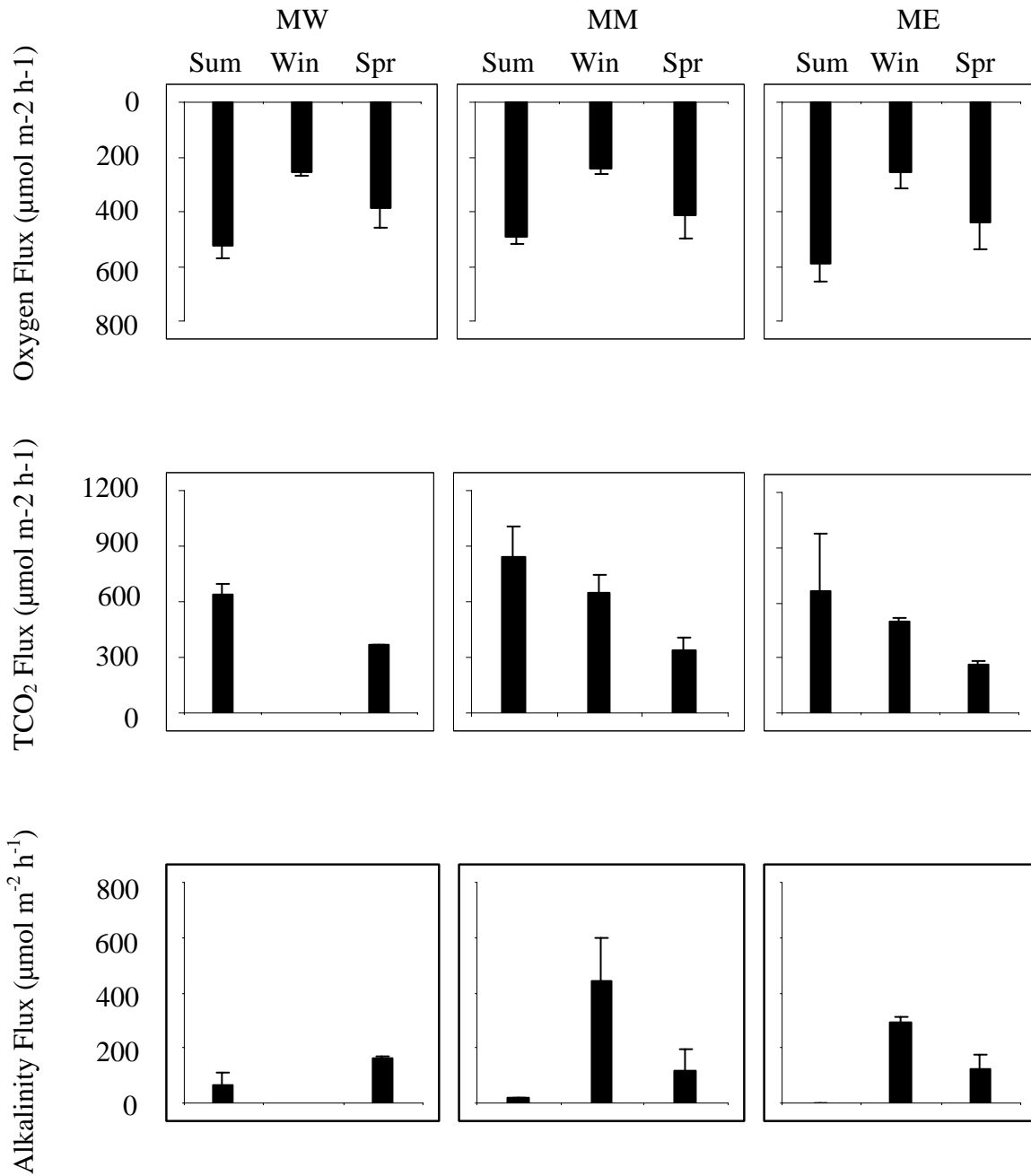


**Figure 8. Oxygen,  $\Sigma\text{CO}_2$  and alkalinity fluxes at the upper estuary transect during March, July and November. Error bars represent the standard error of the mean ( $n = 2$  or  $3$ ). N.B. where no error bars are present, the data only represent one flux result. This is due to some fluxes being not significant because of erratic changes over the incubation period.**

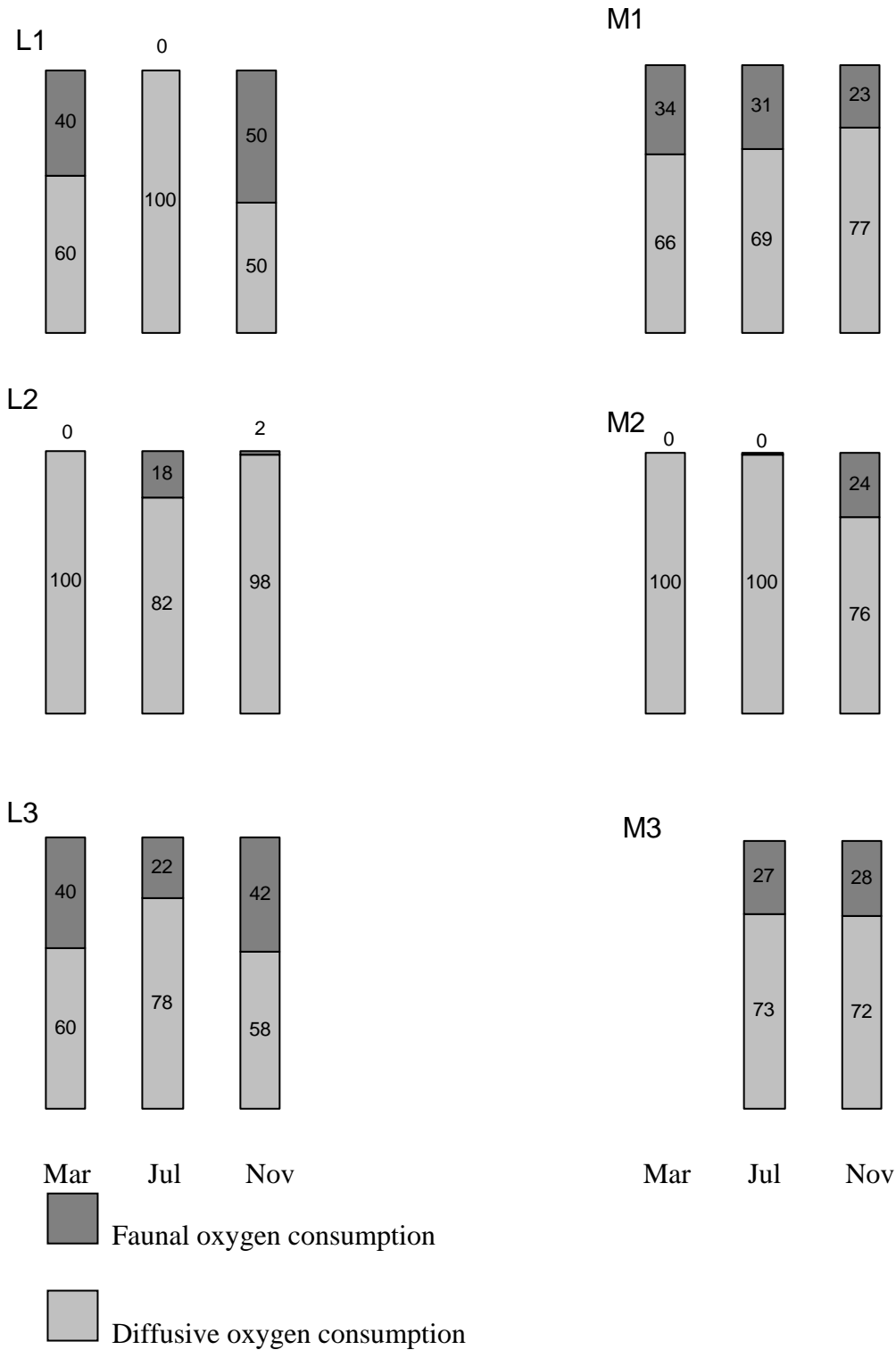


**Figure 9. Comparison of total and diffusive oxygen uptake rates and the role of benthic infauna**

We can use the  $\text{TCO}_2$ :DIN ratio to infer the expected release of DIN to the overlying water column. The ratio of  $\text{TCO}_2$  to DIN flux was always above 6.625, the ratio that would be predicted from the decomposition of organic matter with a “Redfield composition”. The measured ratios ranged between 17.6 – 86.7 at all sites in March and

between 34.1 – 2930.5 at all sites during the July (Figure 13). Assuming that the majority of organic matter decomposed was settled phytoplankton with a Redfield composition, and assuming that  $\text{TCO}_2$  flux reflects decomposition, we calculate from the high  $\text{TCO}_2$ :DIN fluxes that 62.3 – 100% of the nitrogen remineralised in sediments at all stations was not released to the overlying water. This supports the above findings that the majority of nitrogen remineralised in the sediments is released as either nitrate or di-nitrogen gas.

### **New Methodologies for Sediment Biogeochemical Analysis**

Dr Chris Burke was able to refine some of our sediment biogeochemistry techniques through a six month (July to December, 2003) sabbatical in Germany as a fellow of the Hanse Institute for Advanced Studies. This involved a collaborative project with researchers at the Max Planck Institute for Marine Microbiology, Dr Dirk De Beer and Prof. Rudolf Amman and their colleagues. Microelectrodes ( $\text{O}_2$ , pH,  $\text{H}_2\text{S}$ ), molecular biological techniques (DGGE, CARD-FISH, DNA sequencing) and sulphate reduction analysis were used to examine the effects on sediment microbial community structure and function during shock loading with organic carbon (e.g. with feed pellets).

Prior to organic carbon addition, the distribution of  $\text{O}_2$ , pH and  $\text{H}_2\text{S}$  was similar in control and treatment aquaria. The oxic zone was about 2 mm deep in the dark, extending to about 3 mm when aquaria were illuminated.  $\text{H}_2\text{S}$  was not detectable to 12 mm and pH did not vary greatly from neutrality. On addition of organic carbon,  $\text{H}_2\text{S}$  increased considerably, but had a patchy distribution in the sediments. FeS was observed and the sediments were acidic. Rates of sulphate reduction increased by 10 times in a treated aquarium, but did not vary greatly in the control. One treatment aquarium still had an elevated sulphate reduction rate after 43 days! *Bacteriodes* and *Cytophaga* bacteria were common initially, but declined and recovered towards the end of the experiment. *Desulfosarcinales* increased in response to organic carbon loading and were still in high numbers at the sediment surface after 43 days. This combined approach looking at both the microenvironment and the community structure of a sediment looks to be a powerful method for elucidating sedimentary responses to organic enrichment.

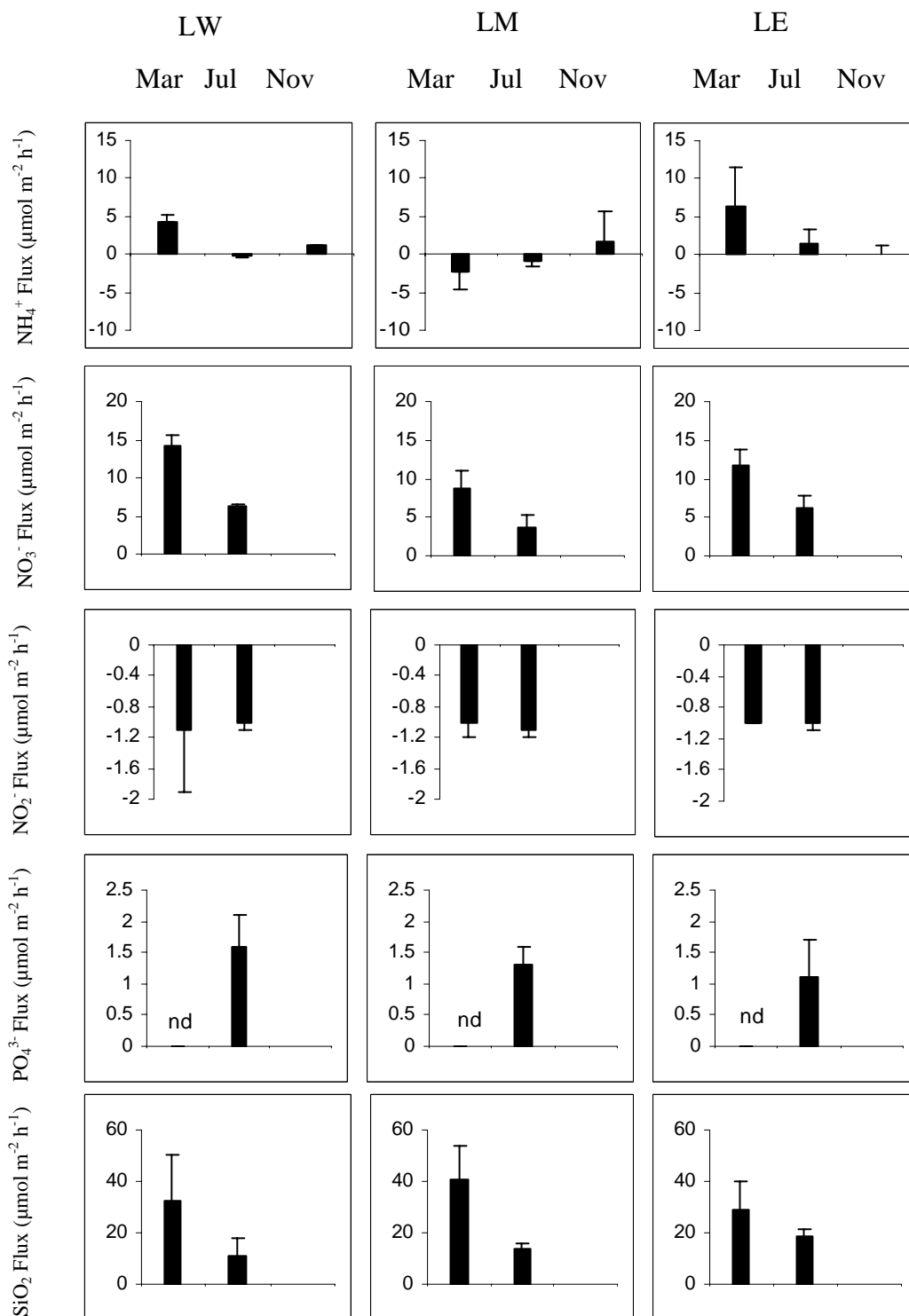


**Figure 10. Fluxes of silicate, phosphate, ammonium, nitrate and nitrite at the sediment – water interface at the six sample sites during March, July and November at the lower estuary sites of the Huon estuary. Error bars represent the standard error of the mean (n = 2 or 3). N.B. where no error bars are present, the data only represent one flux result. N.S = fluxes were not significant because of erratic changes over the incubation period.**

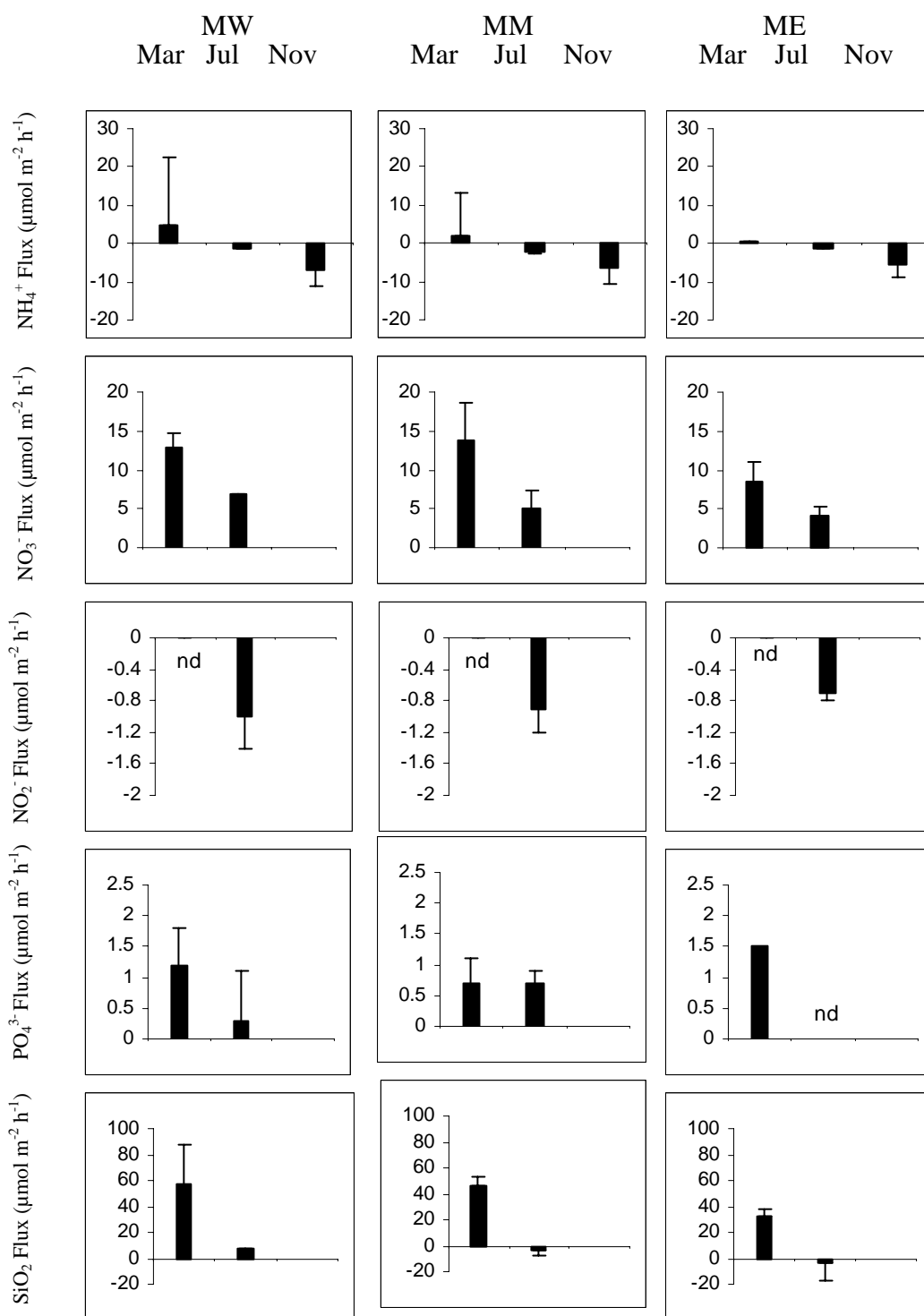
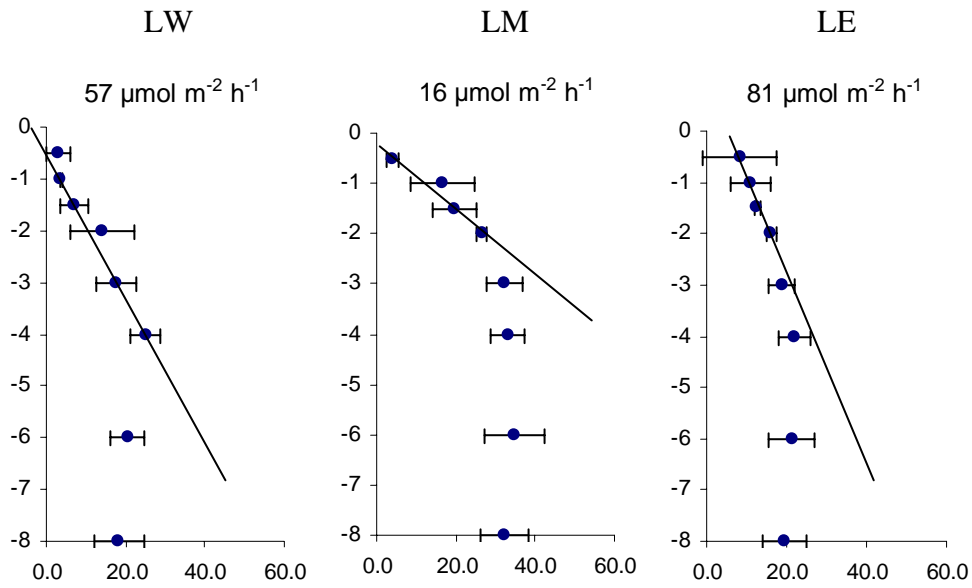


**Figure 11. Fluxes of silicate, phosphate, ammonium, nitrate and nitrite at the sediment – water interface at the six sample sites during March, July and November at the mid estuary sites of the Huon estuary. Error bars represent the standard error of the mean (n = 2 or 3). N.B. where no error bars are present, the data only represent one flux result. N.S = fluxes were not significant because of erratic changes over the incubation period.**

**(a) Lower estuary sites**



**(b) Upper estuary sites**

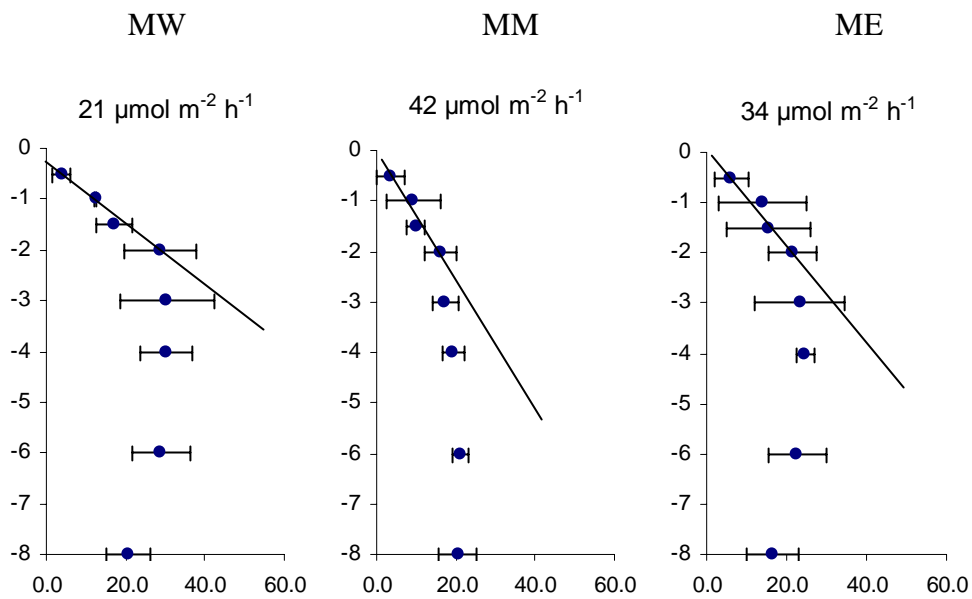


**Figure 12. Porewater profiles of  $\text{NH}_4^+$  and regression lines used to calculate upward fluxes of  $\text{NH}_4^+$  via diffusion and enhanced diffusion at (a) lower estuary sites and (b) upper estuary sites in November (Error bars = standard deviation of mean ( $n = 2$ ))**

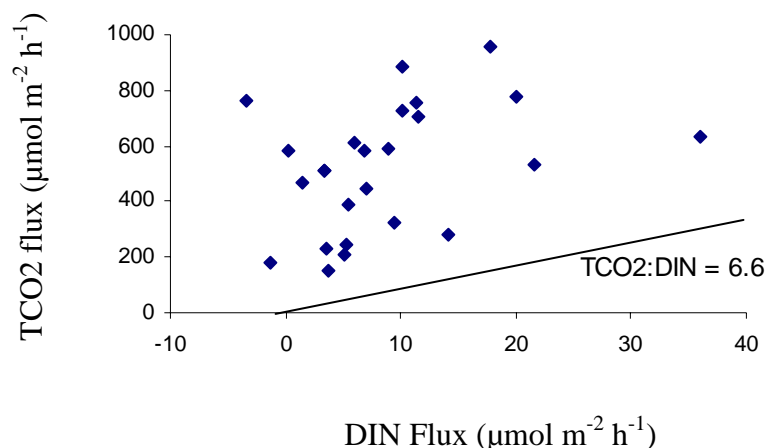


**Figure 13. TCO<sub>2</sub> : DIN flux ratio. Data are represented as individual core incubations for all sites during March and July.**

### Measurement of labile carbon in sediments

A technique was developed for determining the amount of labile carbon in sediments from measurements of sediment oxygen demand (SOD). Two sites in the Tamar estuary were chosen for method development. A predominantly marine sediment was obtained from Kelso. This contained lots of shell grit and sand and had thin algal layer on the surface. A terrestrial sediment was obtained in the Tamar Estuary in front of the University of Tasmania at Launceston. This was very muddy with a dark brown silty surface. Both sediments were obtained in the intertidal zone.

A measured weight of homogenised sediment (ca. 2 g) was placed into a 300 ml BOD bottle and filled with seawater. The oxygen concentration was measured at  $T_0$  and then the sediment was incubated at 20°C for 5 days, after which the oxygen concentration was remeasured. The sediment oxygen demand (SOD) was then determined by the following equation:  $(T_0O_2 - T_5O_2)/g$  of dry sediment. The %TOC and %TN in the sediments were also measured. To assess the proportion of labile material in the carbon pool the SOD is normalised to sediment carbon content (mol C) providing a measure of oxygen consumed relative to carbon content – SOD mol C<sup>-1</sup>. A high SOD mol C<sup>-1</sup> indicates a higher content of labile carbon.

The more “terrestrial” sediment (C/N = 10) gave a measured SOD value of 0.56 ( $\pm 0.02$ ) mmol O<sub>2</sub> mol C<sup>-1</sup>h<sup>-1</sup>, which was considerably less than the value of 1.77 ( $\pm 0.02$ ) found for the more marine sediment (C/N = 7.2). From these preliminary results there does seem to be relationship between SOD and the C/N ratio. The latter has been used as a proxy for sediment quality in past studies, and it is expected that more oxygen would be consumed in sediments with lower C/N ratios and hence more labile carbon.

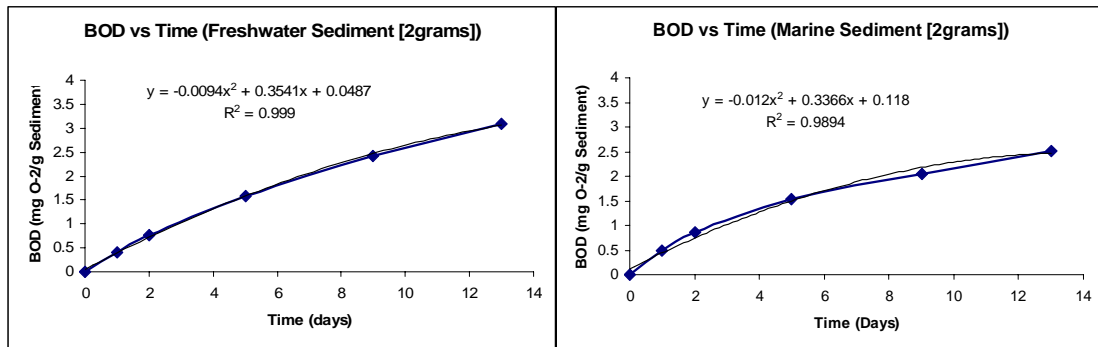


**Figure 14. Evolution of oxygen consumption over time in freshwater and marine sediments from the Tamar River.**

Further studies of this technique will be carried out Huon Estuary sediments where SOD measurements will be related to both molecular biomarkers such as fatty acids and lipids and stable isotopes  $^{13}\text{C}$  and  $^{15}\text{N}$ .

## References

- Abril G., Etcheber H., Lehir P., Bassoullet P., Boutier B., Frankignoulle M. (1999) Oxidic/anoxic oscillations and organic carbon mineralization in an estuarine maximum turbidity zone (The Gironde, France). *Limnology and Oceanography* 44, 1304-1315.
- Berelson W.M., Heggie D., Longmore A., Kilgore T., Nicholson G., Skyring G. (1998) Benthic nutrient recycling in Port Phillip Bay, Australia. *Estuarine, Coastal and Shelf Science* 46, 917-934.
- Berg, P., Risgaard-Petersen, N., Rysgaard, S. (1998). Interpretations of measured concentration profiles in sediment porewater. *Limnology and Oceanography* 81, 289-303.
- Bligh E.G., Dyer W.J. (1959) A rapid method of total lipid extraction and purification. *Canadian Journal of Biochemistry and Physiology* 37, 911-917.
- Bordovskiy O.K. (1965) Accumulation and transformation of organic in marine substances in marine sediments. *Marine Geology* 3, 3-114.
- Boschker H.T.S., Middelburg J.J. (2002) Stable isotopes and biomarkers in microbial ecology. *FEMS Microbiology Ecology* 40, 85-95.
- Butler E.C.V., Parslow J.P., Volkman J.K., Blackburn S.I., Morgan P., Hunter J., Clementson L.A., Parker N.S., Bailey R., Berry K., Bonham P., Featherstone A., Griffin D., Higgins H.W., Holdsworth D., Latham V., Leeming R., McGhie T.K., McKenzie D., Plaschke R., Revill A., Sherlock M., Trenerry L., Turnbull A., Watson R., Wilkes L. (2000) Huon Estuary Study - environmental research for integrated catchment management and aquaculture. Final report to the Fisheries Research and Development Corporation project number 96/284. CSIRO Division of Marine Research, Hobart
- Christensen P.B., Rysgaard S., Sloth N.P., Dalsgaard T., Schwærter S. (2000) Sediment mineralization, nutrient fluxes, denitrification and dissimilatory nitrate reduction to ammonium in an estuarine fjord with sea cage trout farms. *Aquatic Microbial Ecology* 21, 73-84.
- Cook, P.L.M., Butler, E.C.V., Eyre, B.D. (2004a). Carbon and nitrogen cycling on intertidal mudflats of a temperate Australian estuary. I. Benthic metabolism. *Marine Ecology-Progress Series* 280, 25-38.
- Cook, P.L.M., Revill, A.T., Butler, E.C.V., Eyre, B.D. (2004b). Carbon and Nitrogen Cycling on Intertidal Mudflats of a Temperate Australian Estuary. II. Nitrogen Cycling. *Marine Ecology-Progress Series* 280, 39-54.
- Cook P.L.M., Revill A.T., Clementson L.A., Volkman J.K. (2004c) Carbon and nitrogen cycling on intertidal mudflats of a temperate Australian estuary. III. Sources of organic matter. *Marine Ecology Progress Series* 280, 55-72.
- Fry B., Sherr E. (1984)  $\delta^{13}\text{C}$  measurements as indicators of carbon flow in marine and freshwater ecosystems. *Contributions in Marine Science* 27, 15-47
- Glud, R.N., Gundersen, J. K., Roy, H., Jorgensen, B.B. (2003). Seasonal dynamics of benthic O<sub>2</sub> uptake in a semienclosed bay: importance of diffusion and faunal activity. *Limnology and Oceanography* 48, 1265-1276.
- Hansen L.S., Blackburn, T.H. (1992). Effect of algal bloom deposition on sediment respiration and fluxes. *Marine Biology* 112, 147-152.
- Heip C.H.R., Goosen N.K., Herman P.M.J., Kromkamp J., Middelburg J.J., Soetaert K. (1995) Production and consumption of biological particles in temperate tidal estuaries. *Oceanography and Marine Biology - an Annual Review* 33, 1-149.

- Herbert R.A. (1999) Nitrogen cycling in coastal marine ecosystems. *FEMS Microbiology Reviews* 23, 563-590.
- Kharlamenko V.I., Kiyashko S.I., Imbs A.B., Vyshkvartzev D.I. (2001) Identification of food sources of invertebrates from the seagrass *Zostera marina* community using carbon and sulfur stable isotope ratio and fatty acid analyses. *Marine Ecology Progress Series* 220, 103-117.
- Meziane T., Bodineau L., Retiere C., Thoumelin G. (1997) The use of lipid markers to define sources of organic matter in sediment and food web of the intertidal salt-marsh-flat ecosystem of Mont-Saint-Michel Bay, France. *Journal of Sea Research* 38, 47-58.
- Pusceddu A., Cattaneo-Vietti R., Albertelli G., Fabiano M. (1999) Origin, biochemical composition and vertical flux of particulate organic matter under the pack ice in Terra Nova Bay (Ross Sea, Antarctica) during late summer 1995. *Polar Biology* 22, 124-132.
- Schlesinger W.H. (1997) Biogeochemistry. An Analysis of Global Change. Academic Press, San Diego
- Thornton S.F., McManus J. (1994) Application of organic-carbon and nitrogen stable-isotope and C/N ratios as source indicators of organic-matter provenance in estuarine systems - evidence from the Tay Estuary, Scotland. *Estuarine Coastal and Shelf Science* 38:219-233.
- Volkman J.K., Johns R.B., Gillan F.T., Perry G.J., Bavor H.J., Jnr (1980) Microbial lipids of an intertidal sediment - I. Fatty acids and hydrocarbons. *Geochimica et Cosmochimica Acta* 44, 1133-1143.
- Volkman J.K., Farrington J.W., Gagosian R.B. (1987) Marine and terrigenous lipids in coastal sediments from the Peru upwelling region at 15°S: Sterols and triterpene alcohols. *Organic Geochemistry* 11, 463-477.
- Volkman J.K., Barrett S.M., Blackburn S.I., Mansour M.P., Sikes E.L., Gelin F. (1998) Microalgal biomarkers: A review of recent research developments. *Organic Geochemistry* 29:1163-1179.
- Volkman J.K., Rohjans D., Rullkötter J., Scholz-Böttcher B.M., Liebezeit G. (2000) Sources and diagenesis of organic matter in tidal flat sediments from the German Wadden Sea. *Continental Shelf Research* 20, 1139-1158.
- Volkman, J.K. (2005). Polycyclic isoprenoids: source specificity and evolution of biosynthetic pathways. *Organic Geochemistry* 36, 139-159.

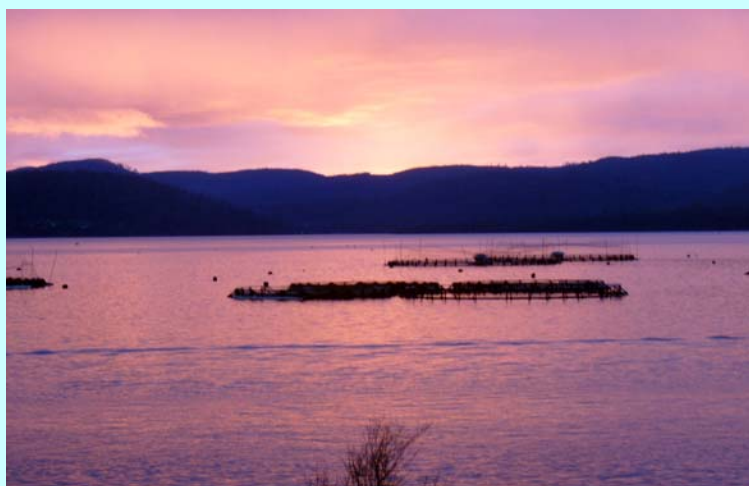
# Technical Report



## **Biogeochemical Modelling of the D'Entrecasteaux Channel and Huon Estuary**

K. Wild-Allen, J. Parslow, Mike Herzfeld, Pavel Sakov, John Andrewartha and Uwe Rosebrock.  
CSIRO Marine and Atmospheric Research

*July 2005  
Aquafin CRC Project 4.2  
(FRDC Project No. 2001/097)*



© Copyright Aquafin Cooperative Research Centre, Fisheries Research and Development Corporation, Commonwealth Scientific and Industrial Research Organisation

**This work is copyright. Except as permitted under the Copyright Act 1968 (Cth), no part of this publication may be reproduced by any process, electronic or otherwise, without the specific written permission of the copyright owners. Neither may information be stored electronically in any form whatsoever without such permission.**

**Every attempt has been made to provide accurate information in this document. However, no liability attaches to Aquafin CRC, its Participant organisations or any other organisation or individual concerned with the supply of information or preparation of this document for any consequences of using the information contained in the document.**

*Published by CSIRO Marine and Atmospheric Research*



# Biogeochemical Modelling of the D'Entrecasteaux Channel and Huon Estuary

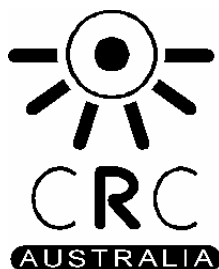
K. Wild-Allen, J. Parslow, Mike Herzfeld, Pavel Sakov,  
John Andrewartha and Uwe Rosebrock.  
CSIRO Marine and Atmospheric Research

*July 2005*

*Aquafin CRC Project 4.2  
(FRDC Project No. 2001/097)*



**Australian Government**  
**Fisheries Research and  
Development Corporation**



## *Executive Summary*

The Huon Estuary Study during 1996-1998 found that annual nitrogen fluxes into the estuary were dominated by natural marine input in winter and reported that intense phytoplankton blooms occurred primarily in summer and autumn, when fish farm loads made a significant contribution to system production. Relatively simple modelling studies in the estuary suggested that in 1997 farm loads increased phytoplankton biomass by about 25% and that a quadrupling of loads could double phytoplankton biomass, although uncertainty remained over conditions in the D'Entrecasteaux Channel. This study considers the Huon Estuary and D'Entrecasteaux Channel as a whole and applies a sophisticated 3D high resolution coupled hydrodynamic, sediment and biogeochemical model, which is validated against observations, to provide an improved basis for understanding and managing nutrient loads into the region.

The biogeochemical model has evolved over the last 10 years through a series of case studies in Australian coastal waters which has generated a diverse range of model components. In this study the biogeochemical code has been restructured into a modular form, with a software core linked to a central library of ecological processes. This allows the biogeochemical model to be dynamically coupled to a high resolution 3D hydrodynamic model 'SHOC' (Herzfeld et al., 2005) and a multilayer sediment model (MECOSED; Margvelashvili, 2003), and incorporated into the CSIRO Environmental Modelling Suite. This is the first time the biogeochemical model has been directly coupled to a 3-D hydrodynamic model in an estuarine application.

The ecological model water column is organised into three 'zones': pelagic, epibenthic and sediment where the epibenthic zone overlaps the lowest pelagic layer and shares the same dissolved and suspended particulate material fields. There are 25 pelagic layers in the model which vary in thickness from 0.25 m at the surface to 4 m at depth. Sediment is modelled as a thin layer of easily resuspendable material overlying a thicker layer of consolidated sediment. Dissolved nutrients are advected and diffused throughout the model domain in an identical fashion to temperature and salinity whilst particulate substances sink and are resuspended in the same way as sediment particles. At each biogeochemical time step, non-conservative rate processes are integrated within the biogeochemical module which returns updated tracer concentrations to the hydrodynamic model via an interface routine. The model is implemented on a curvilinear grid with spatial resolution of 600m – 1.3km.

Non-conservative ecological/biogeochemical processes are organized into pelagic processes of phytoplankton and zooplankton growth and mortality, detritus remineralisation and fluxes of dissolved oxygen, nitrogen and phosphorous; epibenthic processes of macro algae and seagrass growth and mortality; and sediment processes of phytoplankton mortality,

microphytobenthos growth, detrital remineralisation and fluxes of dissolved substances.

The biogeochemical model includes four groups of microalgae (small and large phytoplankton, dinoflagellates and microphytobenthos) and two macrophytes (seagrass and macroalgae) which grow at a 24 hour mean rate determined by access to dissolved nutrients (nitrogen and phosphate) and photosynthetically active radiation (PAR) (Baird 1999). Autotrophs take up ammonium and nitrate with equal preference and phosphate and dissolved inorganic carbon are taken up by phytoplankton at Redfield ratio (106C:16N:1P) and by macrophytes at Atkinson ratio (550C:30N:1P). Ambient PAR is calculated from incident surface 24 hour mean PAR attenuated by sea water, coloured dissolved organic substances, organic and inorganic particles. Chlorophyll concentration is calculated by a fixed nitrogen to chlorophyll ratio (7 mgN/mgChl). Micro- and meso-zooplankton graze on small and large phytoplankton respectively, at rates determined by swimming speed and particle encounter rate. A fraction of grazed material is released as dissolved and particulate carbon, nitrogen and phosphate and further detrital material accumulates through mortality. Detritus and dissolved organic substances are remineralised into inorganic carbon, nitrogen and phosphate with labile detritus transformed most rapidly, refractory detritus slower and dissolved organic material transformed over the longest timescales. The evolution (by photosynthesis) and utilization (by respiration and remineralisation) of dissolved oxygen is also included in the model and depending on prevailing concentrations, facilitates the oxidation of ammonia to nitrate its subsequent denitrification to nitrogen gas which is then lost from the system.

The model was initialized in December 2001 with tracer concentrations derived from observations made throughout the region or historical data. Physical surface and boundary fluxes were supplied as for the hydrodynamical model, except for photosynthetically active radiation (PAR) which was supplied as a 24 hour mean. Nutrient, phytoplankton and oxygen fluxes at the marine boundaries were prescribed as an upstream boundary condition from observations made at monthly intervals at D'Entrecasteaux stations 1 and 12. Flow and nutrient loads were estimated for the Huon, Esperance, Kermandie and Northwest Bay Rivulet based on observations, although many key tracers were poorly known and due to the paucity in data it was not possible to resolve seasonal fluctuations in tracer concentrations. Anthropogenic inputs to the region include sewerage and wastewater discharge and inputs from fin-fish farms. In the context of regional nutrient input sewerage and wastewater discharge is generally small and diffuse along the coast and for this reason it was not included in the model. Fin-fish farm inputs for 2002 were derived from monthly feed data from 20 salmonid farms in the region assuming that all feed pellets were consumed by the fish and that no overfeeding occurred. Of the total feed 5% and 0.8% was discharged by the fish as waste nitrogen and phosphorous respectively in dissolved and particulate forms. Waste was discharged at the farm sites as a point source discharge evenly distributed between 0.5 m and 12 m and diffused spatially throughout the immediate grid cell.

During summer and autumn farm discharges exceeded river fluxes of nutrient into surface waters and seasonal stratification limited the influx of nutrients into surface waters across the marine boundary. Farm waste entered the model as ammonium, dissolved inorganic phosphate and labile detritus which can be rapidly remineralised to dissolved inorganic nutrient and assimilated by phytoplankton; riverine loads were dominated by refractory dissolved and particulate material which is remineralised more slowly. In 2002 farm loads of DIN exceed river loads by more than seven times, and labile particulate detrital farm loads exceed river loads by more than 17 times.

The model was calibrated against nutrient, phytoplankton and dissolved oxygen data collected throughout the region during the Broad Scale Monitoring program (Thompson et al., 2004). Simulated biomass of seagrass, macroalgae and zooplankton, whilst consistent with our understanding of the model system, could not be validated due to lack of observed data and these components should be treated with extreme caution until verification against observations is demonstrated.

The model reproduced the observed spatial and temporal dynamics of dissolved nutrients, chlorophyll, phytoplankton biomass and oxygen in the Huon Estuary and D'Entrecasteaux Channel. Observed nitrogen, chlorophyll and large phytoplankton biomass concentrations were particularly well reproduced in the D'Entrecasteaux Channel and side Bays. The phosphorous cycle, which has a greater number of dissolved and particulate phases, was adequately simulated. Modelled small phytoplankton biomass throughout the region lacked the observed seasonal winter maxima, and dinoflagellate biomass was poorly represented, particularly in the Huon where observed autumn blooms were absent. Modelled oxygen concentrations suggest possible over-estimation of horizontal exchange of bottom waters between D'Entrecasteaux Channel and the mouth of the Huon Estuary.

The sensitivity of the model to the parameterization of zooplankton grazing, denitrification, algal light absorption and dinoflagellate diel vertical migration was assessed. The model was sensitive to the level of zooplankton grazing which impacted simulated regional productivity. Modelled grazing is currently inferred from ancillary data, however proposed observations of zooplankton in the region will allow more direct calibration of zooplankton parameters. The simulated biogeochemistry of the region is less sensitive to changes in denitrification than e.g. Port Phillip Bay, due to the relatively short flushing time of the Huon – D'Entrecasteaux system. Varying phytoplankton light absorption efficiency had small impact on phytoplankton biomass throughout the region as for much of the year and phytoplankton are nutrient and not light limited. Implementing dinoflagellate migration in the model simulated realistic distributions of dinoflagellates throughout the region, although autumn bloom events in the Huon were still not reproduced. A more rigorous model including diurnal cycles in PAR and phytoplankton growth might do better.

The model in its current formulation is considered to provide an adequate simulation and explanation of the seasonal dynamics of nutrient cycling and

phytoplankton abundance in the D'Entrecasteaux Channel and side Bays. However model results in the Huon show poorer agreement with observations, and this is considered to be due to still unresolved aspects of dinoflagellate dynamics in the estuary.

Modelled median annual DIN was  $\sim 10 \text{ mgN m}^{-3}$  in surface waters of the D'Entrecasteaux Channel and about four times that in the Huon Estuary. Bottom water concentrations were highest in the mid Huon Estuary, in relatively shallow water, where the opaque river water limited phytoplankton growth and uptake. In summer surface DIN concentrations were depleted throughout the D'Entrecasteaux Channel and lower Huon Estuary due to phytoplankton assimilation and thermal stratification which limited vertical replenishment. In the mid and upper Huon Estuary nutrients remained in shallow water in summer as local nutrient influx from rivers and farms exceeded algal assimilation. In winter seasonal weather mixed river, farm and marine nutrient throughout the water column and limited phytoplankton growth (by low incident irradiance and vertical mixing) which resulted in elevated surface DIN concentrations. Maximum values occurred in the mid and lower Huon Estuary and at the northern end of the D'Entrecasteaux Channel.

The spatial distribution and concentration of phosphorus (DIP) varied in a similar way to DIN with elevated concentrations simulated in the Huon Estuary and at depth. The 10 percentile surface concentration was elevated compared to nitrogen indicating that the latter controls phytoplankton production in the region.

Modelled annual median chlorophyll concentrations were  $\sim 1 \text{ mgChl m}^{-3}$  in surface waters throughout the D'Entrecasteaux Channel with slightly higher values in the southern basin compared to the northern end of the Channel. In the Huon Estuary modelled chlorophyll concentrations were lower contrary to observations, as dinoflagellates blooms were under-represented. In spring median chlorophyll concentrations were elevated throughout the D'Entrecasteaux Channel and side bays to  $\sim 2 \text{ mg m}^{-3}$  with maximum concentrations simulated in Port Esperance. In autumn highest median concentrations of  $1.5 \text{ mg m}^{-3}$  were simulated in the lower Huon Estuary and southern basin of the D'Entrecasteaux Channel.

Modelled annual median oxygen saturation dropped from  $\sim 100\%$  in surface waters to  $\sim 80\%$  in bottom waters of the lower Huon Estuary. The most oxygen depleted waters were simulated in the upper Huon attributed to the influx of fresh river water. Values in bottom waters of the D'Entrecasteaux Channel were generally higher than in the Huon Estuary. Oxygen saturation was generally high throughout the region and in all seasons as the model system was well flushed [possibly excessively due to the necessarily coarse resolution of the bottom bathymetry]. Some draw-down of oxygen was simulated at depth associated with benthic oxygen demand for remineralisation of organic detritus. Autumn stratification limited surface oxygen exchange with bottom waters and a maximal draw-down of  $\sim 20\%$  occurred in the lower Huon Estuary. In spring the vertical structure was similar

although surface waters were supersaturated with oxygen produced by phytoplankton photosynthesis.

The impacts of farm discharges on the regional biogeochemistry were investigated by comparing scenario simulations with and without farm loads. In general farm discharges had greatest impact on the nutrient and phytoplankton fields in summer and autumn by alleviating seasonal near surface nutrient limitation and thus promoting phytoplankton growth. Riverine and marine fluxes of nutrient into surface waters were comparatively small during this period and the farm discharges enhance the ambient surface nitrogen concentration by >3 times in the lower Huon Estuary ( $\sim 10 \text{ mgN m}^{-3}$ ), and mid- and northern ends of the D'Entrecasteaux Channel ( $< 1 \text{ mgN m}^{-3}$ ). At depth DIN concentrations were elevated by up to  $20 \text{ mgN m}^{-3}$  in the lower Huon and  $8 \text{ mgN m}^{-3}$  at the northern end of the D'Entrecasteaux Channel indicating that vertical exchange of DIN, and/or remineralization of sinking particulate matter, were significant at these locations. Autumn chlorophyll concentrations were enhanced by the farm discharges throughout most of the D'Entrecasteaux Channel, the lower Huon and in Northwest Bay (by  $\sim 50\%$  or  $0.4 \text{ mg Chl m}^{-3}$ ). Farm discharges had little impact on simulated dissolved oxygen concentrations throughout the year and region although some slight variations in concentration were simulated in the upper Huon Estuary likely due to spatial variation in phytoplankton production and degradation of organic material.

Seasonal statistics for sub-regions of the model show a consistent increase in modelled surface DIN and surface chlorophyll concentration across the whole region resulting from the farm discharge. The Huon Estuary had the greatest increase in surface median DIN, followed by Northwest Bay and Barnes Bay. These two Bays also showed the largest response in enhanced chlorophyll concentration, followed by Port Esperance. Regions were most significantly impacted in summer and autumn relative to seasonally depleted surface nutrient and chlorophyll concentrations although in winter and spring the increase in absolute concentration of DIN was greater (table i). The impact of the farm discharge on regional denitrification was comparatively small (+9.4%) which suggested that only 98 tN/y of the 838.7 tN discharged from the farms in 2002 was denitrified.

<b>Season</b>	<b>Relative increase in DIN (%)</b>	<b>Relative increase in chlorophyll (%)</b>	<b>Absolute increase in DIN (<math>\text{mg N m}^{-3}</math>)</b>	<b>Absolute increase in chlorophyll (<math>\text{mg Chl m}^{-3}</math>)</b>
<b>Summer</b>	54	18	1.0	0.14
<b>Autumn</b>	41	19	1.6	0.15
<b>Winter</b>	12	11	3.8	0.07
<b>Spring</b>	24	13	2.1	0.20

*Table (i): Mean increase in surface DIN and chlorophyll concentration due to farm discharges for all sub-regions.*

A second scenario simulation examined the impact of secondary river loads on the regional biogeochemistry. Impacts from the Kermandie, Esperance and Northwest Bay Rivulet discharges were generally small and local to the river mouths. Winter dissolved inorganic nitrogen was elevated (by  $\sim 5 \text{ mg N m}^{-3}$ ) in surface waters of the lower Huon and there was a slight increase in surface nutrients in the southern basin of the D'Entrecasteaux Channel in summer. In the mid D'Entrecasteaux Channel subsurface nutrient concentrations were slightly elevated probably due to regeneration and resuspension of nutrients from river loads. Chlorophyll concentrations were enhanced in spring off Great Taylors Bay and locally in Northwest Bay (by +10%  $\sim 0.3 \text{ mg Chl m}^{-3}$ ). Autumn chlorophyll was also slightly elevated in the lower Huon Estuary and mid D'Entrecasteaux Channel (by  $\sim 0.2 \text{ mg Chl m}^{-3}$ ). Dissolved oxygen concentrations were little impacted by the additional river inputs, although some slight variations in concentration resulted from spatial variation in productivity in the Huon Estuary and remineralisation of organic material in the mid D'Entrecasteaux Channel.

All sub-regions of the model domain showed small increases in seasonal surface median chlorophyll and dissolved inorganic nitrogen in the model with secondary river discharges. Greatest enhancement occurred in spring and summer when additional river nutrients were readily assimilated into phytoplankton (+2% or  $0.02 \text{ mg Chl m}^{-3}$ ). In autumn minimal river flows limited the discharge of nutrients into the model whilst during winter the elevated flow and river loads were dwarfed relative to the considerably greater influx of nutrients from the Huon river and across the marine boundary. The impact of the additional river discharge on the denitrification flux was small (+0.8%) which suggested that 8 tN/y of the 82.8 tN discharged from the secondary rivers in 2002 was denitrified.

The impact of fish farm discharges on the annual median surface dissolved inorganic nitrogen and chlorophyll concentration was consistently greater in all sub-regions than that of the secondary river discharges. On average the impact of farm discharge was 30 times greater than that of rivers for dissolved inorganic nitrogen and 45 times greater for chlorophyll due in part to the wider spatial distribution of farm inputs and in part to the more labile nature of the farm inputs. The seasonal contrast between farm and river impacts was greatest in autumn when river impacts were small coincident with minimum river flow and farm impacts were relatively large. At this time farm discharges supplied additional nutrient to seasonally depleted surface waters which enhanced phytoplankton growth.

This study has shown that fish farm discharges impact the biogeochemistry of the Huon Estuary and D'Entrecasteaux Channel by increasing the supply of nitrogen and phosphorous available for phytoplankton growth. The model has demonstrated that the region is hydrodynamically well connected with a residual circulation from south to north which flushes the whole region over about two and a half weeks. This disperses local nutrient sources widely and results in regional elevation of nutrient and phytoplankton biomass to a modest degree.

# Contents

<b>Executive Summary</b> .....	<b>3</b>
<b>1 Introduction</b> .....	<b>12</b>
<b>2 Biogeochemical Model description</b> .....	<b>13</b>
2.1 History .....	13
2.2 Model Components .....	14
2.3 Primary Production .....	15
2.4 Secondary Production .....	17
2.5 Detritus and nutrient pools .....	18
2.6 Dissolved oxygen .....	20
<b>3 Hydrodynamical Model and Grid</b> .....	<b>20</b>
<b>4 Initialisation</b> .....	<b>20</b>
4.1 Dissolved inorganic material .....	20
4.2 Biomass .....	21
4.3 Detritus .....	21
<b>5 Forcing Data</b> .....	<b>22</b>
5.1 Photosynthetically active radiation .....	22
5.2 Rivers .....	23
Huon River .....	25
Esperance River .....	26
Kermandie River.....	26
Northwest Bay River.....	27
5.3 Marine boundaries .....	28
<b>6 Anthropogenic Inputs</b> .....	<b>28</b>
6.1 Sewerage and wastewater .....	28
6.2 Fin-fish Farm Discharges .....	29
<b>7 Model Calibration against observations</b> .....	<b>33</b>
7.1 Nutrients .....	34
Nutrients in the D'Entrecasteaux Channel .....	34
Nutrients in the side bays of the D'Entrecasteaux Channel.....	36
Nutrients in the Huon Estuary .....	39
7.2 Chlorophyll, Oxygen and Phytoplankton Biomass .....	42
Chlorophyll and phytoplankton biomass in the D'Entrecasteaux Channel .....	42
Vertical structure in observed fluorescence and modelled chlorophyll .....	45
Chlorophyll and phytoplankton biomass in the side bays .....	50
Chlorophyll, oxygen and phytoplankton biomass in the Huon estuary .....	53
7.3 Model Calibration summary .....	57
<b>8 Sensitivity of key processes and parameter values</b> .....	<b>57</b>
8.1 Grazing .....	57
8.2 Denitrification .....	61
8.3 Absorption cross section .....	65
8.4 Dinoflagellate vertical migration and grazing losses .....	70
Simple parameterization.....	70
Reduced grazing pressure .....	71

Surface layer avoidance.....	72
<b>8.5 Summary of model performance</b> .....	<b>81</b>
<b>9 Model Results</b> .....	<b>82</b>
<b>9.1 Annual regional biogeochemistry</b> .....	<b>82</b>
<b>9.2 Seasonal regional biogeochemistry</b> .....	<b>87</b>
Nutrients .....	87
Chlorophyll .....	87
Oxygen .....	88
<b>10 Scenario simulations</b> .....	<b>97</b>
<b>10.1 Impact of fish farm discharges</b> .....	<b>97</b>
Summary .....	109
<b>10.2 Impact of secondary river discharge</b> .....	<b>115</b>
Summary .....	126
<b>10.3 Discussion of scenario simulations</b> .....	<b>127</b>
<b>12 References</b> .....	<b>132</b>

## 1 Introduction

The D'Entrecasteaux Channel and Huon Estuary are located in the south east of Tasmania in a region of low population density and high natural beauty. Water quality is generally high and enjoyed by wildlife, local residents and visitors to the region. It also supports a sizeable aquaculture (shellfish) and is the major centre for the Tasmanian finfish farming industry. Critical to the maintenance of high water quality in the region is the supply and cycling of nutrients through dissolved and particulate phases.

Nutrients enter the system through river run-off, by advection of oceanic waters into the channel, through anthropogenic inputs, and by aeolian supply (not thought to be an important source).

Regional rainfall is moderate and enters the marine system through 4 major rivers and more than 36 smaller rivers, creeks and streams. The largest river is the Huon with annual discharge of  $3.8E+09m^3/y$  and nutrient load of  $1155tN/y$  and  $173tP/y$ . This river drains a large catchment of native forest and moor land giving the river water a distinct tea colour (high concentration of CDOM) and high attenuation coefficient for light.

Oceanic waters are advected north into the channel from the continental shelf south of Tasmania. Ocean and shelf waters in this region undergo a temperate seasonal cycle, with nutrient depletion in surface waters in summer, and elevated surface nutrients in winter. Residual flow through the channel is northwards with a residence/flushing time of  $\sim 2.5$  weeks. The northern end of the D'Entrecasteaux Channel adjoins Storm Bay and the lower Derwent Estuary. Water from these sources is intermittently drawn into the Channel through tidal and wind-driven circulation.

The main direct anthropogenic nutrient inputs into the D'Entrecasteaux Channel and Huon Estuary are from sewerage and waste water treatment works and from finfish farming operations. On a per capita basis nutrient inputs through wastewater are estimated as  $3.6kgN/y$  per person per year. Fish farms in the region discharged an estimated  $839tN/y$  and  $146tP/y$  in 2002.

The capacity of aquatic systems to assimilate nutrient loads is modulated by utilization by primary production, recycling of detrital material, and export to the sediments, through boundaries or by losses to higher trophic levels.

The aim of this modelling study is to simulate the cycling of nitrogen, phosphorous and carbon through dissolved, organic and inorganic forms to better understand the transformations and fate of natural and anthropogenic nutrient sources in the D'Entrecasteaux Channel and Huon Estuary, and the likely response of the system to changing nutrient loads.

The Huon Estuary has previously been the subject of a substantial study (CSIRO, 2000) to quantify nutrient budgets and understand the fate and impact of nutrient loads. That study found that, on an annual basis, nitrogen

fluxes in the Estuary are dominated by (natural) marine inputs of nitrate in winter. However, these are mostly unutilized by phytoplankton, due to low winter temperatures and light intensities. Intense phytoplankton blooms, including harmful algal blooms, occur primarily in summer and autumn, when marine nitrate inputs are low. In these seasons, fish farm loads of nutrients can make a significant contribution to overall system production. Application of simple models suggested that, in 1997, farm loads increased phytoplankton biomass in the Huon Estuary in summer by about 25%, and that a quadrupling of loads could result in approximately a doubling of phytoplankton biomass.

At the end of the Huon Estuary Study, a number of open questions, with potentially important implications for impacts and management of fish farm loads, were identified. In particular, the Huon Estuary Study and modelling stopped at the mouth of the estuary, yet it was increasingly clear that the estuary and D'Entrecasteaux Channel are tightly coupled. As fish farm activity in D'Entrecasteaux Channel increased, it was recognized that the two needed to be studied and modelled as a single system. Uncertainty about the depth at which nutrient excreted by farmed fish is released was also shown to have a significant impact on predicted impacts on phytoplankton biomass. The biogeochemical model used to assess and predict impacts in the Huon Estuary Study was highly simplified. It could not realistically represent the role of sediments as a temporary or permanent sink for nutrients, a role likely to be important in mediating interactions between winter and summer nutrient loads. It included only one phytoplankton functional group, yet experience elsewhere, and observations in the Huon, suggested it could be important to distinguish different phytoplankton functional groups.

This chapter describes the application of a more complex and realistic biogeochemical model to the combined Huon / D'Entrecasteaux system, to address these questions, and provide an improved basis for understanding and managing nutrient loads into the system.

## *2 Biogeochemical Model description*

### **2.1 History**

The biogeochemical model applied here has evolved through a series of case studies including the Port Phillip Bay Environmental Study (Harris et al 1996; Murray & Parslow 1997), the National Land and Water Audit Estuaries Theme, the Gippsland Lakes Environmental Study (Parslow, et al., 2001), the Derwent Estuary ERA (Parslow et al., 2001), and the Ord-Bonaparte Study (Parslow et al., 2003). Each study addressed specific environments and ecological questions resulting in the development, implementation and testing of a diverse range of model components. In these previous studies the biogeochemical model was linked to a box model which represented physical transport with relatively low vertical and horizontal resolution (Walker, 1996). In this study the biogeochemical model has been restructured in modular form, with a software core linked to a central library of ecological processes.

With this structure the code has been incorporated into the CSIRO Environmental Modelling Suite (EMS) and dynamically linked/coupled to a high resolution 3D hydrodynamic model 'SHOC' (Herzfeld et al., 2005) and a multilayer sediment model (MECOSED Margvelashvili 2003). This is the first time the biogeochemical model has been directly coupled to a 3-D hydrodynamic model in an estuarine application, although this was done at continental shelf scales in the North-west Shelf Environmental Study (Herzfeld, et al., 2003). Biogeochemical dissolved tracers are advected and diffused in an identical fashion to physical tracers such as temperature and salinity and ecological particulate tracers sink and are resuspended by the same formulation as sediment particles. At each ecological time step, non-conservative ecological rate processes such as growth, nutrient uptake, grazing and mortality are integrated within the ecological module which returns updated tracer concentrations to the hydrodynamic model via an interface routine.

## 2.2 Model Components

The ecological model water column is organised in 3 'zones': pelagic, epibenthic and sediment. Depending on the grid formulation the pelagic zone may have one or several layers of similar or varying thickness. The epibenthic zone overlaps with the lowest pelagic layer and shares the same dissolved and suspended particulate material fields. The sediment is modelled in 2 layers with a thin layer of easily resuspendable material overlying a thicker layer of consolidated sediment.

Ecological processes are organised into the 3 zones with pelagic processes including phytoplankton and zooplankton growth and mortality, detritus remineralisation and fluxes of dissolved oxygen, nitrogen and phosphorous. Macroalgae and seagrass growth and mortality are included in the epibenthic zone whilst further phytoplankton mortality, microphytobenthos (benthic diatom) growth, detrital remineralisation and fluxes of dissolved substances are included in the sediment layer (figure 2.1).

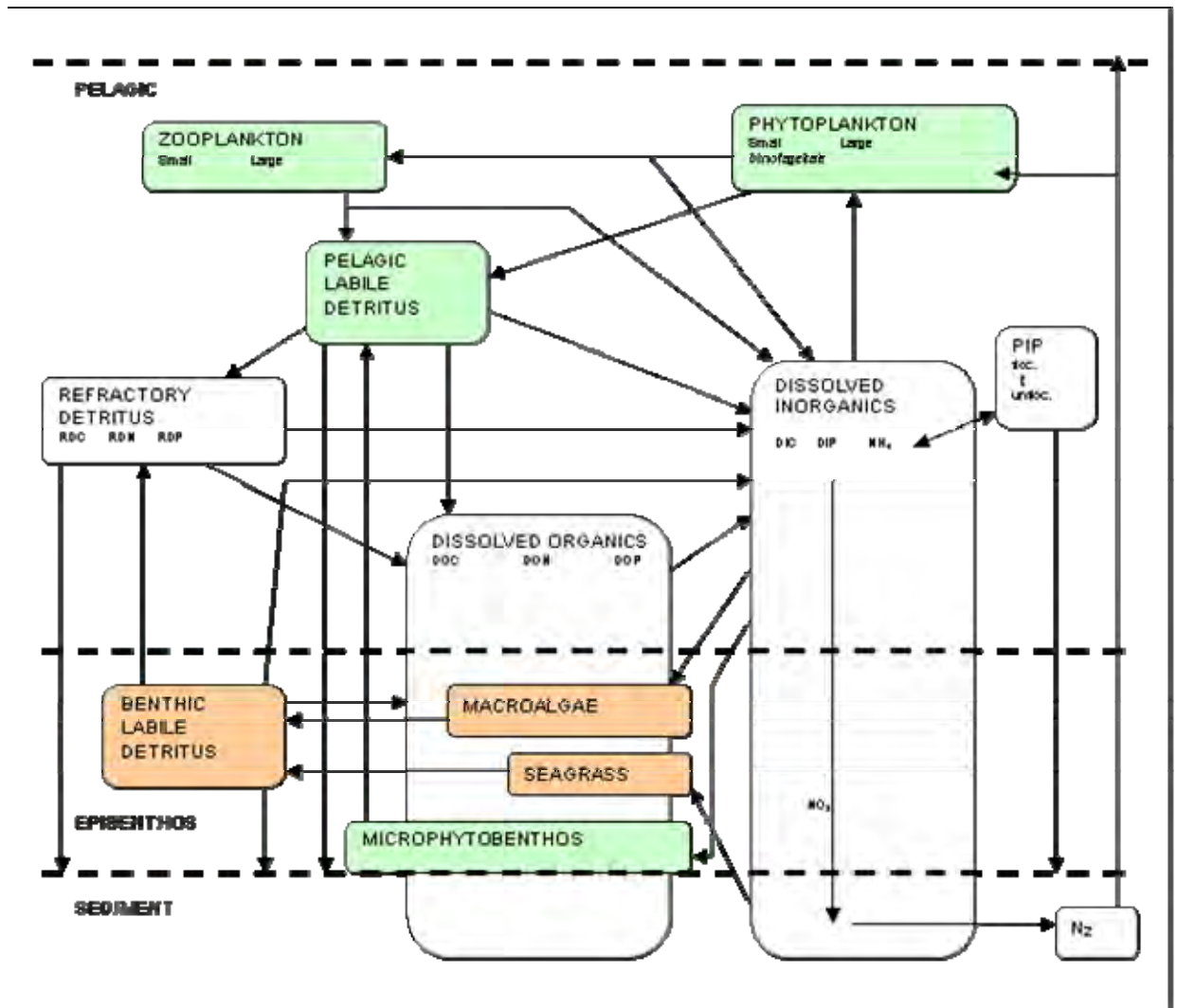


Figure 2.1: Schematic diagram of the biogeochemical model compartments, links and vertical layers. Green compartments have fixed nutrient content at Redfield ratio (106C:16N:1P); brown compartments are fixed at Atkinson ratio (550C:30N:1P).

### 2.3 Primary Production

There are 4 groups of microalgae and 2 macrophytes included in the model:

- ❖ 'Small phytoplankton' representing small flagellates, and photoautotrophic pico- and nano-plankton. These organisms are small, with relatively high growth rates and are typically neutrally buoyant. Their high surface area to volume ratio enables them to uptake nutrients efficiently, even at low concentration, which makes this group of phytoplankton ubiquitous throughout aquatic systems (Fogg 1991). Small phytoplankton are modelled with a fixed nutrient ratio of 106C:16N:1P (Redfield Ratio). The biomass of small phytoplankton is heavily constrained by grazing by tightly coupled small zooplankton. Natural mortality occurs when cells drift into the sediment layer.
- ❖ 'Large phytoplankton' represent diatoms with opportunistic ecological characteristics. They have a high growth rate which allows them to respond rapidly when nutrients and light are available, despite having a lower nutrient uptake efficiency and a tendency to sink out of the euphotic layer. Modelled large phytoplankton have a fixed nutrient ratio of 106C:16N:1P (Redfield Ratio). Large zooplankton graze on

large phytoplankton but their slower growth rate results in a lag in response time allowing bloom events to occur. Large phytoplankton which sink into the sediment layer are assumed to die.

- ❖ 'Dinoflagellates' represent large dinoflagellates with much slower growth rates than the large phytoplankton group. They are either neutrally buoyant or allowed to migrate vertically over a diurnal period to give access to both deep water nutrient and near surface light. To allow 'luxury' uptake and storage of nutrient, dinoflagellates are modelled with independent carbon and nitrogen pools. Large zooplankton graze on dinoflagellates but with a reduced food 'preference' compared with large phytoplankton. Dinoflagellates which sink or drift into the sediment layer are presumed to die.
- ❖ 'Microphytobenthos' are large cells representative of benthic diatoms. They have a high sinking rate and grow in the pelagic and sediment layers where there is sufficient light. In the sediment layer they have access to enhanced concentrations of regenerated nutrients. They are modelled with a fixed nutrient ratio of 106C:16N:1P (Redfield Ratio) and are grazed by large zooplankton when suspended.
- ❖ Seagrass grow in the epibenthic layer where there is sufficient light. They have a fixed carbon to nutrient ratio of 550C:30N:1P (Atkinson Ratio) and utilize nutrients directly from the sediment layer by uptake through their root system. Seagrass mortality occurs when there is insufficient light and/or nutrients to sustain growth in excess of metabolic/respiration requirements.
- ❖ Macroalgae in the model represent both macro- and epiphytic- algal groups that might co-exist with seagrass communities. They have a fixed nutrient ratio of 550N:30N:1P (Atkinson Ratio) and utilize nutrients from the pelagic water column by absorption across the frond surface. Macroalgae mortality occurs when there is insufficient light and/or nutrients to sustain growth in excess of metabolic/respiration requirements.

Modelled autotroph growth is determined by access to essential nutrients (nitrogen and phosphate) and photosynthetically active radiation (PAR) by the chemical reaction (CR) model of (Baird 1999). Dissolved nitrogen is present as ammonium and nitrate and autotrophs take up both equally. Phosphate and dissolved inorganic carbon are also taken up by phytoplankton at Redfield ratio (106C:16N:1P) and by macrophytes at Atkinson ratio (550C:30N:1P). Ambient photosynthetically active radiation (PAR) is calculated from incident surface 24 hour mean PAR attenuated by sea water, coloured dissolved organic substances (CDOM), organic and inorganic particles (optical parameters are shown in table 2.2). Phytoplankton chlorophyll concentration is calculated by assuming a fixed nitrogen to chlorophyll ratio of 7mgN/mgChl.

Parameter	Large Phytoplankton	Small Phytoplankton	Microphyto-benthos	Dino-flagellates	Sea Grass	Macro-algae
Radius (m)	1.0E-5	2.5E-6	1.0E-5	1.0E-5		
Bulk density (mgC m <sup>-3</sup> )	1.0E+9	1.0E+9	1.0E+9	1.0E+9		
Umax (/d)	2.0	1.25	1.35	0.4	0.1	0.02
Respired fraction of umax (-)	0.025	0.025	0.025	0.025	0.025	0.025
Absorption (/m)	30000.0	50000.0	100000.0	40000.0	1.0E-5 m2/mgN	0.001 m2/mgN
Stoichiometry coefficient of phosphorous					2.4E-6	2.4E-6
Mortality term (/d)	0.14	0.14	0.0003	0.14	0.00274	0.1
Half saturation constant for N uptake (mgN m <sup>-3</sup> )	N/A	N/A	N/A	N/A	5.0	
Half saturation constant for P uptake (mgP m <sup>-3</sup> )	N/A	N/A	N/A	N/A	5.0	
Sinking (m/s)	-5.6E-6	0.0	-5.79E-5	diurnal migration	N/A	N/A

Table 2.1: Characteristics of primary producers included in the model.

Parameter	Value
Background attenuation of sea water	0.1
CDOM attenuation coefficient of fresh water (/m)	4.4
Detrital specific attenuation coefficient (/m/mgN m <sup>-3</sup> )	0.0038
TSS specific attenuation coefficient (/m/kg m <sup>-3</sup> )	30.0
Dissolved organic nitrogen specific attenuation coefficient (/m/mgN m <sup>-3</sup> )	0.0009

Table 2.2: Optical parameters.

## 2.4 Secondary Production

There are 2 groups of zooplankton included in the model:

- ❖ 'Small zooplankton' represent microzooplankton less than 200um in size such as zooflagellates, *Tintinnids*, *Ciliates*, *Rotifers*, small copepod nauplii and polychaete larvae. They are mobile, feed on small phytoplankton and have rapid turnover rates. They are modelled with a fixed nutrient ratio of 106C:16N:1P (Redfield Ratio) and grow as a function of maximum specific growth rate and grazing rate. Grazing success depends on the food encounter rate which in turn is based on zooplankton swimming speed, food size and density. Inefficient feeding and excretion returns dissolved and particulate material to the water column at Redfield ratio. A quadratic mortality term is applied to

account for both natural mortality and predation and is the closure term for the models biogeochemical cycling.

- ❖ 'Large Zooplankton' represent mesozooplankton such as copepods and small fish larvae. They are mobile, feed on large phytoplankton, microphytobenthos and with reduced preference on dinoflagellates. They are modelled with a fixed carbon to nutrient ratio of 106C:16N:1P (Redfield Ratio) and have a lower maximum specific growth rate compared with the small zooplankton which results in a lag between enhanced primary and secondary production. Grazing success is a function of food encounter rate and inefficient feeding and excretion returns dissolved and particulate material to the water column at Redfield ratio. Natural mortality and predation of large zooplankton are represented by a quadratic mortality term which is the closure term for the models biogeochemical cycling.

Parameter	Small Zooplankton	Large Zooplankton
Radius (m)	12.5E-6	5.0E-4
Growth efficiency (-)	0.38	0.38
Maximum growth rate at 15°C (/d)	3.0	0.1
Swimming velocity (m)	2.0E-4	2.0E-3
Grazing technique (-)	Rect	Rect
Fraction of growth inefficiency lost to detritus (-)	0.5	0.5
Mortality (quadratic) rate (/d/mgN m <sup>-3</sup> )	0.02	0.0004
Fraction of mortality lost to detritus (-)	0.5	0.5

Table 2.3: Characteristics of secondary producers included in the model.

## 2.5 Detritus and nutrient pools

There are 3 types of particulate detritus and 2 pools of dissolved substances included in the model:

- ❖ 'Pelagic labile detritus' represents fresh detritus which is rapidly broken down by bacteria, viruses and fungi into refractory detritus, dissolved organic and dissolved inorganic substances on the timescale of about a week. It is modelled with a fixed carbon to nutrient ratio of 106C:16N:1P (Redfield Ratio) and generated by inefficient feeding and excretion of large and small zooplankton, and by mortality of phytoplankton and zooplankton. Detrital particles contribute to the attenuation of light, sink and enter the sediment layer where remineralisation processes continue.
- ❖ 'Benthic labile detritus' is similar to pelagic labile detritus but has a fixed carbon to nutrient ratio of 550N:30N:1P (Atkinson Ratio). It is generated by mortality of seagrass and macrophytes. Particles contribute to the attenuation of light, sink and enter the sediment layer where remineralisation processes continue.
- ❖ Refractory detritus represents older detrital material with lower nutrient to carbon content and slower remineralisation time scales of about a year. Refractory material is generated by the breakdown of pelagic and benthic labile detritus (with contrasting carbon to nutrient ratios) which necessitates modelling the carbon, nitrogen and phosphorus components independently. Refractory detrital material is remineralised to dissolved organic and inorganic substances. Particles

contribute to the attenuation of light, sinks and enter the sediment layer where remineralisation processes continue.

- ❖ Dissolved organic material is considered to be a pool of very refractory nature with very slow remineralisation time scales of about two years. Dissolved organic material is generated by remineralisation of pelagic and benthic labile detritus and refractory detritus and is modelled as independent carbon, nitrogen and phosphorus components. This material is remineralised by bacterial and chemical reaction to dissolved inorganic carbon, nitrogen and phosphorus. Enhanced concentrations of detritus in the sediment give rise to gradients in dissolved organic matter which diffuse into the pelagic layer.
- ❖ Dissolved inorganic material is modelled as independent carbon, nitrogen and phosphorous pools. It is generated through inefficient feeding and excretion of zooplankton and by remineralisation of pelagic and benthic labile detritus, refractory detritus and dissolved organic material. These transformations release nitrogen in the form of ammonium which depending on available oxygen, can undergo nitrification to nitrate and denitrification to nitrogen gas, which is then lost to the atmosphere. Dissolved inorganic phosphorous can be adsorbed onto, or desorbed from, suspended sediment particles, which in turn may flocculate into larger particles with different sinking characteristics. Adsorption of phosphorous onto sediment particles limits its availability for algal uptake and growth. Accumulation of labile and refractory detritus in the sediment leads to gradients in dissolved inorganic carbon and nutrient which diffuse back into the pelagic layer at rates enhanced by bio-irrigation. Dissolved inorganic nutrients are the final stage in the recycling process of organic material back into substrate available for algal uptake and growth.

<b>Parameter</b>	<b>Value</b>	<b>Unit</b>
Pelagic labile detritus breakdown rate	0.1	/d
Refractory detritus breakdown rate	0.0036	/d
Dissolved organic matter breakdown rate	0.00176	/d
Fraction of labile detritus converted to DOM	0.01	-
Fraction of labile detritus converted to refractory detritus	0.19	-
Fraction of refractory detritus converted to DOM	0.05	-
DON specific attenuation coefficient	0.0009	/m
Detrital nitrogen specific attenuation coefficient	0.0038	/m
Maximum water column nitrification rate	0.1	/d
Maximum sediment nitrification rate	20.0	/d
Maximum nitrification efficiency	1.0	-
O2 half saturation rate for nitrification	1000.0	mg O m <sup>-3</sup>
Maximum denitrification rate	40.0	/d
O2 content at 50% denitrification rate	4000.0	mg O m <sup>-3</sup>
O2 half saturation rate for aerobic respiration	500.0	mg O m <sup>-3</sup>

*Table 2.4: Modelled detritus parameter values and associated remineralisation rates.*

## 2.6 Dissolved oxygen

The concentration of dissolved oxygen in the model varies with atmospheric exchange at the sea surface, photosynthetic production and respiration of primary producers, respiration of secondary producers and utilization during remineralisation processes. Surface waters are typically oxygen rich, whilst deeper waters and the sediment layer may become depleted in oxygen depending on vertical mixing and flushing of the sediment.

## 3 Hydrodynamical Model and Grid

The hydrodynamical model is described in (Herzfeld et al., 2005). For coupling with the ecological and sediment modules a coarse grid version was implemented (Herzfeld et al., 2005) to achieve an acceptable run time ratio of >100:1. Biogeochemical model tracers are advected and diffused through the 3D flow field in an analogous fashion to temperature and salinity. Tracers with a sinking (or swimming velocity) are passed to the sediment module (Margvelashvili 2003) for vertical displacement. The hydrodynamical model is calculated with a 2D time step of 6 minutes and a 3D time step of 2 hours for accurate representation of physical processes. Biological processes are evaluated using a 5<sup>th</sup> order adaptive integration scheme.

## 4 Initialisation

The biogeochemical model is initialized in December 2001 with tracer concentrations derived (where possible) from observations made throughout the region. Where suitable observations were unavailable historical data and literature values were used. Initialising a model in mid summer is more difficult as most biogeochemical tracers have strong vertical gradients associated with gradients in light, nutrients and mixing. To obtain the initialization fields at the required high vertical resolution, sparse nutrient and biomass observations were interpolated vertically and weighted against profiles of density structure. This gave the initialization field some vertical structure, although at best, gave a crude representation of the real depth of any nutricline and/or subsurface biomass feature. Results from the first month of the simulation should therefore be disregarded as during this period the model is adjusting internally to bring the initialization fields into balance.

### 4.1 Dissolved inorganic material

Nutrient concentrations for nitrate (sum of nitrate and nitrite), ammonium and phosphate were obtained from observations made in surface and bottom waters at 12 stations throughout the D'Entrecasteaux Channel (Thompson ref earlier chapter) on 5 Jan 2002. These data were interpolated horizontally and vertically weighted against observed profiles of density structure. Concentrations of phosphate adsorbed onto flocculated and unflocculated particles had not been observed and were initialized at spatially uniform concentrations of  $1\text{mgP m}^{-3}$  and  $0\text{mgP m}^{-3}$  respectively in the water column and  $5000\text{mgP m}^{-3}$  and  $100\text{mgP m}^{-3}$  respectively in the sediment. Immobilised

particulate inorganic phosphate was initialized as zero. Dissolved inorganic carbon was initialized as  $2.4E4\text{mgC m}^{-3}$  throughout the model domain.

## 4.2 Biomass

Phytoplankton biomass was estimated from phytoplankton counts made from integrated surface layer water samples collected at 12 stations throughout the D'Entrecasteaux Channel on 5 January 2002. Phytoplankton samples were counted and identified (see methods section in earlier chapter) and then converted to biovolumes by assuming a mean size for each species of phytoplankton from previous observations (HES study, literature values and personal communication). Biovolumes were then summed for each model compartment so that 'large phytoplankton' contained mostly diatoms, 'small phytoplankton' mostly flagellates and 'dinoflagellates' contained large dinoflagellates. Observed chlorophyll concentrations were then partitioned between the relative fractions of each algal group and translated to nitrogen biomass assuming a fixed nitrogen:chlorophyll ratio of 7.0 mgN/mgChl. For the dinoflagellate compartment the carbon concentration was calculated by assuming a fixed ratio of 106C:16N. Surface and bottom values of phytoplankton biomass were then interpolated vertically and weighted against the observed profile of density.

No observations of microphytobenthos were available to initialize the model so they were set as a spatially uniform  $700\text{mgN m}^{-3}$  in the sediment and  $0.3\text{mgN m}^{-3}$  in the water column. Similarly the biomass of small and large zooplankton was unknown and these were initialized at spatially uniform concentrations of  $15\text{mgN m}^{-3}$  and  $2\text{mgN m}^{-3}$  respectively in the water column.

Seagrass and macroalgae grow along the periphery of the coast and in shallow inlets and bays throughout the region where favourable substrate exists. No comprehensive data set was available to map onto the model grid which poorly resolves much of the coastal fringe. Seagrass and macroalgae were therefore initialized as  $100\text{mgN m}^{-2}$  and  $500\text{mgN m}^{-2}$  respectively and allowed to evolve in the model system.

## 4.3 Detritus

Few observations of detritus have been made in the region. The model was therefore initialized with horizontally and vertically uniform concentrations of detritus and dissolved organic substances (listed in table 4.1) and allowed to evolve.

Substance	Initial water column concentration	Initial Sediment concentration
Pelagic labile detritus mgN m <sup>-3</sup>	2.0	200
Benthic labile detritus mgN m <sup>-3</sup>	0.0	200
Refractory detrital carbon mgC m <sup>-3</sup>	50.0	8.0E4
Refractory detrital nitrogen mgN m <sup>-3</sup>	5.0	8.0E3
Refractory detrital phosphorous mgP m <sup>-3</sup>	0.7	1.1E3
Dissolved organic carbon mgC m <sup>-3</sup>	1.5E3	0.0
Dissolved organic nitrogen mgN m <sup>-3</sup>	150.0	500.0
Dissolved organic phosphorous mgP m <sup>-3</sup>	20.0	0.0

*Table 4.1: Spatially and depth uniform initialisation field for detritus and dissolved organic material.*

## 5 Forcing Data

### 5.1 Photosynthetically active radiation

Incident sea surface PAR is supplied as a time series of daily averaged values. The data are obtained by taking a 24 hour mean of the short wave radiation supplied to the hydrodynamical model (detailed in section 6.2) and applying a factor 0.43 to convert total short wave solar radiation to PAR (eg. Tett 1990). Fluctuations in daily insolation were derived from variations in cloud cover as observed at Hobart airport. Comparison of calculated and observed surface PAR are shown in figure 5.1.

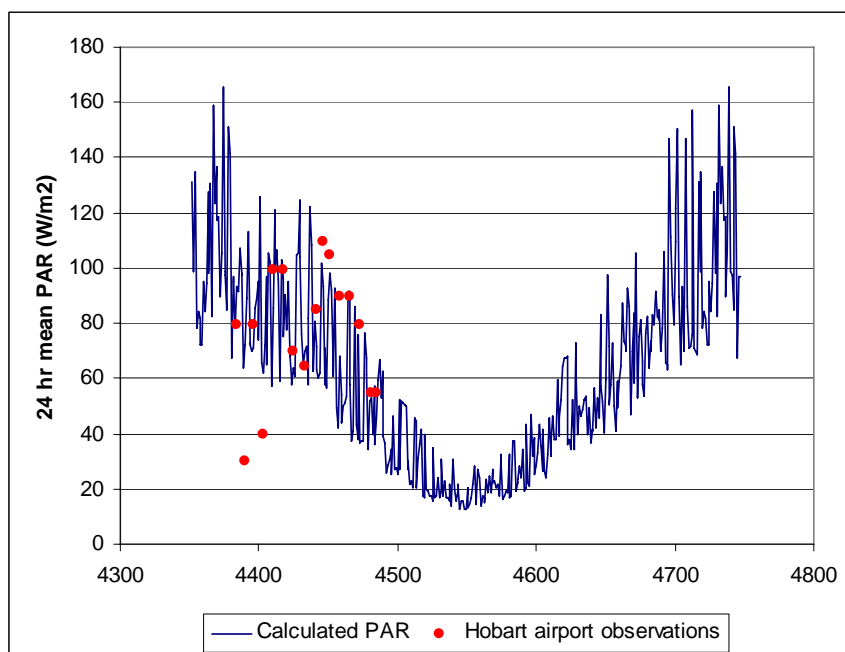


Figure 5.1: Calculated incident sea surface PAR (blue), and observations (red) from Hobart airport.

## 5.2 Rivers

There are 4 major rivers and more than 36 smaller rivers, creeks and streams draining into the region. Of the major rivers the Huon had by far the largest annual discharge ( $3.8E09$  m<sup>3</sup> in 2002) whilst the Esperance discharge was only 4% of this and Northwest Bay and Kermadie rivers just 1% of the Huon discharge. The numerous smaller rivers, creeks and streams have comparatively trivial flows and were not included in the model. For the biogeochemical model it was deemed necessary to include the additional discharges of the Kermadie River, Esperance River and Northwest Bay Rivulet. Whilst their flow rates are comparatively small with respect to the Huon and have little impact on the hydrodynamics, the dissolved and particulate nutrient loads from these rivers are significant. The Huon River is specified as an open boundary condition, however as the flows associated with the other rivers are much smaller they are more reliably simulated as point source discharges.

Seasonal variations in river loads of key biogeochemical tracers are poorly known and there is a paucity of data for all rivers in the region. Where possible data for 2002 are used but in general values have been estimated from literature and observations in other years. It was not possible to resolve seasonal fluctuations in tracer concentrations and annual mean values were estimated for all rivers. The limitations in current monitoring of catchment loads represent a significant handicap for attempts to assess or predict the response of the Huon / D'Entrecasteaux system to changing terrestrial and marine loads. We return to this point in the Discussion.

<b>Substance</b>	<b>Huon</b>	<b>Esperance</b>	<b>Kermandie</b>	<b>NW Bay</b>
<b>flow m<sup>3</sup>/y</b>	3.8E+09	1.5E+08	6.0E+07	2.2E+07
<b>unfloculated total suspended solid kg m<sup>-3</sup></b>	0.0035	0.0035	0.0120	0.0450
<b>Dissolved inorganic phosphate mgP m<sup>-3</sup></b>	2.1	1.2	15.2	13.6
<b>Ammonia mgN m<sup>-3</sup></b>	6.1	5.2	131.2	60
<b>Nitrate mgN m<sup>-3</sup></b>	13.6	5.3	150.2	171
<b>unfloculated particulate inorganic phosphate mgP m<sup>-3</sup></b>	0.6	1.1	45.3	20.6
<b>Large phytoplankton nitrogen mgN m<sup>-3</sup></b>	0.01	0.01	0.01	0.01
<b>Small phytoplankton nitrogen mgN m<sup>-3</sup></b>	0.01	0.01	0.01	0.01
<b>Dinoflagellate nitrogen mgN m<sup>-3</sup></b>	0.001	0.001	0.001	0.001
<b>dinoflagellate carbon mgC m<sup>-3</sup></b>	0.001	0.01	0.01	0.01
<b>pelagic labile detritus mgN m<sup>-3</sup></b>	1.0	0.0	2.4	0.0
<b>Benthic labile detritus mgN m<sup>-3</sup></b>	0.0	16.6	0.0	34.4
<b>small zooplankton nitrogen mgN m<sup>-3</sup></b>	0.001	0.001	0.001	0.001
<b>large zooplankton nitrogen mgN m<sup>-3</sup></b>	0.001	0.001	0.001	0.001
<b>dissolved organic carbon mgC m<sup>-3</sup></b>	3782.8	3210.0	2721.0	3606.0
<b>dissolved organic nitrogen mgN m<sup>-3</sup></b>	237.0	201.0	170.0	225.4
<b>dissolved organic phosphate mgP m<sup>-3</sup></b>	35.7	3.1	6.8	7.7
<b>refractory detrital carbon mgC m<sup>-3</sup></b>	796.7	497.0	1138.0	1100.0
<b>refractory detrital nitrogen mgN m<sup>-3</sup></b>	49.2	31.0	71.0	68.8
<b>refractory detrital phosphate mgP m<sup>-3</sup></b>	7.5	1.9	4.5	2.3

*Table 5.1: Annual mean concentrations of modelled substances in rivers discharging into the model.*

<b>Substance</b>	<b>Huon</b>	<b>Esperance</b>	<b>Kermandie</b>	<b>NW Bay</b>
<b>flow m<sup>3</sup>/y</b>	3.8E+09	1.5E+08	6.0E+07	2.2E+07
<b>unflocculated total suspended solid t/y</b>	13.18	0.53	0.72	0.97
<b>dissolved inorganic phosphate kgP/y</b>	7906.2	180.7	915.6	294.3
<b>Ammonia kgN/y</b>	22965.7	783.1	7903.2	1298.5
<b>Nitrate kgN/y</b>	51202.2	798.2	9047.7	3700.6
<b>unflocculated particulate inorganic phosphate kgP/y</b>	2258.9	165.7	2728.8	445.8
<b>large phytoplankton nitrogen kgN/y</b>	37.65	1.51	0.60	0.22
<b>small phytoplankton nitrogen kgN/y</b>	37.65	1.51	0.60	0.22
<b>dinoflagellate nitrogen kgN/y</b>	3.76	0.15	0.06	0.02
<b>dinoflagellate carbon kgC/y</b>	3.76	1.51	0.60	0.22
<b>pelagic labile detritus kgN/y</b>	3764.9	0.0	144.6	0.0
<b>benthic labile detritus kgN/y</b>	0.0	2499.9	0.0	744.5
<b>small zooplankton nitrogen kgN/y</b>	3.76	0.15	0.06	0.02
<b>large zooplankton nitrogen kgN/y</b>	3.76	0.15	0.06	0.02
<b>dissolved organic carbon kgC/y</b>	14241561.0	483409.0	163907.3	78037.7
<b>dissolved organic nitrogen kgN/y</b>	892238.0	30269.5	10240.4	4877.9
<b>dissolved organic phosphate kgP/y</b>	134354.3	459.3	407.2	166.6
<b>refractory detrital carbon kgC/y</b>	2999571.7	74845.6	68550.7	23805.2
<b>refractory detrital nitrogen kgN/y</b>	185099.1	4668.4	4276.9	1488.9
<b>refractory detrital phosphate kgP/y</b>	28297.8	286.1	268.1	49.8

*Table 5.2: Annual load of model substances discharged from rivers entering the model domain.*

### Huon River

Flow data for the Huon were kindly supplied by the Department of Primary Industries, Water and Environment (DPIWE) and described in the earlier chapter on the hydrodynamical model.

Load estimates were derived using concentration values suggested by SERM, observations made by DPIWE and data collected during the HES (CSIRO, 2000). Observations made in the Mountain River, which joins the Huon upstream of Huonville, were included in the assessment. No data were available for 2002 and it was assumed that tracer concentrations in 2002 were similar to more recent observation made in 2003 and 2004.

### Esperance River

Flow data for the Esperance river were not available for 2002. Data collected between 1983 and 1993 were regressed on Huon flow for the same period and found to vary consistently, presumably due to similar rainfall in the 2 regions. As the Esperance catchment area is considerably smaller than that of the Huon, Esperance flow rate could be approximated as  $0.04 * \text{Huon flow rate}$ .

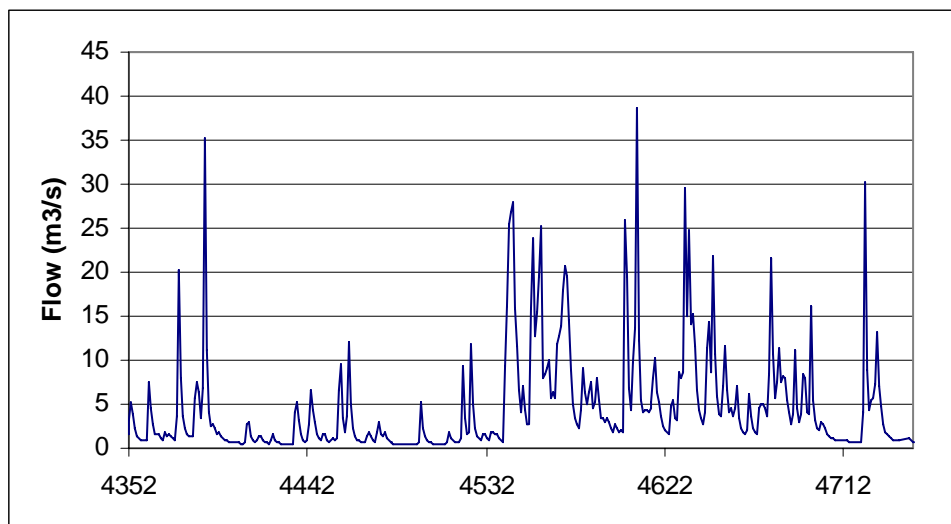


Figure 5.2: Esperance River flow estimated for 2003.

Load data were derived from values suggested by SERM using catchment clearance values suggested by OZ Estuaries, observations made by DPIWE and relationships between parameters observed during the HES.

### Kermandie River

Flow data for the Kermandie were estimated as  $7.1 * \text{flow at Riley's Creek Gauging Station}$  (as in HES study). Data were not available for 2003 but observations made between 1987 and 1989 were scaled against Huon river flow and found to approximate to  $0.0097 * \text{the Huon river flow}$ . This relationship was then used to estimate river flows in 2003.

Load data were derived from observations made by DPIWE between 1996-97 and during the HES study. No data were available for 2002. Nutrient concentrations reported by DPIWE were considerably higher than those reported during the HES study and the values were difficult to reconcile, possibly due to the variable discharge of a sewerage treatment plant operating at the mouth of the river. The load data estimated for 2003 relied

more heavily on observations made during HES which provided a more conservative estimate of nutrient discharge from the river.

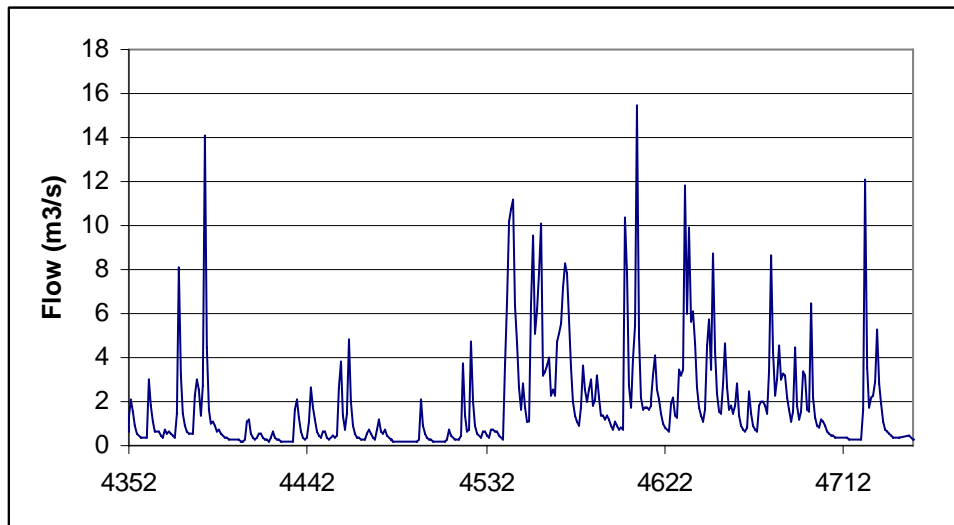


Figure 5.3: Kermadie River flow estimated for 2002.

#### Northwest Bay River

Flow data for the Northwest Bay River were estimated in the same way as for the Northwest Bay Environmental Study. This lagged rainfall data collected at Longley (on the side of Mount Wellington) and scaled the rainfall by a factor of 0.39.

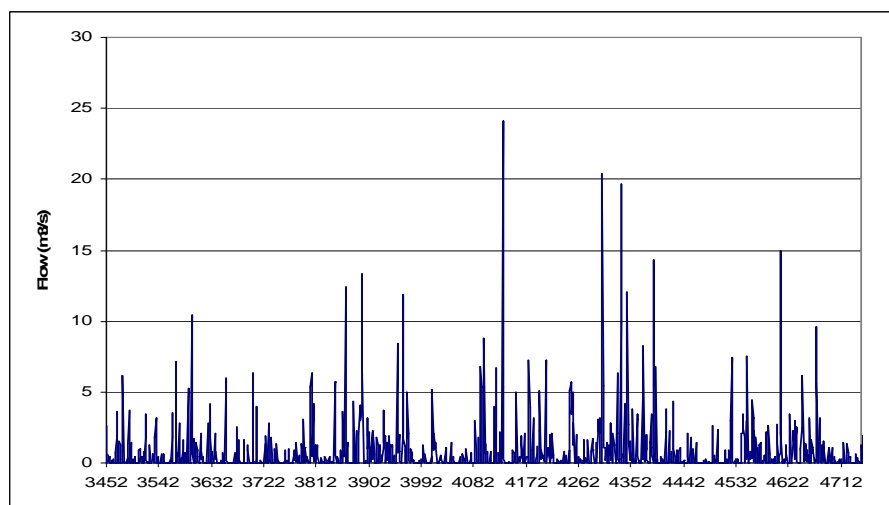


Figure 5.4: Estimated flow for Northwest Bay River in 2003.

Tracer concentrations were estimated from assumptions used in the SERM model and observations made during the Northwest Bay Environmental Study in 1997-98 and Olive (1973). No data were available for 2002.

		Huon	Esperance	Kermandie	NW Bay
<b>Total Nitrogen</b>	<b>tN/y</b>	1155.4	39.0	31.6	12.1
<b>Total Dissolved Nitrogen</b>	<b>tN/y</b>	966.4	31.9	27.2	9.9
<b>Total Particulate Nitrogen</b>	<b>tN/y</b>	189.0	7.2	4.4	2.2
<b>Total Phosphate</b>	<b>tP/y</b>	173.3	1.3	4.3	1.0
<b>Total Dissolved Phosphate</b>	<b>tP/y</b>	142.3	0.6	1.3	0.5
<b>Total Particulate Phosphate</b>	<b>tP/y</b>	31.1	0.6	3.0	0.6

Table 5.3: Summary statistics of nutrient loads discharged from rivers into the model domain.

### 5.3 Marine boundaries

There are 2 marine open boundaries in the model domain at the southern and northern ends of the D'Entrecasteaux Channel. Both boundaries have no gradient boundary conditions supplied for the majority of biogeochemical tracers. This assumes that water entering the model domain has the same concentrations as that leaving the model. The exceptions to this are inorganic nutrients, oxygen and phytoplankton biomass which are specified as an upstream condition. With this formulation, concentrations of dissolved and particulate substances flow out of the model at the simulated concentration but flow into the model only at values specified in a time series data file.

Time series of vertical profiles of phytoplankton biomass and dissolved inorganic nutrient are derived from phytoplankton, chlorophyll, nutrient and dissolved oxygen observations made at monthly intervals throughout the year at stations 1 and 12 (Thompson 2005). These observations are interpolated vertically against profiles of density to give high resolution vertical profiles of concentration. At each time step the model linearly interpolates in time between the observed (monthly) profiles to provide a suitable profile for the model time. In the model simulation incorporating dinoflagellate diel vertical migration, the time series of dinoflagellate carbon and nitrogen biomass was specified every 12 hours to reproduce the simulated depth distribution of alternating aggregations of biomass at depth and close to the surface.

## 6 Anthropogenic Inputs

### 6.1 Sewerage and wastewater

In general the region is sparsely populated, there are however several small towns of note including Margate, Huonville and Dover with local STP facilities. During the HES sewerage discharge at Ranelagh Treatment Plant corresponded to ~10gN/person/d for about 2000 people and totalled ~7tN/y. This input is 2 orders of magnitude smaller than annual river nitrogen input and a similarly small fraction of fin-fish farm nutrient discharge. In the context of regional nutrient input sewerage and wastewater discharge is generally

small and diffuse along the coast and for this reason it has not been included in the model.

## 6.2 Fin-fish Farm Discharges

In 2002 there were 20 salmonid farms operating in the region (DPIWE). Each farm supplied various concentrations of pelleted food to their caged fish and discharged waste material in the form of uneaten feed pellets, fish urea and faeces. We thank Tassal Limited, Huon Aquaculture Limited, Aquatas, Nortas Salmonid Products and Seafarms, who all operate farms in the region, and supplied feed data, and Skretting, who supplied information on feed composition.

Assuming that all feed pellets are consumed by the fish and that no overfeeding occurs then 5% and 0.8% of the total feed is discharged by the fish as waste nitrogen and phosphorous respectively. For nitrogen 85% is assumed to be dissolved in the form of ammonia and 15% as particulate labile detritus. The phosphorus is partitioned between particulate labile detritus (at a fixed Redfield ratio of 16N:1P) and dissolved inorganic phosphorus. Waste material is discharged at the farm sites as a point source discharge evenly distributed between 0.5 m and 12 m (or less where the site is located in shallower water) and diffused spatially throughout the grid cell in which the farm is located.

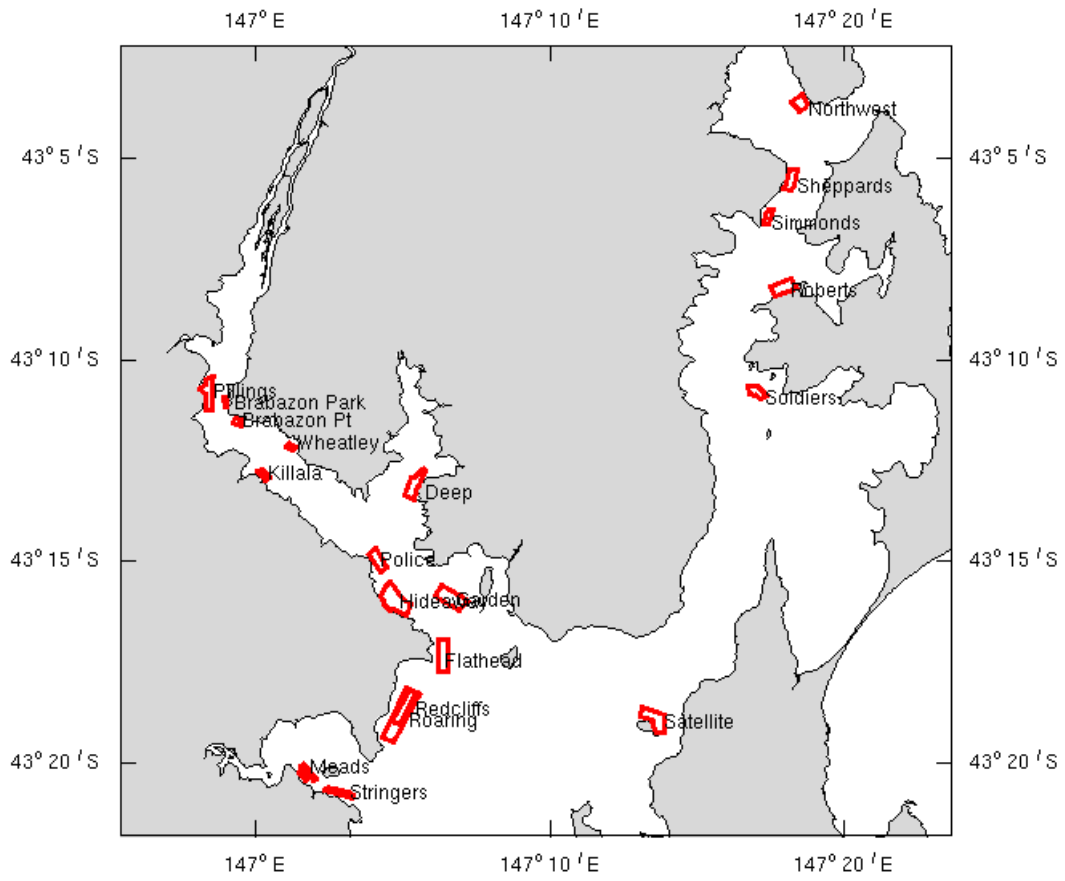


Figure 6.1: Location of farm sites.

<b>Site</b>	<b>Longitude</b>	<b>Latitude</b>	<b>Depth (m)</b>
<b>Pillings Brabazon Park</b>	146.976	-43.178	13.0
<b>Brabazon Pt</b>	146.981	-43.183	11.7
<b>Pt</b>	146.990	-43.191	13.4
<b>Killala</b>	147.008	-43.213	19.3
<b>Wheatley</b>	147.019	-43.202	13.3
<b>Deep</b>	147.090	-43.219	11.5
<b>Police</b>	147.067	-43.246	24.0
<b>Hideaway</b>	147.075	-43.265	12.7
<b>Garden</b>	147.115	-43.264	28.0
<b>Redcliffs</b>	147.092	-43.308	23.9
<b>Roaring</b>	147.085	-43.317	24.0
<b>Stringers</b>	147.051	-43.349	9.7
<b>Meads</b>	147.030	-43.336	13.2
<b>Roberts</b>	147.294	-43.133	16.9
<b>Soldiers</b>	147.286	-43.177	11.7
<b>Flathead</b>	147.109	-43.288	32.0
<b>Satellite</b>	147.230	-43.314	5.9
<b>Northwest</b>	147.312	-43.061	12.0
<b>Sheppards</b>	147.302	-43.087	12.0
<b>Simmonds</b>	147.288	-43.111	12.0

*Table 6.1: Farm site locations and (model) depth of water.*

Farm Site	TN tN/y	TDN tN/y	TPN tN/y	TP tP/y	TDP tP/y	TPP tP/y
<b>Brazbon Pk</b>	10.02	8.59	1.43	1.74	0.82	0.93
<b>Brazbon Pt</b>	15.98	13.69	2.28	2.78	1.30	1.48
<b>Deep</b>	41.16	35.28	5.88	7.16	3.36	3.80
<b>Flathead</b>	13.72	11.76	1.96	2.39	1.12	1.27
<b>Garden</b>	75.54	64.75	10.79	13.15	6.17	6.98
<b>Hideway</b>	71.60	61.37	10.23	11.81	5.50	6.31
<b>Killala</b>	28.88	24.76	4.13	5.03	2.36	2.67
<b>Pillings</b>	34.84	29.86	4.98	6.06	2.84	3.22
<b>Police</b>	5.16	4.42	0.74	0.90	0.42	0.48
<b>Wheatleys</b>	15.91	13.64	2.27	2.77	1.30	1.47
<b>Total Huon</b>	312.81	268.12	44.69	53.79	25.19	28.60
<b>Meads</b>	15.77	13.52	2.25	2.74	1.29	1.46
<b>Northwest</b>	71.05	60.90	10.15	12.37	5.80	6.57
<b>Redcliffs</b>	96.59	82.79	13.80	16.81	7.88	8.93
<b>Roaring</b>	56.33	48.28	8.05	9.80	4.60	5.21
<b>Roberts</b>	87.15	74.70	12.45	15.17	7.11	8.05
<b>Satellite</b>	0.01	0.01	0.00	0.00	0.00	0.00
<b>Sheppards</b>	71.05	60.90	10.15	12.37	5.80	6.57
<b>Simmonds</b>	35.52	30.45	5.07	6.18	2.90	3.28
<b>Soldiers</b>	38.63	33.11	5.52	6.72	3.15	3.57
<b>Stringers</b>	58.05	49.76	8.29	10.10	4.74	5.36
<b>Total Channel</b>	530.15	454.41	75.74	92.27	43.28	49.00
<b>Total Farms</b>	<b>842.96</b>	<b>722.54</b>	<b>120.42</b>	<b>146.06</b>	<b>68.47</b>	<b>77.60</b>

*Table 6.2: Annual dissolved and particulate nitrogen and phosphate discharges from fish farms in the region for 2002.*

The maximum monthly farm discharge occurred in October and nitrogen discharged from farms exceeded river inputs through summer and autumn (figure 6.2). During this period near surface flux of nutrients into the region across the marine boundary is also small due to seasonal stratification and so farm discharges dominate the surface nutrient flux throughout the region.

Waste material discharged from the farm sites enters the biogeochemical model as ammonium which is readily assimilated into algal growth, and labile detrital particles which can be rapidly remineralised to dissolved inorganic nutrient. The flux of nutrients entering the model from the river discharge is dominated by refractory dissolved and particulate material which is remineralised very slowly to inorganic nutrient. Comparing these 2 sources of dissolved inorganic nitrogen the farm loads exceed the river loads by >7 times and for labile particulate detritus by >17 times (figure 6.3).

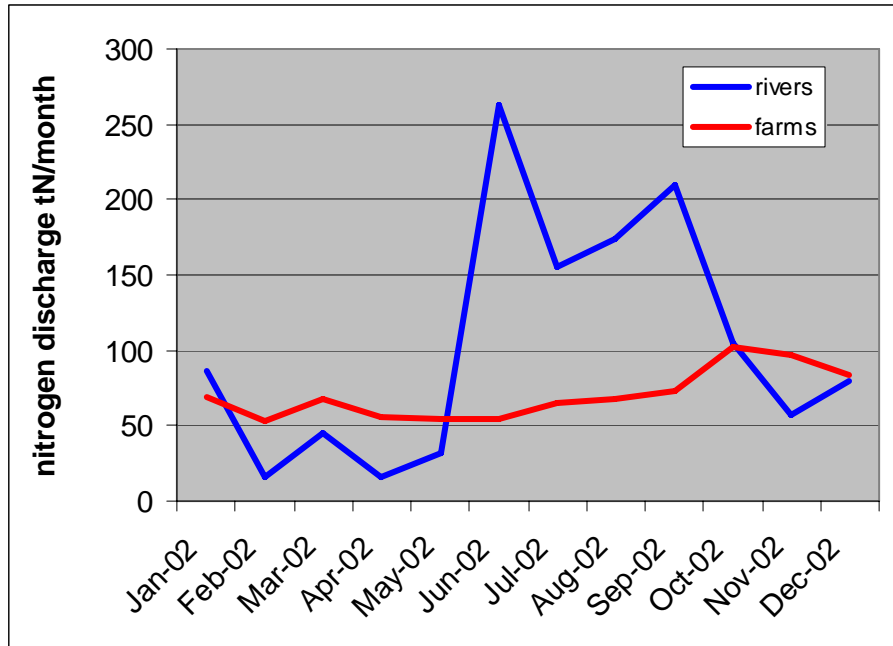


Figure 6.2: Monthly nitrogen input into the model domain for the sum of all farm sites and the sum of the Huon, Kermandie, Esperance and Northwest Bay rivers in 2002.

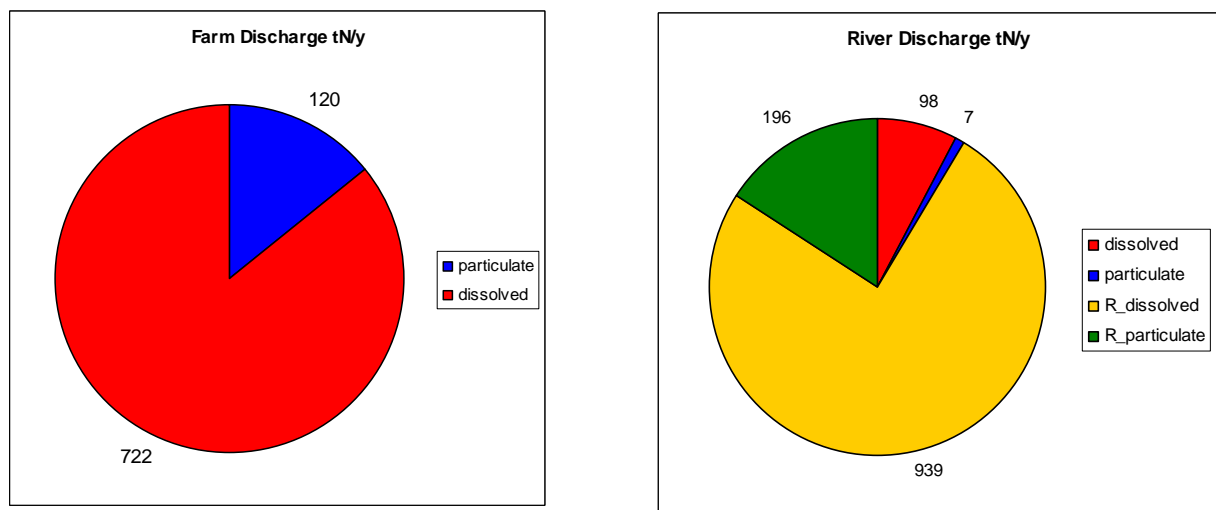


Figure 6.3: Composition of nitrogen component of (a) the farm discharge and (b) the river discharge. Values indicate tones nitrogen per year.

## 7 Model Calibration against observations

The model was compared with data collected during the system wide monitoring program (Thompson 2005). Broadly this consisted of monthly data collected at 12 stations in the D'Entrecasteaux Channel and 4 stations in the Huon Estuary for nutrients (ammonia, nitrate and phosphate), dissolved oxygen, chlorophyll and phytoplankton species. [The time series of data collected at Channel stations 1 and 12, at the northern and southern ends of the D'Entrecasteaux Channel respectively, were used to prescribe

concentrations of nutrients, oxygen and phytoplankton biomass entering the model domain at the northern and southern model boundaries.] Additionally, bottom water temperature, salinity and oxygen were recorded continuously at 3 sites in the Huon estuary for the latter part of 2002 (Thompson 2005). It was not possible to verify the model predictions of seagrass, macroalgae or zooplankton due to absence of observed data. Simulated biomass of these components, whilst consistent with our understanding of the model system, should be treated with extreme caution until verification against observations is demonstrated.

## 7.1 Nutrients

Observations of ammonia, dissolved inorganic nitrate and phosphate made in surface and bottom waters at stations throughout the region (see Thompson, 2005 for methods) were compared with model output.

### Nutrients in the D'Entrecasteaux Channel

Nutrient concentrations in the channel have a distinct seasonal cycle with elevated surface concentrations in winter and reduced (frequently to near zero in the case of nitrogen), concentrations at other times of the year. A similar cycle is evident in bottom waters particularly in the shallower northern end of the channel. In the deeper southern part of the channel elevated winter concentrations prevail for longer as they are isolated from the surface waters by stratification. Variations in deep water nutrient concentration at the southern boundary appear to relate to fluctuations in the nutrient concentration of shelf waters advected into the channel.

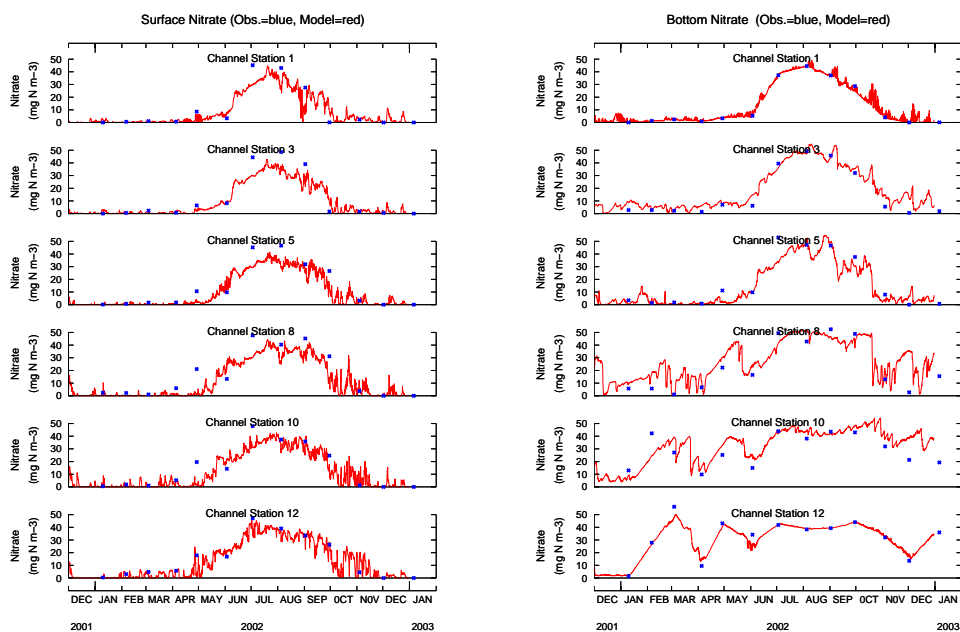
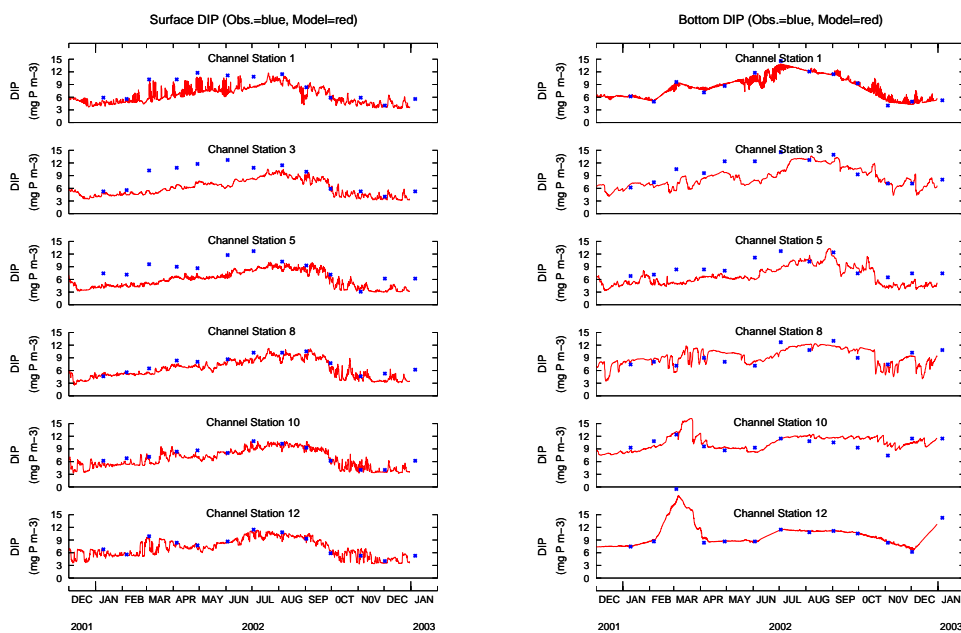


Figure 7.1: Time series of observed and simulated surface and bottom inorganic nitrate concentration at stations throughout the D'Entrecasteaux Channel (station 1 is at the northern end of the channel).

The model reproduces the observed seasonal cycle of nitrate in the channel well although modelled winter concentrations in surface waters are slightly lower than observed in the northern end of the channel. This could be due to an over estimation of modelled phytoplankton uptake and growth in winter, which in turn may result from inaccuracies in the simulated in-situ PAR. Alternatively this discrepancy may result from the under-representation of a surface nitrate source in the model, for example oxidation/nitrification of ammonia. The observed variability in bottom water nitrate at stations 8 and 10 is reproduced by the model, however the exact timing of this variation is not always achieved, possibly due to inaccuracies in simulating the exact flux of nitrate crossing the southern boundary and discharging from the Huon Estuary.



*Figure 7.2: Time series of observed and simulated surface and bottom inorganic phosphate concentration at stations throughout the D'Entrecasteaux Channel (station 1 is at the northern end of the channel).*

The model reproduces the seasonal cycle in dissolved inorganic phosphate, although modelled concentrations in the northern part of the channel are lower than observed in Autumn and early Winter. This discrepancy may result from over-estimation of modelled phytoplankton uptake and growth and/or inefficient simulation of phosphate recycling through dissolved and particulate phases and/or omission of a local discharge. In the southern part of the channel at station 10 there is slight over estimation of modelled dissolved inorganic phosphate in September and October.

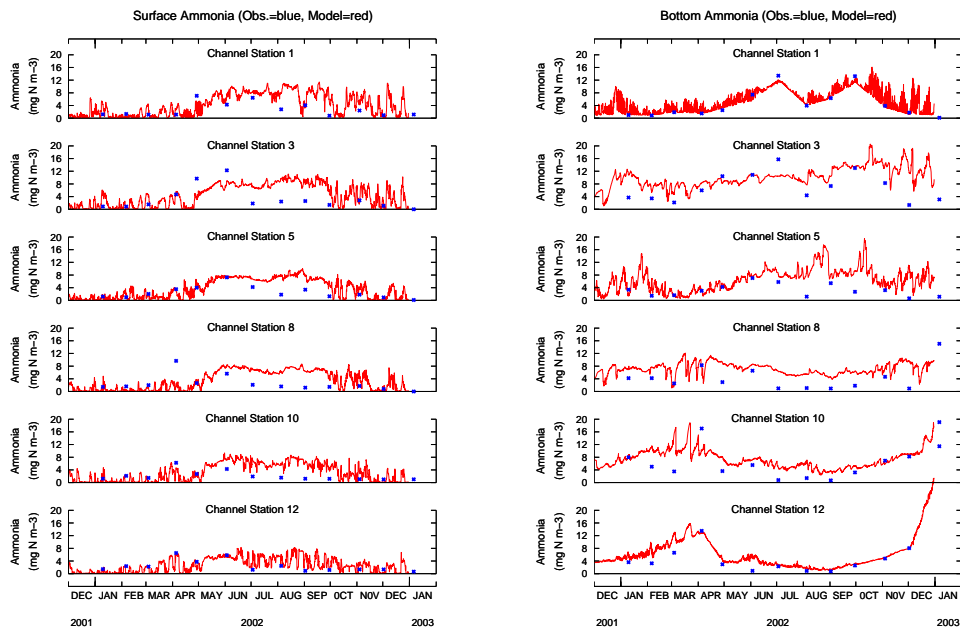


Figure 7.3: Time series of observed and simulated surface and bottom ammonia concentration at stations throughout the D'Entrecasteaux Channel (station 1 is at the northern end of the channel).

The model reproduces a realistic range of surface and bottom water ammonia concentrations in the D'Entrecasteaux Channel, although winter concentrations are typically greater than observed (particularly evident in surface waters). Recalling that nitrogen in the form of nitrate was slightly underestimated by the model in surface waters over winter, then the surplus of ammonia may simply reflect the under estimation of oxidation/nitrification processes in the modelled water column. Alternatively the surplus of modelled ammonia may result from underutilization by phytoplankton. Some groups of phytoplankton have been observed to preferentially uptake nitrogen in the form of ammonia over nitrate as it is metabolically easier to process. In the current version of the model phytoplankton utilize ammonia and nitrate equally which could lead to overestimation of nitrate, and under-representation of ammonia assimilation.

#### Nutrients in the side bays of the D'Entrecasteaux Channel

The seasonal cycle of nutrients in the side bays of the D'Entrecasteaux Channel is similar to the main Channel. Elevated concentrations are observed in winter with reduced concentrations (to near zero nitrogen) at other times of the year. Surface and bottom water concentrations are similar as the bays are typically well mixed throughout most of the year.

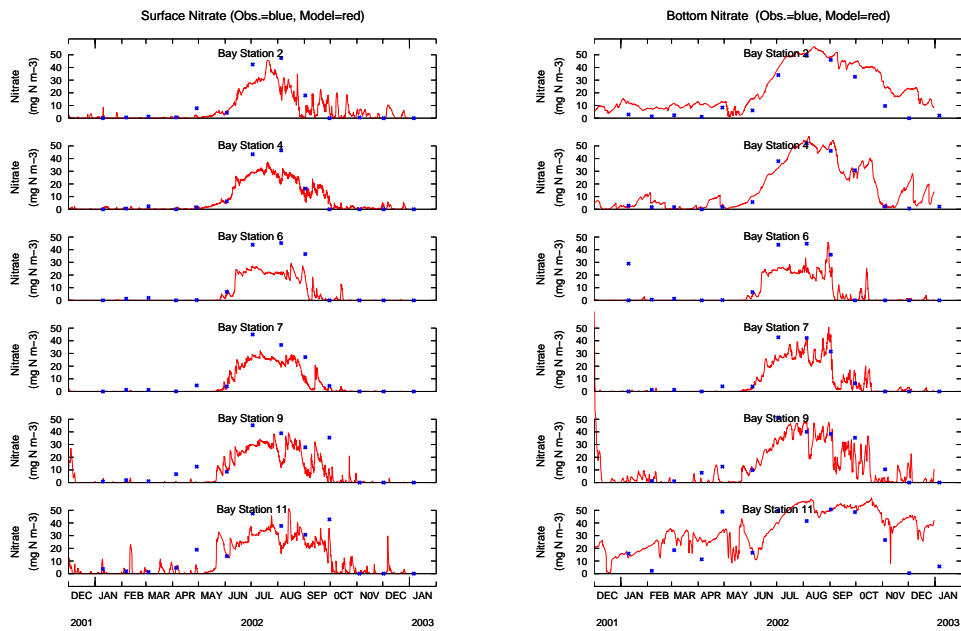


Figure 7.4: Time series of observed and simulated surface and bottom inorganic nitrate concentration in Bays adjacent to the D'Entrecasteaux Channel (station 2 is in Northwest Bay, and station 11 in Great Taylors Bay).

The observed seasonal cycle in nitrate concentration is reproduced by the model although surface nitrate concentrations are generally under-estimated in winter. This results in part from the slightly reduced concentrations of nitrate simulated in the northern part of the channel which supply the bays. Further contributing factors in the bays could be enhanced modelled phytoplankton uptake and growth and/or sub-optimal nutrient recycling and/or omission of additional nitrate sources, for example from small seasonal creeks and rivers.

It is interesting to note that except in Great Bay (and to a lesser extent Isthmus Bay), modelled bottom water nitrate concentrations closely match the observations. The observed surface and bottom concentrations are in general similar, indicating well mixed conditions, however modelled concentrations are reduced at the surface and elevated at depth suggesting an under-representation of vertical mixing in the bays. In the current version of the model enhanced mixing due to wind and swell waves is not included; this may be an important process in the shallow side bays of the D'Entrecasteaux Channel.

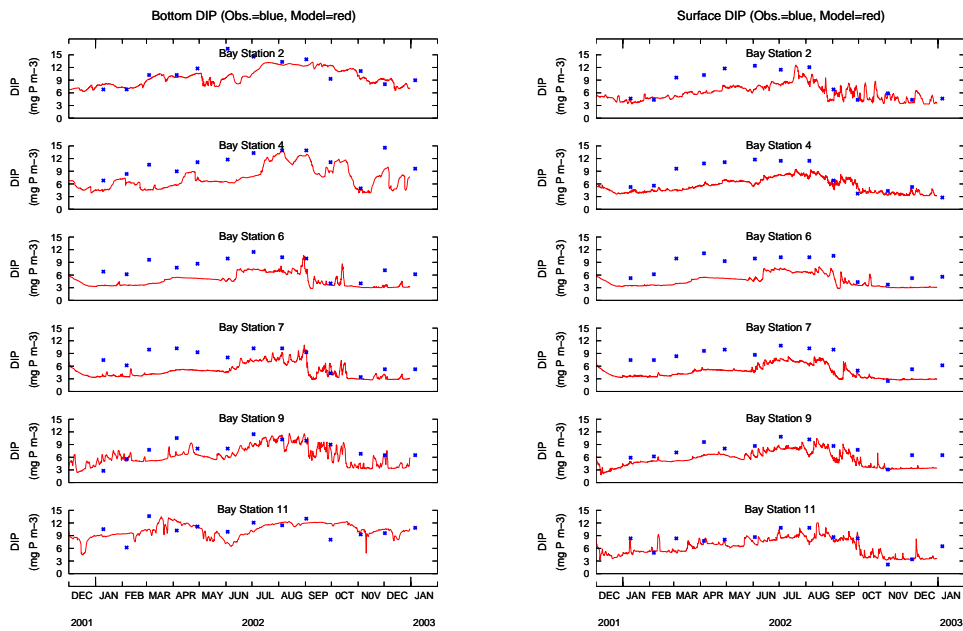


Figure 7.5: Time series of observed and simulated surface and bottom dissolved inorganic phosphate concentration in Bays adjacent to the D'Entrecasteaux Channel (station 2 is in Northwest Bay, and station 11 in Great Taylors Bay).

The reproduction of observed dissolved inorganic phosphate concentration in the side Bays is similar to that in the channel. Modelled concentrations are lower than observed in Autumn and early Winter in Bays towards the northern end of the channel. The discrepancy results in part from the reduced concentrations of dissolved inorganic phosphate simulated in the northern end of the channel. In addition over-estimation of modelled phytoplankton uptake and growth and/or inefficient simulation of phosphate recycling through dissolved and particulate phases and/or omission of a local discharge may also contribute. In the model dissolved inorganic phosphate can be adsorbed onto suspended particulate material; possible overestimation of this process could also contribute to the model deficit.

The comparison between modelled and observed ammonia concentrations in the bays is similar to that in the main channel. In winter modelled ammonia is slightly higher than observed, whilst modelled nitrate is lower than observed. In bottom waters an excess of modelled ammonia prevailed for much of the year in Northwest Bay and Great Taylors Bay. This situation is possibly due to under-representation of oxidation/nitrification processes in the water column as discussed previously, and could be compounded by under-estimation of phytoplankton uptake and growth, perhaps due to excessive attenuation in the water column limiting available PAR for growth.

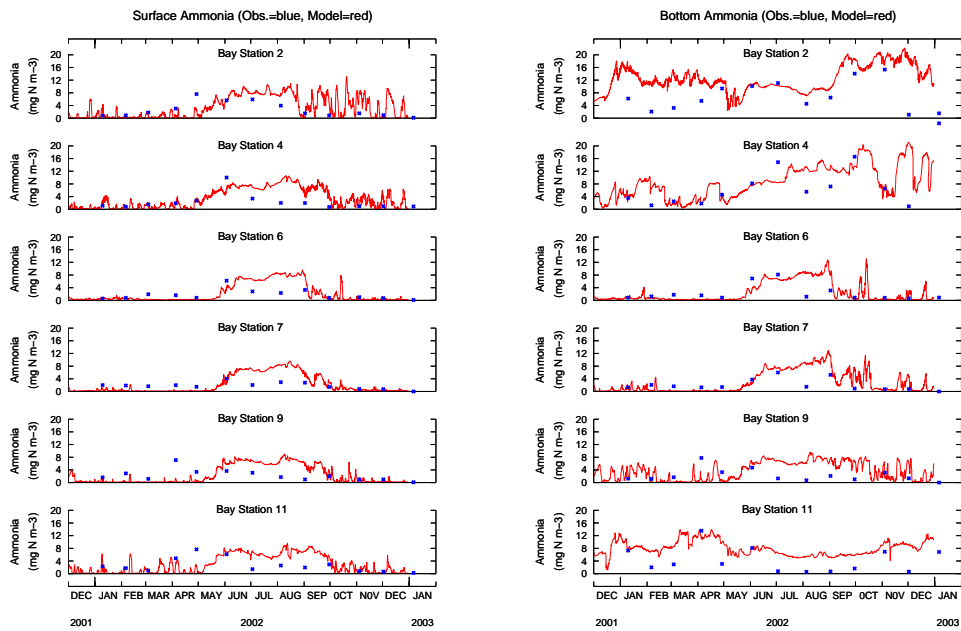


Figure 7.6: Time series of observed and simulated surface and bottom ammonia concentration in Bays adjacent to the D'Entrecasteaux Channel (station 2 is in Northwest Bay, and station 11 in Great Taylors Bay).

### Nutrients in the Huon Estuary

In the Huon estuary the seasonal variation in nutrient concentration is modified by the nutrient loads discharged by the Huon and Kermandie rivers. Whilst the Huon river contributes the largest volume of water the smaller Kermandie river (which discharges mid-estuary) has higher nutrient concentrations. Both flows are greater in winter and spring although episodic high flow events, lasting just a few days, occur throughout the year. No observations of bottom water nutrient were made at station 12.

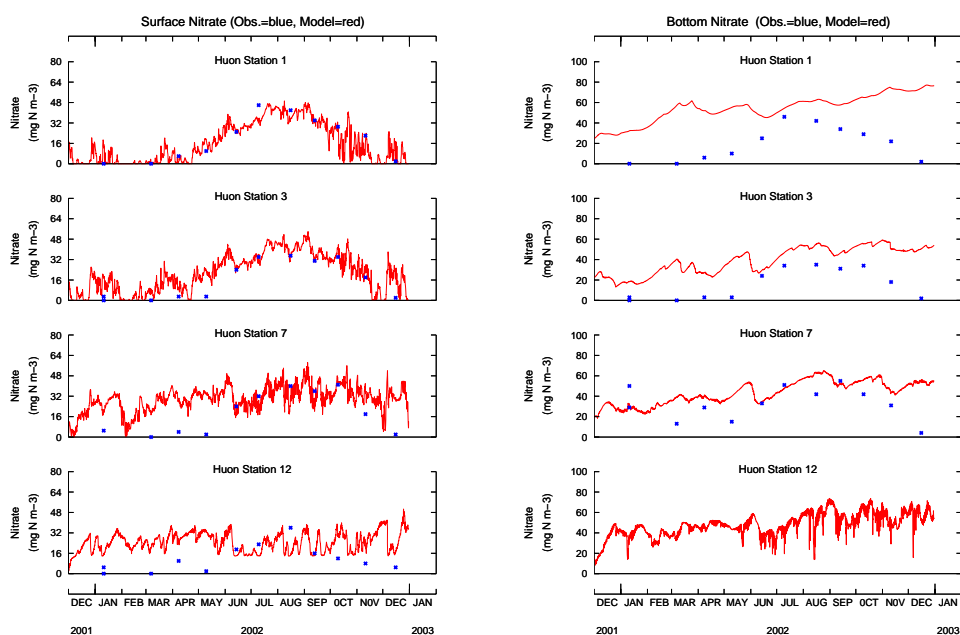


Figure 7.7: Time series of observed and simulated surface and bottom inorganic nitrate concentration at stations in the Huon Estuary (station 1 is at the mouth, and station 12, in the middle of the estuary).

Modelled nitrate concentrations are in the range of observed values. At the lower end of the estuary the model reproduces the observed surface nitrate well, although deep water values are overestimated and similar in concentration to the southern basin of the D'Entrecasteaux Channel. Station 1 at the mouth of the estuary was located in an area of deeper water resolved in the model as a single deep grid square surrounded by shallower bathymetry. This configuration may limit horizontal exchange of bottom water at this site and result in unrealistic accumulation of nitrate. Alternatively the relatively coarse grid representation of the narrow deep water channel linking the D'Entrecasteaux Channel and lower Huon Estuary may result in an overestimation of bottom water ventilation and deep water nitrate flux into the estuary

Towards the upper end of the estuary bottom water nitrate concentrations are better simulated although surface nitrate appears to be overestimated in summer and autumn, suggesting an underestimation of phytoplankton uptake and growth at this time. Modelled phytoplankton growth in the upper estuary is limited by light, but also by advection in the estuarine circulation. Huon river water entering the estuary is characteristically dark in colour, due to high CDOM content draining from the adjacent catchment, and forms a surface plume which flushes water from the upper estuary.

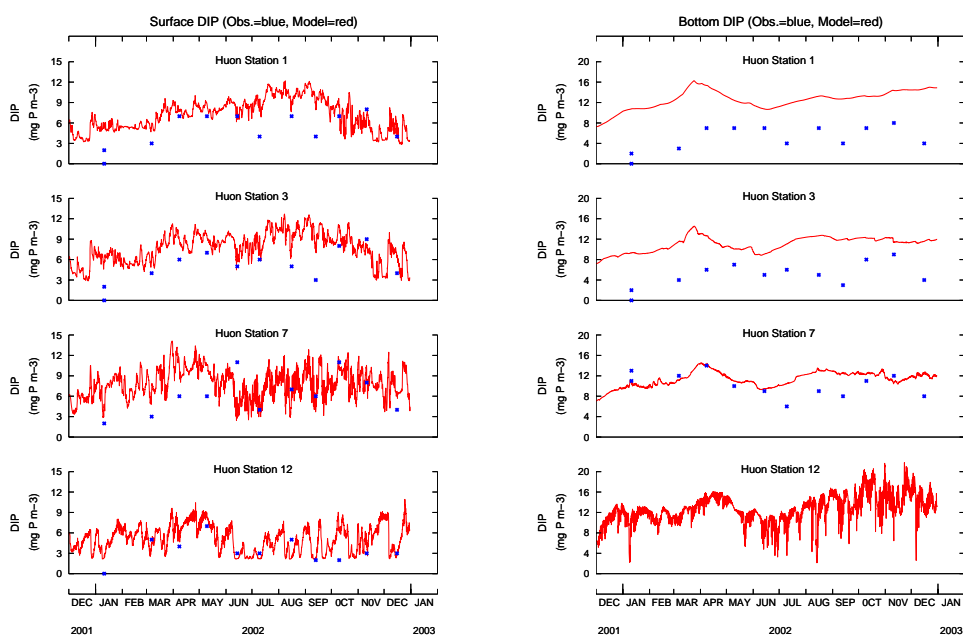


Figure 7.8: Time series of observed and simulated surface and bottom inorganic phosphate concentration at stations in the Huon Estuary (station 1 is at the mouth, and station 12, in the middle of the estuary).

The comparison between modelled and observed dissolved inorganic phosphate is similar to that of nitrate. Modelled values are greater than observed in the lower estuary, but reproduce the observations fairly well in the upper estuary. The over estimation of dissolved inorganic phosphate by the model probably results from under-estimation of phytoplankton uptake and growth in the estuary (as discussed above).

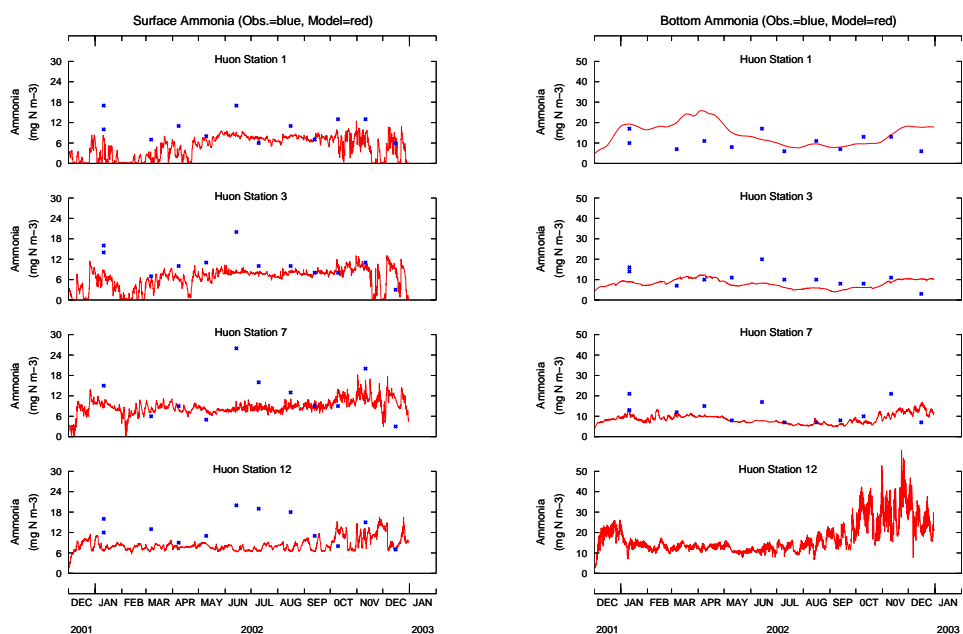


Figure 7.9: Time series of observed and simulated surface and bottom ammonia concentration at stations in the Huon Estuary (station 1 is at the mouth, and station 12, in the middle of the estuary).

The model reproduces the observed concentrations of ammonia in the estuary reasonably well, although winter concentrations in surface waters are underestimated in the upper estuary. At the mouth of the estuary modelled surface ammonia is also underestimated for much of the year. These results are a little puzzling as other nutrients in the estuary had a tendency to be overestimated. Comparing the range of ammonia concentrations observed in the estuary with observations made in the D'Entrecasteaux Channel and side bays shows that the Huon values are higher than those observed elsewhere. Different sample processing and analysis methods were used for ammonia measurements in the Huon and in D'Entrecasteaux and this may contribute to the observed differences (see discussion in chapter on broad scale monitoring program).

The failure of the model to reproduce elevated surface ammonia concentrations in winter may be due to insufficient mixing of bottom water ammonia into the surface layer, although observed bottom water concentrations were often less than surface concentration. An alternative explanation could be the underestimation of ammonia concentrations in the Huon and Kermadec rivers, which have higher flow in winter and enter the surface layer. Concentrations of nutrients in the Huon and Kermadec rivers used for model input are poorly known.

## 7.2 Chlorophyll, Oxygen and Phytoplankton Biomass

Observations of surface and bottom water chlorophyll and phytoplankton biomass were made at 6 stations in the D'Entrecasteaux Channel, 6 stations in the side bays off the D'Entrecasteaux Channel and 4 stations in the Huon Estuary. In addition vertical profiles of chlorophyll-a fluorescence were obtained at stations in the main D'Entrecasteaux Channel and continuous records of bottom water oxygen were obtained at 3 stations in the Huon Estuary (see (Thompson 2005)).

Observations of phytoplankton biomass were divided into 3 groups of species broadly corresponding to modelled 'large phytoplankton', 'small phytoplankton' and 'dinoflagellates', based on microscope cell counts and observed chlorophyll concentration. Species were identified, counted and multiplied by a species specific cell bio-volume to give cell biomass. Groups of species corresponding to the model parameterisation were then summed and the totals normalized against observed chlorophyll assuming a nitrogen to chlorophyll ratio of 7mg N/mg Chl.

**Chlorophyll and phytoplankton biomass in the D'Entrecasteaux Channel**  
The D'Entrecasteaux Channel has fairly low concentrations of surface chlorophyll ( $\sim 1\text{mg m}^{-3}$ ) for most of the year, except during spring when concentrations increase up to fourfold. In deep water concentrations are much lower as there is insufficient light for in-situ growth.

Observations of phytoplankton biomass show distinct seasonal variation with large phytoplankton prominent in spring, small phytoplankton evident throughout the year, but especially in winter and small amounts of dinoflagellates present during autumn and also briefly in spring. This type of

succession is not unusual in temperate waters with fast growing ‘opportunistic’ species such as diatoms (represented in the large phytoplankton) utilizing spring nutrient, slower growing dinoflagellates prevailing in nutrient limited summer/autumn conditions and small picoplankton ubiquitous throughout the year.

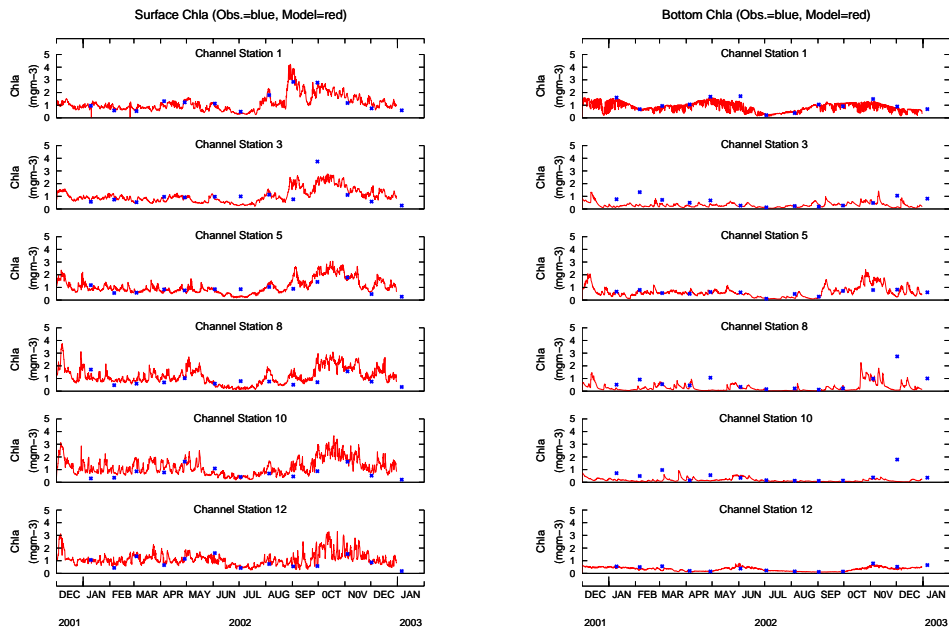


*Figure 7.10: Time series of observed and simulated surface and bottom chlorophyll concentration at stations throughout the D'Entrecasteaux Channel (station 1 is at the northern end of the channel).*

The model simulated the observed temporal evolution of surface and bottom water chlorophyll concentration in the D'Entrecasteaux Channel well. The magnitude and timing of the spring increase in surface chlorophyll concentration was well reproduced, although the model under-estimated spring chlorophyll concentration in bottom waters of the southern basin. A possible explanation for this could be poor resolution of a mixing event which transferred enhanced surface concentrations into deep water and/or coherent sinking of the surface phytoplankton bloom.

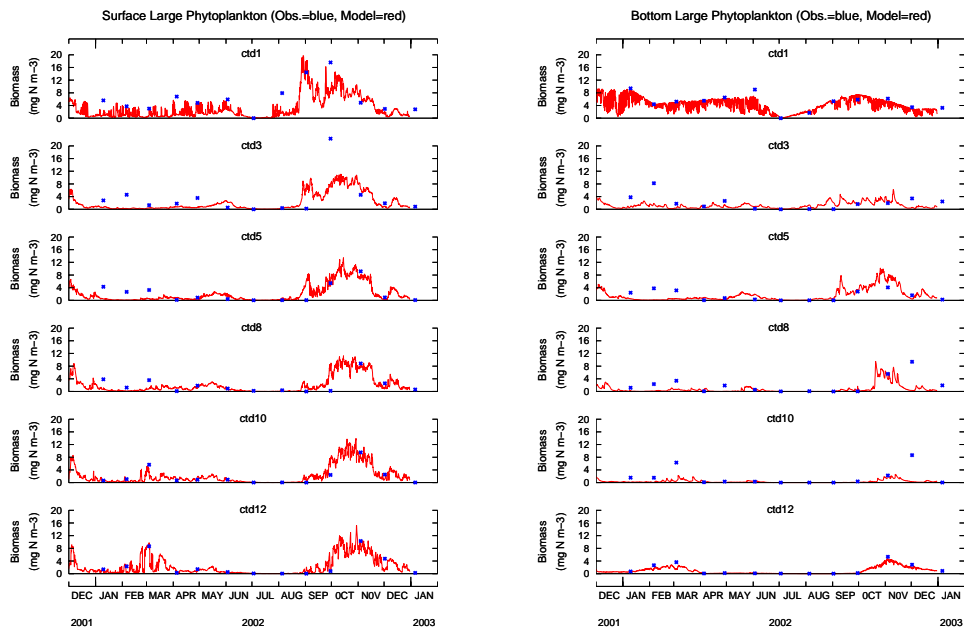


Figure 7.11: Time series of observed and simulated surface and bottom large phytoplankton biomass at stations throughout the D'Entrecasteaux Channel (station 1 is at the northern end of the channel).

The model reproduces the observed seasonal variation in large phytoplankton biomass well. The timing and magnitude of the spring increase in surface waters is well reproduced, except at station 3 where a particularly high value was observed. Small increases in large phytoplankton biomass in late summer in surface and bottom waters are not reproduced by the model, although similar concentrations are simulated throughout autumn.

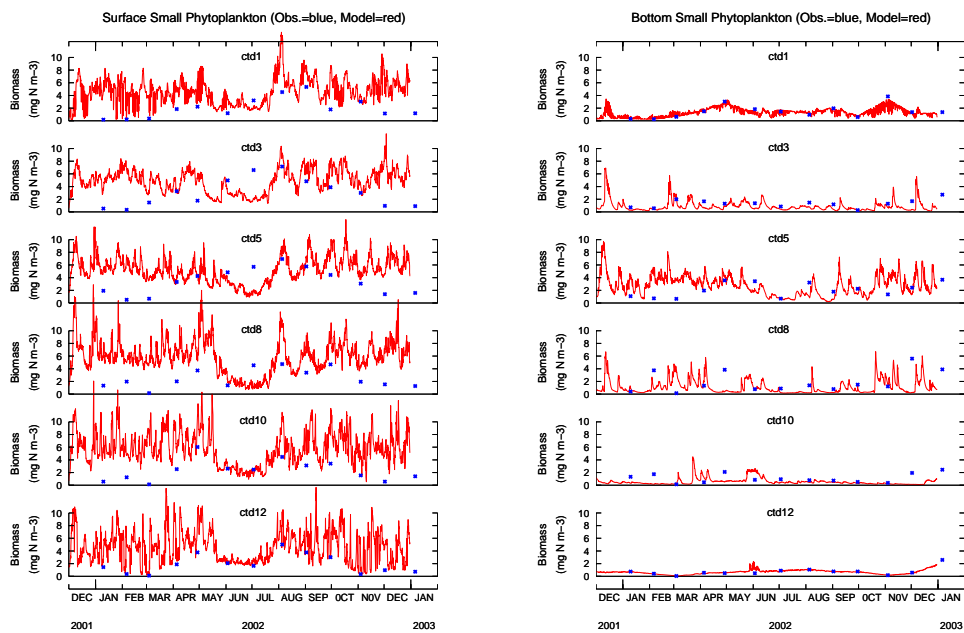


Figure 7.12: Time series of observed and simulated surface and bottom small phytoplankton biomass at stations throughout the D'Entrecasteaux Channel (station 1 is at the northern end of the channel).

The modelled simulates the observed range of small phytoplankton biomass, although the seasonal variation in surface concentration is not well reproduced. The model has a tendency to under-predict small phytoplankton biomass in July and over-predict concentrations in spring and summer. There is also considerable variation in concentration over timescales of a few days possibly due to a combination of predator-prey interactions, tidal advection of patches of enhanced concentration and variations in growth related to nutrient supply over a springs-neaps cycle of tidal currents.

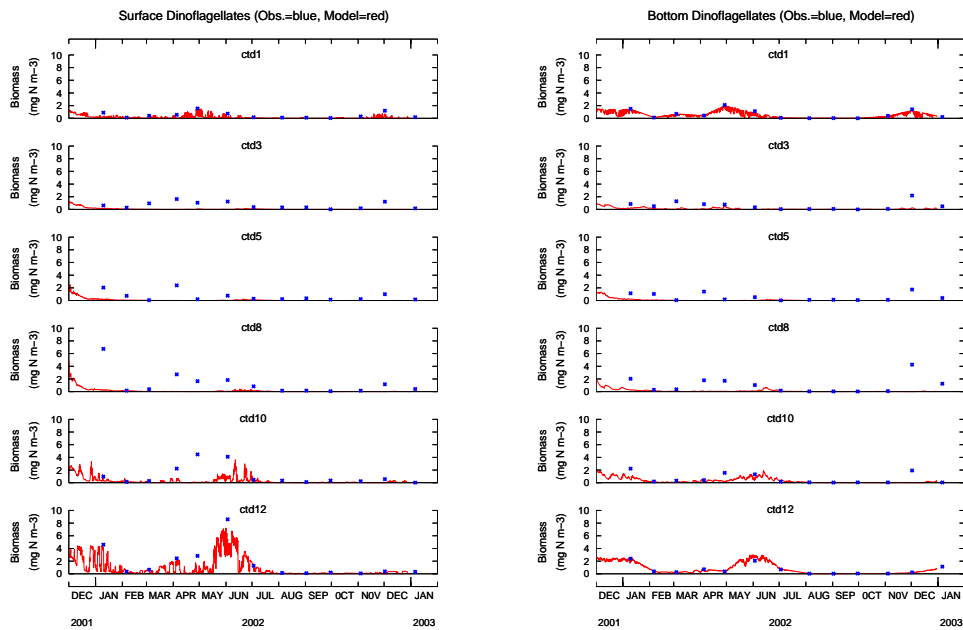


Figure 7.13: Time series of observed and simulated surface and bottom dinoflagellate biomass at stations throughout the D'Entrecasteaux Channel (station 1 is at the northern end of the channel).

Modelled dinoflagellates are in the range of observed values, however for much of the year observed and modelled concentrations are very low. An exception to this is in late autumn in the southern basin when an influx of dinoflagellates enters the model domain across the southern boundary. This injection of dinoflagellate biomass propagates northward and diminishes. Earlier autumn increases in dinoflagellate biomass in the channel are not reproduced. The dinoflagellate functional group comprises of a diverse assemblage of species with distinct life strategies including vertical migration, prey avoidance and cyst resting stages. Any one of these life strategies may facilitate access to resources and avoidance of prey and give rise to an episodic bloom. Modelled dinoflagellates are necessarily parameterized with group mean characteristics which may be insufficient to capture species-specific bloom events.

Vertical structure in observed fluorescence and modelled chlorophyll  
 Vertical profiles of fluorescence were made at monthly intervals at stations throughout the D'Entrecasteaux Channel. Fluorescence is plotted on a relative scale between 0 -1 and would include fluorescence from living and

dead particles containing chlorophyll-a and pheophytin. No calibration against bottle chlorophyll-a measurements has been made but as chlorophyll is likely to be the dominant fluorescent pigment, observed fluorescence will be used as a proxy for (relative) chlorophyll concentration.

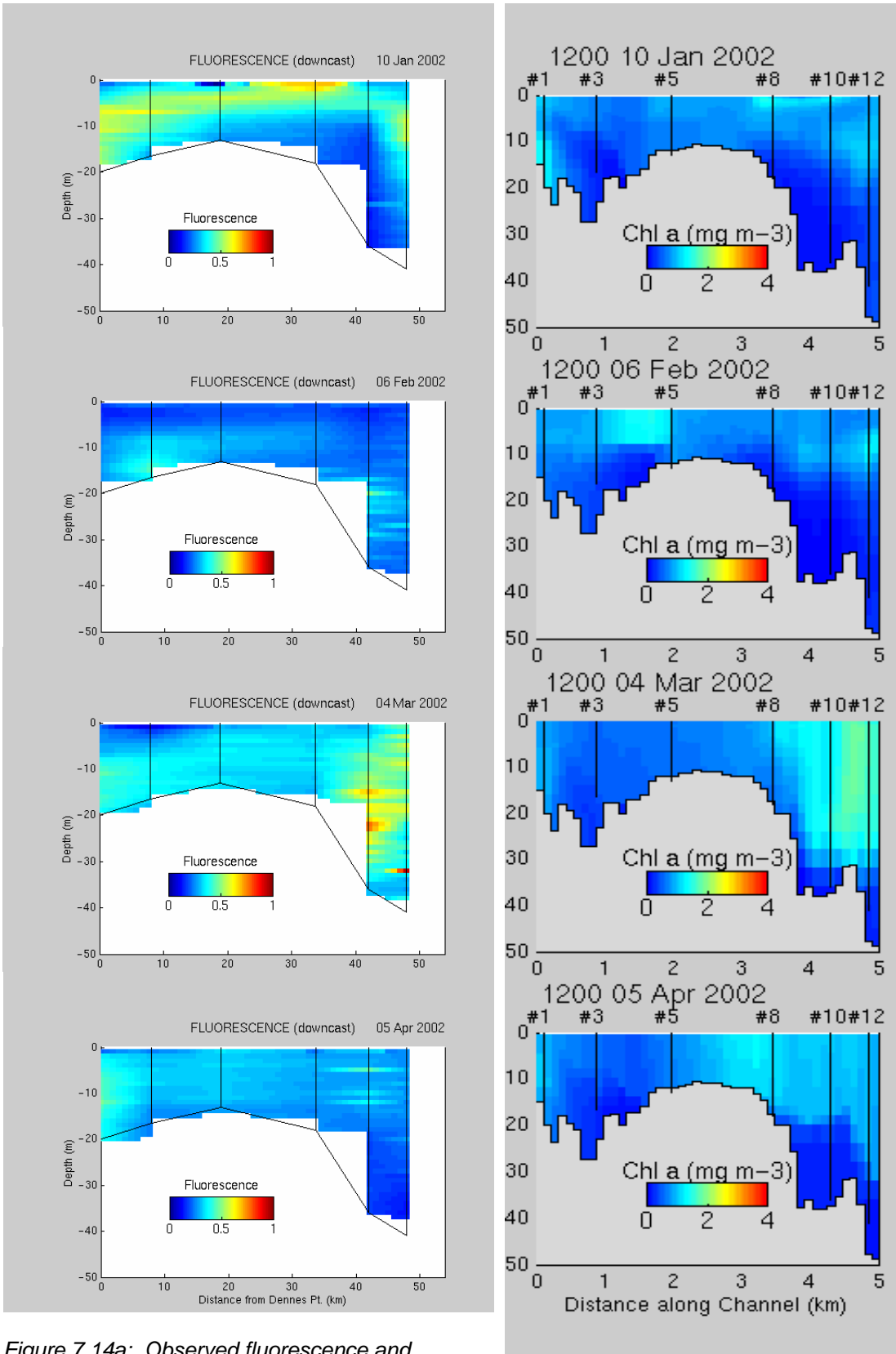


Figure 7.14a: Observed fluorescence and modelled chlorophyll along a north-south transect through the D'Entrecasteaux Channel at monthly intervals through 2002.

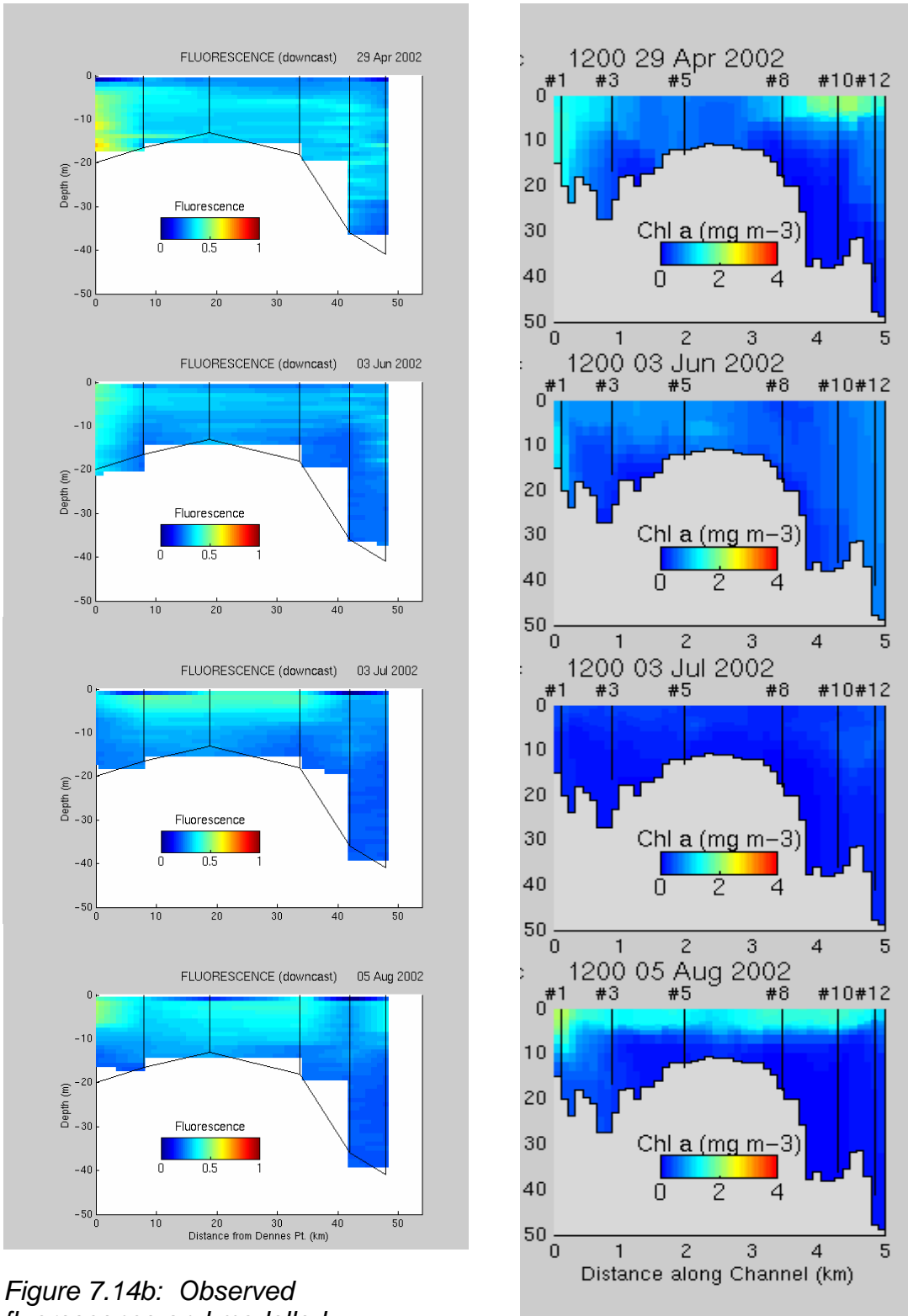
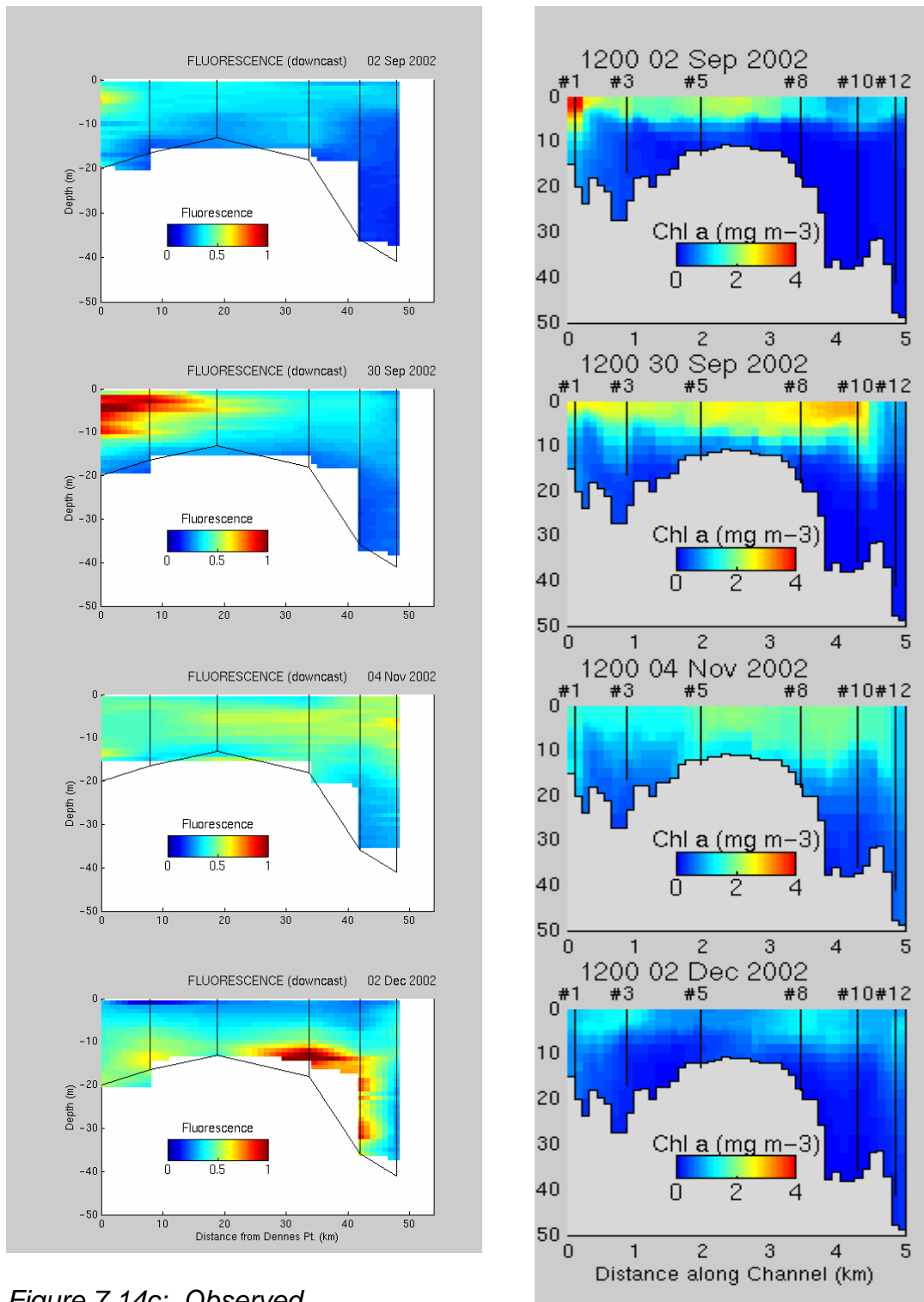


Figure 7.14b: Observed fluorescence and modelled chlorophyll along a north-south transect through the D'Entrecasteaux Channel at monthly intervals through 2002.



*Figure 7.14c: Observed fluorescence and modelled chlorophyll a north-south transect through the D'Entrecasteaux Channel at monthly intervals through 2002.*

The observed and modelled vertical section of fluorescence/chlorophyll along the D'Entrecasteaux Channel shows distinct vertical structure at various sites and times throughout the year. In January a clear subsurface peak in fluorescence was observed at the northern end of the channel which shoaled and outcropped on the surface towards the south. The model produced a subsurface peak in chlorophyll concentration at the northern end of the channel at this time and a surface signature in the south however there was no band of enhanced concentration linking these features.

In February the observations show enhanced fluorescence at depth, but the model distribution of chlorophyll is concentrated at the surface. In March both model and observations indicate enhanced chlorophyll/fluorescence throughout the water column at the southern end of the channel. The fluorescence signal is maximal at depth suggesting an accumulation of phytoplankton biomass or perhaps enhanced chlorophyll content of shade adapted cells.

Through autumn and winter observed fluorescence is generally low and distributed through the water column. Modelled chlorophyll is similarly low in concentration and vertically spread although a patch of enhanced concentration was simulated in surface waters in the southern basin in April.

In August the onset of the spring bloom is first observed at the northern end of the channel. This intensifies and extends south with a band of elevated fluorescence throughout the channel in November. A month later high fluorescence is observed at depth either due to in-situ production, or sinking and (possibly resuspension) of phytoplankton biomass. The model produces a very similar sequence of enhanced spring chlorophyll concentrations. High concentrations are first simulated in surface waters in the north and progress southwards. In September the modelled surface bloom occupies most of the channel with maximal concentration in the southern basin. This contrasts with the observed maximal September fluorescence in the north probably due to slight model offsets in many terms affecting the onset of the spring bloom (attenuation of light, availability of nutrients, advection, zooplankton biomass, etc). In November the observed spatial distribution of fluorescence and modelled chlorophyll have better agreement although the observations suggest a slightly deeper distribution of biomass. By December modelled chlorophyll concentrations have diminished and the observed high fluorescence/chlorophyll at depth is not reproduced. As the model includes resuspension processes (but not enhance bottom water chlorophyll), the observed fluorescence/chlorophyll signal is more likely to be either a transient sinking event, or result from shade adaptation (enhanced chlorophyll content) of phytoplankton at depth.

#### Chlorophyll and phytoplankton biomass in the side bays

The model reproduces the observed seasonal variation in surface chlorophyll concentration in the side bays off the D'Entrecasteaux Channel well. The timing of the spring bloom is generally well simulated although the modelled

bloom occurs a little early in Great Bay and the magnitude is slightly over predicted in Northwest Bay, Little Taylors Bay and Great Taylors Bay. Observed bottom water chlorophyll concentrations are similarly well reproduced by the model except for occasional enhanced concentrations in spring and autumn in Northwest Bay, Barnes Bay and Great Taylors Bay. During these periods bottom water chlorophyll concentrations exceed their surface value suggesting accumulation of sinking and/or resuspended viable phytoplankton and/or shade adaptation of phytoplankton. Sinking and resuspension processes are included in the model, although their importance may be underestimated in these Bays.

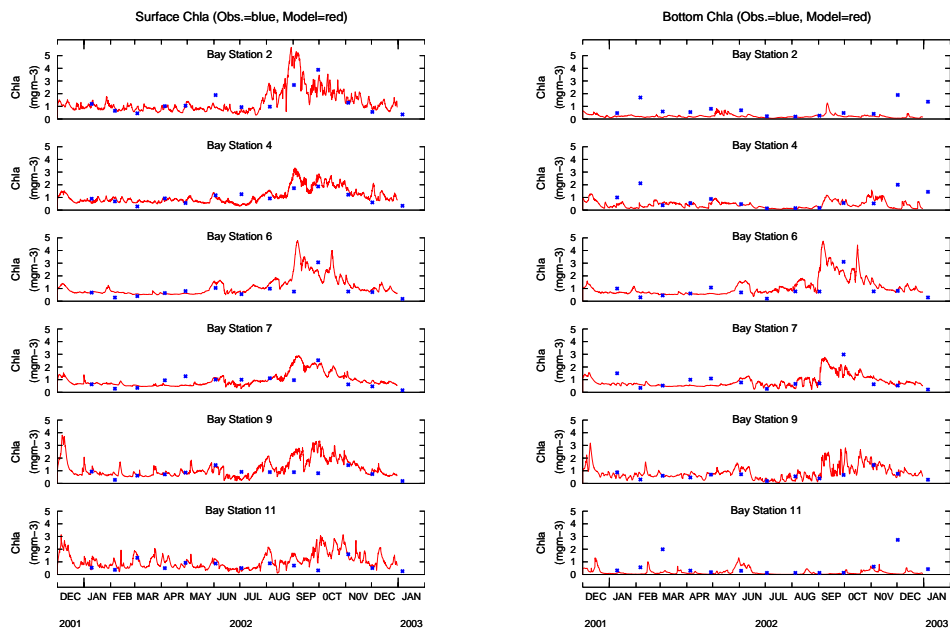


Figure 7.15: Time series of observed and simulated surface and bottom chlorophyll concentration in Bays adjacent to the D'Entrecasteaux Channel (station 2 is in Northwest Bay, and station 11 in Great Taylors Bay).

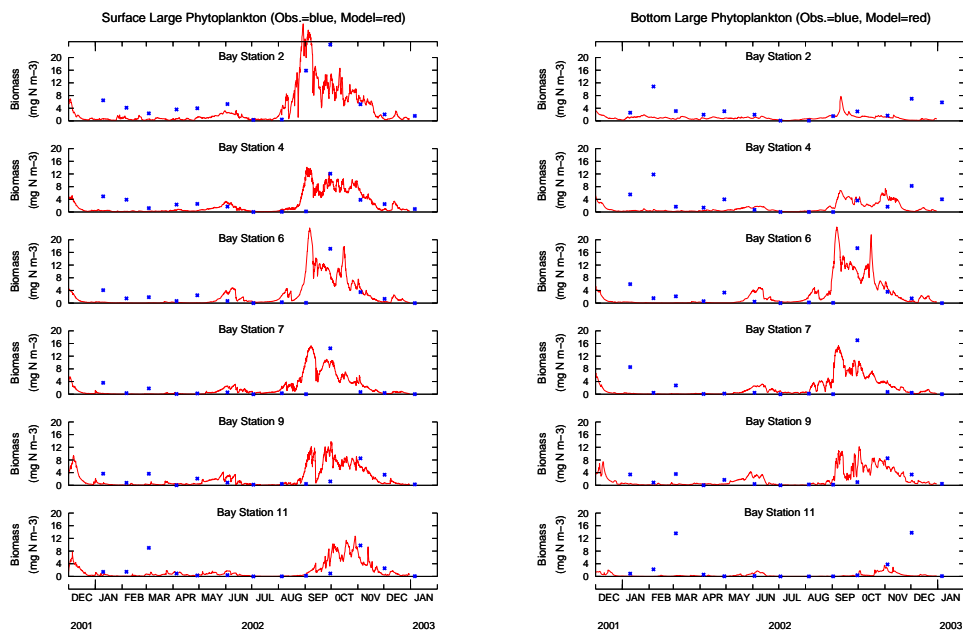


Figure 7.16: Time series of observed and simulated surface and bottom large phytoplankton biomass in Bays adjacent to the D'Entrecasteaux Channel (station 2 is in Northwest Bay, and station 11 in Great Taylors Bay).

The observed biomass of large phytoplankton in the Bays off the D'Entrecasteaux Channel is well simulated by the model. Modelled autumn values are a little low in bays at the northern end of the Channel and the enhanced deep water values observed in February are not reproduced. The spring increase in concentration is simulated a little early in most of the bays, but with the correct magnitude.

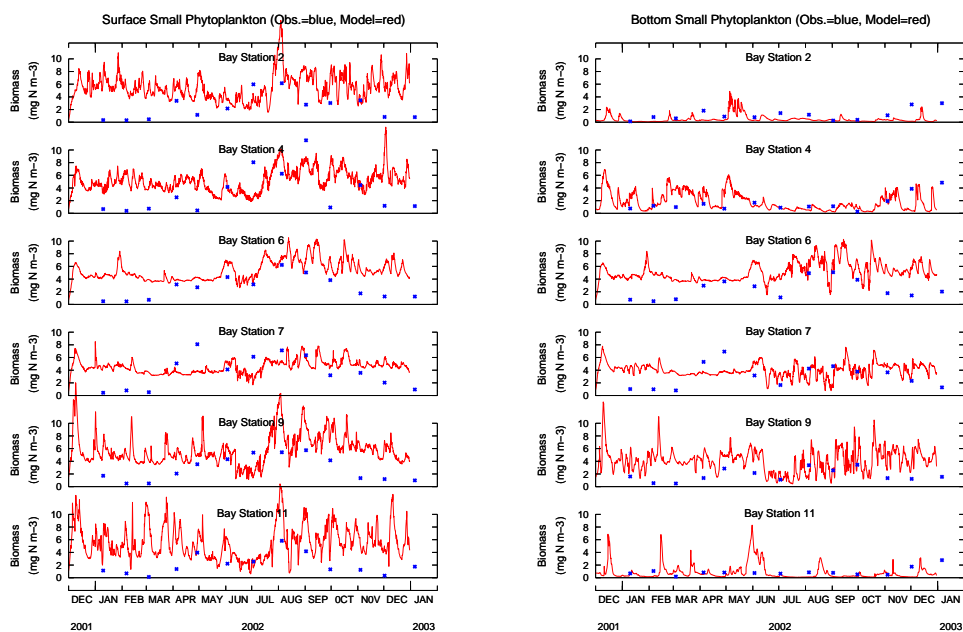


Figure 7.17: Time series of observed and simulated surface and bottom small phytoplankton biomass in Bays adjacent to the D'Entrecasteaux Channel (station 2 is in Northwest Bay, and station 11 in Great Taylors Bay).

The model simulated a realistic magnitude of small phytoplankton biomass throughout the year but failed to reproduce the observed seasonal variation in biomass in surface waters. This same situation occurred in the main Channel and suggests some omission/inaccuracy in the parameterization of small phytoplankton growth and/or loss terms in the model.

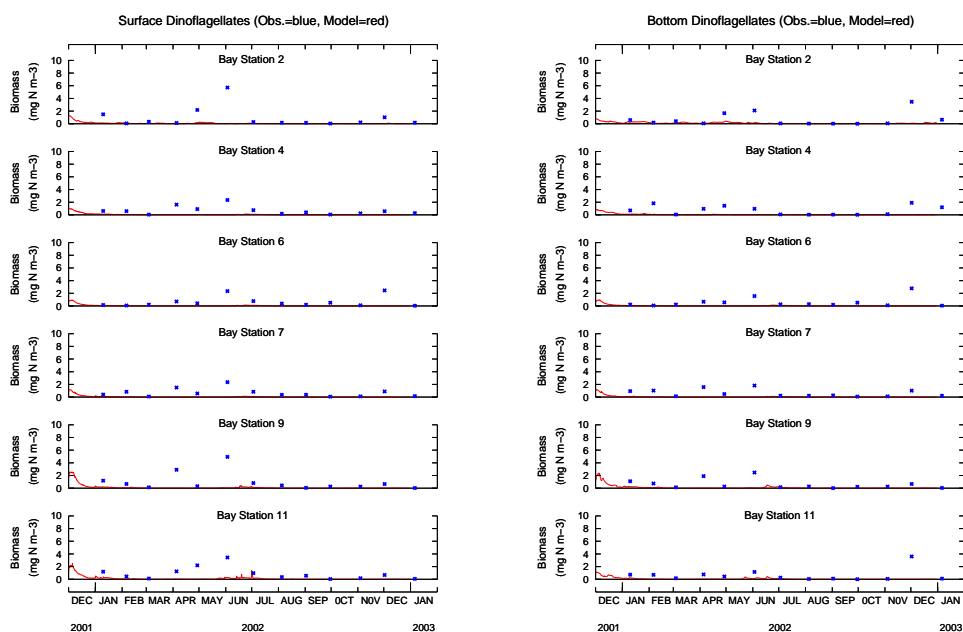


Figure 7.18: Time series of observed and simulated surface and bottom dinoflagellate biomass in Bays adjacent to the D'Entrecasteaux Channel (station 2 is in Northwest Bay, and station 11 in Great Taylors Bay).

The observed biomass of dinoflagellates in the Bays off the D'Entrecasteaux Channel is not well simulated by the model which fails to reproduce the observed autumn increase. This is partially due to the underestimation of dinoflagellates biomass in the main channel for much of the year. It is interesting to note that a very small influx of dinoflagellates into several Bays occurs in late autumn, however this biomass is not fast growing enough to develop into a bloom of the observed magnitude.

Chlorophyll, oxygen and phytoplankton biomass in the Huon estuary  
 Chlorophyll concentration and phytoplankton samples were observed at 4 stations in the Huon Estuary throughout 2002 by Simon Willcox and Sam Foster et al. (see TAFI section in (Thompson 2005)). Pigment samples were collected in surface and bottom waters (except station 12), whilst phytoplankton samples for identification were collected using an integrated water column sampler that collected water from the surface to a maximum of 12 metres. Microscope analysis resolved cells  $> 10 \mu\text{m}$  and cell species and number were converted to biomass using estimated biovolumes for each species group and summing the groups into large phytoplankton, small phytoplankton and dinoflagellates. [Small phytoplankton will be under

represented as many species are  $< 10 \mu\text{m}$  and unresolved during the analysis].

In addition bottom water oxygen concentration (and concurrent temperature and salinity) were recorded continuously at 3 stations in the lower estuary for the latter part of 2002. During the deployment instruments were recovered for maintenance and cleaning on the 11 November and 16 December. On both occasions the probes were found to be heavily encrusted with fouling organisms which may have influenced the data.

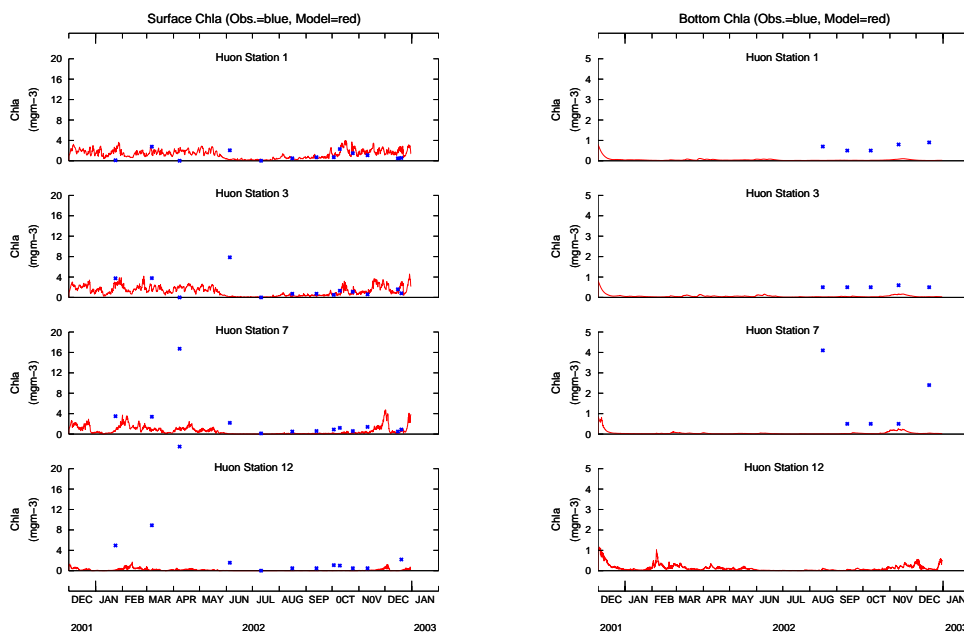


*Figure 7.19: Time series of observed and simulated surface and bottom chlorophyll concentration at stations in the Huon Estuary (station 1 is at the mouth, and station 12, in the middle of the estuary).*

The model simulates realistic chlorophyll concentrations at the mouth of the Huon Estuary, although deep water concentrations are lower than observed. In the mid estuary observed autumn blooms of significant concentration (up to  $24 \text{ mg m}^{-3}$ ) are not reproduced by the model although background concentrations throughout the rest of the year are of the right magnitude.

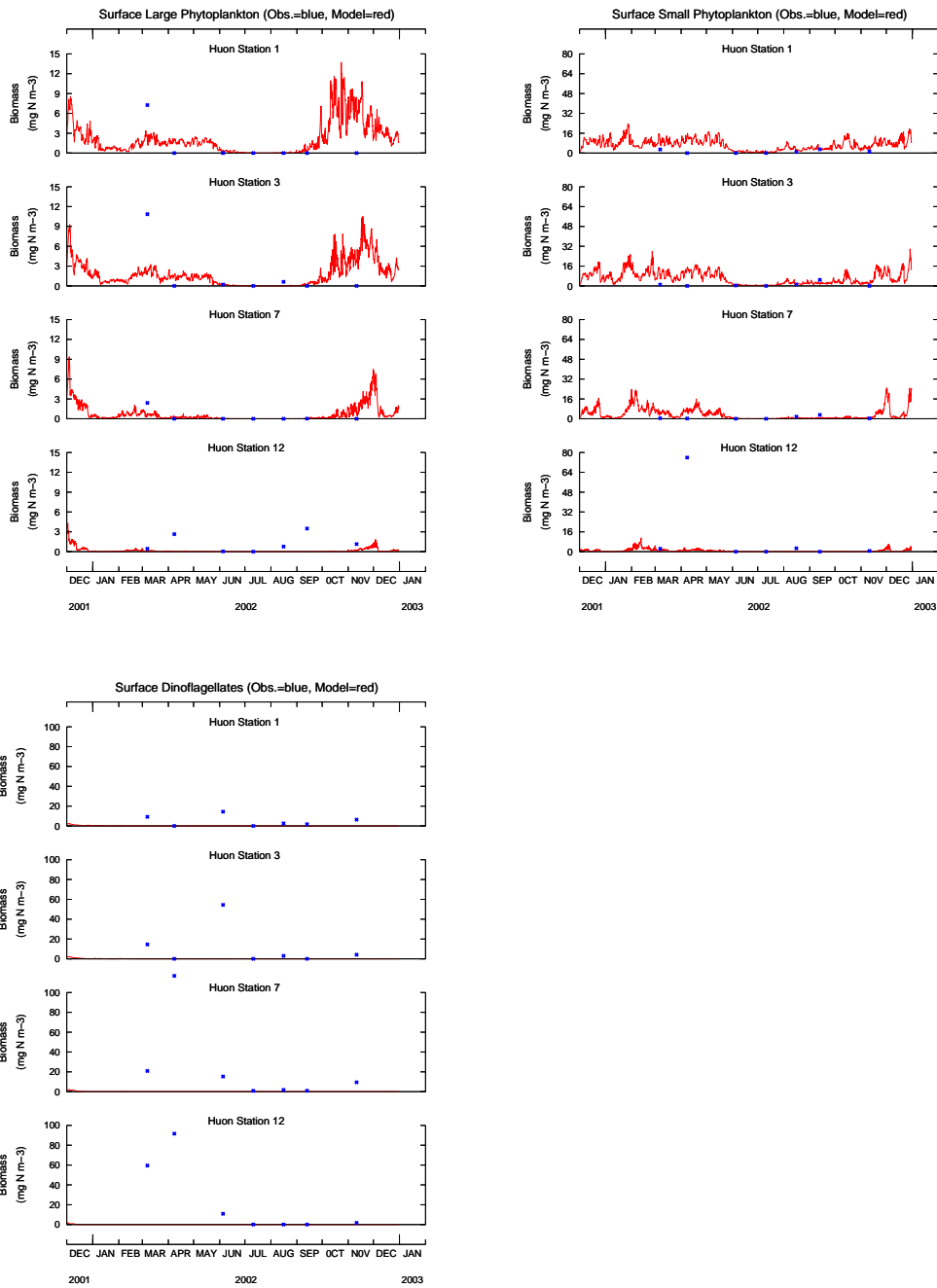
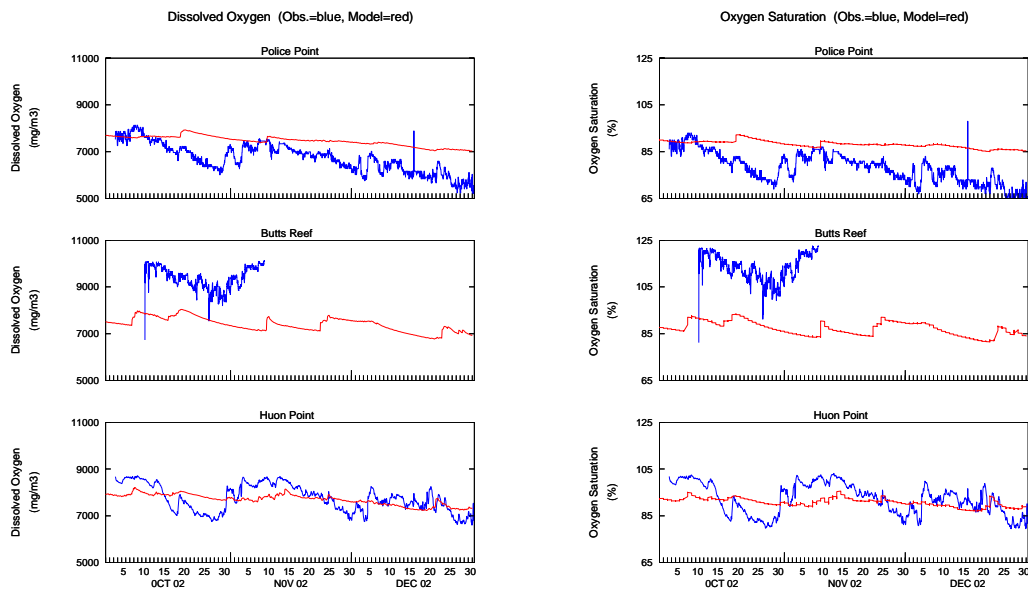


Figure 7.20: Time series of observed and simulated phytoplankton biomass in surface waters at stations in the Huon Estuary (station 1 is at the mouth, and station 12, in the middle of the estuary).

The model fails to reproduce realistic seasonal variation in biomass concentrations in the 3 modelled phytoplankton groups in the Huon Estuary. Large and small phytoplankton are simulated at approximately the observed magnitudes however the autumn bloom period is not reproduced and a spurious spring increase is simulated. [In 2003 a spring bloom dominated by diatoms was observed and 2002 might be anomalous in this respect.] The observed huge biomass of dinoflagellates in autumn is not simulated, and

modelled dinoflagellates are in general absent from the estuary. These discrepancies between model and observations may result from inaccuracies in the both the model flow field and attenuation of light. Retention of phytoplankton in the estuary depends on the estuarine circulation drawing water into the estuary at depth, whilst surface waters are continuously discharged. Modelled fast growing small and large phytoplankton are able to survive in this environment, however dinoflagellates with slower growth rate are advected out of the estuary and do not accumulate. This situation is compounded by high attenuation of PAR in the near surface layer due to humic substances in the river water. For dinoflagellates to accumulate to the observed high concentrations they need to both spend time in the deep water, for upstream advection into the estuary, and in the surface waters to access sufficient PAR for growth. In the Huon the most successful species of dinoflagellate are those that migrate vertically in the water column and achieve this life strategy. The model has demonstrated that without vertical migration dinoflagellates do not prevail in the estuary. [This hypothesis is examined further in a scenario simulation including dinoflagellate vertical migration (in section 8.3).]



*Figure 7.21: Time series of observed and simulated dissolved oxygen in bottom waters at mooring stations in the Huon Estuary (Huon Point is close to the mouth of the Estuary the other stations are further upstream).*

Modelled dissolved oxygen concentrations in bottom waters of the lower estuary in the latter part of 2002 are of similar magnitude to the observations although much of the short term variability is absent. At Police Point the model slightly overestimates oxygen concentration and saturation, whilst at Butts Reef the converse is true. The best fit between model and observations is at Huon Point close to the mouth of the estuary although the magnitude of observed monthly fluctuations, possibly associated with varying ventilation of

bottom waters over a springs-neaps cycle, are not well reproduced by the model. Whilst this could be a production-consumption issue it is more likely to result from over estimation of bottom water exchange between the D'Entrecasteaux Channel and Huon Estuary due to the necessarily coarse resolution of the bottom bathymetry. In this case bottom waters in the Huon would more closely and consistently resemble those in the Channel (which have fairly high oxygen content) rather than reflecting localized oxygen draw-down.

### 7.3 Model Calibration summary

The model reproduces the observed spatial and temporal dynamics of dissolved nutrients, chlorophyll, phytoplankton biomass and oxygen in the Huon Estuary and D'Entrecasteaux Channel. Observed nitrogen, chlorophyll and large phytoplankton biomass concentrations are particularly well reproduced in the D'Entrecasteaux Channel and side Bays. The phosphorous cycle, which has a greater number of dissolved and particulate phases, is adequately simulated. Modelled small phytoplankton biomass throughout the region lacks the observed seasonal winter maxima, and dinoflagellate biomass is poorly represented, particularly in the Huon where observed autumn blooms are absent. Modelled oxygen concentrations suggest over-estimation of horizontal mixing in bottom waters at the mouth of the Huon Estuary.

## 8 *Sensitivity of key processes and parameter values*

### 8.1 Grazing

Micro- and meso-zooplankton grazing exerts 'top-down' control on phytoplankton populations in the model. It plays an important role in curtailing the spring bloom and recycling nutrient through waste products and detritus. Whilst the important role of zooplankton is recognized and implemented in the model, the magnitudes of grazing rates are poorly known.

Model zooplankton grazing is calculated as the least of the maximum ingestion rate and the phytoplankton encounter rate. The encounter rate depends on the concentration of prey, the size of predator and prey, the zooplankton swimming speed and method of feeding, and ambient turbulence and viscosity. Maximum ingestion rate depends on the zooplankton maximum specific growth rate, cell biomass and growth efficiency.

To examine the sensitivity of the model to variations in grazing rate, simulations were made with micro- and meso-zooplankton swimming speed doubled.

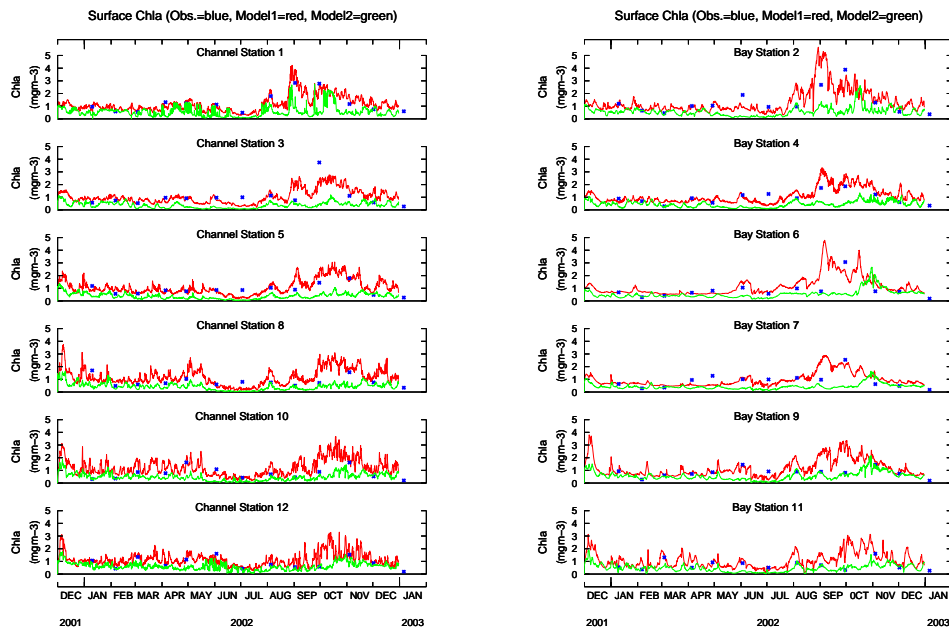
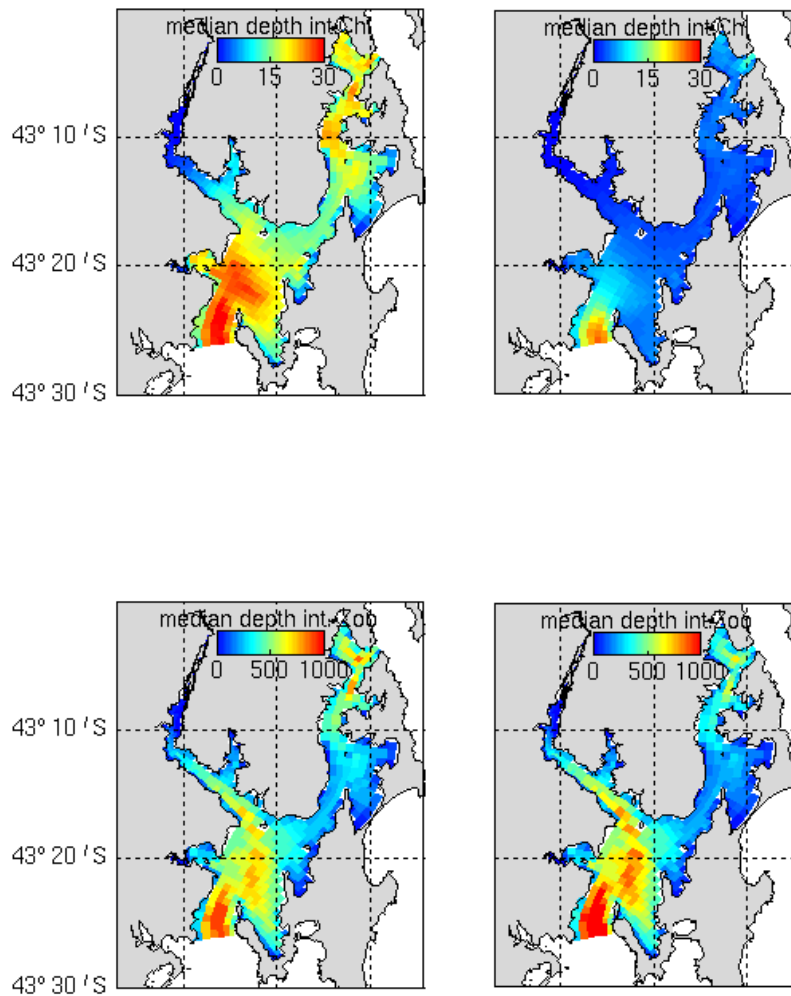


Figure 8.1: Time series of observed and simulated surface chlorophyll concentrations at stations throughout the D'Entrecasteaux Channel (station 1 is at the northern end of the channel) and Bays adjacent to the Channel (station 2 is in Northwest Bay, and station 11 in Great Taylors Bay). The original model values are in red and the model results from the simulation with enhanced micro- and meso-zooplankton swimming speed are shown in green.

In the simulation with doubled zooplankton swimming speeds the additional grazing tightly controlled phytoplankton growth throughout the year. Phytoplankton biomass was lower and there was no spring bloom in contrast to the original model run and observations. At the same time dissolved nutrient concentrations were elevated throughout the domain compared with the original model run and observations; the presence of excess nutrient in surface waters throughout the spring and summer was directly related to reduced phytoplankton uptake and growth.



*Figure 8.2: Spring median depth integrated chlorophyll ( $\text{mg Chl m}^{-2}$ ) (top) and zooplankton biomass ( $\text{mg N m}^{-2}$ ) (bottom) for the original model run (left) and model run with enhanced zooplankton swimming speed (right).*

Depth integrated chlorophyll and phytoplankton biomass were reduced in the model run with doubled zooplankton swimming speed. Despite an excess of surface nutrient, phytoplankton biomass was curtailed by the intensified zooplankton grazing. Depth integrated zooplankton biomass was slightly elevated in the model run with enhance zooplankton swimming speed. This increase resulted from the additional grazing, however as the prey concentration was significantly depleted the increase in zooplankton biomass was only marginal.

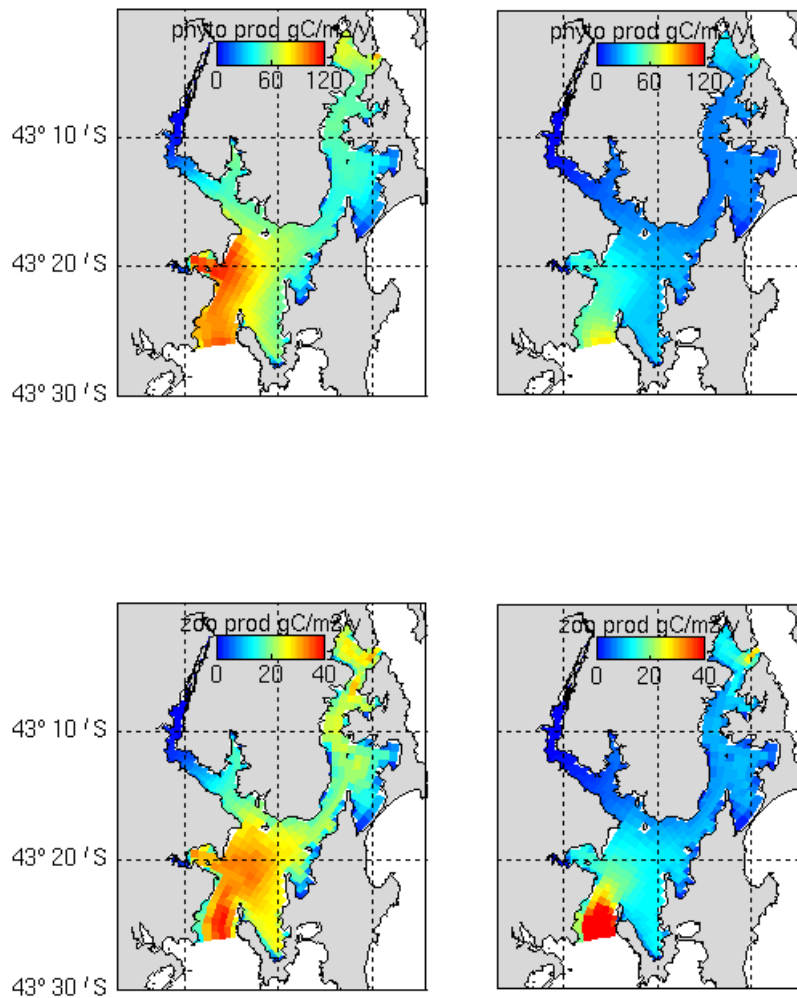


*Figure 8.3: Annual depth integrated phytoplankton primary production (top) and zooplankton secondary production (bottom) for the original model run (left) and model run with enhanced zooplankton swimming speed (right).*

In both simulations the southern basin of the D'Entrecasteaux Channel appears to be the most productive sub-region in the domain, and in the case of zooplankton production the southern boundary is particularly productive. The southern basin has the deepest bathymetry of the region which accounts in part for the greater depth integrated productivity. At the southern boundary the flux of phytoplankton biomass into the model domain is specified as an upstream condition constrained to observed values. Zooplankton, in contrast, have a statistical no flux condition at the boundary and the local population respond dynamically to the influx of fresh phytoplankton biomass. An improved formulation might be to prescribe concentrations of zooplankton biomass as an upstream boundary condition in quasi-steady state with the observed phytoplankton biomass. In this respect observations of zooplankton biomass in the region would be extremely useful.

Annual phytoplankton primary production was reduced by approximately 50% in the model run with enhanced zooplankton swimming and associated grazing. This impacted the zooplankton production which was similarly reduced over much of the region. Under intense zooplankton grazing the productivity of the whole ecosystem was reduced as grazing limited the biomass of primary producers in the system.

The model is sensitive to the rate of zooplankton swimming and associated grazing which controls the amount of phytoplankton biomass and productivity of the system. Grazing rate also impacts the ambient nutrient concentration by limiting phytoplankton biomass available to take up nutrients and efficiently recycling a portion of the grazed material. The results suggest that high zooplankton swimming speeds / clearance rates, which result in tight grazing control of phytoplankton biomass, are not compatible with the observed seasonal cycle in phytoplankton biomass.

## 8.2 Denitrification

Denitrification occurs in the sediment when ammonium is oxidized/nitrified to nitrate and subsequently denitrified to nitrogen gas. Nitrogen gas is released to the atmosphere and lost from the model system effectively reducing the pool of nitrogen available for phytoplankton growth. The rate at which these transformations occur depends on the ambient concentration of dissolved oxygen in the sediment. Nitrification increases with oxygen concentration, however denitrification is maximal under anaerobic conditions. For the standard parameter values used here, maximum denitrification efficiency occurs at sediment oxygen concentrations of  $\sim 1900 \text{ mg m}^{-3}$  and is regulated by the half saturation constants for nitrification and denitrification. The exact value of these parameters is not well known and may vary regionally and with time. Current values used in the model are  $500$  and  $10000 \text{ mg O m}^{-3}$  for the half saturation constants for nitrification and denitrification respectively.

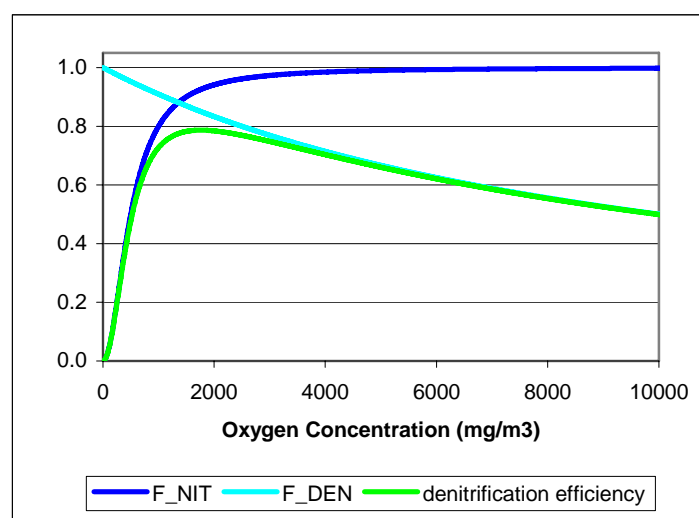


Figure 8.4: Proportion of available ammonium nitrified (dark blue), and proportion of nitrified ammonium denitrified (cyan) plotted against ambient oxygen concentration. The green line is the net denitrification (half saturation coefficient for nitrification  $500 \text{ mg O m}^{-3}$  and denitrification  $10000 \text{ mg O m}^{-3}$ ).

To assess the model sensitivity to denitrification a simulation was made with the half saturation coefficient for denitrification reduced by an order of magnitude. This reduced the maximum denitrification efficiency by ~50% compared to the original model run and significantly reduced denitrification (>70%) at elevated oxygen concentrations.

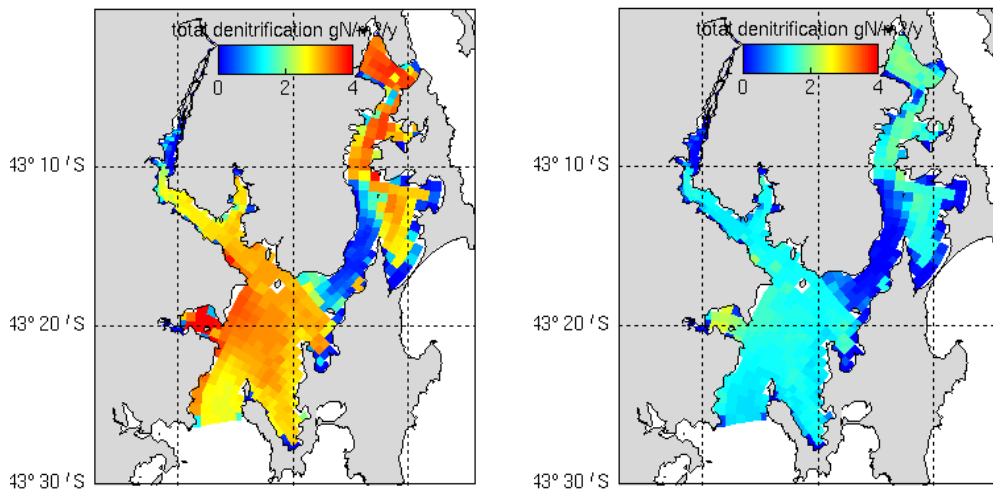


Figure 8.5: Annual denitrification flux ( $\text{gN m}^{-2}/\text{y}$ ) for original model run (left) and model run with reduced denitrification (right).

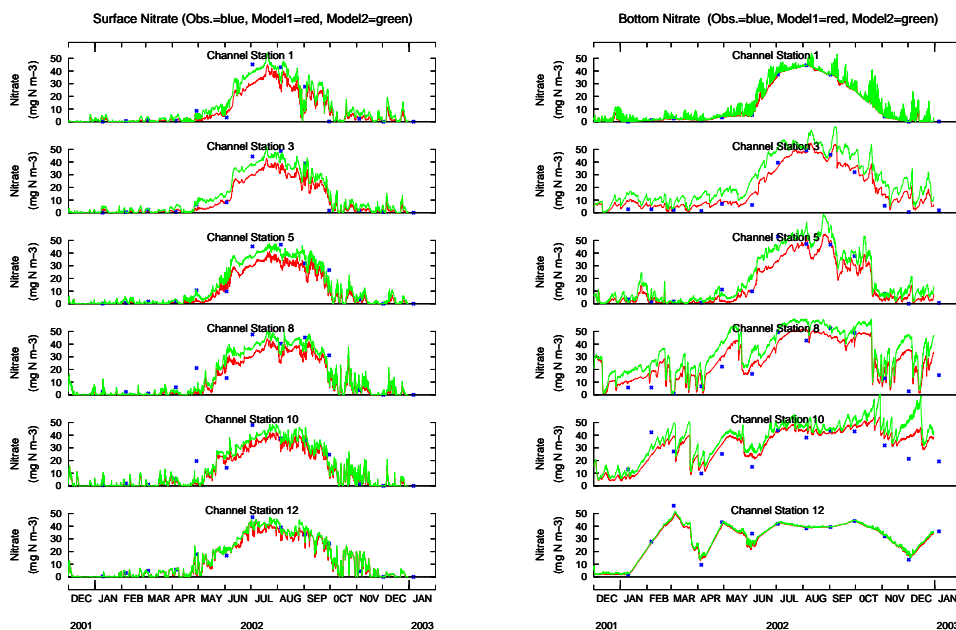


Figure 8.6: Time series of observed and simulated surface and bottom nitrate concentration at stations throughout the D'Entrecasteaux Channel (station 1 is at the northern end of the channel). The original model values are in red and the model results from the simulation with reduced denitrification are in green.

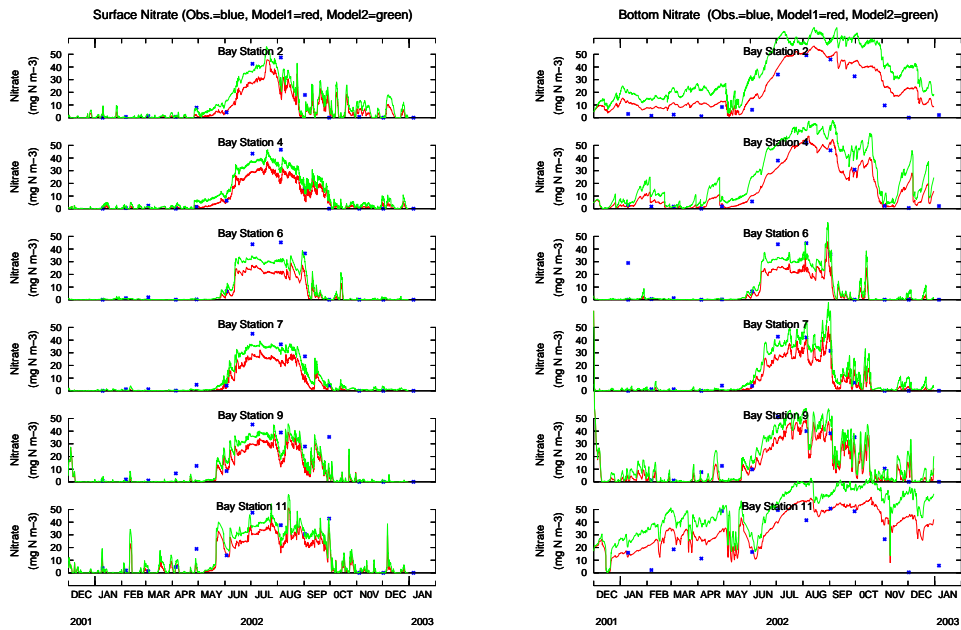
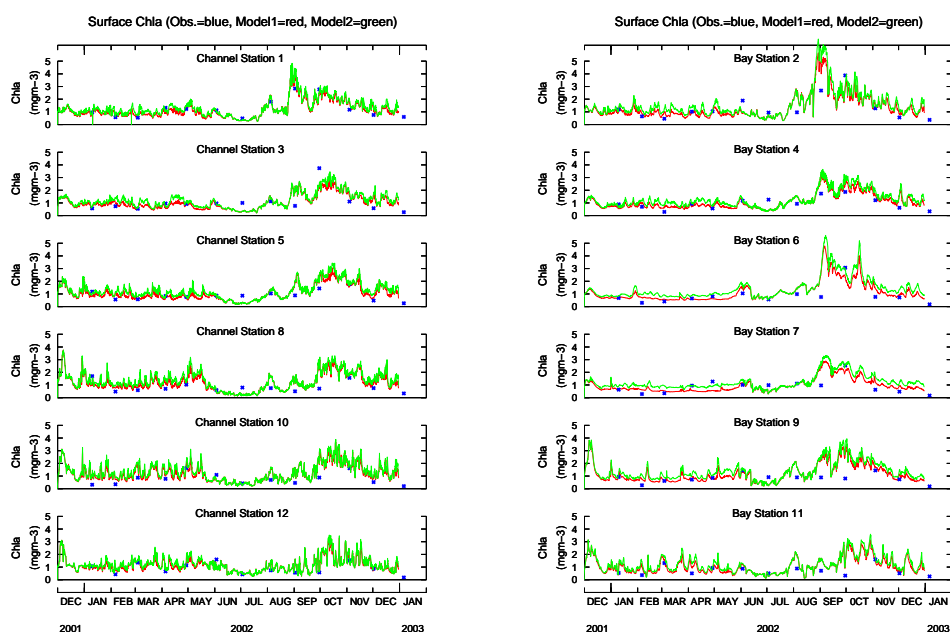


Figure 8.7: Time series of observed and simulated surface and bottom nitrate concentration in Bays adjacent to the D'Entrecasteaux Channel (station 2 is in Northwest Bay, and station 11 in Great Taylors Bay); original model: red; model with reduced denitrification: green.

The model run with reduced denitrification simulates consistently higher bottom water nitrogen values than the original model. Bottom water nitrate concentrations were elevated by  $\sim 10\text{mgN m}^{-3}$  and ammonium by up to  $5\text{mgN m}^{-3}$ . Surface nitrogen values were only enhanced during winter as algal primary production utilized the additional nutrient at other times of year, and generated slightly more algal biomass than in the original simulation.



*Figure 8.8: Time series of observed and simulated surface chlorophyll concentration at stations throughout the D'Entrecasteaux Channel and in Bays adjacent to the D'Entrecasteaux Channel; original model: red; model with reduced denitrification: green.*

Comparing the model run with reduced denitrification with observations demonstrates that this parameterization over estimates bottom water nitrate concentrations in the D'Entrecasteaux Channel and several of the Bays. In Great Bay and Isthmus Bay however the model with reduced denitrification appears to be a better fit to the observations suggesting that sediment denitrification may indeed be less in these Bays, possibly due to variations in sediment type and in fauna. In surface waters the enhanced nitrate values better fit the observations in winter, however model over estimation of algal uptake and production and/or under estimation of ammonium nitrification are thought to be more likely causes of the deficit in the original model.

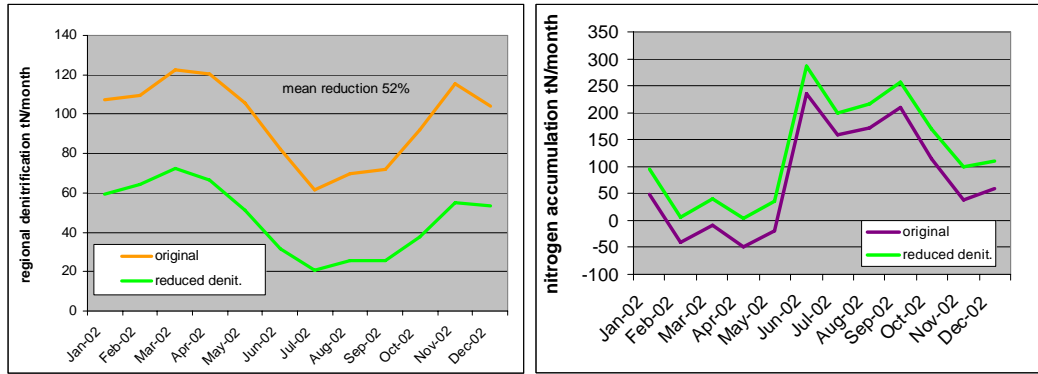


Figure 8.8: Seasonal regional denitrification (left) net accumulation of nitrogen (right).

	tN/y
River discharge into region	1239.6
Fish farm discharge into region	838.7
Denitrification in original model	1161.5
Denitrification in model with reduced denitrification	562.5
Accumulation in original model	920.5
Accumulation in model with reduced denitrification	1519.4

Table 8.1: Relative fluxes of nitrogen into and out of the model region.

For the whole model region denitrification accounted for 56% of the combined river and farm nitrogen load. This is less than estimated for Port Phillip Bay, where denitrification accounts for 80 to 90% of nitrogen loads. Halving the denitrification efficiency had a relatively minor effect on the water column biogeochemistry despite increasing the net flux of nitrogen into the region by 65%. This suggests that the modelled ecosystem is robust to increased nitrogen load, probably due to the relatively short flushing time of the D'Entrecasteaux / Huon system. Further analysis of the model results are required to calculate a definitive nitrogen budget for the region and clarify the fate of nutrient loads.

### 8.3 Absorption cross section

Absorption of PAR by algae determines their growth rate under nutrient replete conditions. The absorption cross section ( $aA$ ) is evaluated from the size and shape of the algae and its pigment content (absorption coefficient) eg. Baird (2003). Absorption cross sections are typically normalized to units of chlorophyll ( $m^2/mgChl$ ) and the model values are shown in table 8.2. Comparatively microphytobenthos have the largest absorption cross section and large phytoplankton the smallest. In general the absorption cross sections used in the model are small compared to literature values (eg.  $0.035 m^2/mgChl$  Lee et al 2003).

	radius m	absorption /m	aA m <sup>2</sup> /cell	conversion molP/cell	absorption cross section m <sup>2</sup> /mgChl
<b>Small Phytoplankton</b>	2.50E-06	50000	2.99E-12	5.64E-15	0.0165
<b>Large Phytoplankton</b>	1.00E-05	30000	1.01E-10	3.61E-13	0.0088
<b>Microphytobenthos</b>	1.00E-05	100000	2.21E-10	3.61E-13	0.0191
<b>Dinoflagellate</b>	1.00E-05	40000	1.26E-10	3.61E-13	0.0109

Table 8.2: Modelled microalgae size and absorption characteristics.

The model is parameterized with fixed absorption characteristics for each algae group, although in reality algae are known to adjust their pigment content depending on light history and cell nutrient content to optimize photosynthesis. It is not possible, within the scope of this project, to include a detailed pigment adaptation model, however, simulations were made to ascertain the sensitivity of the model to algal absorption parameterization.

Results from a simulation with phytoplankton absorption doubled for small phytoplankton, large phytoplankton, microphytobenthos and dinoflagellates, follow. The impacts were most obvious in the surface layer.

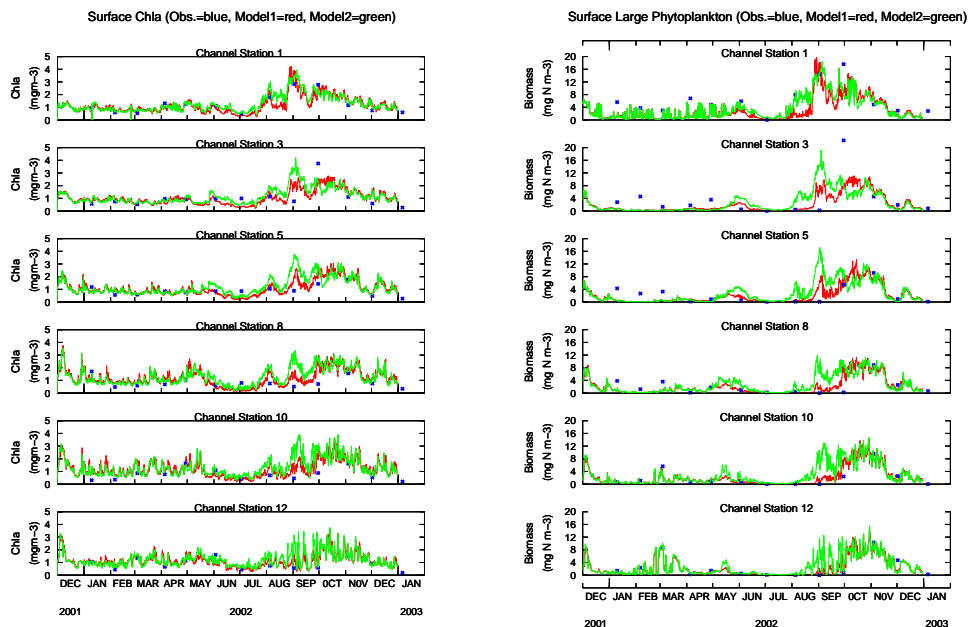


Figure 8.9: Time series of observed and simulated surface chlorophyll and large phytoplankton biomass at stations throughout the D'Entrecasteaux Channel (station 1 is at the northern end of the channel). The original model values are in red and the model results from the simulation with doubled phytoplankton absorption in green.

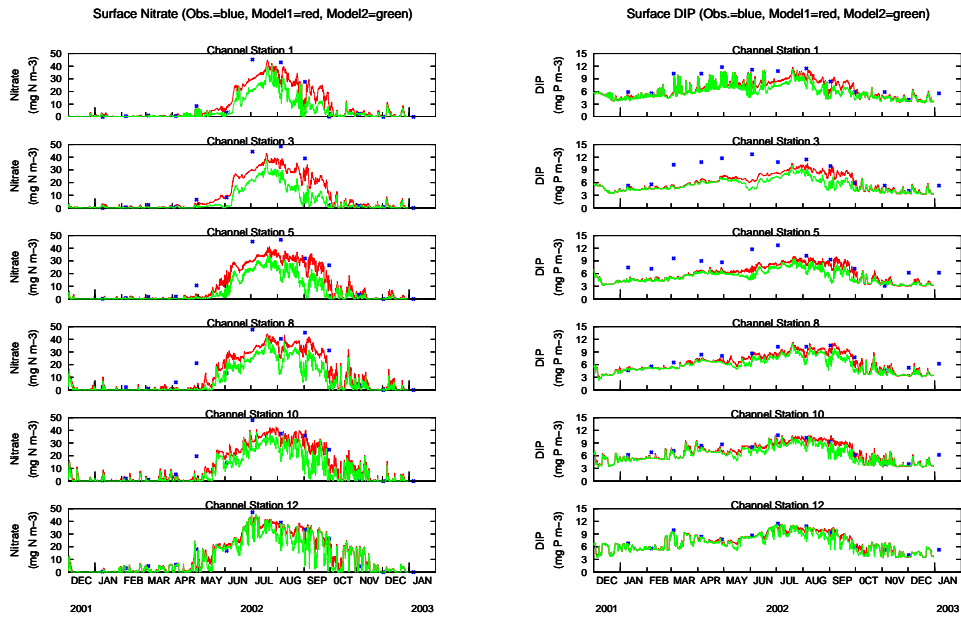
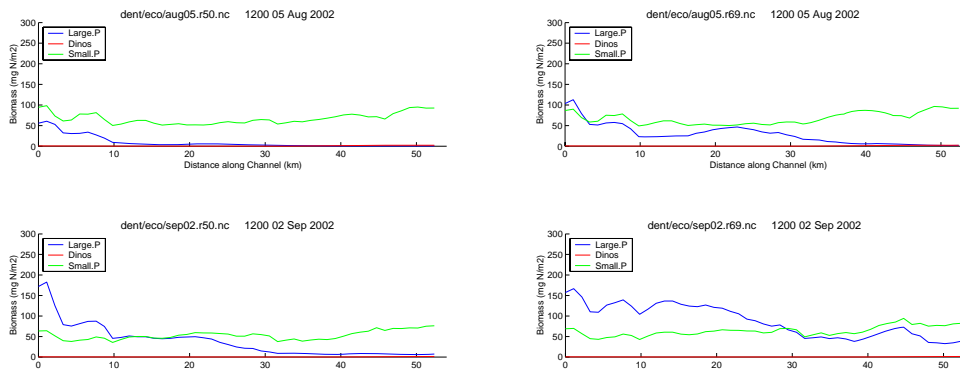


Figure 8.10: Time series of observed and simulated surface nitrate and phosphate at stations throughout the D'Entrecasteaux Channel (station 1 is at the northern end of the channel). The original model values are in red and the model results from the simulation with double phytoplankton absorption in green.

The overall impact of doubling phytoplankton absorption was relatively small. There was a small increase in chlorophyll concentration throughout the year and the spring bloom, dominated by large phytoplankton, occurred ~ 1 month earlier. Nutrient concentrations in surface waters were consistently less than in the original model run associated with the additional phytoplankton uptake. The model already tended to underestimate observed surface nitrate values, and doubling phytoplankton absorption exacerbated this disagreement.



*Figure 8.11: Depth integrated phytoplankton biomass along a transect through the D'Entrecasteaux Channel from north (left) to south (right) in August (top) and September (bottom). Results from the original model run are shown on the left and from the simulation with enhanced phytoplankton absorption on the right.*

Doubling phytoplankton absorption enhanced phytoplankton production and biomass at depth where ambient PAR was less. These cells which also had better access to deep water nutrient increased in their biomass and enhanced productivity compared to the original model run particularly during spring.

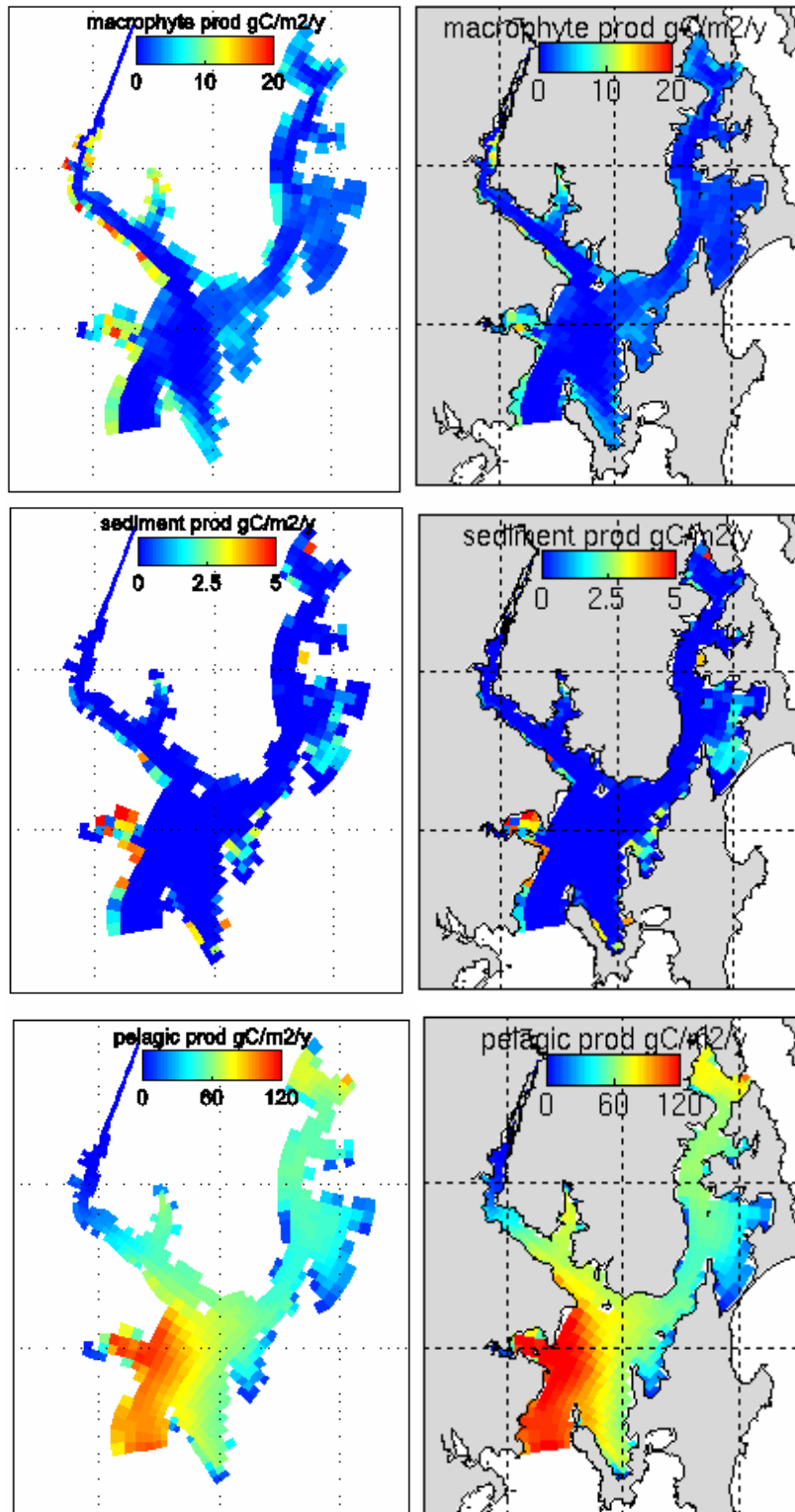


Figure 8.12: Annual macrophyte production (top) and depth integrated sediment (middle) and pelagic (bottom) primary production for the original model (left) and the model with double phytoplankton absorption

Depth integrated primary production shows a slight increase in pelagic production in the simulation with double phytoplankton absorption, however microphytobenthos production in the sediment is similar probably due to additional shading by the extra pelagic production, limiting growth. Macrophyte production is slightly reduced probably for the same reasons.

Doubling the absorption coefficients for phytoplankton had a limited impact on phytoplankton biomass in the model system. This is because for much of the year the phytoplankton are nutrient and not light limited in both simulations. The exception to this situation is in spring when winter nutrients and increasing day length provide optimal conditions for growth. In the simulation with double phytoplankton absorption coefficients the phytoplankton growth in spring occurred earlier and generated more biomass than in the former simulation.

#### 8.4 Dinoflagellate vertical migration and grazing losses

Vertical migration is thought to give some species of dinoflagellate a competitive advantage by allowing them access to both deep water nutrient and high near surface PAR levels. In particular the species *Gymnodinium catenatum* has been observed vertically migrating in concentrated blooms in the Huon Estuary during the HES study. As the model poorly simulated dinoflagellate populations in the Huon a number of simulations were made to examine the role of vertical migration and mesozooplankton grazing on dinoflagellates in the region.

##### Simple parameterization

Dinoflagellate vertical migration was initially parameterized as a positive (upwards) and negative (downwards) vertical swimming speed which switched on a 12 hour cycle. The maximum vertical swimming velocity was set to 4m/hr in mid water, estimated from fluorescence observations in the Huon Estuary Study. Above and below mid-depth the swimming velocity declined linearly to zero at the surface and sea bed (or 25m in deeper water). In waters below 25m the swimming velocity was fixed at a constant 0.4m/hr upwards. By this parameterization dinoflagellate biomass accumulated at the surface for ~10 hours and at the bottom (or ~25m) for ~10 hours.

Results from the simulation of dinoflagellate biomass with simple diel vertical migration were essentially similar to the original model run. The dinoflagellates rapidly declined from their initial concentration and apart from minor events associated with the influx of biomass at the marine boundaries, they were unsustainable in the model domain and absent from the Huon Estuary. A probable explanation for this is associated with the parameterization of irradiance and phytoplankton growth at day mean rates. In the context of day mean irradiance and growth, migrating dinoflagellates were limiting their access to PAR by as much as 50% in deep water (less in shallower zones). To compensate for this a number of model runs were made with enhanced dinoflagellate maximum growth rate, however, even doubling

the growth rate to 0.8/d had very little effect and the population remained unsustainable.

### Reduced grazing pressure

A number of authors have hypothesized that some species of dinoflagellate are less palatable to grazing mesozooplankton and are avoided as a food source in preference to other microplankton (eg. Stoecker & Sanders 1985). Considering this hypothesis a model run was made with selective reduction of mesozooplankton grazing on dinoflagellates. This was parameterized by reducing the successful predator prey encounters between large zooplankton and dinoflagellates to 80% [successful predator-prey encounters between large zooplankton and large phytoplankton, and small zooplankton and small phytoplankton remained at 100%]. Dinoflagellate vertical migration was parameterized as before and dinoflagellate maximum growth rate was set at 0.8/d.

The results from this simulation generated a dinoflagellate spring bloom throughout the D'Entrecasteaux Channel and in the side bays off the main channel. Significant concentrations of dinoflagellates were not observed at these locations in spring, and the observed autumn blooms in the Huon were not reproduced by the model.

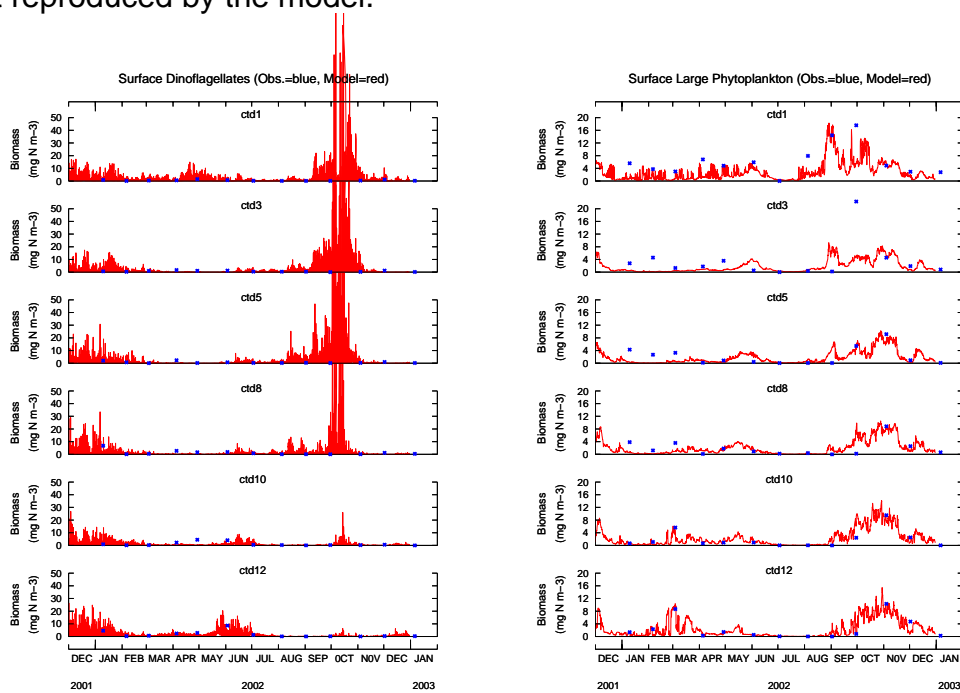


Figure 8.13: Time series of observed and simulated surface dinoflagellate phytoplankton biomass at stations throughout the D'Entrecasteaux Channel (station 1 is at the northern end of the channel). The surface concentration of dinoflagellate biomass varies over a diurnal cycle as vertical migration alternately concentrates and disperses biomass at the surface.

For dinoflagellates to occur in the Huon they must either grow in-situ and/or be advected into the estuary by the estuarine circulation. The typically large volumes of water discharged from the Huon results in a net export of material from the estuary, particularly in the buoyant fresher surface layer. The relatively small tidal range generates oscillatory flow predominantly in the bottom water where denser saltier water flows into the estuary forming a salt wedge intrusion at the head of the estuary. For slow growing dinoflagellates to remain in the estuary they must physically spend more time in the bottom layer of oscillating tidal flow than in the surface layer of water which is constantly being flushed from the estuary.

In this simulation dinoflagellates growing in the D'Entrecasteaux Channel would have been advected into the estuary in the bottom water. However during every 12 hours they spent at the surface they were efficiently flushed out of the estuary and so biomass failed to accumulated in the estuary.

### Surface layer avoidance

Fluorescence profiles observed at several times during the Huon Estuary study depict a subsurface concentration of pigments at ~4m. At this depth phytoplankton biomass may avoid being flushed out of the estuary in the buoyant surface river water, but still gain access to both deep water nutrients and PAR. A model run was made with the vertical migration parameterization updated so that dinoflagellates between 0-4m always swam down at a constant speed of 0.4m/hr.

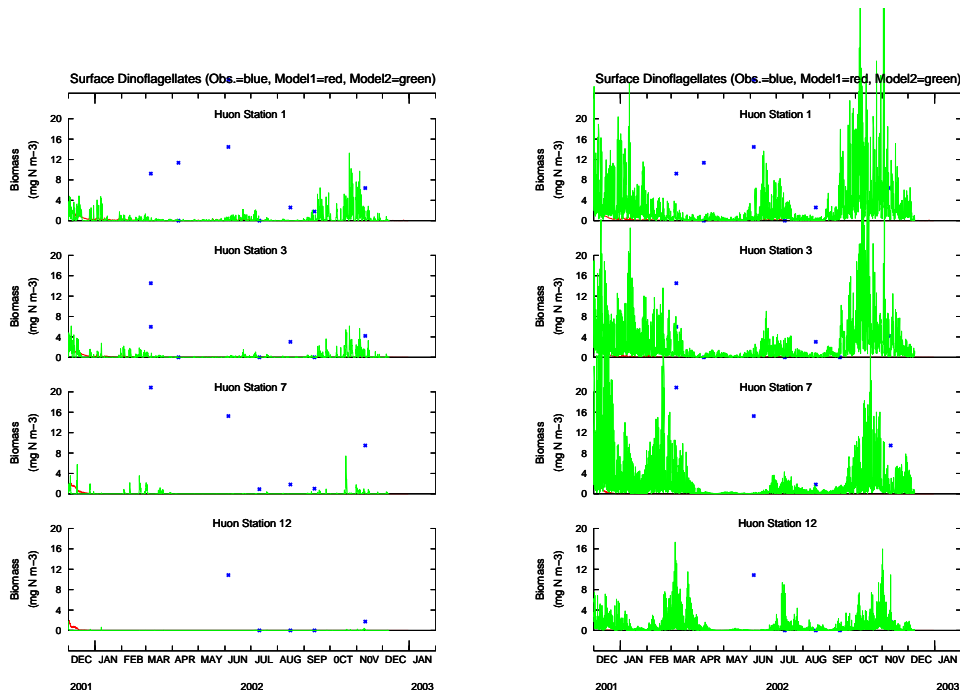


Figure 8.14: Time series of observed and simulated dinoflagellate concentration at the surface (left) and at 4m (right) at stations in the Huon Estuary (station 1 is at the mouth, and station 12, in the middle of the estuary). Model run with no vertical migration (red), with vertical migration (green) and observations (blue).

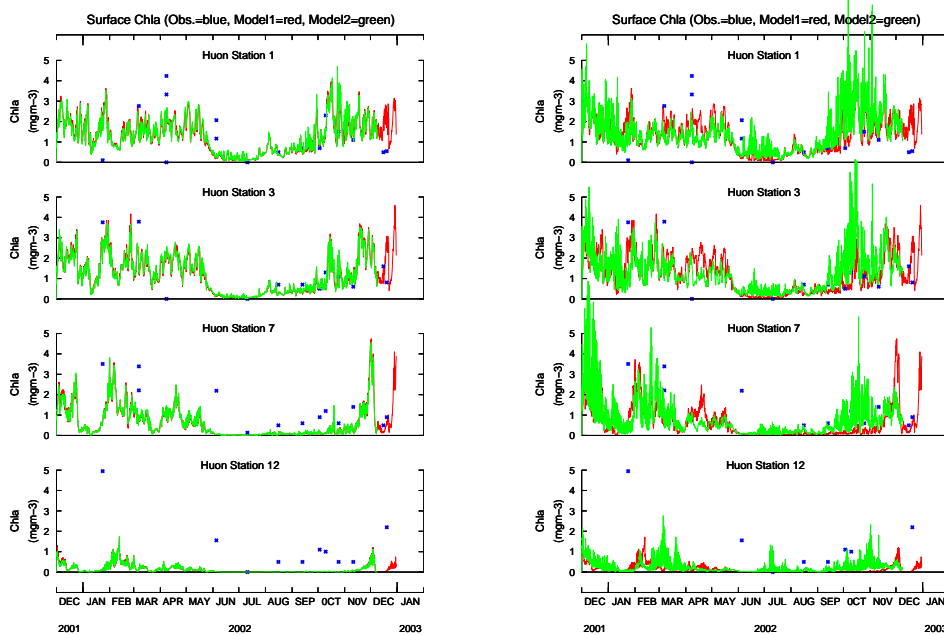


Figure 8.15: Time series of observed and simulated chlorophyll concentration at the surface (left) and at 4m (right) at stations in the Huon Estuary (station 1 is at the mouth, and station 12, in the middle of the estuary). Model with no vertical migration (red), with vertical migration (green) and observations (blue).

In this simulation there was little difference in surface chlorophyll concentration compared to the model run with no vertical migration, however at ~4m there was a significant increase in dinoflagellate biomass and a corresponding increase in chlorophyll concentration. In the Huon Estuary this was most sustained in spring, but the observed autumn dinoflagellate blooms were not reproduced.

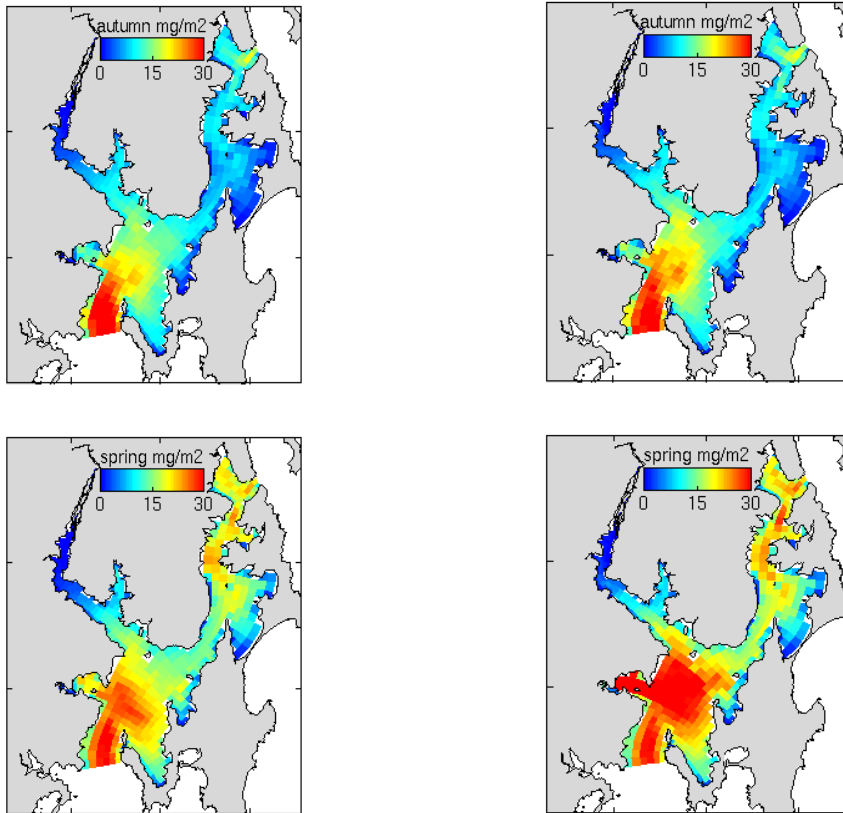


Figure 8.16: Autumn (top) and spring (bottom) mean depth integrated chlorophyll for the model run with no dinoflagellate vertical migration (left) and with vertical migration (right).

Dinoflagellate vertical migration increased the depth integrated chlorophyll concentration throughout the region most significantly in spring. Values throughout the D'Entrecasteaux channel, particularly the southern basin and Port Esperance were elevated by  $>20\text{mg m}^{-2}$ . In the Huon Estuary concentrations were slightly elevated in the mid and lower estuary. In shallow water and most of the side bays depth integrated chlorophyll concentrations were similar in both model runs as dinoflagellate concentrations were not favoured in shallow waters by the downward swimming response of surface cells. An exception to this was in Port Esperance which has relatively deep water and close proximity to the marine boundary where influx of seed populations of dinoflagellates might occur.

In autumn depth integrated chlorophyll concentrations in the lower Huon were enhanced by dinoflagellate vertical migration, however the observed highly concentrated blooms of dinoflagellates and the associated chlorophyll concentrations of  $>20\text{mg m}^{-3}$  were not reproduced.

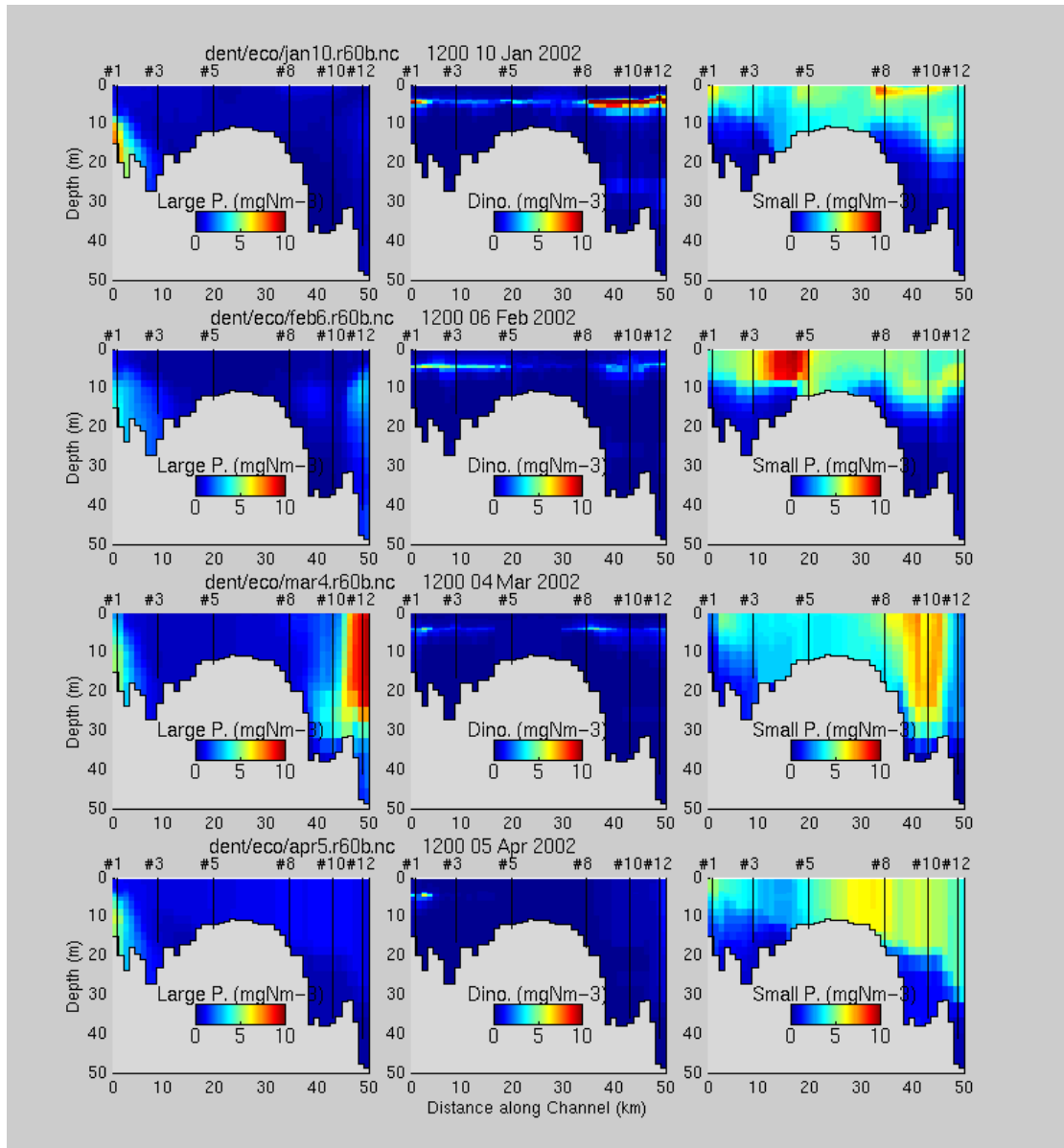


Figure 8.17a: Sections of modelled large phytoplankton, dinoflagellates and small phytoplankton through the D'Entrecasteaux Channel from north (left) to south (right). Dates and station marks correspond to the fieldwork program.

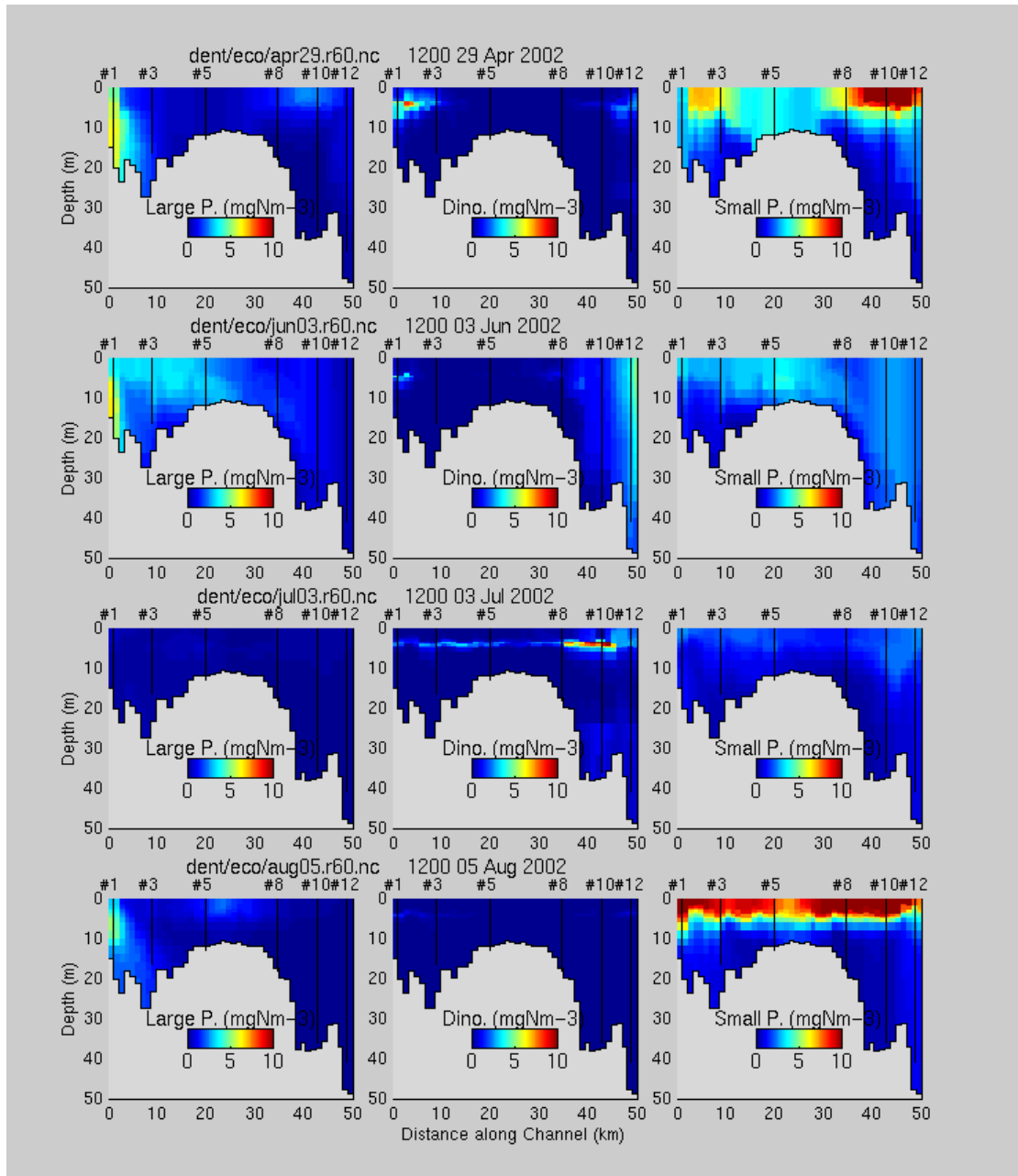


Figure 8.17b: Sections of modelled large phytoplankton, dinoflagellates and small phytoplankton through the D'Entrecasteaux Channel from north (left) to south (right). Dates and station marks correspond to the fieldwork program.

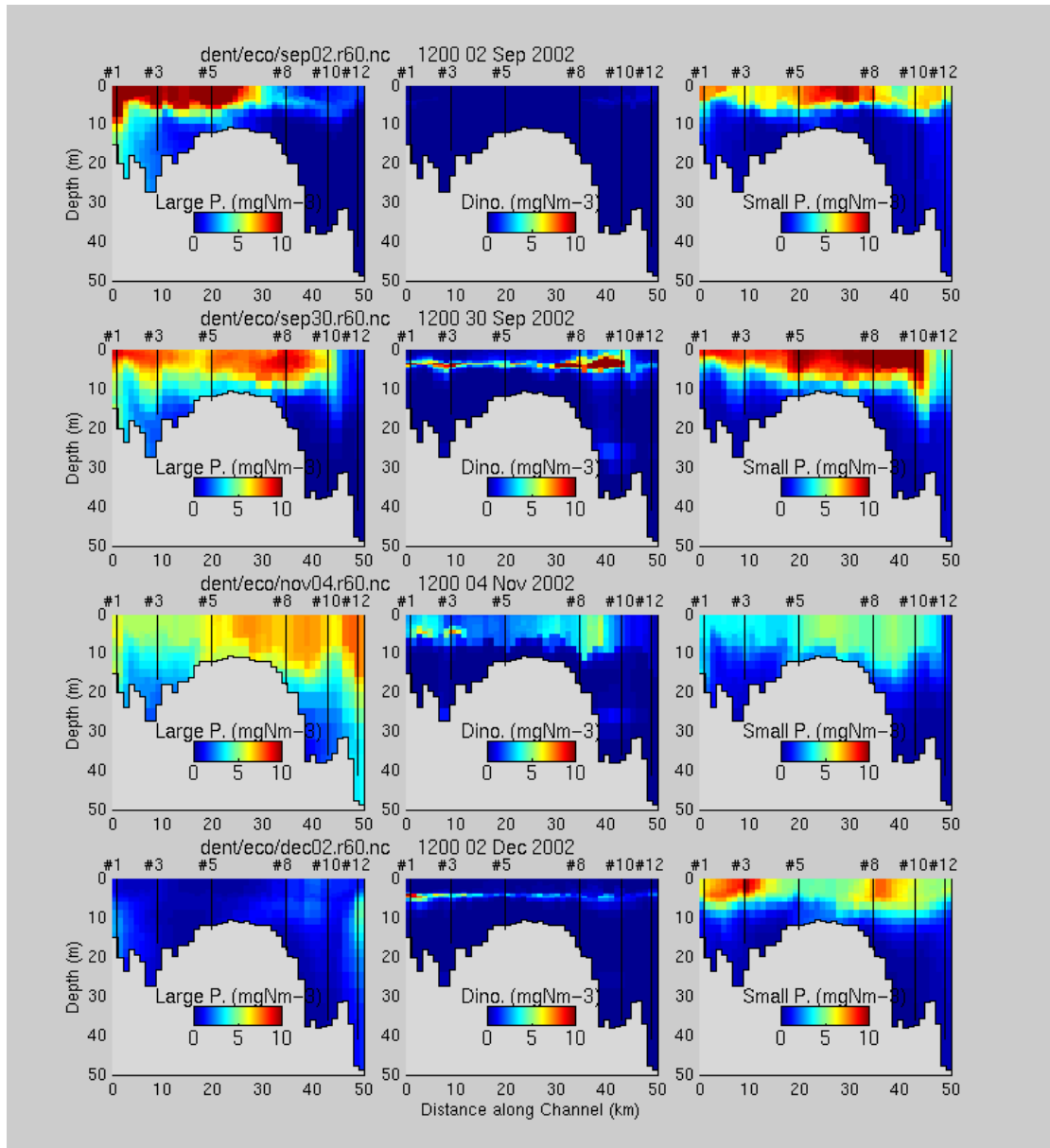


Figure 8.17c: Sections of modelled large phytoplankton, dinoflagellates and small phytoplankton through the D'Entrecasteaux Channel from north (left) to south (right). Dates and station marks correspond to the fieldwork program.

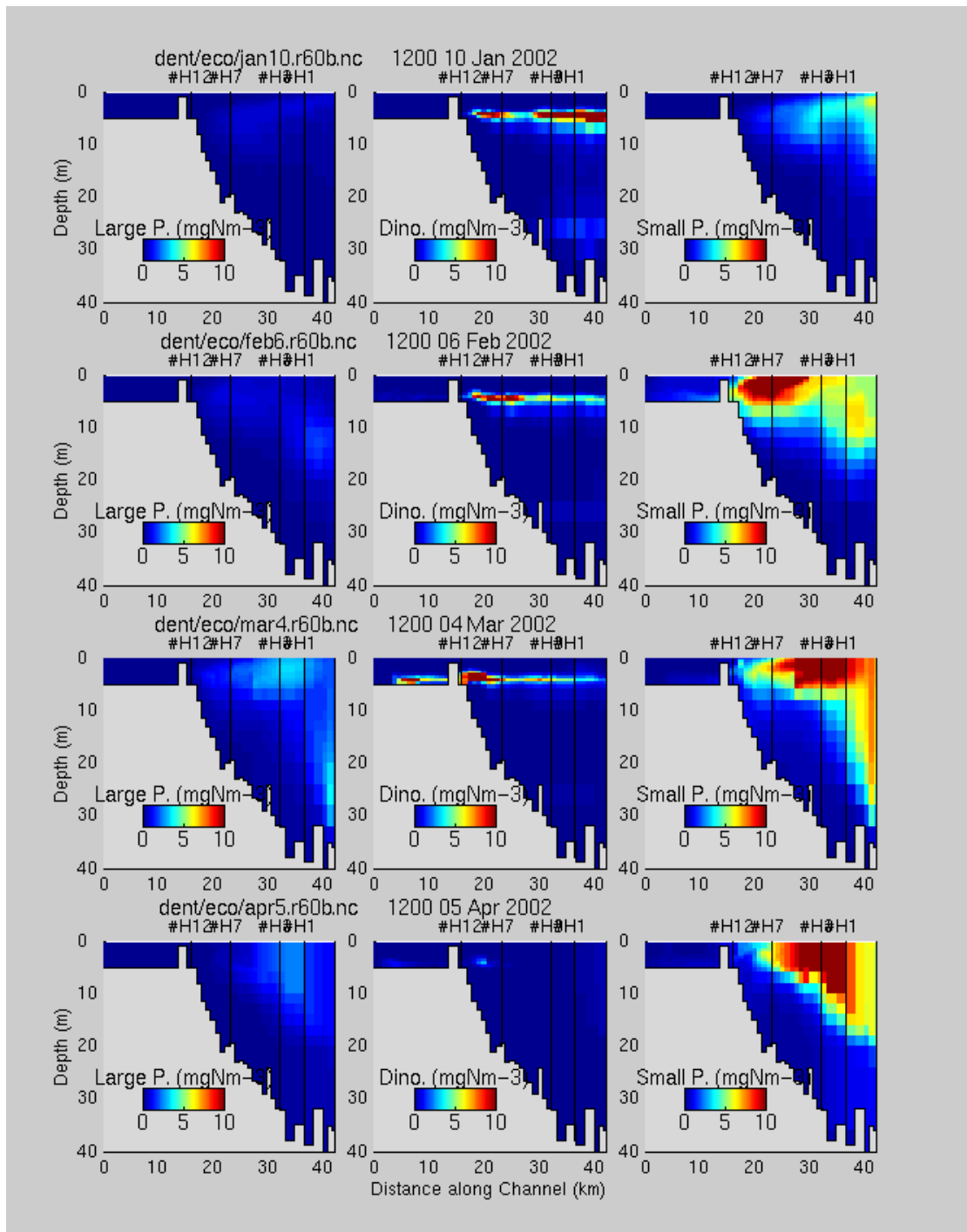


Figure 8.18a: Sections of modelled large phytoplankton, dinoflagellates and small phytoplankton through the Huon Estuary from the Huon River (left) to the D'Entrecasteaux Channel (right). Dates and station marks correspond to the fieldwork program.

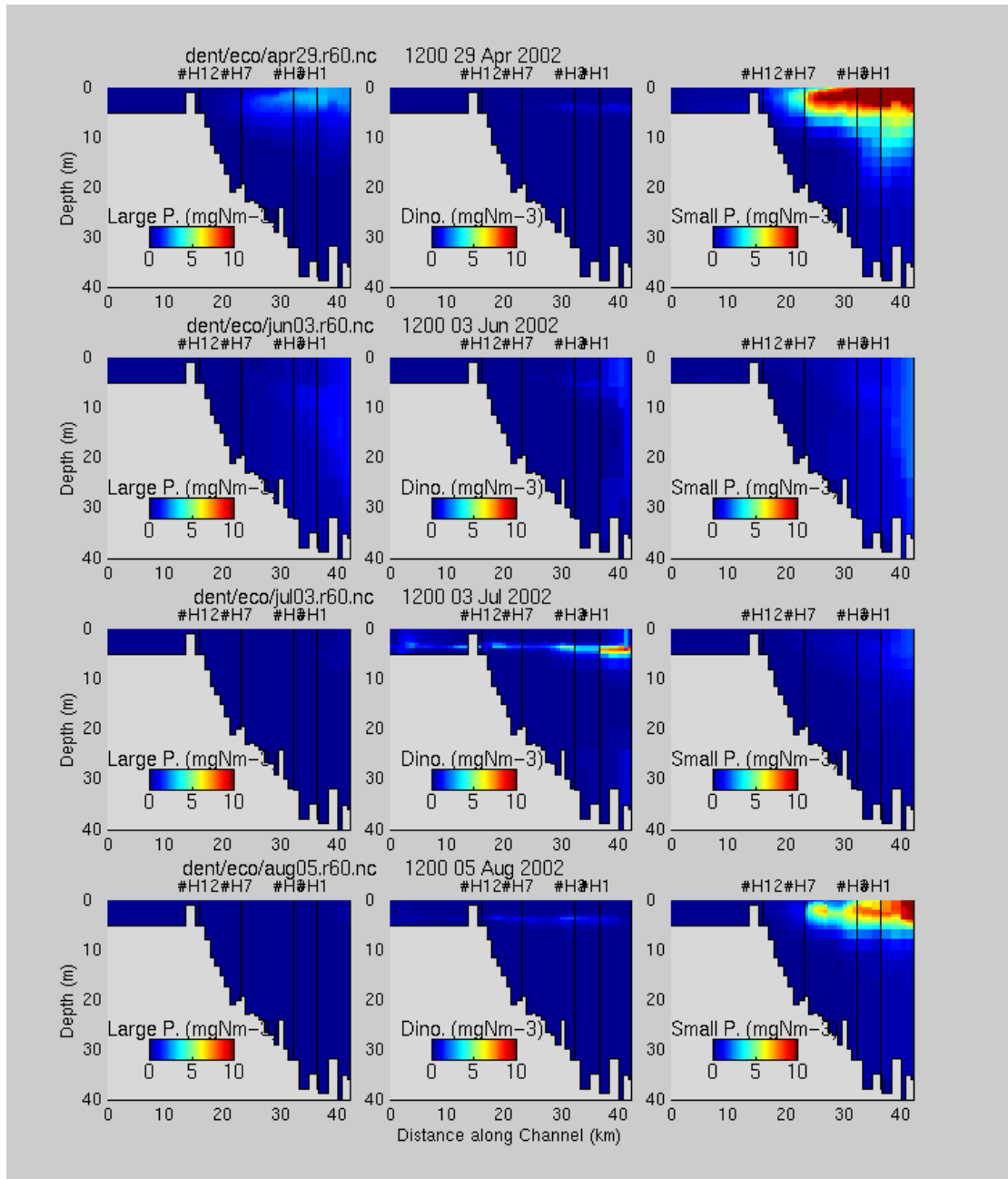


Figure 8.18b: Sections of modelled large phytoplankton, dinoflagellates and small phytoplankton through the Huon Estuary from the Huon River (left) to the D'Entrecasteaux Channel (right). Dates and station marks correspond to the fieldwork program.

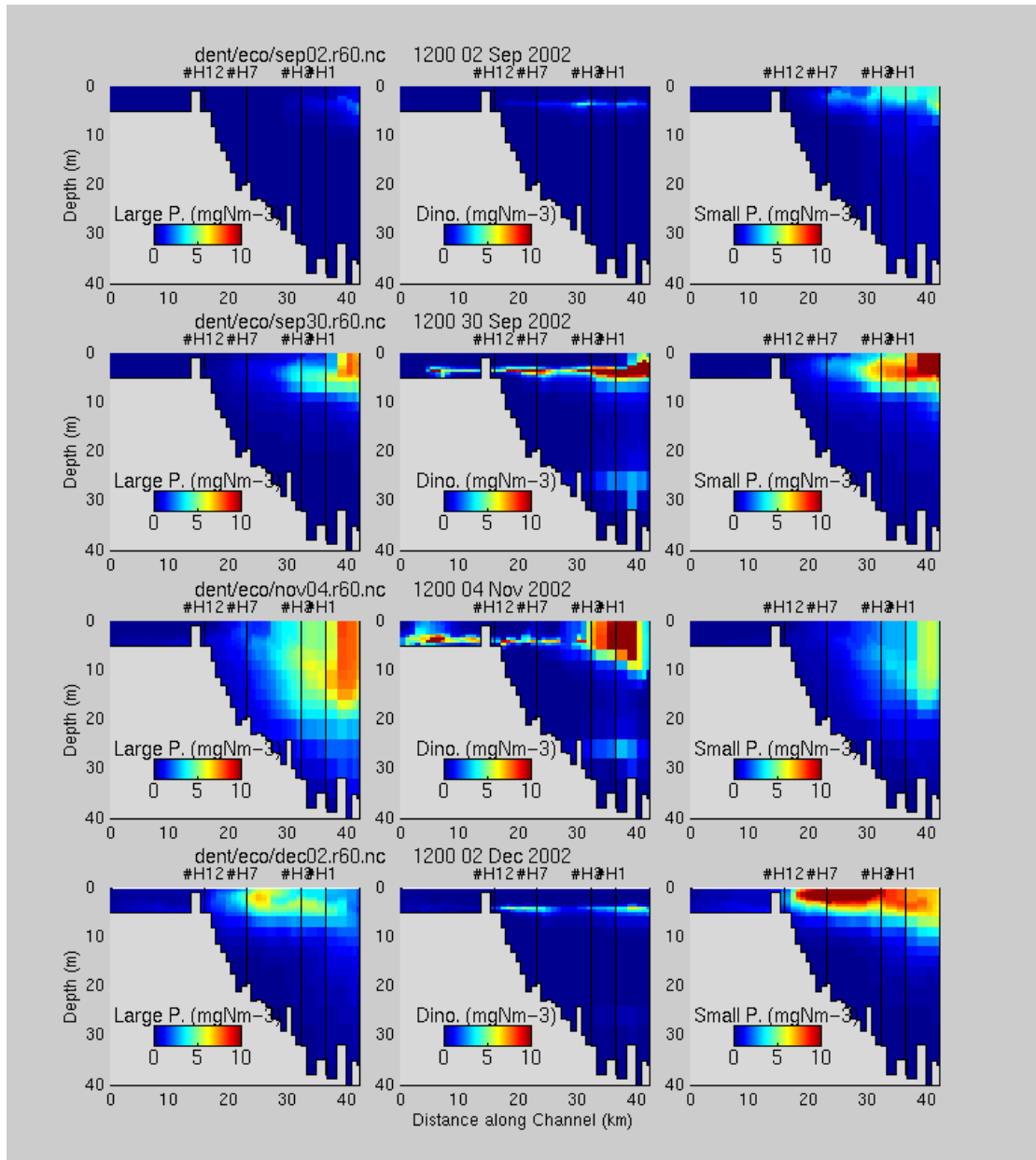


Figure 8.18c: Sections of modelled large phytoplankton, dinoflagellates and small phytoplankton through the Huon Estuary from the Huon River (left) to the D'Entrecasteaux Channel (right). Dates and station marks correspond to the fieldwork program.

The formulation for dinoflagellate migration capped with downward swimming above 4m simulated realistic distributions of dinoflagellates in the Huon Estuary throughout the year. Capping the upward swimming of dinoflagellates at 4m effectively retained them in the estuarine circulation through all seasons, however the simulated autumn biomass was considerably lower than that observed. Two possible explanations immediately present themselves: firstly the migration cap of 4m may at times be either too deep, therefore limiting dinoflagellate exposure to light and the resulting growth rate, or too shallow causing too much biomass to be swept out of the estuary in the

surface river plume. An improved formulation might cap migration as a function of fresh water so that dinoflagellates could have greater exposure to PAR when the surface river plume was very shallow or absent but remain below the plume during flood events. Whilst this formulation might be appropriate for an estuarine situation, in the fully marine D'Entrecasteaux Channel and in particular the shallow side bays, dinoflagellates would rapidly dominate the phytoplankton community. As this has not been observed, salinity may not cap vertical migration in the region.

An alternative explanation is that vertical migration in the model effectively halves dinoflagellate exposure to PAR, which is modelled as a 24 hour mean intensity, as migrating biomass accumulates at the bottom or beyond the euphotic layer for ~10 hours per day. In a system where growth is limited by exposure to PAR and nutrients are generally replete vertical migration would be disadvantageous to growth. To examine this hypothesis further a more realistic model is required which simulates diurnal cycles in ambient PAR, nutrient uptake, and resulting growth and respiration.

Finally there remains the possibility that some other aspect of the dinoflagellate lifecycle (in particular *Gymnodinium catenatum*) is having a fundamental impact on the occurrence of blooms in the region. Such a characteristic might be a requirement for a riverine micronutrient(s), the avoidance of a marine predator or successful cycles of encystment and excystment which in turn might depend on spatially variable sediment type and benthic fauna.

## 8.5 Summary of model performance

The model is sensitive to the rate of zooplankton swimming and associated grazing which controls the amount of phytoplankton biomass and productivity of the system. Grazing rate also impacts the ambient nutrient concentration by limiting phytoplankton biomass available to take up nutrients and efficiently recycling a portion of the grazed material. The results suggest that high zooplankton swimming speeds / clearance rates, which result in tight grazing control of phytoplankton biomass, are not compatible with the observed seasonal cycle in phytoplankton biomass.

The relatively minor effect of halving denitrification efficiencies in the model reflects the relatively short flushing times of the D'Entrecasteaux / Huon system. Flushing rather than denitrification constitutes the major control on the accumulation of nitrogen loads in this system, in contrast for example with Port Phillip Bay, where denitrification accounts for 80 to 90% of nitrogen loads.

Doubling the absorption coefficients for phytoplankton had a limited impact on phytoplankton biomass in the model system. This is because for much of the year the phytoplankton are nutrient and not light limited in both simulations. The exception to this situation is in spring when winter nutrients and increasing day length provide optimal conditions for growth. In the simulation

with double phytoplankton absorption coefficients the phytoplankton growth in spring occurred earlier and generated more biomass than in the former simulation.

## *9 Model Results*

### **9.1 Annual regional biogeochemistry**

Modelled annual median chlorophyll concentrations are  $\sim 1\text{mgChl m}^{-3}$  in surface waters throughout the D'Entrecasteaux Channel with slightly higher values in the southern basin compared to the northern end of the Channel. In the Huon Estuary modelled chlorophyll concentrations are lower contrary to observations. There are significant differences in spatial distribution between the 10 and 90 percentile concentrations with consistently higher chlorophyll concentrations simulated off Cygnet and Port Esperance.

Modelled annual median oxygen saturation drops from  $\sim 100\%$  in surface waters to  $\sim 80\%$  in bottom waters of the lower Huon Estuary. The most oxygen depleted waters were simulated in the upper Huon attributed to the influx of fresh river water. Values in bottom waters of the D'Entrecasteaux Channel were generally higher than in the Huon Estuary.

Median annual dissolved inorganic nitrogen is  $\sim 10\text{mgN m}^{-3}$  in surface waters of the D'Entrecasteaux Channel and about four times that in the Huon Estuary. Bottom water concentrations were highest in the mid Huon Estuary and in relatively shallow water, where the opaque river water limited phytoplankton growth and uptake. The considerable range in concentration between the 10 and 90 percentile concentrations results from utilization of nutrients by phytoplankton over an annual cycle.

The spatial distribution of phosphorus concentration is similar to that for nitrogen with the larger concentrations simulated in the Huon Estuary and at depth. The 10 percentile surface concentrations are elevated compared to nitrogen indicating that the latter is controlling phytoplankton production in the region.

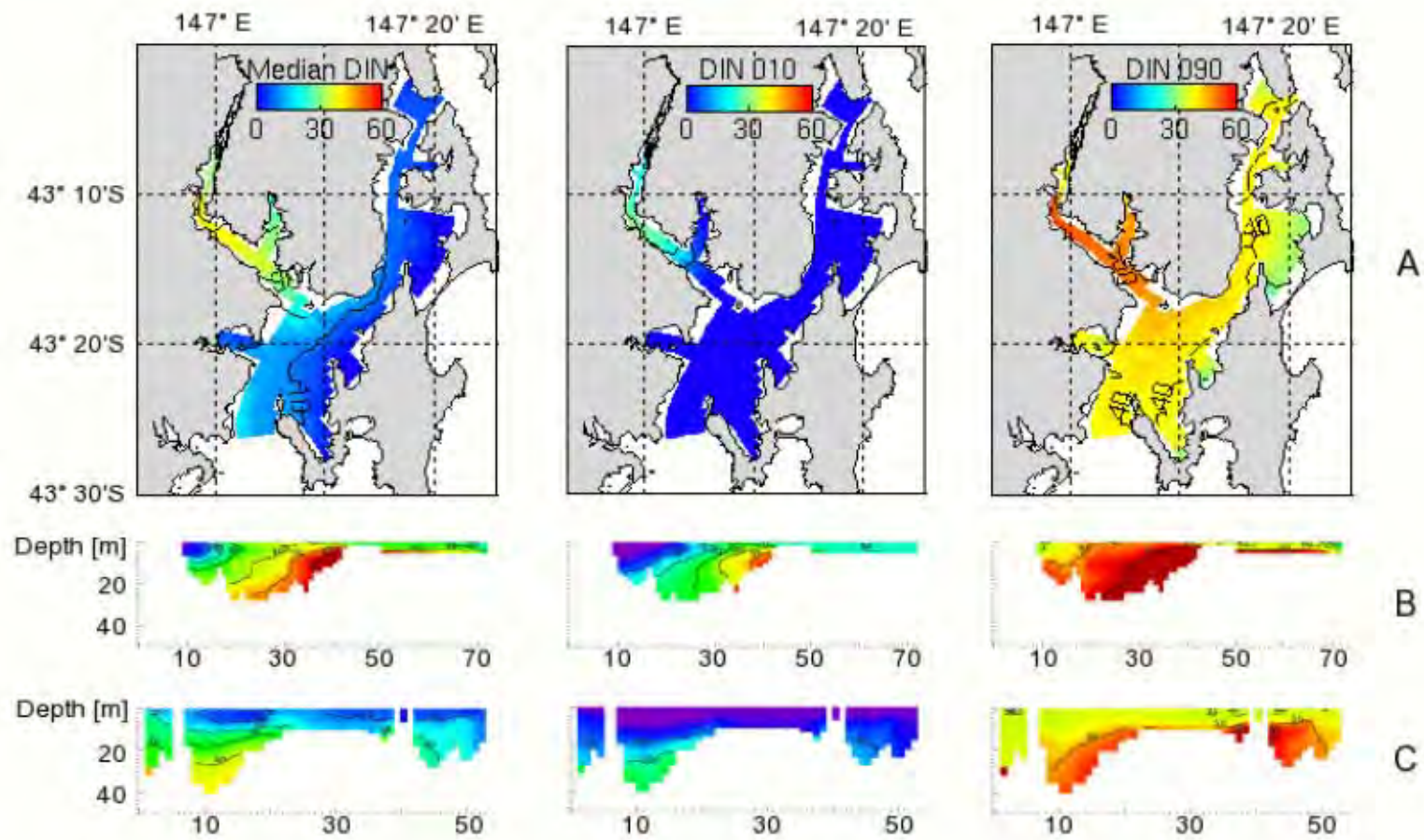


Figure 9.1: A) Surface concentration of annual median, 10 and 90 percentile dissolved inorganic nitrogen with (B) vertical cross sections through the Huon Estuary [from D'Entrecasteaux Channel (left) to Huon river (right)] and (C) the D'Entrecasteaux Channel [from south (left) to north (right)].

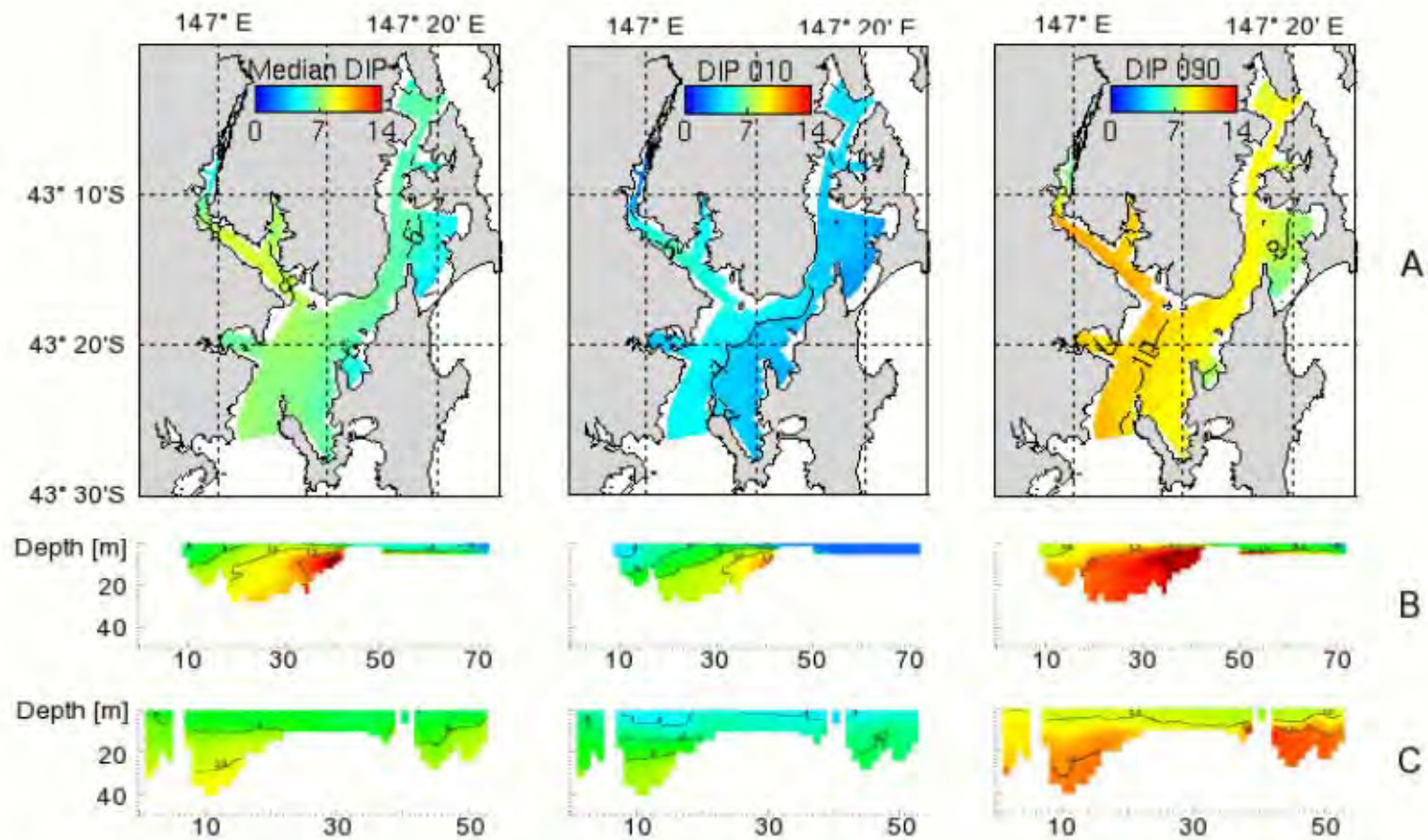


Figure 9.2: A) Surface concentration of annual median, 10 and 90 percentile dissolved inorganic phosphate with (B) vertical cross sections through the Huon Estuary [from D'Entrecasteaux Channel (left) to Huon river (right)] and (C) the D'Entrecasteaux Channel [from south (left) to north right)].

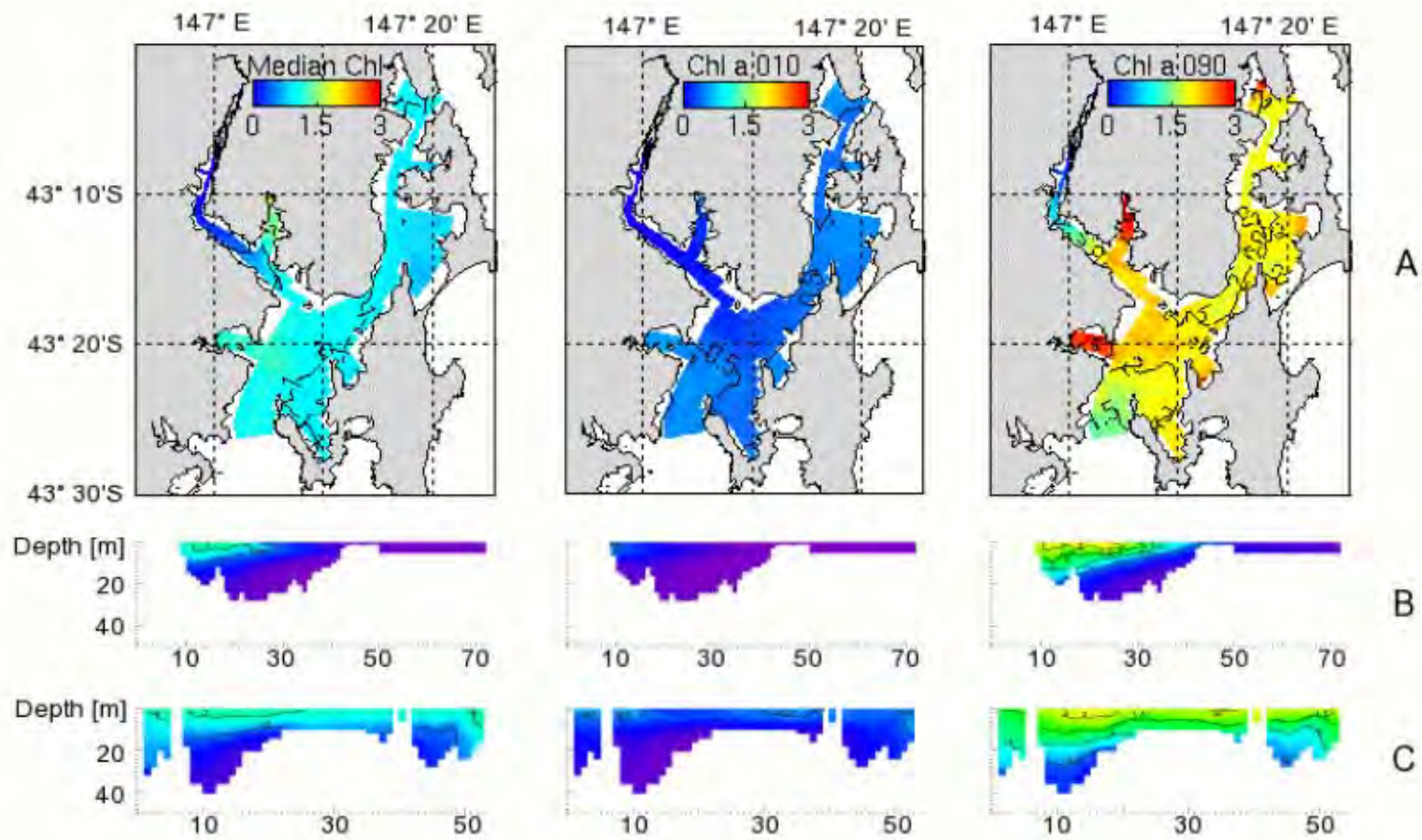


Figure 9.3: A) Surface concentration of annual median, 10 and 90 percentile chlorophyll concentration with (B) vertical cross sections through the Huon Estuary [from D'Entrecasteaux Channel (left) to Huon river (right)] and (C) the D'Entrecasteaux Channel [from south (left) to north (right)].

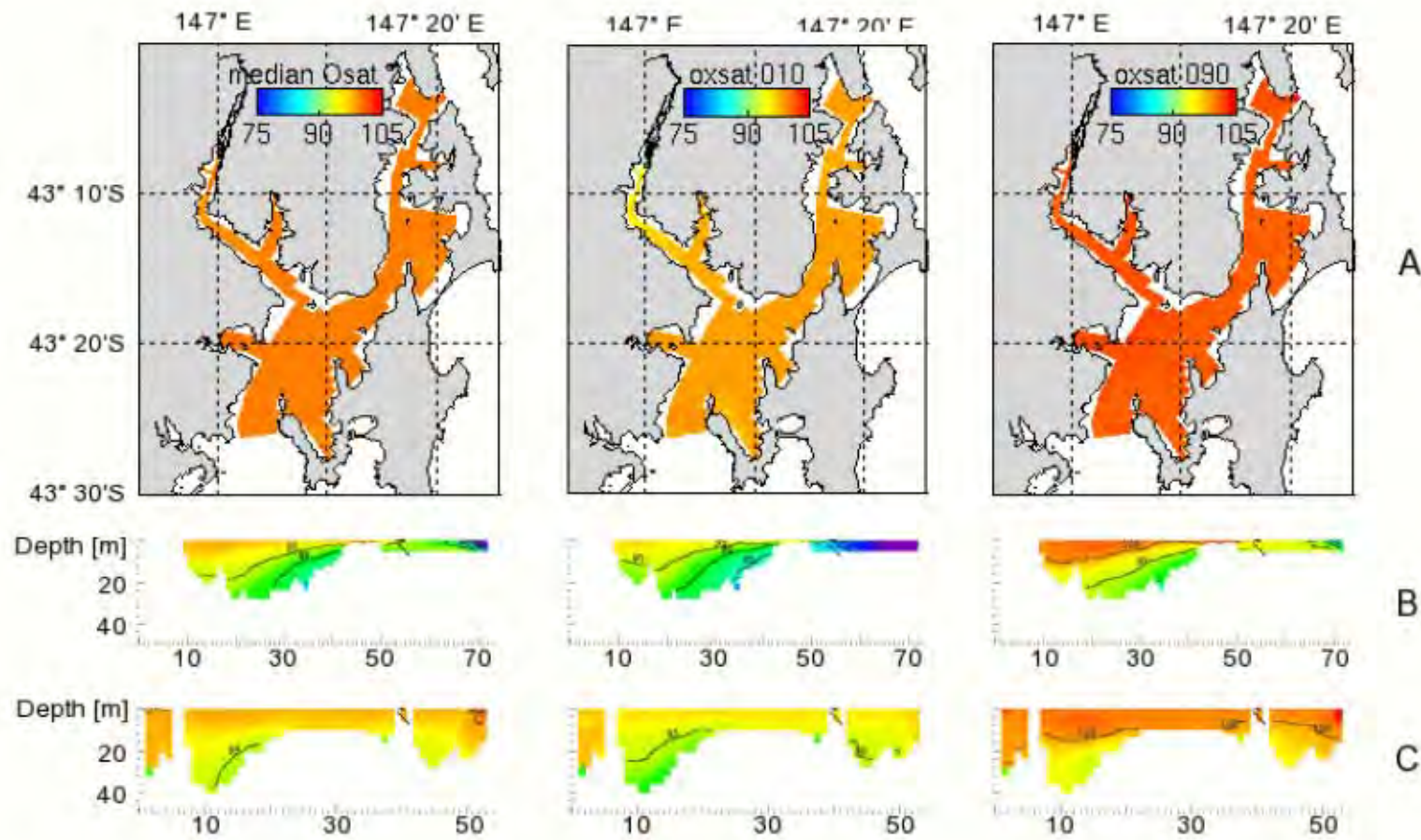


Figure 9.4: A) Surface concentration of annual median, 10 and 90 percentile oxygen saturation with (B) vertical cross sections through the Huon Estuary [from D'Entrecasteaux Channel (left) to Huon river (right)] and (C) the D'Entrecasteaux Channel [from south (left) to north (right)].

## 9.2 Seasonal regional biogeochemistry

### Nutrients

In summer and autumn surface DIN and DIP concentrations are depleted throughout the D'Entrecasteaux Channel and lower Huon Estuary due to phytoplankton assimilation and thermal stratification limiting vertical mixing. In the mid and upper Huon Estuary shallow water nutrients remain during this period as phytoplankton assimilation in the opaque river water is low [and probably under predicted by the model] and local nutrient influx from the river water and fish farm discharge exceeds algal uptake. The distinct subsurface peak in nutrient concentration in the mid estuary is formed by the accumulation of nutrients from the Huon and Kermadec River [which is enhanced by a local sewerage treatment plant] in the opaque river water.

In winter the seasonal weather mixes river, farm and marine nutrient into surface waters and as phytoplankton growth is limited (by low incident irradiance and enhanced vertical mixing) surface concentrations are elevated. Maximum nutrient concentrations are found in the mid and lower Huon Estuary and at the northern end of the D'Entrecasteaux Channel.

During spring incident irradiance increases and the water column becomes more stable which favours phytoplankton growth. Nutrients in the euphotic layer are rapidly utilized by the phytoplankton and concentrations in surface waters become depleted.

### Chlorophyll

Chlorophyll concentrations are elevated in surface waters during summer and autumn with highest median concentrations of  $1.5\text{mg m}^{-3}$  found in autumn in the lower Huon Estuary and southern basin of the D'Entrecasteaux Channel. In autumn phytoplankton growth is limited by surface nutrient supply and diminishing incident irradiance as winter approaches. [Simulated chlorophyll concentrations in the Huon Estuary are lower than observed as the model fails to capture the dynamics of dinoflagellate blooms which can be significant in autumn.]

Over winter phytoplankton growth is limited by seasonally low irradiance and enhanced vertical mixing and chlorophyll concentrations are low throughout the region.

In spring median chlorophyll concentrations are higher throughout the D'Entrecasteaux Channel and side bays  $\sim 2\text{mg m}^{-3}$  with maximum concentration simulated in Port Esperance. Spring chlorophyll concentrations in the Huon Estuary are lower due to the strongly attenuating river water which limits available PAR for phytoplankton growth.

## Oxygen

Oxygen saturation is generally high throughout the region in all seasons as the model system is well flushed [possibly excessively due to the necessarily coarse resolution of the bottom bathymetry]. Example sections show some draw-down of oxygen saturation at depth associated with benthic oxygen demand for remineralisation of organic detritus. In summer and autumn stratification limits surface oxygen exchange with bottom waters and maximal draw-down of ~20% occurs in the lower Huon Estuary.

In winter seasonally strong mixing mixes well oxygenated surface waters to the bottom where it is utilized by benthic remineralisation of organic material. During spring vertical gradients in oxygen are enhanced as surface waters become supersaturated with oxygen produced by phytoplankton photosynthesis.

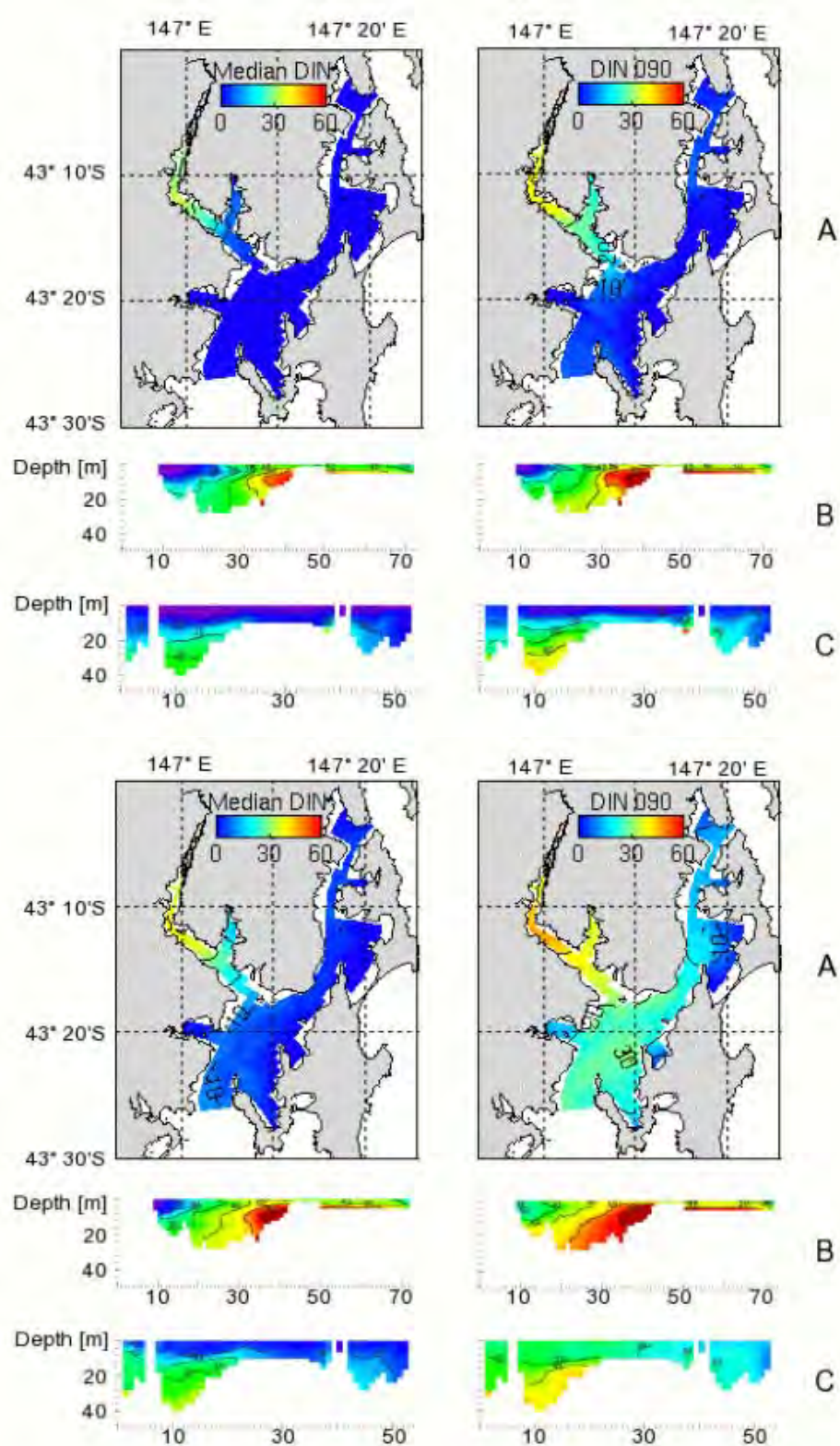


Figure 9.5: Summer (top) and autumn (bottom) (A) surface concentration of median and 90 percentile dissolved inorganic nitrogen with (B) vertical cross sections through the Huon Estuary [from D'Entrecasteaux Channel (left) to Huon river (right)] and (C) the D'Entrecasteaux Channel [from south (left) to north (right)].

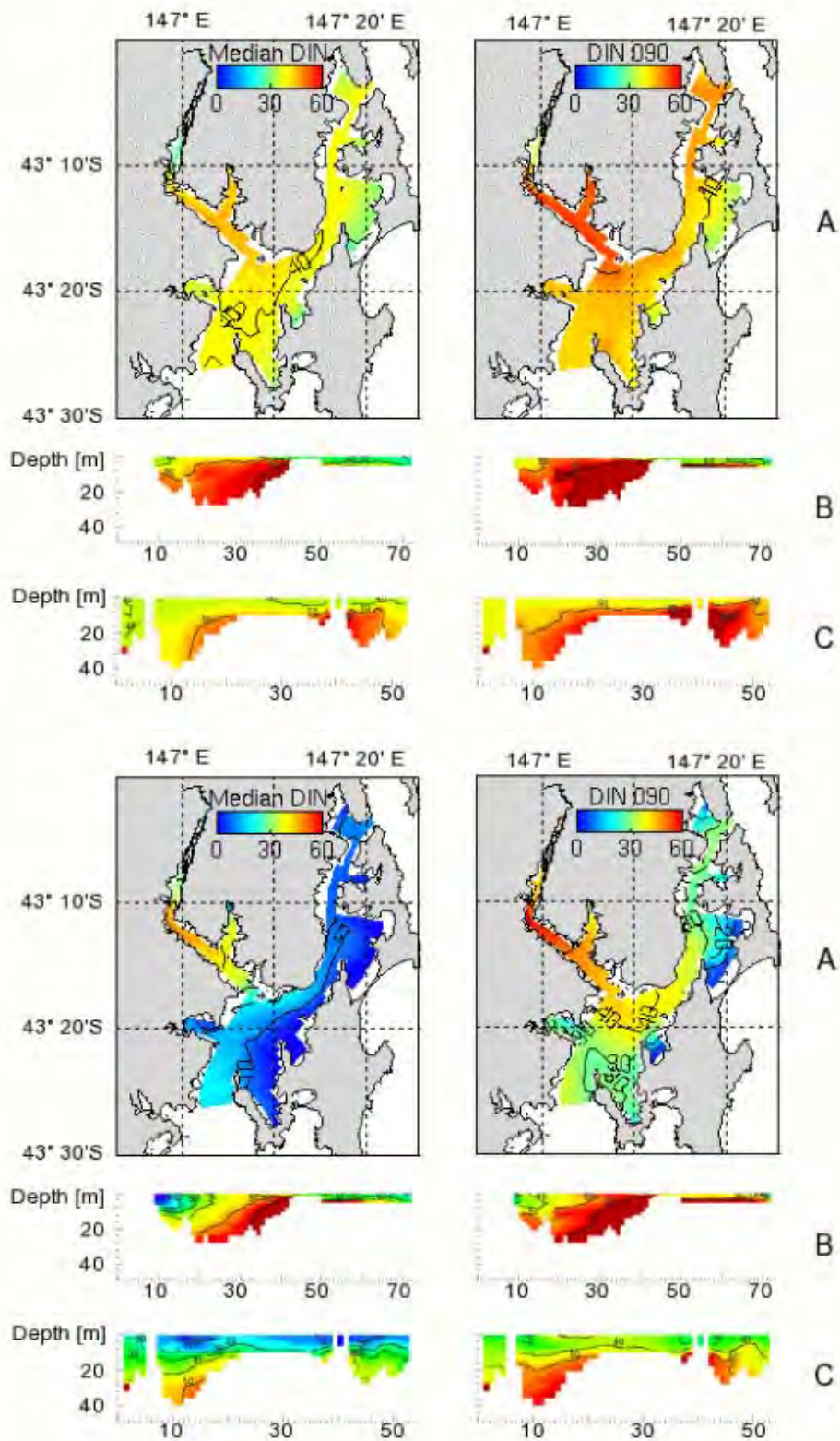


Figure 9.6: Winter (top) and spring (bottom) (A) surface concentration of median and 90 percentile dissolved inorganic nitrogen with (B) vertical cross sections through the Huon Estuary [from D'Entrecasteaux Channel (left) to Huon river (right)] and (C) the D'Entrecasteaux Channel [from south (left) to north (right)].

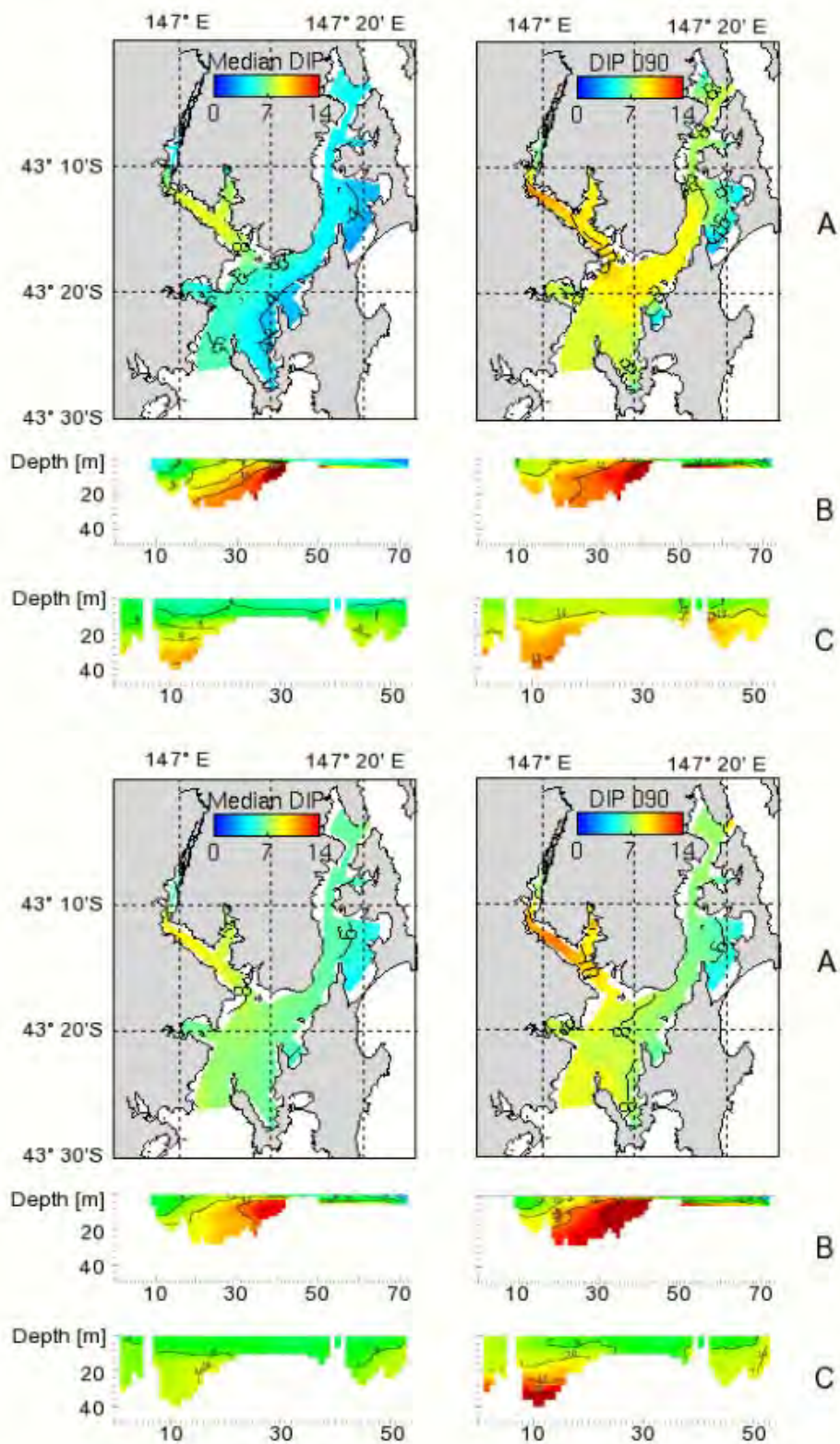


Figure 9.7: Summer (top) and autumn (bottom) (A) surface concentration of median and 90 percentile modelled dissolved inorganic phosphate with (B) vertical cross sections through the Huon Estuary [from D'Entrecasteaux Channel (left) to Huon river (right)] and (C) the D'Entrecasteaux Channel [from south (left) to north (right)].

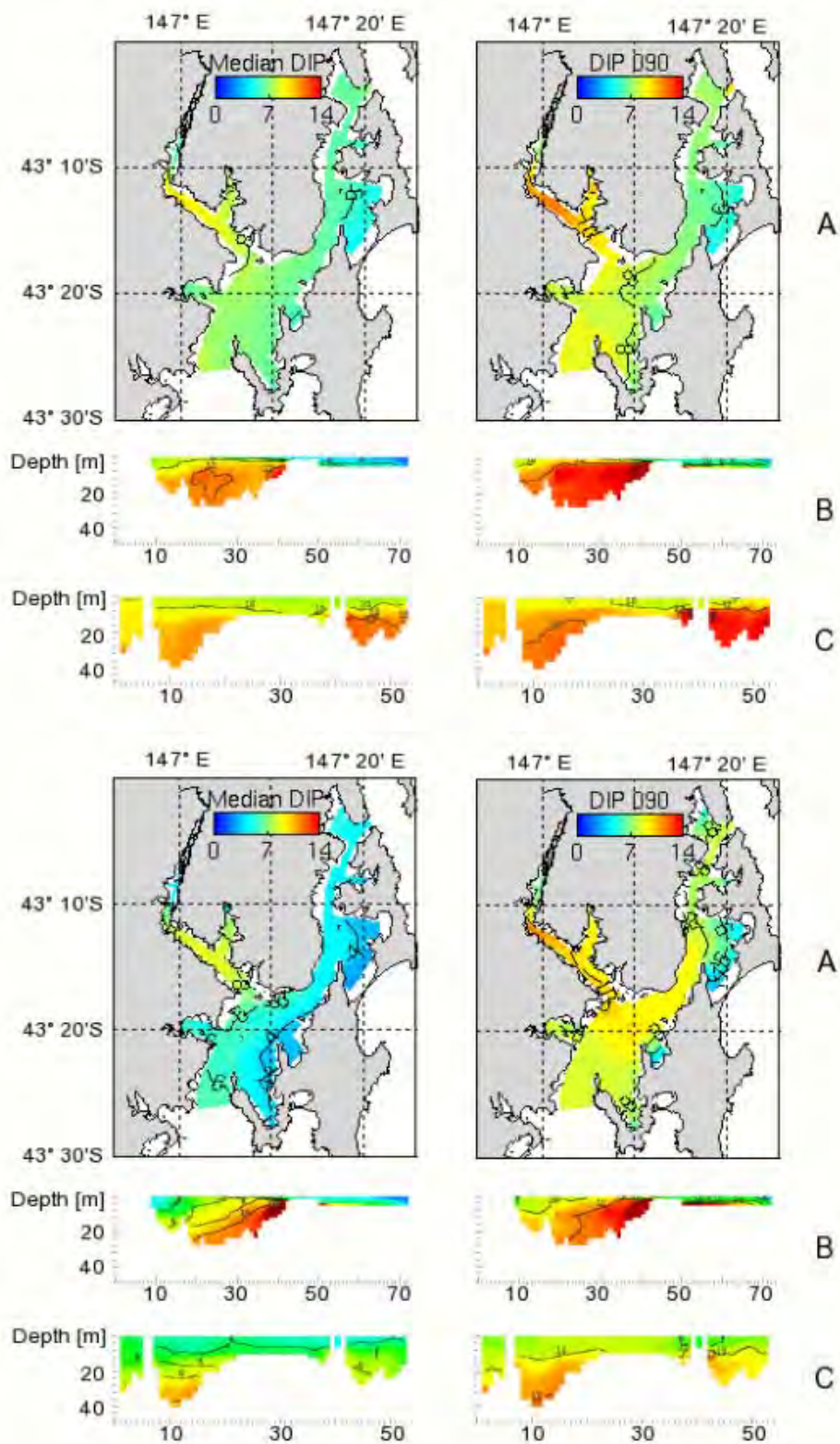


Figure 9.8: Winter (top) and spring (bottom) (A) surface concentration of median and 90 percentile modelled dissolved inorganic phosphate with (B) vertical cross sections through the Huon Estuary [from D'Entrecasteaux Channel [from D'Entrecasteaux Channel (left) to Huon river (right)] and (C) the D'Entrecasteaux Channel [from south (left) to north (right)].

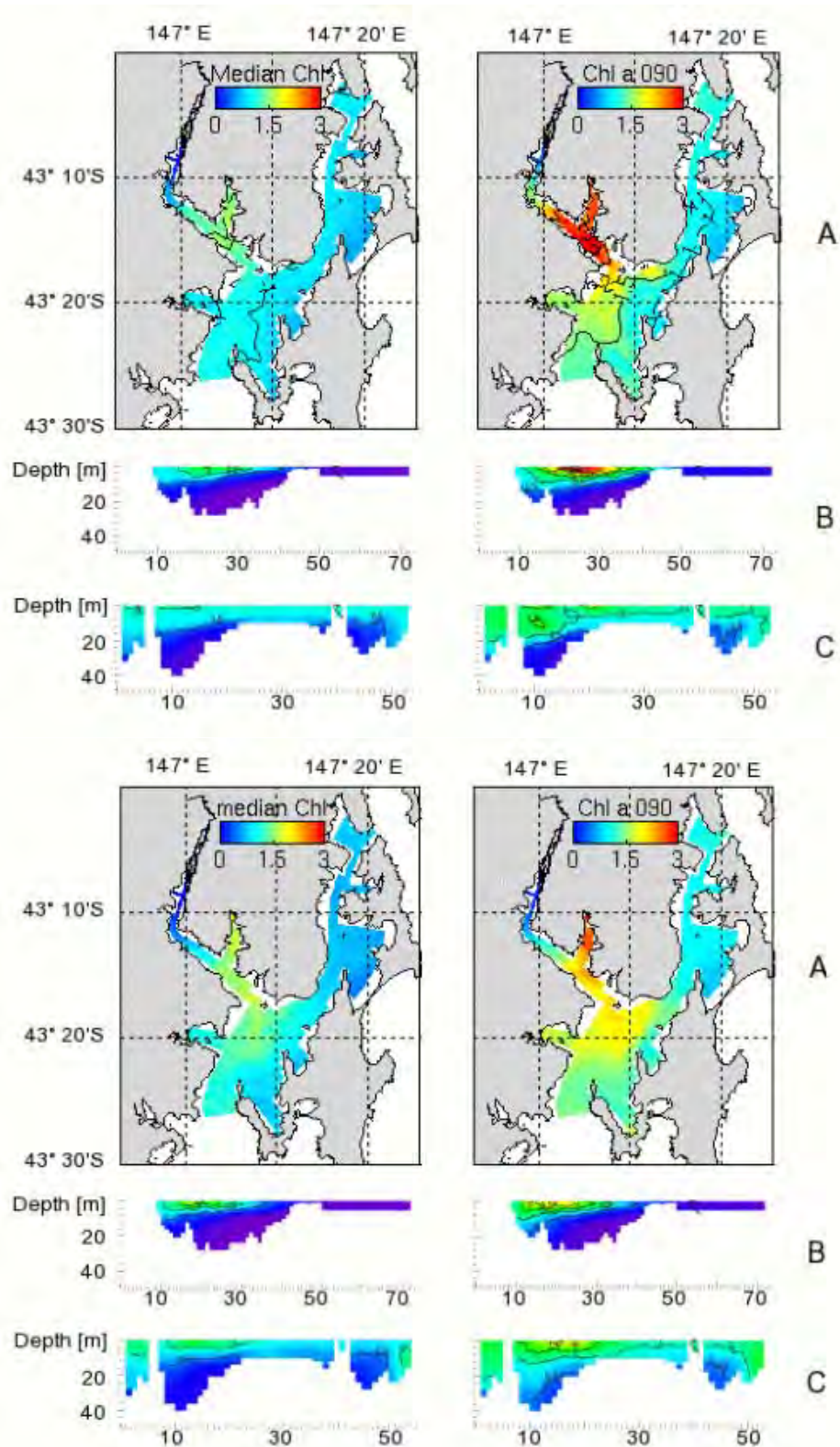


Figure 9.9: Summer (top) and autumn (bottom) (A) surface concentration of median and 90 percentile chlorophyll concentration with (B) vertical cross sections through the Huon Estuary [from D'Entrecasteaux Channel (left) to Huon river (right)] and (C) the D'Entrecasteaux Channel [from south (left) to north (right)].

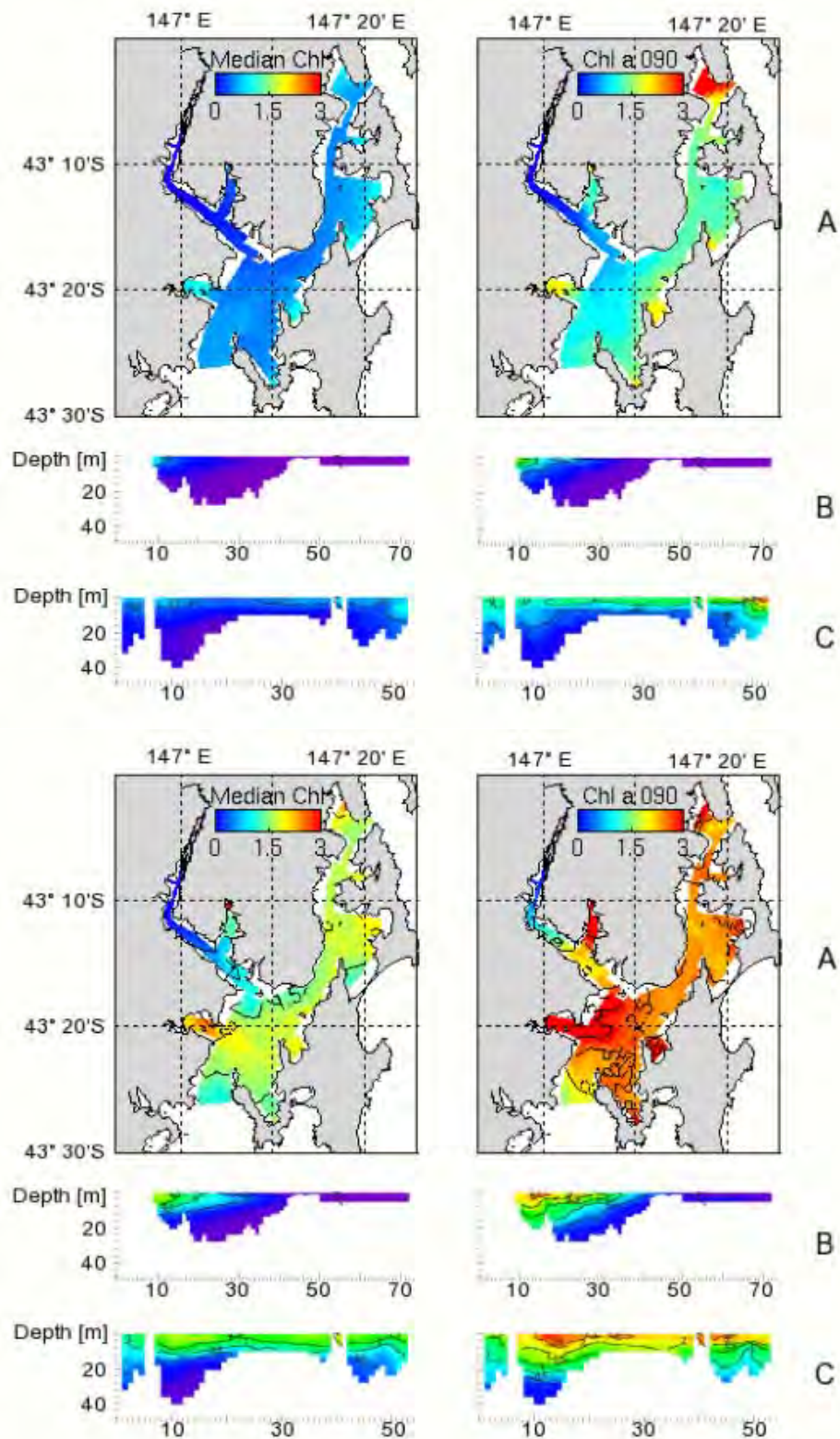


Figure 9.10: Winter (top) and spring (bottom) (A) surface concentration of median and 90 percentile chlorophyll concentration with (B) vertical cross sections through the Huon Estuary [from D'Entrecasteaux Channel (left) to Huon river (right)] and (C) the D'Entrecasteaux Channel [from south (left) to north (right)].

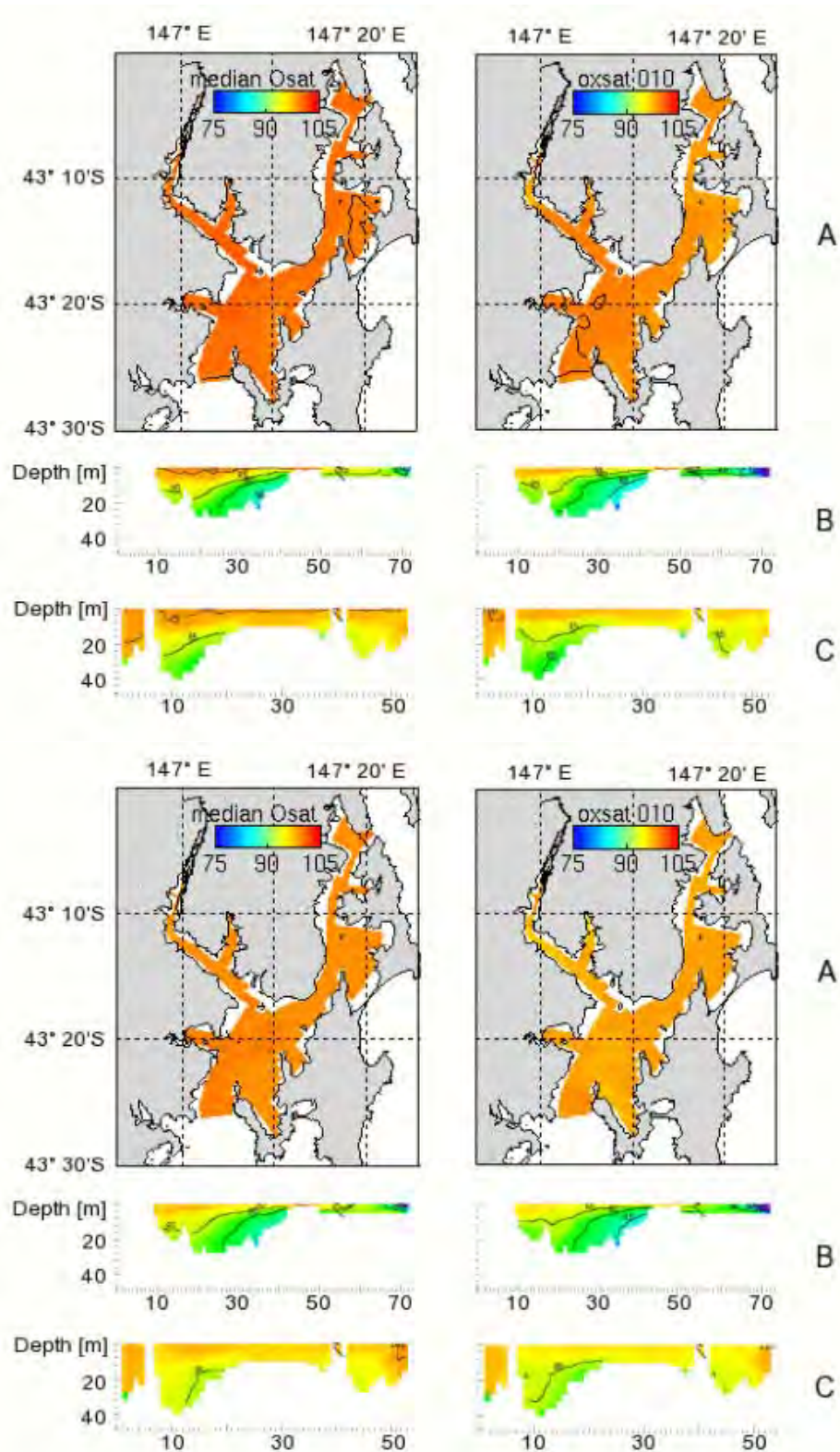


Figure 9.11: Summer (top) and autumn (bottom) (A) surface concentration of median and 10 percentile oxygen saturation with (B) vertical cross sections through the Huon Estuary [from D'Entrecasteaux Channel (left) to Huon river (right)] and (C) the D'Entrecasteaux Channel [from south (left) to north (right)].

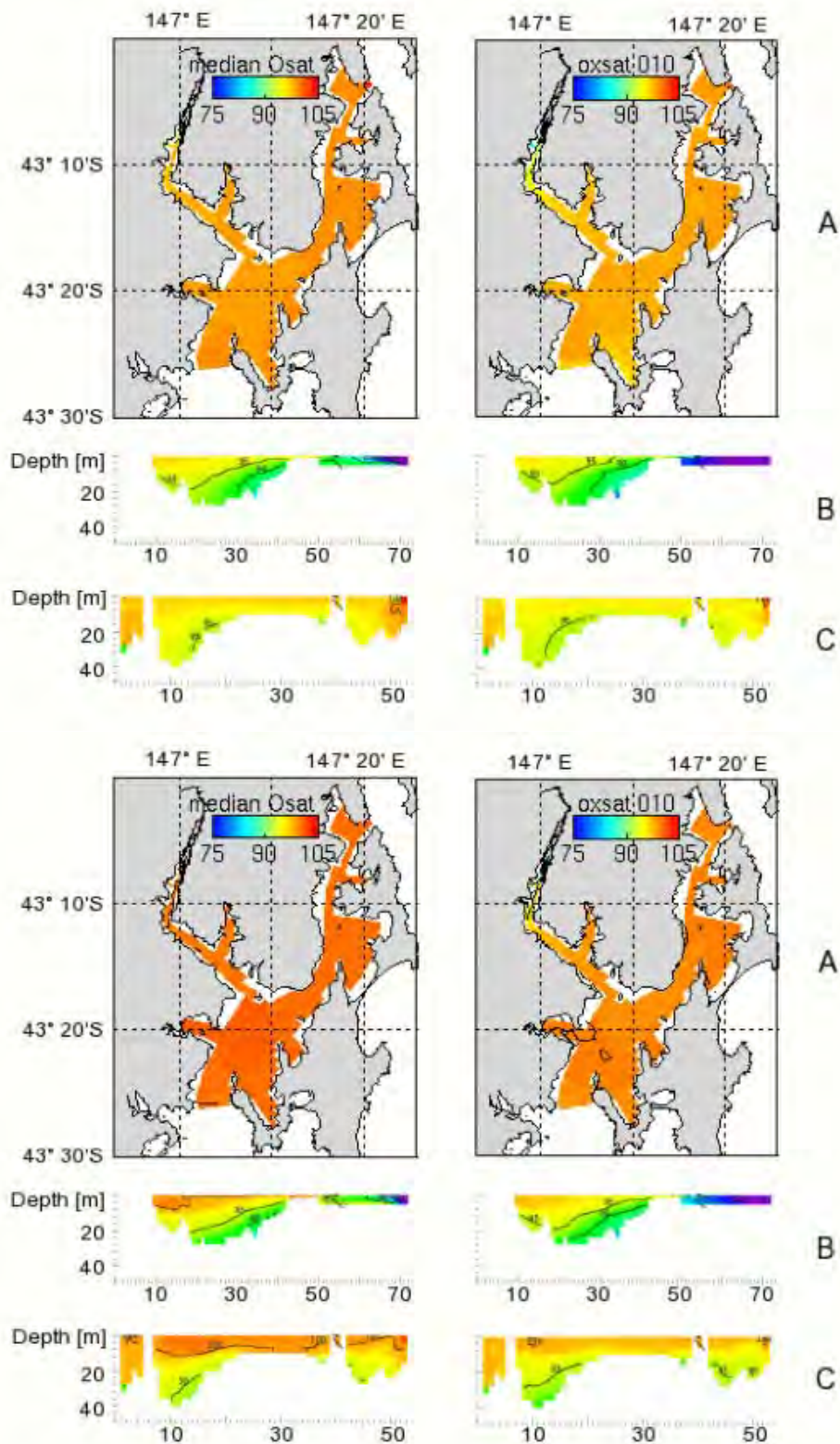


Figure 9.12: Winter (top) and spring (bottom) (A) surface concentration of median and 10 percentile oxygen saturation with (B) vertical cross sections through the Huon Estuary [from D'Entrecasteaux Channel (left) to Huon river (right)] and (C) the D'Entrecasteaux Channel [from south (left) to north (right)].

## 10 Scenario simulations

To clearly demonstrate the impact in the model of fish farm and river discharges on the biogeochemical cycling and water quality of the Huon Estuary and D'Entrecasteaux Channel model simulations were made with contrasting nutrient loads. For the first scenario discharges from the fish farms were omitted, whilst dissolved and particulate inputs from the Huon, Kermandie, Esperance and Northwest Bay Rivers remained. By comparing this simulation with the original model run the impacts of fish farm discharges throughout the region are clearly shown.

In a second scenario simulation both fish farm and secondary river discharges (from the Kermandie, Esperance and Northwest Bay Rivers) of dissolved and particulate substances were omitted. Discharges from the Huon river were included in the simulation as this river dominates the circulation and biogeochemistry of the region. By comparing the first and second scenario simulations the impact of river loads from the Kermandie, Esperance and Northwest Bay River are clearly shown.

Model Run	Description	Results
Original model	Fish farm and all river discharges included	Baseline simulation
First scenario	Fish farm discharges omitted	Impact of fish farm discharges
Second scenario	Fish farm and secondary river discharges omitted	Impact of secondary river discharges

Table 10.1: Summary of model scenario simulations.

### 10.1 Impact of fish farm discharges

The simulation with fish farm discharges omitted is compared with the original model simulation and differences between the simulations are presented. Comparisons are presented as maps and tables of both relative changes (ratios) and absolute changes (differences) in indicators.

For the ratio plots:

<1 = reduced concentration; 1 = no difference; > 1 = enhanced concentration.

For the difference plots:

-ve value = reduced concentration; 0 = no difference; +ve value = enhanced concentration.

In general farm discharges had greatest impact on the nutrient fields in summer and on the phytoplankton in autumn. Results are shown for dissolved nutrients in winter and summer and for chlorophyll and oxygen in spring and autumn.

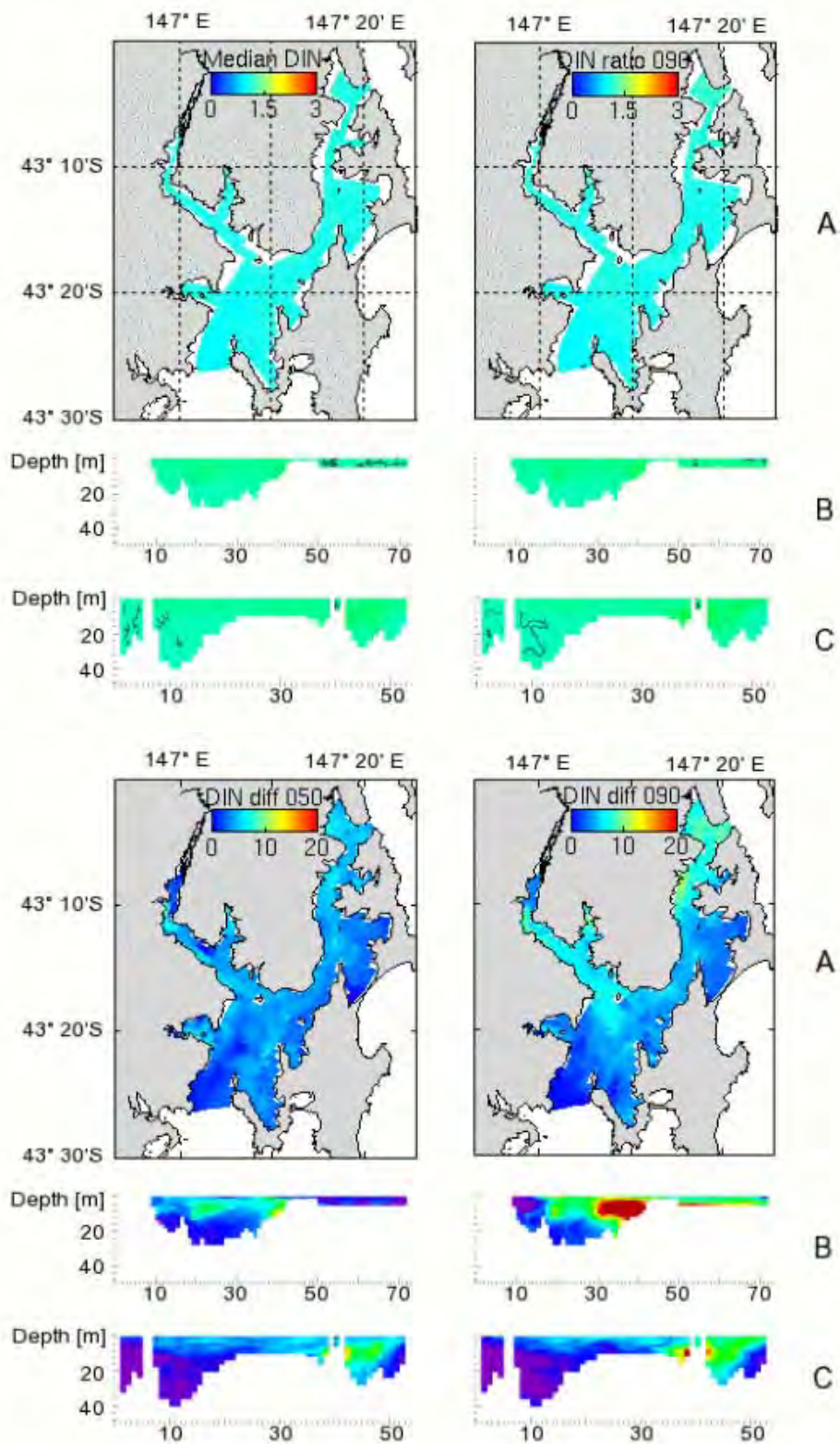


Figure 10.1: Ratio (top) and absolute difference (bottom) in winter median and 90 percentile dissolved inorganic nitrogen between the model run with and without fish farm discharges (A) surface distribution, (B) vertical cross section through the Huon Estuary [from D'Entrecasteaux Channel (left) to Huon river (right)] and (C) vertical cross section through the D'Entrecasteaux Channel [from south (left) to north (right)].

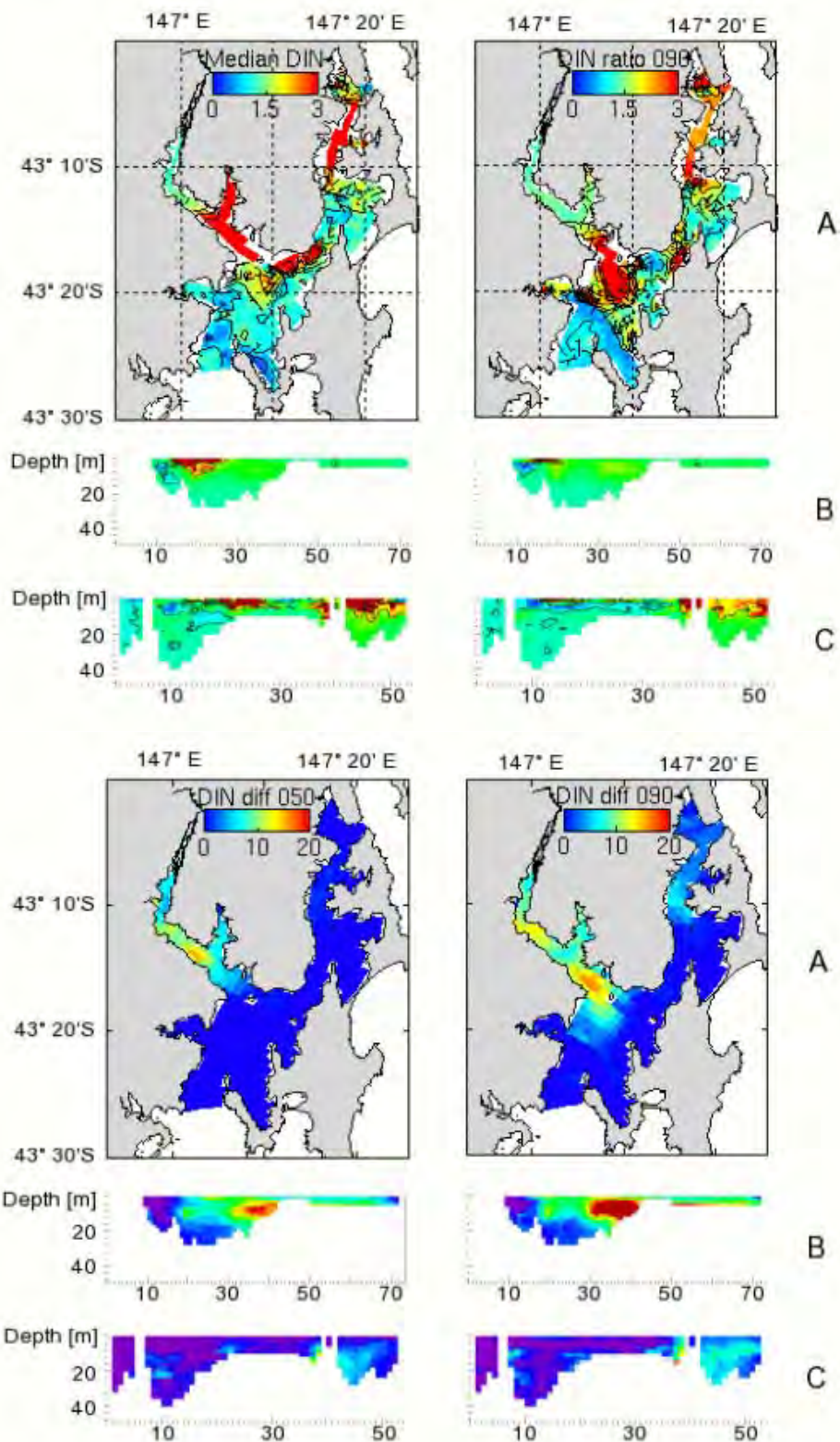


Figure 10.2: Ratio (top) and absolute difference (bottom) in summer median and 90 percentile dissolved inorganic nitrogen between the model run with and without fish farm discharges (A) surface distribution, (B) vertical cross section though the Huon Estuary [from D'Entrecasteaux Channel (left) to

*Huon river (right)] and (C) vertical cross section through the D'Entrecasteaux Channel [from south (left) to north (right)].*

Fish farm discharges had little impact on median dissolved inorganic nitrogen concentrations throughout the region in winter. Concentrations were similar or only slightly elevated in surface waters compared to the standard model run. During this period river and marine nutrient inputs are significant and stormy weather mixes the water column which disperses additional farm discharge. In the lower Huon and northern end of the D'Entrecasteaux Channel subsurface median dissolved inorganic nitrogen concentrations were elevated by farm discharge, by a small amount in comparison to the seasonally high winter concentration  $>60\text{mgN m}^{-3}$ . The greatest impact of farm discharge on the dissolved inorganic nitrogen field was on the subsurface 90 percentile concentration indicating sporadic injection of farm nutrient to these depths probably by resuspension and ventilation of sediment rich in particulate farm waste and degradation products.

In summer seasonal stratification restricts vertical mixing and dissolved inorganic nitrogen discharged from farms accumulates in surface waters. Riverine and marine fluxes of nutrient into surface waters are comparatively small during this period and the farm discharges enhance the ambient surface nitrogen concentration by  $>3$  times in the lower Huon Estuary, and mid- and northern ends of the D'Entrecasteaux Channel. This corresponds to an absolute increase of  $\sim 10\text{mgN m}^{-3}$  in the Huon, but  $<1\text{mgN m}^{-3}$  in the D'Entrecasteaux Channel where surface nutrients are seasonally depleted to near zero concentration. At depth dissolved inorganic nitrogen concentrations are elevated by up to  $20\text{mgN m}^{-3}$  in the lower Huon and  $8\text{mgN m}^{-3}$  at the northern end of the D'Entrecasteaux Channel suggesting that resuspension processes continue to be significant at these locations.

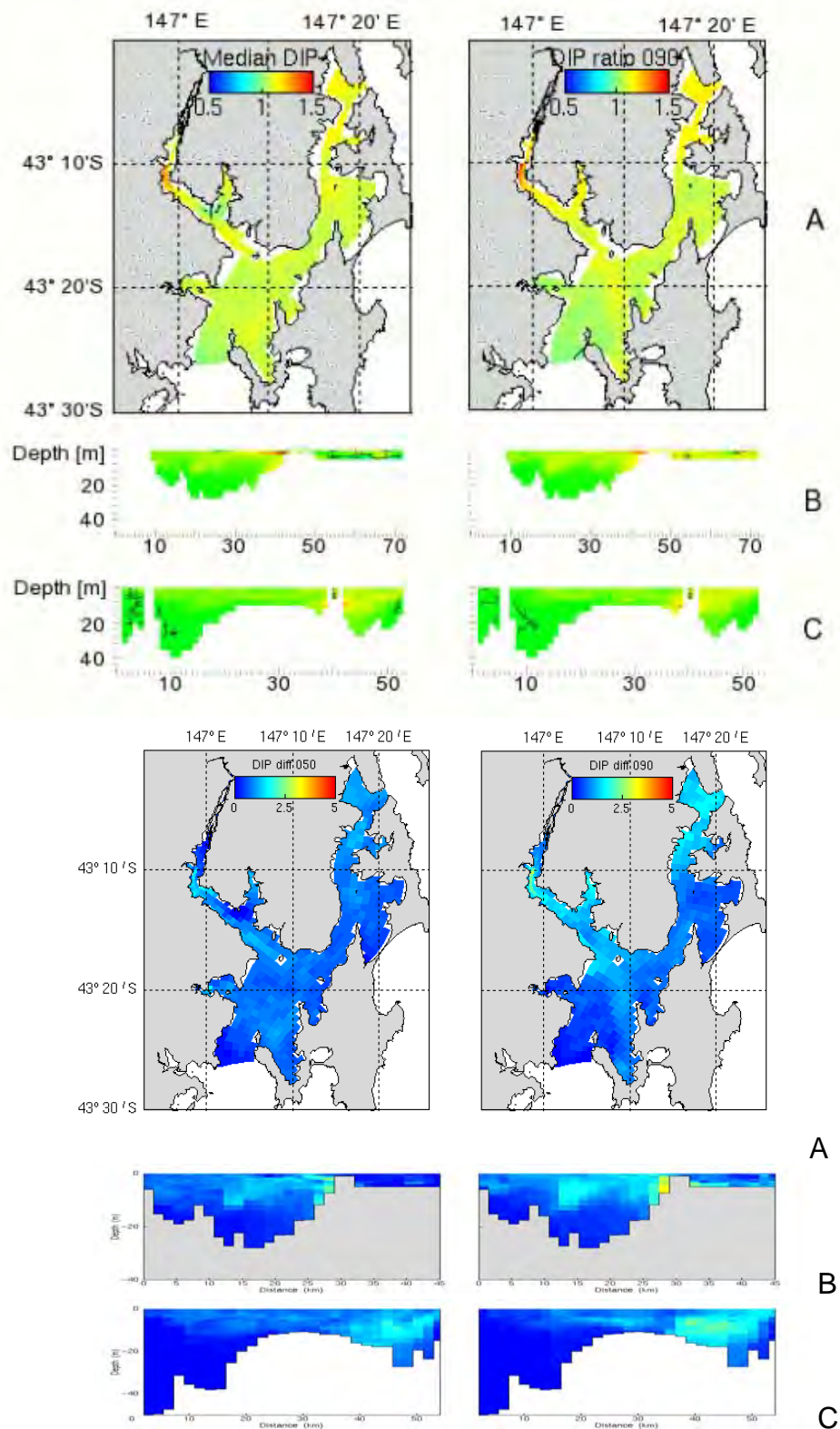


Figure 10.3: Ratio (top) and absolute difference (bottom) in winter median and 90 percentile dissolved inorganic phosphate between the model run with and without fish farm discharges (A) surface distribution, (B) vertical cross section though the Huon Estuary [from D'Entrecasteaux Channel (left) to Huon river (right)] and (C) vertical cross section through the D'Entrecasteaux Channel [from south (left) to north (right)].

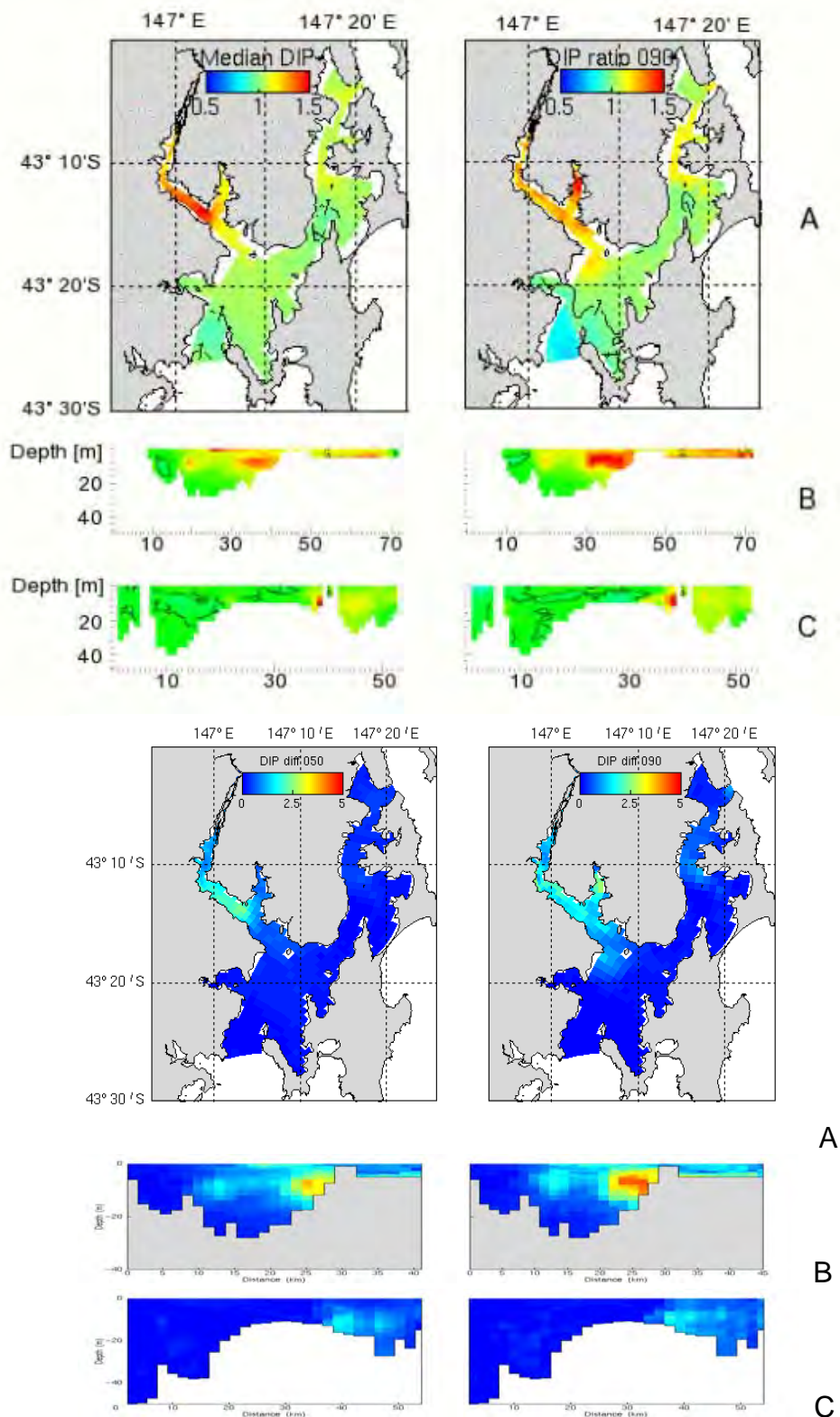


Figure 10.4: Ratio (top) and absolute difference (bottom) in summer median and 90 percentile dissolved inorganic phosphate between the model run with and without fish farm discharges (A) surface distribution, (B) vertical cross section through the Huon Estuary [from D'Entrecasteaux Channel (left) to Huon river (right)] and (C) vertical cross section through the D'Entrecasteaux Channel [from south (left) to north (right)].

Dissolved inorganic phosphate discharged from farms has small impact on the ambient phosphate concentration during winter when seasonal weather and river flows vertically mix and flush the region efficiently. Slight elevation of dissolved inorganic phosphate is simulated in surface waters in the mid Huon estuary (+20%) and in deeper waters towards the northern end of the D'Entrecasteaux Channel. The elevated sub-surface phosphate concentrations likely result from resuspension/ventilation of sediment containing elevated phosphate concentrations in comparison to the standard model run. Farm discharges appear to have greater impact on ambient phosphate than nitrate which reflects their relatively rich phosphate content compared with natural elemental ratios.

Summer farm discharge of phosphate accumulated in the surface layer in the upper and mid Huon Estuary with ambient concentrations enhanced by ~50%. During this period seasonal stratification limited dispersion of the farm discharges which were significant compared to the seasonally low influx of phosphate from marine and river sources. Elevated concentrations were also simulated in deep waters towards the northern end of the D'Entrecasteaux Channel similar to the winter situation.

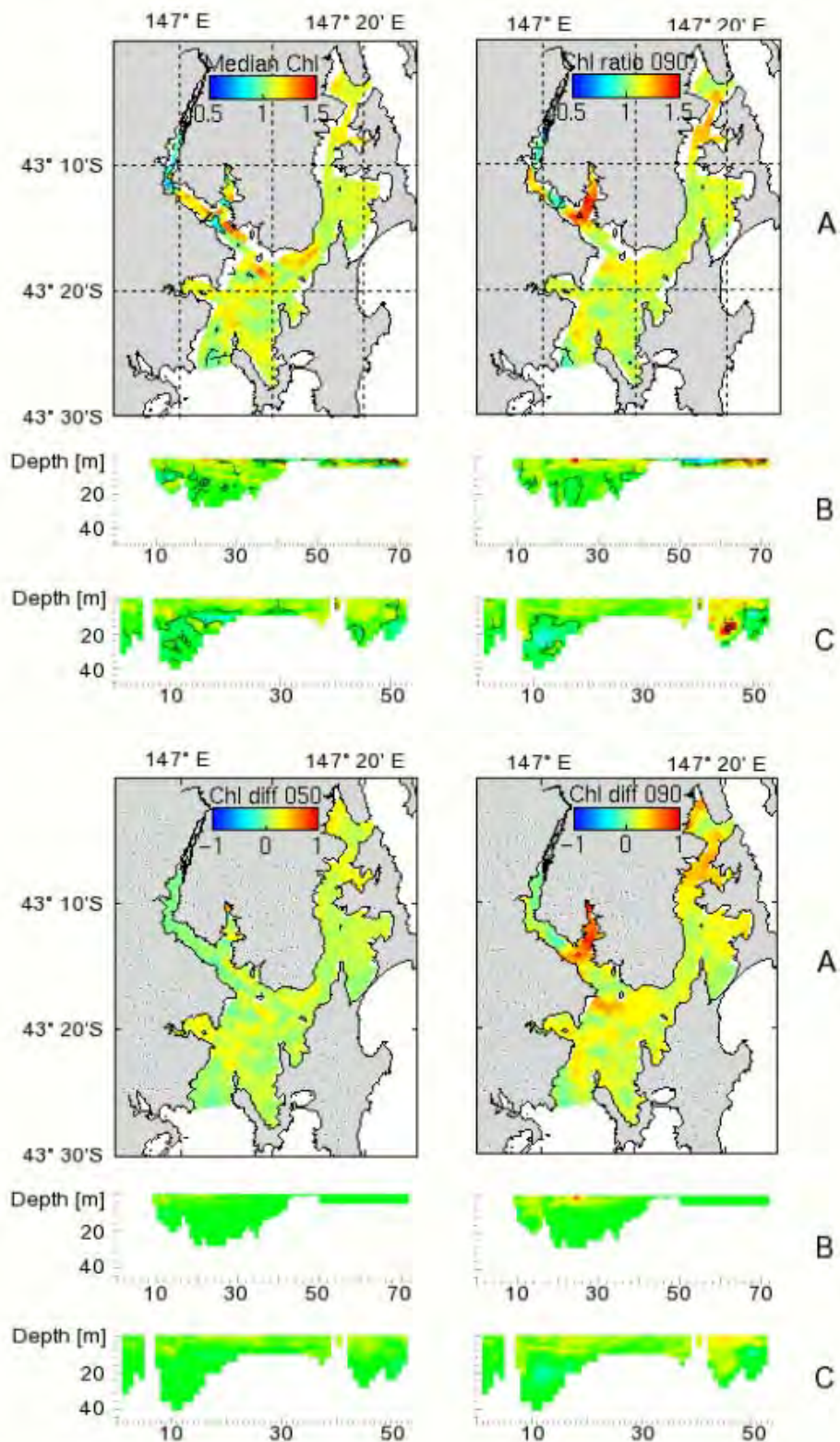


Figure 10.5: Ratio (top) and absolute difference (bottom) in spring median and 90 percentile chlorophyll concentration between the model run with and without fish farm discharges (A) surface distribution, (B) vertical cross section through the Huon Estuary [from D'Entrecasteaux Channel (left) to Huon river (right)] and (C) vertical cross section through the D'Entrecasteaux Channel [from south (left) to north (right)].

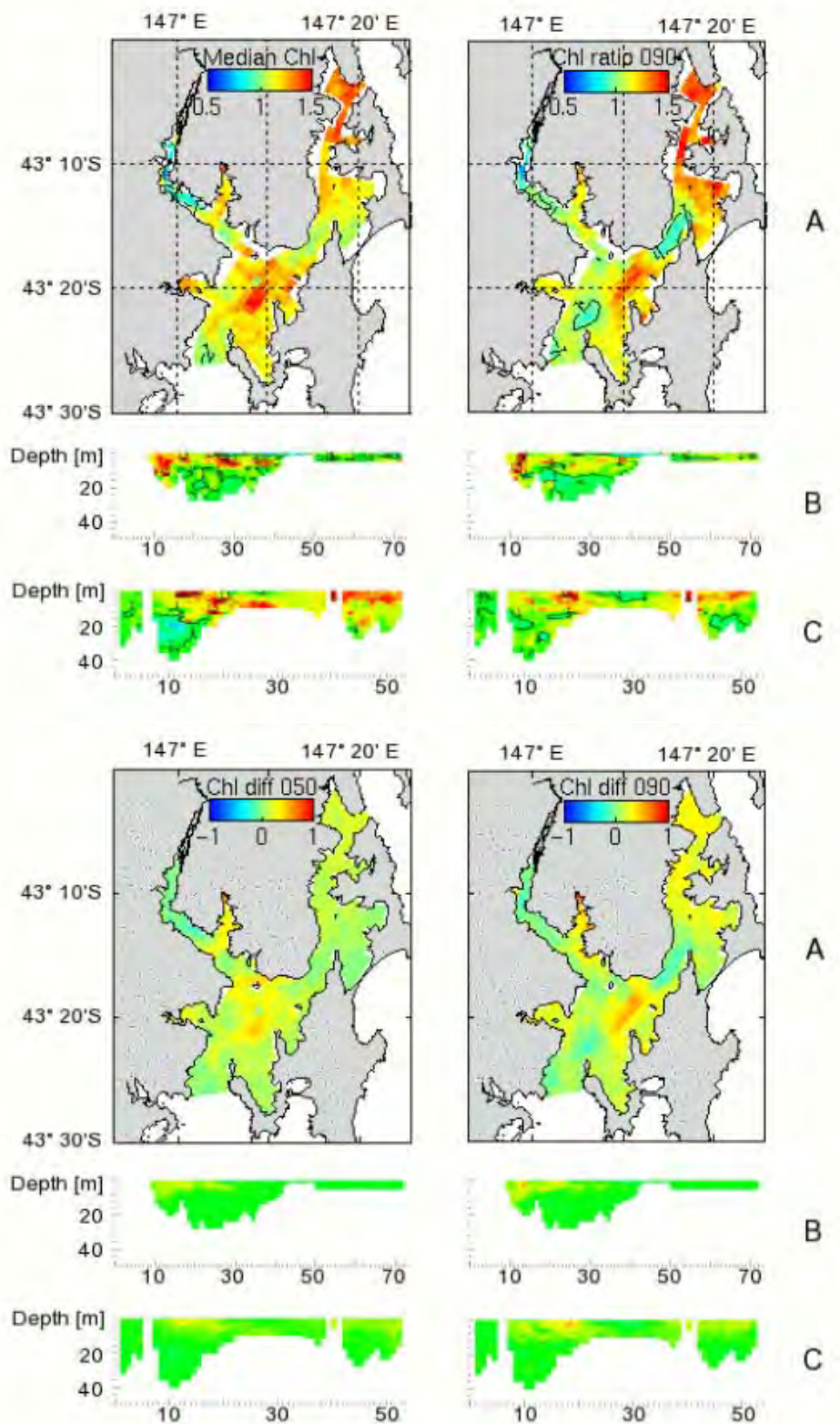


Figure 10.6: Ratio (top) and absolute difference (bottom) in autumn median and 90 percentile chlorophyll concentration between the model run with and without fish farm discharges (A) surface distribution, (B) vertical cross section through the Huon Estuary [from D'Entrecasteaux Channel (left) to Huon river (right)] and (C) vertical cross section through the D'Entrecasteaux Channel [from south (left) to north (right)].

In general spring median chlorophyll concentrations were enhanced by  $\sim 0.2 \text{ mg Chl m}^{-3}$  by farm nutrient discharge throughout the region. A few localised 'hot spots' of greater impact ( $< 20\%$ , or  $\sim 0.5 \text{ mg Chl m}^{-3}$ ) were simulated in the lower Huon and mid D'Entrecasteaux Channel. The 90 percentile chlorophyll concentration was also elevated by  $\sim 30\%$ ,  $1 \text{ mg m}^{-3}$  off Cygnet and by  $\sim 0.7 \text{ mg Chl m}^{-3}$  in the northern end of the D'Entrecasteaux Channel suggesting an increase in bloom events at these locations. Regional spring phytoplankton biomass primarily reflects the ambient winter nutrient concentrations which are dominated by seasonally high river discharge, marine influx and vertical mixing. Winter farm discharges were comparatively small and rapidly dispersed throughout most of the region however by late spring farm discharge exceeded riverine nitrogen supply and localised enrichment of surface nutrient enhanced phytoplankton chlorophyll. In a few locations spring chlorophyll concentration declined in the simulation with farm discharges. The most likely explanation for this is slight variation in zooplankton patchiness between the model runs although elevated concentrations of suspended particulate material may also contribute by reducing the ambient light available for phytoplankton growth.

Autumn chlorophyll concentrations were enhanced by the farm discharges throughout most of the D'Entrecasteaux Channel, the lower Huon and in Northwest Bay. At this time seasonal river and marine nutrient fluxes into surface waters were small, although farm discharges were comparatively high. Median chlorophyll was enhanced by  $\sim 50\%$ ,  $\sim 0.4 \text{ mg Chl m}^{-3}$  in the central and northern end of the Channel and the 90 percentile concentrations indicate an increase in bloom events.

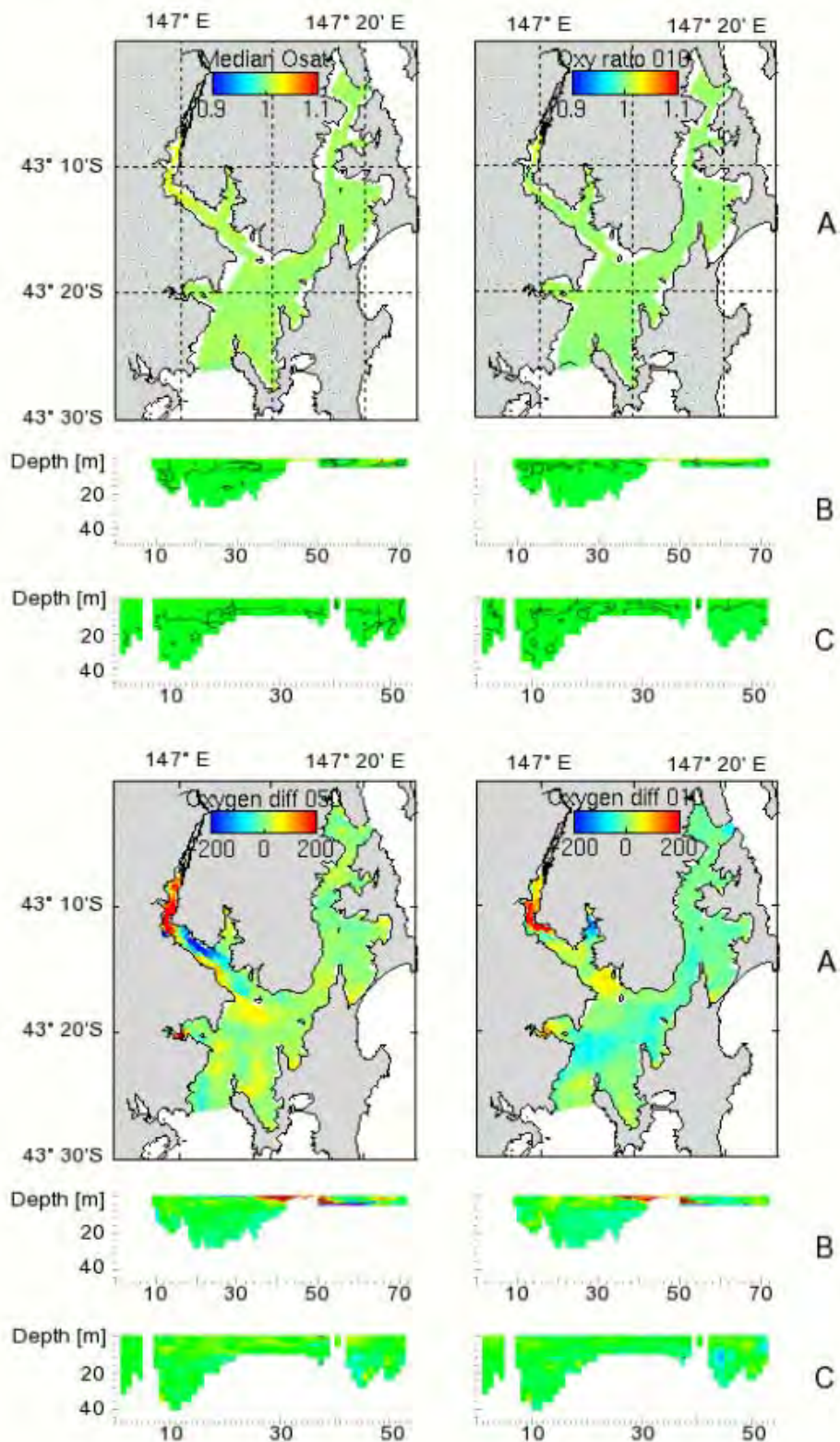


Figure 10.7: Ratio (top) and absolute difference (bottom) in spring median and 10 percentile dissolved oxygen saturation (top) and concentration (bottom) between the model run with and without fish farm discharges (A) surface distribution, (B) vertical cross section through the Huon Estuary [from D'Entrecasteaux Channel (left) to Huon river (right)] and (C) vertical cross section through the D'Entrecasteaux Channel [from south (left) to north (right)].

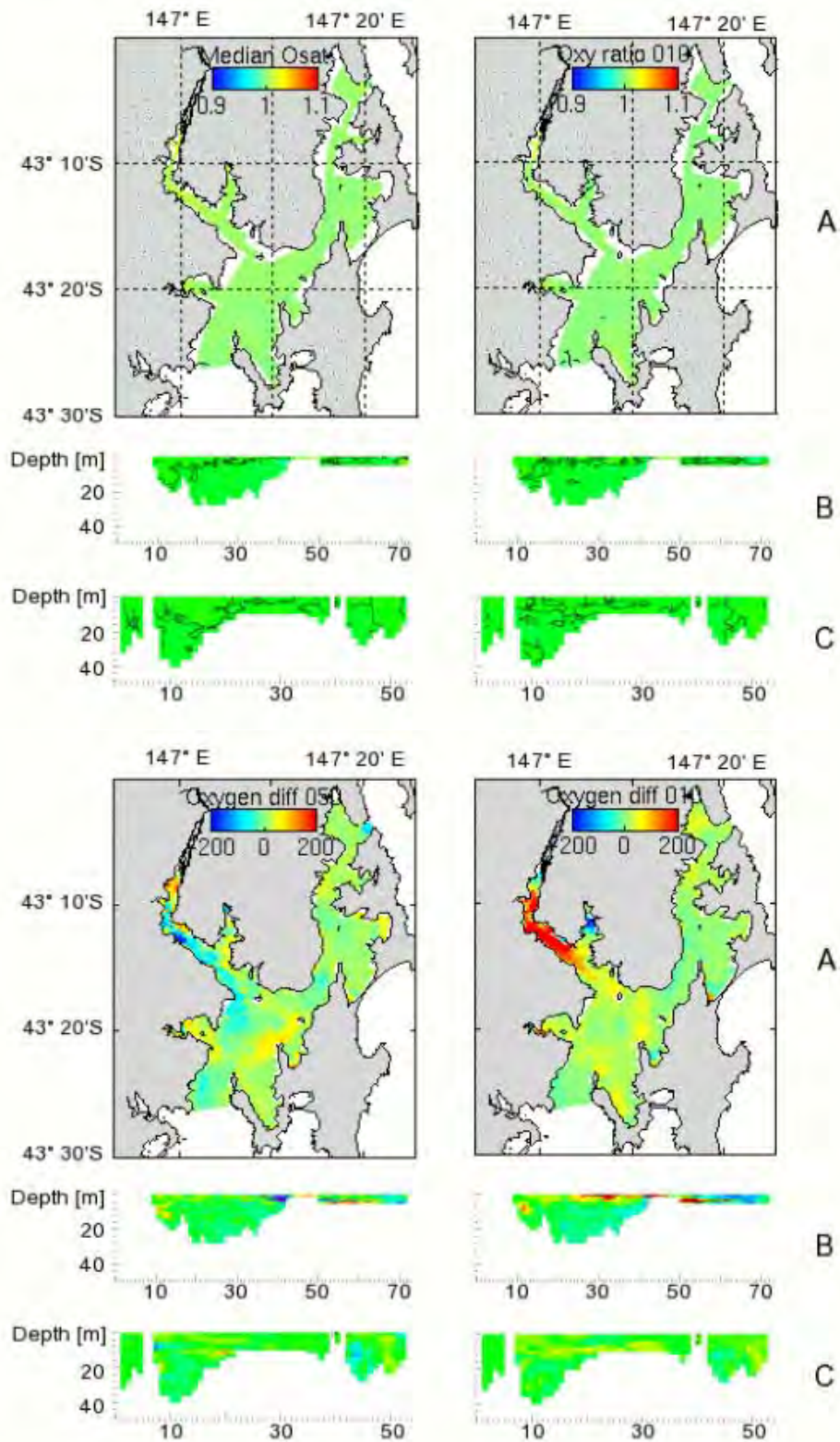


Figure 10.8: Ratio (top) and absolute difference (bottom) in autumn median and 10 percentile dissolved oxygen saturation (top) and concentration (bottom) between the model run with and without fish farm discharges (A) surface distribution, (B) vertical cross section through the Huon Estuary [from D'Entrecasteaux Channel (left) to Huon river (right)] and (C) vertical cross section through the D'Entrecasteaux Channel [from south (left) to north (right)].

Farm discharges had little impact on simulated dissolved oxygen concentrations throughout the year in the D'Entrecasteaux Channel. In the upper Huon Estuary farm discharge resulted in some variation in absolute concentration  $\pm 200 \text{ mg O m}^{-3}$  or  $<2\%$  of the ambient concentration. This likely resulted from spatial differences in phytoplankton production and degradation of organic material between the 2 model runs. Whilst dissolved oxygen concentrations were depleted at depth due to benthic oxygen demand, this was consistent in both simulations indicating that farm discharges do not impact the modelled oxygen field which is well ventilated throughout the year [possibly excessively compared to observations – see section 7.1].

### Summary

The impacts of farm discharges throughout the Huon Estuary and D'Entrecasteaux Channel statistics were prepared for sub-regions of the model domain from the 2 model runs with and without farm discharges.

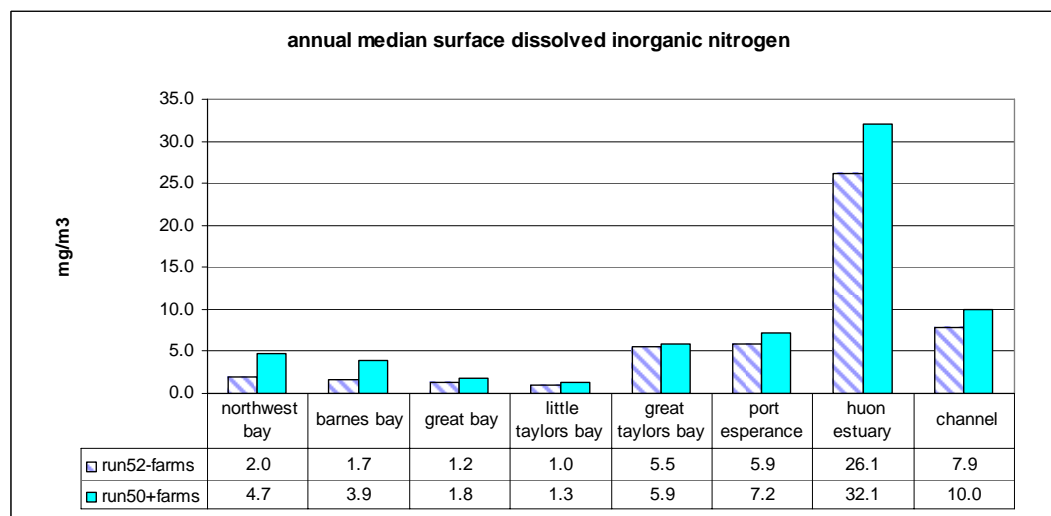
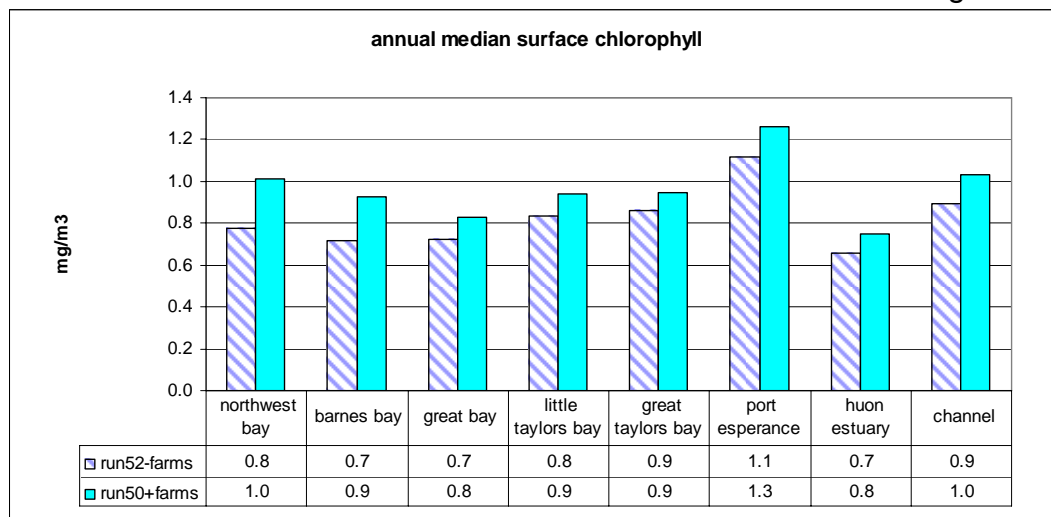


Figure 10.9: Annual median surface chlorophyll (top) and dissolved inorganic nitrogen (bottom) for sub-regions of the model.

Summary statistics for all sites give a mean increase of 17% in annual median surface chlorophyll and 30% for annual median surface dissolved inorganic nitrogen in the model run with farm discharges. The Huon Estuary had the greatest increase in surface dissolved inorganic nitrogen, followed by Northwest Bay and Barnes Bay. These 2 Bays also showed the largest response in enhanced chlorophyll concentration, followed by Port Esperance.

Seasonal statistics for each sub-region show a consistent increase in modelled surface dissolved inorganic nitrogen and surface chlorophyll concentration across the whole region resulting from the farm discharge. The maximum increase in seasonal median surface dissolved inorganic nitrogen occurred in summer (+54%) when surface concentrations were seasonally depleted to near zero concentration. Surface chlorophyll concentrations were most enhanced in autumn and summer when surface nutrient concentrations were augmented with the farm discharge.

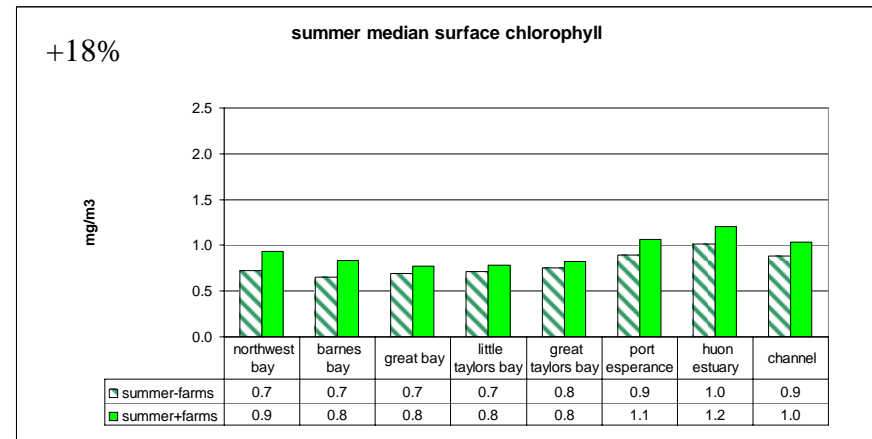
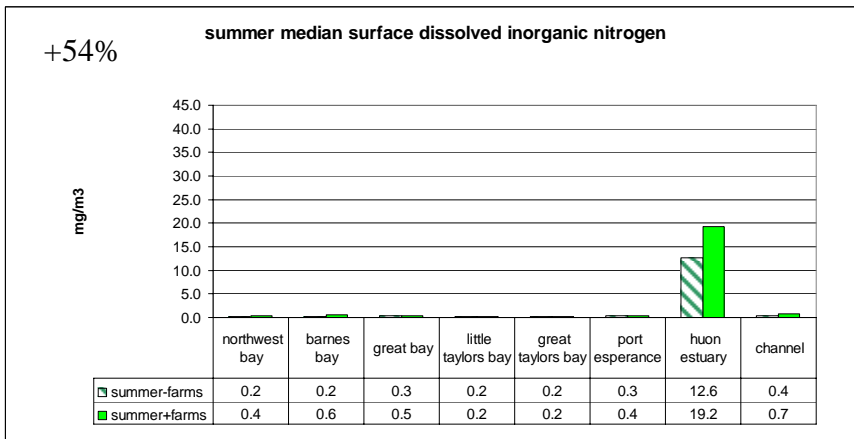
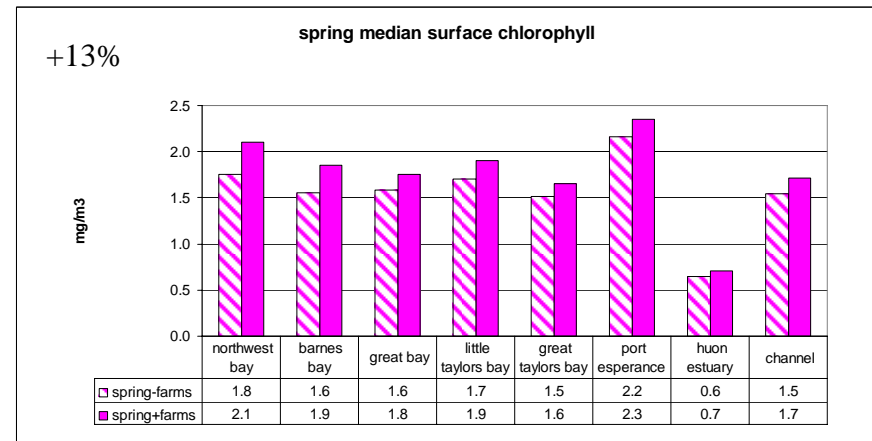
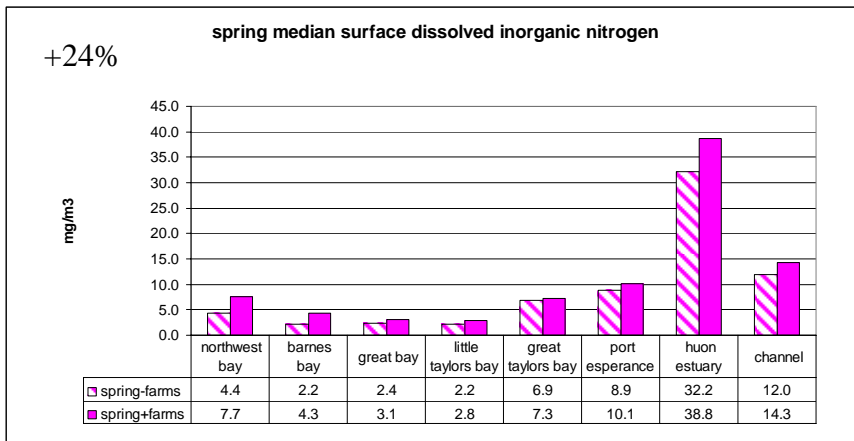


Figure 10.10a: Seasonal surface median dissolved inorganic nitrogen (left) and chlorophyll (right) concentration for sub-regions of the model. Summary statistics for average increase in concentration (with simulation of farm discharges) across all sites are inset.

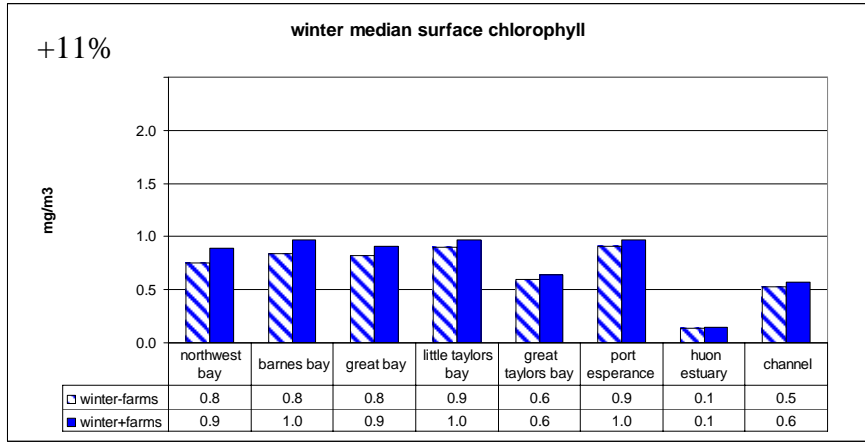
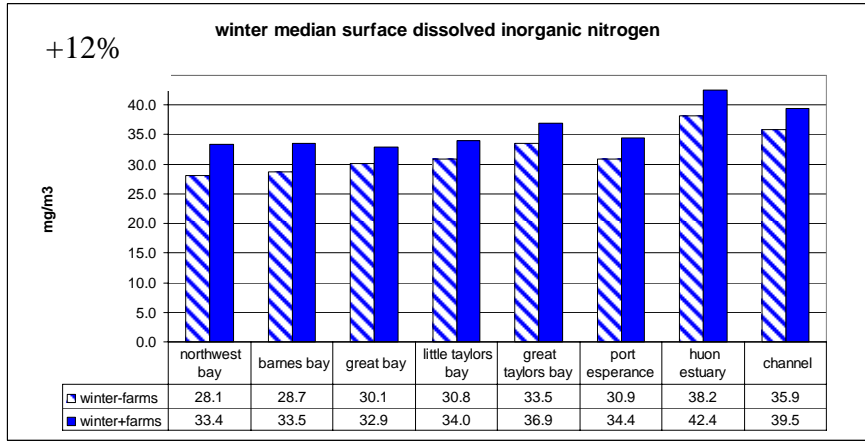
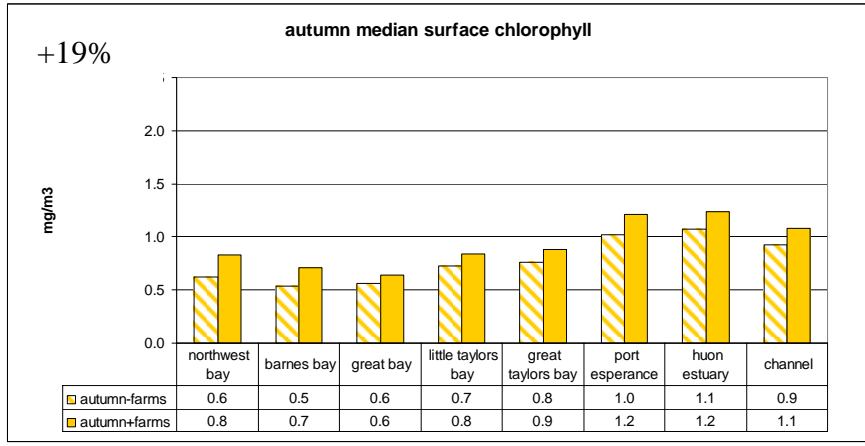
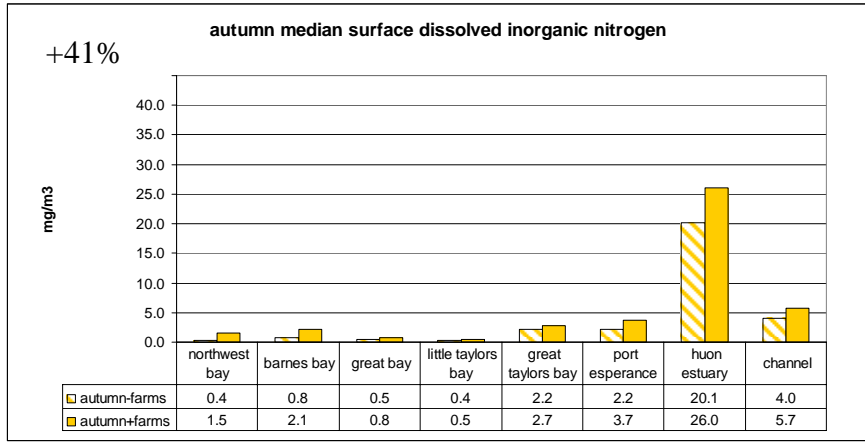


Figure 10.10b: Seasonal surface median dissolved inorganic nitrogen (left) and chlorophyll (right) concentration for sub-regions of the model. Summary statistics for average increase in concentration (with simulation of farm discharges) across all sites are inset.

On an annual basis regional denitrification in tN/y exceeded nitrogen discharged from the fish farms in 2002. Regional denitrification was compared for the simulations with and without farm discharges to evaluate what fraction of the farm waste was being denitrified.

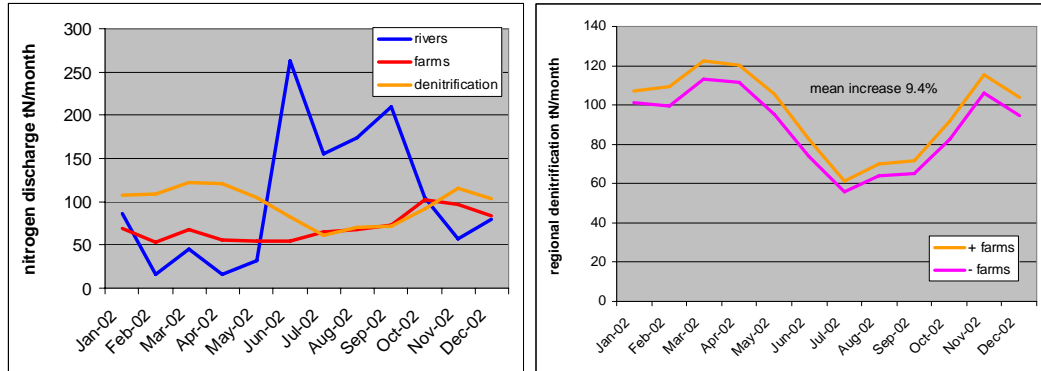


Figure 10.11: Regional denitrification compared to river and farm loads (left) and for the model runs with and without farm loads (right).

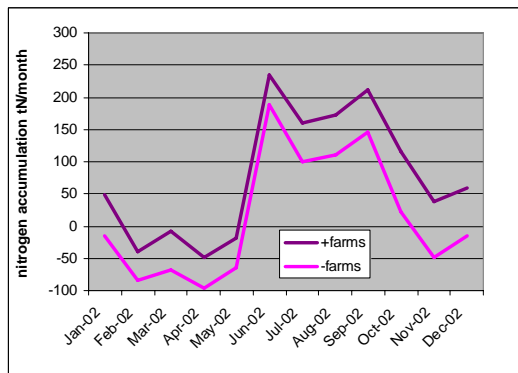


Figure 10.12: Seasonal nitrogen accumulation

	tN/y
River discharge into region	1239.6
Fish farm discharge into region	838.7
Modelled denitrification with farm discharge	1161.5
Modelled denitrification without farm discharge	1062.9
Net gain with farm discharge	920.5
Net gain without farm discharge	176.8

Table 10.2: Relative fluxes of nitrogen into and out of the model region.

Seasonal denitrification throughout the region exceeded the nitrogen discharge from fish farms by 323 tN/y however the impact of the farm discharge on the denitrification flux was comparatively small. Comparing denitrification between the 2 simulations indicated a mean increase in

denitrification flux of 9.4% with farm discharges. This increase indicates that 98tN/y or 11.8% of the 838.7 tN discharged from the farms in 2002 was denitrified.

## 10.2 Impact of secondary river discharge

A simulation with the secondary river (Kermandie, Esperance and Northwest Bay Rivulet) discharges omitted is compared with a simulation including these rivers. In both cases the Huon River, which has a significant impact on the regional dynamics and biogeochemistry, was included and additional fish farm discharges were omitted. Differences between the simulations are presented in ratio plots to emphasise regions where the simulations differ and as absolute differences to quantify the magnitude of any change.

For the ratio plots:

<1 = reduced concentration; 1 = no difference; > 1 = enhanced concentration.

For the difference plots:

-ve value = reduced concentration; 0 = no difference; +ve value = enhanced concentration.

In general secondary river discharges had greatest impact on the nutrient fields in spring-summer and on the phytoplankton in spring. Results are shown for dissolved nutrients in winter and summer and for chlorophyll and oxygen in spring and autumn.

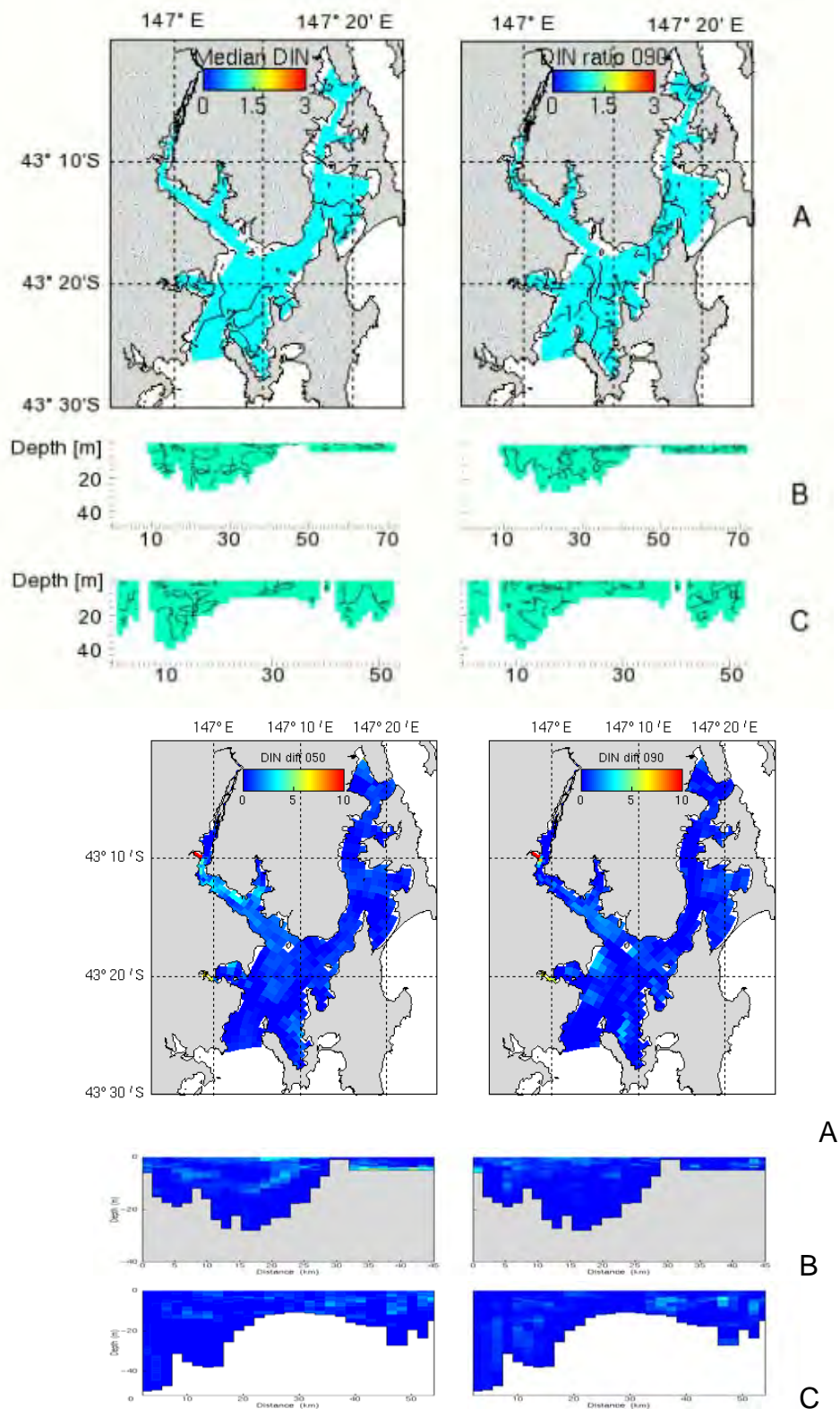


Figure 10.13: Ratio (top) and absolute difference (bottom) in summer median and 90 percentile dissolved inorganic nitrogen between the model run with and without secondary river discharges (A) surface distribution, (B) vertical cross section through the Huon Estuary [from D'Entrecasteaux Channel (left) to Huon river (right)] and (C) vertical cross section through the D'Entrecasteaux Channel [from south (left) to north (right)].

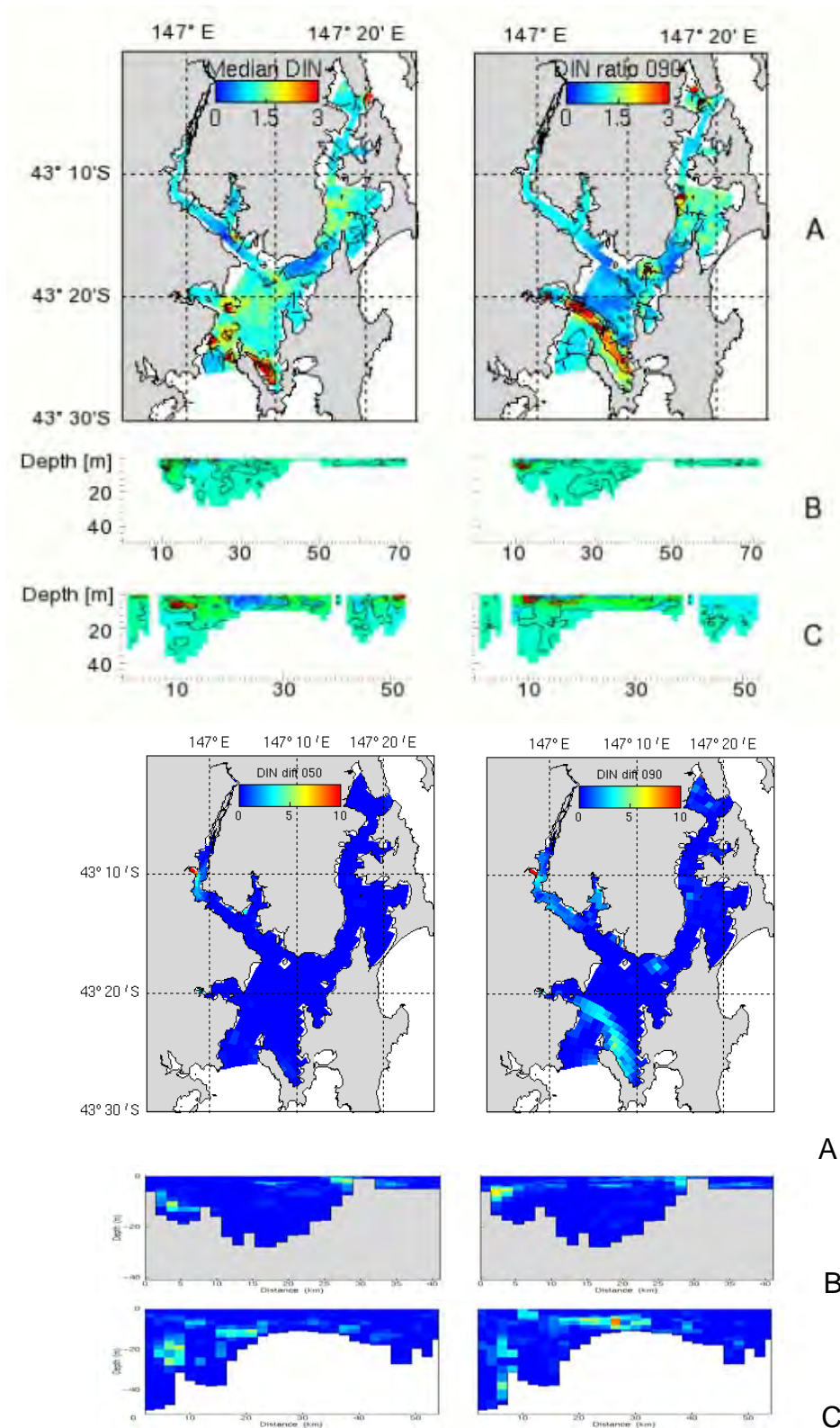


Figure 10.14: Ratio (top) and absolute difference (bottom) in summer median and 90 percentile dissolved inorganic nitrogen between the model run with and without secondary river discharges (A) surface distribution, (B) vertical cross section through the Huon Estuary [from D'Entrecasteaux Channel (left) to Huon river (right)] and (C) vertical cross section through the D'Entrecasteaux Channel [from south (left) to north (right)].

The Kermandie, Esperance and Northwest Bay Rivulet discharges had little impact on the winter dissolved inorganic nitrogen concentration throughout the region although concentrations were slightly elevated (by  $\sim 5\text{mg m}^{-3}$ ) in surface waters of the lower Huon and local enhancement was apparent at the mouth of the Kermandie and Esperance rivers. During winter nutrient fluxes into the region are dominated by inputs from the Huon and marine boundary and the system is vertically well mixed and horizontally well flushed.

In summer the ratio plots indicate that median dissolved inorganic nitrogen concentrations were elevated at the southern end of the D'Entrecasteaux Channel across to Great Taylors Bay and also towards the northern end of the Channel. The difference plots indicate that the magnitude of these changes was actually very small as the near surface layer was seasonally depleted to near zero nutrient concentration. The 90 percentile plots show a distinct band of enhanced surface nitrogen concentration across the southern basin of the D'Entrecasteaux Channel which probably relates to an episodic discharge of dissolved inorganic nitrogen propagated from the Esperance river across the channel associated with heavy rains and high river flow in the 1<sup>st</sup> week of January. There is also an increase in the subsurface 90 percentile nitrogen concentration in the mid D'Entrecasteaux Channel which could relate to an increase in resuspension events due to the additional flux of fresh water flux, or to enhanced regeneration of dissolved inorganic nitrogen from nutrient rich river loads or both.

The secondary river discharges had little impact on the dissolved inorganic phosphate concentrations throughout the region in winter, although there was some local enhancement at the mouth of the Kermandie and Esperance rivers.

In summer there was slight enhancement of surface phosphorous concentration near the Kermandie river and south of Port Esperance. The 90 percentile concentrations indicate episodic phosphate enrichment extending south of the Esperance to the model boundary. This could result from phosphate discharge from the Esperance during periods of southerly flow in the D'Entrecasteaux Channel, or possibly from a difference in the marine boundary flux for dissolved inorganic phosphate between the 2 model runs.

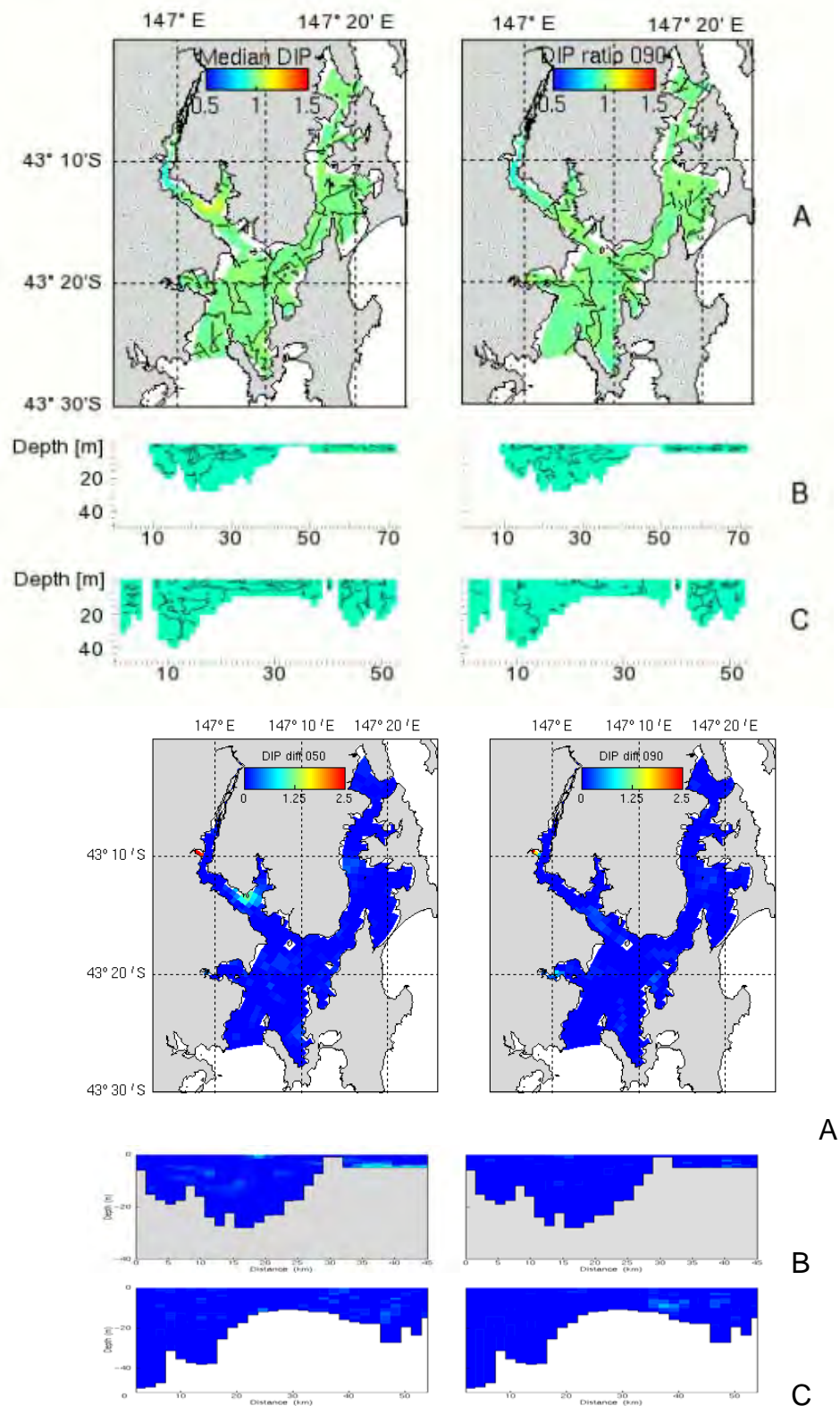


Figure 10.15: Ratio (top) and absolute difference (bottom) in winter median and 90 percentile dissolved inorganic phosphorous between the model run with and without secondary river discharges (A) surface distribution, (B) vertical cross section through the Huon Estuary [from D'Entrecasteaux Channel (left) to Huon river (right)] and (C) vertical cross section through the D'Entrecasteaux Channel [from south (left) to north (right)].

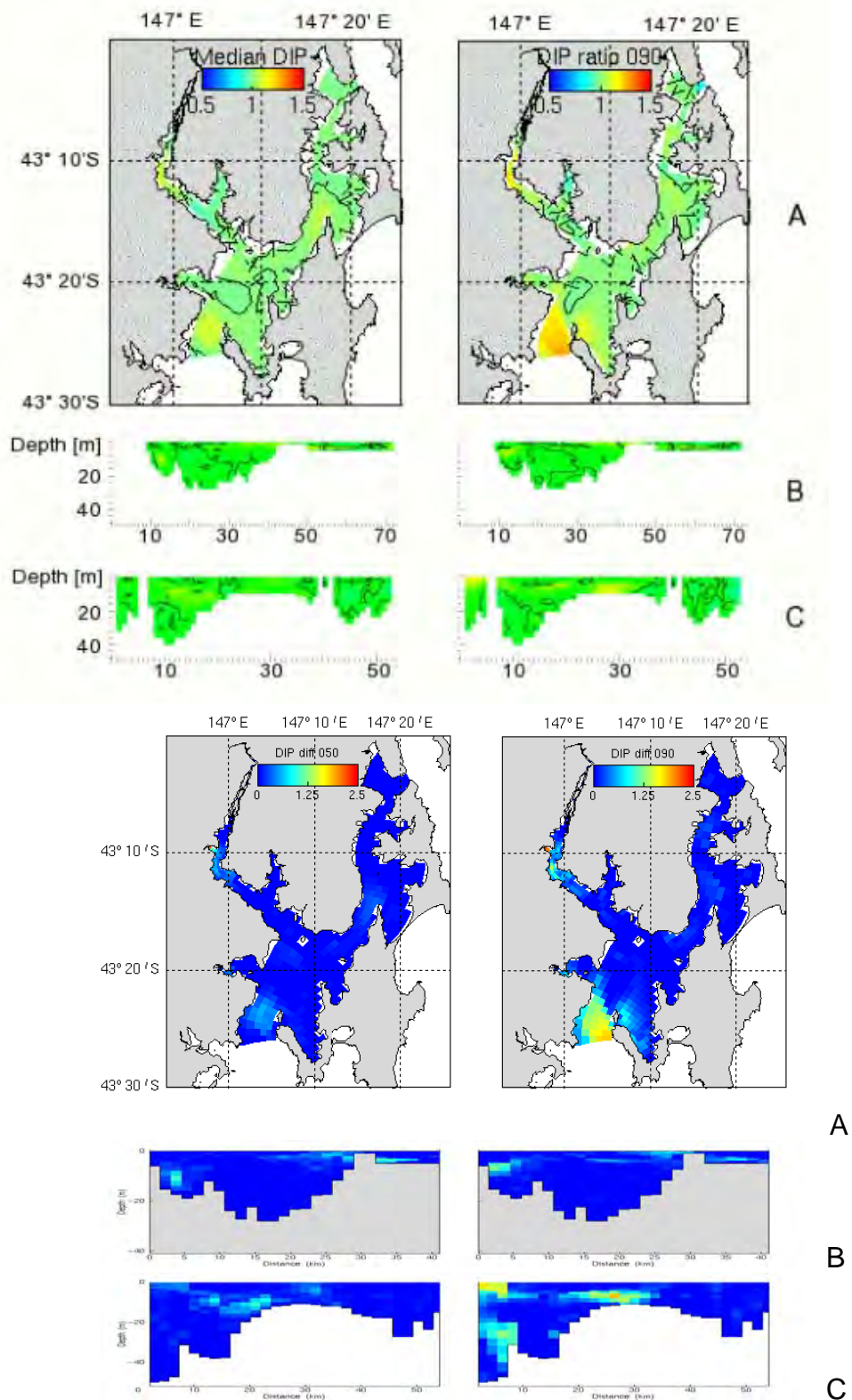


Figure 10.16: Ratio (top) and absolute difference (bottom) in summer median and 90 percentile dissolved inorganic phosphorus between the model run with and without secondary river discharges (A) surface distribution, (B) vertical cross section through the Huon Estuary [from D'Entrecasteaux Channel (left) to Huon river (right)] and (C) vertical cross section through the D'Entrecasteaux Channel [from south (left) to north (right)].

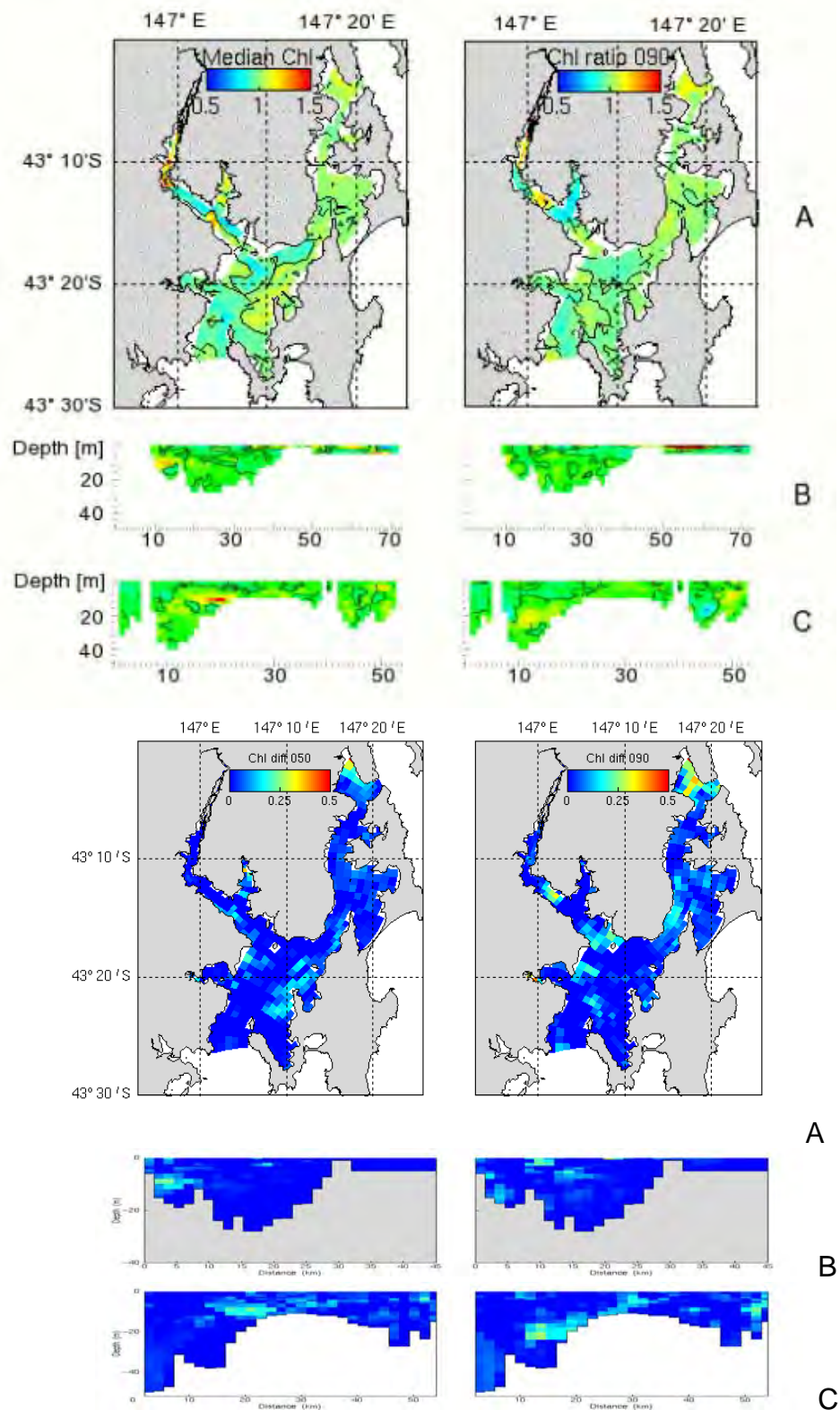


Figure 10.17: Ratio (top) and absolute difference (bottom) in spring median and 90 percentile chlorophyll between the model run with and without secondary river discharges (A) surface distribution, (B) vertical cross section through the Huon Estuary [from D'Entrecasteaux Channel (left) to Huon river (right)] and (C) vertical cross section through the D'Entrecasteaux Channel [from south (left) to north (right)].

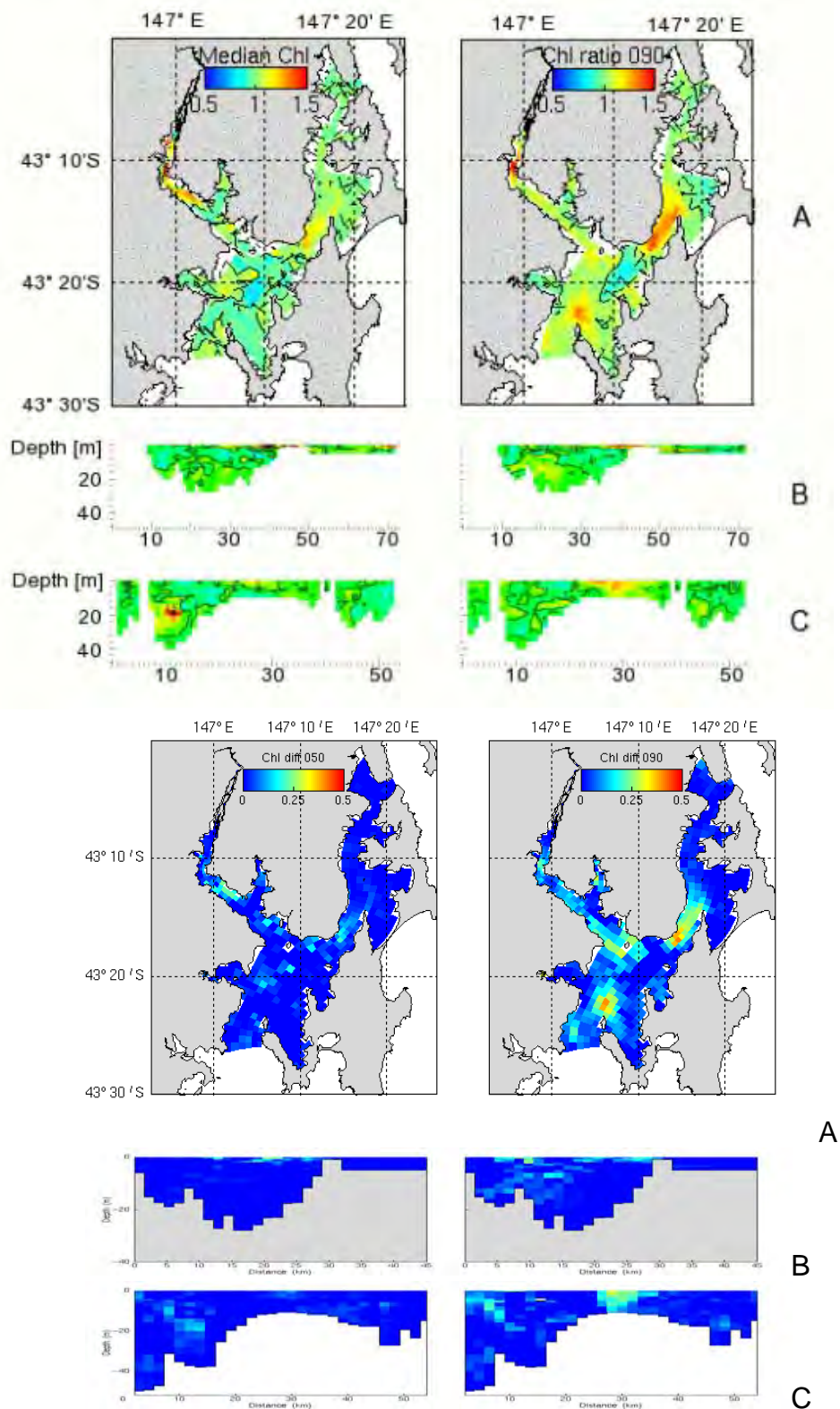


Figure 10.18: Ratio (top) and absolute difference (bottom) in autumn median and 90 percentile chlorophyll between the model run with and without secondary river discharges (A) surface distribution, (B) vertical cross section through the Huon Estuary [from D'Entrecasteaux Channel (left) to Huon river (right)] and (C) vertical cross section through the D'Entrecasteaux Channel [from south (left) to north (right)].

The secondary river discharges elevated spring chlorophyll in the D'Entrecasteaux Channel slightly (+10%) with greatest impact off Great Taylors Bay and locally in Northwest Bay (+0.3mg Chl m<sup>-3</sup>). In the upper Huon Estuary the ratio plots show a significant increase in surface chlorophyll although absolute concentrations in this region were very low (as light limited phytoplankton growth in the highly attenuating river water) so the actual increase in chlorophyll was slight.

In autumn enhanced median concentrations of chlorophyll (+0.2mg Chl m<sup>-3</sup>) were simulated in the lower Huon Estuary and mid D'Entrecasteaux Channel in the model run with secondary river discharges. The increase in chlorophyll in the Huon probably relates to enhanced nutrient supply from the Kermandie river. Its location downstream from the mouth of the Kermandie river suggests that light limitation, due to the highly attenuating river water, is reduced in the lower estuary. In the mid D'Entrecasteaux Channel the enhanced chlorophyll concentrations probably relate to the elevated nitrogen concentrations simulated in the same region, possibly due to enhanced resuspension and or nutrient remineralisation.

Secondary river discharges had little impact on simulated dissolved oxygen concentrations throughout the year and region, although there were small differences (<5%) in the mid-lower Huon Estuary. The reduction of dissolved oxygen in the mid estuary probably relates to the omission of the Kermandie river as an oxygen source with slightly higher oxygen content compared to the estuarine water. In the lower estuary oxygen concentrations increased in the simulation with secondary river discharges due to additional phytoplankton growth resulting from the increased nutrient supply from the Kermandie river.

In the D'Entrecasteaux Channel bottom water oxygen concentrations showed slight local variation in autumn between the model runs. Towards the northern end of the channel bottom water oxygen concentrations increased with secondary river discharge whilst in the mid channel they were slightly reduced. These variations probably arise from slight differences in the spatial distribution and remineralisation of detrital material.

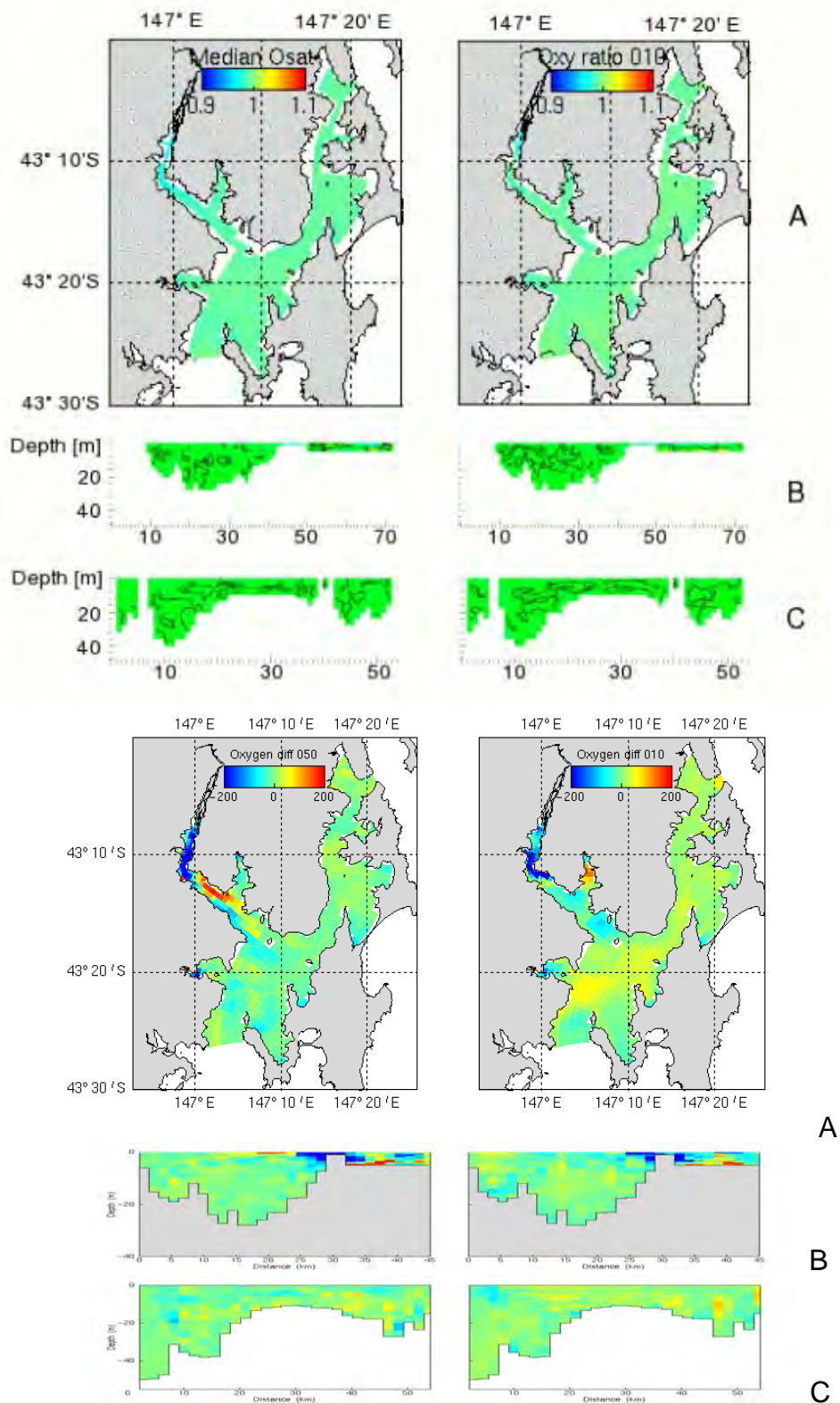


Figure 10.19: Ratio (top) and absolute difference (bottom) in spring median and 10 percentile dissolved oxygen saturation (top) and concentration (bottom) between the model run with and without secondary river discharges (A) surface distribution, (B) vertical cross section through the Huon Estuary [from D'Entrecasteaux Channel (left) to Huon river (right)] and (C) vertical cross section through the D'Entrecasteaux Channel [from south (left) to north (right)].

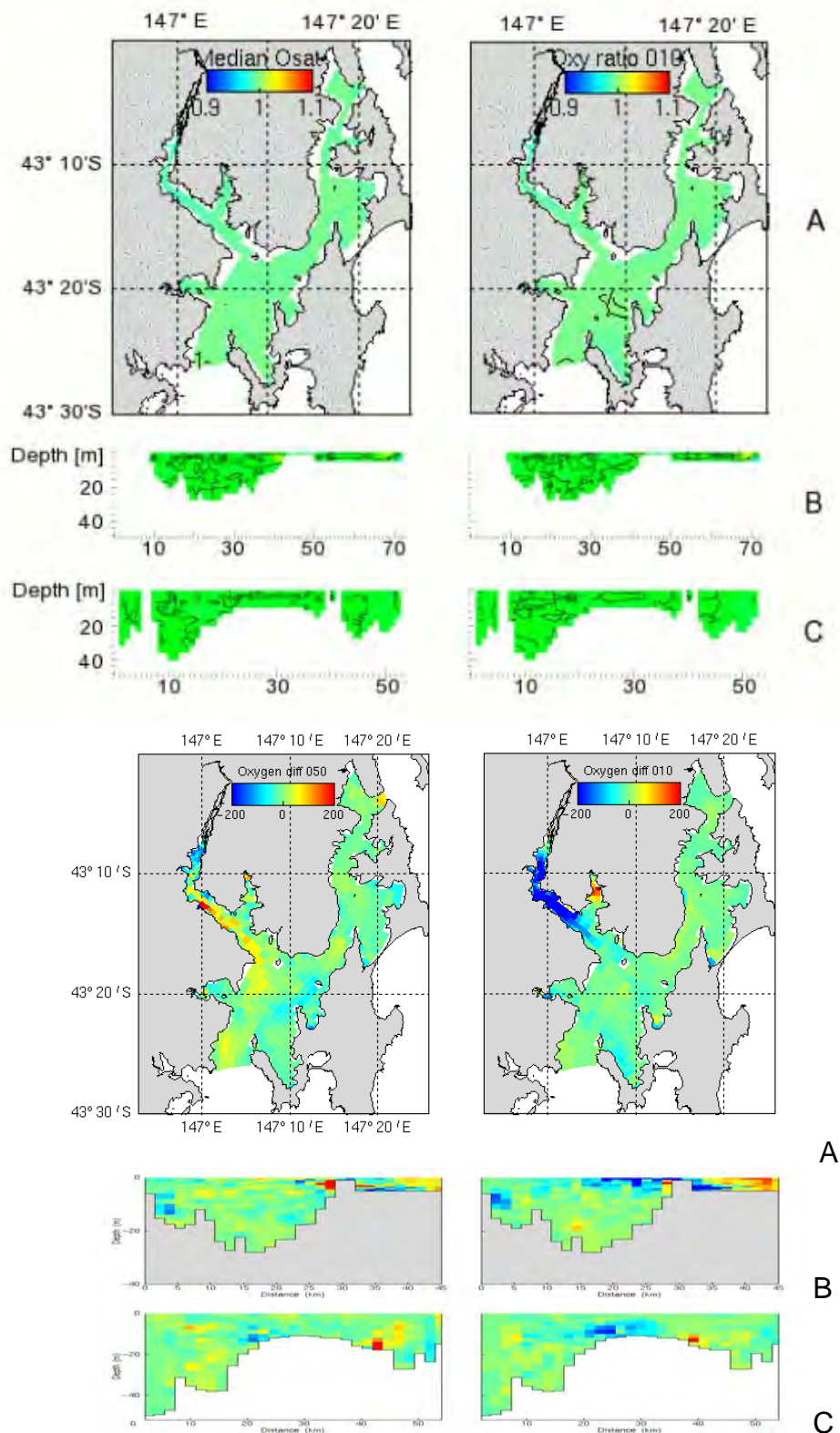


Figure 10.20: Ratio (top) and absolute difference (bottom) in autumn median and 10 percentile dissolved oxygen saturation (top) and concentration (bottom) between the model run with and without secondary river discharges (A) surface distribution, (B) vertical cross section through the Huon Estuary [from D'Entrecasteaux Channel (left) to Huon river (right)] and (C) vertical cross section through the D'Entrecasteaux Channel [from south (left) to north (right)].

## Summary

Annual surface median chlorophyll and dissolved inorganic nitrogen concentrations were calculated for sub regions of the model domain. Over all sub regions there was an increase of 1% in chlorophyll and 4% in dissolved inorganic nitrogen concentration associated with the secondary river discharges (fig.10.22).

The seasonal variation in surface median chlorophyll and dissolved inorganic nitrogen were calculated for sub regions of the model domain. In all cases the simulation with secondary river discharges generated enhanced surface nitrogen and chlorophyll concentrations although the increases were typically small (Fig. 10.24). Secondary river discharges had greatest impact on surface nitrogen and chlorophyll concentrations in spring and summer. In spring additional surface nutrients were readily assimilated into the actively growing phytoplankton population whilst in summer additional surface nutrients alleviated near surface nutrient limitation. The smallest increase in surface nitrogen from secondary rivers occurred in autumn as seasonal river flow was minimal. In contrast during maximal winter river discharge the impact of the secondary rivers on the surface nitrogen field was relatively small due to the considerably greater influx of nutrients from the Huon river and across the marine boundary.

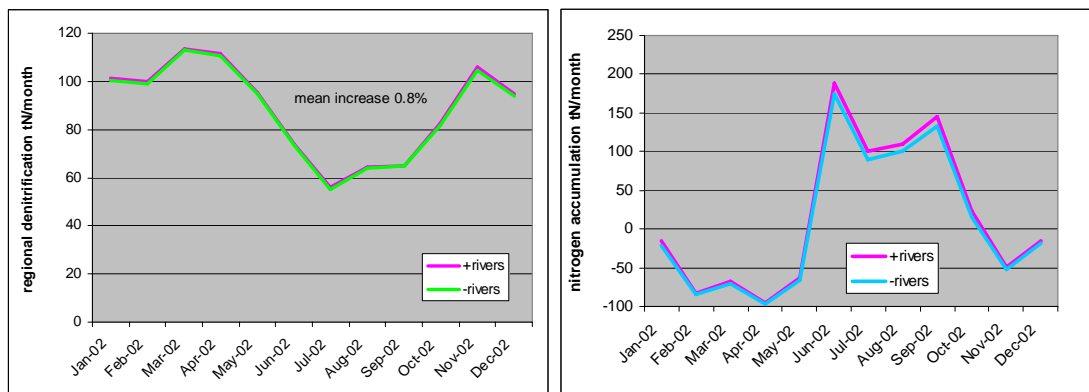


Figure 10.21: Regional denitrification for the model runs with and without secondary river loads (left) and seasonal nitrogen accumulation (right).

	<b>tN/y</b>
Huon River discharge into region	1156.8
Secondary river discharge into region	82.8
Modelled denitrification with secondary river discharge	1062.9
Modelled denitrification without secondary river discharge	1054.8
Net gain with secondary river discharge	176.8
Net gain without secondary river discharge	102.0

*Table 10.2: Relative fluxes of nitrogen into and out of the model region.*

Seasonal denitrification throughout the region exceeded the additional nitrogen discharge from the secondary rivers by 980 tN/y however the impact of the additional river discharge on the denitrification flux was comparatively small. Comparing denitrification between the 2 simulations indicated a mean increase in denitrification flux of just 0.8% with secondary river discharges. This indicates that 8tN/y or 9.7% of the 82.8 tN discharged from the secondary rivers in 2002 was denitrified.

### 10.3 Discussion of scenario simulations

The impact of fish farm discharges on the annual median surface dissolved inorganic nitrogen and chlorophyll concentration was consistently greater in all sub-regions than that of the secondary river discharges. On average the impact of farm discharge was 30 times greater than that of rivers for dissolved inorganic nitrogen and 45 times greater for chlorophyll. This was partly due to the spatial distribution of farm inputs which were more widely spread throughout the region compared to the secondary river locations. The higher ratio for chlorophyll compared with dissolved inorganic nitrogen likely reflects the fact that a larger fraction of the farm nutrient was rapidly assimilated by the phytoplankton. In contrast the river discharge contained a proportion of refractory nitrogen which could only contribute to the dissolved inorganic nutrient pool following remineralisation.

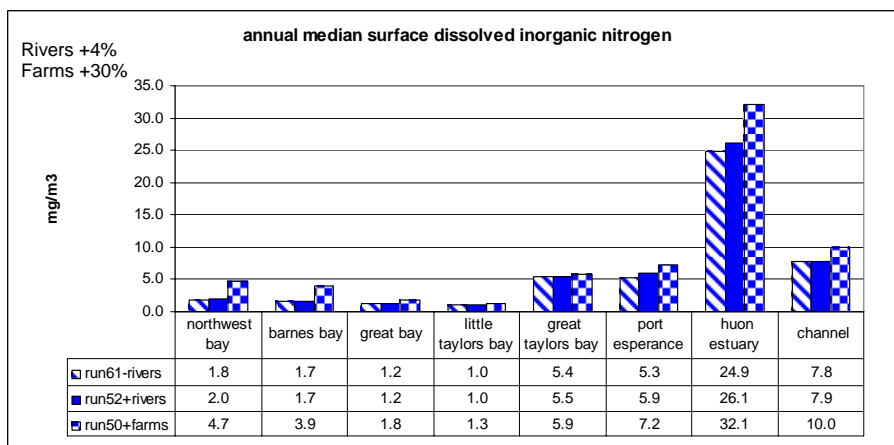
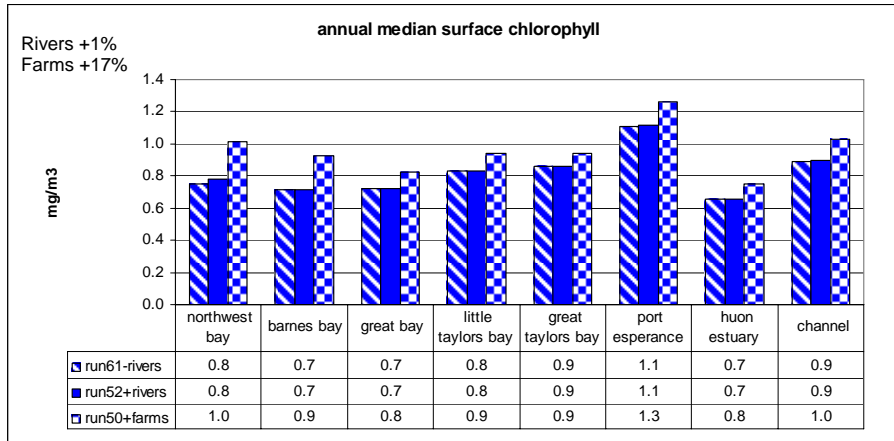


Figure 10.22: Annual median surface chlorophyll (top) and dissolved inorganic nitrogen (bottom) for sub-regions of the model. Mean % increase in concentration inset.

In all seasons and sub-regions fish farm discharges had greater impact on surface nitrogen and chlorophyll than secondary river discharges. The seasonal contrast between farm and river impacts was greatest in autumn when river impacts were small coincident with minimum river flow and farm impacts were relatively large as they supplied nutrient to seasonally depleted surface waters which resulted in additional phytoplankton growth. During this period farm discharges contributed on average to 17 times more dissolved inorganic nitrogen and 46 times more chlorophyll than secondary river discharges. The farm impact on chlorophyll was greater due in part to the more labile nature of the farm discharges which were more rapidly assimilated into phytoplankton.

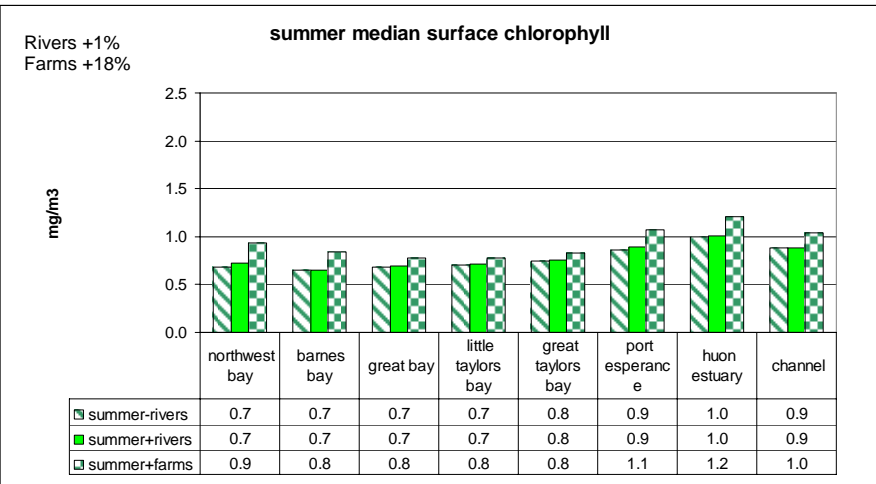
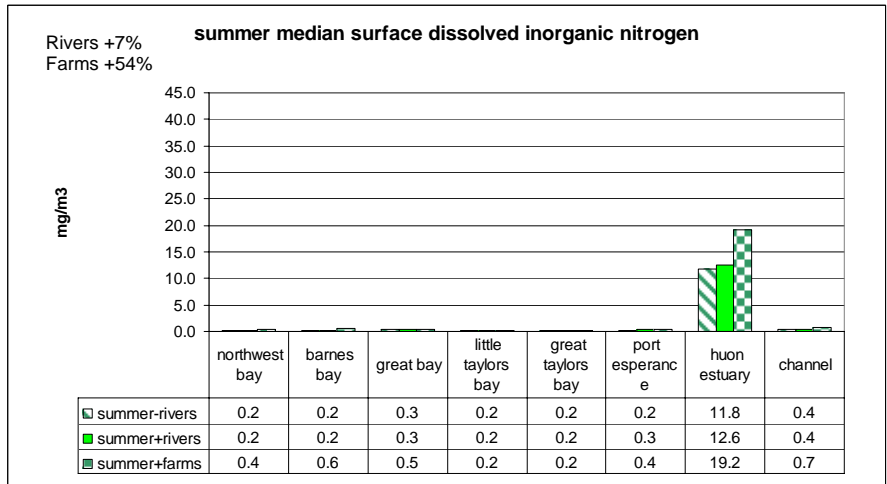
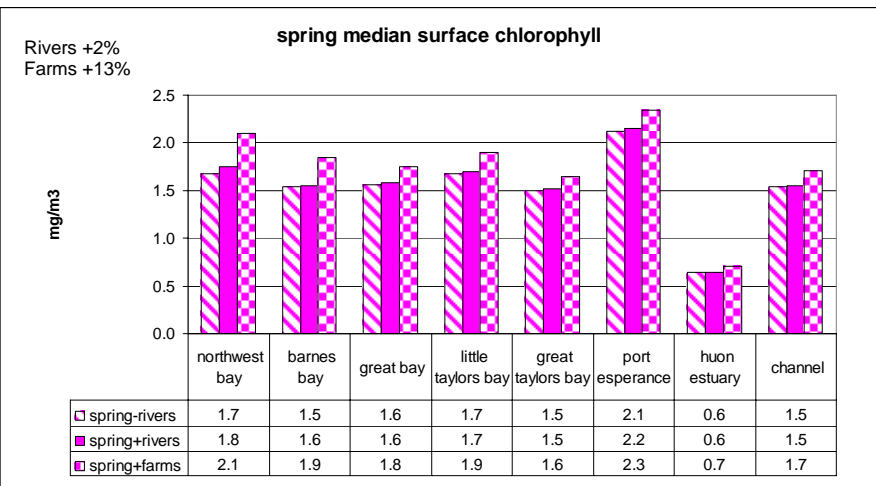
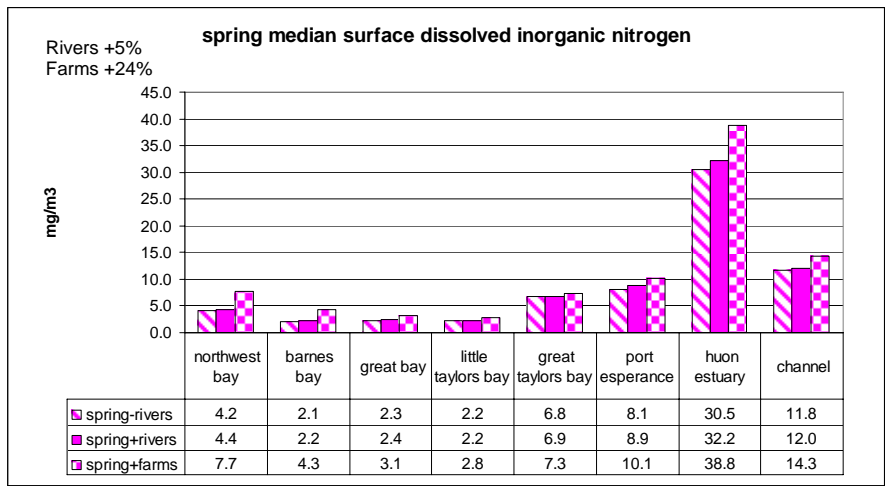


Figure 10.23a: Seasonal surface median dissolved inorganic nitrogen (left) and chlorophyll (right) concentration for sub-regions of the model. The mean % increases in concentration due to secondary river and farm discharges across all sites are inset.

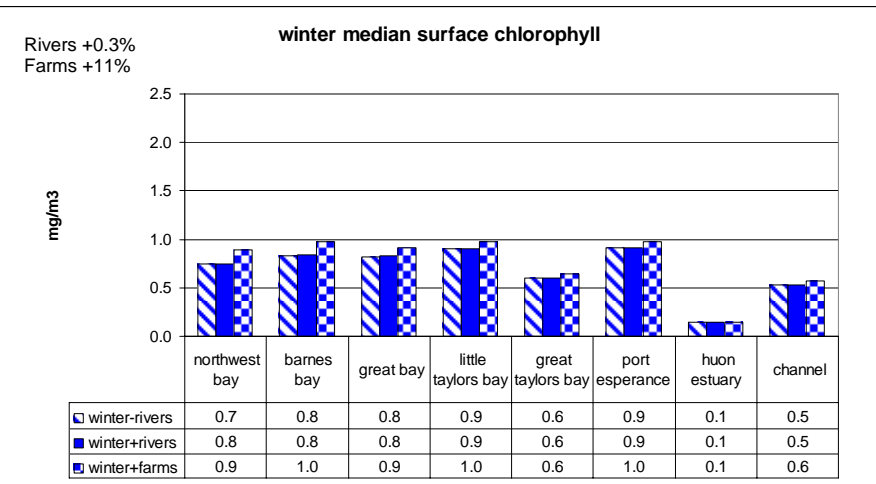
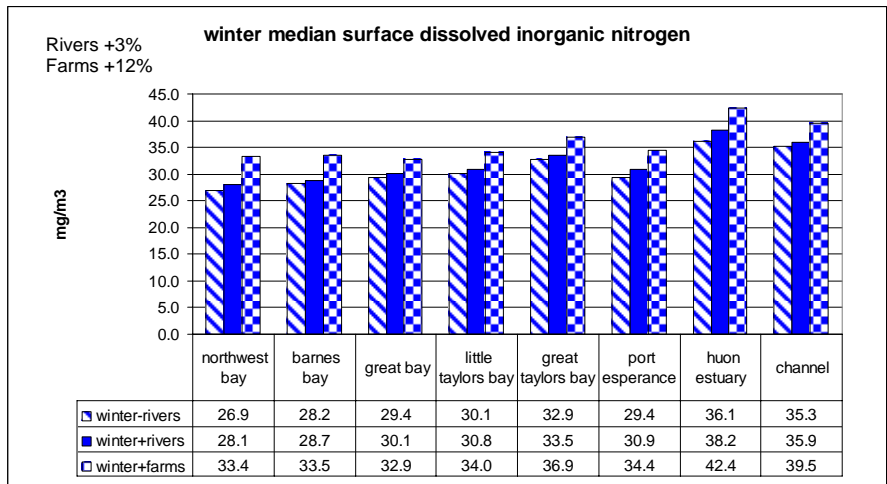
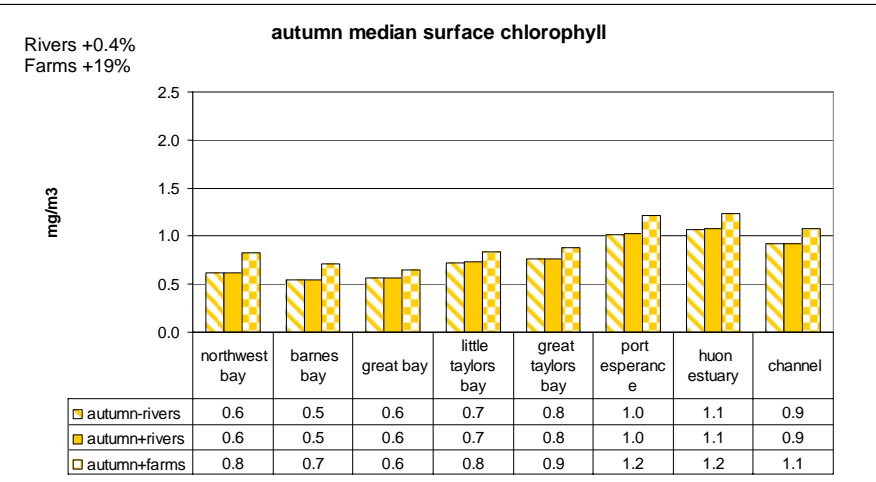
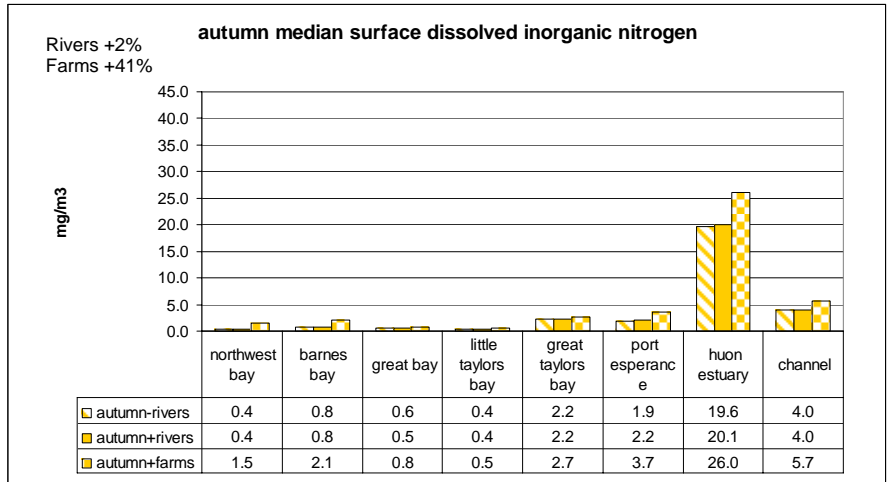


Figure 10.23b: Seasonal surface median dissolved inorganic nitrogen (left) and chlorophyll (right) concentration for sub-regions of the model. The mean % increases in concentration due to secondary river and farm discharges across all sites are inset.

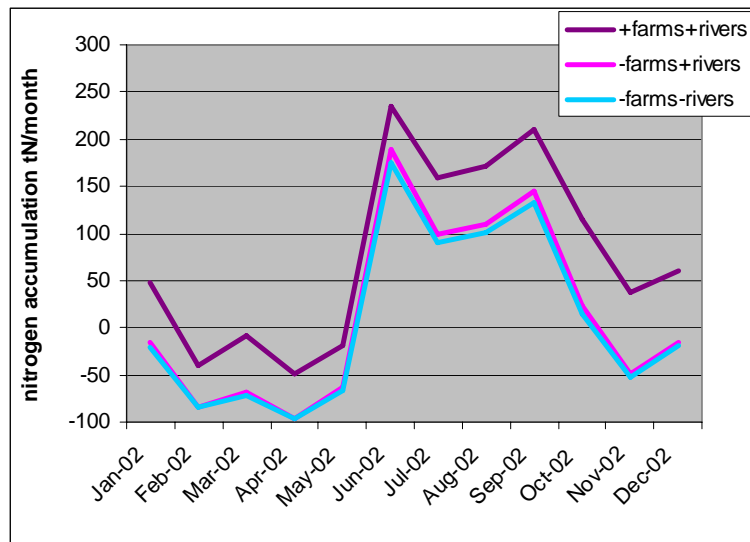


Figure 10.24: Modelled regional nitrogen accumulation for scenario simulations.

Model Run	accumulation tN/y
With Huon River, secondary river & farm discharges into region	920.5
With Huon River & secondary river discharges into region	176.8
With Huon River discharge into region	102.0

Table 10.3: Net accumulation of nitrogen in the model domain.

The net accumulation of nitrogen in the region was greatest in the simulation including secondary river and fish farm discharges. Whilst the secondary rivers contributed an additional 75tN over the year the fish farms added 744tN which is an order of magnitude more nitrogen to the system. It should be noted that whilst these budgets include regional denitrification they do not account for fluxes at the marine model boundaries which likely disperse a portion of the additional nutrient into the broader region. Further analysis of the model results are required to calculate a definitive nitrogen budget for the region and fully define the fate of river and farm nutrient loads.

## 12 References

- Baird, M.E., S.J. Walker, B.B. Wallace, I.T. Webster, J.S. Parslow, 2003. The use of mechanistic descriptions of algal growth and zooplankton grazing in an estuarine eutrophication model. *Estuarine, Coastal and Shelf Science* 56:685–695.
- Baird, M. 2001. CSIRO Simple Estuarine Response Model: Technical Description of the Ecological Model. CSIRO Marine, PO Box 1538, Hobart, TAS 7001. Nov 1.
- Baird, M. E. and Emsley S. M. 1999. Towards a mechanistic model of plankton population dynamics. *Journal of Plankton Research*. 21:85-126.
- Fogg, G. E. 1991. Tansley Review No.30: The phytoplanktonic ways of life. *New Phytology*. 118:191-232.
- CSIRO Huon Estuary Study Team. 2000 Huon Estuary Study – environmental research for integrated catchment management and aquaculture. Final report to Fisheries Research and Development Corporation. Project number 96/284, June 2000. CSIRO Division of Marine Research. Marine Laboratories, Hobart.
- Harris G., Batley, G., Fox, D., Hall, D., Jernakoff, P., Molloy, R., Murray, A., Newell, B., Parslow, J., Skyring, G. & Walker, S. 1996. Port Phillip Bay Environmental Study Final Report. CSIRO, Canberra, Australia.
- Herzfeld, M., Parslow, J., Sakov, P. Andrewartha, J.R. 2005. Numerical hydrodynamic modelling of the D'Entrecasteaux Channel and Huon Estuary. Aquafin CRC Technical report, CSIRO, Hobart, Australia.
- Herzfeld, M., Parslow, J., Sakov, P. and Andrewartha, J.R. 2003 Biogeochemical Modelling of the North West Shelf of Australia. North West Shelf Joint Environmental Management Study. Milestone Report 2.5, CSIRO, Hobart, Australia.
- Jordan, A., Doole, J., Archer, L., Lawler, M., Halley, V. & Sanderson, C. 2002. Assessment and monitoring of nutrients and habitats in North West Bay – Supporting Sustainable management. Kingborough Council Natural Resource Management Strategy, Hobart, 94p.
- Lee, J-Y. Tett P. Jones K. Jones S. Luyten P. Smith C. & Wild-Allen K. 2002. The PROWQM physical-biological model with benthic-pelagic coupling applied to the northern North Sea. *Journal of Sea Research*. 48:287-331.
- Margvelashvili, N. 2003. MECOSSED: Model for estuarine and coastal sediment transport. CSIRO Report pp53.
- Murray, A. G. and Parslow J. S. 1997. Port Phillip Bay Integrated model: Final Report. Port Phillip Bay Environment Study Technical Report No. 44, Melbourne.
- Olive 1973
- Parslow, J., Sakov, P. & Andrewartha, J. 2001. Gippsland Lakes Environmental Study Integrated Model development and Calibration. Technical Report. CSIRO, Hobart, Australia.
- Parslow, J., N. Margvelashvili, D. Palmer, A. Revill, B. Robson, P. Sakov, J. Volkman, R. Watson, I. Webster. 2003. The Response of the Lower Ord River and Estuary to Management of Catchment Flows and

- Sediment and Nutrient Loads. Ord Bonaparte Program, Project 3.4\_4.1\_4.2B Final Science report. CSIRO, Hobart.
- Parslow, J., M. Herzfeld, J.R. Hunter, J.R. Andrewartha, P. Sakov, J. Waring. 2001. Mathematical Modelling of the Dispersal and Fate of CES Discharge from the Boyer Mill in the Upper Derwent Estuary. Final Report. CSIRO Marine Research, Hobart.
- Pavel Sakov 'New Ecology', manuscript CSIRO Division of Marine Research, Marine Laboratories, Hobart.
- Tett, P. 1990. The Photic Zone. In Light and Life in the Sea (ed. Herring, P. J., Campbell, A. K., Whitfield, M. & Maddock, L.), 59-87. Cambridge University Press, Cambridge, U.K.
- Thompson, P. A. Bonham P. Willcox S. Crawford C. 2005. Baseline environmental data for the D'Entrecasteaux Channel. 2005; Aquafin CRC Technical report.